

**STRUCTURAL SYSTEMS
RESEARCH PROJECT**

Final Report
SSRP-19/03

**Alternative Weld Details and Design for
Continuity Plates and Doubler Plates for
Applications in Special and Intermediate
Moment Frames**

by

**MATHEW REYNOLDS
CHIA-MING UANG**

Final Report Submitted to AISC

November 2019

Department of Structural Engineering
University of California, San Diego
La Jolla, California 92093-0085

University of California, San Diego
Department of Structural Engineering
Structural Systems Research Project

Final Report

**Alternative Weld Details and Design for Continuity Plates and
Doubler Plates for Applications in Special and Intermediate
Moment Frames**

by

Mathew Reynolds

Graduate Student Researcher

Chia-Ming Uang

Professor of Structural Engineering

Final Report Submitted AISC

Department of Structural Engineering
University of California, San Diego
La Jolla, California 92093-0085

ABSTRACT

Cyclic testing of ten full-scale steel moment frame connections was conducted to evaluate the efficacy of economized continuity plate and doubler plate weld details. Phase 1 of the testing included six one-sided RBS connections tested in the upright position. Phase 2 of the testing included two-sided WUF-W connections tested in the horizontal position. The rolled shapes were of A992 steel and the plate material was A572 Gr. 50 steel. The testing was performed in displacement control to impose a prescribed drift according to the AISC 341-16 cyclic loading sequence.

The Phase 1 specimens were carefully designed to investigate the applicable column limit states of Flange Local Bending (FLB) and Web Local Yielding (WLY). Three of these specimens were designed to directly challenge a criterion in AISC 341-16, which imposes a minimum thickness of an unstiffened column flange to be equal to the adjacent beam flange width divided by 6. One specimen was designed to use a doubler plate to reinforce the column for the WLY limit state. This doubler plate was designed using a proposed methodology to design the vertical welds in lieu of the stringent requirement imposed by AISC 314-16. One specimen was a nominally identical specimen that was hot-dipped galvanized prior to the simulated field welding of the beam flange CJP welds. The Phase 2 specimens were designed to subject the continuity plates to a higher level of force that is realized by the WUF-W connection and investigate the effect of a continuity plate stiffening of two-sided connections. All of the Phase 1 and 2 specimens that used continuity plate used two-sided fillet welds to attach the continuity plate to the column flange and column web. Most of these specimens (7 of 9) used the proposed fillet weld size of $(3/4)t$, where t is the continuity plate thickness.

All of the specimens passed the AISC Acceptance Criteria for Special Moment Frame applications. The Phase 1 specimens failed either through low-cycle fatigue of the beam in the reduced beam section (Specimens C4, C6-G, and C7) or through fracture of the beam top flange CJP weld (Specimens C3, C5, and C6). After passing the Acceptance Criteria, all Phase 2 specimens all failed eventually through fracture of the beam top flange CJP weld. This fracture primarily initiated at the edge of the beam flange CJP weld root, where the root of the weld met the backing bar.

ACKNOWLEDGMENTS

This project was sponsored by the American Institute of Steel Construction (AISC). The Herrick Corporation donated the fabrication of the specimens and the Smith & Emery Company donated inspection services. The authors also would like to acknowledge the advice from the Advisory Committee composed of Tim Fraser, Tom Kuznik, Kim Roddis, Subhash Goel, and Brian Volpe with James Malley as the Chair.

TABLE OF CONTENTS

ABSTRACT	i
ACKNOWLEDGMENTS	ii
TABLE OF CONTENTS	iii
LIST OF TABLES	vii
LIST OF FIGURES	viii
1 INTRODUCTION	1
1.1 Introduction.....	1
1.2 Research Objective and Scope.....	4
1.3 Literature Review	5
1.3.1 The Pre-Northridge Connection.....	5
1.3.2 The Northridge Earthquake Damage	6
1.3.3 The Post-Northridge Connection	7
1.3.4 Development of Fracture Mechanics to Simulate Beam-to-Column Fracture	10
1.3.5 Continuity Plate and Doubler Plate Research.....	13
1.4 Flexibility-Based Formulation.....	20
1.5 Historical Review of AISC Requirements on Continuity Plate and Doubler Plate Design	22
1.5.1 Lehigh Criterion.....	24
1.5.2 Development of Column Stiffening Limit States	26
1.6 Summary.....	30
2 SPECIMEN DESIGN	38
2.1 General.....	38
2.2 Design Philosophy.....	39
2.2.1 Continuity Plate Design	39
2.2.2 Continuity Plate Weld Design	39
2.2.3 Doubler Plate Vertical Weld Design.....	43
2.3 Specimen Design and Details	44
3 TEST PROGRAM	54

3.1	General.....	54
3.2	Test Setup	55
3.3	Specimen Sizes and Test Order	56
3.4	Specimen Construction and Inspection	56
3.5	Material Properties.....	56
3.6	Instrumentation	57
3.7	Data Reduction	58
3.8	Loading Sequence.....	60
3.9	Acceptance Criteria	60
4	TEST RESULTS.....	92
4.1	General.....	92
4.2	Specimen C3.....	92
4.2.1	General.....	92
4.2.2	Observed Performance.....	92
4.2.3	Recorded Response.....	93
4.3	Specimen C4.....	112
4.3.1	General.....	112
4.3.2	Observed Performance.....	112
4.3.3	Recorded Response.....	113
4.4	Specimen C5.....	134
4.4.1	General.....	134
4.4.2	Observed Performance.....	134
4.4.3	Recorded Response.....	135
4.5	Specimen C6.....	159
4.5.1	General.....	159
4.5.2	Observed Performance.....	159
4.5.3	Recorded Response.....	160
4.6	Specimen C6-G.....	184
4.6.1	General.....	184
4.6.2	Observed Performance.....	184
4.6.3	Recorded Response.....	185

4.7	Specimen C7	198
4.7.1	General	198
4.7.2	Observed Performance	198
4.7.3	Recorded Response	199
4.8	Specimen W1	222
4.8.1	General	222
4.8.2	Observed Performance	222
4.8.3	Recorded Response	223
4.9	Specimen W2	254
4.9.1	General	254
4.9.2	Observed Performance	254
4.9.3	Recorded Response	255
4.10	Specimen W3	285
4.10.1	General	285
4.10.2	Observed Performance	285
4.10.3	Recorded Response	286
4.11	Specimen W4	317
4.11.1	General	317
4.11.2	Observed Performance	317
4.11.3	Recorded Response	318
4.12	Specimen Macroetching	348
4.13	Lateral Bracing Force	353
5	DISCUSSION OF TEST RESULTS	357
5.1	General	357
5.2	Observed Response and Governing Failure Modes	358
5.3	Effect of Galvanization	360
5.4	Continuity Plate Response	360
5.5	Doubler Plate Response	361
5.6	Column Limit States	362
5.6.1	Web Local Yielding (WLY)	362
5.6.2	Flange Local Bending (FLB)	363

5.7	RBS Lateral Bracing Force.....	364
6	SUMMARY AND CONCLUSIONS	379
6.1	Summary.....	379
6.2	Conclusions.....	381
	REFERENCES.....	385
	APPENDIX A: DESIGN DRAWINGS.....	391
	APPENDIX B: WELD INSPECTION REPORTS	400
	APPENDIX C: CERTIFIED MILL TEST REPORTS.....	415
	APPENDIX D: TENSION COUPON TESTING.....	441
	APPENDIX E: WELDING PROCEDURE SPECIFICATIONS.....	454

LIST OF TABLES

Table 1.1 Limit State Matrix (W14 Column and W36 Beam; One-Sided RBS Connection).....	32
Table 2.1 Research Objective Matrix	48
Table 2.2 Phase 1 Specimen RBS Dimensions.....	49
Table 2.3 Continuity Plate Design Metric	50
Table 2.4 Doubler Plate Design Metric	51
Table 3.1 Phase 1 Exterior RBS Connection Test Matrix	62
Table 3.2 Phase Two Interior WUF-W Connection Test Matrix.....	62
Table 3.3 Member Cross-Sectional Dimensions	63
Table 3.4 Base Metal Mechanical Properties	65
Table 3.5 Chemical Compositions for Components from Mill Certificates.....	69
Table 3.6 Weld Metal Charpy V-Notch Test Results	71
Table 4.1 Specimen C3: Lateral Bracing Force.....	354
Table 4.2 Specimen C4: Lateral Bracing Force.....	354
Table 4.3 Specimen C5: Lateral Bracing Force.....	355
Table 4.4 Specimen C6: Lateral Bracing Force.....	355
Table 4.5 Specimen C6-G: Lateral Bracing Force.....	356
Table 5.1 Specimen Performance Comparison.....	365
Table 5.2 Continuity Plate Design and Experimentally Determined Forces	366
Table 5.3 Doubler Plate Design and Experimentally Determined Forces	367
Table 5.4 Specimen Lateral Bracing Force Comparison	368

LIST OF FIGURES

Figure 1.1 Pre-Northridge Connection (Hamburger et al. 2016).....	33
Figure 1.2 Fracture at Beam Bottom Flange Backing Bar (Hamburger et al. 2016).....	33
Figure 1.3 Prequalified Moment Connections (Hamburger et al. 2016)	34
Figure 1.4 Plastic Strain versus Triaxiality Ratio (Ricles et al. 2000).....	34
Figure 1.5 Net-Section Failure of Beam Flange (Ricles et al. 2000).....	35
Figure 1.6 Continuity Plate Free Body Diagram (Mashayekh 2017)	35
Figure 1.7 Flexibility Method Verification (Mashayekh and Uang 2018)	35
Figure 1.8 WLY Limit State (Carter 1999)	36
Figure 1.9 FLB Limit State (Tran et al. 2013).....	36
Figure 1.10 Yield Line Mechanism	36
Figure 1.11 Flange Local Bending Comparison	37
Figure 2.1 Continuity Plate Force Prediction	52
Figure 2.2 Continuity Plate Diagrams	52
Figure 2.3 Continuity Plate Weld <i>DCR</i> Including Shear	52
Figure 2.4 Doubler Plate Free Body Diagram	53
Figure 2.5 Doubler Plate Vertical Fillet Welds	53
Figure 3.1 Exterior Moment Connection Test Setup (Phase 1).....	72
Figure 3.2 Column Support (Phase 1).....	73
Figure 3.3 Lateral Bracing at Loading End (Phase 1)	73
Figure 3.4 Top Flange Intermediate Lateral Restraint (Specimens C3 and C5).....	74
Figure 3.5 Top Flange Intermediate Lateral Restraint (Specimens C4, C6, C6-G, and C7)	74
Figure 3.6 Interior Moment Connection Test Setup (Phase 2).....	75
Figure 3.7 Test Setup (Phase 2)	76
Figure 3.8 Column Supports (Phase 2).....	76
Figure 3.9 Beam Lateral Restraint and Loading End (Phase 2)	77
Figure 3.10 Beam Bottom Flange and Web CJP Weld Preparation (Specimen C5).....	78
Figure 3.11 Beam Top Flange CJP Weld Preparation (Specimen C5).....	78
Figure 3.12 Beam Flange CJP Weld during Groove Welding (Specimen C5)	79

Figure 3.13 Beam Bottom Flange Underside CJP Weld Treatment (Specimen C5).....	80
Figure 3.14 Beam Top Flange Underside CJP Weld Treatment (Specimen C5)	80
Figure 3.15 Beam Web Weld (Specimen C5)	81
Figure 3.16 Continuity Plate Fillet Welds (Specimen C5)	81
Figure 3.17 Exterior Moment Connection (Specimens C3 to C7) Transducer Layout	82
Figure 3.18 Interior Moment Connection (Specimens W1 to W4) Transducer Layout ...	83
Figure 3.19 Specimen C3: Instrumentation	84
Figure 3.20 Specimen C4: Instrumentation	85
Figure 3.21 Specimen C5: Instrumentation	86
Figure 3.22 Specimen C6: Instrumentation	87
Figure 3.23 Specimen C6-G: Instrumentation	88
Figure 3.24 Specimen C7: Instrumentation	89
Figure 3.25 Interior Frame (Specimen W1 to W4): Instrumentation	90
Figure 3.26 AISC Loading Protocol	91
Figure 4.1 Specimen C3: Specimen before Testing.....	96
Figure 4.2 Specimen C3: East Side of Connection.....	97
Figure 4.3 Specimen C3: Beam Top Flange Weld Tearing.....	98
Figure 4.4 Specimen C3: Beam Web Buckling	99
Figure 4.5 Specimen C3: Beam Top Flange Fracture.....	99
Figure 4.6 Specimen C3: Connection at End of Test.....	100
Figure 4.7 Specimen C3: Beam Lateral-Torsional Buckling (End of Test)	101
Figure 4.8 Specimen C3: Beam Top Flange CJP Weld Fracture (End of Test).....	101
Figure 4.9 Specimen C3: Recorded Loading Sequence.....	102
Figure 4.10 Specimen C3: Applied Load versus Beam End Displacement Response ...	102
Figure 4.11 Specimen C3: Moment at Column Face versus Story Drift Response.....	103
Figure 4.12 Specimen C3: Moment at Column Face versus Plastic Rotation	103
Figure 4.13 Specimen C3: Panel Zone Shear Deformation	104
Figure 4.14 Specimen C3: Column Rotation.....	104
Figure 4.15 Specimen C3: Energy Dissipation.....	105
Figure 4.16 Specimen C3: Topside of Beam Top Flange Strain Profile	106
Figure 4.17 Specimen C3: Underside of Beam Bottom Flange Strain Profile	107

Figure 4.18 Specimen C3: Column Flange Warping	108
Figure 4.19 Specimen C3: Panel Zone Response	109
Figure 4.20 Specimen C3: Column Flange Strain Profile	111
Figure 4.21 Specimen C4: Specimen before Testing.....	116
Figure 4.22 Specimen C4: East Side of Connection.....	117
Figure 4.23 Specimen C4: Beam Bottom Flange Yielding and Buckling.....	118
Figure 4.24 Specimen C4: Beam Web Yielding at +0.02 rad (2 nd Cycle).....	119
Figure 4.25 Specimen C4: Beam Top Flange at -0.04 rad (1 st Cycle).....	119
Figure 4.26 Specimen C4: Beam Flange and Web Yielding at -0.04 rad (1 st Cycle).....	120
Figure 4.27 Specimen C4: Beam Web Buckling at -0.04 rad (1 st Cycle).....	120
Figure 4.28 Specimen C4: Beam Bottom Flange Fracture after one cycle at 0.06 rad ..	121
Figure 4.29 Specimen C4: Beam Top Flange at -0.06 rad (2 nd Cycle).....	121
Figure 4.30 Specimen C4: Connection at End of Test.....	122
Figure 4.31 Specimen C4: Beam Bottom Flange Fracture (End of Test).....	123
Figure 4.32 Specimen C4: Column Flange (End of Test)	123
Figure 4.33 Specimen C4: Recorded Loading Sequence.....	124
Figure 4.34 Specimen C4: Applied Load versus Beam End Displacement Response ...	124
Figure 4.35 Specimen C4: Moment at Column Face versus Story Drift Response.....	125
Figure 4.36 Specimen C4: Moment at Column Face versus Plastic Rotation	125
Figure 4.37 Specimen C4: Panel Zone Shear Deformation	126
Figure 4.38 Specimen C4: Column Rotation.....	126
Figure 4.39 Specimen C4: Energy Dissipation.....	127
Figure 4.40 Specimen C4: Topside of Beam Top Flange Strain Profile	128
Figure 4.41 Specimen C4: Underside of Beam Bottom Flange Strain Profile	129
Figure 4.42 Specimen C4: Column Flange Warping.....	130
Figure 4.43 Specimen C4: Column Panel Zone Response	131
Figure 4.44 Specimen C4: Column Web Strain Profiles	132
Figure 4.45 Specimen C4: Column Flange Strain Profiles.....	133
Figure 4.46 Specimen C5: Specimen before Testing.....	139
Figure 4.47 Specimen C5: East Side of Connection.....	140
Figure 4.48 Specimen C5: Beam Top Flange.....	141

Figure 4.49 Specimen C5: Beam Top Flange CJP Weld Fracture Progression.....	142
Figure 4.50 Specimen C5: Column Kinking due to Panel Zone Deformation	143
Figure 4.51 Specimen C5: Beam Web Buckling (End of Test).....	144
Figure 4.52 Specimen C5: Beam Lateral-Torsional Buckling (End of Test)	144
Figure 4.53 Specimen C5: Continuity Plate (End of Test)	145
Figure 4.54 Specimen C5: Recorded Loading Sequence.....	146
Figure 4.55 Specimen C5: Applied Load versus Beam End Displacement Response ...	146
Figure 4.56 Specimen C5: Moment at Column Face versus Story Drift Response.....	147
Figure 4.57 Specimen C5: Moment at Column Face versus Plastic Rotation	147
Figure 4.58 Specimen C5: Panel Zone Shear Deformation	148
Figure 4.59 Specimen C5: Column Rotation	148
Figure 4.60 Specimen C5: Energy Dissipation.....	149
Figure 4.61 Specimen C5: Topside of Beam Top Flange Strain Profile	150
Figure 4.62 Specimen C5: Underside of Beam Bottom Flange Strain Profile	151
Figure 4.63 Specimen C5: Column Flange Warping.....	152
Figure 4.64 Specimen C5: Panel Zone Response	153
Figure 4.65 Specimen C5: Continuity Plate at Column Flange Edge Strain Profile	154
Figure 4.66 Specimen C5: Continuity Plate at Column Flange Edge Shear Strain Profile	155
Figure 4.67 Specimen C5: Continuity Plate Strain Gauge Rosette R09 Response	156
Figure 4.68 Specimen C5: Continuity Plate at Column Web Edge Shear Strain Profile	157
Figure 4.69 Specimen C5: Bottom Continuity Plate Bending.....	158
Figure 4.70 Specimen C6: Specimen before Testing.....	163
Figure 4.71 Specimen C6: East Side of Connection.....	164
Figure 4.72 Specimen C6: Beam Top Flange.....	165
Figure 4.73 Specimen C6: Beam Top Flange CJP Weld Fracture Progression.....	166
Figure 4.74 Specimen C6: Beam Bottom Flange Yielding	167
Figure 4.75 Specimen C6: Panel Zone Yielding	168
Figure 4.76 Specimen C6: Beam Web and Flange Local Buckling at +0.04 rad (2 nd Cycle).....	168
Figure 4.77 Specimen C6: Connection at End of Test.....	169

Figure 4.78 Specimen C6: Continuity Plate (End of Test)	170
Figure 4.79 Specimen C6: Recorded Loading Sequence.....	171
Figure 4.80 Specimen C6: Applied Load versus Beam End Displacement Response ...	171
Figure 4.81 Specimen C6: Moment at Column Face versus Story Drift Response.....	172
Figure 4.82 Specimen C6: Moment at Column Face versus Plastic Rotation	172
Figure 4.83 Specimen C6: Panel Zone Shear Deformation	173
Figure 4.84 Specimen C6: Column Rotation.....	173
Figure 4.85 Specimen C6: Energy Dissipation.....	174
Figure 4.86 Specimen C6: Topside of Beam Top Flange Strain Profile	175
Figure 4.87 Specimen C6: Underside of Beam Bottom Flange Strain Profile	176
Figure 4.88 Specimen C6: Column Flange Warping.....	177
Figure 4.89 Specimen C6: Panel Zone Response	178
Figure 4.90 Specimen C6: Continuity Plate at Column Flange Edge Strain Profile	179
Figure 4.91 Specimen C6: Continuity Plate at Column Flange Edge Shear Strain Profile	180
Figure 4.92 Specimen C6: Continuity Plate Strain Gauge Rosette R09 Response	181
Figure 4.93 Specimen C6: Continuity Plate at Column Web Edge Shear Strain Profile	182
Figure 4.94 Specimen C6: Bottom Continuity Plate Bending.....	183
Figure 4.95 Specimen C6-G: Specimen before Testing	187
Figure 4.96 Specimen C6-G: East Side of Connection.....	188
Figure 4.97 Specimen C6-G: Cracks in Galvanization Coating.....	189
Figure 4.98 Specimen C6-G: Hairline Crack at Beam Top Flange CJP Weld.....	189
Figure 4.99 Specimen C6-G: Flange Local Buckling.....	190
Figure 4.100 Specimen C6-G: Web Local Buckling	191
Figure 4.101 Specimen C6-G: Beam Flange Partial Fracture at -0.06 rad (1 st Cycle) ...	191
Figure 4.102 Specimen C6-G: Complete Beam Fracture at -0.06 rad (1 st Cycle).....	192
Figure 4.103 Specimen C6-G: East Side of Connection at End of Test.....	193
Figure 4.104 Specimen C6-G: Continuity Plate Welds at End of Test	193
Figure 4.105 Specimen C6-G: Recorded Loading Sequence	194
Figure 4.106 Specimen C6-G: Applied Load versus Beam End Displacement Response	194

Figure 4.107 Specimen C6-G: Moment at Column Face versus Story Drift Response .	195
Figure 4.108 Specimen C6-G: Moment at Column Face versus Plastic Rotation.....	195
Figure 4.109 Specimen C6-G: Panel Zone Shear Deformation.....	196
Figure 4.110 Specimen C6-G: Column Rotation.....	196
Figure 4.111 Specimen C6-G: Energy Dissipation.....	197
Figure 4.112 Specimen C7: Specimen before Testing.....	202
Figure 4.113 Specimen C7: East Side of Connection.....	203
Figure 4.114 Specimen C7: Beam Bottom Flange Yielding	204
Figure 4.115 Specimen C7: Beam Top Flange Yielding at -0.015 rad (2 nd Cycle).....	205
Figure 4.116 Specimen C7: Beam Top Flange Yielding at -0.02 rad (2 nd Cycle).....	205
Figure 4.117 Specimen C7: Colum WLY at Beam Top Flange Level.....	205
Figure 4.118 Specimen C7: Colum WLY at End of Test.....	206
Figure 4.119 Specimen C7: Beam Flange Local Bucking.....	206
Figure 4.120 Specimen C7: Connection at End of Test.....	207
Figure 4.121 Specimen C7: Beam Flange Partial Fracture.....	208
Figure 4.122 Specimen C7: Column Yielding (End of Test)	209
Figure 4.123 Specimen C7: Doubler Plate at End of Test.....	210
Figure 4.124 Specimen C7: Recorded Loading Sequence.....	211
Figure 4.125 Specimen C7: Applied Load versus Beam End Displacement Response .	211
Figure 4.126 Specimen C7: Moment at Column Face versus Story Drift Response.....	212
Figure 4.127 Specimen C7: Moment at Column Face versus Plastic Rotation	212
Figure 4.128 Specimen C7: Panel Zone Shear Deformation	213
Figure 4.129 Specimen C7: Column Rotation.....	213
Figure 4.130 Specimen C7: Energy Dissipation.....	214
Figure 4.131 Specimen C7: Topside of Beam Top Flange Strain Profile	215
Figure 4.132 Specimen C7: Underside of Beam Bottom Flange Strain Profile	216
Figure 4.133 Specimen C7: Column Flange Warping.....	217
Figure 4.134 Specimen C7: Panel Zone Response	218
Figure 4.135 Specimen C7: Column Web Strain Profiles	219
Figure 4.136 Specimen C7: Doubler Plate Response	220
Figure 4.137 Specimen C7: Column Flange Response	221

Figure 4.138 Specimen W1: Connection before Testing	226
Figure 4.139 Specimen W1: Connection during Testing.....	227
Figure 4.140 Specimen W1: East Beam Bottom Flange Yielding	228
Figure 4.141 Specimen W1: West Beam Bottom Flange Yielding	228
Figure 4.142 Specimen W1: East Beam Bottom Flange Local Buckling.....	229
Figure 4.143 Specimen W1: Panel Zone Yielding at +0.03 rad (2 nd Cycle)	229
Figure 4.144 Specimen W1: Lateral-Torsional Buckling.....	230
Figure 4.145 Specimen W1: East Beam Top Flange CJP Weld Fracture at -0.04 rad (2 nd Cycle).....	231
Figure 4.146 Specimen W1: East Beam Top Flange CJP Weld Fracture Progression...	232
Figure 4.147 Specimen W1: East Beam Top Flange CJP Weld Fracture Surface	233
Figure 4.148 Specimen W1: Connection at End of Test	234
Figure 4.149 Specimen W1: Top Flange Continuity Plate (End of Test).....	234
Figure 4.150 Specimen W1: Bottom Flange Continuity Plate (End of Test)	235
Figure 4.151 Specimen W1: Underside Continuity Plates (End of Test)	235
Figure 4.152 Specimen W1: Recorded Loading Sequence	236
Figure 4.153 Specimen W1: Column Shear versus Story Drift Angle	236
Figure 4.154 Specimen W1: Applied Load versus Beam End Displacement Response	237
Figure 4.155 Specimen W1: Moment at Column Face versus Story Drift Response.....	238
Figure 4.156 Specimen W1: Moment at Column Face versus Plastic Rotation.....	239
Figure 4.157 Specimen W1: Panel Zone Shear Deformation.....	240
Figure 4.158 Specimen W1: Column Rotation.....	240
Figure 4.159 Specimen W1: Energy Dissipation.....	241
Figure 4.160 Specimen W1: Topside of East Beam Top Flange Strain Profile	242
Figure 4.161 Specimen W1: Underside of East Beam Bottom Flange Strain Profile ...	243
Figure 4.162 Specimen W1: Topside of West Beam Top Flange Strain Profile	244
Figure 4.163 Specimen W1: Underside of West Beam Bottom Flange Strain Profile...	245
Figure 4.164 Specimen W1: Column Flange Warping.....	246
Figure 4.165 Specimen W1: Panel Zone Strain Profile	247
Figure 4.166 Specimen W1: Panel Zone Shear Strain Profile.....	248
Figure 4.167 Specimen W1: Continuity Plate at Column Flange Edge Strain Profile ...	249

Figure 4.168 Specimen W1: Continuity Plate at Column Flange Edge Shear Strain Profile	250
Figure 4.169 Specimen W1: Continuity Plate Strain Gauge Rosette Response	251
Figure 4.170 Specimen W1: Continuity Plate at Column Web Edge Shear Strain Profile	252
Figure 4.171 Specimen W1: Beam Shear Response.....	253
Figure 4.172 Specimen W2: Connection before Testing.....	258
Figure 4.173 Specimen W2: Connection during Testing.....	259
Figure 4.174 Specimen W2: East Beam Bottom Flange Yielding	260
Figure 4.175 Specimen W2: West Beam Bottom Flange Yielding	260
Figure 4.176 Specimen W2: East Beam Top Flange Local Buckling	261
Figure 4.177 Specimen W2: East Beam Top Flange CJP Weld Tear at -0.03 rad (2 nd Cycle).....	261
Figure 4.178 Specimen W2: East Beam Top Flange CJP Weld Tear Progression.....	262
Figure 4.179 Specimen W2: West Beam Bottom Flange CJP Weld Fracture at: -0.05 rad (2 nd Cycle).....	262
Figure 4.180 Specimen W2: East Beam Bottom Flange CJP Weld Fracture at: +0.06 rad (1 st Cycle).....	263
Figure 4.181 Specimen W2: East Beam Bottom Flange Lateral-Torsional Buckling at: -0.06 rad (1 st Cycle)	263
Figure 4.182 Specimen W2: East Beam Top Flange Partial Fracture during Excursion to -0.06 rad (2 nd Cycle)	264
Figure 4.183 Specimen W2: East Beam Top Flange Weld Access Hole Tear at -0.06 rad	264
Figure 4.184 Specimen W2: West Beam Bottom Flange Fracture during Excursion to -0.06 rad (2 nd Cycle)	265
Figure 4.185 Specimen W2: Connection at End of Test	265
Figure 4.186 Specimen W2: Panel Zone (End of Test).....	266
Figure 4.187 Specimen W2: Continuity Plate Fillet Welds (End of Test)	266
Figure 4.188 Specimen W2: Recorded Loading Sequence	267
Figure 4.189 Specimen W2: Column Shear versus Story Drift Angle	267

Figure 4.190 Specimen W2: Applied Load versus Beam End Displacement Response	268
Figure 4.191 Specimen W2: Moment at Column Face versus Story Drift Response.....	269
Figure 4.192 Specimen W2: Moment at Column Face versus Plastic Rotation.....	270
Figure 4.193 Specimen W2: Panel Zone Shear Deformation.....	271
Figure 4.194 Specimen W2: Column Rotation.....	271
Figure 4.195 Specimen W2: Energy Dissipation.....	272
Figure 4.196 Specimen W2: Topside of East Beam Top Flange Strain Profile	273
Figure 4.197 Specimen W2: Underside of East Beam Bottom Flange Strain Profile	274
Figure 4.198 Specimen W2: Topside of West Beam Top Flange Strain Profile	275
Figure 4.199 Specimen W2: Underside of West Beam Bottom Flange Strain Profile...	276
Figure 4.200 Specimen W2: Column Flange Warping.....	277
Figure 4.201 Specimen W2: Panel Zone Strain Profile	278
Figure 4.202 Specimen W2: Panel Zone Shear Strain Profile.....	279
Figure 4.203 Specimen W2: Continuity Plate at Column Flange Edge Strain Profile ...	280
Figure 4.204 Specimen W2: Continuity Plate at Column Flange Edge Shear Strain Profile	281
Figure 4.205 Specimen W2: Continuity Plate Strain Gauge Rosette Response	282
Figure 4.206 Specimen W2: Continuity Plate at Column Web Edge Shear Strain Profile	283
Figure 4.207 Specimen W2: Beam Shear Response.....	284
Figure 4.208 Specimen W3: Connection before Testing.....	289
Figure 4.209 Specimen W3: Connection during Testing.....	290
Figure 4.210 Specimen W3: East Beam Bottom Flange Yielding	291
Figure 4.211 Specimen W3: West Beam Bottom Flange Yielding	291
Figure 4.212 Specimen W3: East Beam Top Flange Local Buckling	292
Figure 4.213 Specimen W3: East Beam Top Flange Weld Access Hole Tearing at -0.05 rad (1 st Cycle)	292
Figure 4.214 Specimen W3: Web Local Buckling at +0.05 rad (1 st Cycle).....	293
Figure 4.215 Specimen W3: Flange Local Buckling at -0.05 rad (1 st Cycle).....	293
Figure 4.216 Specimen W3: East Beam Top Flange CJP Weld Tear Progression.....	294
Figure 4.217 Specimen W3: East Beam Top Flange Weld Access Hole Tear.....	294

Figure 4.218 Specimen W3: East Beam Top Flange Fracture at +0.06 rad (1 st Cycle)..	295
Figure 4.219 Specimen W3: East Beam Top Flange Fracture.....	295
Figure 4.220 Specimen W3: Connection at End of Test	296
Figure 4.221 Specimen W3: West Beam Top Flange (End of Test)	296
Figure 4.222 Specimen W3: Top Flange Continuity Plate (End of Test).....	297
Figure 4.223 Specimen W3: Bottom Flange Continuity Plate (End of Test)	297
Figure 4.224 Specimen W3: Continuity Plate Fillet Welds (End of Test)	298
Figure 4.225 Specimen W3: Recorded Loading Sequence	299
Figure 4.226 Specimen W3: Column Shear versus Story Drift Angle	299
Figure 4.227 Specimen W3: Applied Load versus Beam End Displacement Response	300
Figure 4.228 Specimen W3: Moment at Column Face versus Story Drift Response.....	301
Figure 4.229 Specimen W3: Moment at Column Face versus Plastic Rotation.....	302
Figure 4.230 Specimen W3: Panel Zone Shear Deformation.....	303
Figure 4.231 Specimen W3: Column Rotation.....	303
Figure 4.232 Specimen W3: Energy Dissipation.....	304
Figure 4.233 Specimen W3: Topside of East Beam Top Flange Strain Profile	305
Figure 4.234 Specimen W3: Underside of East Beam Bottom Flange Strain Profile	306
Figure 4.235 Specimen W3: Topside of West Beam Top Flange Strain Profile	307
Figure 4.236 Specimen W3: Underside of West Beam Bottom Flange Strain Profile...	308
Figure 4.237 Specimen W3: Column Flange Warping.....	309
Figure 4.238 Specimen W3: Panel Zone Strain Profile	310
Figure 4.239 Specimen W3: Panel Zone Shear Strain Profile.....	311
Figure 4.240 Specimen W3: Continuity Plate at Column Flange Edge Strain Profile ...	312
Figure 4.241 Specimen W3: Continuity Plate at Column Flange Edge Shear Strain Profile	313
Figure 4.242 Specimen W3: Continuity Plate Strain Gauge Rosette Response	314
Figure 4.243 Specimen W3: Continuity Plate at Column Web Edge Shear Strain Profile	315
Figure 4.244 Specimen W3: Beam Shear Response.....	316
Figure 4.245 Specimen W4: Connection before Testing.....	321
Figure 4.246 Specimen W4: Connection during Testing.....	322

Figure 4.247 Specimen W4: East Beam Bottom Flange Yielding	323
Figure 4.248 Specimen W4: West Beam Bottom Flange Yielding	323
Figure 4.249 Specimen W4: West Beam Bottom Flange Local Buckling	324
Figure 4.250 Specimen W4: West Beam Web Buckling at +0.04 rad (1 st Cycle).....	324
Figure 4.251 Specimen W4: East Beam Top Flange CJP Weld Fracture at -0.04 rad (2 nd Cycle).....	325
Figure 4.252 Specimen W4: West Beam Top Flange CJP Weld Tear at +0.05 rad (1 st Cycle).....	325
Figure 4.253 Specimen W4: East Beam Lateral-Torsional Buckling at +0.05 rad (1 st Cycle).....	326
Figure 4.254 Specimen W4: East Beam Top Flange Fracture during First Excursion of -0.05 rad.....	326
Figure 4.255 Specimen W4: East Beam Top Flange Weld Access Hole Fracture during First of -0.05 rad	327
Figure 4.256 Specimen W4: West Beam Top Flange Fracture (End of Test).....	327
Figure 4.257 Specimen W4: East Beam Top Flange Fracture.....	328
Figure 4.258 Specimen W4: Connection at End of Testing	328
Figure 4.259 Specimen W4: Continuity Plates (End of Test)	329
Figure 4.260 Specimen W4: Panel Zone (End of Test).....	329
Figure 4.261 Specimen W4: Recorded Loading Sequence	330
Figure 4.262 Specimen W4: Column Shear versus Story Drift Angle.....	330
Figure 4.263 Specimen W4: Applied Load versus Beam End Displacement Response	331
Figure 4.264 Specimen W4: Moment at Column Face versus Story Drift Response.....	332
Figure 4.265 Specimen W4: Moment at Column Face versus Plastic Rotation.....	333
Figure 4.266 Specimen W4: Panel Zone Shear Deformation.....	334
Figure 4.267 Specimen W4: Column Rotation.....	334
Figure 4.268 Specimen W4: Energy Dissipation.....	335
Figure 4.269 Specimen W4: Topside of East Beam Top Flange Strain Profile	336
Figure 4.270 Specimen W4: Underside of East Beam Bottom Flange Strain Profile	337
Figure 4.271 Specimen W4: Topside of West Beam Top Flange Strain Profile	338
Figure 4.272 Specimen W4: Underside of West Beam Bottom Flange Strain Profile...	339

Figure 4.273 Specimen W4: Column Flange Warping.....	340
Figure 4.274 Specimen W4: Panel Zone Strain Profile	341
Figure 4.275 Specimen W4: Panel Zone Shear Strain Profile.....	342
Figure 4.276 Specimen W4: Continuity Plate at Column Flange Edge Strain Profile ...	343
Figure 4.277 Specimen W4: Continuity Plate at Column Flange Edge Shear Strain Profile	344
Figure 4.278 Specimen W4: Continuity Plate Strain Gauge Rosette Response	345
Figure 4.279 Specimen W4: Continuity Plate at Column Web Edge Shear Strain Profile	346
Figure 4.280 Specimen W4: Beam Shear Response.....	347
Figure 4.281 Macroetch of Specimen C3 Beam Bottom Flange CJP Weld.....	349
Figure 4.282 Macroetch of Specimen C5 Welds	349
Figure 4.283 Macroetch of Specimen C6 Welds	350
Figure 4.284 Macroetch of Specimen W1 Welds (East Beam)	351
Figure 4.285 Macroetch of Specimen C7 Welds	352
Figure 5.1 Summary of Specimen Story Drift Capacity.....	369
Figure 5.2 Summary of Measured Peak Connection Strength Factor, C_{pr}	369
Figure 5.3 Summary of Normalized Energy Dissipation Capacity	370
Figure 5.4 Summary of Reserve Energy Ratio	370
Figure 5.5 Summary of Beam Clear Span-to-Depth Ratio	371
Figure 5.6 Comparison of Specimens C6 and C6-G Responses.....	371
Figure 5.7 Continuity Plate Principal Strains	372
Figure 5.8 Doubler Plate Shear Strain Profiles (Positive Drift).....	373
Figure 5.9 Specimen C4: Column Web Strain Profiles	374
Figure 5.10 Specimen C7: Comparison of Column Web and Doubler Plate Strains	375
Figure 5.11 Specimen W4: Panel Zone Strain Profile.....	376
Figure 5.12 Specimen W4: Continuity Plate at Column Flange Edge Strain Profile	377
Figure 5.13 Specimen C4: Observed Column Flange Localized Yielding (End of Test)	378
Figure 5.14 Recorded Column Flange Response (Positive Drift)	378

1 INTRODUCTION

1.1 Introduction

Steel moment frames are a common Seismic Force-Resisting System (SFRS) because of the architectural freedom they offer. Moment frames permit open bays and eliminate the need for braced frames or shear walls. These systems develop plastic hinging through the plastification of the beams and the base of the first story-column. The use of relatively stocky width-to-thickness ratios prevents undesirable levels of strength degradation due to local buckling of the flange or web of the beam. Stable hysteretic behavior of the frames is encouraged by providing lateral bracing of the beams, which prevents lateral-torsional instability. These SFRS have excellent levels of ductility which allow designers significant reductions of the required elastic seismic design forces. However, after the 1994 Northridge Earthquake, significant damage to steel moment frames was observed at drift levels far below their assumed capacity. The observed damage instigated a significant research effort, which made significant changes to the detailing of steel moment frames.

The magnitude 6.7 Northridge Earthquake (1994) in the San Fernando Valley resulted in numerous fractures at the complete-joint-penetration (CJP) groove weld between the beam flanges and column flange of a steel moment frame connection. Similar fractures were also observed in steel moment frame buildings following the magnitude 6.9 Kobe Earthquake (1995) in Japan. An after-earthquake survey of the damage found nearly 1000 weld fractures. Following this, a consortium of associations and researchers known as the SAC Joint Venture initiated an 6-year research program to investigate the source of the fractures. They found that a combination of low fracture toughness weld metals, a lack of control of base metal properties, and connection geometries susceptible to high localized strain conditions were the main cause of the fractures. After the findings of the SAC Joint Venture, strict control of the use of steel moment frames has been imposed through AISC 341, the Seismic Provisions for Structural Steel Buildings (AISC 2016b), AISC 358, the Prequalified Connections for Special and Intermediate Steel Moment Frames for Seismic Applications (AISC 2016c), and AWS D1.8 the Structural Welding Code-Seismic Supplement (AWS 2016).

These controls involve mandatory use of notch-tough weld electrodes for welds designated as Demand Critical (DC), modified access hole geometries, and weld root

treatments to minimize sharp discontinuities. However, the most important provision requires that Special Moment Frames (SMF) and Intermediate Moment Frames (IMF) match the dimensions and detailing of previously qualified connections. For example, the Seismic Provisions stipulate that Special Moment Frames (designated as special due to their ‘special’ detailing requirements) must complete one cycle of 0.04 radian (rad) drift without significant strength degradation. The imposed drift follows a standard loading protocol, which gradually ramps up the imposed displacement. Due to their high ductility, SMF enjoys a high Response Modification Factor, R , and have no height limits for any Seismic Design Category tabulated in ASCE 7-16 (ASCE 2016).

The Prequalified Connections document (AISC 358) summarizes the geometry limitations and detailing requirements of prequalified connections since connection testing would be prohibitively expensive to perform on a project basis. A number of these connections are proprietary, wherein the intellectual property is licensed during the design phase. Two standard non-proprietary connections are the Reduced Beam Section (RBS) and the Welded Unreinforced Flange with Welded Web (WUF-W). When the prescriptive detailing requirements are adhered to, these two connections demonstrate the ability to satisfy the ductility requirements of SMF. Some of the prescriptive detailing requirements enacted after the Northridge Earthquake are recognized to be conservative. Specifically, the welding requirements of continuity plates and doubler plates for SMF and IMF. These plates are installed between the column flanges to stiffen the connection and ensure the desired inelastic behavior of the frame. The stiffening elements accomplish this by preventing excessive column flange deformation which would otherwise lead to premature failure of the connection, and by reinforcing the high shear panel zone such that plastic hinging occurs in the beam.

The Seismic Provisions have two requirements dictating when a continuity plate shall be used in a connection. They are: (1) when the available strength of the column as computed for the Web Local Yielding (WLY) or the Flange Local Bending (FLB) limit states of Section J10 of the Specification for Structural Steel Buildings (AISC 2016) are insufficient to resist the flange force from the moment connection, and (2) when the column flange thickness is less than the beam flange width divided by 6. The latter requirement is referred to as the ‘Lehigh’ Criterion herein for the institution of the founding study. When

either of these requirements dictates the use of a continuity plate, the plate thickness shall be 50% of the adjacent beam flange thickness for exterior (one-sided) connections or 75% of the thicker adjacent beam flange for interior (two-sided) connections. The current requirement of the weld between the continuity plate and the column flange is shall be a CJP groove weld; the use of a CJP weld rather than a fillet weld has significant economic implications. These welds require additional fabrication to bevel the edge of the plates and install a backing bar, additional weld volume, and more stringent inspection requirements. As per Section N of the AISC Specifications, CJP welds in Risk Category III or IV (as defined in ASCE 7-16) require 100% Ultrasonic Testing (UT). This inspection requirement for CJP welds significantly increases the cost of fabricating the continuity plates—an increase so significant that some designers prefer to increase the size of the column to mitigate the need for additional stiffening elements (Carter 1999).

Adequately designing the fillet welds for continuity plates would require the reconciliation of the flow of forces through the joints. A CJP weld does not possess this requirement as the weld develops the strength of adjacent plates—implying that failure of the plate would occur before the weld. Intimately linked to the continuity plate is the doubler plate. When present, this plate acts to double up the web to resist the high shear forces that develop within the panel zone of the moment connection. The high shear force is a result of the concentrated flange forces which resolve the beam moment as a force-couple. These flange forces flow through the column flanges into the continuity plates before ultimately loading the panel zone in shear. According to the Seismic Provisions, vertical weldments of the doubler plates to the column flanges are required to develop the shear strength of the plate—irrespective of the demand that may exist for the plate.

A pilot study that used a flexibility design method (Tran et al. 2013) tested two exterior RBS connections with fillet welded continuity plates (Mashayekh and Uang 2018). The flexibility design methodology was developed under the assumption that the continuity plates remain elastic. However, intentional under sizing of a continuity plate demonstrated excellent performance when continuity plates are permitted to yield. The inception of this testing program occurred after the preliminary success of the pilot study.

1.2 Research Objective and Scope

The objective of the research project was to conduct full-scale testing to explore more efficient design methodologies for the welding of the column stiffening. The physical testing forms the phenomenological evidence to adopt a plastic methodology in the design of continuity plates, and the weldments of continuity and doubler plates. Included in this are vertical doubler plate welds that do not develop the strength of the plate and fillet welds for the continuity plate to column connection. Two types of prequalified connections tested in interior and exterior configurations are used to explore these two objectives. Phase 1 of the research includes RBS exterior connections (only one beam attached to the column) using both shallow and deep columns. Phase 2 of the research includes WUF-W interior connections (two beams attached to the column). For Phase 2, shallow columns were not considered as the AISC 341 requirement of Strong Column Weak Beam (SCWB) to prevent soft story mechanisms force thick flanges that do not require stiffening. The specimens with continuity plates were designed using a plastic methodology similar to that which exists in AISC 360-16 §J10. The ultimate continuity plate strength is verified by using a plastic interaction equation. These specimens used fillet welds to join the continuity plates to the column flanges using a simple fillet weld design rule.

The Phase 1 specimens are also designed to explore the current limit states of column stiffening (FLB and WLY) by omitting continuity plates in three specimens. The omission of the continuity plates in these specimens violates the Lehigh Criterion. This criterion is found to be the only code provision that requires the use of a continuity plate for these specimens (i.e., the strength limit state of FLB does not require a stiffening plate). For one of these specimens, the WLY limit state shows that the column web alone is insufficient for the concentrated flange force. A doubler plate instead of the convention of using a continuity plate was used to reinforce the column web. A new procedure was used to design vertical welds that do not develop the shear strength of the doubler plate. The Phase 2 specimens endeavored to test fillet welded continuity plates in WUF-W connections. These connections typically see much higher flange forces than an RBS connection, thereby challenging the continuity plate welds. Table 2.1 shows the test matrix for both phases of the testing.

1.3 Literature Review

1.3.1 The Pre-Northridge Connection

Before exploring the changes that occurred after 1994, a brief history of steel moment frames is provided. The use of steel moment frames for lateral force-resisting systems has been in everyday use since the turn of the 20th century. Construction of the first moment frames used built-up ‘H’ shapes made from riveting four angles to a plate that formed the web. Connections were stiffened using gusset plates at the connection to provide a fully-restrained connection. Concrete encasement of the steel framing in these structures was standard for added fire protection of the steel skeleton. The 1906 San Francisco Earthquake and devastating fires demonstrated the excellent ductility of steel moment frames—some of the only surviving buildings in the downtown core were steel buildings. However, it is possible this was primarily due to the internal redundancy of these steel frames due to the riveted connections and built-up shapes, and the concrete encasement providing superior fire resistance (Hamburger et al. 2016).

After World War II, the predominant architectural style began to change with a transition to the use of glass curtain walls. This transition saw the robust gusseted connection replaced with smaller angles and ‘T’ sections to form the connection. In the 1960s, there was a preferential use of steel moment frames over other systems due to their previously demonstrated excellent performance and lack of height of limits governing their use; nearly every tall building constructed in this era on the west coast of the United States employed steel moment frames. Innovative research at this time focusing on several different configurations of field welded moment connections demonstrated sufficient ductility (Popov and Pinkney 1969). In the 1970s, riveting fell out of everyday use, which led to using high-strength bolted shear tabs and CJP welds on each beam flange. Shielded Metal Arc Welded (SMAW) was the welding process of choice for field welding as tanks of inert gas were not required when performing the field welding.

During the 1980s, a sharp increase in the cost of labor resulted in engineers attempting to minimize the amount of welding. Concentrating the lateral force-resisting system into a limited number of bays was a common measure to decrease the cost of construction. Decreasing the number of moment frames in a building decreases the system-level redundancy. In 1988 the Uniform Building Code (UBC) codified the prequalified

bolted web-welded flange moment connection, this connection has become known as the “pre-Northridge” moment connection (UBC 1988). Additionally, during this time, fabricators transitioned to using a self-shielded variety of Flux-Core Arc Welding (FCAW). This welding process has high deposition rates and does not require the welder to interrupt welding to reinsert a new stick electrode. Figure 1.1 shows a typical pre-Northridge Connection. Prior to events of 1994 there was little indication that the modern moment frame connection would develop less ductility than expected. The only known indication came in 1993 with a testing program which demonstrated significant variability in ductility capacity when using common FCAW welding electrodes and bolted shear tabs (Englehardt and Hussan 1993).

1.3.2 The Northridge Earthquake Damage

The 1994 magnitude 6.7 Northridge Earthquake saw many steel moment frame structures with brittle fractures in the connection region. Figure 1.2 shows an example of one of the fractures observed after the earthquake. Many of these fractures occurred after being subjected to rotations not more than 0.01 rad (Englehart and Sabol 1997). The damage due to the earthquake was immediately apparent as several of the buildings which experienced fractured connections were under construction, and as such, the steel frame was easily accessible. Similar fractures were observed in Japan after the 1995 magnitude 6.9 Kobe Earthquake.

The Northridge Earthquake caused an estimated 30 billion dollars of damage in Southern California (FEMA 2000e). Although damage to structures, especially older structures, was not peculiar, extensive damage to steel moment frames, once thought invulnerable, troubled the engineering community. Steel structures had performed well in previous earthquakes, which had precipitated significant changes in seismic detailing of other building materials. For example, the 1971 San Fernando Earthquake is seen as an incipient event for prescriptive ductile detailing of concrete in the United States (Hamburger 2006). These previous earthquakes did not demonstrate the steel fractures observed in 1994 since relatively few steel buildings were present in the areas affected by the most severe ground motions. After the Northridge earthquake, a significant inspection effort revealed fractures in moment frames in the San Francisco Bay area that were believed the result of the 1989 Loma Prieta Earthquake (FEMA 2000e). In response to the

unanticipated damage, the Federal Emergency Management Agency (FEMA), with coordinated efforts from the National Science Foundation (NSF) and the National Institute of Standards and Technology (NIST), sponsored the SAC Joint Venture to investigate the fractures. The SAC Joint Venture consisted of the Structural Engineers Association of California (SEAOC), the Applied Technology Council (ATC), and California Universities for Research in Earthquake Engineering (CUREe) made up of eight academic institutions in California at the time.

1.3.3 The Post-Northridge Connection

Over the 6 years following the Northridge Earthquake, the findings of the SAC Joint Venture were published in over 50 reports. The results from the SAC reports are distilled in a series of reports published by FEMA:

- FEMA 350–Recommended Seismic Design Criteria for New Steel Moment-Frame Buildings (FEMA 2000a).
- FEMA 351–Recommended Seismic Evaluation and Upgrade Criteria for Existing Welded Steel Moment Frame Buildings (FEMA 2000b).
- FEMA 352–Recommended Postearthquake Evaluation and Repair Criteria for Welded Steel Moment-Frame Buildings (FEMA 2000c).
- FEMA 353–Recommended Specifications and Quality Assurance for Steel Moment Frame Construction for Seismic Applications (FEMA 2000d).
- FEMA 354–A Policy Guide to Steel Moment Frame Construction (FEMA 2000e).

The first four reports are abridged recommendations, with the fifth report, FEMA 354, provided as a non-technical guide to explain the inherent risk and mitigation strategies. Detailed reports which show the basis of the first four reports are published as reports FEMA 355A through FEMA 355F (FEMA 2000f).

The organized research effort looked critically at the standard pre-Northridge connection fabricated during the 1970s and 1980s. It became apparent as the steel moment frames evolved with emerging technologies and were influenced by the higher cost of labor that their behavior drifted from the earlier demonstrably ductile steel frames. Some of the fundamental underlying causes and resulting modifications which define a post-Northridge connection are as follows:

- The most common weld electrodes in the pre-Northridge era were either E70T-4 or E70T-7 using the self-shielded FCAW process (Engelhardt and Sabol 1997). Although these electrodes realize the minimum specified strength of 70 ksi, they typically have poor toughness, achieving a Charpy V-Notch (CVN) Toughness of 5 to 10 ft-lbs at room temperature. Experimental testing of SMF connections with weld electrodes that realize a higher notch toughness (E70TG-K2 or E70T-6) demonstrates significantly higher inelastic drift capabilities (Johnson et al. 2000). A Post-Northridge connection classifies the CJP welds adjoining the beam-to-column as Demand Critical (DC). AWS D1.8 stipulates that DC welds must achieve a CVN toughness of 20 ft-lbs at 0°F and 70 ft-lbs at 70°F (AWS 2016).
- The use of bolted shear tabs and welded beam flanges was found not to be conducive to the intended behavior transmitting the beam shear through the web. Experimental testing demonstrated that bolted shear tabs permit relative slip at the faying surface. This slip has two consequences: (1) flexural forces are carried almost entirely through the beam flanges, and (2) the web does not carry the shear of the section as assumed. Carrying the beam shear through the flanges results in high secondary bending stresses, which exacerbate the strain condition at the extreme fiber of the flange. Most post-Northridge connections use field welded beam webs to prevent slip. Field welding of the beam web is readily accomplished by using the shear tab with bolts to frame and plumb the structure as before but also act as a backing bar for a vertically orientated CJP weld to fasten the web of the beam to the column web. In some connection types, it is also required to supplement this weld with a perimeter weld around the shear tab to stiffen the web of the section. The welding of the beam web has not eliminated the issue of secondary stresses due to a complicated stress pattern in the beam adjacent to a moment connection. Goel et al. (1997) showed that classical beam theory fails to capture the behavior in this region and that a modest portion of shear transfers through the flanges regardless of the welded beam web.

- A survey of the damage following the Northridge Earthquake revealed that a significant portion of the damage originated at the bottom flange backing bar and propagated through the column flange or beam flange. The column fractures either propagated transversely through the column or by taking a divot out of the column face (Engelhardt and Sabol 1997). Backing bars are required in most CJP welds to catch the molten weld metal during the initial passes of the weld. These backing bars would commonly be left in place as their presence was not believed to greatly influence the performance of the connection. However, research has shown that the discontinuity between fused and unfused portions of metal at the weld root results in a notch-like condition, increasing the fracture potential (Chi et al. 1997). This imperfection is impossible to detect visually, and UT testing has a low sensitivity to flaw detection at the root (Paret 2000). This notch-like condition is the most critical at the beam bottom flange where it exists at the extreme fiber. A post-Northridge connection requires removal of the bottom flange backing bar after welding the CJP weld. A reinforcing fillet weld is added after the removal of the backing bar to reinforce the root of the CJP. A concession is made at the top flange, wherein the backing bar can remain, but a reinforcing fillet must be made to underside of the backing bar.

The most significant impact on the steel moment frame construction following the Northridge Earthquake is the requirement that connections intended for use in Special or Intermediate Moment Frames must be shown to demonstrate an adequate level of ductility through full-scale testing. For SMF, the drift requirement is 0.04 rad, while for IMF, the drift requirement is 0.02 rad in AISC 341 (AISC 2016b). The Prequalified Connections for Special and Intermediate Steel Moment Frames for Seismic Applications (AISC 358) was released to assist engineers in selecting an appropriate connection (AISC 2016c). These connections adopt one of two strategies to improve the ductility of steel moment frames: they may reinforce the connection at the face of the column, or they may weaken the beam. In either strategy, the goal is to force the plastic hinge to occur away from the face of the column to limit the strain demand on the beam-to-column CJP welds. There are limitations to these connections based on the geometry of the connections that have successfully

demonstrated adequate performance through testing. The prequalification requirement has spawned several proprietary connections that have been developed by private enterprises. All SMF and IMF connections are reviewed by a standards committee, the Connection Prequalification Review Panel (CPRP) of AISC. Figure 1.3 shows examples of prequalified RBS and WUF-W connections.

During the experimental testing of the SAC Joint Venture, most of the moment connections utilized continuity plates with CJP welds—a response to the surveyed damage of the Northridge Earthquake, revealing that more damage occurred in frames that did not have continuity plates (Tremblay et al. 1998). Since the initial development of the prequalified connections, several relaxations have been made to the provisions. These concessions are: (1) the CJP weld fastening the continuity plate to the column flange may have its backing bar in place, and (2) the weld fastening the continuity plate the column web (or doubler plate) may be any weld that develops the strength of the plate.

1.3.4 Development of Fracture Mechanics to Simulate Beam-to-Column Fracture

The beam-to-column moment connection is a highly restrained location subjected to large scale cyclic strains. Traditional fracture mechanics, either Linear Elastic Fracture Mechanics (LEFM) or Elastic-Plastic Fracture Mechanics (EPFM), are based on the nature of the stress field around a pre-existing flaw and are valid only in situations where the stress fields in the vicinity of the crack behave in a bijective manner. For example, the critical stress intensity, K_{IC} , or the critical value of the J-integral, J_{IC} , must resemble the singularity stress field derived using Elasticity in their respective regions (Kanvinde 2017). Generally, this is true under small-scale yielding, where the plastic region around a crack tip is small. When the stress fields lose their uniqueness in a significant region during large scale plastic flow, or when a pre-existing flaw is not present, these methods fail to provide a reliable fracture metric. In these situations, local fracture models can characterize the fracture potential. To build local fracture models, researchers have turned to work done by Rice and Tracy (1969), which solved for the rate of growth of a spherical microvoid in a stress field or the Gurson-Tvergaard-Needleman (GTN) metal plasticity model which models the metal as a softening porous medium (Anderson 2017). The drawback to these local models is that a high-fidelity finite element simulation with calibrated plasticity models must be used to track the related indices.

These ductile fracture models attempt to fracture as the nucleation, growth, and coalescence of microvoids. The nucleation of these microvoids is due to plastic flow around material inclusion or dislocation pileups at grain boundaries. The growth of microvoids occurs due to the localization of strain around the void. Ductile fracture propagates as the plastic strain localizes across a dominate plane of voids. Rice and Tracy derived the growth rate of a spherical void in the stress field as a function of the triaxiality of the stress state (see Eq. 1.1).

$$\frac{dR}{dR_0} = 0.283 d\bar{\epsilon}^p e^{1.5T} \quad (1.1)$$

where R and R_0 are the current and original radius of a void and T is the triaxiality ratio, expressed as the ratio of hydrostatic stress, σ_H , to von Mises stress, σ_{vm} :

$$T = \frac{\sigma_H}{\sigma_{vm}} \quad (1.2)$$

The hydrostatic stress is related to the Cauchy stress tensor as $\sigma_H = \sigma_{\alpha\alpha}/3$, and the von Mises stress is given as $\sigma_{vm} = \sqrt{\frac{3}{2}\sigma'_{ij}\sigma'_{ij}}$ where σ'_{ij} are the deviatoric components of the Cauchy stress tensor. Finally, $d\bar{\epsilon}^p$ is an increment of effective plastic strain (*PEEQ*):

$$\bar{\epsilon}^p = \sqrt{\frac{2}{3}\epsilon'_{ij}\epsilon'_{ij}} \quad (1.3)$$

Hancock and Mackenzie (1976) postulated that the plastic strain at failure is inversely proportional to the rate of void growth:

$$\bar{\epsilon}^f = \alpha e^{-1.5T} \quad (1.4)$$

where α is a material property typically between 1 and 3 for plain steel. Hancock and Mackenzie demonstrated reasonable predictions of ductile fracture using this approach. They were also able to demonstrate a significantly lower failure strain of a hot-rolled material when loaded through-thickness rather than parallel to the direction of rolling. The interpretation of Rice and Tracey's work to generate a failure strain by Hancock and Mackenzie forms the foundation of the Stress Modified Critical Strain (SMCS) model to predict fracture. Using triaxiality ratio allows the characterization of the stress state into high ($T \geq 1.5$), moderate ($0.75 \leq T < 1.5$), and low ($T < 0.75$). The connection region of a SMF demonstrates high triaxiality—resulting in a low plastic strain at fracture.

Several researchers leveraged ductile fracture mechanics by using indices rooted from the work of Rice and Tracy. For Example, Ricles et al. (2003) used the $PEEQ$ Index (Eq. 1.5) and detailed finite element analysis to compare differences in the detailing of the weld access holes in WUF-W connections.

$$PEEQ_I = \frac{\bar{\epsilon}^p}{\epsilon_y} \quad (1.5)$$

El-Tawil et al. (2000) used the rupture index to investigate the required thickness of continuity plates and the size of weld access holes:

$$RI = \frac{\frac{\bar{\epsilon}^p}{\epsilon_y}}{e^{-1.5T}} \quad (1.6)$$

A key unknown in using these fracture metrics to determine the point of fracture is a characteristic length in which the metric has a positive indication (Hancock and Cowling 1980, and El-Tawil et al. 1999). The characteristic length is a well-known issue, as ductile fracture occurs only when an associated finite volume of material has reached a critical void growth rate (Kanvinde 2017). Using a representative characteristic length avoids erroneous conclusions that occur due to strain localizations that occur near strain risers in a finite element model. The suggested characteristic length is 2-10 times the material grain size; for mild steel, the characteristic length is suggested to be 0.005 in. The work done by Ricles and El-Tawil used either $PEEQ_I$ or RI as a relative metric to compare details without trying to predict the instance of fracture. Han et al. (2017) calibrated the RI from observed fractures of WUF-W specimens to determine a critical value of RI as 1,150 for the E71TG-1C notch-tough electrode. It was not cited what the characteristic length was used to determine this value.

Modern local fracture models that can capture the low-cycle fatigue condition at the beam-to-column interface are the Cyclic Void Growth Model (CVGM) discussed by Kanvinde and Deierlein (2004), and more recently the Stress-Weighted Damage Model (SWDM) discussed by Smith et al. (2014). These two methods have shown viability in predicting ductile fracture in the high inelastic strain regions of SMF subjected to accidental defects (Abbas 2015). These modern methods integrate separately the plastic strain histories of tension and compression strain cycles. This separate is important as the assumed uniform expansion of a microvoid under tension is not simply equal and opposite

when subjected to the reverse excursion. Instead compression strains compress the minor direction of the voids resulting in an oblate void perpendicular to the direction of loading. Locally increasing the curvature of the voids results in a stress riser which further localizes strains, or can lead to decohesion and cleavage (Kanvinde 2004).

1.3.5 Continuity Plate and Doubler Plate Research

Prior research related to the size and welding of continuity plates and doubler plates is summarized below.

- Popov et al. (1986) tested 8 half-scale, two-sided pre-Northridge connections. The tests compared the performance of the connection with and without continuity plates, with and without doubler plates, and with a fillet welded or CJP welded continuity plate. All of these specimens fractured near or at the beam flange CJP weld—most of them demonstrating little ductility. The authors observed that the presence of a continuity plate improved the performance. These continuity plates were designed based on the AISC Specifications at the time, using the nominal yielding flange force entering the column as a concentrated load. Two specimens used fillet-welded continuity plates with double-sided fillet welds of size $5/8$ times the thickness of the continuity plate, t_{cp} . Of the two fillet welded specimens tested, one experienced a brittle fracture of the fillet welds. However, the same column experienced lamellar tearing when retested with a CJP welded continuity plate; poor metallurgy is likely a culprit. Based on the results of this test, the authors recommended that CJP welds should be used for continuity plates. Additionally, the authors stipulate that designing a continuity plate based on the nominal yielding strength of the beam is unconservative based on the observed yielding and buckling of the continuity plates.
- Kaufman et al. (1996) tested several moment frame connections and determined that fillet-welded continuity plates were adequate when notch-tough electrodes were used for the beam flange CJP welds.
- In 1997 AISC released an advisory that welding of stiffeners and doubler plates must not be made within the k-area of the rolled column due to several observed fractures during fabrication (AISC 1997). Malley and Frank (2000)

documented the fracture toughness of k-area of W-shaped sections of A992 steel. They determined that this area has 25% lower upper-shelf CVN toughness, which is postulated to be due to of the cold-working of the material during the straightening process. The authors determine that the lower toughness of the k-area material coupled with the high restraint of welding continuity plates and doubler plates leads to unanticipated fractures during fabrication. Tide (2000) corroborated this conclusion and reproduced the lower toughness material by straining a coupon of material to 15% and performing CVN testing after aging the material.

This research is the premise of AWS D1.8 §4.2, which dictates that continuity plate corner clips must extend at least 1.5 in. into the web from the tabulated *k* dimension. AISC 358 §3.6 repeats the corner clip criteria. Yee et al. (1998) further demonstrated by modeling the thermomechanical effects of welding that the high weld volumes associated with CJP-welded continuity plates develop higher residual stresses than a fillet-welded continuity plate. However, Deierlein and Chi (1999) found that the effect of welding residual stress is most significant during the elastic behavior of the connection. This conclusion was corroborated by Matos and Dodds (2000), who found that the effects of residual stress have minimal effect on the connection after the beam has reached its plastic limit state.

- Engelhardt et al. (1998) tested five one-sided RBS connections using continuity plates matching the flange thickness of the adjacent beams and fastened to the column flanges using CJP welds. In an article summarizing testing of RBS connections during the SAC Joint Venture, Engelhardt et al. explains that no connections have been tested so far without continuity plates. As a cost-saving measure, it was mentioned that the removal of the steel backing of the continuity plate CJP weld is not required (Engelhardt 1999). More recent testing of exterior RBS connections using continuity plates of thickness equal to be the beam flange thickness was also only tested using CJP welds fastening the continuity plate to the column flange [Chi and Uang (2002) and Lee et al. (2005)]. Chi and Uang found that even continuity plates

equal to the beam flange thickness may yield when using A36 steel plate. This research also found that RBS-type connections framing into deep columns are more susceptible to lateral-torsional buckling instability due to the lower warping stiffness of the column.

- Bjorhovde et al. (1999) tested nine different moment frame connections using fillet-welded continuity plates. All of the specimens utilized W14×176 columns and W21×122 beams with welded cover plates to reinforce the connection. Double-sided fillet welds of size $5/8t_{cp}$ were used to fasten continuity plates matching the thickness of the adjacent beam flange.
- El-Tawil et al. (1999) performed finite element analysis on a pre-Northridge connection tested during the SAC Joint Venture (Specimen PN3). This specimen was a W36×150 beam attached to a W14×257 column that only achieved 0.01 rad of inelastic drift before experiencing a brittle fracture (Popov et al. 1996). By comparing values of RI during a parametric finite element analysis, the authors concluded that a weak panel zone results in a higher fracture potential at the beam-to-column interface at high drift levels.
- El-Tawil et al. (2000) continued work on their finite element analysis of Specimen PN3. The authors concluded by comparing the RI at the beam flange-to-column interface that a continuity plate equal to 50% of the adjacent beam flange thickness was adequate in stiffening the joint. Continuity plates of thicknesses greater than this saw diminishing returns. Furthermore, the authors postulated that thicker continuity plates might result in a k-area fracture of the column due to the increased volume of welds required.
- Dexter et al. (2001) tested 47 pull plate specimens consisting of a monotonically loaded plate welded on each face of a column. The focus of the research was on the through-thickness strength of a heavy rolled section subjected to a tension force coming from a beam flange. In efforts to force a failure in the through-thickness direction, 100 ksi material was used for the pull plates. No instances of lamellar tearing were observed, which is postulated to be a consequence of modern material manufacturing processes. Only 1 of 12 specimens using a fillet-welded continuity plate demonstrated a

fracture of the fillet welds. This specimen had inadequate corner clips of the continuity plate resulting in the continuity plate welds extending into the k-area of the column. The resulting fracture propagated through the fillet-welded continuity plate and the k-area of the column.

- Ricles et al. (2002) tested 6 one-sided (Specimens T1 to T6) and 5 two-sided (Specimens C1 to C6) moment frame connections. All of the specimens tested in this study utilized a W36×150 beam. These connections were the first WUF-W specimens tested with the modified welded access hole developed by Mao et al. (2000). Several specimens did not use the modern shear tab connection detail with supplemental fillet welds—these specimens performed markedly worse than those with the modern shear tab connection. Additionally, one specimen fractured prematurely in the beam plastic hinge due to the presence of a welded shear stud. Four specimens (Specimens T5 and T6 with a W14×311 column, Specimen C1 with a W14×398 column and Specimen C3 with a W27×258 column) were tested without a continuity plate. All four of these specimens achieved at least 0.05 rad drift. Specimens C2 and C4 were nominally identical to Specimens C1 and C3, respectively, except that they used a continuity plate that matched the thickness of the adjacent beam flange. Both specimens achieved one cycle higher drift when tested with a pair of continuity plates. CJP welds were used to affix all of the continuity plates. In the case of Specimen C3 the beam flange width-to-column flange thickness ratio (b_{bf}/t_{cf}) was equal to 6.8—significantly over the suggested limit of 6.0 of the Lehigh Criterion.
- Ricles et al. (2003) provided a detailed finite element study of the previously tested 11 specimens. The study compared the *PEEQ* demand at the root of the CJP weld across the testing cohort. Finite element results demonstrated that when the $b_{bf}/t_{cf} < 6.0$, the addition of a continuity plate only marginally influenced the *PEEQ* across the width of the CJP weld; the only observed effect was that the *PEEQ* demands became more uniform across the flange with the same resulting peak value. When the specimen with b_{bf}/t_{cf} of 6.8 was tested, the peak value of *PEEQ* was observed to decrease when adding a

continuity plate. However, whether a continuity plate was equal to one-half or the full thickness of the adjacent beam flange did not influence the results. Note that the clear beam span-to-depth ratio of Specimens C3 and C4 is equal to 9.1; this specimen is similar to Specimen W1 tested and to be reported in Chapter 4. The study also corroborated an earlier conclusion from El-Tawil et al. (1999) that a weak panel zone with column kinking tends to exacerbate the fracture potential.

- Hajjar et al. (2003) tested a series of monotonic pull plate specimens to investigate the WLY and FLB limit states. Two of these specimens were fabricated with continuity plates half the thickness of the pull plate with fillet welds of size equal to $(2/3)t_{cp}$. The column size of these specimens was W14×132. It was observed that yielding occurred in the continuity plate and fracture of the fillet welds did not occur.
- Lee et al. (2005a) tested six two-sided WUF-W specimens. All of the specimens used a W24×94 beam, while the column size and column stiffening detail were varied. Three of these specimens (Specimens CR1, CR2, and CR5) did not use continuity plates, while Specimens CR2 and CR5 violated the FLB criterion by using the hardened beam flange force as a demand. All three of these specimens completed at least one cycle of 0.04 rad. Given this observation, the authors discuss that the FLB limit state contained in ASIC 360 §J10, developed for non-seismic applications, appears satisfactory for seismic demands when notch-tough electrodes are used. Specimen CR3 used a fillet-welded continuity plate with a thickness equal to 60% of the adjacent beam flange thickness. This thickness was chosen based on satisfying the width-to-thickness requirement of unstiffened plates subjected to axial compression:

$$\frac{b}{t} < 0.56 \sqrt{\frac{E}{F_y}} \quad (1.7)$$

The fillet weld was sized to develop the strength of the continuity plate and resulted in a double-sided fillet weld of size $0.75t_{cp}$. This specimen

completed 14 cycles of 0.04 rad drift before low-cycle fatigue occurred in the beam flange CJP weld. Strain gauging of the continuity plate revealed that the continuity plate did not yield across its breadth. Based on this observation, it was concluded that fillet welds might not need to develop the strength of the plate. The authors also observed ductile tearing at 0.03 rad of the beam flange CJP weld at the toe of the last weld pass, which creates a radius at the re-entrant corner of the CJP weld. One specimen of this study, Specimen CR4, experienced a brittle fracture at 0.02 rad drift. Material testing revealed that the CJP weld of this specimen had low toughness—despite being performed using an E70T-6 notch tough electrode.

Further investigation also revealed that Specimen CR1 failed to meet the notch toughness requirements of a post-Northridge connection. No conclusion was made regarding why these specimens had a lower notch toughness than expected despite using a qualified electrode. A companion paper published looked at the relative strength of the panel zones and concluded that weak panel zones could develop excellent inelastic performance (Lee et al. 2005b). These panel zones used doubler plates that utilized fillet welds sized to develop the shear strength of the doubler plate for the vertical weld attaching the doubler plate to the column. The doubler plates were beveled such that they cleared the radius of the column flange to column web junction.

- Shirsat and Englehardt (2012) investigated the attachment details for the doubler plate. This work was performed using finite element analysis and explored the effect of welding different edges of the doubler plate, extending the doubler plate beyond the connection region, and of using asymmetric doubler plates. This research effort demonstrated that welding the top horizontal edges of extended doubler plates provided minimal benefit beyond stabilizing doubler plates about to buckle. The authors also found that the demands imposed on the vertical welds were between 0.5 and 1.3 times the expected shear yielding strength of the plate—an effect attributed to the strain hardening of the doubler plate. Gupta (2013) continues this research and

further demonstrates that the loading condition at the flange level of a doubler plate is mostly in the transverse direction and well beyond the nominal yielding strength of the plate. The author observed that the welding of the continuity plate to the doubler plate does not result in overstressing the doubler plate. The final remark was that extending the doubler plates beyond the level of the beam flanges demonstrates better panel zone behavior.

- Han et al. (2014) tested four exterior WUF-W connections using beam depths of 27 in. and 35 in. The authors found that the deeper beam depths failed to satisfy the 0.04 rad drift requirement. They postulated that the root cause of this was due to two reasons: (1) the weld access hole, although still compliant to the AISC 358 (2016) detailing requirements, was quite steep relative to those shown to be satisfactory by Ricles et al. (2002); and (2) that the clear span-to-depth ratio was 6.8, slightly below the minimum value of 7.0 required by AISC 358 (2016). The continuity plates in these specimens matched the thickness of the beam flange and used CJP welds for the weldment to column flange. Han et al. later tested the same two specimens with shallower weld access holes and found satisfactory performance (Han et al. 2016). The authors then demonstrated using detailed finite element models and the Rupture Index, RI , that shallow welded access holes have less propensity to fracture (Han et al. 2017).
- Shim (2017) performed experimental testing on nine WUF-W connections and one Bolted Flange Plate (BFP) connection. The research explored the role of relative panel zone strength to the overall ductile performance of the moment frame and the role of axial tension on the panel zone strength. The columns tested were either W33×263, W14×398, or W12×106. The only specimen which did not achieve at least 0.04 rad drift was Specimen UT05, which used a 1/16-in. tungsten electrode embedded into the doubler plate CJP weld as an intentional defect. It is unclear whether this intentional defect was the source of the fracture, as the fracture appeared to originate at the termination of the beam web to column flange CJP weld before propagating through the column flange. The author concluded that weak panel zones are

a reliable and effective means of generating ductility capacity. Furthermore, the panels with weak panel zones demonstrated less beam buckling and required less lateral bracing. The study demonstrates that although the specimens with the weak panel zones generate higher fracture potential according to the Rupture Index, RI , experimental evidence does not support this conclusion.

1.4 Flexibility-Based Formulation

In response to uncertainty on how design fillet welds to fasten continuity plates to the column flanges of Special Moment Frames, Tran et al. (2013) developed a flexibility formulation. This method allows the designer to design the continuity plate and its weldments based on its relative stiffness dictating the proportion of hardened beam flange force, P_f , acting on the plate. The fundamental assumption in this theory is that the continuity plate remains elastic. The force entering a continuity plate is determined as:

$$P_{cp} = \left(\frac{P_f}{2}\right) \left(\frac{b_{bf} - t_{pz} - 2t_{cf}}{b_{bf}}\right) \left(\frac{B_{cf}}{B_{cf} + B_{cp}}\right) \quad (1.8)$$

where B_{cp} is the flexibility coefficient of the continuity plate and B_{cf} is the out-of-plane column flexibility coefficient. Given the short ‘span’ of the column flange and continuity plate, the flexibility coefficients include both a flexural and shear components. The second term of Eq. 1.8 refers to the amount of force that is assumed to transmit directly into the column web, assuming a 1:1 catchment through the column flange. The continuity plate was then designed based on satisfying an M-V-P interaction equation (Doswell 2015):

$$\frac{M_r}{M_c} + \left(\frac{P_r}{P_c}\right)^2 + \left(\frac{V_r}{V_c}\right)^4 < 1.0 \quad (1.9)$$

Axial force in the continuity plate is computed using Eq. 1.8. Shear in the continuity plate develops due to the moment equilibrium of the plate (see Figure 1.6); it was assumed that P_{cp} is centered about 0.6 the width of the continuity plate, b_n . The 0.6 was derived based on an assumed trapezoidal elastic stress distribution on the edge of the plate. Mashayekh (2017) identified an additional moment that is generated by the clipping of the continuity plate.

The strength of the weld connecting the continuity plate to column flange is designed to resist the resultant force:

$$R_{cp} = \sqrt{P_{cp}^2 + V_{cp}^2} \quad (1.10)$$

The strength of a fillet weld of size, w , and length, l_w , is then designed as per §J2.4 of AISC 360 (2016):

$$R_n = 2(0.6F_{EXX})wl_w \left(1 + \frac{1}{2} \sin(\theta)^{1.5}\right) \quad (1.11)$$

where F_{exx} is the weld electrode strength, and θ is the orientation of the fillet with respect to the orientation of the vector R_{cp} :

$$\theta = \tan^{-1} \left(\frac{P_{cp}}{V_{cp}} \right) \quad (1.12)$$

Mashayekh and Tran et al. both recommended designing for a maximum shear flow of the fillet weld:

$$q_{max} = \frac{1.6P_{cp}}{b} \quad (1.13)$$

which originates from the peak of the assumed trapezoidal force distribution on the edge of the continuity plate. The strength of the weld adjoining the continuity plate to the column web (or doubler plate) is designed for P_{cp} for an exterior connection or $\sum P_{cp}$ for an interior connection. The orientation of this weld suggests $\theta = 0^\circ$ in Eq. 1.11.

Mashayekh and Uang (2018) validated the flexibility methodology with two exterior full-scale RBS connections. Specimen C1 was a W30×116 beam and a W24×176 column and Specimen C2 was a W36×150 beam and a W14×257 column. The thickness of the continuity plates tested were 1.8 and 1.3 times thicker than the recommended minimum thickness of 50% of the beam flange for an exterior connection. The large continuity plates are a consequence of the flexibility methodology whereby keeping the continuity plates elastic results in the attraction of significant load due to the relatively higher axial stiffness of the continuity plate versus the out-of-plane flexure of the column flange. Specimen C2 was designed such that the plastic interaction (Eq. 1.9) was violated, a conclusion which is corroborated by observed yielding of the continuity plates. The fillet weld sizes of Specimens C1 and C2 were $0.75t_{cp}$ and $0.8t_{cp}$, respectively. Both specimens performed well, achieving a maximum story drift of 0.05 rad and 0.07 rad, respectively.

Despite the success of the flexibility method, there are some critiques:

- The assumption that the continuity plate remains elastic is conservative, resulting in continuity plates thicker than those that have demonstrated adequate performance through prequalification. Several researchers during these tests have observed the yielding of the continuity plates.
- The flexibility formulation tends to be iterative, as the stiffness of the continuity plate is typically an order of magnitude larger than that of the column flange. This results in a runaway procedure as the continuity plate attracts more load as it's size is increased.

Testing of Specimens C1 and C2 in 2016 was a pilot project to verify the flexibility-based method of design (Mashayekh and Uang, 2018). Although the research objective of this study has pivoted, the performance of Specimens C1 and C2 are still presented herein as evidence of the efficacy of fillet-welded continuity plate.

1.5 Historical Review of AISC Requirements on Continuity Plate and Doubler Plate Design

A brief review of the requirement of continuity plates and weld attachments to the column in AISC 341 is summarized below.

- AISC 341 (1992) (pre-Northridge): continuity plate is sized such that $1.8F_{yb}b_f t_{bf} \leq 6.25(t_{cf})^2 F_{yf}$ which relates an assumed beam flange force to the flange local bending limit state (§J10.1 of AISC 360). The attachment welds are not specified.
- AISC 341 (1997): continuity plates shall be provided to match the tested connection; almost all of the tested continuity plates which satisfy the drift requirement of SMF at this point equal in size to the beam flange thickness and use CJP welds to connect the plates to the beam flanges.
- AISC 341 (2005): the seismic specifications (AISC 341) refer to AISC 358 for the design of continuity plates in Special Moment Frames. The AISC 358 (2005) specification specifies that continuity plates are required unless both of the following are satisfied:

$$t_{cf} \geq 0.4 \sqrt{1.8b_{bf} t_{bf} \frac{F_{yb} R_{yb}}{F_{yc} R_{yc}}} \quad (1.14)$$

$$t_{cf} \geq \frac{b_{bf}}{6} \quad (1.15)$$

The latter (Eq. 1.15) is referred to as the Lehigh Criterion herein. The required thickness of the continuity plates shall be one half of t_{bf} in an exterior connection, or equal to the larger t_{bf} in an interior connection. Additionally, the continuity plates were also required to conform to §J10 of AISC 360. The welds to the column flanges were required to be CJP welds.

- AISC 341 (2010): the continuity plate requirements are the same as listed in AISC 358 (2005).

According to the latest edition of AISC 341 (2016b), continuity plates are required if the predicted flange force exceeds the design strength at the column face as per §J10 AISC 360 (2016) or if the column flange thickness is less than one-sixth of the adjoining beam flange width [see Eq. (1.15)]. The strength requirement is equivalent to the previous proportion limit from AISC 341-05 (Eq. 1.14).

$$t_{cf} \geq \frac{b_{bf}}{6} \quad (1.16)$$

AISC 358 (2016c) generates the predicted flange force of a cyclically hardened beam undergoing large inelastic strains for the appropriate connection. For example, the flange force, P_f , for an RBS connection with a CJP-welded web connection is computed as:

$$P_f = \frac{0.85M_f}{d^*} = \frac{0.85}{d^*} (M_{pr} + V_{RBS}S_h) = \frac{0.85}{d - t_{bf}} (Z_{RBS}F_yR_yC_{pr} + V_{RBS}S_h) \quad (1.17)$$

The thickness of the continuity plates, according to §E3.6f.2(b) of AISC 341 (2016b), is determined as:

$$t_{cp} = \begin{cases} 0.5t_{bf} & \text{for exterior connections} \\ 0.75t_{bf} & \text{for interior connections} \end{cases} \quad (1.18)$$

§E3.6f.2(b) of AISC 341 (2016b) stipulates that the width of continuity plates shall at least extend to the edge of the beam flange.

As per the current specifications, the weld connecting the continuity plate to the column flange is required to be a CJP groove weld. However, the continuity plate to the column web can be either a groove weld or fillet weld. Currently, this weld must be sized

to develop the lesser of the tension or shear strength of the continuity plate or the shear capacity of the doubler plate (if applicable) that it attaches to in the column panel zone.

The use of doubler plates are dictated when the panel zone shear, derived from the equilibrium between the flange force, P_f , and the column shear, exceeds the design strength as per §J10.6 of AISC 360 (2016):

$$R_n = 0.6F_y d_c t_{pz} \left(1 + \frac{3b_{cf} t_c f^3}{d_b d_c t_p} \right) \quad (1.19)$$

Note that the resistance factor, ϕ , for panel zone shear has been equal to 1.0 since the 1997 Seismic Provisions (AISC 1997). When a doubler plate is required, the groove or fillet welds connecting the doubler plate to the column are required to develop the design shear yielding strength of the doubler plate thickness. This requirement has been the same since the first edition of the Seismic Provisions (AISC 1992). When fillet welds are used, the plate thickness must be maintained through the combined thickness of the weld throat and plate bevel at the inside radius of the column. To prevent premature instability of the doubler plate, AISC recommends the following stability limit:

$$t_{dp} \geq \frac{d_z + w_z}{90} \quad (1.20)$$

Up until the 2010 edition of AISC 341, horizontal welds at the top and bottom of the doubler plates were required regardless of the configuration. Modern requirements waive the requirements for these welds unless the stability limit (Eq. 1.20) is violated when the doubler plate is extended at least 6 in. beyond the beam flange.

1.5.1 Lehigh Criterion

The Lehigh Criterion of §E3.6f.1(b) of AISC 341 stipulates that a continuity plate must be used when the column flange thickness is less than the beam flange width framing in divided by six (see Eq. 1.16). The source of this requirement is from Ricles et al. (2000), who explored the performance of WUF-W connections through finite element analysis and an experimental testing program of interior and exterior connections. This experimental testing program utilized the newly developed modified weld access hole by Mao et al. (2000). To develop the criterion, the authors leveraged ductile fracture mechanic indices.

Ricles et al. calibrated the material factor in Eq. 1.4 by testing A572 Gr. 50 material and two different weld metals, E70T-4 and E70TG-K2 (see Figure 1.4). The pre-

Northridge electrode, E70T-4, demonstrates significantly less fracture strain for all triaxiality ratios. The research also demonstrates that the critical plastic strain is much lower for higher triaxiality, a condition which is typical for highly restrained regions. The authors selected a material constant of $\alpha = 2$, which is similar to the value of 2.6 selected by Chi et al. (2006). The authors developed a criterion for fracture based on the net section rupture of the material. A critical crack length is defined from Figure 1.5 as:

$$a_f = \left(1 - \frac{F_y}{F_u}\right) t \quad (1.21)$$

where t is the thickness of the material. To develop a model for cyclic loading, a fatigue law for constant strain range was assumed:

$$\ln(\Delta\epsilon^p) = \ln(\epsilon_f) - \frac{1}{k} \ln(n) \quad (1.22)$$

where $\Delta\epsilon^p$ is the strain range and ϵ_f is the engineering strain at failure. Converting the plastic strain at failure, $\bar{\epsilon}^f$, into engineering strain at failure allows the determination of k , a material parameter that now depends on triaxiality through the previously calibrated material parameter α . The authors found that for a triaxiality of 1.3, the value of k equals 2.26 for the A572 Gr. 50 steel and high-toughness weld electrode. Using a Paris fatigue law based on the effective plastic strain using two material parameters, C and B :

$$\frac{da}{dn} = C a (\Delta\epsilon^p)^k \quad (1.23)$$

inverting this equation:

$$C = \frac{\ln a |_{a_0}^{a_f}}{\epsilon_f^k} \quad (1.24)$$

Substituting the results from before and using an initial flaw size equal to 0.0012 in., an average flaw size observed at the root of the weld, allows for the determination of constant C . Eq. 1.18 to track the growth of a crack or the number of constant amplitude cycles to failure, N_f can be solved for as:

$$N_f = \left(\frac{\epsilon_f}{\Delta\epsilon^p}\right)^k \quad (1.25)$$

Using the results of the low-cycle fatigue analysis, the authors correlated their findings to column flange flexural deformations. The authors found that at least 0.03rad of inelastic

story drift ratio could be obtained if the column flange deflection at the edge of the beam flange, Δ_A , was limited to $l/520$, where l is the clear distance from the column web to the edge of the beam flange. Assuming that the moment of inertia of a cantilever section of the column flange has a width of $9t_{cf}$ and that the flange force is evenly distributed results in the criteria:

$$t_{cf} \geq 0.26[F_y t_{bf} l^3]^{\frac{1}{4}} \quad (1.26)$$

It was found that the beam size of W36×150, with a W14×311 column, satisfies Eq. 1.26 and achieved at least 0.03 rad of inelastic drift during their experimental testing. Therefore, to simplify the criterion, it was instead decided to set the b_{bf}/t_{cf} ratio of this specimen (equal to 5.2) to the limiting b_{bf}/t_{cf} ratio. This ratio was rounded up to 6.0 in FEMA 350 (2000).

This criterion was explicitly derived using WUF-W connections, which tend to have higher flange forces. Table 1.1 shows the results of a typical one-sided RBS connection using beams from the W36 shape family and columns from the W14 shape family. The figure demonstrates that the Lehigh Criterion is triggered for a significant number of combinations, while only a few violate the flange local bending limit state. Therefore, the Lehigh Criterion may be overly conservative for a significant number of potential RBS connections.

1.5.2 Development of Column Stiffening Limit States

The design of continuity plates uses either the minimum thickness as per Eq. 1.18 extending to at least the width of the beam flange or is designed as a typical stiffener using the concentrated force limit states of §J10 of AISC 360. Three limit states are applicable: Flange Local Bending (§J10.1), Web Local Yielding (§J10.2), and Web Local Crippling (§J10.3). The limit state of Web Local Crippling seldom governs and is not discussed in detail. A brief discussion of FLB and WLY follows.

1.5.2.1 Web Local Yielding (WLY)

The WLY yielding was first described in the AISC ASD Specifications in the 1937 Edition to prevent local yielding and crippling of the web of a wide flange shape subjected to a concentrated compressive load (Prochnow et al. 2000). At that time, the WLY limit

state was combined with the Web Local Crippling Limit State. The stress in the column web was to be limited to 24 ksi, and the assumed spread of the bearing force was assumed to be 1:1 through the column flange. Later, testing by Sherbourne and Jensen (1957) found that the 1:1 slope was conservative and recommended a 2:1 slope. In 1960 Graham et al. (1960) found that a 2.5:1 slope provided a better fit to the experimental data. To explain the 2.5:1 slope, the authors used an elastic stress distribution along the k-line of a rolled section. The incorporation of this slope did not occur until the 9th Edition of the AISC ASD Specifications in 1989 and the 1st Edition of the AISC LRFD Specifications in 1986. At this time, the Web Local Crippling limit state was separated from WLY. The WLY of AISC 360 (2016) for interior connections is:

$$R_n = (5k + N)F_y t_{cw} \quad (1.27)$$

where k is the dimension from the outside face of the column to the termination of the fillet, and N is the bearing width. Exterior connections have a similar expression except that the leading term takes on the value of $2.5k$. For moment frames it is a convention to take N as the thickness of the adjacent beam flange, t_{bf} . Figure 1.8 shows the WLY limit state of an interior connection.

1.5.2.2 Flange Local Bending (FLB)

The FLB is a tension limit state where insufficient stiffening of a column flange results in a concentration of the tension load at the center stiffer portion of the flange above the web of the column (Carter 1999). Figure 1.11 shows the FLB and the role of continuity plates in preventing it. The combined bending of the flanges with the concentration of the load leads to the rupture of the beam flange weld. Graham et al. (1960) developed the FLB limit state by using a yield line analysis to determine the strength of a column flange. The FLB as first specified in the 8th Edition of the AISC ASD Specification, which required stiffeners if:

$$t_{cf} < 0.4 \sqrt{\frac{P_{bf}}{F_y}} \quad (1.28)$$

A set of lower bound values of key geometric variables from available section shapes were used to conservatively derive this equation. The yield line analysis is reposed to convert this expression for use in LRFD design (Prochnow et al. 2000):

$$R_n = 7t_{cf}^2 F_c + t_{bf} k F_y \quad (1.29)$$

where the first term describes the strength of the column flanges in bending, and the latter describes the capacity of the web directly below the adjacent beam flange. After taking a 20% reduction in capacity and imposing the experimental results of pull plate testing, the following equation for FLB in AISC 360 (2016) is realized:

$$R_n = 6.25t_{cf}^2 F_y \quad (1.30)$$

As an alternative derivation, Prochnow et al. (2000) developed a yield line analysis informed from the results of an experimental testing program of pull plates welded to W-shapes. Following their methodology, a yield line analysis was developed such that four hinges form on each side of the web to form a tent (see Figure 1.10). The clear span of the flange, q , is taken as:

$$q = \frac{b_{cf}}{2} - k_1 \quad (1.31)$$

The authors recommend the same value as Graham et al. used for the longitudinal length of the yield lines of:

$$p = 12t_{cf} \quad (1.32)$$

Defining the length of the inclined yield line as:

$$r = \sqrt{\left(\frac{p}{2}\right)^2 + q^2} \quad (1.33)$$

Solving for the internal energy of the yield lines results in:

$$W_I = M_p \Delta \left[\frac{p}{q} + \frac{8q}{p} \right] \quad (1.34)$$

Substituting with $M_p = \frac{1}{4} t_{cf}^2 F_y$ results in:

$$W_I = t_{cf}^2 \left[\frac{p}{4q} + \frac{2q}{p} \right] \Delta F_y \quad (1.35)$$

Solving for the external energy as:

$$W_E = \int_0^h w \left(\frac{\Delta}{q} \right) x dx = \frac{w\Delta}{2q} h^2 \quad (1.36)$$

where $h = \frac{b_{bf}}{2} - k_1$, and w is the assumed uniform load applied by the beam flange.

Finally, equating the internal and external energy results in:

$$w = \frac{t_{cf}^2}{h^2} \left[\frac{p}{2} + \frac{4q^2}{p} \right] F_y \quad (1.37)$$

Solving for the maximum flange force then produces:

$$R_n = 2k_1 t_{bf} F_y + 2wh \quad (1.38)$$

Substituting in the result for w :

$$R_n = 2k_1 t_{bf} F_y + \frac{2}{h} \left[\frac{p}{2} + \frac{4q^2}{p} \right] t_{cf}^2 F_y \quad (1.39)$$

Prochnow et al. (2000) simplified Eq. 1.39 by taking the average minus one standard deviation of parameters for common column and girder combinations to find:

$$R_n = F_y (0.8 + 5.9 t_{cf}^2) \quad (1.40)$$

Graham et al. and Prochnow et al. both used the simplification that $p = 12t_{cf}$; however, if the critical value of p is found by taking the derivative of 1.37 with respect to p :

$$\frac{dw}{dp} = \frac{t_{cf}^2}{h^2} F_y \left[\frac{1}{2} - \frac{4q^2}{p^2} \right] \quad (1.41)$$

Then solving for the minimum value by setting equal to zero:

$$p = 2\sqrt{2}q \quad (1.42)$$

This minimum value of p , as a function of q , results in a capacity for FLB of:

$$R_n = 2k_1 t_{bf} F_y + \frac{2}{h} \left[\sqrt{2}q + \frac{2q}{\sqrt{2}} \right] t_{cf}^2 F_y \quad (1.43)$$

Prochnow et al. found that Eq. 1.40 predicted the results of their pull plate specimens with greater accuracy. Figure 1.11 compares Eq. 1.30 and Eq. 1.40 to Eq. 1.43 for a W36×150 beam framing into either a W14 or W27 column. It is observed that the bounding performed by Prochnow et al. (2000) is very close to that performed by Graham et al. (1960). Both of these equations are conservative for the columns tested (W14×132 to W14×159) when compared with the unsimplified yield line equation (Eq. 1.43). Their experimental testing program corroborates this as none of the pull-plate specimens fractured (Hajjar et al. 2003). These specimens used E70T-6 weld electrodes for their CJP welds with a measured CVN toughness of 63.7 ft-lb at 70°F and 19.0 ft-lb at 0°F. It is noted that Eq. 1.40 and Eq. 1.30 both use a reduction factor of 0.8 which has not been incorporated into Eq. 1.43. This reduction factor was applied to original derivation in an attempt to make the upper bound strength estimate from the yield line method conservative.

The previous discussion indicates that the FLB is conservative when using notch-tough weld electrodes for monotonic pull-plate tests. The level of conservatism diminishes for heavier sections—sections that would be common in a modern moment frame subjected to a Strong Column Weak Beam (SCWB) philosophy. An additional concern when using an FLB derived based on a monotonic pull plate test is that the beam flange CJP rupture of a seismic moment frame is significantly different than from a pull-plate test. Firstly, the connection of a moment frame experiences large scale cyclic strains resulting in strain hardening and, secondly, significant secondary bending exists in the flanges of a moment frame connection.

1.6 Summary

The 1994 Northridge Earthquake was a pivotal event for the design of steel moment frames as an SFRS. Observation of brittle fractures in the connection region of the frames precipitated necessary changes in the detailing of these moment frames, including the use of notch-tough electrodes, careful treatment of backing bars, and welding of the beam web to the column to facilitate the shear transfer from the beam web. The most significant modification was the requirement that connections for SMF and IMF be prequalified to achieve a prescribed level of drift. Most of these early tests, which set the foundation for prequalified connections, utilized conservative column stiffening details, including the use of continuity plates as thick as the beam flange and the use of CJP groove welds for the continuity plate weldments.

Research in the 2000s attempted to set conservative bounds as to when a continuity plate was required and set minimum required thicknesses of the continuity plate. Several researchers have demonstrated the efficacy of using fillet welds for this joint in monotonic pull-plate specimens as well as full-scale cyclic moment frame tests. However, the use of a CJP groove for the weldment of the continuity plate to the column flange is still required. This weld tends to be costly due to the increased preparation to bevel the plate and install a backing bar, and the required UT testing of the joint after welding. In response to the steel industry's push to economize the connection, a new method was derived using the flexibility of the continuity plate and column. This new flexibility method was validated using the full-scale testing of two exterior RBS connections and relies on the assumption that continuity plates must remain elastic. This assumption results in relatively thick

continuity plates, which are often thicker than plates that have already demonstrated adequate performance.

In response, this research program is designed to explore a plastic design methodology to design continuity plates and their welds. This program explored the currently defined limit states for stiffening columns as per the AISC Specifications and validates a simple design rule for designing fillet welds. The next chapter describes the design of each specimen.

Table 1.1 Limit State Matrix (W14 Column and W36 Beam; One-Sided RBS Connection)

		Beam: W36x									
		302	282	262	247	231	194	182	170	160	150
Column: W14x	455										
	425										
	398										
	370										
	342										
	311										
	283										
	257										
	233							FLB	FLB		
	211									FLB	FLB
	193										FLB
	176										

	No CP Req'd	FLB	Governed by AISC 360 §J10.1
	Eq. (1.1) Triggered	WLY	Governed by AISC 360 §J10.2
	Violates SCWB		Phase 1 Testing

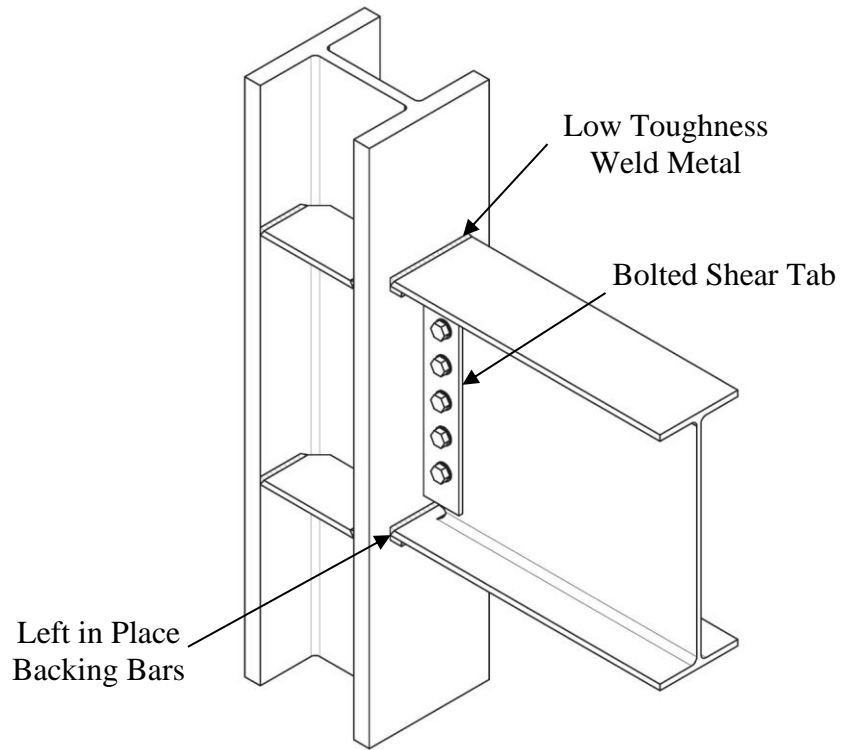


Figure 1.1 Pre-Northridge Connection (Hamburger et al. 2016)



Figure 1.2 Fracture at Beam Bottom Flange Backing Bar (Hamburger et al. 2016)

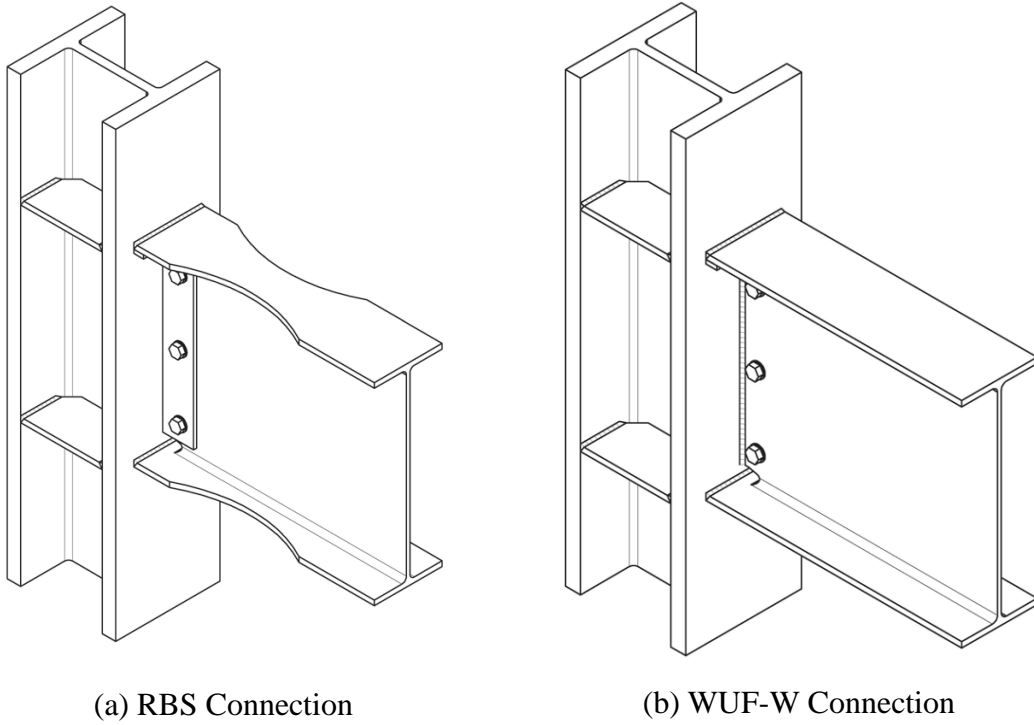


Figure 1.3 Prequalified Moment Connections (Hamburger et al. 2016)

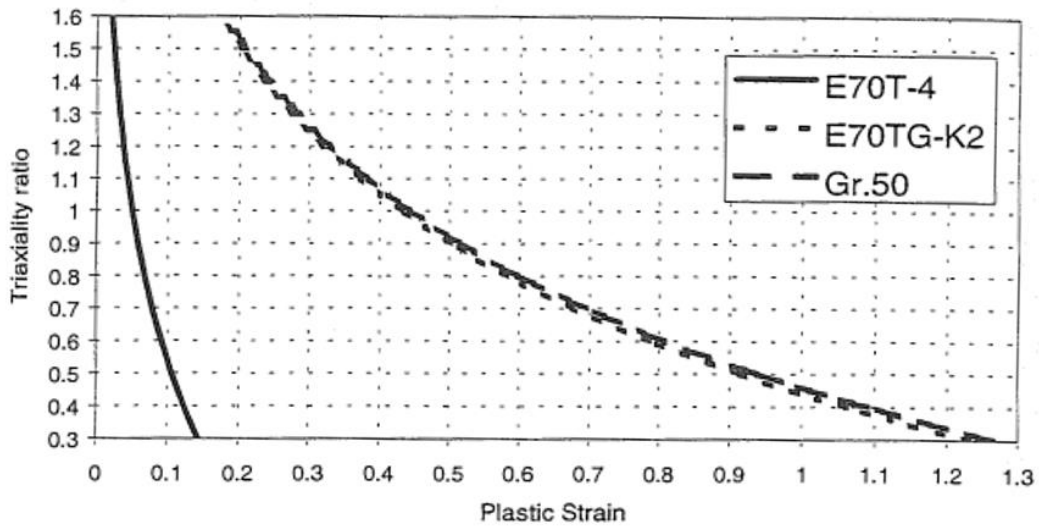


Figure 1.4 Plastic Strain versus Triaxiality Ratio (Ricles et al. 2000)

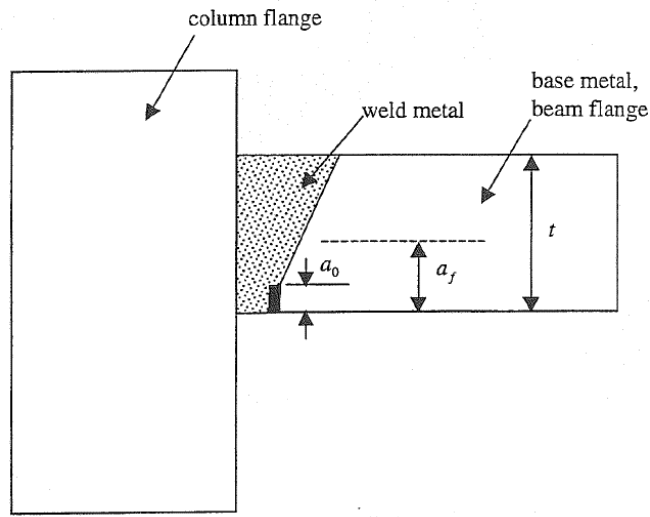
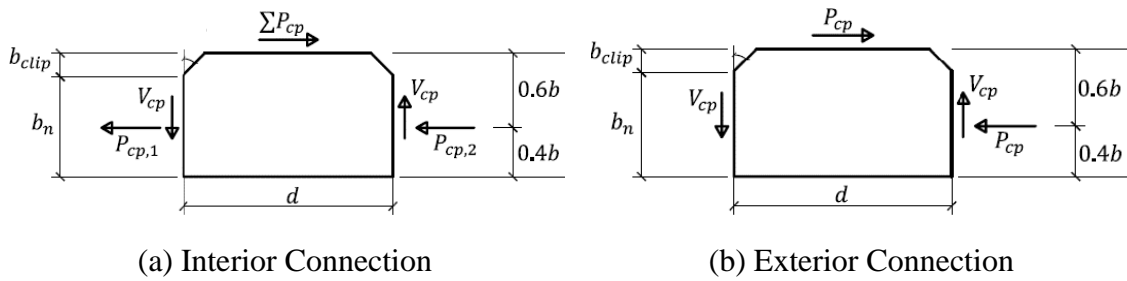


Figure 1.5 Net-Section Failure of Beam Flange (Ricles et al. 2000)



(a) Interior Connection

(b) Exterior Connection

Figure 1.6 Continuity Plate Free Body Diagram (Mashayekh 2017)



(a) Specimen C1



(b) Specimen C2

Figure 1.7 Flexibility Method Verification (Mashayekh and Uang 2018)

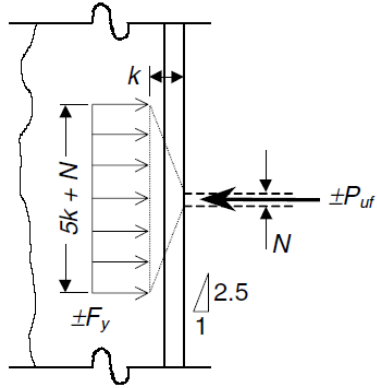
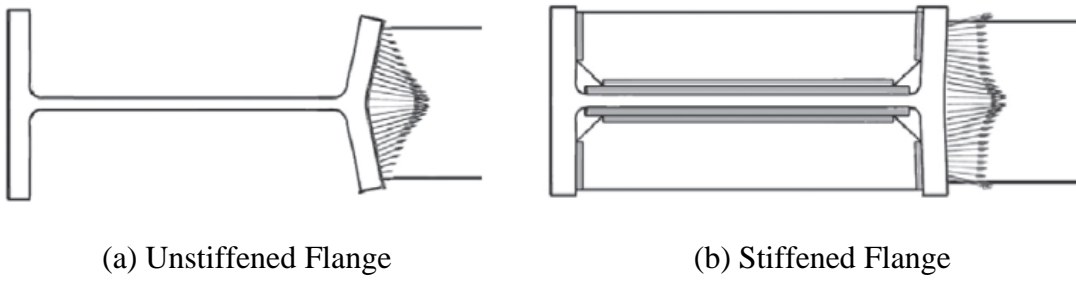


Figure 1.8 WLY Limit State (Carter 1999)



(a) Unstiffened Flange

(b) Stiffened Flange

Figure 1.9 FLB Limit State (Tran et al. 2013)

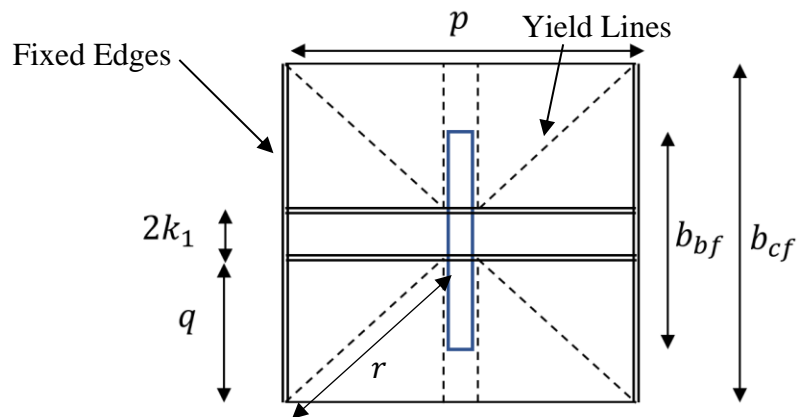


Figure 1.10 Yield Line Mechanism

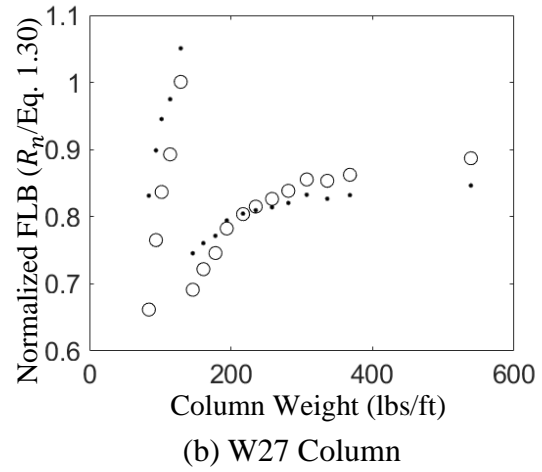
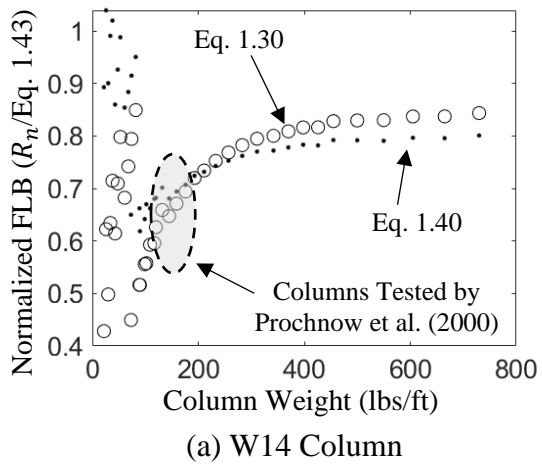


Figure 1.11 Flange Local Bending Comparison

2 SPECIMEN DESIGN

2.1 General

This chapter discusses the design philosophy and research objective of Phase 1 (Specimens C3, C4, C5, C6, C6-G, and C7) and Phase 2 (Specimens W1, W2, W3, and W4). The Phase 1 specimens are one-sided specimens simulating an exterior moment frame RBS connection. These six specimens are engineered to characterize the limit states surrounding continuity plates. Specimens C1 and C2 were previously tested as part of the verification of the flexibility design method in 2016 (Mashayekh 2017). Although the research objective of this study has pivoted, the satisfactory performance of Specimens C1 and C2 are presented as evidence of the usability of fillet welds for the continuity plate-to-column flange weld. The Phase 2 specimens are two-sided WUF-W connections simulating an interior moment frame connection. These four specimens are engineered to challenge the continuity plate and its weldments with high flange forces.

The primary objective of this research is to economize the detailing of continuity plates. Improving the economy of continuity plates is accomplished in two ways: (1) by exploring the boundaries in which continuity plates are required, and (2) by providing a design methodology to use a fillet weld for the continuity plate-to-column flange weld. It is proposed that the continuity plate is designed for the plastic distribution of forces in accordance with the existing stiffener design procedure of §J10 in AISC 360 (2016) while using the strain hardened beam flange force for the applicable connection as per AISC 358 (2016c). This methodology differs from previous research (Tran et al. 2013, Mashayekh and Uang 2018), which used the elastic distribution of forces in the connection to size the continuity plates and their weldments. Subscription to this methodology requires a reevaluation of the Lehigh Criterion (Eq. 1.16), which often necessitates continuity plates in connections with relatively low flange forces. These relatively low flange forces result in connections where a strength limit state (either WLY or FLB) do not govern, This effect is demonstrated in Table 1.1, which illustrates the cohort of possible single-sided RBS connections between a W14 shape column and a W36 shape beam.

The second objective of the research program is to economize the detailing of doubler plates. Doubler plates are incorporated into this research because of their prevalence of use in conjunction with continuity plates. Doubler plate economy is improved by providing a

design methodology to size the weld for the proportion of the panel zone shear in the doubler plate.

2.2 Design Philosophy

With the exception of the test parameters (see Table 2.1), the specimens are designed according to AISC 341 (2016b) and AISC 358 (2016c).

2.2.1 Continuity Plate Design

The continuity plate design uses the plastic design method, where the force demand, P_{cp} , imposed on the continuity plate is:

$$P_{cp} = (P_f - \min(FLB, WLY))/2 \quad (2.1)$$

where P_f is the hardened flange force as per AISC 358 (Eq. 1.17), and FLB and WLY are the column strengths associated with the limit states as per AISC 360 (Eqs. 1.27 and 1.30). The resistance factors are $\phi = 0.9$ and $\phi = 1.0$ for the FLB and WLY limit states, respectively. When the resultant plastic demand on the continuity plate is negative, which occurs when the column capacity according to FLB and WLY is greater than the flange force, a continuity plate is not required. The strength of the continuity plate is based on a plastic interaction equation (Eq. 2.2) between the shear and axial force in the continuity plate (Doswell 2015).

$$\left(\frac{P_{cp}}{P_c}\right)^2 + \left(\frac{V_{cp}}{V_c}\right)^4 \leq 1.0 \quad (2.2)$$

Shear forces in the continuity plate are found from the equilibrium of the continuity plate. The capacity of the continuity plate in axial compression, P_c , and shear, V_c , are evaluated as per the yielding limit states of AISC 360 §J4.1 and §J4.2 on the edge of the continuity plate in contact with the column flange. When the ratio of $V_{cp}/V_c \leq 0.4$ the shear contribution to the interaction is less than 2.5% and can be neglected for design purposes. Finite element analysis shows that the small amount of moment that exists at the edge of the continuity plate vanishes as the plate achieves its ultimate state.

2.2.2 Continuity Plate Weld Design

The high in-plane stiffness of the continuity plate relative to the out-of-plane stiffness of the column flange results in a significant portion of the beam flange force being transmitted to the plate. Extending the flexibility method (Section 1.4) for an elastic-plastically designed continuity plate allows for the prediction of the continuity plate force,

P_{cp} . Figure 2.1 demonstrates this using Specimens C5 and C6 of this testing program. The figure shows that, for these two cases, the continuity plate is expected to yield until a thickness above the minimum specified in AISC 341 is reached (Eq. 1.18). Specimen C2 demonstrates this effect, where the plastic method does not require a continuity plate, but the flexibility method shows that a 5/8-in. thick continuity plate yields. Yielding of this continuity plate was confirmed by the experimental testing of this specimen. Additionally, the presence of high residual stresses due to the thermal stresses induced by welding promotes continuity plate yielding. Therefore, the continuity plate fillet welds fastening the continuity plate to the column flange are designed to develop the strength of the continuity plate. Traditionally a $(5/8)t$ rule, where t is the thickness of the plate in question, would be used to design a double-sided fillet weld that would develop the strength of a plate in tension. To verify this rule, we equate the strength of a transversely orientated double-sided fillet weld of size, w , to the yield limit state of a plate:

$$\phi_w 0.6 F_{EXX} A_{we} (1.0 + 0.5 \sin^{1.5} \theta) = \phi_t F_y A_g \quad (2.3)$$

$$\phi_w 0.6 F_{EXX} 2 \frac{w}{\sqrt{2}} l_w (1.5) = \phi_t F_y t_{cp} l_w \quad (2.4)$$

$$w = 0.786 \frac{\phi_t F_y}{\phi_w F_{EXX}} t_{cp} \quad (2.5)$$

which for a Gr. 50 steel plate with a matched electrode ($F_{EXX} = 70$ ksi) results in:

$$w = \frac{5}{8} t_{cp} \quad (2.6)$$

However, to be consistent with a capacity design philosophy, the fillet weld of the specimen continuity plates is designed for the nominal yielding, not design, strength of the continuity plate such that:

$$\phi_w 0.6 F_{EXX} A_{we} (1.0 + 0.5 \sin^{1.5} \theta) = F_y A_g \quad (2.7)$$

$$w = 0.786 \frac{F_y}{\phi_w F_{EXX}} t_{cp} \quad (2.8)$$

which for a Gr. 50 steel plate with a matched electrode ($F_{EXX} = 70$ ksi) results in:

$$w = \frac{3}{4} t_{cp} \quad (2.9)$$

Since the column flange edges of the continuity plate experiences shear, V_{cp} , the assumption that the weld is only loaded in tension appears not be conservative. But

including the shear in the analysis also modifies the design strength of the plate. Assuming that the continuity plate observes an elastic-plastic response (i.e., the plate will not be subjected to significant cyclic strains that would induce strain hardening) it will be shown below that the modified yield condition of the continuity plate offsets the decrease in the weld strength.

The direction-dependent term used for fillet welds, $(1.0 + 0.5 \sin^{1.5} \theta)$, decays as additional shear modifies the direction of the resultant force vector, P_r , (see Eq. 2.10 and 2.11).

$$P_r = \sqrt{P_{cp}^2 + V_{cp}^2} \quad (2.10)$$

$$\theta = \tan^{-1} \left(\frac{P_{cp}}{V_{cp}} \right) \quad (2.11)$$

The shear at the forward edge of the plate is found as:

$$V_{cp} = \gamma P_{cp} \quad (2.12)$$

Assuming that P_{cp} acts at the center of the plate edge results in the following expressions for γ :

$$\gamma = \begin{cases} \frac{(b_{clip} + \frac{b_n}{2})}{d} & \text{for exterior connections} \\ \frac{2(b_{clip} + \frac{b_n}{2})}{d} & \text{for interior connections} \end{cases} \quad (2.13)$$

where b_{clip} is the distance clipped off the continuity plate to clear the radius of the column web-to-flange junction, and d is the depth of the continuity plate: $d = d_c - 2t_{bf}$ (see Figure 2.2). Assuming the continuity plate does not demonstrate significant strain hardening, the resultant force P_r must exist on the initial yield surface defined by the nominal yield strength of the material. For metal plasticity it is common to assume a von Mises yield surface:

$$\sigma_{vm}^2 = \frac{1}{2} [(\sigma_{11} - \sigma_{22})^2 + (\sigma_{22} - \sigma_{33})^2 + (\sigma_{33} - \sigma_{11})^2 + 6(\sigma_{23}^2 + \sigma_{31}^2 + \sigma_{12}^2)] \quad (2.14)$$

Assuming plane stress and conservatively setting $\sigma_{22} = 0$ results in:

$$F_y^2 = \sigma_{11}^2 + 3\sigma_{12}^2 \quad (2.15)$$

The average tension stress is $\sigma_{11} = P_{cp}/A_{cp}$ and the average shear stress is $\sigma_{12} = V_{cp}/A_{cp}$, where $A_{cp} = b_n t_{cp}$ is the area of the continuity plate in contact with the column flange. Substituting these expressions into Eq. 2.15 produces:

$$P_{cp} = \frac{P_y}{\sqrt{1 + 3\gamma^2}} \quad (2.16)$$

$$V_{cp} = \frac{\gamma P_y}{\sqrt{1 + 3\gamma^2}} \quad (2.17)$$

where $P_y = F_y A_{cp}$. Substituting these expressions into Eq. 2.10 results in:

$$\frac{P_r}{P_y} = \sqrt{\frac{1 + \gamma^2}{1 + 3\gamma^2}} \quad (2.18)$$

$$\theta = \tan^{-1}\left(\frac{1}{\gamma}\right) \quad (2.19)$$

The ratio of strengths of a transversely orientated ($\theta = 90^\circ$) weld versus a resultant angle according to Eq. 2.19 is:

$$\frac{R_n(\theta = 90^\circ)}{R_n(\theta)} = \frac{\frac{3}{2}}{1.0 + 0.5 \sin^{1.5}\left(\tan^{-1}\left(\frac{1}{\gamma}\right)\right)} \quad (2.20)$$

The ratio of Eq. 2.18 to Eq. 2.20 represents the resulting demand-capacity ratio, DCR between a weld subjected to a vector resultant of axial and shear forces, limited by a von Mises yield criterion, to a weld design solely for tension:

$$DCR_{Weld} = \frac{3 \sqrt{\frac{1 + \gamma^2}{1 + 3\gamma^2}}}{2 \left[1.0 + 0.5 \sin^{1.5}\left(\tan^{-1}\left(\frac{1}{\gamma}\right)\right)\right]} \quad (2.21)$$

Since $DCR_{Weld} \leq 1.0$ for all admissible values of γ , it is conservative to neglect the shear force acting on the weld (see Figure 2.3). Finite element analysis has also revealed that before the continuity plate yields, a small amount of moment is generated at the edge of the plate. This moment vanishes as the continuity plate yields due to the axial force. The weld fastening the continuity plate to the web of the continuity plate is designed to develop the strength of the axially loaded portion of the continuity plate. For an exterior connection,

this is equal to $A_{cp}F_y$, while for an interior connection, the force is doubled. Therefore, it is conservative to assume this weld is orientated longitudinally ($\theta = 0^\circ$).

The continuity plate fillet welds in this research program were typical welds with no special requirements regarding the treatments at weld terminations. This use of typical detailing was intentional to represent a conservative fabrication case where the fillet weld may be fabricated with a start and stop of each weld pass contained within the breadth of the continuity plate.

2.2.3 Doubler Plate Vertical Weld Design

The vertical welds of a doubler plate are designed to resist the appropriate proportion of the panel zone shear based on the relative elastic shear stiffness of the doubler plate:

$$V_{dp} = \left(\frac{Gt_{dp}}{Gt_{dp} + Gt_{cw}} \right) V_{pz} = \left(\frac{t_{dp}}{t_{dp} + t_{cw}} \right) V_{pz} \quad (2.22)$$

where V_{dp} is the shear force in the doubler plate(s), and t_{dp} and t_{cw} are the thicknesses of the doubler plate and column web, respectively. The panel zone shear, V_{pz} is derived from the equilibrium between the flange force, P_f and the column shear, V_{col} . Assuming that the stress of the doubler plate is uniformly distributed across a shear area equal to $t_{dp}d_c$ results in shear flow of $q_{dp} = V_{dp}/d_c$. Moment equilibrium of the doubler plate itself results in (see Figure 2.4):

$$\frac{V_{dp}}{d_c} h_c d^* = V_{dp,v} h_c \quad (2.23)$$

$$V_{dp,v} = \frac{V_{dp}}{d_c} d^* \quad (2.24)$$

For design purposes, assume that the shear flow along the vertical edge is uniform:

$$q_{dp,v} = \frac{V_{dp,v}}{d^*} = q_{dp} \quad (2.25)$$

It is observed that the uniform shear flow along the vertical edge of the doubler plate is equal to the uniform shear flow along the horizontal edge. The above approach may result in a vertical shear force in excess of the shear yielding strength of the plate—a paradox that occurs because of the inelastic behavior assumed in the second term of Eq. 1.19. Therefore, the following requirement is necessary:

$$q_{dp,v} = \frac{V_{dp}}{d_c} \leq 0.6F_y t_{dp} \quad (2.26)$$

In practice, economic doubler plates designed solely for panel zone shear would not be designed differently than the current practice of sizing the weld to develop the shear strength of the doubler plate. However, there are two instances where the proposed approach realizes greater economy:

- (1) When the strength design (Eq. 1.19) would suggest a doubler plate that would violate the stability limit (Eq. 1.20) and instead of using plug welds to stabilize the plate, a thicker doubler plate may be specified.
- (2) When WLY governs the need for column stiffening, a doubler plate may be used in lieu of a continuity plate. Specimen C7 of this research project utilized this approach.

An additional complication to using fillet welds as the vertical weld to fasten the doubler plate to the column is maintaining the effective throat of the weld through the beveled portion of the doubler plate [see Figure 2.5(a)]. The commentary of §E3.6e.3 in AISC 341 (2016b) discusses the issue and recommends that the fillet weld size should be increased to accommodate any reductions in the effective throat due to the bevel of the doubler plate. For Specimen C7, a bevel angle of 45° was specified to circumvent this issue [see Figure 2.5(b)]. No fit-up issues of the 5/8-in. doubler plate on the W24×192 column was reported.

2.3 Specimen Design and Details

Table 2.1 summarizes the research objective of the specimens in both phases. The first two specimens of Phase 1 (Specimens C3 and C4) challenge the need for the Lehigh Criterion (Eq. 1.16) for a shallow and a deep column configuration. While Specimen C4 has a much higher SCWB ratio indicating a stiffer column, the deep column may be more susceptible to warping once a lateral-torsional instability is developed at the plastic hinge in the beam. Specimen C4 also possesses a markedly stronger panel zone than Specimen C3. Specimen C5 was designed with a continuity plate as per Eq. 2.2, resulting in a continuity plate that is 1/8 in. thinner than that required per Eq. 1.18. The resulting continuity plate has a high width-to-thickness ratio of 16.0; high width-to-thickness ratio plates are susceptible to local buckling. Specimen C5 also used a weak panel zone ($DCR = 1.18$). The combination of column kinking and continuity plate buckling while the continuity plate is cycled plastically challenges the ductility capacity of the continuity plate

fillet welds. The continuity plate-to-column flange fillet weld was the nearest standard weld size to satisfy $w = (3/4)t_{cp}$.

Specimen C6 was designed with a continuity plate as per Eq. 2.2, resulting in a continuity plate that is equal to that required per Eq. 1.18. The continuity plate fillet welds in this specimen were equal to t_{cp} . This was done to ensure that premature failure of the specimen did not occur such that Specimen C6-G, which was a duplicate specimen that was hot-dip galvanized, would have meaningful results when comparing the effects of galvanization. To maintain consistency for later comparison, Specimen C6-G is fabricated identically to Specimen C6—including maintaining metallurgical similarity by using rolled shapes from the same heat number. Specimen C7 aims to satisfy the governing column limit state, WLY, by the addition of a doubler plate in lieu of a continuity plate. The *DCR* for the FLB limit state is 0.92, which according to the plastic design methodology does not require a continuity plate. The doubler plate fillet weld has been sized to resist the proportion of panel zone shear transmitted to the doubler plate based on its ratio of shear stiffness to the column web, according to Eq. 2.22 and Eq. 2.26. Table 2.2 shows the RBS dimensions of the Phase 1 specimens. Included in this table is the ratio of moment at the column face to the expected plastic moment, M_f/M_{pe} , which indicates the utilization of the RBS including hardening.

Specimen W1 used a 1/2-in. continuity plate as per Eq. 2.2, which violates the current minimum thickness criterion for two-sided connections as per Eq. 1.18. This specimen used a pair of 5/8-in. extended doubler plates with a vertical PJP weld. Specimen W2 used a 3/4-in. continuity plate as per the minimum thickness of AISC 341 (Eq. 1.18). The plastic methodology predicts this plate as overloaded, with a *DCR* of 1.43. Overloading of the continuity plate was done intentionally to observe any negative consequences. This specimen used a pair of 3/4-in. extended doubler plates with a vertical PJP weld. Specimen W3 used a 1/2 -in. continuity plate as per Eq. 2.2 which violates the current minimum thickness criterion for two-sided connections as per Eq. 1.18. This specimen used a pair of 1/2-in. extended doubler plates, which were insufficient based on the predicted panel zone shear (see Eq. 1.19) and violated the stability criteria (see Eq. 1.20). The weak and slender panel zone was designed intentionally to investigate any negative consequences. The slope of the weld access hole from the beam flange for WUF-W connections has been shown to

be a critical parameter (Han et al. 2014). AWS D1.8 (2016) §6.11.1.2 is not explicit in specifying the slope of the weld access hole—only imposing a limit of 25° degrees. The design drawings for Phase 2 detailed the weld access as a standard weld access for WUF-W connections following the Alternate Geometry of AWS D1.8. As-built slopes of the access holes for the Phase 2 specimens were approximately 15°.

Specimen W4 used a 3/4-in. continuity plate as per Eq 2.2, which satisfied the current minimum thickness criterion for two-sided connections as per Eq. 1.18. This specimen used a doubler plate placed within the continuity plates. The vertical welds of the doubler plates were designed to develop the shear strength of the doubler plate. Only Specimen W4 used horizontal fillet welds to fasten the doubler plate to the continuity plate. This fillet weld was sized based on 75% of the available shear capacity of the doubler plate as per §E3.6e.3(b)(2) in AISC 341 (2016b).

Concrete slabs were not used in this testing as their presence significantly complicates the testing and impairs the visual assessment of the connection during testing. Experimental testing of SMFs using concrete slabs have demonstrated that their presence is generally beneficial by stabilizing the plastic hinge (Englehardt et al. 2000). In positive flexure the addition of a composite slab can increase the plastic strain demand at the beam bottom flange extreme fiber (Hajjar et al. 1998). However, a modern connection which prohibits the use of shear studs in the beam plastic hinge region lacks the shear transfer capability to develop significant composite behavior. Uang et al. (2000) found that the shift in the neutral axis for partially composite beams to be minor.

Table 2.3 shows the following specimen and continuity plate design metrics:

- The clear Span-to-Depth Ratio. AISC 358 (2016c) §5.3.j requires the ratio for SMF using RBS connections to be limited to 7 or greater. Similarly, AISC 358 (2016c) §8.3.j requires the ratio for SMF using WUF-W connections to be limited to 7 or greater.
- The Strong Column Weak Beam (SCWB) Moment Ratio. AISC 341 (2016b) §E3.4a requires that the ratio of the summation of projected column strengths to the summation of projected beam strengths shall be larger than one. The ratio listed in the table is:

$$SCWB = \frac{\sum M_{pc}^*}{\sum M_{pb}^*} \quad (2.27)$$

- The flange force, P_f as per Eq. 1.17 using the appropriate clause of AISC 358 (2016c) to compute the moment at the face of the column, M_f . Specifically, §5.8 in AISC 358 for RBS connections and §8.7 in AISC 358 for WUF-W connections.
- The resistance of the FLB, WLY column limit states computed as per §J10 in AISC 360 (2016) (Eq. 1.30 and Eq. 1.27) using the designed thickness of the panel zone (i.e., $t_{cw} + \sum t_{dp}$). The WLC limit state has been omitted since it does not govern.
- The resultant continuity plate force, P_{cp} , computed as per Eq. 2.1.
- The continuity plate DCR expressed as the resultant of the P-V interaction equation (Eq. 2.2).
- The continuity plate width-to-thickness ratio (b/t).
- The fillet weld size, w , adjoining the continuity plate to the column flange.
- The ratio of fillet weld size to continuity plate thickness, w/t_{cp} .

Table 2.4 shows the following panel zone and doubler plate design metrics:

- The panel zone shear force, V_{pz} determined as the equilibrium between the flange force(s) and the column shear.
- The panel zone DCR expressed as the ratio of V_{pz} and R_n as per Eq. 1.19.
- The ratio of the combination of the panel zone width and depth to its thickness (see Eq. 1.20) computed for the column web and doubler plate.
- The vertical weld shear flow as computed per Eq. 2.26 and the upper bound of the shear flow defined as $0.6F_y t_{dp}$.

Table 2.1 Research Objective Matrix

Spec. No.	Beam	Column	Connection Type	Research Objective
C1 ^a	W30×116	W24×176	One-sided RBS	Continuity plate designed using the flexibility method (Section 1.4).
C2 ^a	W36×150	W14×257	One-sided RBS	Continuity plate designed using the flexibility method (Section 1.4). Continuity plate expected to yield.
C3	W36×150	W14×257	One-sided RBS	Specimen violates Lehigh Criterion (Eq. 1.16). Strength Limit states predict plate not required (Eq. 2.1).
C4	W30×116	W27×235	One-sided RBS	Specimen violates Lehigh Criterion (Eq. 1.16). Strength Limit states predict plate not required (Eq. 2.1).
C5	W36×150	W14×211	One-sided RBS	Size of continuity plate designed as per Eq. 2.2. Column designed to have a weak panel zone to exacerbate column kinking. Beam designed to deliver a probable maximum beam flange force that results in a continuity plate thinner than Eq. 1.18. Continuity plate welds designed as the per the $w = (3/4)t_{cp}$ rule.
C6	W30×116	W24×176	One-sided RBS	Size of continuity plate designed per Eq. 2.2. The continuity plate also satisfied the minimum thickness as per Eq. 1.18. Welds conservatively designed ($w = t_{cp}$).
C6-G	W30×116	W24×176	One-sided RBS	Identical as Specimen C6 but, except all plates and the beam and column members were hot dip galvanized.
C7	W30×116	W24×192	One-sided RBS	Size of doubler plate to satisfy WLY limit state. FLB limit state satisfied without stiffening. Welds designed according to Eq. 2.22 and Eq. 2.26.
W1	W36×150	W27×258	Two-sided WUF-W	Size of continuity plate designed per Eq. 2.2. Extended doubler plate welded with PJP. Continuity plate welds designed as per the $w = (3/4)t_{cp}$ rule.
W2	W33×141	W27×217	Two-sided WUF-W	Size of continuity plate under-designed based per Eq. 2.2 ($DCR=1.16$). Continuity plate satisfied minimum thickness as per Eq. 1.18. Extended doubler plate welded with PJP. Continuity plate welds designed as per the $w = (3/4)t_{cp}$ rule.
W3	W30×116	W24×207	Two-sided WUF-W	Size of continuity plate designed per Eq. 2.2. Weak panel zone (DCR of 1.07) per Eq. 1.19. Doubler plate stability criterion violated (Eq. 1.20). Extended doubler plate welded with vertical fillet welds to develop shear capacity. Continuity plate welds designed as per the $w = (3/4)t_{cp}$ rule.
W4	W24×94	W24×182	Two-sided WUF-W	Size of continuity plate designed per Eq. 2.2. Continuity plate satisfied minimum thickness as per Eq. 1.18. Doubler plate welds placed within continuity plates with vertical fillet welds to develop shear capacity. Continuity plate welds designed as per the $w = (3/4)t_{cp}$ rule.

a) Specimens tested and reported in Mashayekh and Uang (2018).

Table 2.2 Phase 1 Specimen RBS Dimensions

Spec. No.	a (in.)	b (in.)	c (in.)	R (in.)	$\frac{M_f}{M_{pe}}$
C1 ^a	7.0	25.0	2.00	40.0	0.95
C2 ^a	7.0	25.0	2.50	32.5	0.92
C3	6.0	24.0	2.50	30.0	0.91
C4	6.0	20.0	2.00	26.0	0.93
C5	6.0	24.0	2.00	37.0	0.88
C6	6.0	20.0	2.00	36.0	0.93
C6-G ^b	6.0	20.0	2.00	36.0	0.93
C7	6.0	20.0	2.25	23.3	0.89

a) Specimens tested and reported in Mashayekh and Uang (2018).

b) Specimen beam and column are galvanized.

Table 2.3 Continuity Plate Design Metric

Specimen No.	Span-to-Depth Ratio ^a	SCWB Ratio	t_{cp} (in.)	P_f (kips)	FLB (kips)	WLY (kips)	P_{cp}^b (kips)	V_{cp}^b (kips)	Cont. Plate DCR	b/t	w^c (in.)	w/t_{cp}
C1	11.2	2.41	0.75	577	505	377	100	15.5	0.35	8.0	9/16	0.75
C2	9.6	1.58	0.63	719	1005	790	-36	-10.2	-	9.6	1/2	0.80
C3	9.9	1.60	-	709	1005	790	-41	-	-	-	-	-
C4	11.4	3.70	-	563	729	585	-11	-	-	-	-	-
C5	9.9	1.19	0.38	681	684	575	53	15.3	0.45	16.0	5/16	0.83
C6	11.6	2.48	0.50	563	505	377	93	14.5	0.68	12.0	1/2	1.00
C6-G	11.6	2.48	0.50	563	505	377	93	14.5	0.68	12.0	1/2	1.00
C7	11.6	2.84	-	538	600	764	-31	-	-	-	-	-
W1	6.8	1.05	0.50	1088	881	1532	104	28.4	0.86	12.0	3/8	0.75
W2	7.3	0.99	0.75	1040	633	1446	204	53.2	1.43	7.8	9/16	0.75
W3	8.2	1.11	0.50	849	693	1047	78	67.5	0.6	11.0	3/8	0.75
W4	10.1	1.22	0.75	710	419	926	146	41.9	0.95	7.3	9/16	0.75

a) Span-to-depth ratio for two-sided specimens listed for the shorter span.

b) Negative values result when continuity plates not required per §J10 in AISC 360 regarding the FLB and WLY limit states.

c) Weld size, w , tabulated for the continuity plate-to-column flange fillet weld.

Table 2.4 Doubler Plate Design Metric

Specimen No.	t_{dp} (in.)	V_{pz} (kips)	Panel Zone DCR	$\frac{d_z + w_z}{t_{cw}}$	$\frac{d_z + w_z}{t_{dp}}$	$q_{dp,v}$ (kips/in)	$0.6F_y t_{dp}$ (kips/in)	Doubler Plate Vertical Weld
C1	-	576	0.90	68	-	-	-	-
C2	-	692	0.96	40	-	-	-	-
C3	-	683	0.94	40	-	-	-	-
C4	-	562	0.63	59	-	-	-	-
C5	-	656	1.18	48	-	-	-	-
C6	-	562	0.88	68	-	-	-	-
C6-G	-	562	0.88	68	-	-	-	-
C7	0.63	537	0.43	63	81	9.2	18.8	7/16 in.
W1	0.63	2003	0.98	61	95	18.8	18.8	PJP
W2	0.75	1957	0.94	68	76	22.2	22.5	PJP
W3	0.50	1640	1.07	58	102	15.0	15.0	11/16 in.
W4	0.63	1431	0.93	64	72	18.3	18.3	7/8 in.

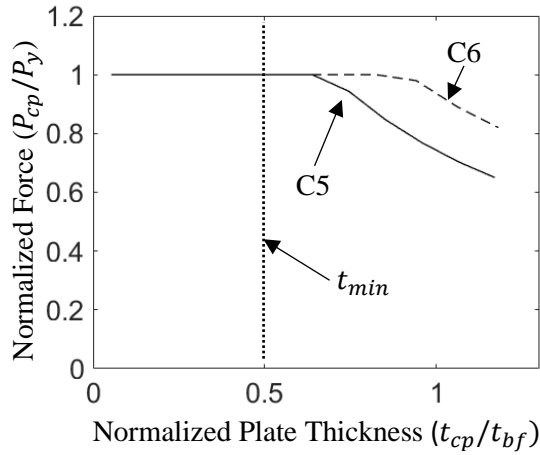
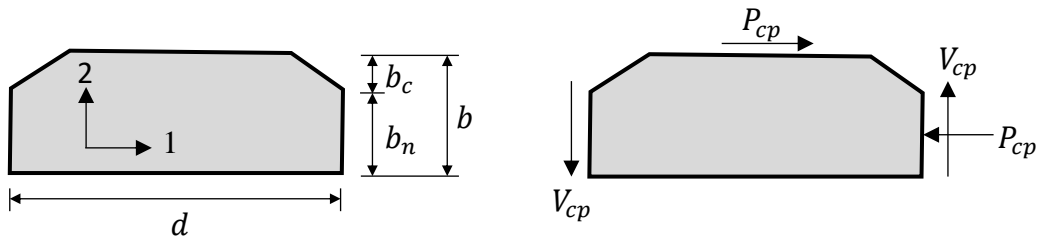


Figure 2.1 Continuity Plate Force Prediction



(a) Dimensions and Sign Convention

(b) Free Body Diagram (Exterior)

Figure 2.2 Continuity Plate Diagrams

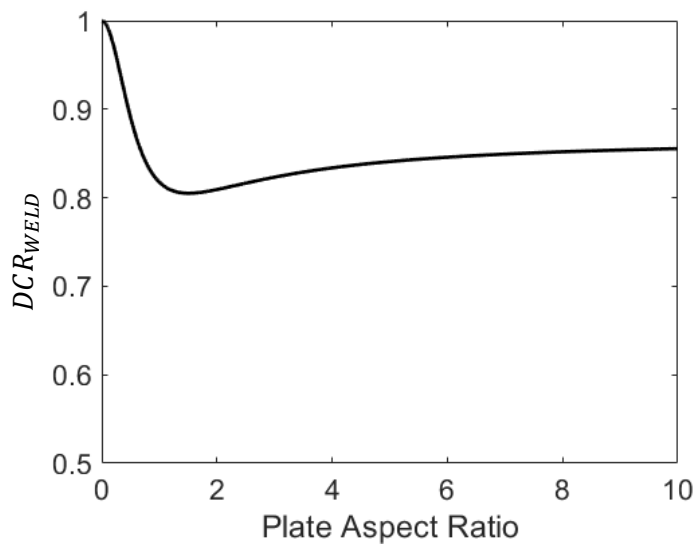


Figure 2.3 Continuity Plate Weld DCR Including Shear

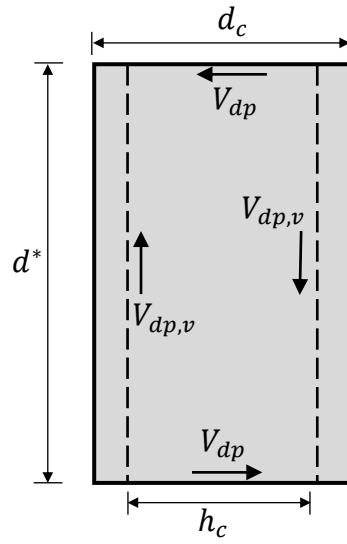
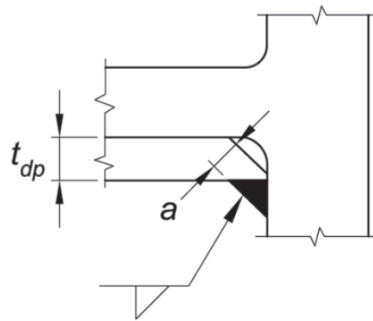


Figure 2.4 Doubler Plate Free Body Diagram



(a) Fig. C-E3.6.(b) AISC 341 (2016b)



(b) Specimen C7

Figure 2.5 Doubler Plate Vertical Fillet Welds

3 TEST PROGRAM

3.1 General

The testing was conducted in accordance with Section K2 of AISC 341 (2016b) at the Charles Lee Powell Structural Systems Laboratories of the University of California, San Diego (UCSD). The full-scale testing program was divided into two phases. Phase 1 consisted of exterior (one-sided) beam-column subassemblies with Reduced Beam Section (RBS) moment connections. Table 3.1 shows the test matrix for the exterior RBS connections. The specimens used either a W36×150 beam or a W30×116 beam. Several shallow columns (W14×211 and W14×257) and several deeper column shapes (W24×176, W24×192, and W27×235) were tested. Three of the Phase 1 specimens (Specimens C5, C6, and C6-G) used a continuity plate that either met or was undersized according to §E3.6f.2(b) of AISC 341. The three specimens which did not use a continuity plate (Specimens C3, C4, and C7) violated the continuity plate requirement of §E3.6f.1(b) of AISC 341. Specimen C6-G was nominally identical to Specimen C6, except this specimen was hot-dip galvanized before simulated field welding. Specimen C7 was the only specimen of Phase 1 to use a doubler plate. Fillet welds were used for the vertical welds of this doubler plate.

Phase 2 consisted of four interior (two-sided) beam-column subassemblies with Welded Unreinforced Flange with a Welded Web (WUF-W) connections. Table 3.2 shows the beams and columns selected for the specimens. Specimen W1 used two W36×150 beams welded to a W27×258 column. Specimen W2 used two W33×141 beams welded to a W27×217 column. Specimen W3 used two W30×116 beams welded to a W24×207 column. Finally, Specimen W4 used two W24×94 beams welded to a W24×182 column. Specimens W2 and W4 used continuity plates which satisfied the minimum thickness as per AISC 341. The other two specimens used continuity plates thinner than the minimum thickness requirement. All four specimens used doubler plates as symmetric plates placed on either side of the column. All of the doubler plates were extended 6 in. beyond the beam flange level, except for Specimen W4, which placed a doubler plate within the continuity plates. Specimens W1 and W2 used a PJP weld for the vertical welds, while Specimens W3 and W4 used fillet welds for the vertical welds.

All of the members satisfy the requirements of AISC 341 Section D1. Specifically, the members are proportioned to satisfy the requirements of a highly-ductile member. Except for Beam 1 of Specimen W1, all the specimens satisfy the clear span-to-depth ratio specified in either Chapter 5 or Chapter 8 of AISC 358-16. The remaining design details, including but not limited to Demand Critical (DC) welding of CJP beam-to-column welds, supplemental fillet welds, shear tab thickness, and continuity plate corner clips, satisfy the design requirements of AISC 341 or the connection-specific requirements of AISC 358.

3.2 Test Setup

The Phase 1 test setup is shown in Figure 3.1; each specimen was tested in the upright position. Frame inflection points are assumed to exist at the mid-height of each story, which are simulated by using three W14×257 hinge supports. The W14 shapes were mounted under the column and at the top and bottom as shown in Figure 3.2. The beam length represents half of the bay width, assuming an inflection point at the midspan of the beam. The loading end (south end of the specimen) is loaded through a 220-kip hydraulic actuator with an inline load cell. The load from the actuator is delivered to the free end of the beam through a loading corbel (see Figure 3.3). An intermediate top flange lateral restraint placed about 18 in. away from the RBS cut used for Specimens C3 and C5 is seen Figure 3.4. The top-flange lateral bracing outside of the RBS simulates the lateral restraint provided by a composite concrete slab in a real application. To increase the stiffness of the intermediate lateral restraint, the two lateral columns were tied together. For the remainder of the specimens both the top and bottom flange of the beam was braced as the same location just beyond the reduced beam section (see Figure 3.5). A modular frame provides lateral bracing at the loading corbel at the end of the beam. All lateral restraints use a polished, greased sliding surface to minimize friction.

The Phase 2 test setup is shown in Figure 3.6; each specimen was tested in the horizontal position. As in Phase 1, frame inflection points are assumed to exist at the mid-height of each story. The lower end of the specimen is mounted in a clevis while the upper end uses a W14×311 hinge (see Figure 3.8). The clevis uses a 9-in. greased pin and a matching tang, which was designed to attach to the bottom of the specimens through a bolted base plate. The beam ends are loaded through loading corbels which slide on a greased plate elevated by a sliding block (see Figure 3.9). The load is delivered to the

loading corbels through a 500-kip hydraulic actuator on each side of the specimen. Lateral restraint of the beam is achieved by sandwiching the beams between two HSS sections. These HSS sections are bolted to an HSS post which is post-tensioned to the laboratory strong floor.

3.3 Specimen Sizes and Test Order

Table 3.1 shows the member sizes and stiffening element details for the five specimens tested in Phase 1 as well as the two specimens previously tested by Mashayekh and Uang (2018). The Phase 2 specimens consisted of two identical beam shapes framing into a common column using the WUF-W connection. Table 3.2 summarizes the specimens of Phase 2. Table 3.3 shows the member cross-sectional dimensions for each test specimen. Detailed engineering drawings are included in Appendix A.

3.4 Specimen Construction and Inspection

The San Bernardino location (San Bernardino Steel) of The Herrick Corporation fabricated the test specimens. For reasons of economy, the field welding was simulated at Herrick's shop. The simulated field welding of Specimen C5 was observed on October 25 of 2018. Figure 3.10 to Figure 3.16 show the observed simulated field welding. At the time of welding, a visual inspection was performed by West Coast Inspection Services. After a 24-hour cool-down period, UT and magnetic particle testing were also performed by West Coast Inspection Services. Weld inspection of the Phase 2 specimens was completed by the Smith & Emery Company. See Appendix B for all Weld Inspection Reports. The inspections did not reveal any actionable flaws in the welding.

3.5 Material Properties

The W-shaped beams and columns were fabricated from ASTM A992 steel, while the continuity and doubler plates were fabricated from ASTM A572 Gr. 50 steel. Table 3.4 shows the mechanical properties of the base materials. Table 3.5 shows the chemical composition of the materials obtained from the Certified Mill Test Reports (see Appendix C). Appendix D shows the stress-strain response of the tensile coupon testing performed at UCSD.

The simulated field welding of the beam top and bottom flange CJP welds used an E70T-6 (Lincoln Electric NR-305) electrode in the flat position. The beam web CJP, beam

top flange backing bar fillet, and beam bottom flange reinforcing fillet was welded with an E71T-8 (Lincoln Electric NR-232) electrode in the vertical and overhead positions. Continuity plate and doubler plate welds were shop-welded with an E70T-9C (Lincoln Electric OSXLH-70) electrode. These electrodes satisfy the requirements of AWS D1.8 (2016) for Demand Critical welds. Specifically, they satisfy the minimum Charpy V-Notch toughness requirements of 20 ft-lb at 0°F and 40 ft-lb at 70°F. Table 3.6 shows the Charpy V-Notch toughness from the beam flange and beam web welds. Charpy samples were extracted in the transverse direction of a weld mockup fabricated on the same day as the Phase 2 specimens. Appendix E shows the Welding Procedure Specifications for shop and the simulated field welding.

3.6 Instrumentation

A combination of displacement transducers, strain gauge rosettes, and uniaxial strain gauges were used to measure global and local responses. Figure 3.17 shows the location of the displacement transducers for the Phase 1 specimens. Displacement transducer L1 measured the displacement and controls the actuator for displacement-control testing. Transducer L2 was used to quantify slip, if any, between the loading corbel and beam tip. Panel zone deformations were measured from transducers L3 and L4. Column rotations were measured from transducers L5 and L6. Transducers L7 through L9 were used to monitor displacements at the supports, which were anticipated to be negligible.

Figure 3.18 shows the location of displacement transducers for the Phase 2 specimens. L1 and L2 measured the displacements and controlled the two actuators. Transducers L3 and L4 were used to quantify slip between the loading corbels and the beam ends. Column rotations were measured using transducers L5 and L6, while the panel zone deformation was measured by transducers L7 and L8. Transducers L12, L13, and L14 were used to monitor the out-of-plane displacement of the column. The remaining transducers were used to monitor the displacements at the supports, which were anticipated to be negligible.

Various rosettes and uniaxial strain gauges were used to measure the strains in the connection region. Figure 3.19 to Figure 3.25 show the instrumentation layout for the connection region of each specimen. Additionally, several gauges were placed on the intermediate lateral restraint columns to characterize the lateral bracing force.

It is typical practice to whitewash the specimens in the connection region prior to loading such that yielding can be photographed during testing. As part of a pilot project to test the capabilities of Digital Imaging Correlation (DIC) software, the first two specimens tested (Specimens C3 and C5) were not whitewashed. Instead, a random speckle pattern was applied to key areas of the specimen. The remaining specimens were whitewashed to provide visual evidence of yielding.

3.7 Data Reduction

The Story Drift Angle (*SDA*) is the ratio between δ_{total} and L :

$$SDA = \delta_{total}/L \quad (3.1)$$

where δ_{total} is the total beam tip deflection measured by displacement transducer L1 (and L2 for Phase 2), and L is the length of the beam measured from the beam tip (i.e., loading point) to the centerline of the column.

The total plastic rotation (θ_p) of the specimen is calculated by dividing the plastic component (δ_p) of the beam tip displacement by L .

$$\theta_p = \frac{\delta_p}{L} = \frac{1}{L}(\delta_{total} - \delta_e) = \frac{1}{L}\left(\delta_{total} - \frac{P}{K}\right) \quad (3.2)$$

where P is the applied load, δ_e is the elastic component of beam tip displacement, and K is the elastic stiffness determined from the initial low-amplitude response of P vs. δ_{total} .

The components of the beam tip displacement are separated into the displacements due to the flexure of the beam, the flexure of the column, and the shearing of the panel zone. Panel zone deformation, γ is computed using L3 and L4 in Phase 1 or L7 and L8 in Phase 2. Assigning the displacement recorded by L3 or L7 to δ_a and the displacement from L4 or L8 to δ_b , the average panel zone shear deformation is computed by:

$$\gamma = \frac{\sqrt{w_{pz}^2 + d_{pz}^2}}{2w_{pz}d_{pz}}(\delta_b - \delta_a) \quad (3.3)$$

where w_{pz} and d_{pz} are the width and depth of the panel zone measure points. For specimens without a continuity plate, the transducers were placed within the panel zone to avoid spurious displacement caused by column out-of-plane flange flexure. Otherwise, the transducers were placed at the center of the cruciform formed by the beam flange, continuity plate, and column flange. A rigid-body correction is required when extrapolating

the influence of the panel zone deformation on the beam tip deformation (Uang and Bondad 1996):

$$\delta_{pz} = \gamma L - \gamma d - \frac{d_b}{H} \left(L + \frac{d_c}{2} \right) \quad (3.4)$$

The contribution of the beam tip deformation due to the column flexure is found by transducers L5 and L6 in either phase. Assigning the displacement recorded by these transducers to δ_c and δ_d , respectively, results in:

$$\delta_{col} = \frac{\delta_d - \delta_c}{d_b} L - \gamma d_b \left(1 - \frac{d_b}{H} \right) \quad (3.5)$$

where the latter term is the correction to remove the panel zone deformation from the flexural deformations. Finally, the components of the beam tip deformation are as follows:

$$\delta_{total} = \delta_{beam} + \delta_{pz} + \delta_{col} \quad (3.6)$$

The contribution due to the beam can then be solved for as:

$$\delta_{beam} = \delta_{total} - \delta_{pz} - \delta_{col} \quad (3.7)$$

In the Phase 2 specimens an additional component of deformation exists due to the gap between the clevis and the pin, δ_{clevis} . The rigid-body motion of this is removed by incorporating the displacement recorded by transducer L15. Assigning δ_p to be the displacement recorded by transducer L15 results in:

$$\delta_{clevis} = \frac{2\delta_p}{H} L \quad (3.8)$$

Which gives the beam tip deformation for Phase 2 as:

$$\delta_{beam} = \delta_{total} - \delta_{pz} - \delta_{col} - \delta_{clevis} \quad (3.9)$$

The dissipated hysteretic energy is computed by integrating the load-displacement response such that:

$$E_{h,total} = E_{h,beam} + E_{h,pz} + E_{h,col} - E_{elastic} \quad (3.10)$$

where $E_{elastic}$ is the recoverable elastic energy. By convention, the integration of the dissipated energy includes only the drift cycles where the moment at the face of the column has not degraded beyond $0.8M_{pn}$, where M_{pn} equals the beam nominal plastic moment. This cutoff is imposed because strength degradation beyond this limit does not satisfy the SMF requirements of AISC 341. From the dissipated energy the cumulative plastic drift can be determined as:

$$\Sigma\theta_p = \frac{E_{h,total}}{M_p} \quad (3.11)$$

where M_p is the actual plastic moment of the section. The Reserved Energy Ratio, Ω_E , represents the amount of energy dissipated in excess of the first-cycle, 0.04 rad story drift angle requirement of SMF based on AISC 341. Setting the dissipated energy capacity, $E_{h,min}$, to be the dissipated energy after completing one cycle of 0.04 rad story drift results in:

$$\Omega_E = \frac{E_{h,total}}{E_{h,min}} \quad (3.12)$$

The peak connection strength factor, C_{pr} , accounting for strain hardening and local restraint, is used in predicting the seismic flange forces of the beams framing into the column (AISC 2016b). Specimen design has used the values provided in AISC 358-16 as 1.15 and 1.4 for the RBS and WUF-W connections, respectively. After testing of each specimen, C_{pr} is computed by normalizing the experimentally determined moment at the plastic hinge location by the expected moment, M_{pe} . For RBS connections, $M_{pe} = Z_{RBS}F_{ya}$, and for WUF-W connections, $M_{pe} = Z_xF_{ya}$, where F_{ya} is the measured yield strength of the material. Per AISC 358-16 The plastic hinge location is assumed to take place at the center of the reduced section for RBS cuts and at the face of the column for WUF-W connections.

3.8 Loading Sequence

Testing is conducted in a displacement-control mode. The loading sequence used for all specimens was the standard AISC loading sequence specified in Section K2 of AISC 341 (2016). The AISC loading sequence specifies a series of load cycles at different $SDAs$. The loading history begins with six cycles each at 0.00375, 0.005, and 0.0075 rad drifts. These are followed by four cycles at 0.01 rad drifts, two cycles at 0.015 rad drifts, two cycles at 0.02, 0.03, 0.04 rad drifts, and etc., up until failure. Figure 3.26 shows the loading sequence.

3.9 Acceptance Criteria

According to Section E3.6b of the AISC Seismic Provisions for Structural Steel Buildings (AISC 2016b), beam-to-column connections used in special moment frames shall satisfy the following requirements:

- (1) The connection shall be capable of accommodating a story drift angle of at least 0.04 rad.
- (2) The measured flexural resistance of the connection, determined at the column face, shall equal at least $0.8M_{pn}$ of the connected beam at a story drift angle of 0.04 rad, where M_{pn} is the nominal plastic moment of the beam.

Table 3.1 Phase 1 Exterior RBS Connection Test Matrix

Spec. No.	Beam	Column	Continuity Plate (in.)	Continuity Plate Fillet Weld (in.)	Doubler Plate	Test Date
C1 ^a	W30×116	W24×176	3/4	9/16	-	04/28/2016
C2 ^a	W36×150	W14×257	5/8	1/2	-	04/04/2016
C3	W36×150	W14×257	-	-	-	11/02/2018
C4	W30×116	W27×235	-	-		1/29/2019
C5	W36×150	W14×211	3/8	5/16		11/14/2018
C6	W30×116	W24×176	1/2	1/2		2/08/2019
C6-G ^b	W30×116	W24×176	1/2	1/2		2/15/2019
C7	W30×116	W24×192	-	-	1 × 5/8"	2/04/2019

a) Specimens tested and reported in Mashayekh et al. (2017).

b) Specimen beam and column are galvanized.

Table 3.2 Phase Two Interior WUF-W Connection Test Matrix

Spec. No.	Beam	Column	Continuity Plate (in.)	Continuity Plate Fillet Weld (in.)	Doubler Plate	Test Date
W1	W36×150	W27×258	1/2	3/8	2 × 5/8"	8/08/2019
W2	W33×141	W27×217	3/4	9/16	2 × 3/4"	7/31/2019
W3	W30×116	W24×207	1/2	3/8	2 × 1/2"	7/26/2019
W4	W24×94	W24×182	3/4	9/16	2 × 5/8"	7/22/2019

Table 3.3 Member Cross-Sectional Dimensions

Specimen No.	Member	d (in.)	t_w (in.)	b_f (in.)	t_f (in.)	Width-Thickness Ratio	
						Web	Flange
C1 ^a	Beam (W30×116)	30.0	0.57	10.5	0.85	47.8	6.17
	Column (W24×176)	25.2	0.75	12.9	1.34	28.7	4.81
C2 ^a	Beam (W36×150)	35.9	0.625	12.0	0.94	51.9	6.37
	Column (W14×257)	16.4	1.18	16.0	1.89	9.71	4.23
C3	Beam (W36×150)	35.9	0.625	12.0	0.94	51.9	6.37
	Column (W14×257)	16.4	1.18	16.0	1.89	9.71	4.23
C4	Beam (W30×116)	30.0	0.57	10.5	0.85	47.8	6.17
	Column (W27×235)	28.7	0.91	14.2	1.61	26.2	4.41
C5	Beam (W36×150)	35.9	0.625	12.0	0.94	51.9	6.37
	Column (W14×211)	15.7	0.98	15.8	1.56	11.6	5.06
C6, C6-G	Beam (W30×116)	30.0	0.57	10.5	0.85	47.8	6.17
	Column (W24×176)	25.2	0.75	12.9	1.34	28.7	4.81
C7	Beam (W30×116)	30.0	0.57	10.5	0.85	47.8	6.17
	Column (W24×192)	25.5	0.81	13.0	1.46	26.6	4.43

a) Specimens tested and reported in Mashayekh et al. (2017).

Table 3.3 Member Cross-Sectional Dimensions (continued)

Specimen No.	Member	d (in.)	t_w (in.)	b_f (in.)	t_f (in.)	Width-Thickness Ratio	
						Web	Flange
W1	Beam (W36×150)	35.9	0.625	12.0	0.94	51.9	6.37
	Column (W27×258)	29.0	0.980	14.3	1.77	24.4	4.03
W2	Beam (W33×141)	33.3	0.605	11.5	0.96	49.6	6.01
	Column (W27×217)	28.4	0.830	14.1	1.50	28.7	4.71
W3	Beam (W30×116)	30.0	0.565	10.5	0.85	47.8	6.17
	Column (W24×207)	25.7	0.870	13.0	1.57	24.8	4.14
W4	Beam (W24×94)	24.3	0.515	9.07	0.88	41.9	5.18
	Column (W24×182)	25.0	0.705	13.0	1.22	30.6	5.31

Table 3.4 Base Metal Mechanical Properties

Spec. No.	Component	Steel Type/ Heat No.	Yield Stress ^a (ksi)	Tensile Strength (ksi)	Elong. ^b (%)
C1	Beam Flange (W30×116)	A992 443484	56.9 (56.5) ^b	75.6 (72.0) ^b	34.5 (28.0) ^b
	Beam Web (W30×116)		58.5	73.2	39.5
	Column Flange (W24×176)	A992 442208	57.2 (57.5) ^b	70.6 (72.5) ^b	39.1 (27.0) ^b
	Column Web (W24×176)		58.5	72.2	37.3
	Continuity Plate (3/4 in.)	A572 Gr. 50 SB15106	68.1 (58.0) ^b	85.6 (81.0) ^b	36.9 (25.0) ^b
C2	Beam Flange (W36×150)	A992 60114091/04	53.5 (57.0) ^b	74.9 (75.1) ^b	38.3 (26.4) ^b
	Beam Web (W36×150)		57.9	74.7	38.1
	Column Flange (W14×257)	A992 317275	52.3 (57.0) ^b	74.3 (75.0) ^b	37.7 (26.0) ^b
	Column Web (W14×257)		54.8	74.8	38.6
	Continuity Plate (5/8 in.)	A572 Gr. 50 813K75180	54.1 (57.6) ^b	79.8 (82.6) ^b	35.1 (22.5) ^b
C3	Beam Flange (W36×150)	A992 421418	57.2 (57.0) ^b	72.4 (72.0) ^b	25.7 (26.0) ^b
	Beam Web (W36×150)		67.8	78.8	21.8
	Column Flange (W14×257)	A992 N039862	60.0 (59.0) ^b	80.4 (78.0) ^b	22.3 (28.0) ^b
	Column Web (W14×257)		52.6	75.5	29.6
C4	Beam Flange (W30×116)	A992 3G7361	59.7 (60.7) ^b	82.0 (82.8) ^b	22.7 (24.5) ^b
	Beam Web (W30×116)		65.7	85.4	-
	Column Flange (W27×235)	A992 488640	(53.0) ^b	(71.0) ^b	(27.0) ^b
	Column Web (W27×235)		60.0	75.0	24.8

Table 3.4 Base Metal Mechanical Properties (continued)

Spec. No.	Component	Steel Type/ Heat No.	Yield Stress ^a (ksi)	Tensile Strength (ksi)	Elong. ^b (%)
C5	Beam Flange (W36×150)	A992 440889	(55.0) ^b	(71.0) ^b	(28.0) ^b
	Beam Web (W36×150)		65.6	77.1	23.2
	Column Flange (W14×211)	A992 452443	54.3 (59.0) ^b	71.5 (75.0) ^b	24.2 (28.5) ^b
	Column Web (W14×211)		57.0	75.1	24.2
	Continuity Plate (3/8 in.)	A572 Gr. 50 N17266	59.9 (63.3) ^b	79.0 (82.0) ^b	20.5 (31.0) ^b
C6, C6-G	Beam Flange (W30×116)	A992 426935	56.9 (58.0) ^b	69.9 (72.0) ^b	24.3 (28.5) ^b
	Beam Web (W30×116)		62.8	76.4	22.2
	Column Flange (W24×176)	A992 463912	54.2 (57.0) ^b	73.0 (75.0) ^b	25.5 (26.5) ^b
	Column Web (W24×176)		61.0	74.3	23.6
	Continuity Plate (1/2 in.)	A572 Gr. 50 1202005567	(54.9) ^b	(75.2) ^b	(34.0) ^b
C7	Beam Flange (W30×116)	A992 A127163	57.1 (58.0) ^b	72.5 (72.0) ^b	24.3 (28.5) ^b
	Beam Web (W30×116)		61.7	74.2	23.7
	Column Flange (W24×192)	A992 H53207	57.6 (60.0) ^b	80.0 (80.0) ^b	22.8 (23.5) ^b
	Column Web (W24×192)		60.0	80.7	22.6
	Doubler Plate (5/8 in.)	A572 Gr. 50 N17707	51.2 (51.8) ^b	72.2 (70.8) ^b	23.9 (28.0) ^b

Table 3.4 Base Metal Mechanical Properties (continued)

Spec. No.	Component	Steel Type/ Heat No.	Yield Stress ^a (ksi)	Tensile Strength (ksi)	Elong. ^b (%)
W1	Beam Flange (W36×150)	A992 3110558	52.3 (57.0) ^b	78.8 (78.2) ^b	23.3 (26.1) ^b
	Beam Web (W36×150)		68.9	85.7	20.1
	Column Flange (W27×258)	A992 321553	52.6 (56.0) ^b	72.8 (74.0) ^b	25.3 (28.0) ^b
	Column Web (W24×258)		59.49	74.0	23.8
	Continuity Plate (1/2 in.)	A572 Gr. 50 N21707	(64.0) ^b	(80.2) ^b	(31.0) ^b
	Doubler Plate (2 × 5/8 in.)	A572 Gr. 50 N20741	(62.0) ^b	(80.5) ^b	(21.0) ^b
W2	Beam Flange (W33×141)	A992 506190	54.9 (53.0) ^b	70.4 (68.5) ^b	26.3 (29.5) ^b
	Beam Web (W33×141)		67.8	76.2	21.0
	Column Flange (W27×217)	A992 494737	59.7 (58.0) ^b	76.0 (75.0) ^b	24.2 (26.0) ^b
	Column Web (W27×217)		63.9	77.4	23.1
	Continuity Plate (3/4 in.)	A572 Gr. 50 S27292	(58.0) ^b	(81.0) ^b	(40.0) ^b
	Doubler Plate (2 × 3/4 in.)	A572 Gr. 50 S27292	(58.0) ^b	(81.0) ^b	(40.0) ^b
W3	Beam Flange (W30×116)	A992 504994	56.3 (53.5) ^b	71.3 (69.0) ^b	23.9 (27.5) ^b
	Beam Web (W30×116)		66.6	76.4	22.5
	Column Flange (W24×207)	A992 399018	58.3 (58.0) ^b	76.8 (76.5) ^b	22.9 (26.5) ^b
	Column Web (W24×207)		60.2	75.9	21.8
	Continuity Plate (1/2 in.)	A572 Gr. 50 N21707	(64.0) ^b	(80.2) ^b	(31.0) ^b
	Doubler Plate (2 × 1/2 in.)	A572 Gr. 50 N21707	(64.0) ^b	(80.2) ^b	(31.0) ^b

Table 3.4 Base Metal Mechanical Properties (continued)

Spec. No.	Component	Steel Type/ Heat No.	Yield Stress ^a (ksi)	Tensile Strength (ksi)	Elong. ^b (%)
W4	Beam Flange (W24×94)	A992 N 042176	53.5 (57.7) ^b	79.0 (76.6) ^b	21.6 (27.2) ^b
	Beam Web (W24×94)		60.5	81.3	23.6
	Column Flange (W24×182)	A992 H77491	57.4 (56.6) ^b	80.1 (76.9) ^b	22.3 (25.0) ^b
	Column Web (W24×182)		66.3	83.5	24.0
	Continuity Plate (3/4 in.)	A572 Gr. 50 S27292	(58.0) ^b	(81.0) ^b	(40.0) ^b
	Doubler Plate (2 × 5/8 in.)	A572 Gr. 50 N20741	(62.0) ^b	(80.5) ^b	(21.0) ^b

^a Yield stress determined by 0.2% strain offset method

^b Values in parentheses from Certified Mill Test Reports, others from testing at UCSD

Table 3.5 Chemical Compositions for Components from Mill Certificates

Spec. No.	Member	C	Mn	P	S	Si	Cu	Ni	Cr	Mo	V	CE (%)
C3	Beam (W36×150)	0.08	1.10	0.019	0.028	0.25	0.24	0.08	0.12	0.03	0.01	0.32
	Column (W14×257)	0.13	1.39	0.008	0.002	0.19	0.15	0.05	0.07	0.01	0.04	0.40
C4	Beam (W30×116)	0.17	1.03	0.021	0.010	0.13	0.23	0.10	0.15	0.02	0.028	0.40
	Column (W27×235)	0.08	1.31	0.013	0.022	0.20	0.27	0.13	0.19	0.05	0.04	0.38
C5	Beam (W36×150)	0.07	1.12	0.110	0.022	0.22	0.29	0.09	0.11	0.02	0.0	0.31
	Column (W14×211)	0.08	1.31	0.016	0.021	0.26	0.27	0.16	0.14	0.04	0.04	0.37
	Continuity Plate (3/8 in.)	0.14	1.08	0.011	0.004	0.22	0.01	0.05	0.02	0.00	0.016	0.33
C6, C6-G	Beam (W30×116)	0.08	1.10	0.013	0.023	0.25	0.23	0.09	0.12	0.04	0.0	0.32
	Column (W24×176)	0.08	1.36	0.018	0.022	0.21	0.25	0.12	0.14	0.05	0.05	0.37
	Continuity Plate (1/2 in.)	0.14	1.07	0.011	0.004	0.25	0.01	0.05	0.02	0.00	0.018	0.33
C7	Beam (W30×116)	0.07	1.23	0.014	0.025	0.23	0.30	0.10	0.10	0.031	0.035	0.33
	Column (W24×192)	0.26	1.03	0.013	0.011	0.22	0.20	0.09	0.09	0.017	0.03	0.40
	Doubler Plate (5/8 in.)	0.14	1.03	0.010	0.006	0.22	0.01	0.05	0.02	0.00	0.016	0.32

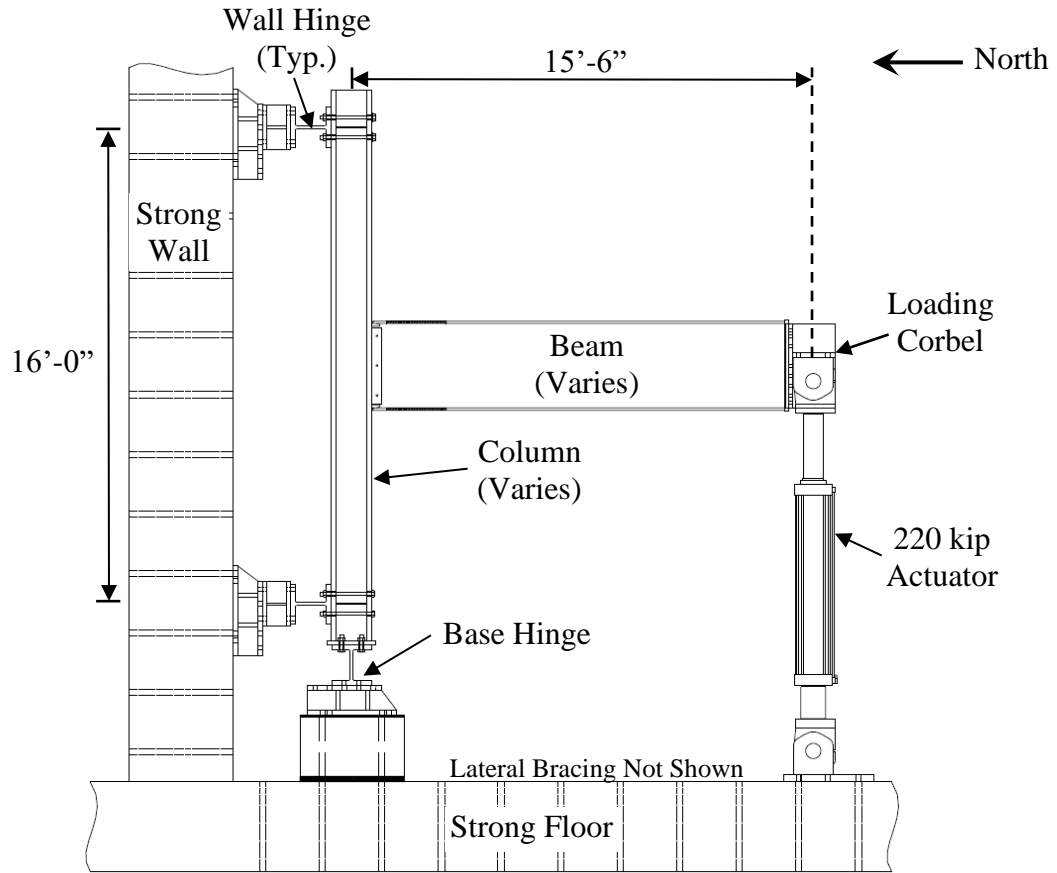
Table 3.5 Chemical Compositions for Components from Mill Certificates (continued)

Spec. No.	Member	C	Mn	P	S	Si	Cu	Ni	Cr	Mo	V	CE (%)
W1	Beam (W36×150)	0.17	1.02	0.072	0.011	0.14	0.24	0.08	0.13	0.02	0.032	0.39
	Column (W27×258)	0.07	1.38	0.022	0.020	0.24	0.30	0.09	0.11	0.03	0.05	0.37
	Continuity Plate (1/2 in.)	0.17	1.06	0.015	0.007	0.22	0.01	0.04	0.03	0.00	0.018	0.36
	Doubler Plate (2 × 5/8 in.)	0.14	1.10	0.017	0.006	0.23	0.01	0.05	0.02	0.00	0.048	0.38
W2	Beam (W33×141)	0.07	1.01	0.011	0.024	0.21	0.30	0.10	0.12	0.02	0.01	0.29
	Column (W27×217)	0.07	1.35	0.016	0.020	0.26	0.29	0.11	0.13	0.03	0.05	0.36
	Continuity Plate (3/4 in.)	0.14	1.34	0.012	0.003	0.31	0.010	0.010	0.020	0.00	0.07	0.39
	Doubler Plate (2 × 3/4 in.)	0.14	1.34	0.012	0.003	0.31	0.010	0.010	0.020	0.00	0.07	0.39
W3	Beam (W30×116)	0.08	1.00	0.010	0.024	0.20	0.32	0.13	0.10	0.04	0.01	0.31
	Column (W24×207)	0.07	1.35	0.012	0.025	0.29	0.25	0.11	0.15	0.04	0.05	0.37
	Continuity Plate (1/2 in.)	0.17	1.06	0.015	0.007	0.22	0.01	0.04	0.03	0.00	0.018	0.36
	Doubler Plate (2 × 1/2 in.)	0.17	1.06	0.015	0.007	0.22	0.01	0.04	0.03	0.00	0.018	0.36
W4	Beam (W24×94)	0.18	0.94	0.020	0.008	0.15	0.21	0.08	0.12	0.02	0.13	0.39
	Column (W24×182)	0.15	1.10	0.012	0.006	0.19	0.22	0.07	0.09	0.02	0.12	0.38
	Continuity Plate (3/4 in.)	0.14	1.34	0.012	0.003	0.31	0.010	0.010	0.020	0.00	0.07	0.39
	Doubler Plate (2 × 5/8 in.)	0.14	1.10	0.017	0.006	0.23	0.01	0.05	0.02	0.00	0.048	0.38

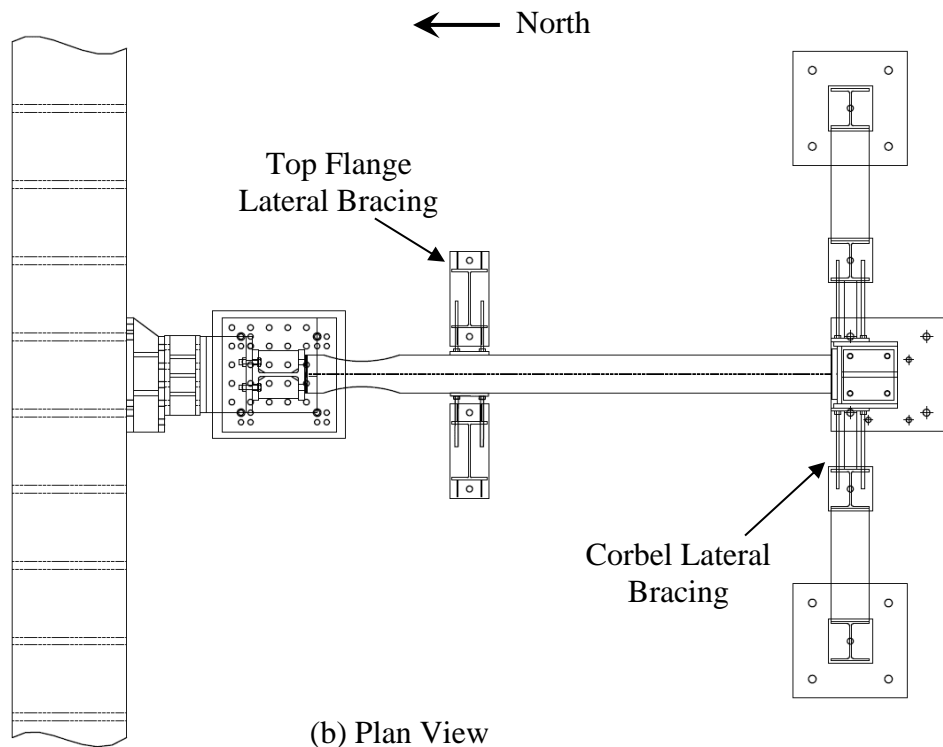
$$CE = C + \frac{Mn}{6} + \frac{Cr + Mo + V}{5} + \frac{Ni + Cu}{15}$$

Table 3.6 Weld Metal Charpy V-Notch Test Results

Weld Electrode	Energy (ft-lbs)							
	at 0°F				at 70°F			
E71T-8 (Lincoln Electric NR 232)	62	60	57		84	73	76	
	Average: 60				Average: 78			
E70T-6C (Lincoln Electric NR 305)	44	44	44	45	62	62	59	58
	Average: 44				Average: 60			



(a) Elevation View



(b) Plan View

Figure 3.1 Exterior Moment Connection Test Setup (Phase 1)



(a) Lower End

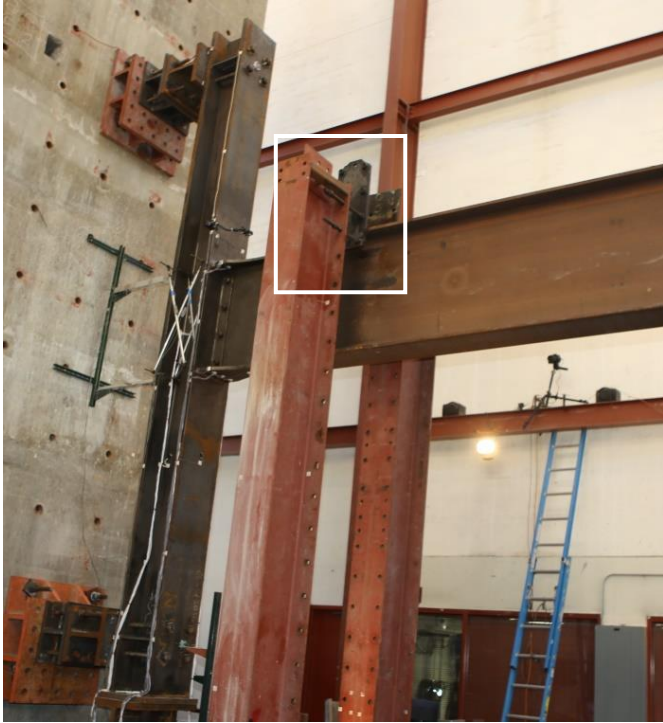


(b) Upper End

Figure 3.2 Column Support (Phase 1)



Figure 3.3 Lateral Bracing at Loading End (Phase 1)



(a) Overview



(b) Detail

Figure 3.4 Top Flange Intermediate Lateral Restraint (Specimens C3 and C5)



Figure 3.5 Top Flange Intermediate Lateral Restraint (Specimens C4, C6, C6-G, and C7)

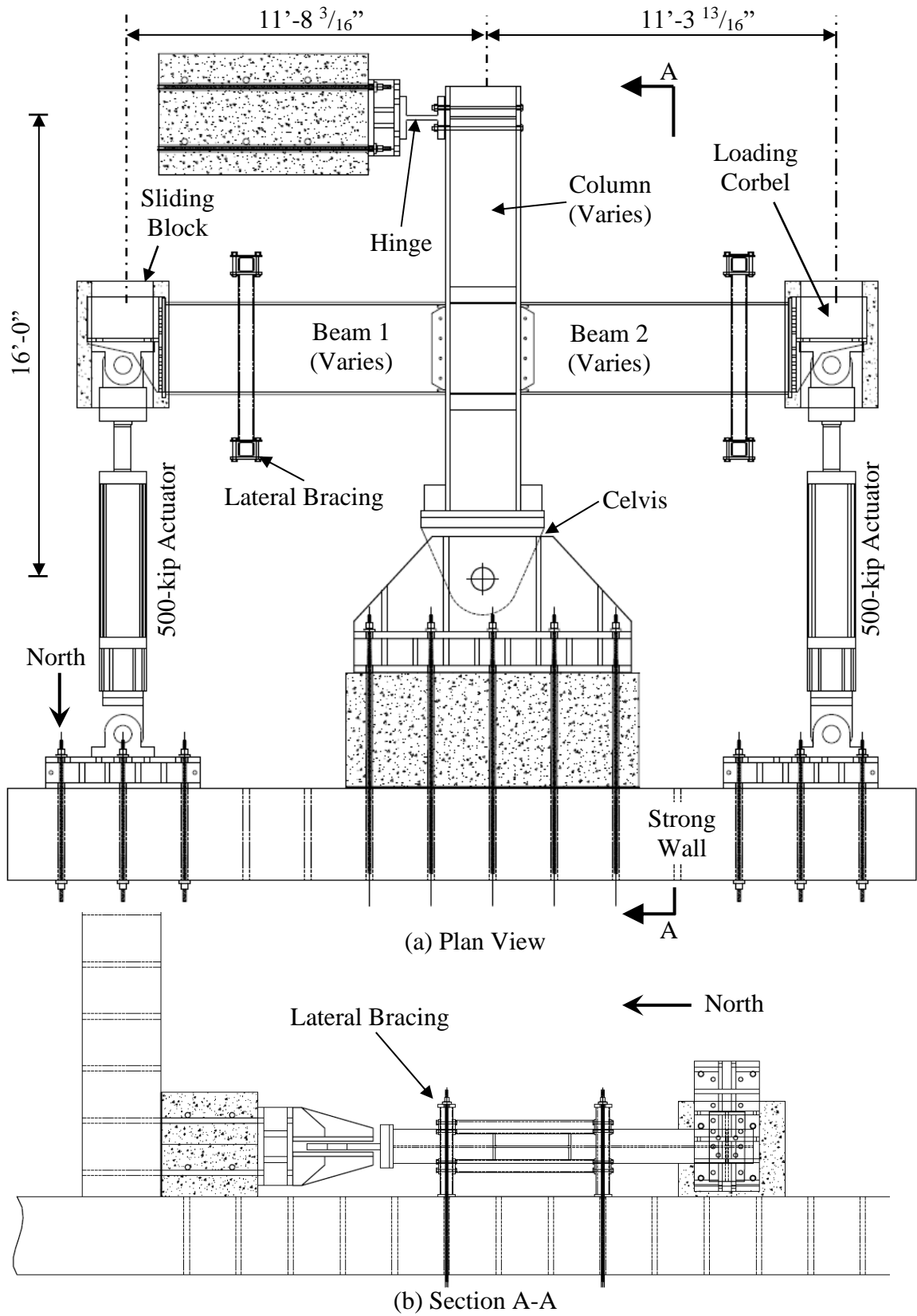


Figure 3.6 Interior Moment Connection Test Setup (Phase 2)

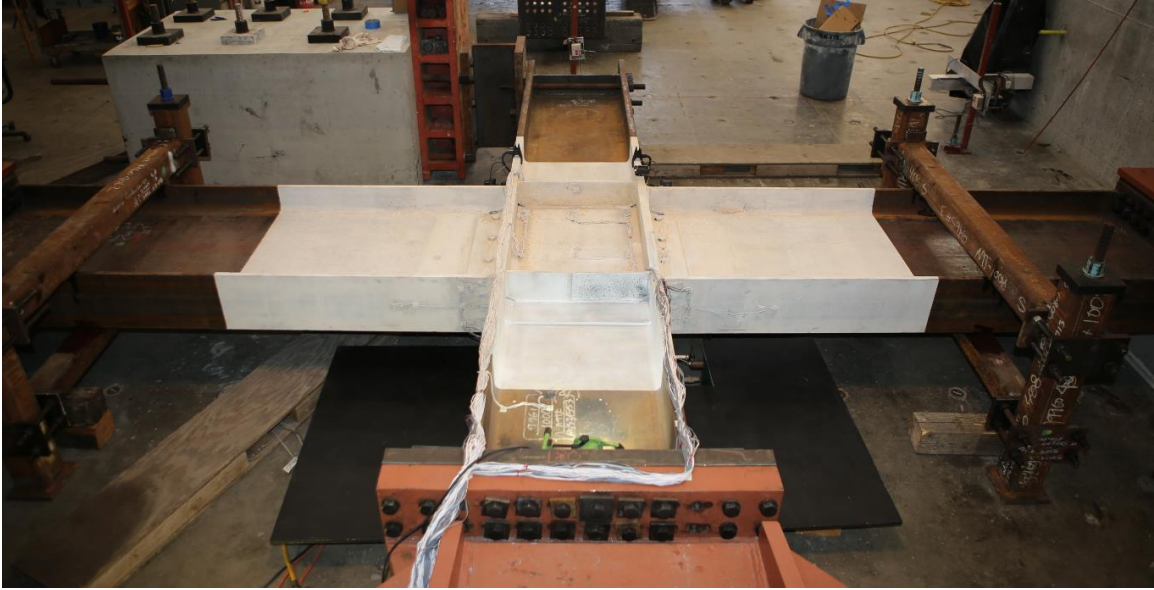


Figure 3.7 Test Setup (Phase 2)



(a) Column Base Support Clevis



(b) Top Column Support

Figure 3.8 Column Supports (Phase 2)

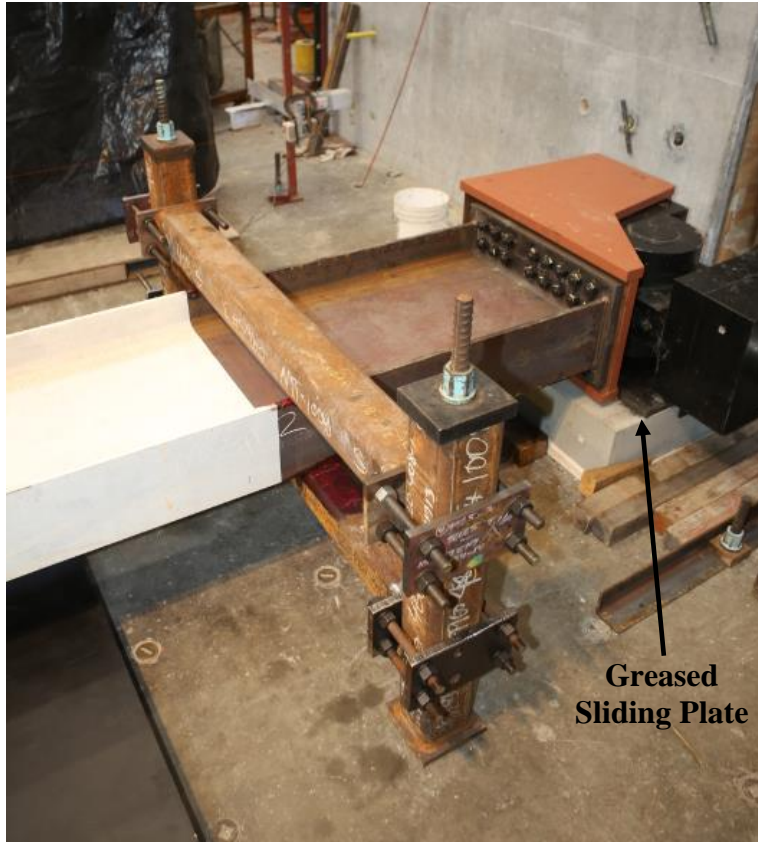


Figure 3.9 Beam Lateral Restraint and Loading End (Phase 2)



(a) Overview



(b) Weld Access Hole



(c) Run off Tab

Figure 3.10 Beam Bottom Flange and Web CJP Weld Preparation (Specimen C5)



(a) Backing Bar

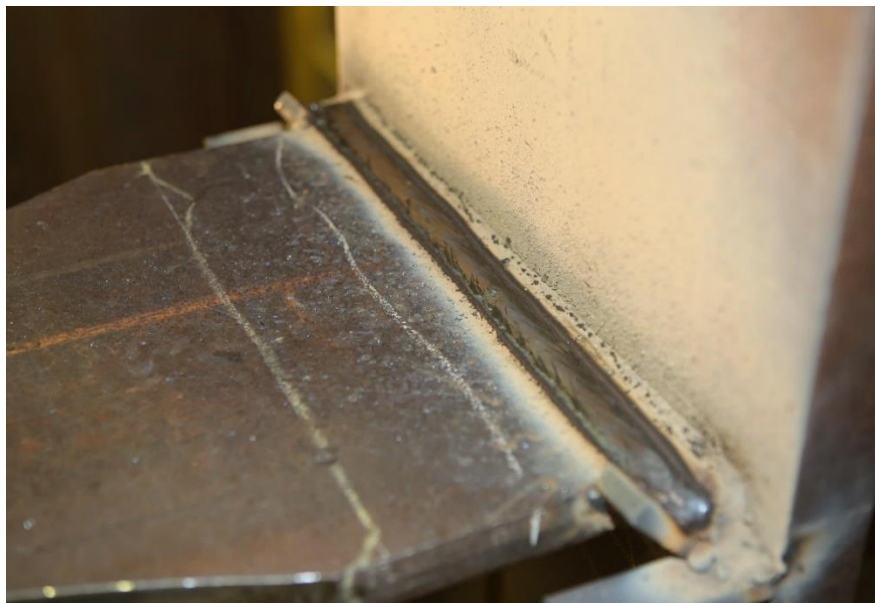


(b) Groove

Figure 3.11 Beam Top Flange CJP Weld Preparation (Specimen C5)



(a) Beam Bottom Flange



(b) Beam Top Flange

Figure 3.12 Beam Flange CJP Weld during Groove Welding (Specimen C5)



(a) Backgouging



(b) Reinforcing Fillet

Figure 3.13 Beam Bottom Flange Underside CJP Weld Treatment (Specimen C5)

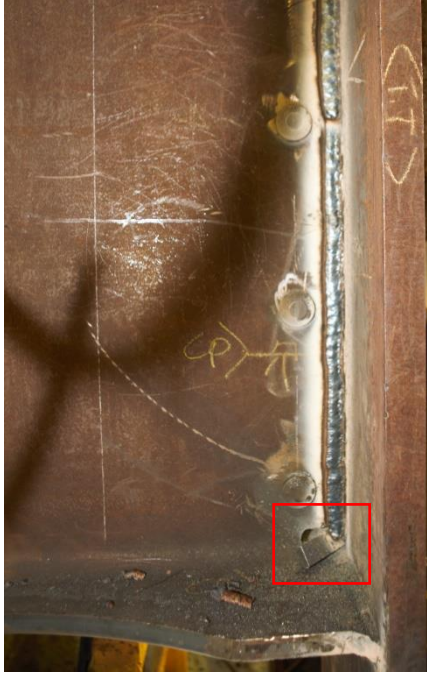


(a) Reinforcing Fillet



(b) after Cleanup

Figure 3.14 Beam Top Flange Underside CJP Weld Treatment (Specimen C5)



(a) Completed Weld



(b) after Cleanup

Figure 3.15 Beam Web Weld (Specimen C5)



Figure 3.16 Continuity Plate Fillet Welds (Specimen C5)

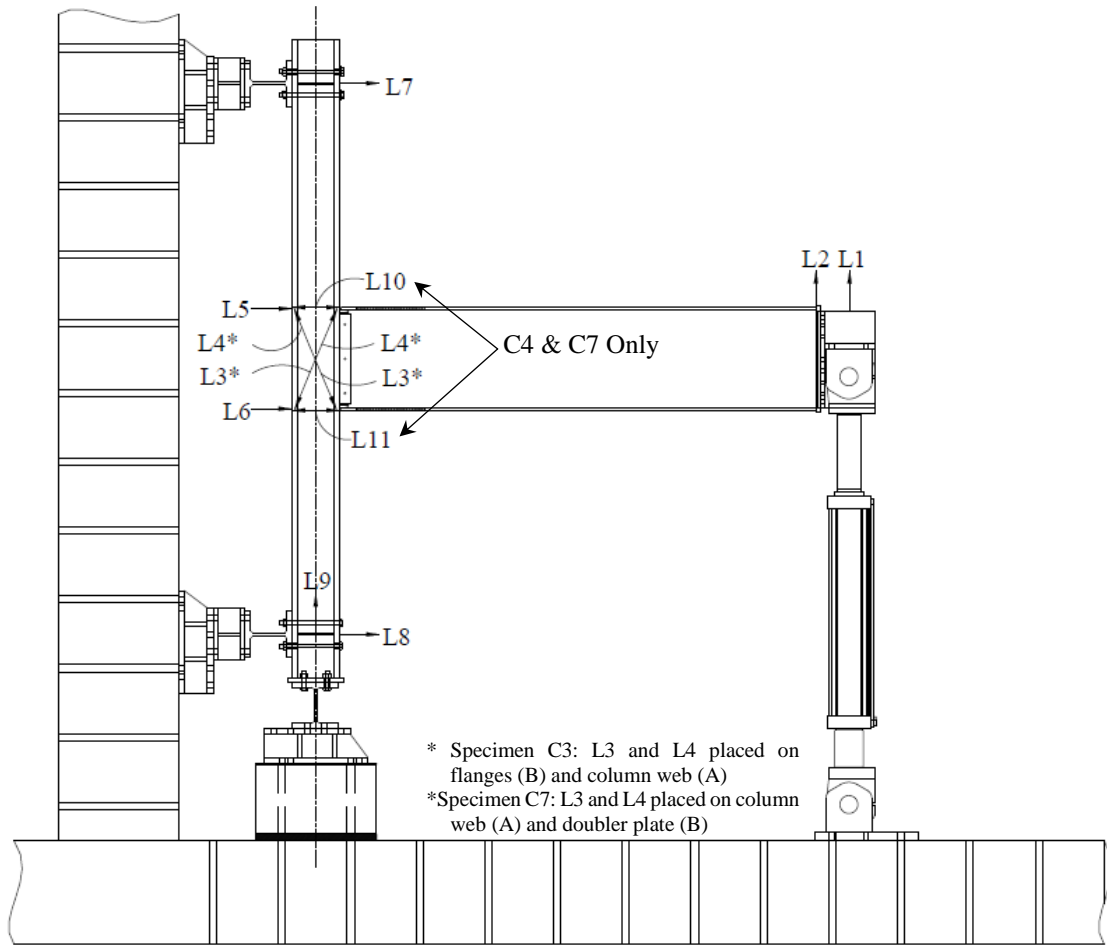


Figure 3.17 Exterior Moment Connection (Specimens C3 to C7) Transducer Layout

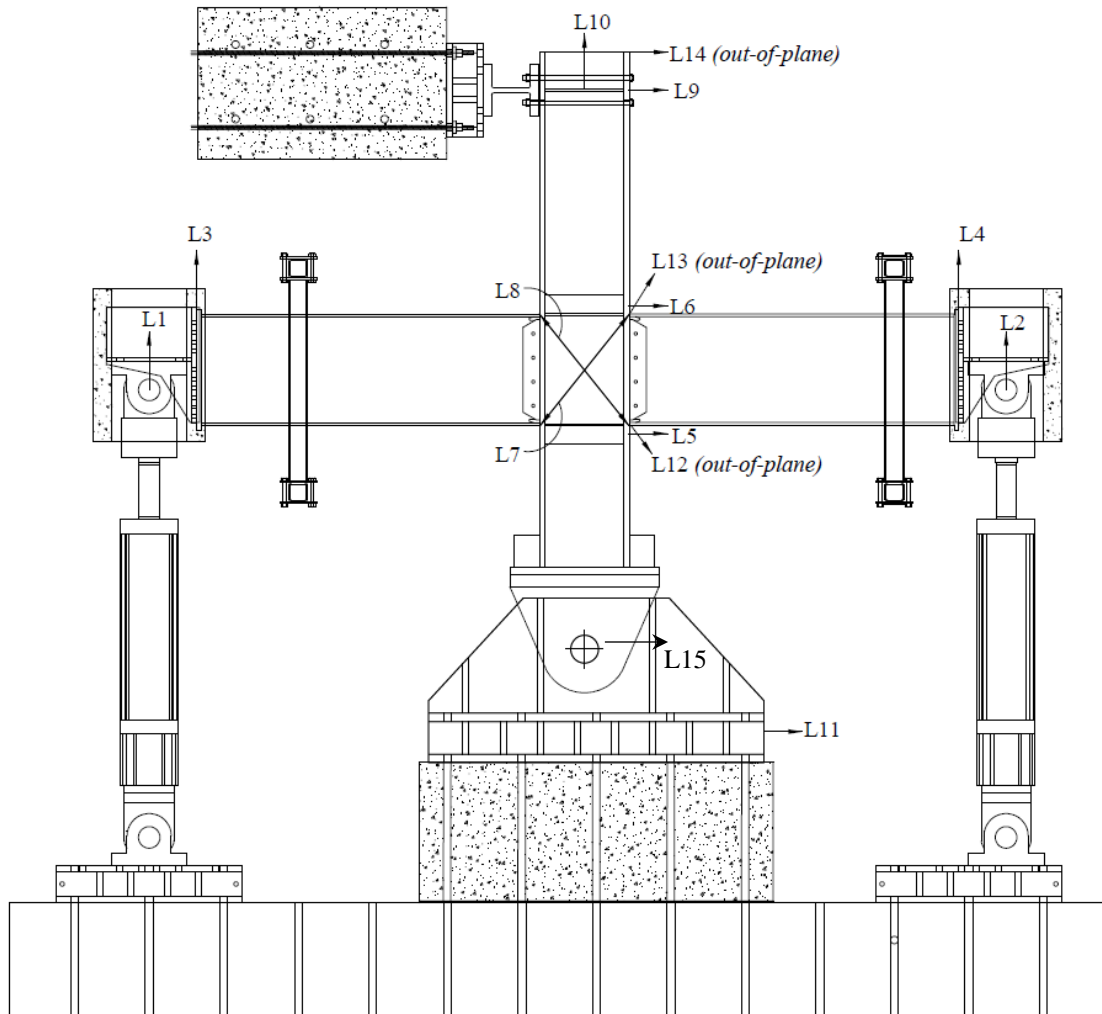


Figure 3.18 Interior Moment Connection (Specimens W1 to W4) Transducer Layout

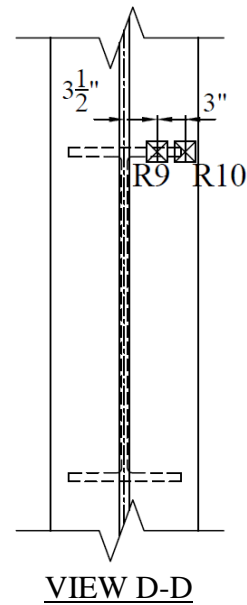
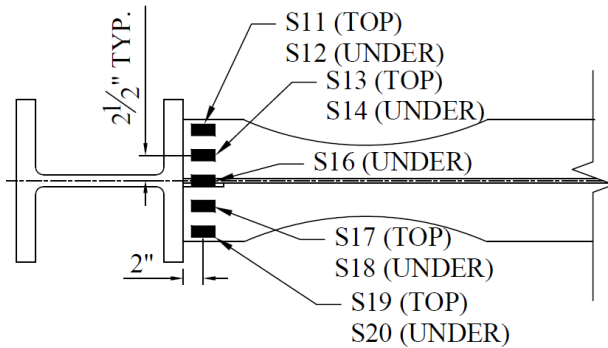
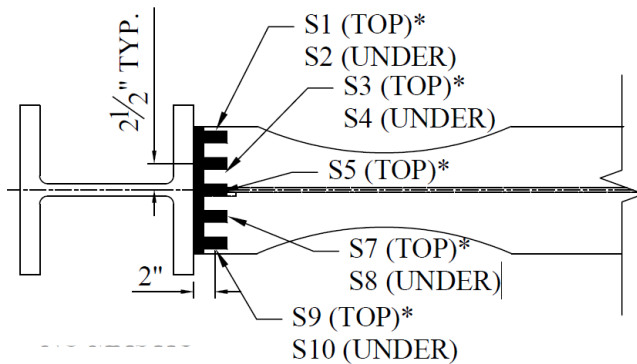
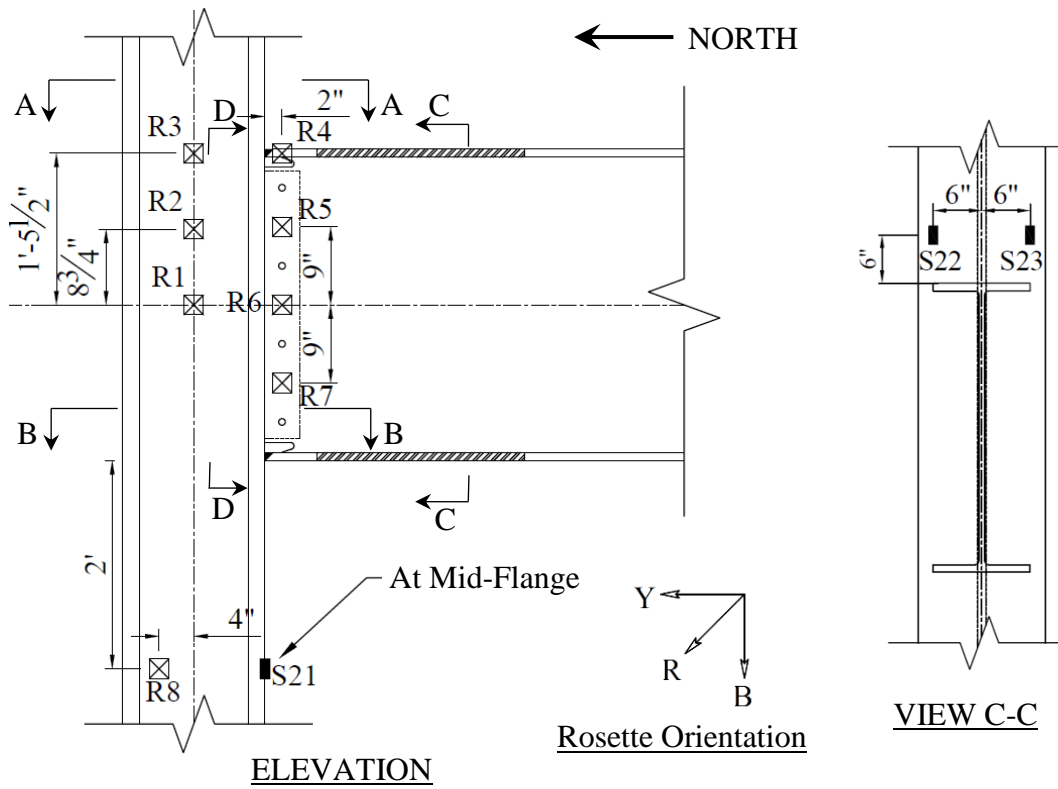


Figure 3.19 Specimen C3: Instrumentation

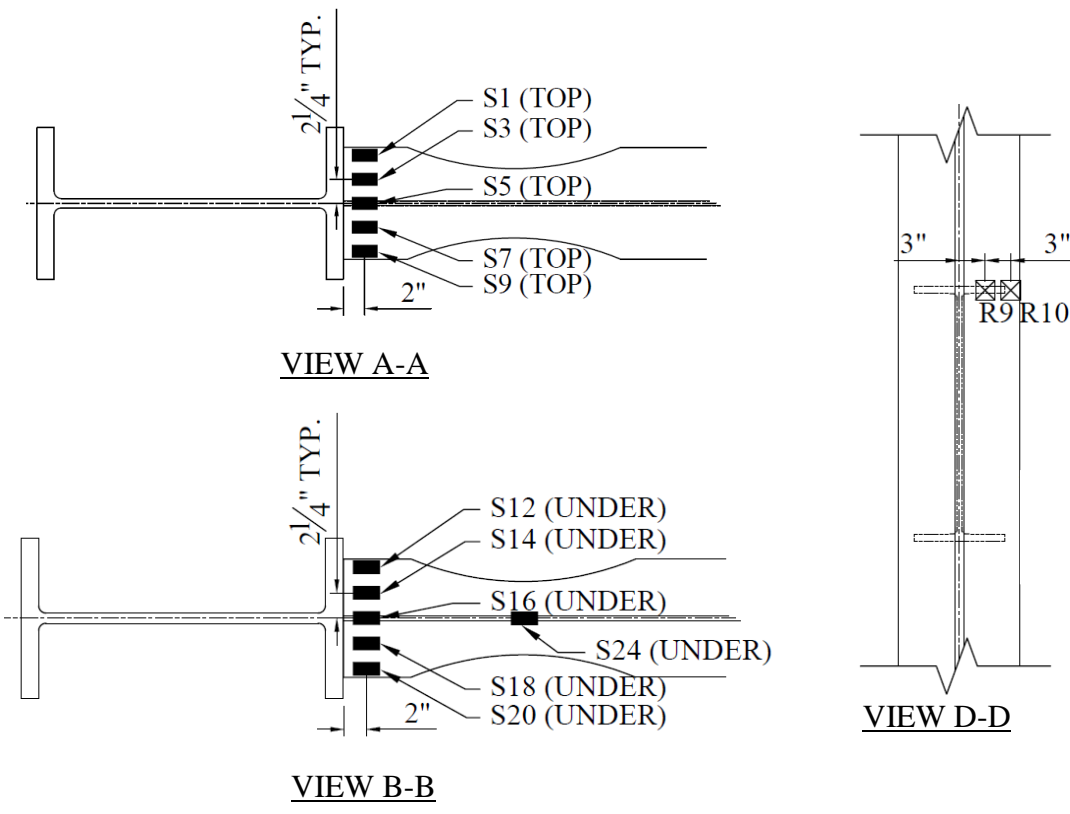
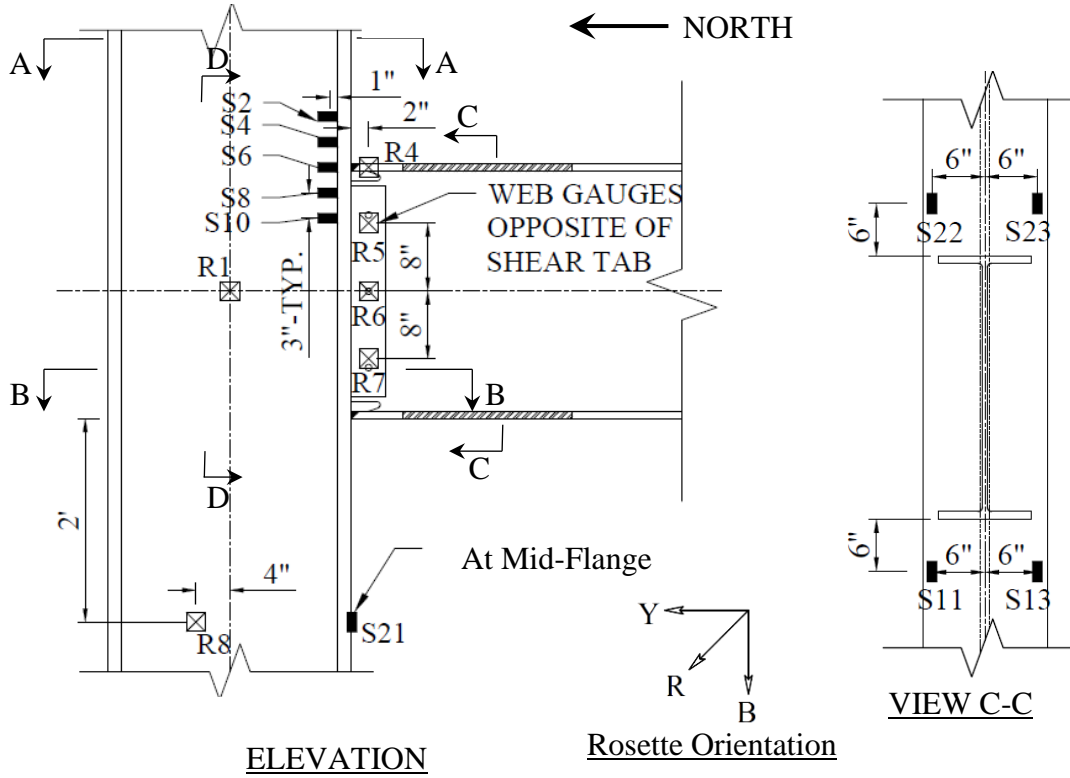


Figure 3.20 Specimen C4: Instrumentation

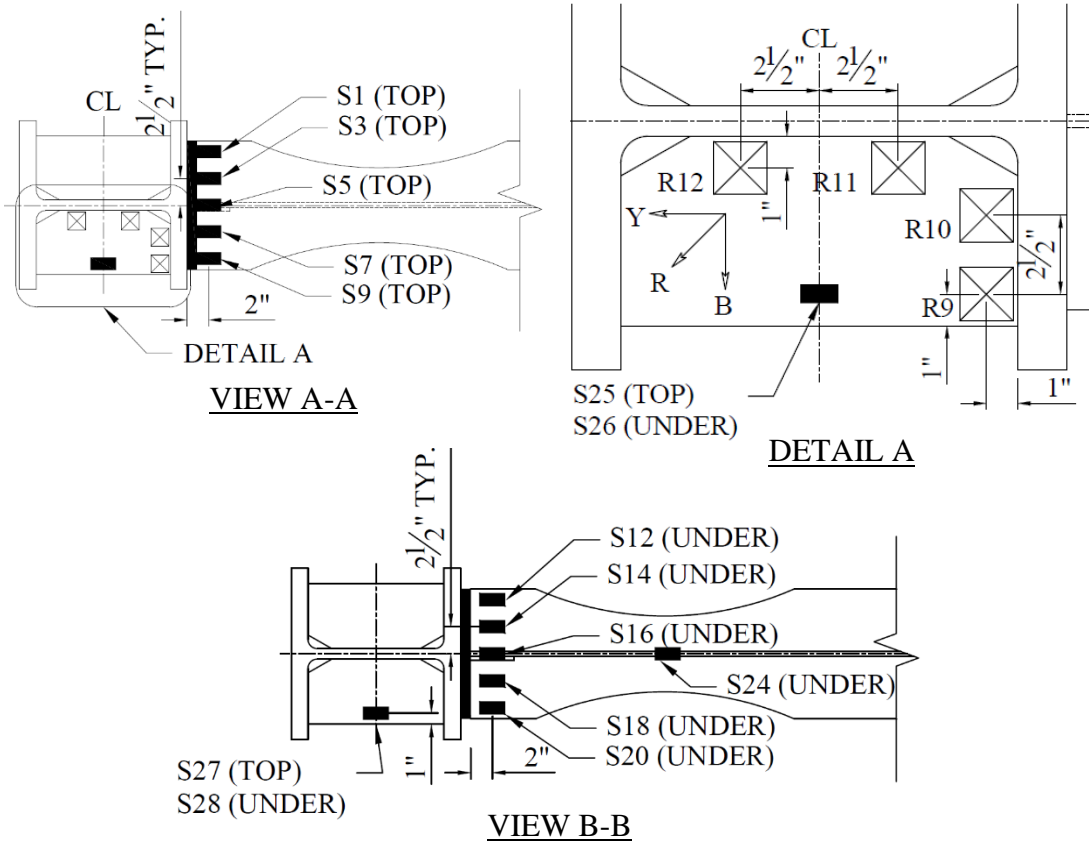
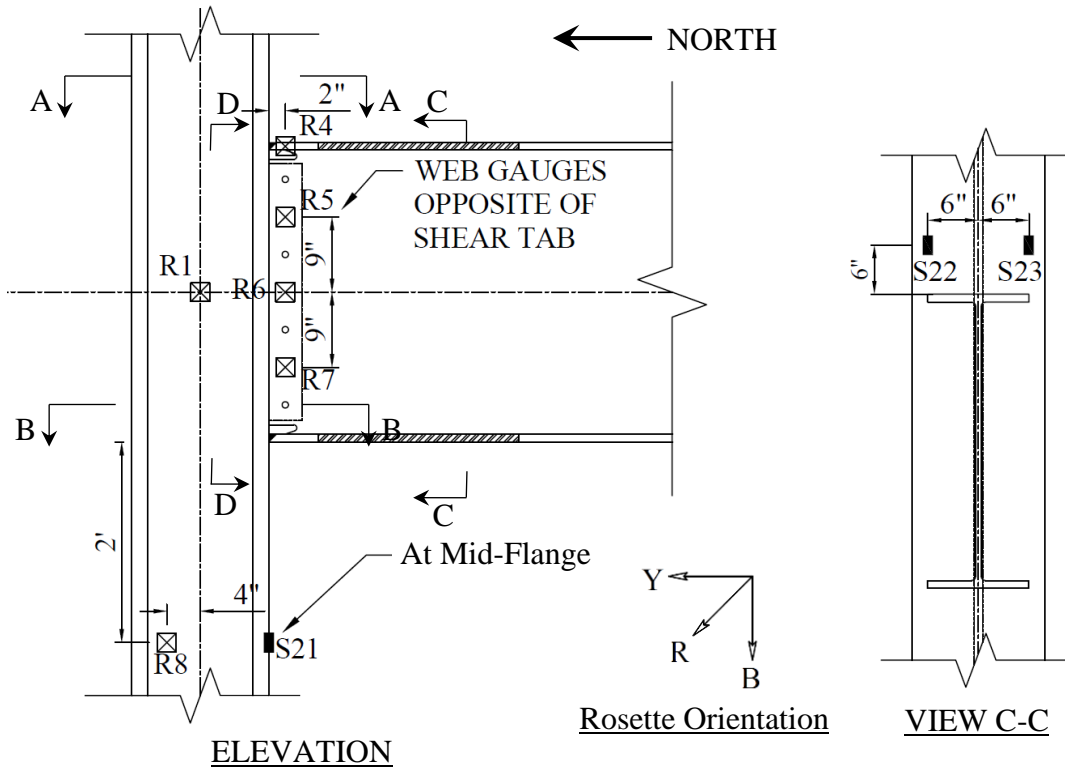


Figure 3.21 Specimen C5: Instrumentation

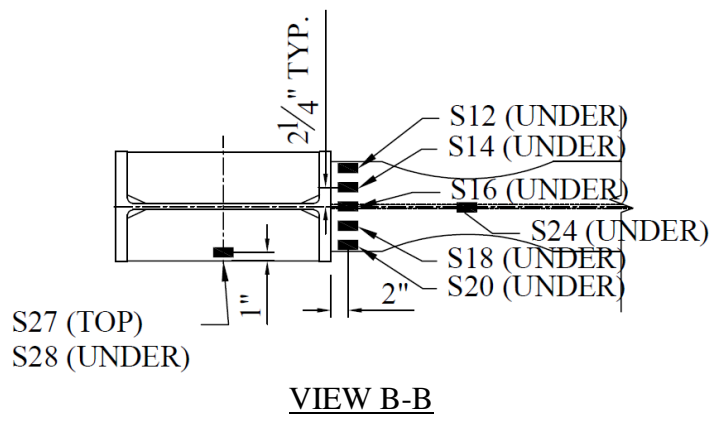
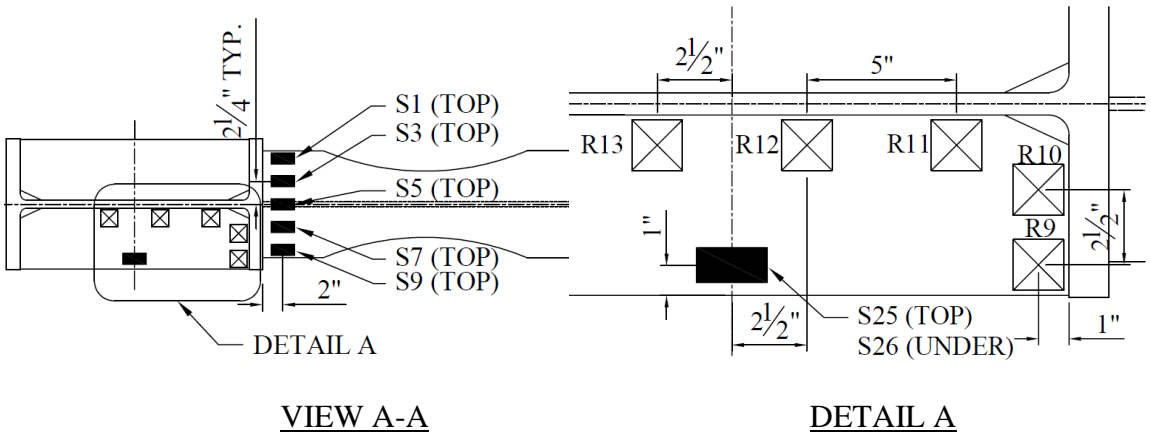
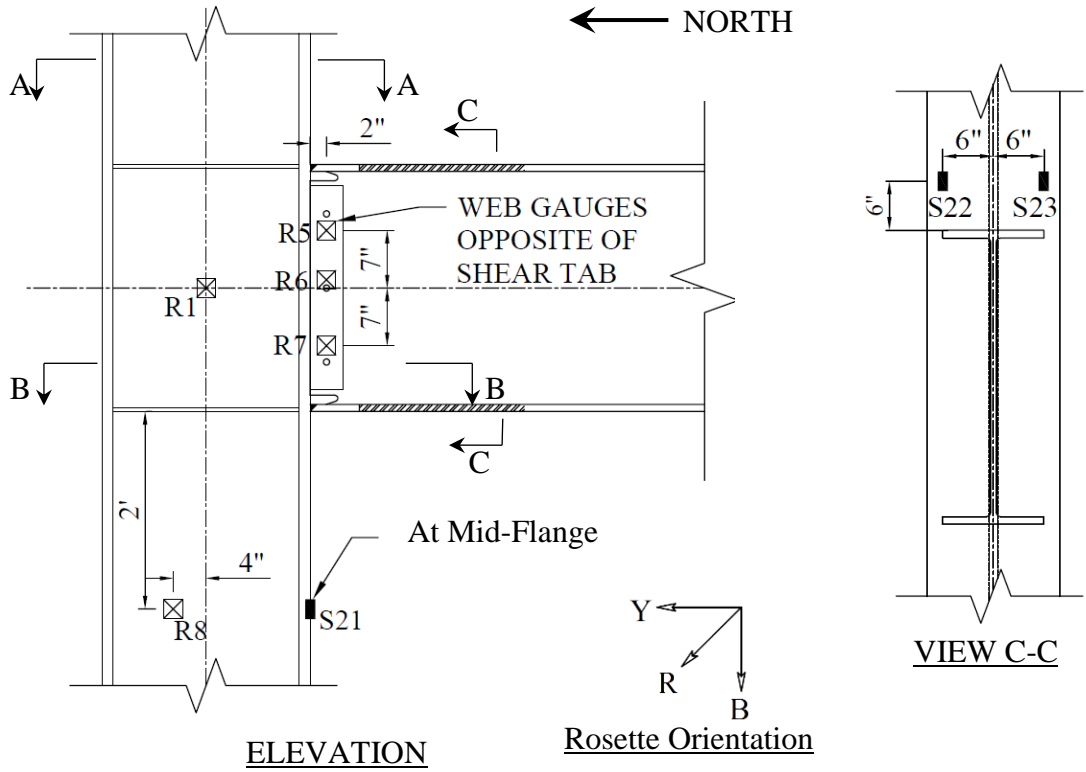


Figure 3.22 Specimen C6: Instrumentation

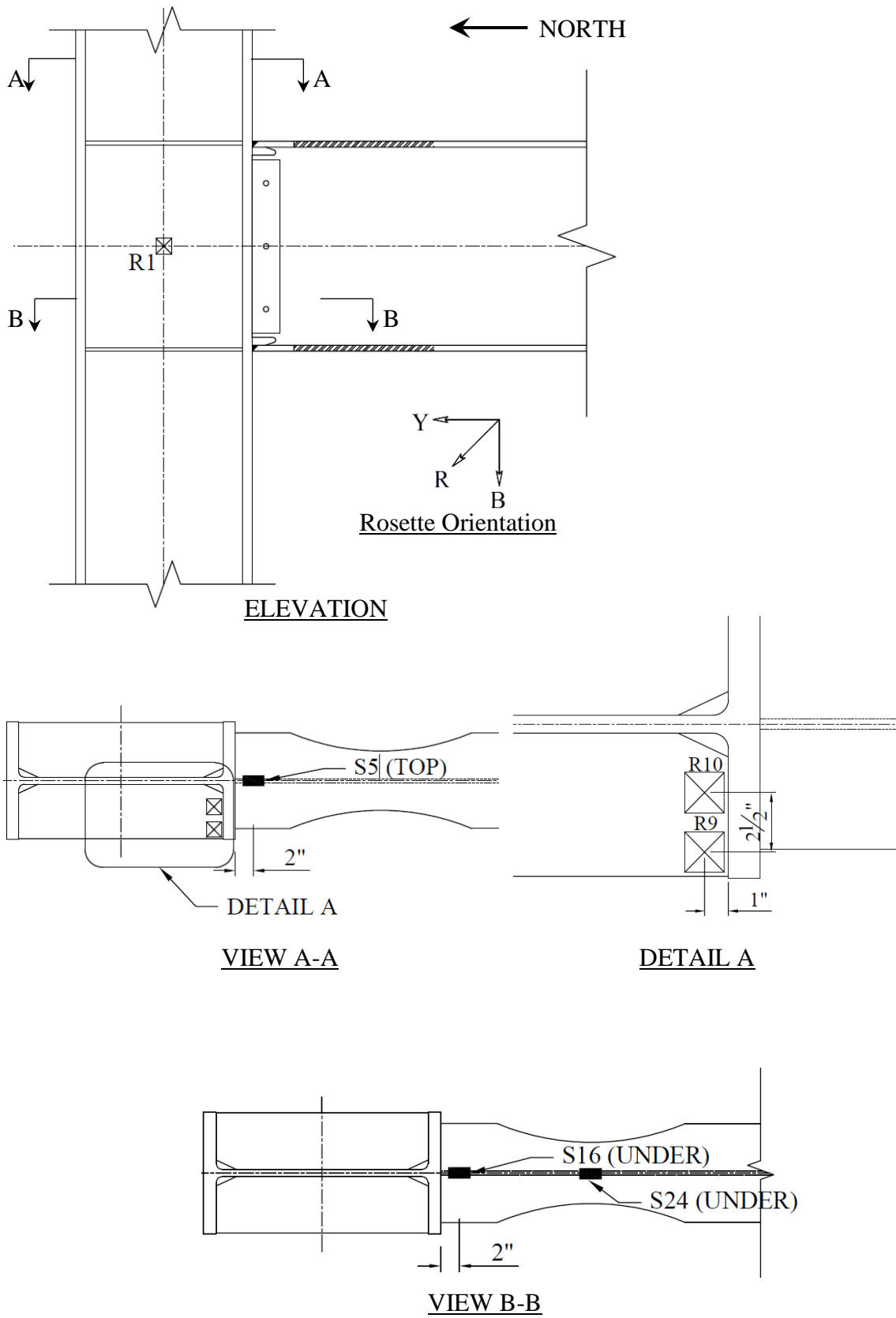


Figure 3.23 Specimen C6-G: Instrumentation

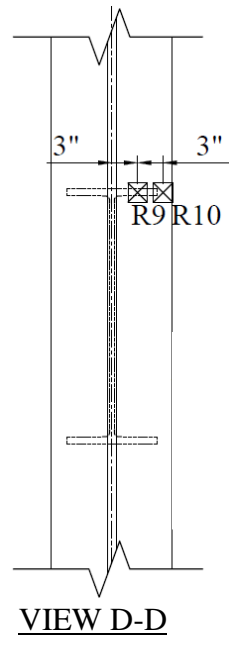
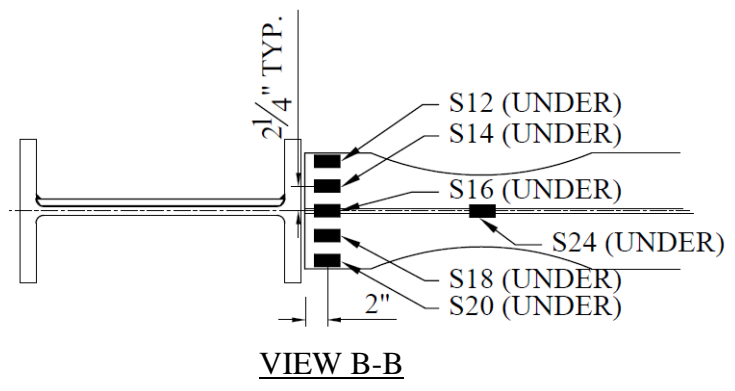
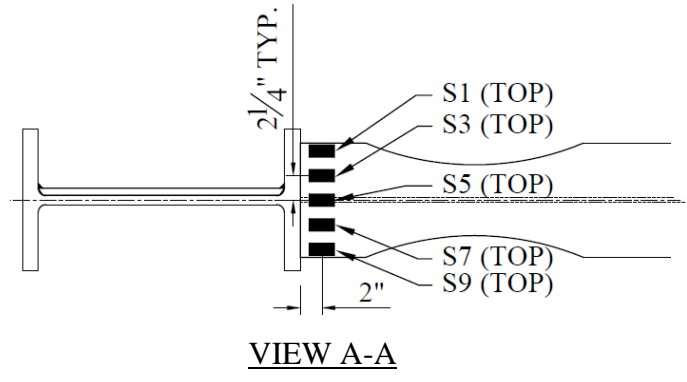
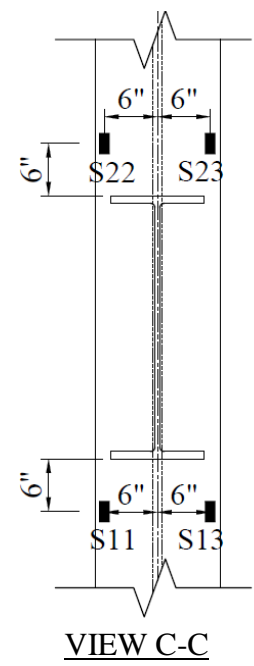
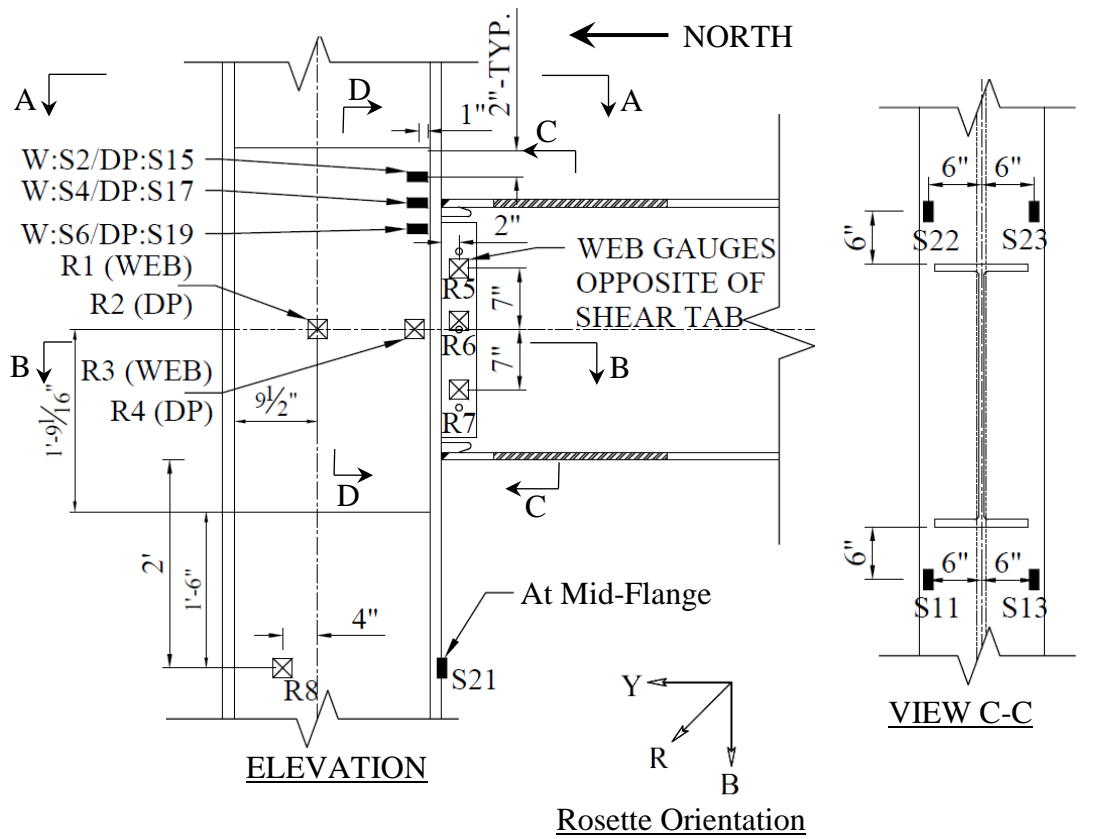


Figure 3.24 Specimen C7: Instrumentation

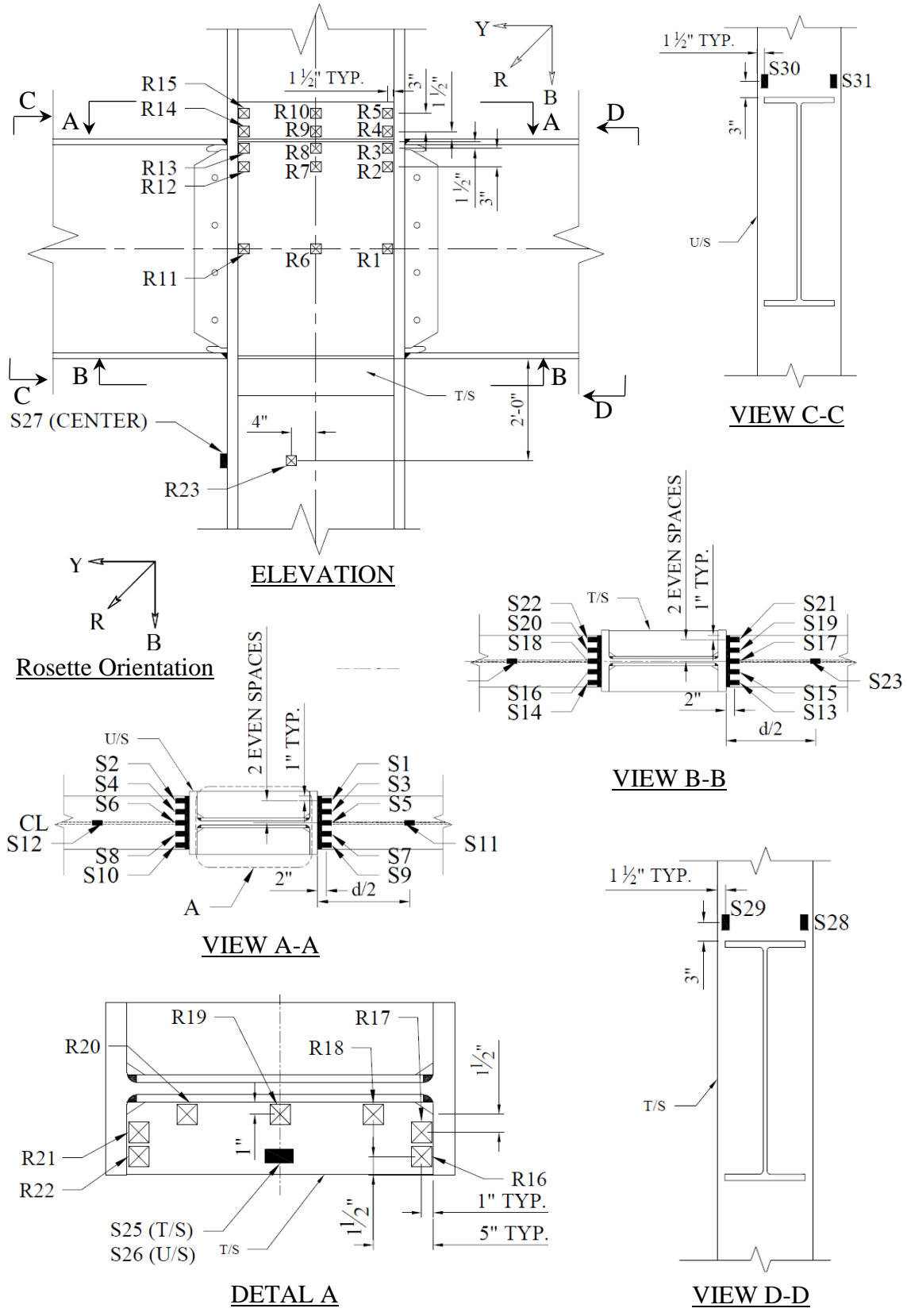


Figure 3.25 Interior Frame (Specimen W1 to W4): Instrumentation

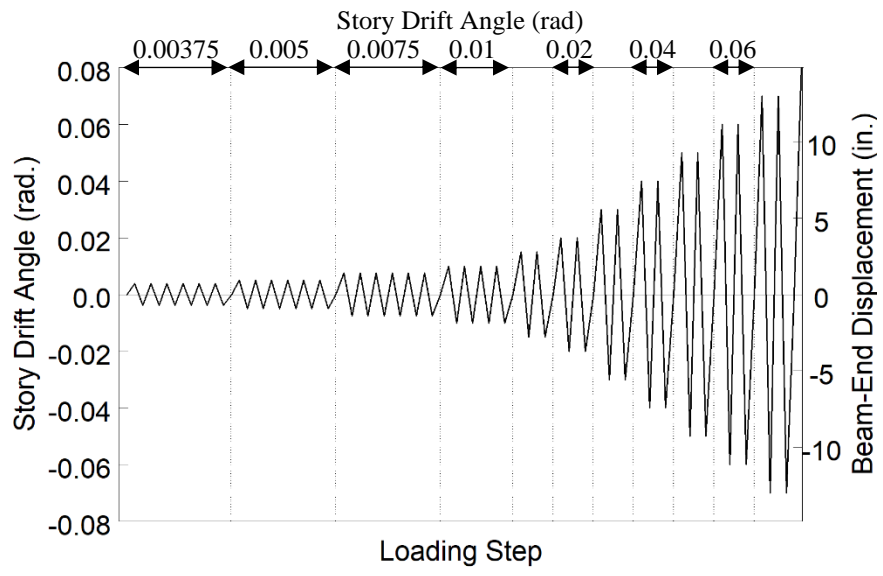


Figure 3.26 AISC Loading Protocol

4 TEST RESULTS

4.1 General

This section contains the observed and recorded response for the Phase 1 and 2 specimens. during the imposed AISC Loading protocol.

4.2 Specimen C3

4.2.1 General

Specimen C3 was designed to challenge the Lehigh Criterion. This was the only requirement of AISC 341 (2016) that would necessitate a continuity plate in this specimen; the flange force computed from AISC 358 (2016) for this connection does not exceed any column limit state of AISC 360 §J10 (2016). The specimen also closely matches Specimen C2 tested during the verification of the flexibility method, except that Specimen C2 used a 5/8-in. continuity plate. The panel zone of Specimen C3 has a high DCR of 0.94. Figure 4.1 shows the specimen before testing. The specimen failed by a complete fracture of the beam top flange CJP weld during the second cycle of 0.05 rad drift.

4.2.2 Observed Performance

The observed response for Specimen C3 is described below.

- Figure 4.2 shows the east side of the specimen at the peak excursions during the later cycles of the loading protocol. The specimen met the AISC acceptance criteria by completing one complete cycle at 0.04 rad drift while the flexural strength at the column face did not degrade below 80% of the beam nominal flexural strength. It was observed that beam web buckling initiated during the first cycle of 0.04 rad drift. Flange local buckling initiated at the beam bottom flange within the RBS cut during the second cycle of 0.04 rad drift. By 0.05 rad drift flange local buckling was observed in both flanges.
- Figure 4.3 shows ductile tearing of the beam top flange CJP weld that was first observed during the 2nd negative excursion of 0.03 rad drift. Minor growth of this fracture occurred during the 0.04 rad cycles occurred during testing.
- Figure 4.4 shows the progression of web buckling. It was observed that the buckling orientation was mirrored in the web between positive and negative excursions.

- Figure 4.5(a) shows an incomplete beam top flange CJP weld fracture, that occurred during the first negative excursion to 0.05 rad extending from the west side of the flange to 2.5 in. beyond the center of the flange. Complete fracture of the CJP weld occurred at -0.013 rad drift of the second cycle of 0.05 rad drift. This shear type fracture originates at a toe of the prominent weld pass against the column and propagates through the flange at a 35-degree angle through the base metal. At the flange tips the fracture takes on a cup and cone with interlocking shear lips through the weld and base metal of the beam. The asymmetry in the fracture pattern was likely due to beam lateral-torsional buckling.
- Figure 4.6 shows the connection after testing. The top flange CJP weld fractured at -0.013 rad of the second cycle of 0.05 rad drift. Tearing of the web through the erection bolts occurred during continued negative excursion. Figure 4.7 shows the beam lateral-torsional buckling at the end of testing. The buckling was most pronounced in the unbraced bottom flange of the beam.
- Figure 4.8 shows the beam top flange CJP weld fracture after testing. The lateral-torsional buckling has produced a latent twist to the beam. A ductile shear fracture through the weld metal was observed at the center of the flange. A small fracture exists perpendicular to the beam at the termination of this fracture at the center of the flange. The ends of the beam flange fractured as a typical tension fracture with interlocking shear lips.

4.2.3 Recorded Response

4.2.3.1 Global Response

- Figure 4.9 shows the recorded displacement response of the beam tip measured with transducer L1. A hairline crack at the centerline of the beam top flange CJP weld was observed at the first negative excursion of 0.03 rad drift. The beam top flange CJP weld experienced an incomplete fracture at -0.029 rad of the first negative excursion of 0.05 rad drift. The beam top flange continued to tear in a ductile manner until the peak excursion was reached. At -0.015 rad drift during the second negative excursion of 0.05 rad drift the remaining portion of the beam top flange CJP weld fractured.

Continued excursion saw tearing of the web which originated at the radius of the weld access hole and propagated through the first two bolt holes in the shear tab.

- Figure 4.10 shows the load-displacement response of the beam.
- Figure 4.11 shows the computed moment at the column face (M_f) versus the story drift angle. Two horizontal axes at 80% of the nominal plastic moment (M_{pn}) of the beam section are also added. In addition, two vertical axes at ± 0.04 rad story drift show the drift required for SMF connections per AISC 341. It was observed that the beam developed its nominal plastic bending moment. If the moment is computed at the plastic hinge location and compared to the expected plastic moment, then the peak connection strength factor (C_{pr}) is 1.13.
- Figure 4.12 shows the plastic response of the specimen. The plastic response is computed using the procedure outlined in Section 3.7. The computed elastic stiffness of the specimen was determined to be 57.9 kips/in.
- Figure 4.13 shows the panel zone deformation determined from transducers L3 and L4. It was observed that modest panel zone yielding occurred.
- Figure 4.14 shows the column rotation determined from transducers L5 and L6 after removing the rigid-body motion due to panel zone deformation. It was observed that negligible hysteretic behavior occurred.
- Figure 4.15 shows the dissipated energy of Specimen C3. The dissipated energy is obtained by integrating the load-displacement response of each constituent deformation. Dotted vertical lines on the graph demonstrate the completion of each group of cycles, and the dashed red vertical line shows the completion of the first cycle of 0.04 rad in the AISC loading. An additional vertical axis normalizes the hysteretic energy by the nominal plastic moment of the beam to determine the cumulative plastic rotation. It is observed that the completion of the first drift cycle of 0.04 rad (the requirement for SMF connections per AISC 341) occurs after 530 kip-ft of energy has been dissipated. The connection does not degrade below $0.8M_{pn}$ until 975 kip-ft of energy has been dissipated. Therefore, only 54% of the energy dissipation capacity was utilized after the completion of the 0.04 rad drift requirement. It is observed that most (71%) of the energy dissipation capacity occurred in the beam.

4.2.3.2 *Local Response*

- Figure 3.19 and Figure 4.17 show the strain gauge response from the extreme fiber of the beam top and beam bottom flange during the testing. At 0.03 rad drift the strain pattern is nearly uniform, while higher drifts show moderate weak axis flexure due to the lateral-torsional buckling of the beam. The top flange results are influenced by the weld tearing which initiates from the center of the top flange. As the weld tears, the tension force concentrates near the peripheral edges of the flange where the weld is still intact. As a result, the gauge at the center of the top flange remains in compression during the peak tension excursion to 0.05 rad drift.
- Figure 4.18 shows the strain gauge response of the column flange which affixes the beam. It is observed that the column flange did not yield, but significant deviation from a 1:1 response demonstrates the torsional demand imposed on the column due to the lateral-torsional buckling of the beam.
- Figure 4.19 shows the shear strain response of the panel zone. The center of the panel demonstrates the most strain with a minor decrease in shear strain magnitude at an intermediate gauge. The outermost gauge, placed in line with the beam flange, shows a significant reduction in shear strain. Significant panel zone yielding was expected with a DCR of 0.94 using the post-yielding panel zone strength permitted in AISC 341.
- Figure 4.20 shows the transverse flexural strain of the column flange. Peak strains on the order of $4\epsilon_y$ demonstrate significant flange yielding behind the beam flange. The strain is significantly higher during positive excursions when the top flange is in compression due to the weak axis bending of the beam.

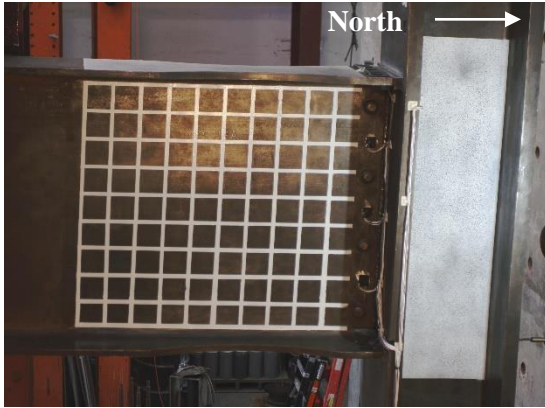


(a) West Side

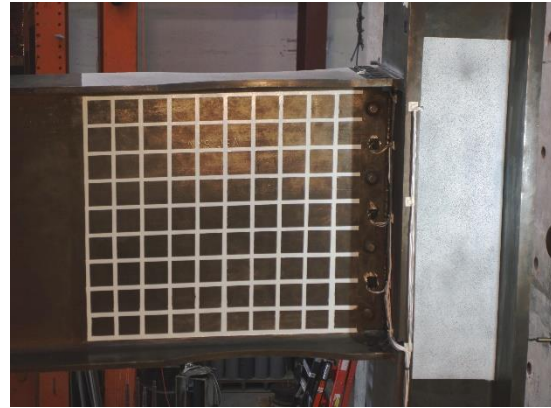


(b) East Side

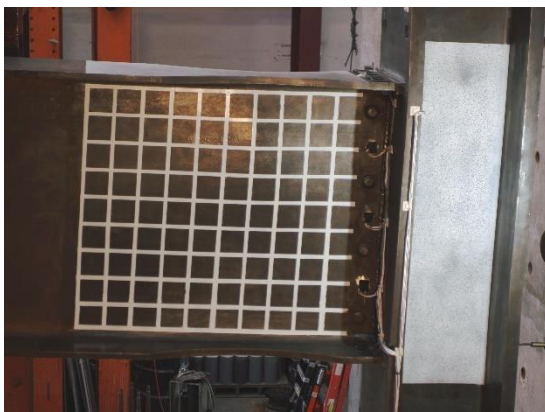
Figure 4.1 Specimen C3: Specimen before Testing



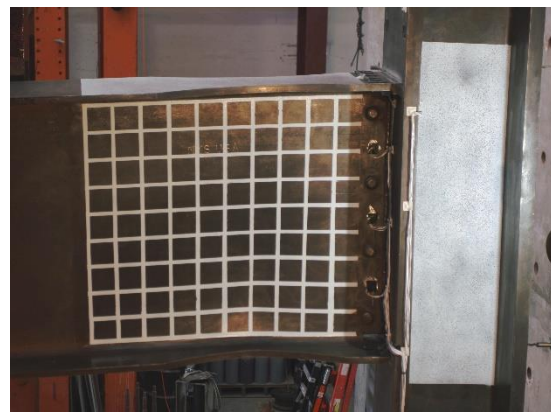
(a) +0.03 rad (2nd Cycle)



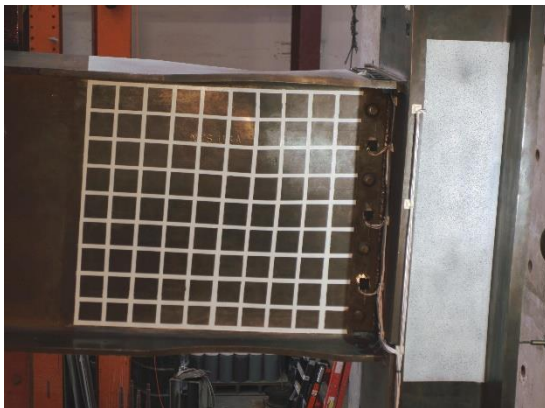
(b) -0.03 rad (2nd Cycle)



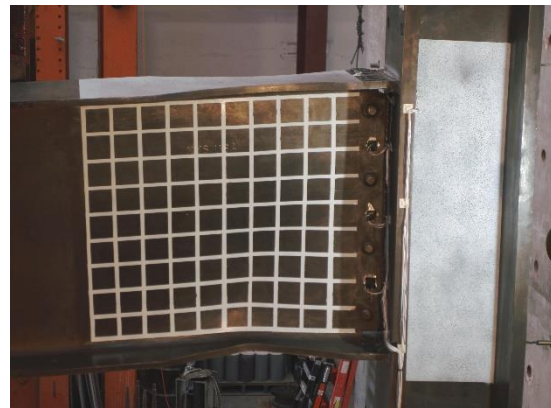
(c) +0.04 rad (2nd Cycle)



(d) -0.04 rad (2nd Cycle)



(e) +0.05 rad (1st Cycle)

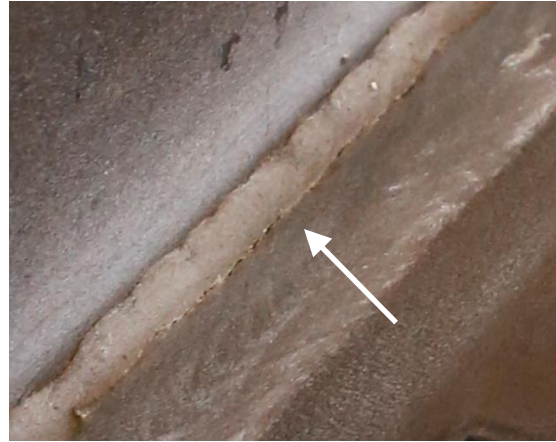


(f) -0.05 rad (1st Cycle)

Figure 4.2 Specimen C3: East Side of Connection



(a) Overview



(b) Tearing at -0.03 rad (2nd Cycle)

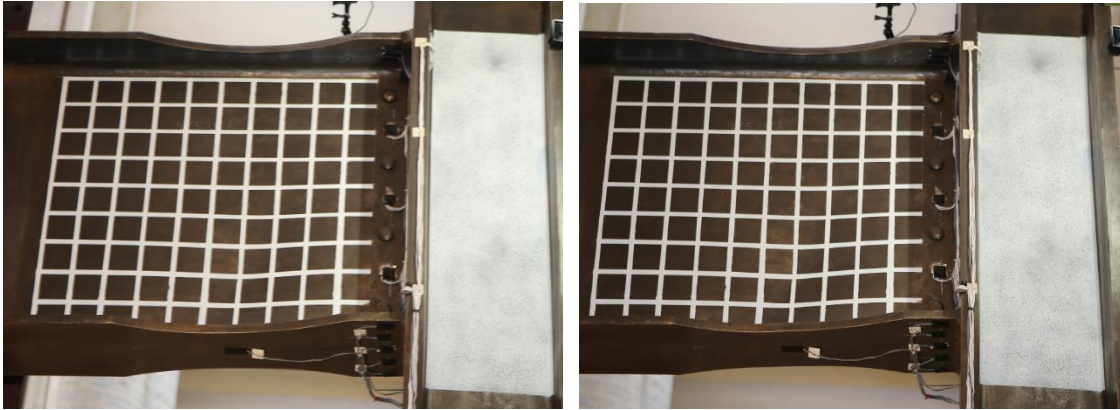


(c) -0.04 rad (1st Cycle)



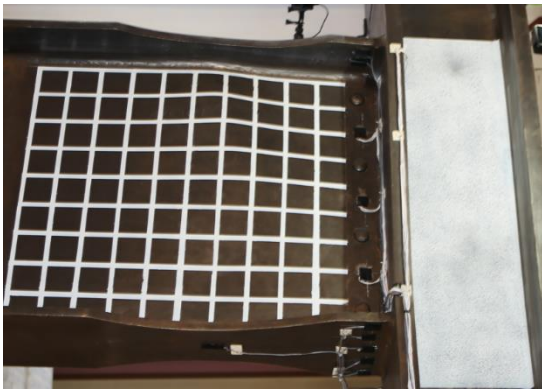
(d) -0.04 rad (2nd Cycle)

Figure 4.3 Specimen C3: Beam Top Flange Weld Tearing

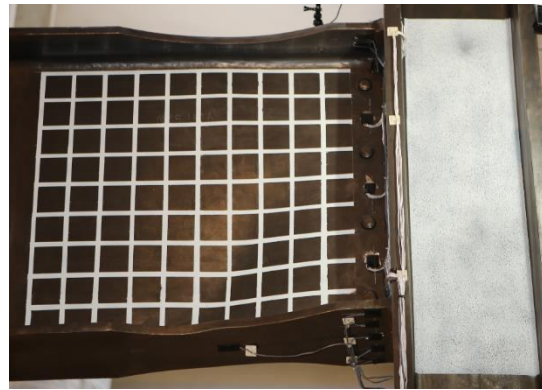


(a) -0.04 rad (1st Cycle)

(b) -0.04 rad (2nd Cycle)



(c) +0.05 rad (1st Cycle)



(d) -0.05 rad (1st Cycle)

Figure 4.4 Specimen C3: Beam Web Buckling

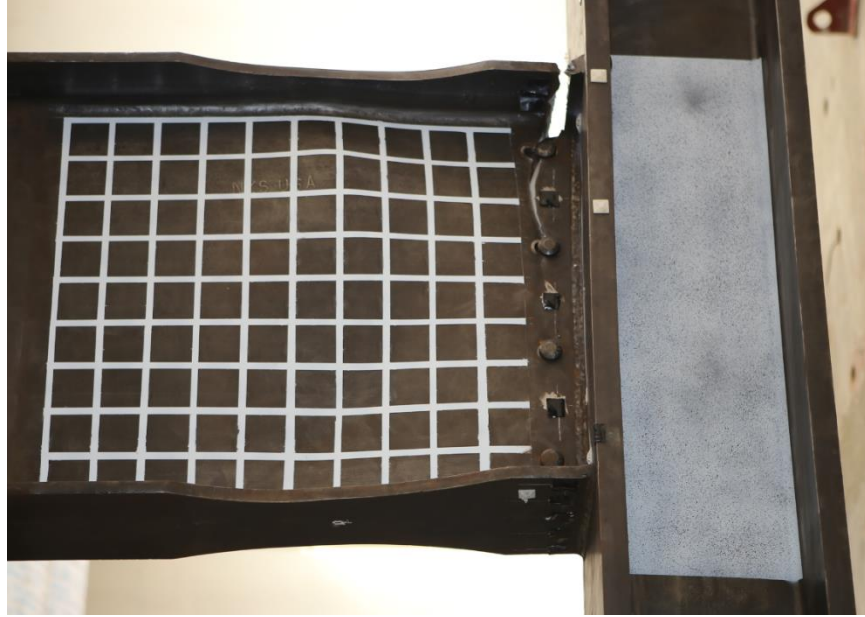


(a) -0.05 rad (1st Cycle)



(b) -0.013 rad (during 2nd Cycle at 0.05 rad Drift)

Figure 4.5 Specimen C3: Beam Top Flange Fracture



(a) East Side



(b) West Side

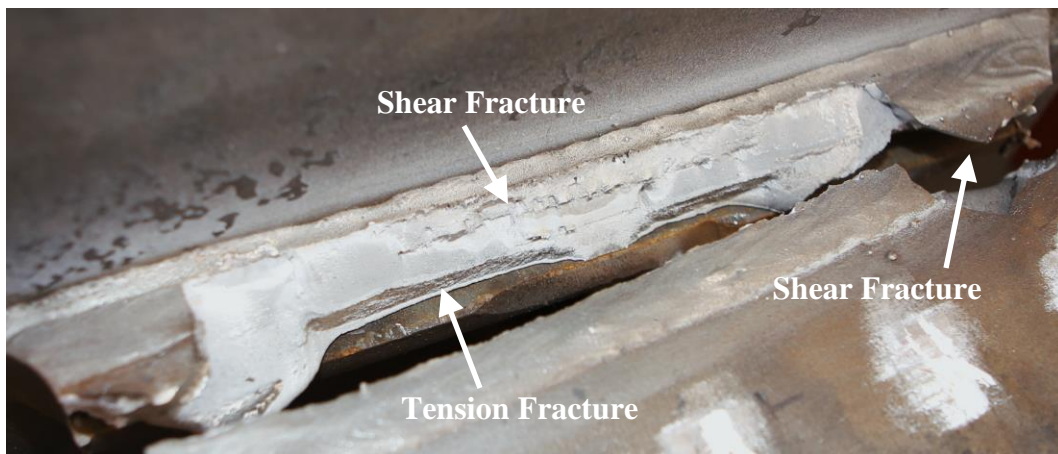
Figure 4.6 Specimen C3: Connection at End of Test



Figure 4.7 Specimen C3: Beam Lateral-Torsional Buckling (End of Test)



(a) Overview



(b) Fracture Surface

Figure 4.8 Specimen C3: Beam Top Flange CJP Weld Fracture (End of Test)

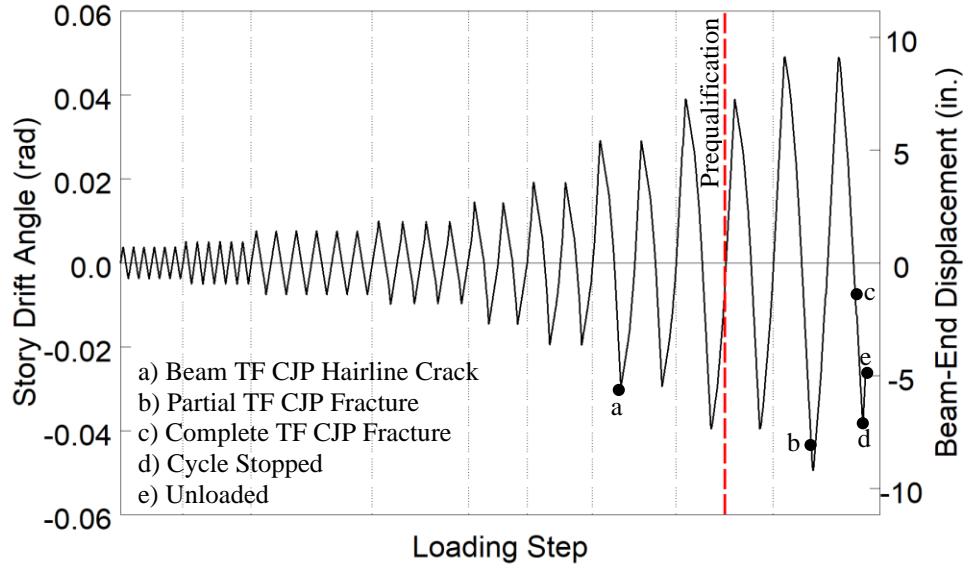


Figure 4.9 Specimen C3: Recorded Loading Sequence

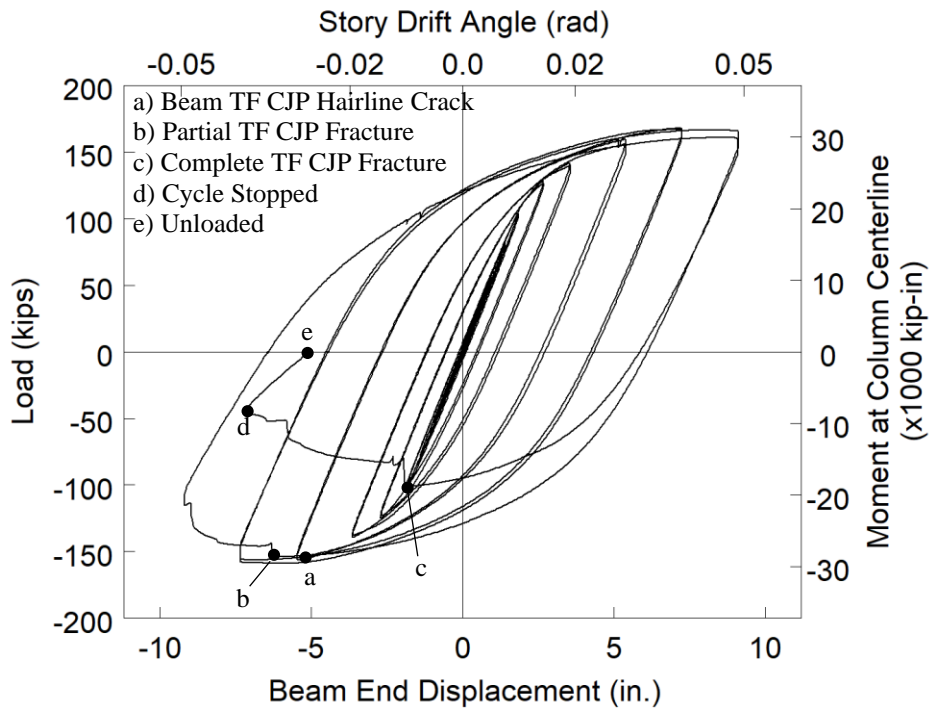


Figure 4.10 Specimen C3: Applied Load versus Beam End Displacement Response

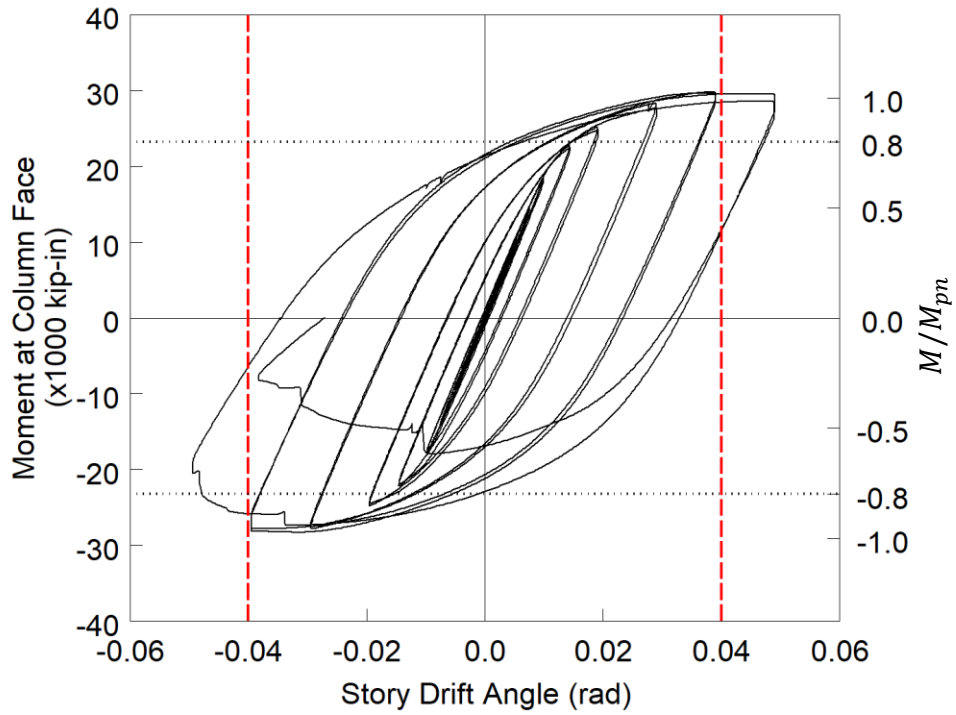


Figure 4.11 Specimen C3: Moment at Column Face versus Story Drift Response

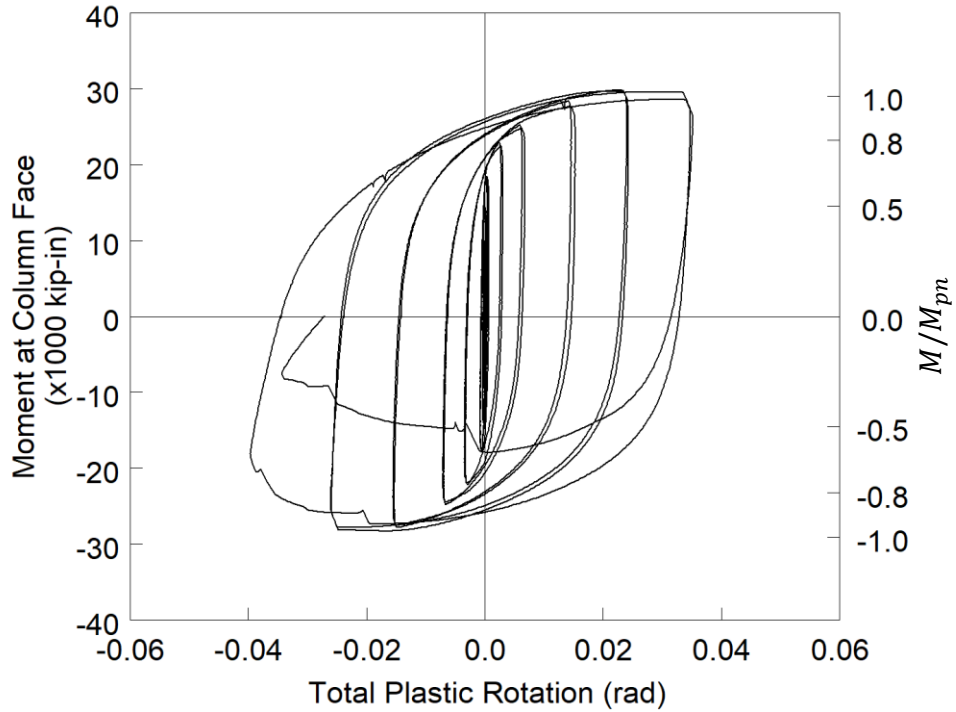


Figure 4.12 Specimen C3: Moment at Column Face versus Plastic Rotation

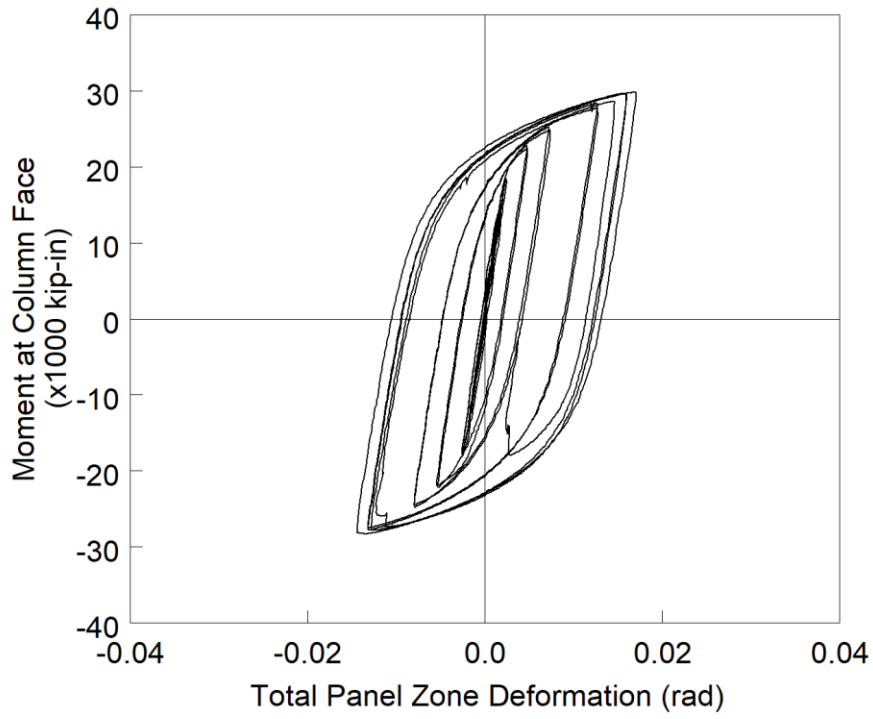


Figure 4.13 Specimen C3: Panel Zone Shear Deformation

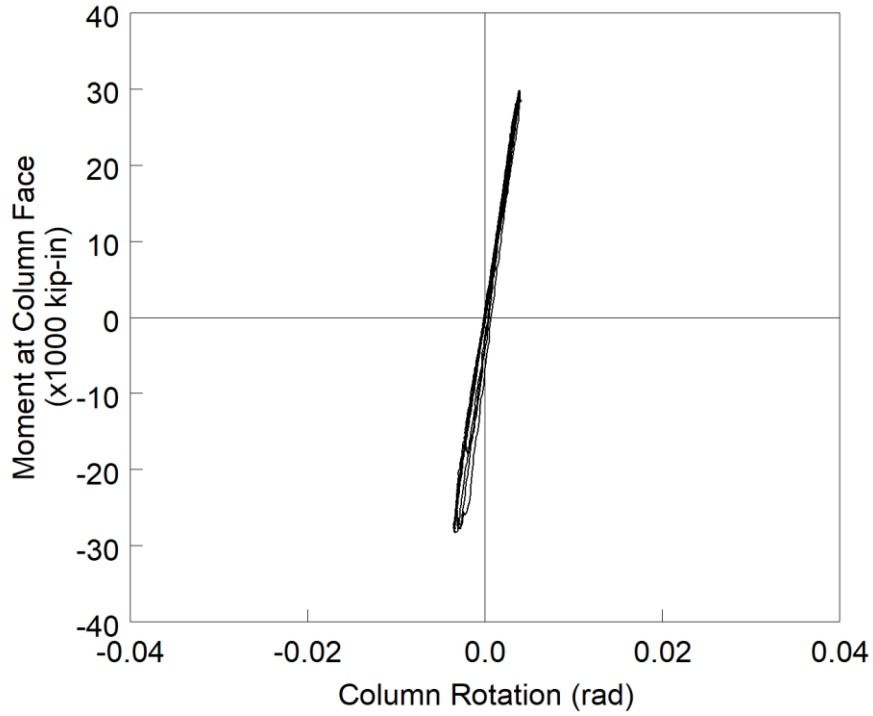


Figure 4.14 Specimen C3: Column Rotation

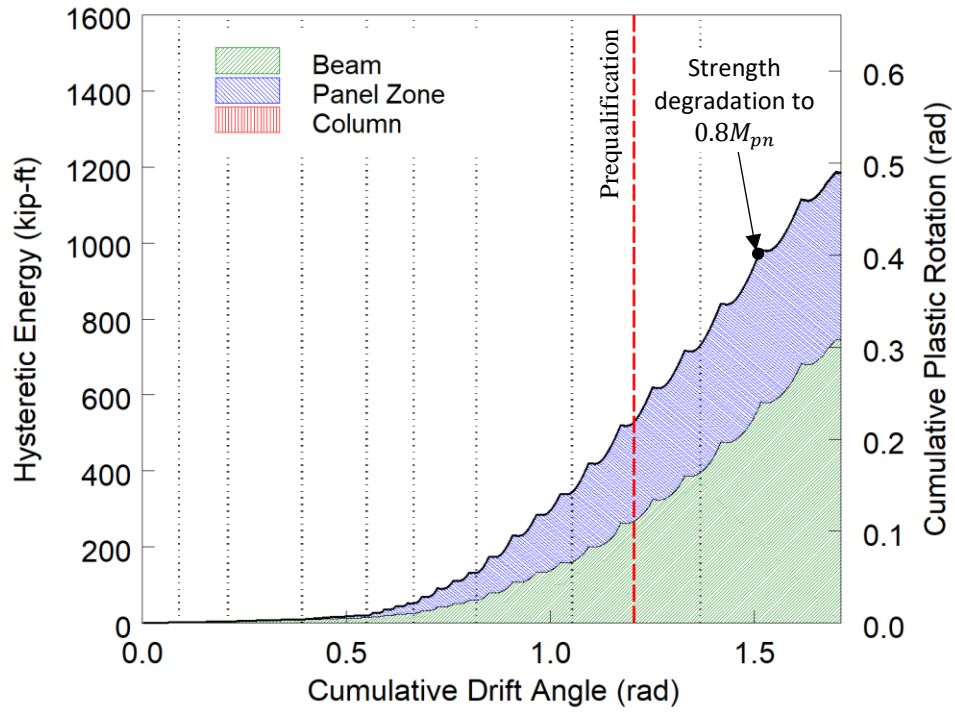
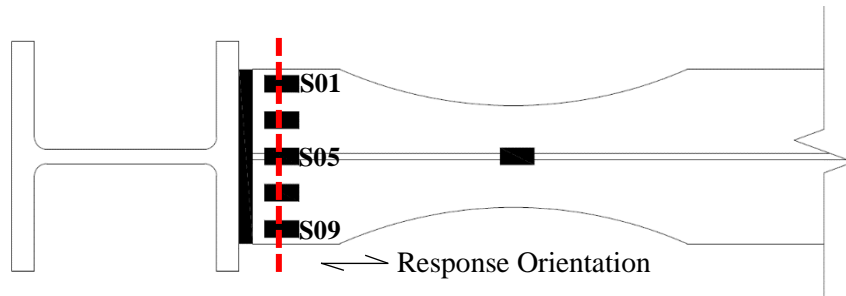
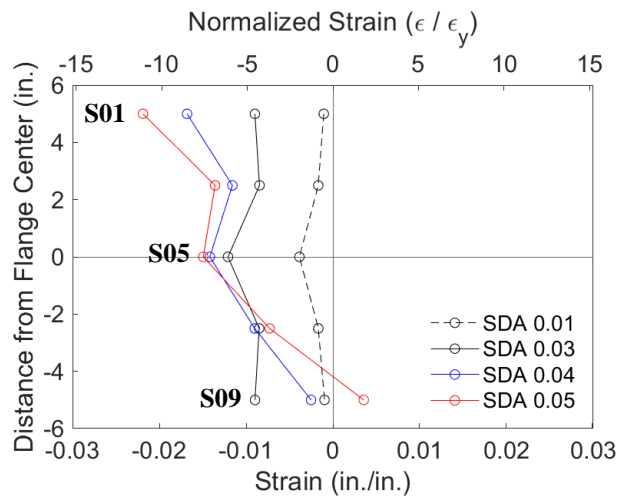


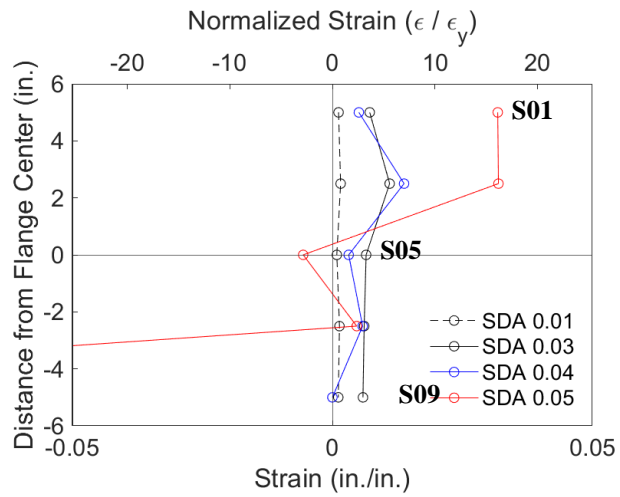
Figure 4.15 Specimen C3: Energy Dissipation



(a) Section

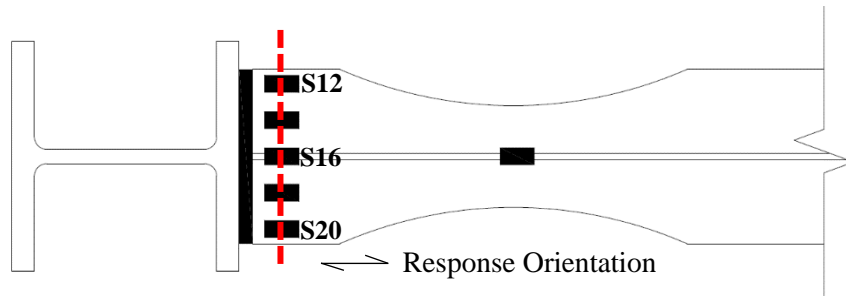


(b) Positive Drift

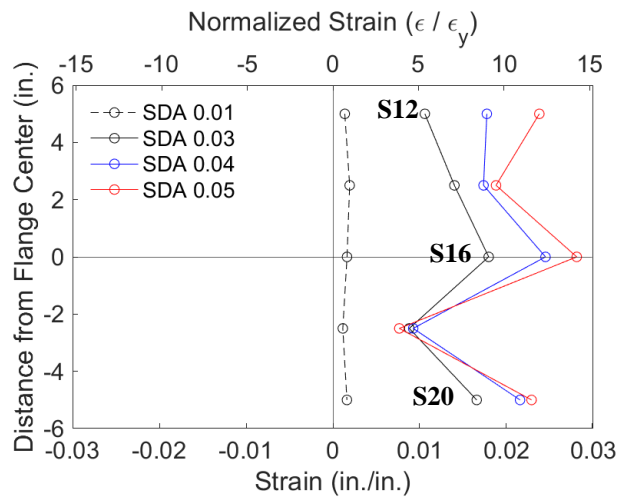


(c) Negative Drift

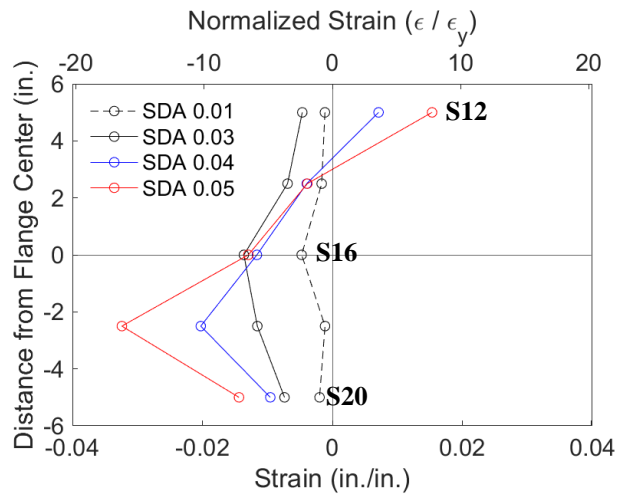
Figure 4.16 Specimen C3: Topside of Beam Top Flange Strain Profile



(a) Section

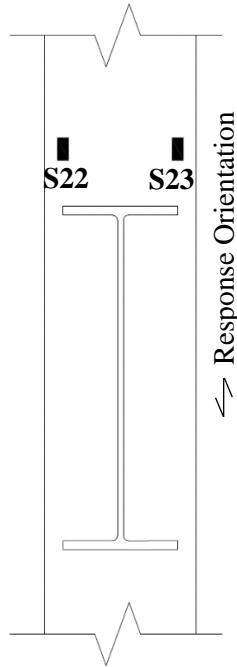


(b) Positive Drift

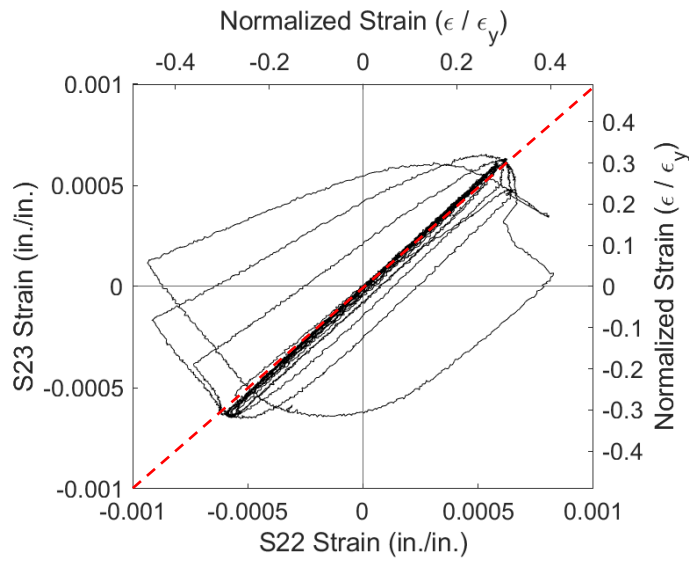


(c) Negative Drift

Figure 4.17 Specimen C3: Underside of Beam Bottom Flange Strain Profile

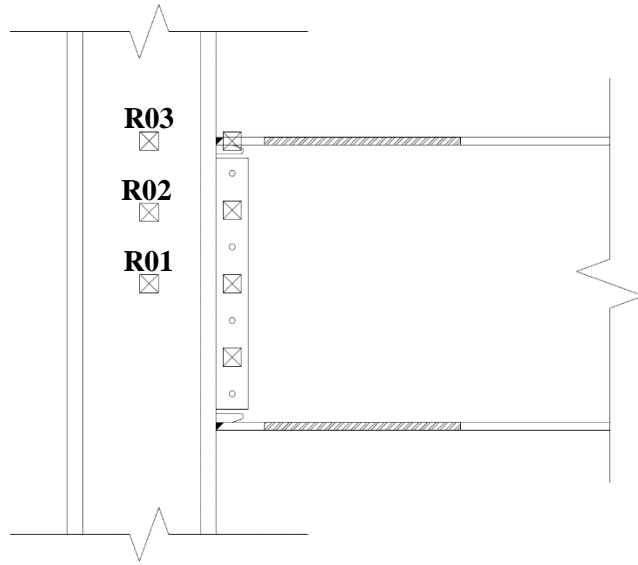


(a) Gauge Layout

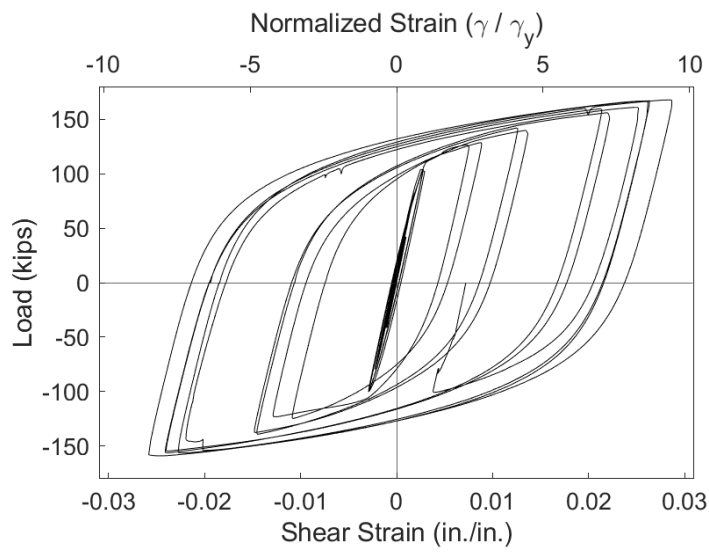


(b) Response

Figure 4.18 Specimen C3: Column Flange Warping

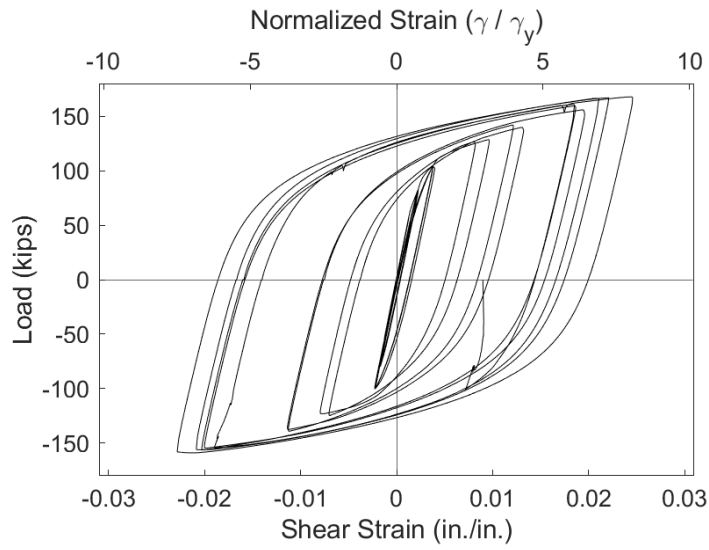


(a) Gauge Layout

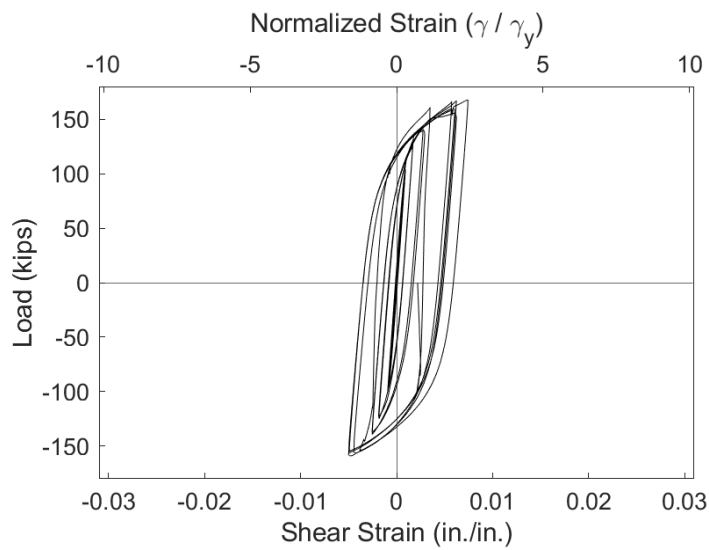


(b) Strain Rosette Gauge R01

Figure 4.19 Specimen C3: Panel Zone Response

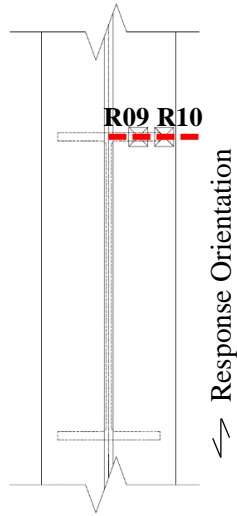


(c) Strain Rosette Gauge R02

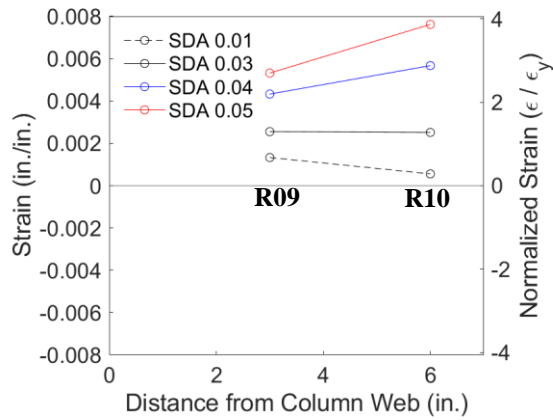


(d) Strain Rosette Gauge R03

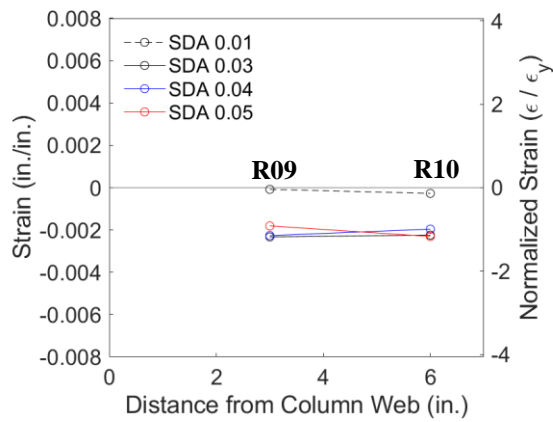
Figure 4.19 Specimen C3: Panel Zone Response (continued)



(a) Section



(b) Positive Drift



(c) Negative Drift

Figure 4.20 Specimen C3: Column Flange Strain Profile

4.3 Specimen C4

4.3.1 General

Specimen C4 was similar to Specimen C3 as it was designed to challenge the Lehigh Criterion. This was the only requirement of AISC 341 (2016) that would necessitate a continuity plate in this specimen; the flange force computed from AISC 358 (2016) for this connection does not exceed any column limit state of AISC 360 §J10 (2016). In contrast to Specimen C3, Specimen C4 uses a deep column to reflect a modern practice in SMFs to control drift. Figure 4.21 shows the specimen before testing. The specimen ultimately failed by low-cycle fatigue of the beam bottom flange in the plastic hinge location during the second cycle of 0.06 rad drift.

4.3.2 Observed Performance

The observed response for Specimen C4 is described below.

- Figure 4.22 shows the east side of the specimen at the peak excursions during the later cycles of the loading protocol. The specimen met the AISC acceptance criteria by completing one complete cycle at 0.04 rad drift while the flexural strength at the column face did not degrade below 80% of the beam nominal flexural strength. Local buckling of the web and flange initiated during the second cycle of 0.03 rad drift. This progressed to result in modest flange local buckling during the 0.04 rad and 0.05 rad drift cycles.
- Beam bottom flange yielding started during the 0.01 rad cycles within the reduced beam section and near the column flange. Figure 4.23 shows the progression of the yielding which concentrates in the reduced beam section. Figure 4.23(c) shows lateral-torsional buckling initiating at the thinnest portion of the reduced beam section. This lateral-torsional buckling was first observed during the 2nd cycle of 0.03 rad drift. Lateral-torsional buckling did not progress significantly beyond this level due to the top and bottom flange lateral restraint just beyond the reduced beam section.
- Beam web yielding was observed inboard of the k-area during the 0.02 rad drift cycles (see Figure 4.24). This was accompanied with observed yielding on the underside of the beam top flange.

- Significant beam top flange yielding was observed during the 0.04 rad drift cycles. Some minor distress was observed at the toe of an unintentional cover weld (see Figure 4.25). This distress did not progress further.
- During the first negative excursion of 0.04 rad drift significant beam flange local buckling was observed (see Figure 4.26). This was accompanied with modest web yielding propagating into the web from the k-area. This yielding occurred at the high double curvature portion of a uniform out-of-plane web buckling (see Figure 4.27).
- During the unloading portion at -0.047 rad after the 1st negative excursion to 0.06 rad the beam bottom flange partially fractured due to load cycle fatigue (see Figure 4.28). This fracture occurred at the apogee of the local buckling as the tension in the flange started to pull the curvature out. It is predicted that the fracture started at the underside of the flange at the most extreme curvature and propagated through. Upon resuming load, the remainder of the beam bottom flange immediately fractured (Figure 4.30). This fracture occurred near the smallest section of the reduced beam. Minor panel zone yielding was observed at the end of test [see Figure 4.30(a)].
- Figure 4.29 shows ductile tearing of the beam top flange similar to the condition of the beam bottom flange prior to fracture. It was observed that significant tearing occurs in the ‘compression’ side of the local buckling during load reversals.
- The complete bottom flange tear was accompanied with a 4-in. propagation into the web (see Figure 4.31). Most of the fracture surface consists of cleavage fracture with shear fracture surfaces at the peripheral edges of the flange.
- Column flange yielding behind the beam flanges, similar to a flange local bending phenomenon, was observed during the 0.05 rad cycles. Figure 4.32 shows the yielding of the column flanges at the end of the test.

4.3.3 Recorded Response

4.3.3.1 Global Response

- Figure 4.33 shows the recorded displacement response of the beam tip measured with transducer L1. A partial beam bottom flange fracture occurred during the unloading portion of the first cycle of 0.06 rad drift. Immediately after resuming loading the remainder of the beam bottom flange fractured.

- Figure 4.34 shows the load-displacement response of the beam.
- Figure 4.35 shows the computed moment at the column face (M_f) versus the story drift angle. Two horizontal axes at 80% of the nominal plastic moment (M_{pn}) of the beam section are also added. In addition, two vertical axes at ± 0.04 rad story drift show the drift required for SMF connections per AISC 341. It is observed that the beam developed 1.2 times its nominal plastic bending moment. If the moment is computed at the plastic hinge location and compared to the expected plastic moment, then the peak connection strength factor (C_{pr}) is 1.23.
- Figure 4.36 shows the plastic response of the specimen. The plastic response is computed using the procedure outlined in Section 3.7. The computed elastic stiffness of the specimen was determined to be 50.6 kips/in.
- Figure 4.37 shows the panel zone deformation determined from transducers L3 and L4. It is observed that negligible panel zone yielding occurred.
- Figure 4.38 shows the column rotation determined from transducers L5 and L6 after removing the rigid-body motion due to panel zone deformation. It is observed that negligible hysteretic behavior occurred.
- Figure 4.39 shows the dissipated energy of Specimen C3. Dotted vertical lines on the graph demonstrate the completion of each group of cycles, and the dashed red vertical line shows the completion of the first cycle of 0.04 rad in the AISC loading. An additional vertical axis normalizes the hysteretic energy by the nominal plastic moment of the beam to determine the cumulative plastic rotation. It is observed that the completion of the first drift cycle of 0.04 rad (the requirement for SMF connections per AISC 341) occurs after 517 kip-ft of energy has been dissipated. The connection does not degrade below $0.8M_{pn}$ until after completing the first positive excursion to 0.06 rad drift dissipating 1,239 kip-ft of energy. Therefore, only 42% of the energy dissipation capacity was utilized after the completion of the 0.04 rad drift requirement. It is observed that all of the energy dissipation capacity occurred in the beam.

4.3.3.2 *Local Response*

- Figure 4.40 and Figure 4.41 show the strain gauge response from the extreme fiber of the beam top and beam bottom flange during the testing. The compression excursions of each flange demonstrate weak axis flexure consistent with the observed deformation.
- Figure 4.42 shows the strain gauge response of the column flange which affixes the beam. It is observed that the column flange did not yield, but significant deviation from a 1:1 response demonstrates the torsional demand imposed on the column due to the lateral-torsional buckling of the beam.
- Figure 4.43 shows the shear strain response of the panel zone. The center of the panel zone achieved yielding levels of shear strain, γ_y , however, hysteretic behavior was not observed. Yielding of the panel zone was not anticipated given the low DCR (0.63) of the panel zone.
- The column web response directly behind the beam flange is shown in Figure 4.44. The observed behavior was close to the expected with yielding level strains extending over a distance of $5k$ as per the WLY limit state. During positive drifts, when the top flange is in compression, the strain distribution is more uniform with strains exceeding ϵ_y by 0.04 rad drift. During negative drifts, when the top flange is in tension, a significantly steeper gradient in the strain response is observed. The peak strain response in either direction is similar. The discrepancy is partially attributed to a complex residual stress pattern in the in the web resulting in a predilection to yielding in compression.
- Figure 4.45 shows the transverse flexural strain of the column flange. Peak strains on the order of $3\epsilon_y$ demonstrate significant yielding of the column flange behind the beam; the DCR of the flange local bending limit state was designed as 0.77.

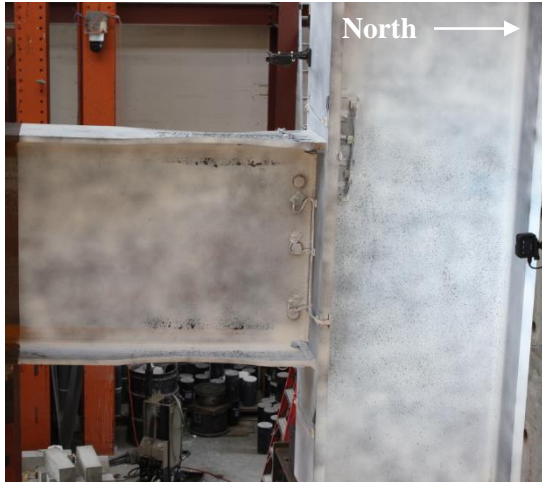


(a) West Side



(b) East Side

Figure 4.21 Specimen C4: Specimen before Testing



(a) +0.03 rad (2nd Cycle)



(b) -0.03 rad (2nd Cycle)



(c) +0.04 rad (2nd Cycle)



(d) -0.04 rad (2nd Cycle)

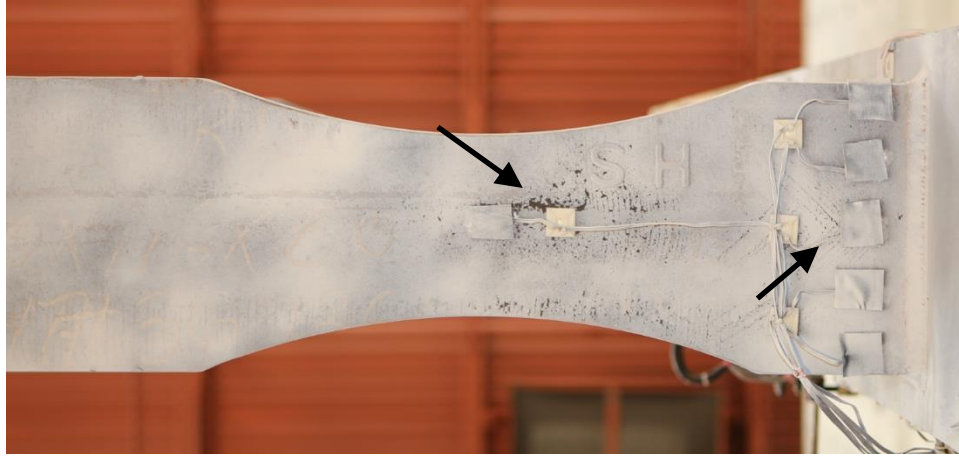


(e) +0.05 rad (1st Cycle)



(f) -0.05 rad (1st Cycle)

Figure 4.22 Specimen C4: East Side of Connection



(a) -0.015 rad (2nd Cycle)



(b) -0.02 rad (2nd Cycle)



(c) -0.04 rad (2nd Cycle)

Figure 4.23 Specimen C4: Beam Bottom Flange Yielding and Buckling

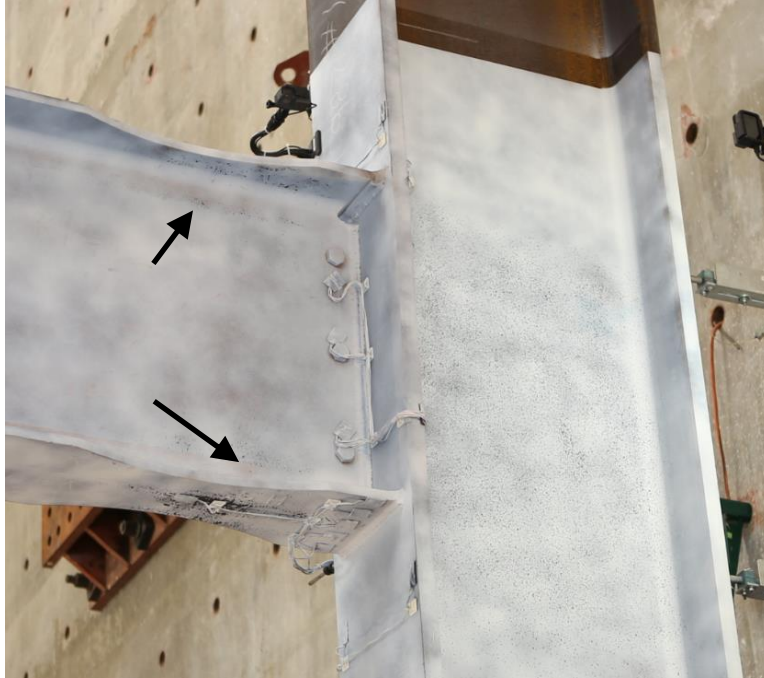


Figure 4.24 Specimen C4: Beam Web Yielding at +0.02 rad (2nd Cycle)



(a) Overview



(b) CJP Weld

Figure 4.25 Specimen C4: Beam Top Flange at -0.04 rad (1st Cycle)

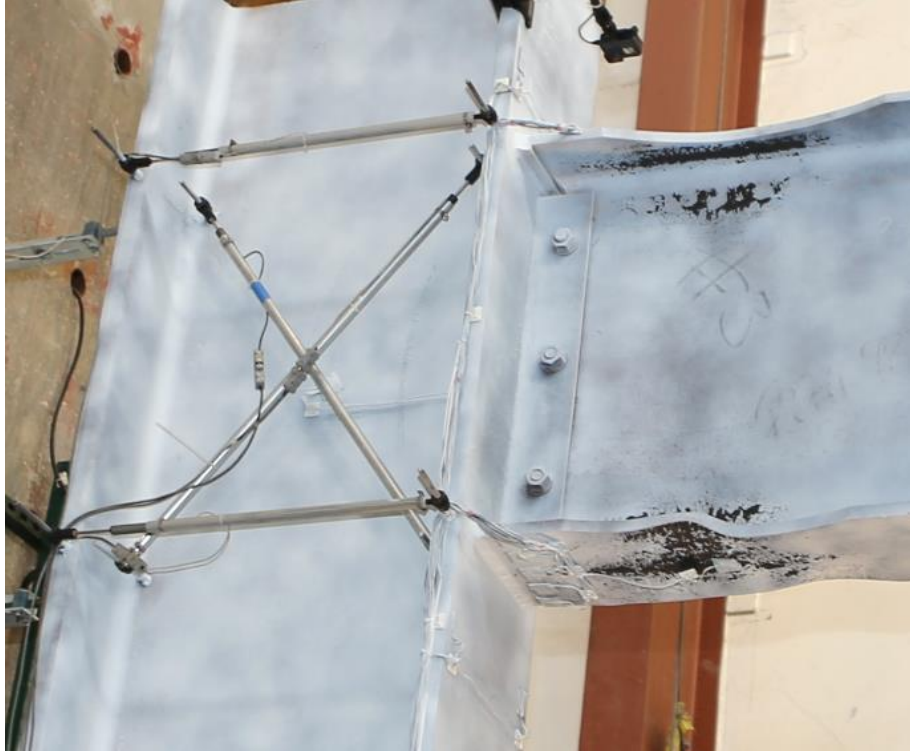


Figure 4.26 Specimen C4: Beam Flange and Web Yielding at -0.04 rad (1st Cycle)

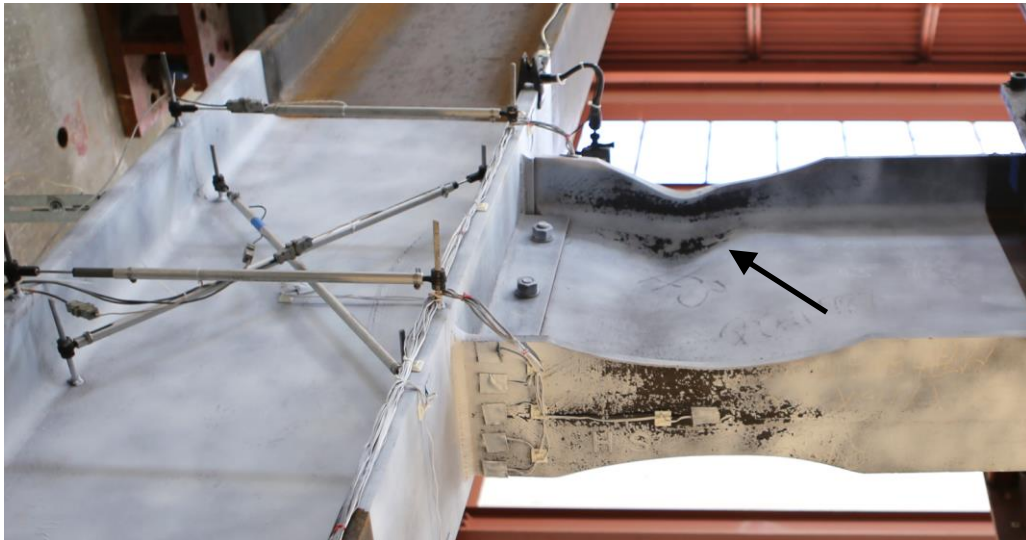


Figure 4.27 Specimen C4: Beam Web Buckling at -0.04 rad (1st Cycle)

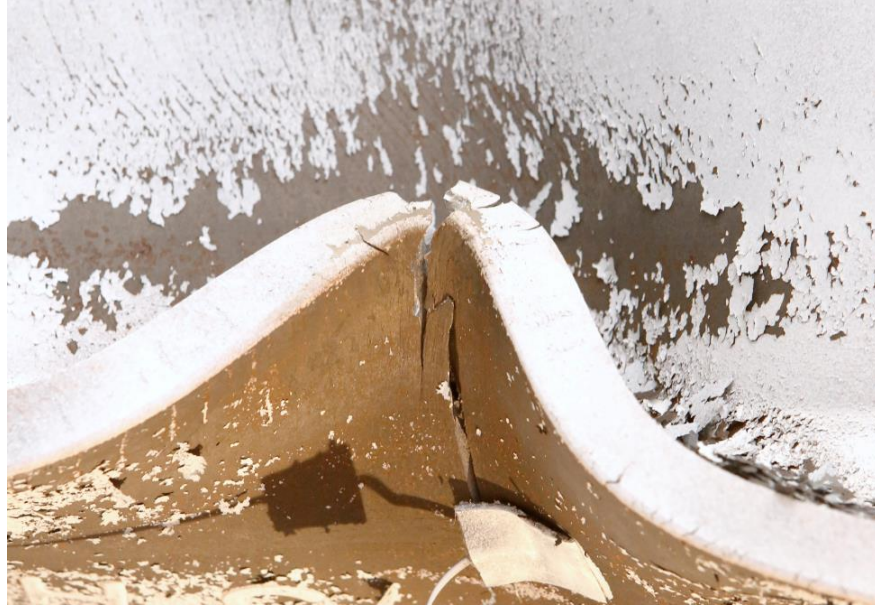


Figure 4.28 Specimen C4: Beam Bottom Flange Fracture after one cycle at 0.06 rad



(a) Overview



(b) Ductile Tearing

Figure 4.29 Specimen C4: Beam Top Flange at -0.06 rad (2nd Cycle)



(a) West Side



(b) East Side

Figure 4.30 Specimen C4: Connection at End of Test



(a) Overview



(b) Fracture Surface

Figure 4.31 Specimen C4: Beam Bottom Flange Fracture (End of Test)



(a) Overview



(b) Flange Local Bending

Figure 4.32 Specimen C4: Column Flange (End of Test)

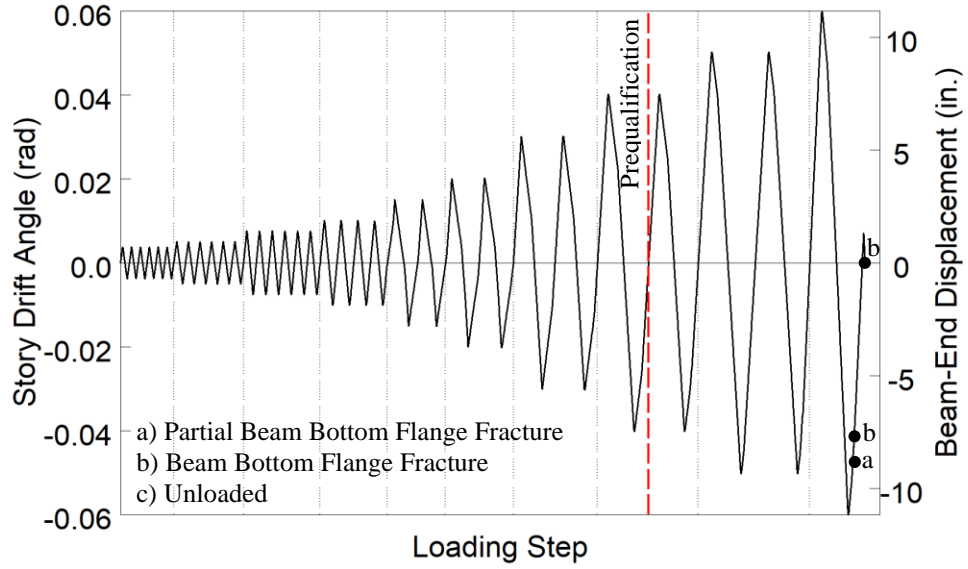


Figure 4.33 Specimen C4: Recorded Loading Sequence

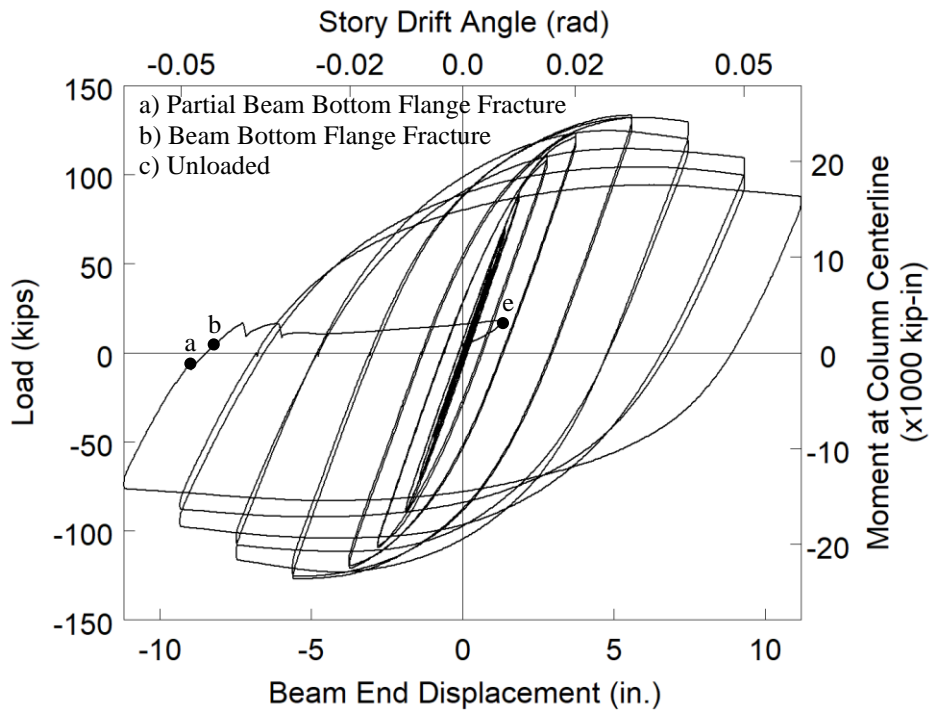


Figure 4.34 Specimen C4: Applied Load versus Beam End Displacement Response

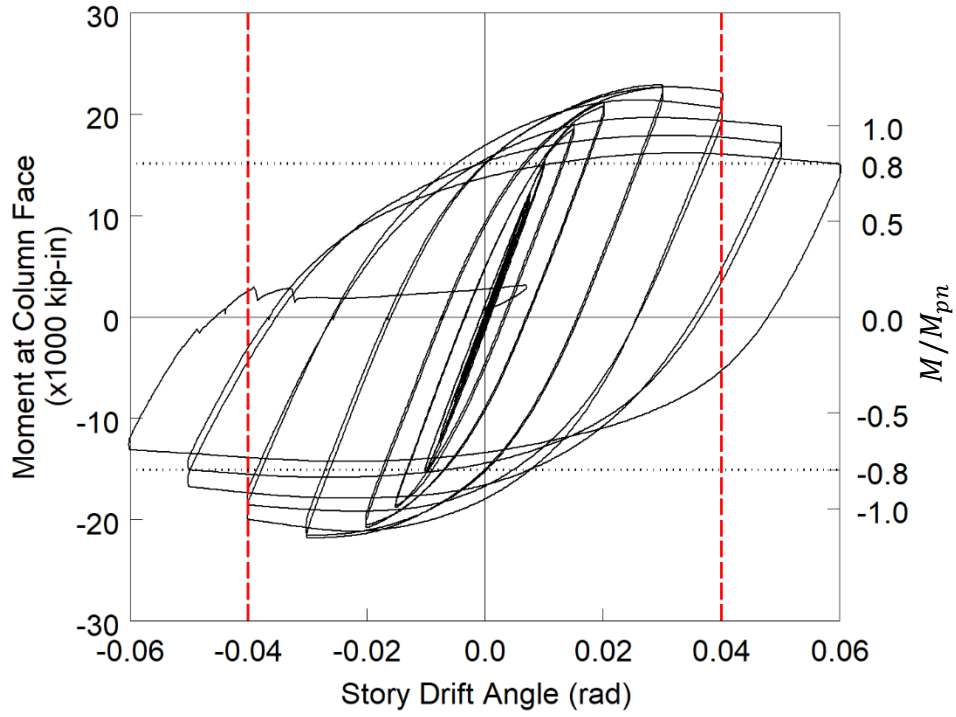


Figure 4.35 Specimen C4: Moment at Column Face versus Story Drift Response

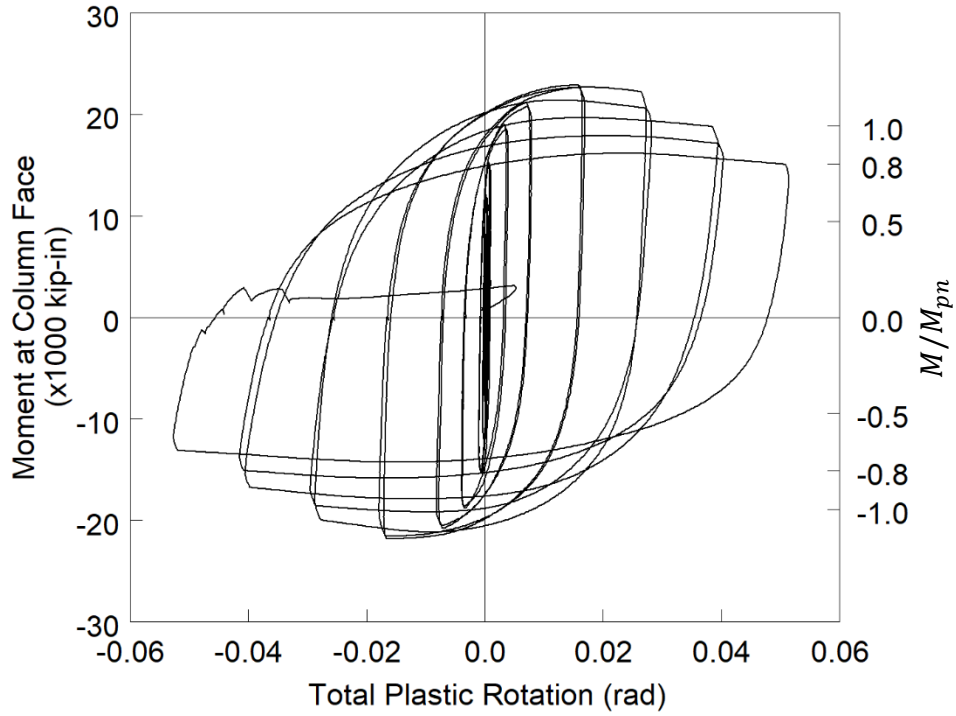


Figure 4.36 Specimen C4: Moment at Column Face versus Plastic Rotation

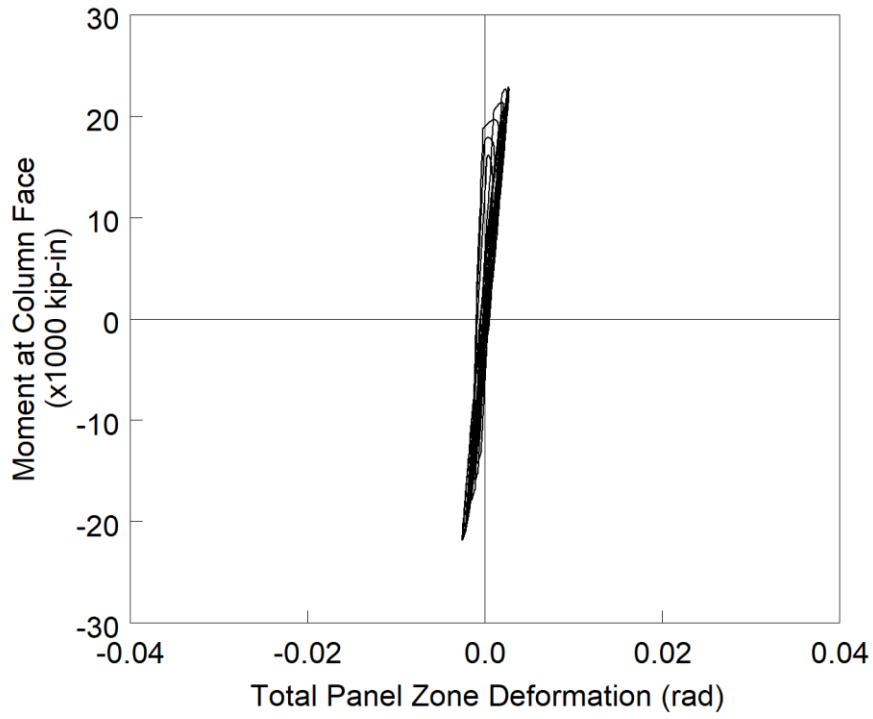


Figure 4.37 Specimen C4: Panel Zone Shear Deformation

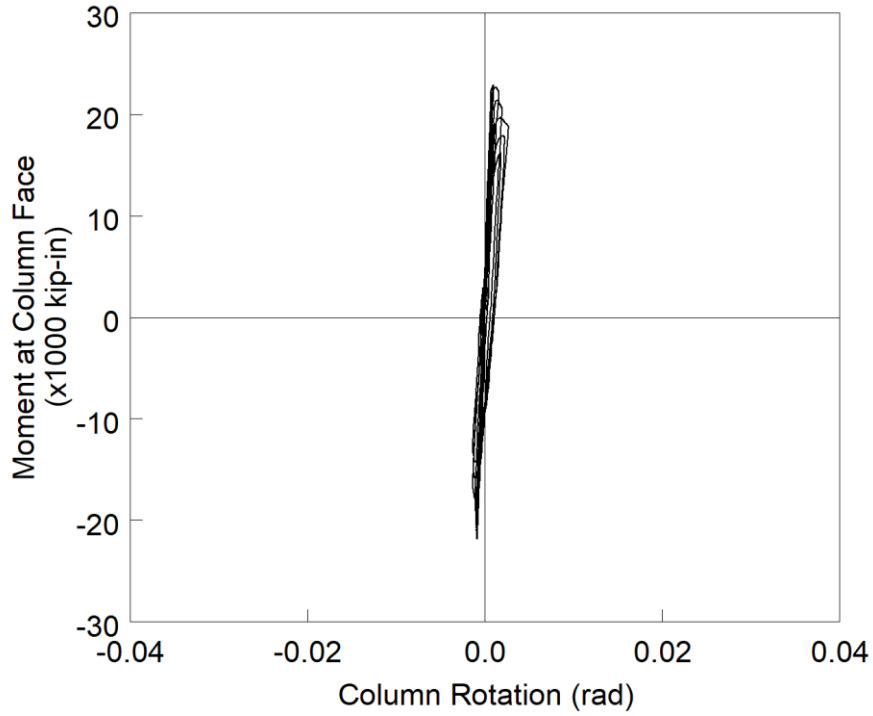


Figure 4.38 Specimen C4: Column Rotation

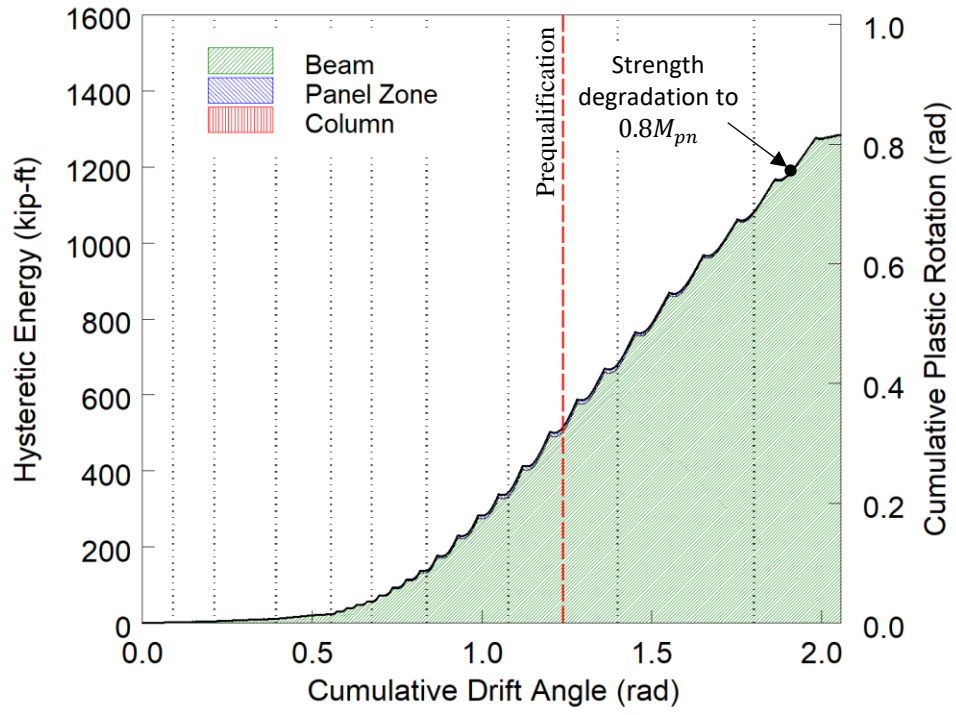
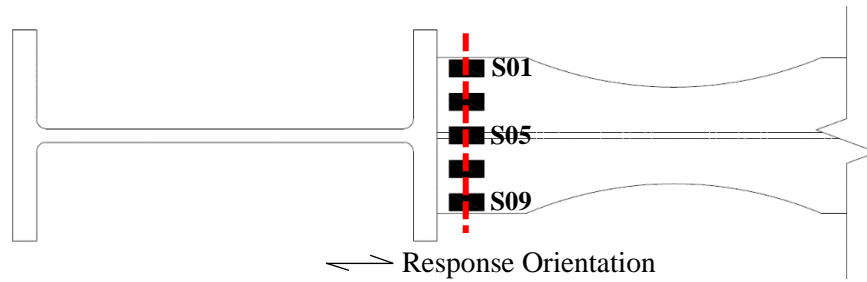
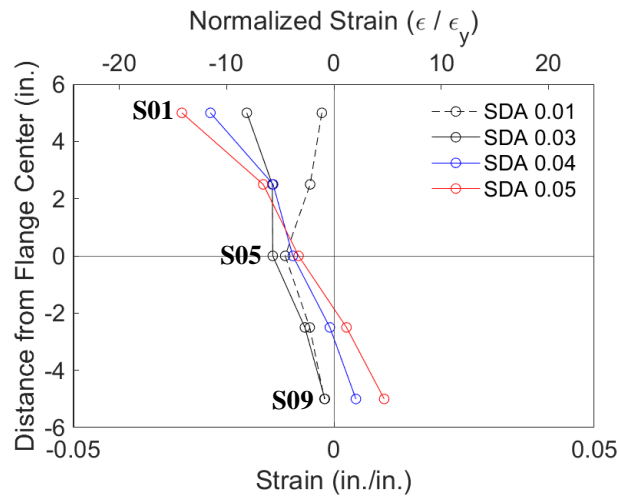


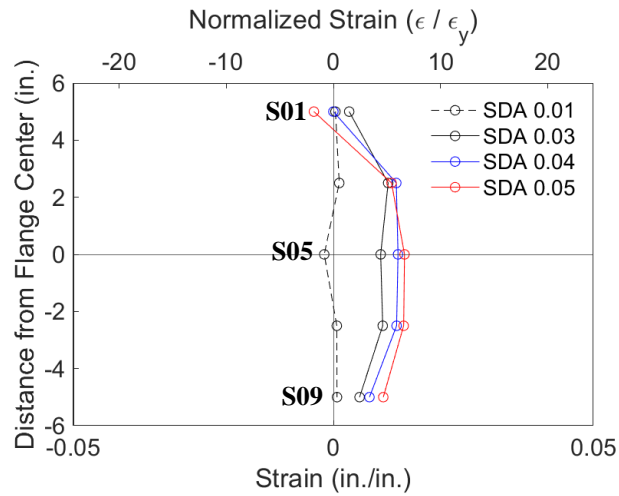
Figure 4.39 Specimen C4: Energy Dissipation



(a) Section

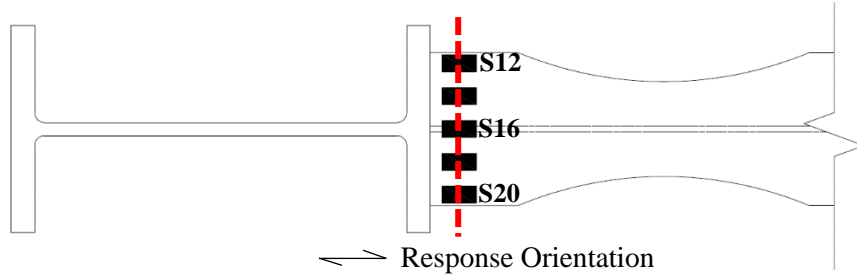


(b) Positive Drifts

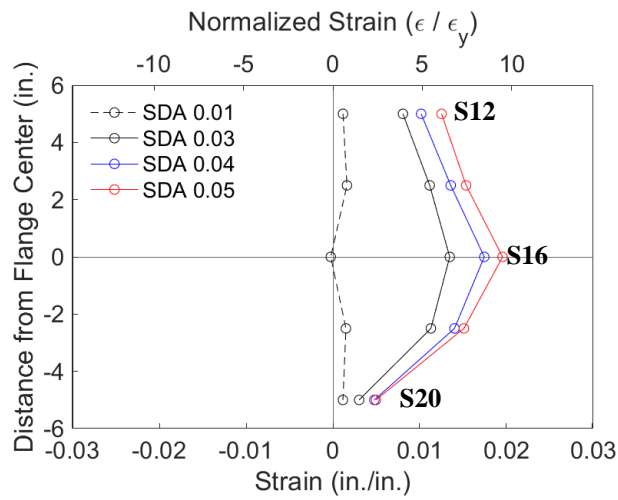


(c) Negative Drifts

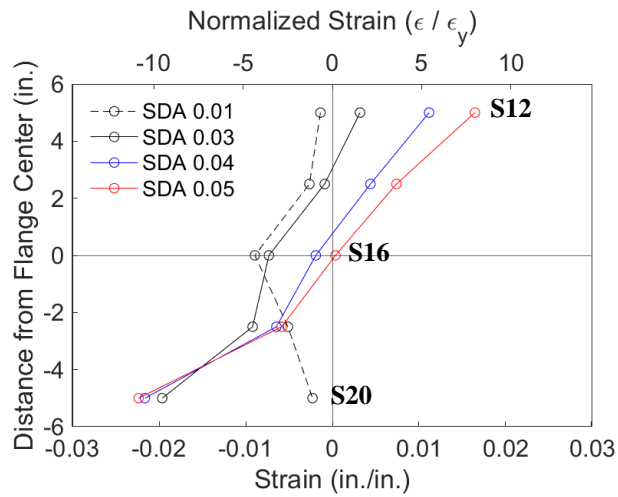
Figure 4.40 Specimen C4: Topside of Beam Top Flange Strain Profile



(a) Section

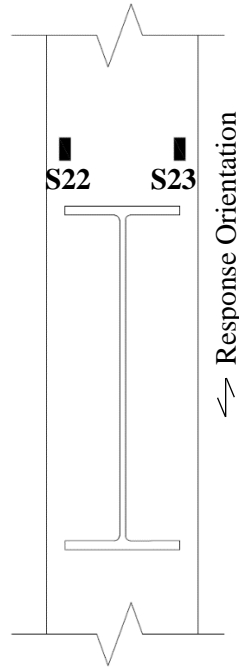


(b) Positive Drifts

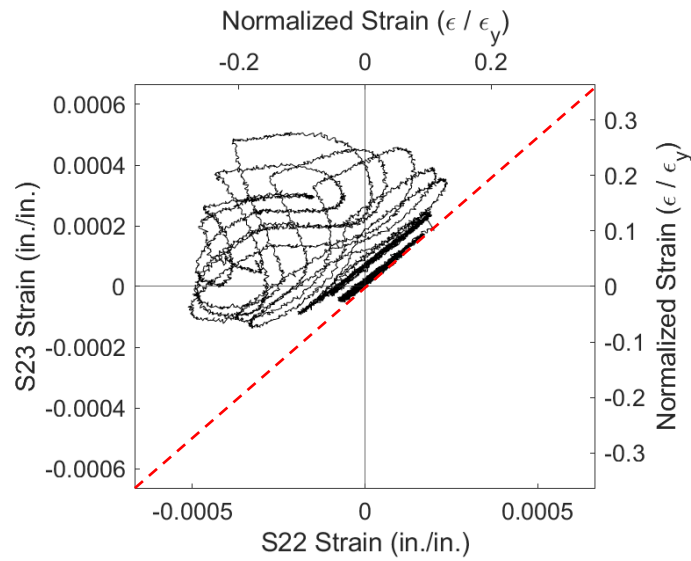


(c) Negative Drifts

Figure 4.41 Specimen C4: Underside of Beam Bottom Flange Strain Profile

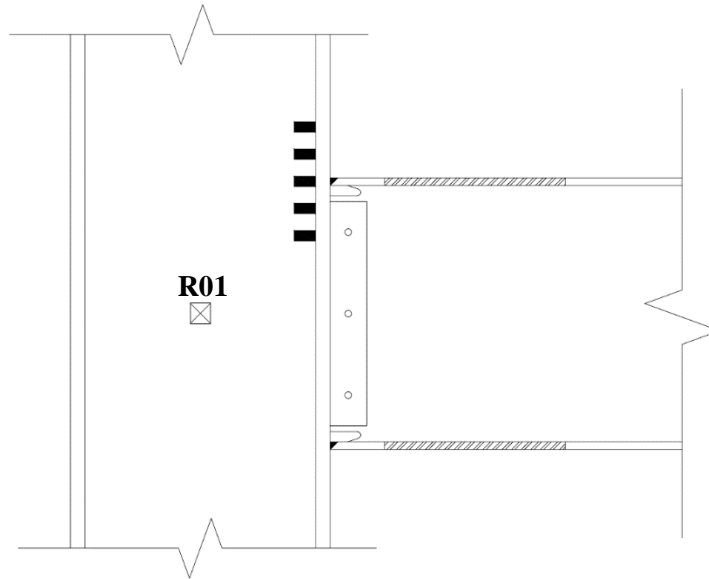


(a) Gauge Layout

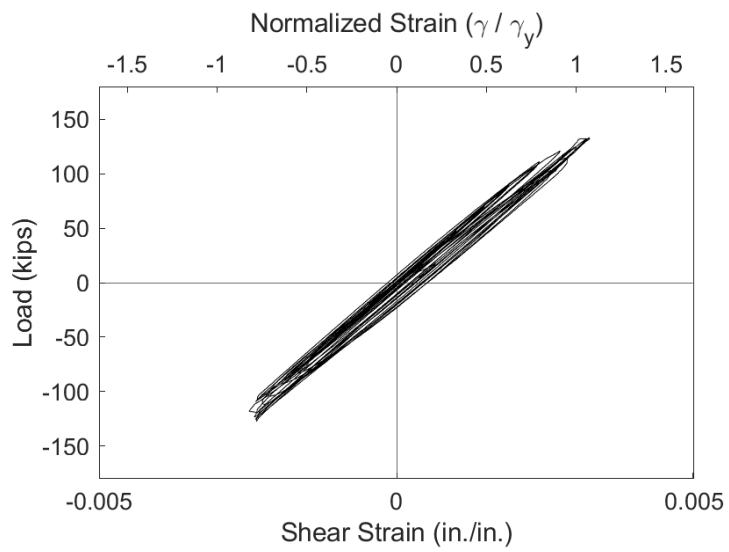


(b) Response

Figure 4.42 Specimen C4: Column Flange Warping

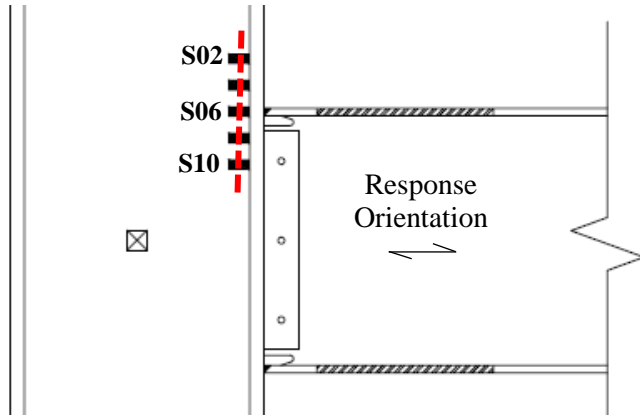


(a) Gauge Layout

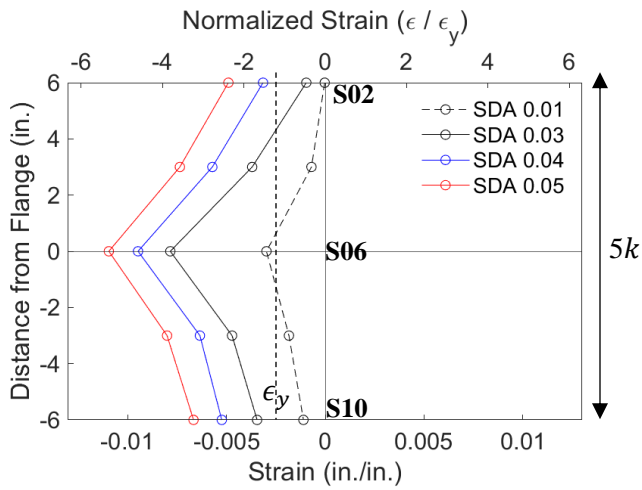


(b) Strain Rosette Gauge R01

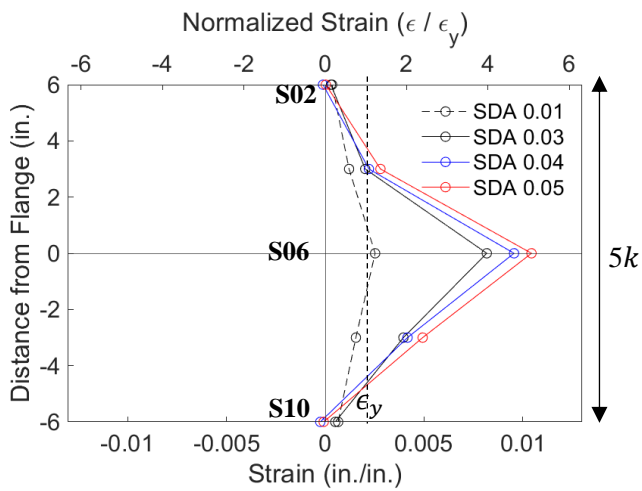
Figure 4.43 Specimen C4: Column Panel Zone Response



(a) Gauge Layout

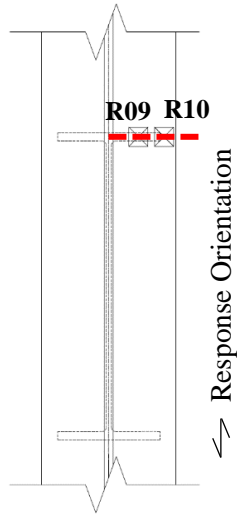


(b) Positive Drift

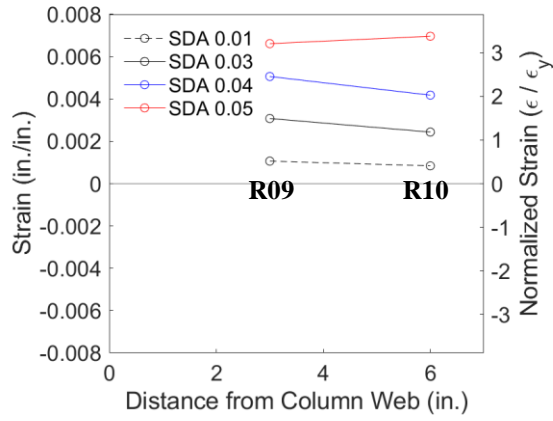


(c) Negative Drift

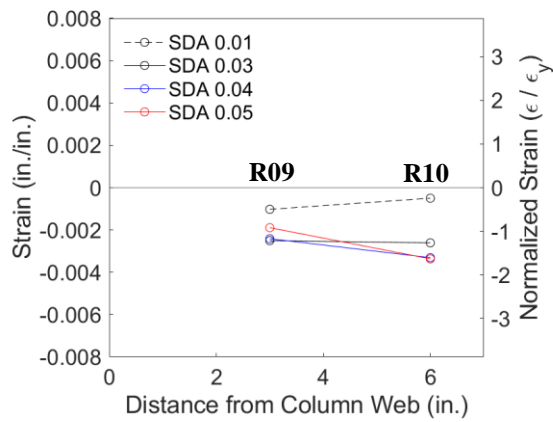
Figure 4.44 Specimen C4: Column Web Strain Profiles



(a) Section



(b) Positive Drift



(c) Negative Drift

Figure 4.45 Specimen C4: Column Flange Strain Profiles

4.4 Specimen C5

4.4.1 General

Specimen C5 was designed to investigate the validity of using the plastic distribution to estimate the required strength of the continuity plate. The continuity plates were designed to satisfy the governing AISC 360 §J10 concentrated force column limit state; WLY, was the governing limit state exceed by the flange force. The panel zone strength of Specimen C5 was intentionally designed weak with a *DCR* of 1.18. The continuity plate was welded to the column flange and web using a fillet weld of size $w = 0.8t_{cp}$, which was the closest standard fillet weld size to $w = 0.75t_{cp}$. The specimen failed by fracture of the beam top flange CJP weld after completing two cycles of 0.05 rad drift. Figure 4.46 shows the connection before testing.

4.4.2 Observed Performance

The observed response for Specimen C5 is described below.

- Figure 4.47 shows the east side of the specimens at the peak excursions during the later cycles of the loading protocol. The specimen met the AISC acceptance criteria. It was observed that beam web buckling initiated during the first cycle of 0.04 rad drift. Flange local buckling initiated at the beam bottom flange within the RBS cut during the second cycle of 0.04 rad drift. By 0.05 rad drift flange local buckling was observed in both flanges.
- Figure 4.48 shows ductile tearing of the beam top flange CJP weld that was first observed during the 2nd negative excursion of 0.03 rad drift. Minor growth of this fracture occurred during the 0.04 rad cycles during testing.
- Figure 4.49 shows gradual progression of tearing of the beam top flange CJP weld. Figure 4.49(e) shows the complete beam top flange fracture. This shear type fracture originated at a toe of the prominent weld pass against the column and propagated through the flange at a 35-degree angle through the base metal. At the flange tips the fracture took on a cup and cone with interlocking shear lips through the base metal of the beam.
- Significant column kinking was observed during the testing of the specimen (see Figure 4.50).

- Minor web buckling was evident at the end of testing [see Figure 4.51(a)]. Continued negative excursion after fracturing the beam top flange produced a fracture of the beam web [see Figure 4.51(b)]. This fracture originated in the weld access hole and propagated down through the erection bolt holes. Local necking was observed near this fracture.
- Figure 4.52 shows the slight beam lateral-torsional buckling at the end of testing.
- At the end of testing no damage was observed in any of the fillet welds fastening the continuity plates to the column. Figure 4.53 shows the continuity plates after testing. The east bottom flange and west top flange continuity plate experienced local plate buckling. The east bottom flange continuity plate started developed local buckling during the first negative excursion of 0.04 rad drift. At the time of failure, the specimen was experiencing a negative excursion which pulled the west top flange continuity plate straight with minor residual deformation. The east bottom flange shows the full extent of the buckling as this plate was in compression at the point of failure. Despite the significant plate buckling and column flange kinking, the continuity plate to column flange welds have remained intact [see Figure 4.53(b)].

4.4.3 Recorded Response

4.4.3.1 Global Response

- Figure 4.54 shows the recorded displacement response of the beam tip measured with transducer L1. A hairline crack at the centerline of the beam top flange CJP weld was observed at the second negative excursion of 0.03 rad drift. A tear through the center of the beam top flange CJP weld was observed at the peak excursion of 0.05 rad drift. At -0.035 rad drift during the second negative excursion of 0.05 rad drift, the remaining portion of the beam top flange CJP weld fractured. Continued excursion saw tearing of the web which originated at the radius of the weld access hole and propagated through the first bolt hole in the shear tab. Unanticipated bolt slip had occurred at the loading corbel during testing of the latter cycles. This slip resulted in a slight undershoot of the target displacements. For example, the computed drift during the targeted 0.04 rad story drift cycles was determined to be 0.0391 rad. It is not believed that this minor discrepancy affects the conclusions of this specimen.

- Figure 4.55 shows the load-displacement response of the beam.
- Figure 4.56 shows the computed moment at the column face (M_f) versus the story drift angle. Two horizontal axes at 80% of the nominal plastic moment (M_{pn}) of the beam section are also added. In addition, two vertical axes at ± 0.04 rad story drift show the drift required for SMF connections per AISC 341. It is observed that the beam developed its nominal plastic bending moment. If the moment is computed at the plastic hinge location and compared to the expected plastic moment, then the peak connection strength factor (C_{pr}) is 1.16.
- Figure 4.57 shows the plastic response of the specimen. The plastic response is computed using the procedure outlined in Section 3.7. The computed elastic stiffness of the specimen was determined to be 56.3 kips/in.
- Figure 4.58 shows extensive inelastic behavior of the panel zone. It is possible that the deformation of the column flanges has erroneously influenced the computation of the panel zone shear given the significant deformation observed of the continuity plates.
- Figure 4.59 shows that minor hysteretic behavior was observed in the column rotation.
- Figure 4.60 shows the dissipated energy of Specimen C5. Dotted vertical lines on the graph demonstrate the completion of each group of cycles, and the dashed red vertical line shows the completion of the first cycle of 0.04 rad in the AISC loading. It is observed that the completion of the first drift cycle of 0.04 rad (the requirement for SMF connections per AISC 341) occurs after 538 kip-ft of energy has been dissipated. The connection did not degrade below $0.8M_{pn}$ until 1,165 kip-ft of energy had been dissipated. Therefore only 46% of the energy dissipation capacity was utilized after the completion of SMF requirement. It is observed that most (65%) of the energy dissipation capacity occurred in the panel zone.

4.4.3.2 Local Response

- Figure 4.61 and Figure 4.62 show the strain gauge response from the extreme fiber of the beam top and beam bottom flange during the testing. The top flange results are influenced by the beam flange CJP weld tear. It is observed that during the 0.04 rad

drift cycles the gauge in the center of the flange experienced very little tension—correlating with the spread of the beam top flange CJP weld tear. During compression excursions the weld tear closes, and the flange can develop compressive yield forces. Subsequent tension excursions result in residual compressive stresses in this location; the weld tear results in a ratcheting of the strain response. During the first cycle of 0.05 rad drift significant weld tearing resulted in a transfer of load to the peripheral edges of the flange. A lateral-torsional response of the beam influences these peripheral gauges. These large cyclic strains on the west edge of the beam top flange result in a ductile shear fracture before the east edge of the flange.

- Figure 4.63 shows the strain gauge response of the column flange which affixes the beam. It is observed that the column flange did not yield, but deviation from a 1:1 response demonstrates the torsional demand imposed on the column due to the lateral-torsional buckling of the beam.
- Figure 4.64 shows the shear strain response of the panel zone. The panel zone saw significant hysteretic behavior with strains on the order of $12\gamma_y$. Significant yielding of the panel zone was anticipated due to the high as-designed DCR of 1.18.
- Significant continuity plate axial yielding was observed at the edge attaching the plate to the column flange (see Figure 4.65). The strains are most significant at the outboard edge of the plate with an amplitude of $12\epsilon_y$. Significant shear response, as predicted from equilibrium, is observed in the plate (see Figure 4.66). Before instability of the continuity plate cyclic principal strains of ϵ_y were observed in the plate [see Figure 4.67(b)]. After instability cyclic strains on the order of $20\epsilon_y$ was observed [see Figure 4.67(c)].
- The shear response of the continuity plate attachment to the web of the plate demonstrates localized shear strains of γ_y at the corner adjacent to the loaded edge of the plate. This peak only occurs when the continuity plate is in compression, which is attributed to a loss of stiffness of the outboard edge of the plate concentrating the shear to the nearest edge of the plate (see Figure 4.68).
- Figure 4.69 shows the response of the outboard edge of the continuity plate. Gauges placed on the topside and underside of the plate provide an indication of the nature

of loading. If the response follows the 1:1 line, shown as a red dashed line, then the plate is responding axially. Deviation from this line indicates flexure of the continuity plate. Significant deviation from this line correlates with the observed buckling of the continuity plate.

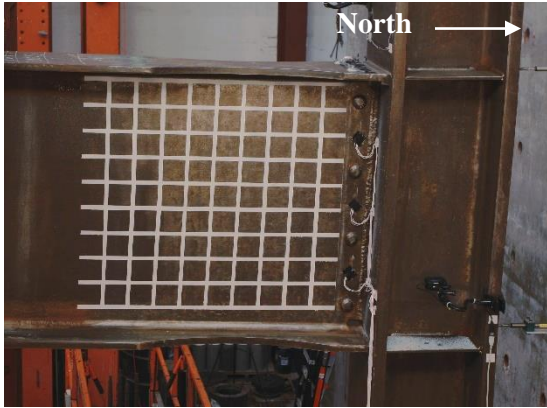


(a) West Side

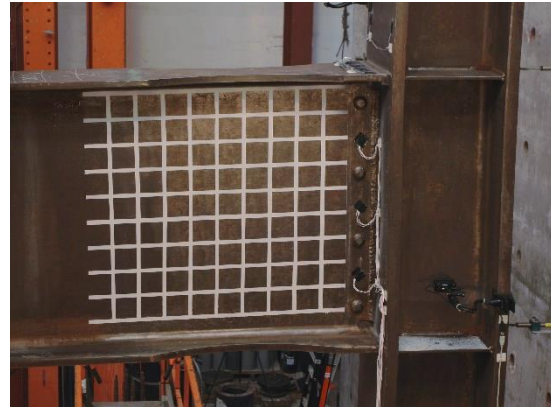


(b) East Side

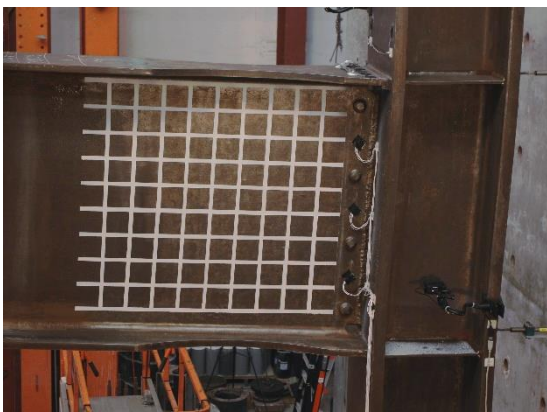
Figure 4.46 Specimen C5: Specimen before Testing



(a) +0.03 rad (2nd Cycle)



(b) -0.03 rad (2nd Cycle)



(c) +0.04 rad (2nd Cycle)



(d) -0.04 rad (2nd Cycle)



(e) +0.05 rad (1st Cycle)



(f) -0.05 rad (1st Cycle)

Figure 4.47 Specimen C5: East Side of Connection



(a) -0.03 rad (1st Cycle)



(b) -0.03 rad (2nd Cycle)



(c) -0.04 rad (1st Cycle)



(d) -0.04 rad (2nd Cycle)

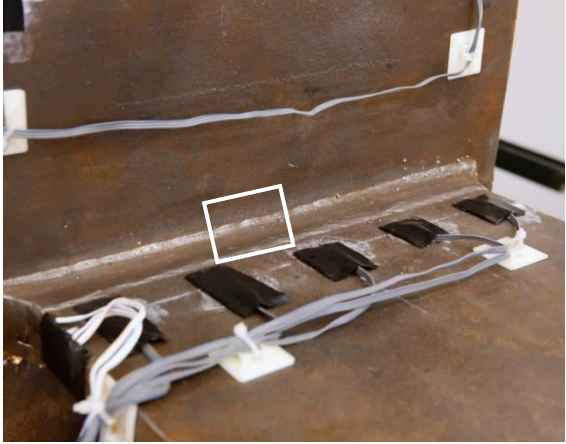


(e) -0.05 rad (1st Cycle)



(f) -0.05 rad (2nd Cycle)

Figure 4.48 Specimen C5: Beam Top Flange



(a) Overview



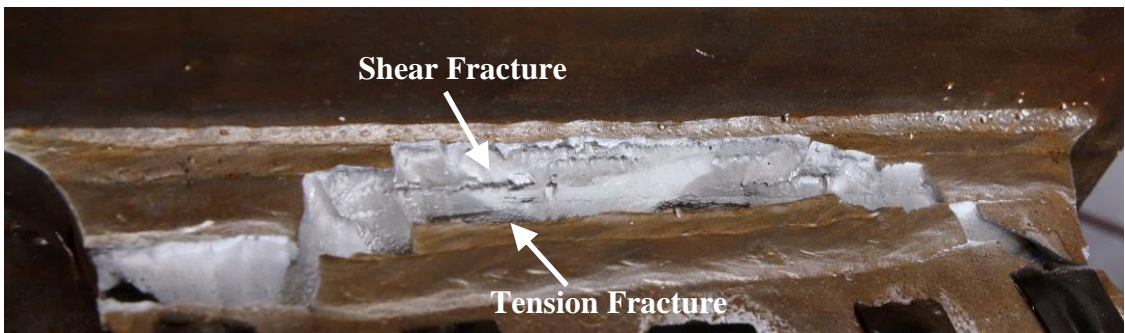
(b) -0.03 rad (2nd Cycle)



(c) -0.04 rad (2nd Cycle)

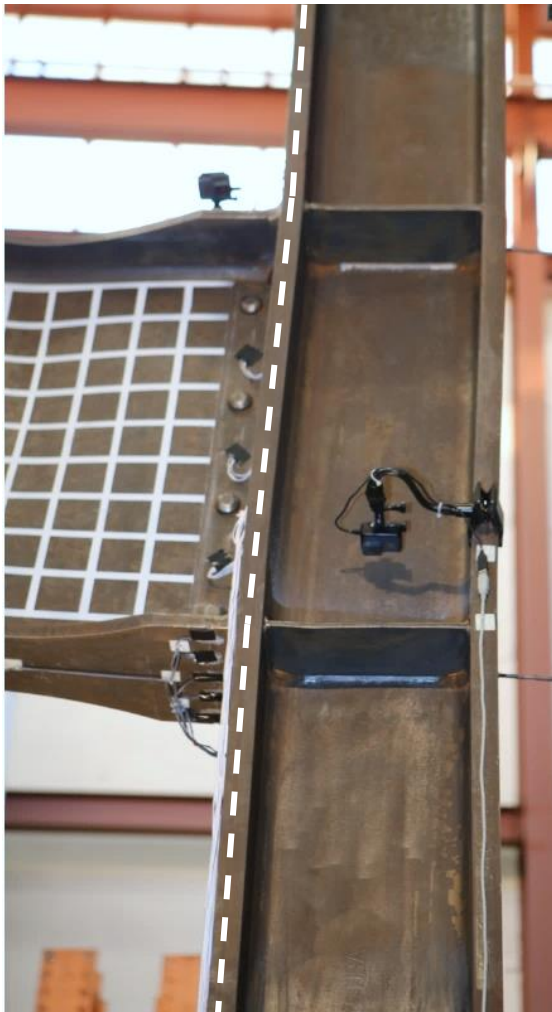


(d) -0.05 rad (1st Cycle)



(e) Fracture (End of Test)

Figure 4.49 Specimen C5: Beam Top Flange CJP Weld Fracture Progression



(a) +0.05 rad (2nd Cycle)



(b) -0.05 rad (2nd Cycle)

Figure 4.50 Specimen C5: Column Kinking due to Panel Zone Deformation



(a) Beam Web Buckling



(b) Web Fracture

Figure 4.51 Specimen C5: Beam Web Buckling (End of Test)



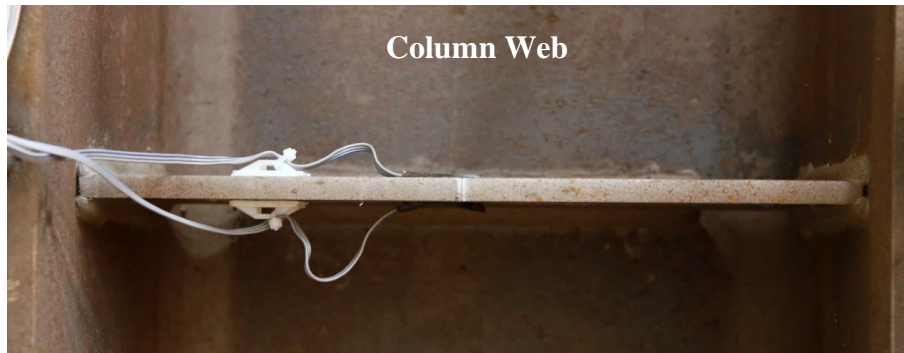
Figure 4.52 Specimen C5: Beam Lateral-Torsional Buckling (End of Test)



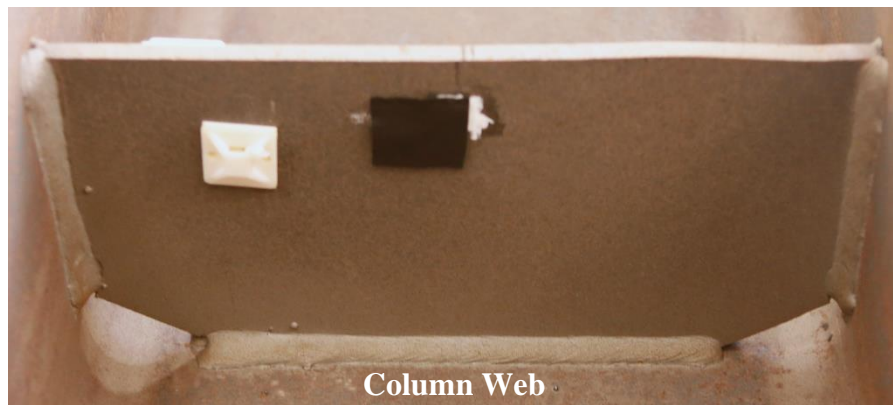
(a) East Bottom Flange Continuity Plate



(b) Enlarged View of Weld



(c) West Bottom Flange Continuity Plate



(d) West Top Flange Continuity Plate

Figure 4.53 Specimen C5: Continuity Plate (End of Test)

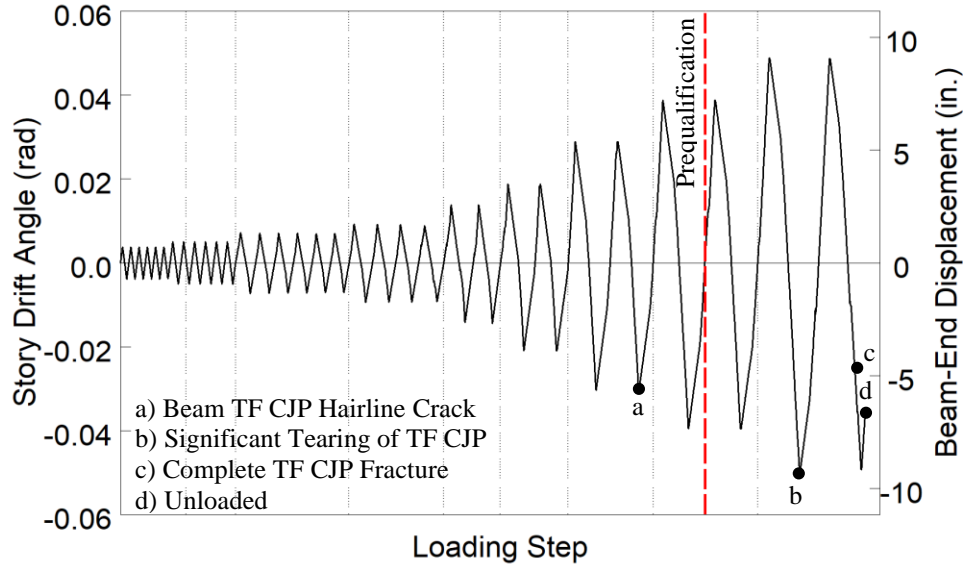


Figure 4.54 Specimen C5: Recorded Loading Sequence

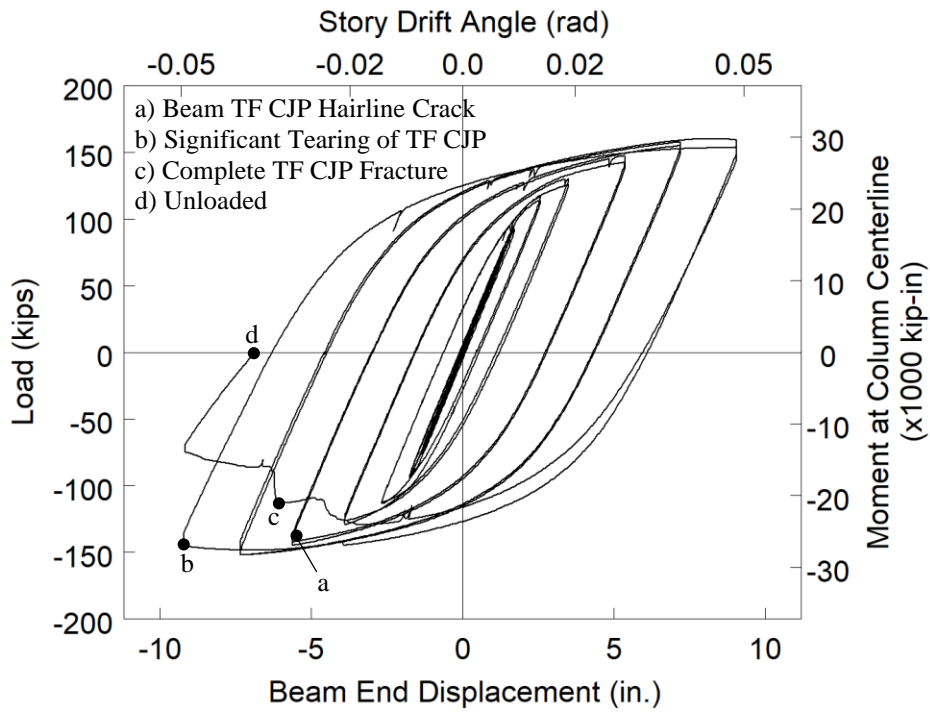


Figure 4.55 Specimen C5: Applied Load versus Beam End Displacement Response

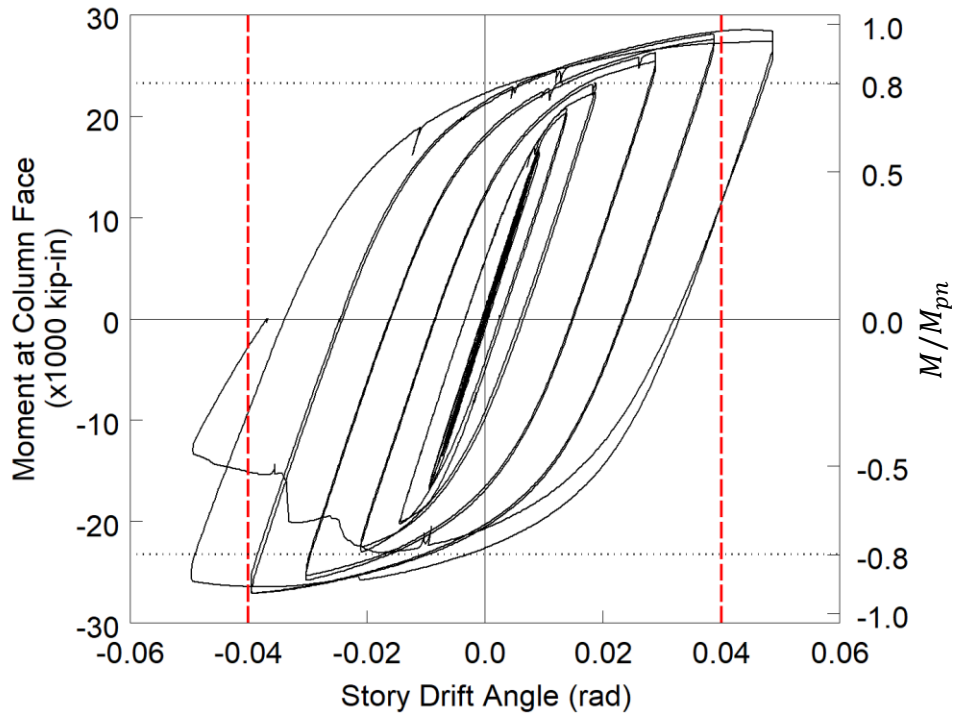


Figure 4.56 Specimen C5: Moment at Column Face versus Story Drift Response

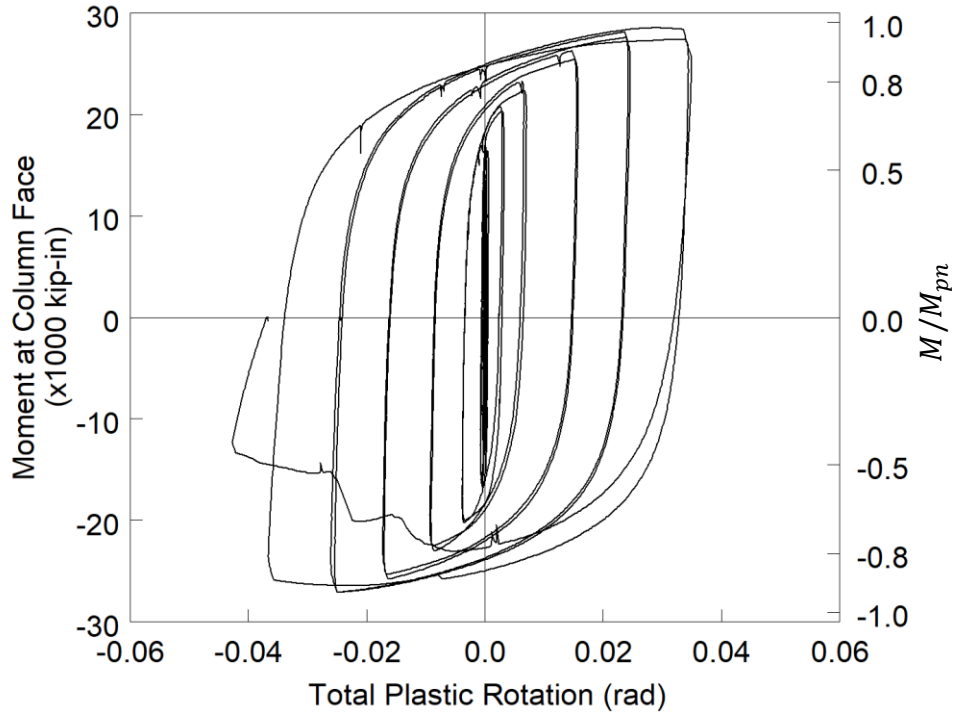


Figure 4.57 Specimen C5: Moment at Column Face versus Plastic Rotation

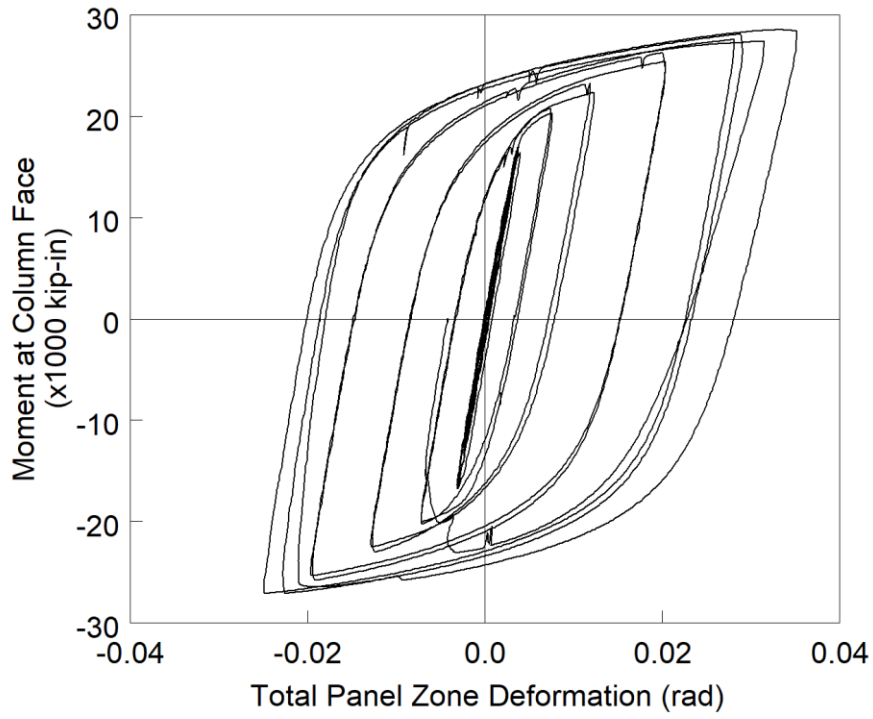


Figure 4.58 Specimen C5: Panel Zone Shear Deformation

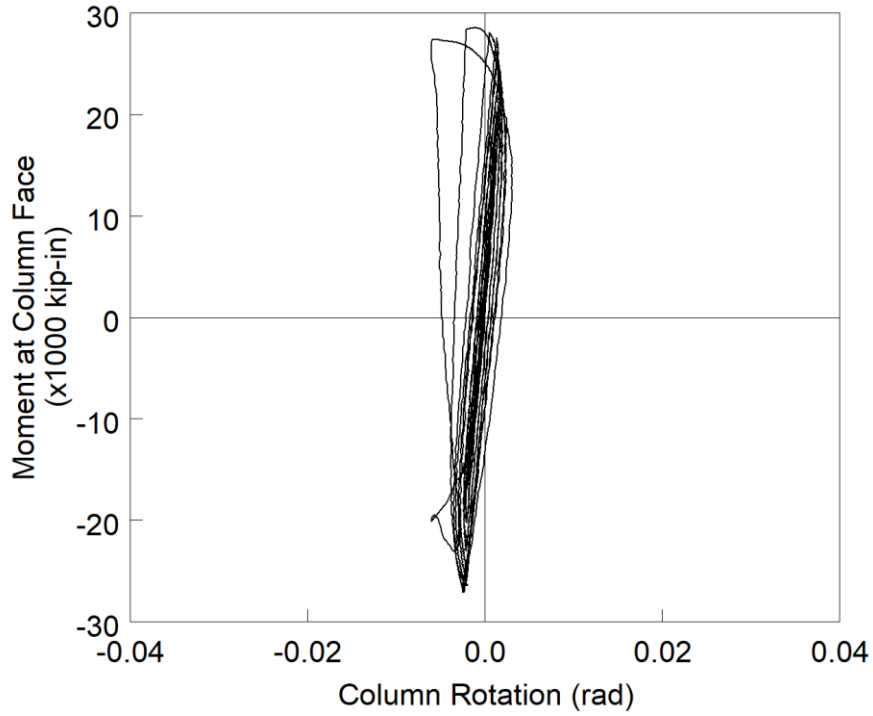


Figure 4.59 Specimen C5: Column Rotation

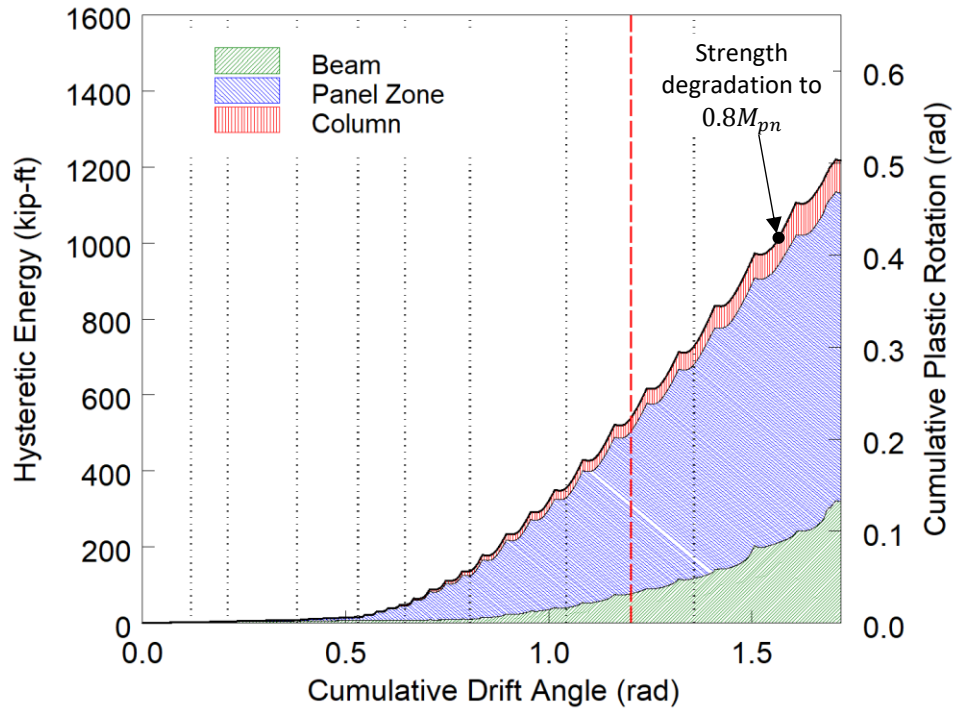
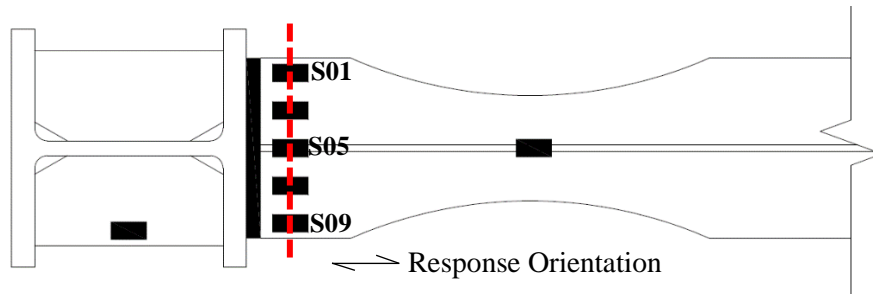
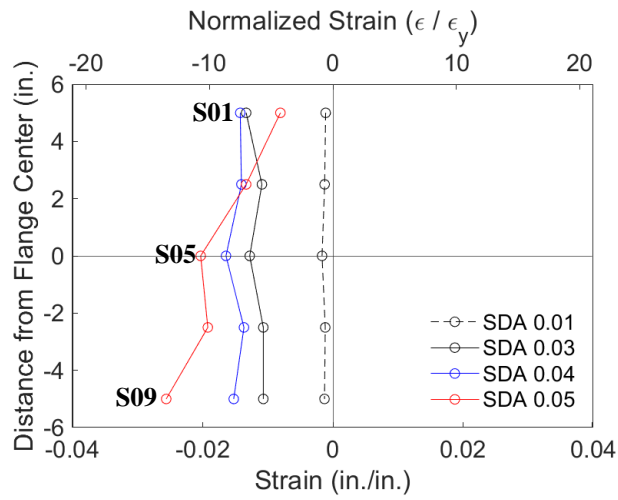


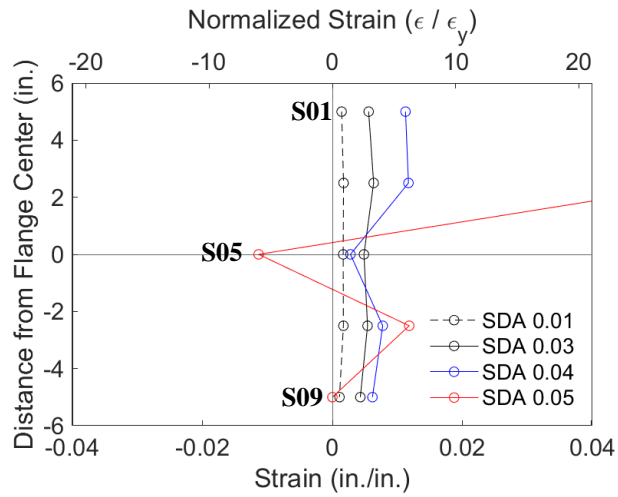
Figure 4.60 Specimen C5: Energy Dissipation



(a) Section

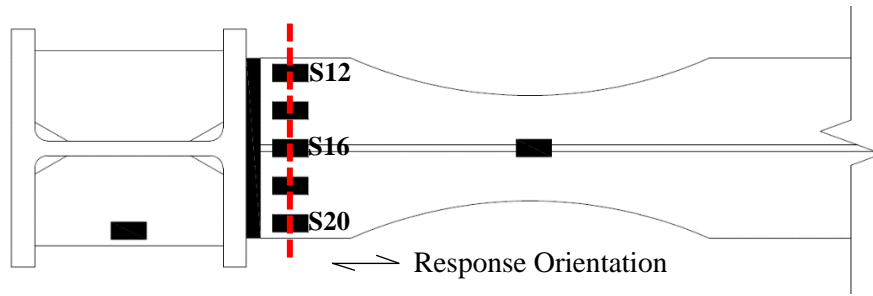


(b) Positive Drift

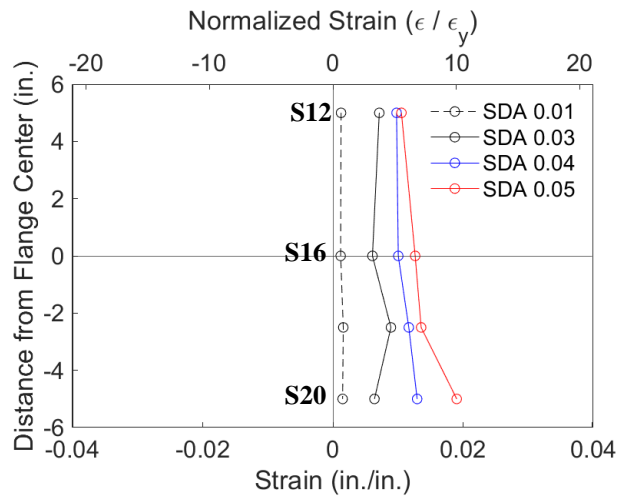


(c) Negative Drift

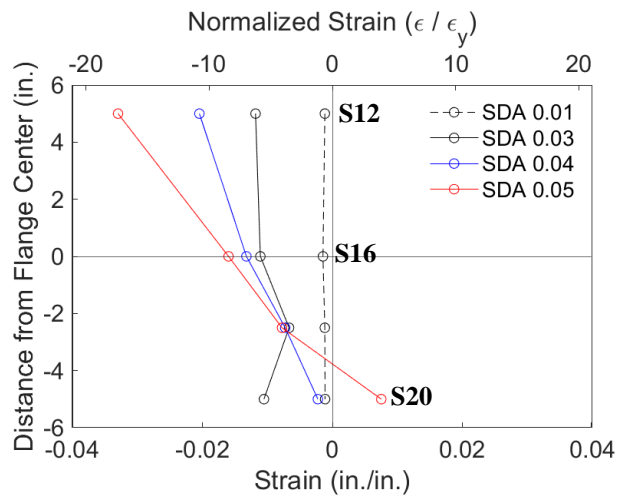
Figure 4.61 Specimen C5: Topside of Beam Top Flange Strain Profile



(a) Section

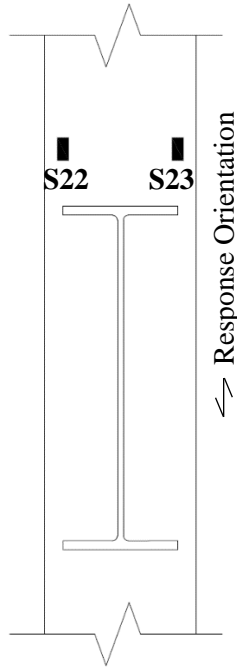


(b) Positive Drift

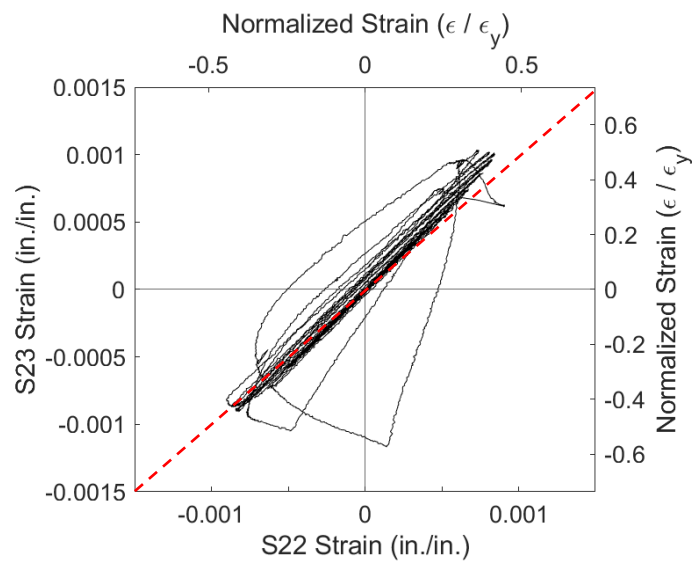


(c) Negative Drift

Figure 4.62 Specimen C5: Underside of Beam Bottom Flange Strain Profile

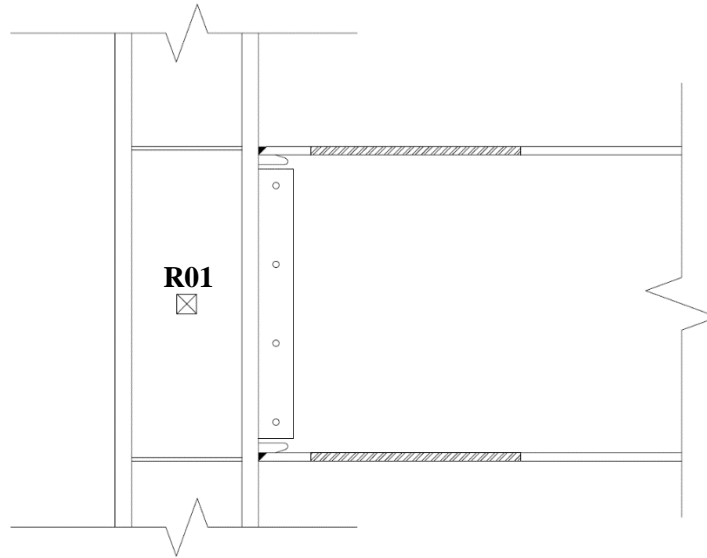


(a) Gauge Layout

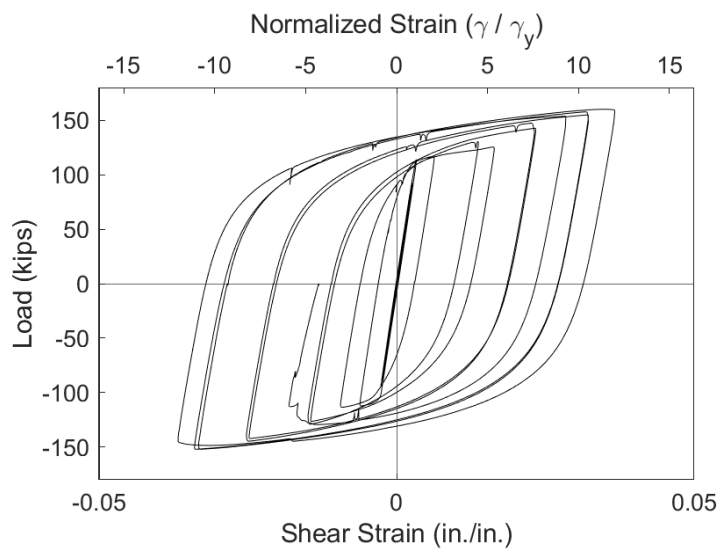


(b) Response

Figure 4.63 Specimen C5: Column Flange Warping

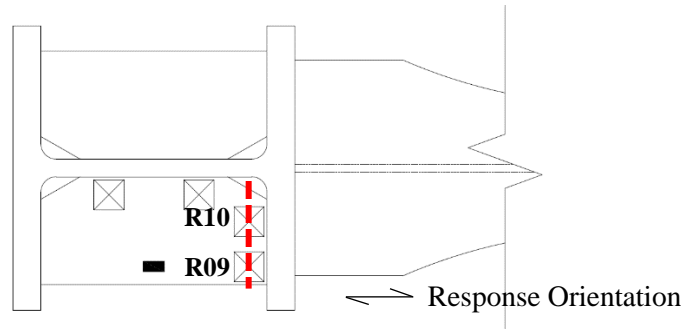


(a) Gauge Layout

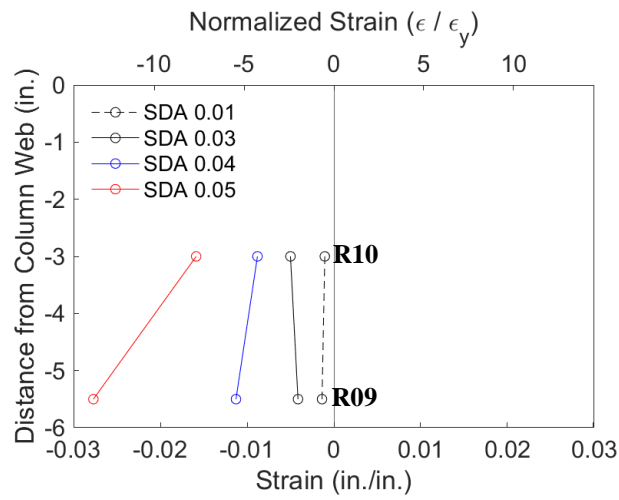


(b) Strain Rosette Gauge R01

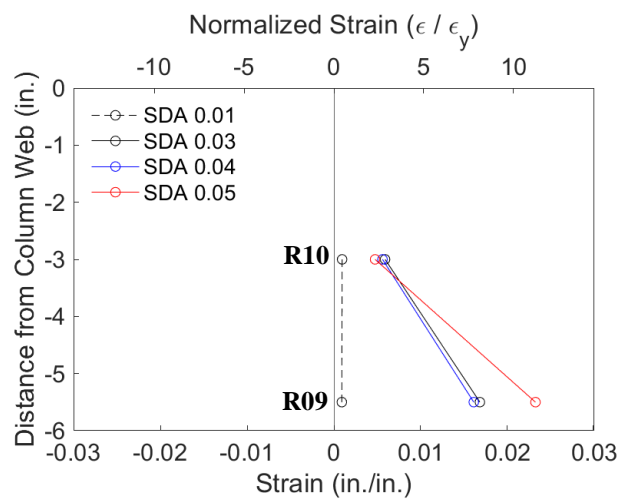
Figure 4.64 Specimen C5: Panel Zone Response



(a) Section

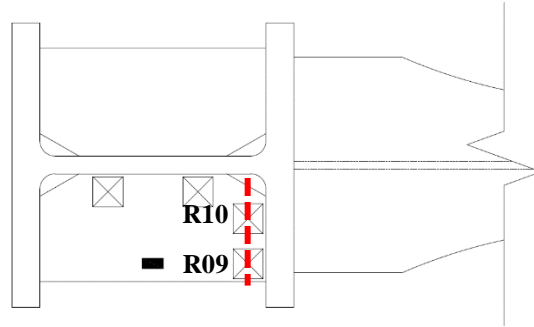


(b) Positive Drift

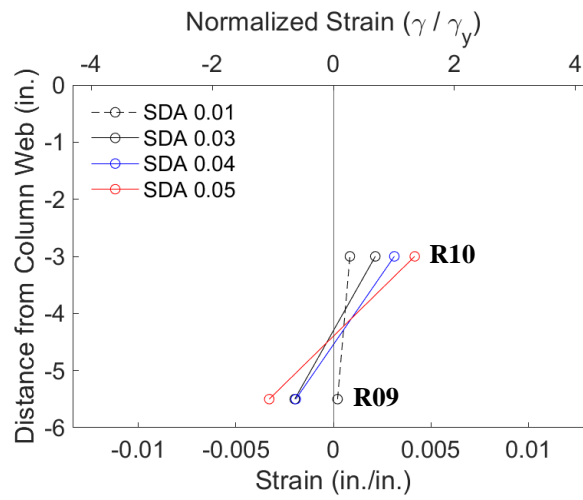


(c) Negative Drift

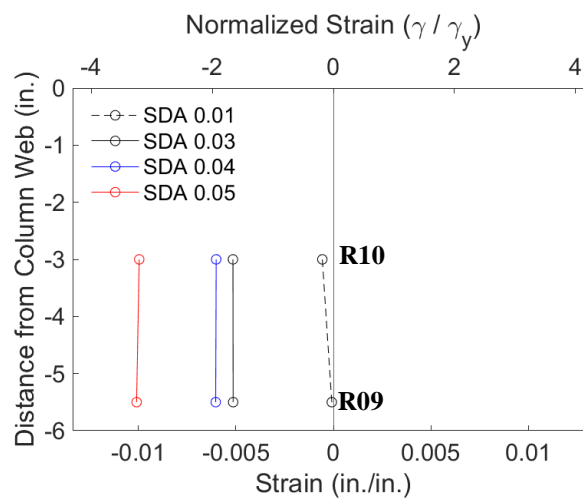
Figure 4.65 Specimen C5: Continuity Plate at Column Flange Edge Strain Profile



(a) Section

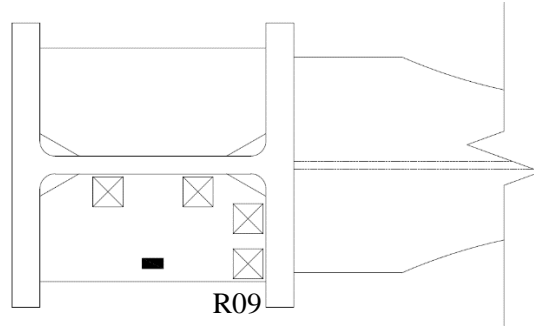


(b) Positive Drift

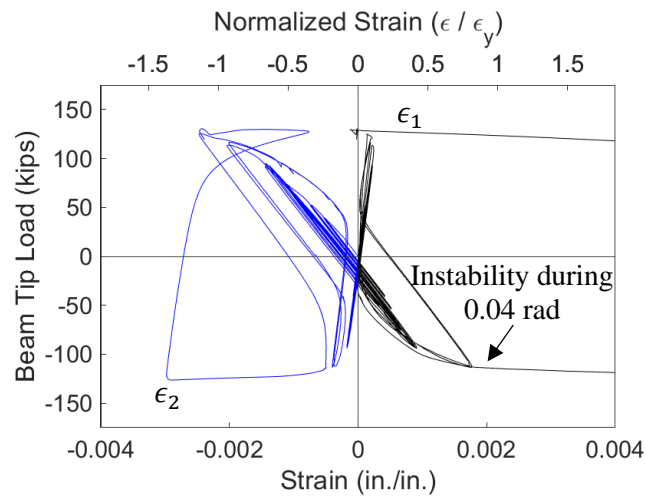


(c) Negative Drift

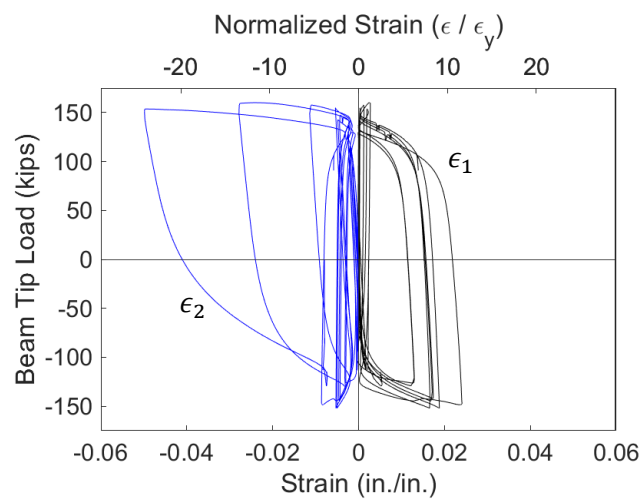
Figure 4.66 Specimen C5: Continuity Plate at Column Flange Edge Shear Strain Profile



(a) Layout

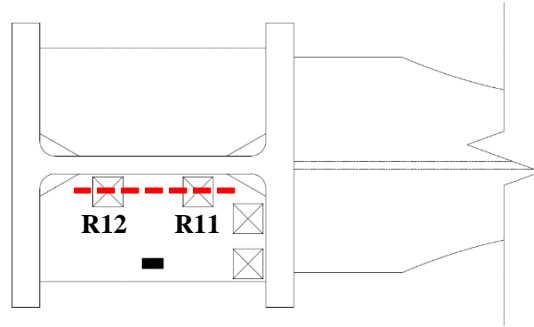


(b) Principal Strains to First Positive Excursion of 0.04 rad drift

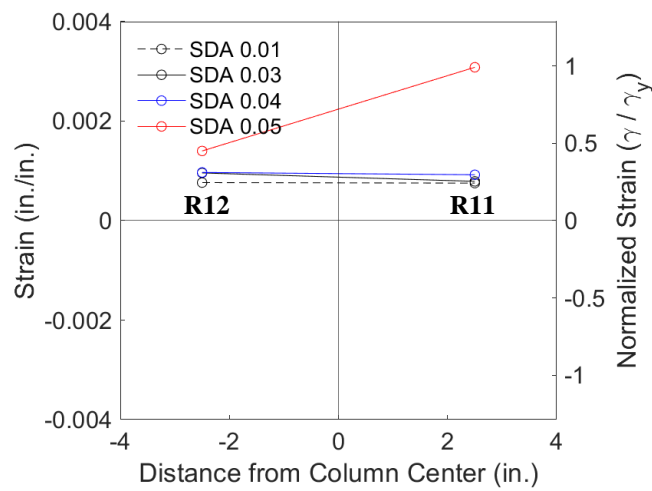


(c) Principal Strains throughout Testing

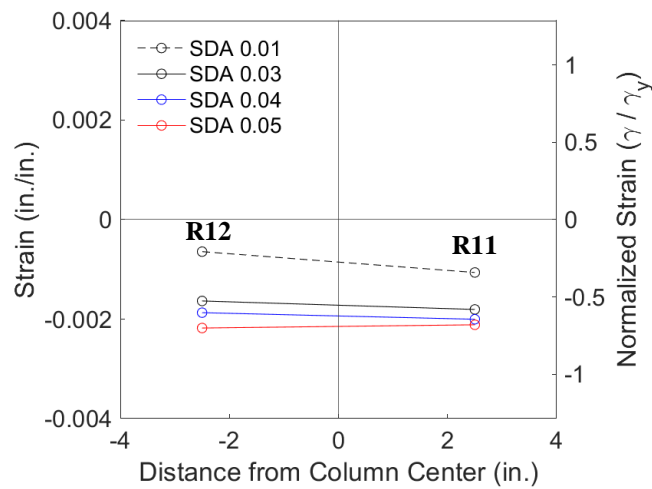
Figure 4.67 Specimen C5: Continuity Plate Strain Gauge Rosette R09 Response



(a) Section

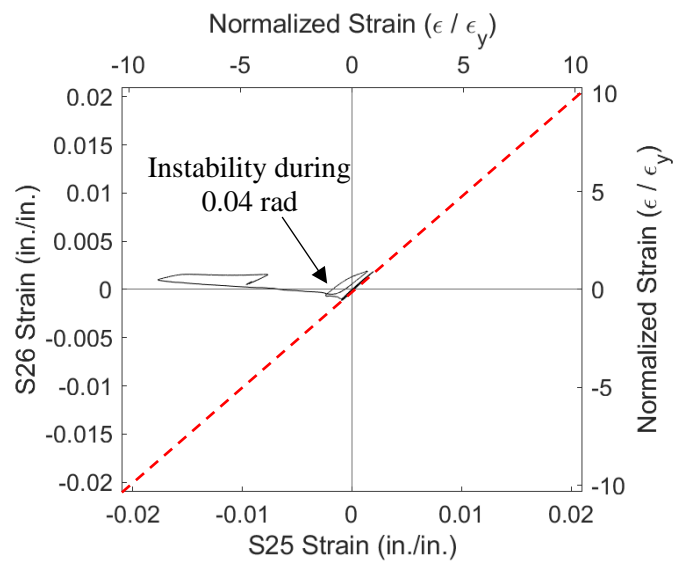
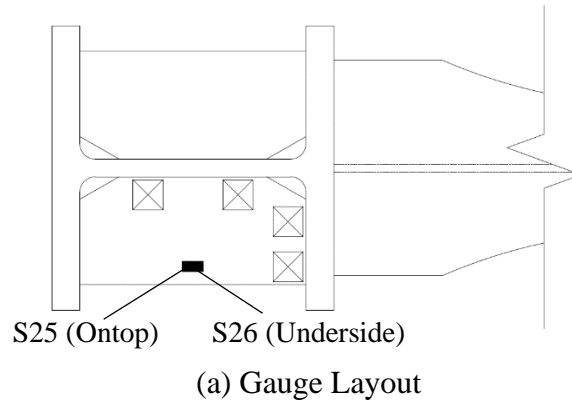


(b) Positive Drift



(c) Negative Drift

Figure 4.68 Specimen C5: Continuity Plate at Column Web Edge Shear Strain Profile



(b) Response

Figure 4.69 Specimen C5: Bottom Continuity Plate Bending

4.5 Specimen C6

4.5.1 General

Specimen C6 was designed to investigate the validity of using the plastic distribution to estimate the required strength of the continuity plate. The continuity plates were designed to satisfy the governing AISC 360 §J10 concentrated force column limit state; both the FLB and WLY limit dictate the need of a continuity plate in this specimen. The continuity plate was welded to the column flange and web using a fillet weld of size $w = 1.0t_{cp}$, which was oversized on purpose to ensure survivability of the fillet weld for this specimen and Specimen C6-G, which was essentially an identical twin of this specimen. The specimen eventually failed by fracture of the beam top flange CJP weld during the first negative excursion to 0.05 rad drift during the first excursion to 0.05 rad. Figure 4.70 shows the connection before testing.

4.5.2 Observed Performance

The observed response for Specimen C6 is described below.

- Figure 4.71 shows the east side of the specimen at the peak excursions during the later cycles of the loading protocol. The specimen met the AISC acceptance criteria. It was observed that beam web buckling and beam flange local buckling both initiated during the first cycle of 0.04 rad drift. Flange local buckling initiated at the beam bottom flange within the RBS cut during the second cycle of 0.04 rad drift. At 0.05 rad drift modest beam flange and beam web local buckling was observed.
- Figure 4.72 shows the progressive tearing of the beam top flange CJP weld. At the first negative excursion to 0.03 rad drift a minor crack was observed at the toe of prominent weld pass on the outward surface of the CJP weld. This crack progressed until -0.037 rad of the first negative excursion of 0.05 rad drift when a sudden fracture of the flange propagated severing the east side of the beam flange connection. Continued excursion to -0.05 rad tore the remainder of the beam flange CJP weld.
- The gradual progression of the weld tearing is shown in Figure 4.73. The final fracture surface was observed to primarily be a shear fracture [see Figure 4.73(e)]. This picture also shows minor column flange yielding which only occurred at the center of the beam top flange location.

- Beam bottom flange yielding started during the 0.01 rad cycles within the reduced beam section and near the column flange (see Figure 4.74). This yielding progresses through testing. Minor lateral-torsional buckling was observed during testing.
- Figure 4.75 shows panel zone yielding on the west side of the specimen. This yielding commenced during the 0.015 rad drift cycles and progressed through testing. Figure 4.76 shows the beam flange and beam web local buckling.
- Figure 4.77 shows the connection after testing. Significant flange local buckling occurred during the first cycle of 0.05 rad drift.
- Figure 4.78 shows the continuity plates and their fillet welds after testing. No damage to the fillet welds was observed. Additionally, yielding of the continuity plates was not observed.

4.5.3 Recorded Response

4.5.3.1 Global Response

- Figure 4.79 shows the recorded displacement response of the beam tip measured with transducer L1. A hairline crack at the centerline of the beam top flange CJP weld was observed at the first negative excursion of 0.03 rad drift. This gradually tore throughout testing until, during the first negative excursion of 0.05 rad drift, the beam top flange partially ruptured at -0.037 rad drift. Continued excursion to -0.05 rad tore the remainder of the flange.
- Figure 4.80 shows the load-displacement response of the beam.
- Figure 4.81 shows the computed moment at the column face (M_f) versus the story drift angle. Two horizontal axes at 80% of the nominal plastic moment (M_{pn}) of the beam section are also added. In addition, two vertical axes at ± 0.04 rad story drift show the drift required for SMF connections per AISC 341. It is observed that the beam developed 1.1 times its nominal plastic bending moment. If the moment is computed at the plastic hinge location and compared to the expected plastic moment, then the peak connection strength factor (C_{pr}) is 1.21.
- Figure 4.82 shows the plastic response of the specimen. The plastic response is computed using the procedure outlined in Section 3.7. The computed elastic stiffness of the specimen was determined to be 46.9 kips/in.

- Figure 4.83 shows modest inelastic behavior of the panel zone.
- Figure 4.84 shows that minimal hysteretic behavior was observed in the column rotation.
- Figure 4.85 shows the dissipated energy of Specimen C6. Dotted vertical lines on the graph demonstrate the completion of each group of cycles, and the dashed red vertical line shows the completion of the first cycle of 0.04 rad in the AISC loading. It is observed that the completion of the first drift cycle of 0.04 rad (the requirement for SMF connections per AISC 341) occurs after 489 kip-ft of energy has been dissipated. The connection did not degrade below $0.8M_{pn}$ until 834 kip-ft of energy had been dissipated. Therefore only 58% of the energy dissipation capacity was utilized after the completion of SMF requirement. It is observed that most (78%) of the energy dissipation capacity occurred in the beam.

4.5.3.2 *Local Response*

- Figure 4.86 and Figure 4.87 show the strain gauge response from the extreme fiber of the beam top and beam bottom flange during the testing. Weak axis flexural response of the beam is observed across the flange consistent with the observed lateral-torsional buckling of the beam. The top flange results are influenced by the weld tearing which initiates from the center of the top flange. As the weld tears, the tension force transmits to the peripheral edges of the flange, and the gauge at the center of the top flange remains in compression.
- Figure 4.88 shows the strain gauge response of the column flange which affixes the beam. It is observed that the column flange did not yield, but deviation from a 1:1 response demonstrates the torsional demand imposed on the column due to the lateral-torsional buckling of the beam.
- Figure 4.89 shows the shear strain response of the panel zone. The panel zone saw significant hysteretic behavior with strains on the order of $6\gamma_y$. Yielding of the panel zone was expected; using the post-elastic panel zone strength results in a DCR of 0.88.
- Modest continuity plate axial yielding ($2\epsilon_y$) was observed at the edge attaching the plate to the column flange (see Figure 4.90). Shear response, as predicted from

equilibrium, is observed in the plate (see Figure 4.91). The principal strain response at the outboard edge of the continuity plate shows cyclic strains limited to $2\epsilon_y$.

- The shear response of the continuity plate attachment to the web of the column shows nearly a uniform response (see Figure 4.93).
- Figure 4.94 shows the response of the outboard edge of the continuity plate. The response conforming to the 1:1 line (shown in red) demonstrates that the continuity plate was loaded axially and did not experience any out of plane flexure.

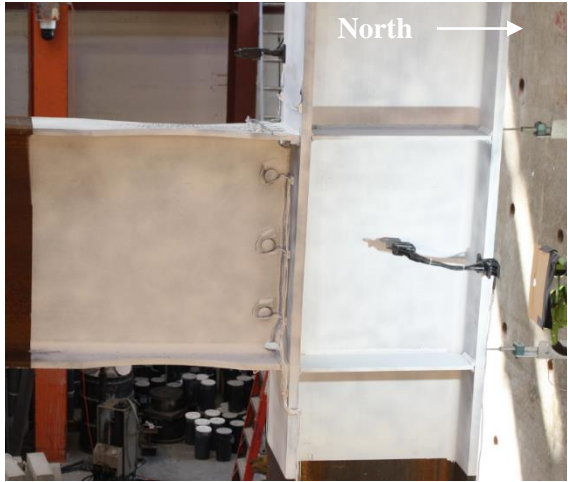


(a) West Side



(b) East Side

Figure 4.70 Specimen C6: Specimen before Testing



(a) +0.03 rad (2nd Cycle)



(b) -0.03 rad (2nd Cycle)



(c) +0.04 rad (2nd Cycle)



(d) -0.04 rad (2nd Cycle)



(e) +0.05 rad (1st Cycle)



(f) -0.05 rad (1st Cycle)

Figure 4.71 Specimen C6: East Side of Connection



(a) -0.03 rad (1st Cycle)



(b) -0.03 rad (2nd Cycle)



(c) -0.04 rad (1st Cycle)



(d) -0.04 rad (2nd Cycle)

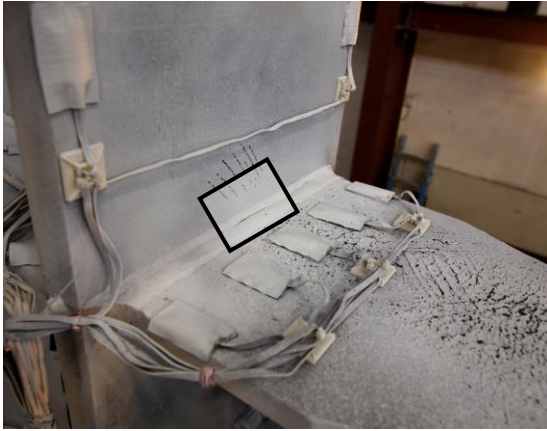


(e) -0.037 rad (1st Cycle of 0.05 rad)

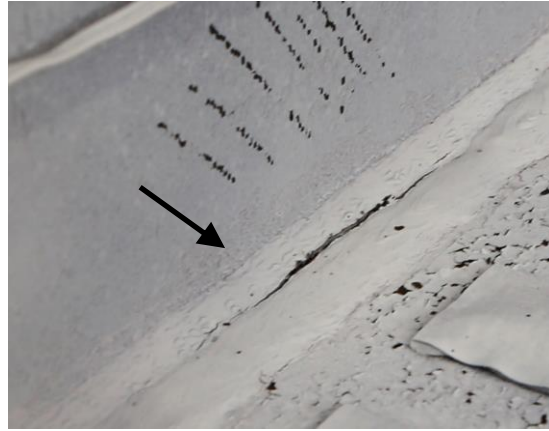


(f) -0.05 rad (1st Cycle)

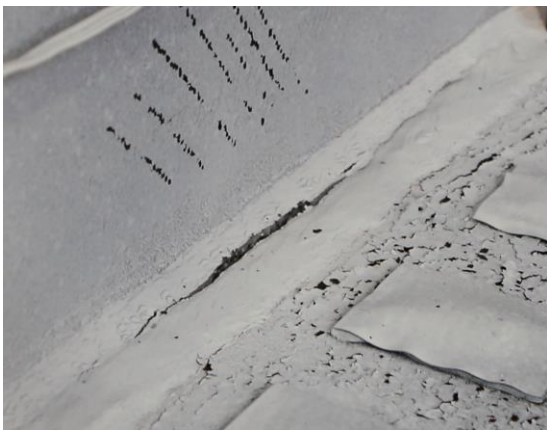
Figure 4.72 Specimen C6: Beam Top Flange



(a) Overview



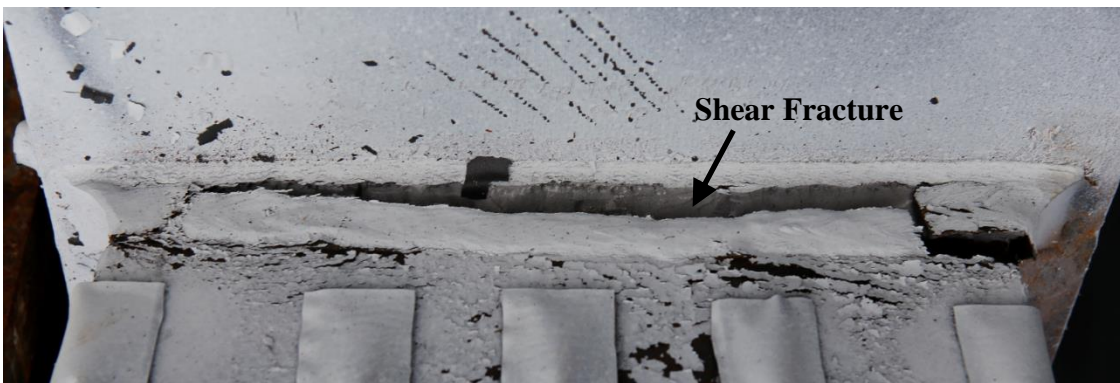
(b) -0.03 rad (2nd Cycle)



(c) -0.04 rad (1st Cycle)

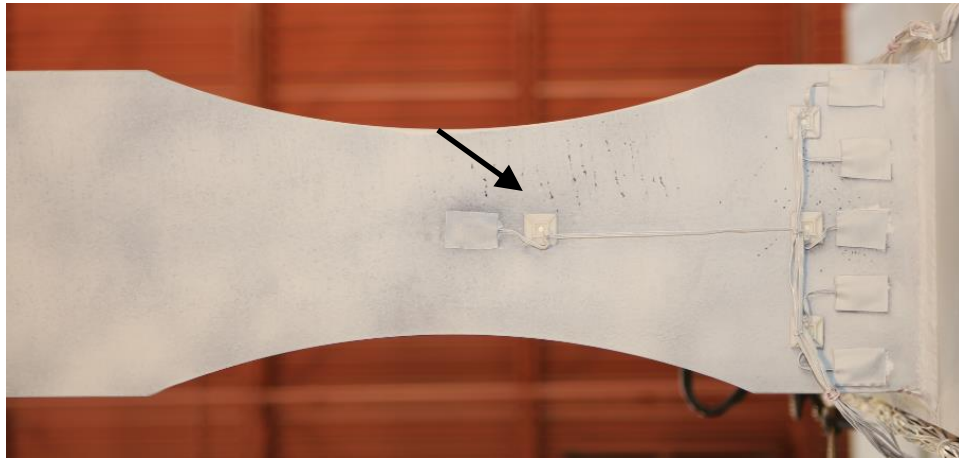


(d) -0.04 rad (2nd Cycle)

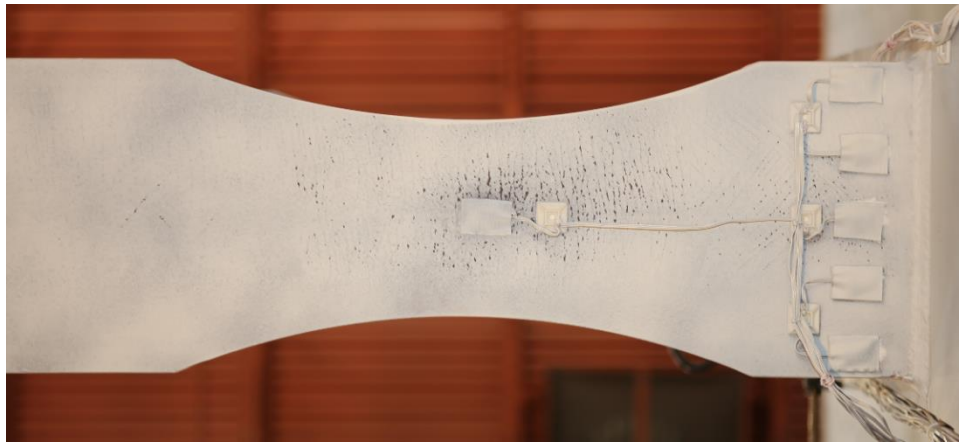


(e) Fracture (End of Test)

Figure 4.73 Specimen C6: Beam Top Flange CJP Weld Fracture Progression



(a) -0.01 rad (4th Cycle)

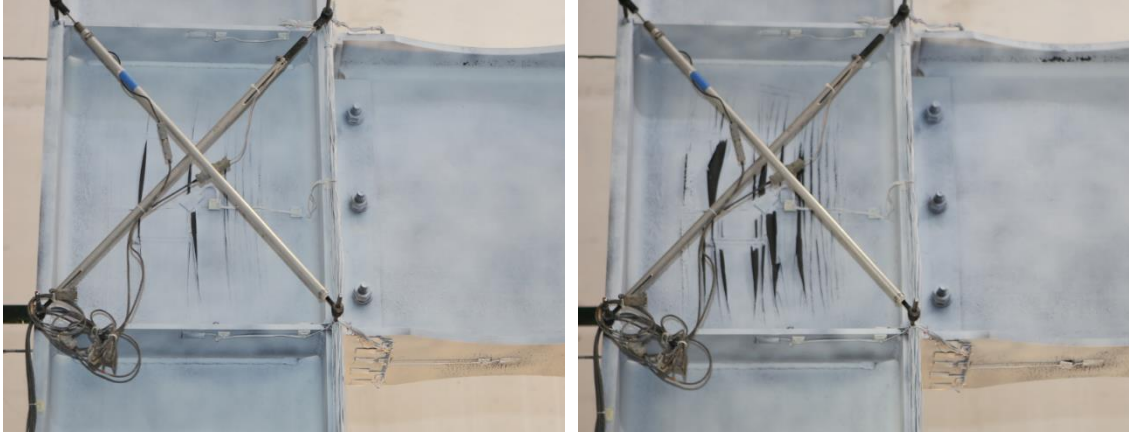


(b) -0.02 rad (2nd Cycle)



(c) +0.04 rad (2nd Cycle)

Figure 4.74 Specimen C6: Beam Bottom Flange Yielding



(a) +0.02 rad (2nd Cycle)

(a) +0.03 rad (2nd Cycle)

Figure 4.75 Specimen C6: Panel Zone Yielding



Figure 4.76 Specimen C6: Beam Web and Flange Local Buckling at +0.04 rad (2nd Cycle)



(a) West Side



(b) East Side

Figure 4.77 Specimen C6: Connection at End of Test



(a) West Bottom Flange Continuity Plate



(b) East Top Flange Continuity Plate



(c) West Top Flange Continuity Plate

Figure 4.78 Specimen C6: Continuity Plate (End of Test)

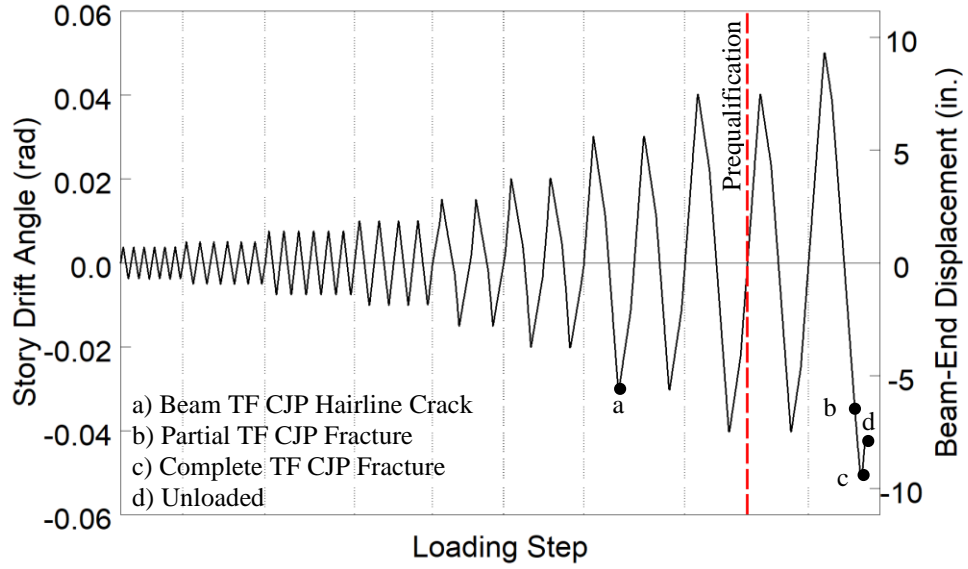


Figure 4.79 Specimen C6: Recorded Loading Sequence

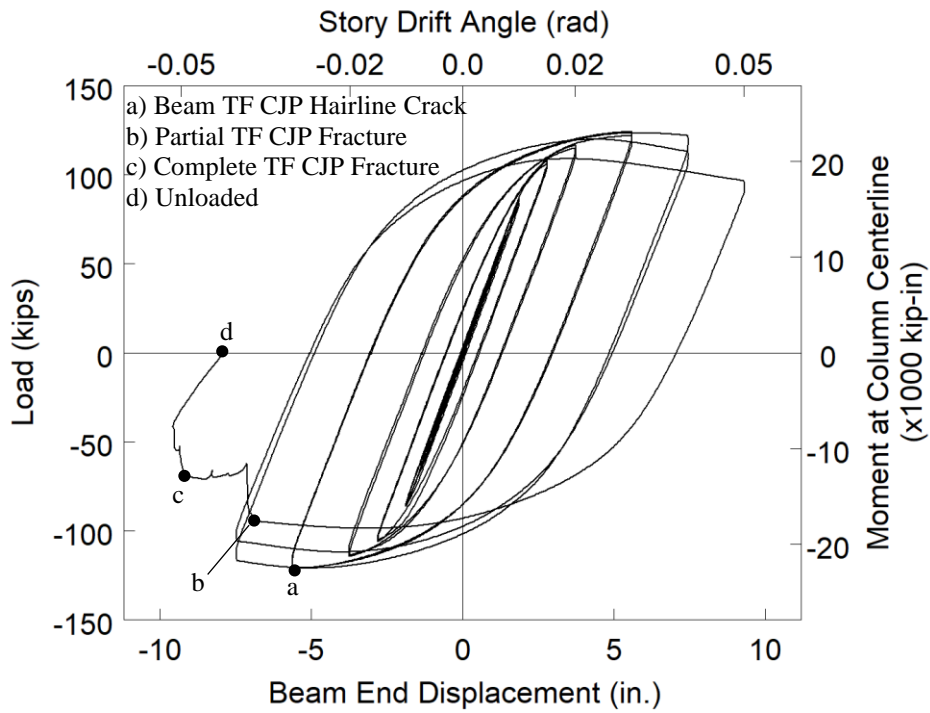


Figure 4.80 Specimen C6: Applied Load versus Beam End Displacement Response

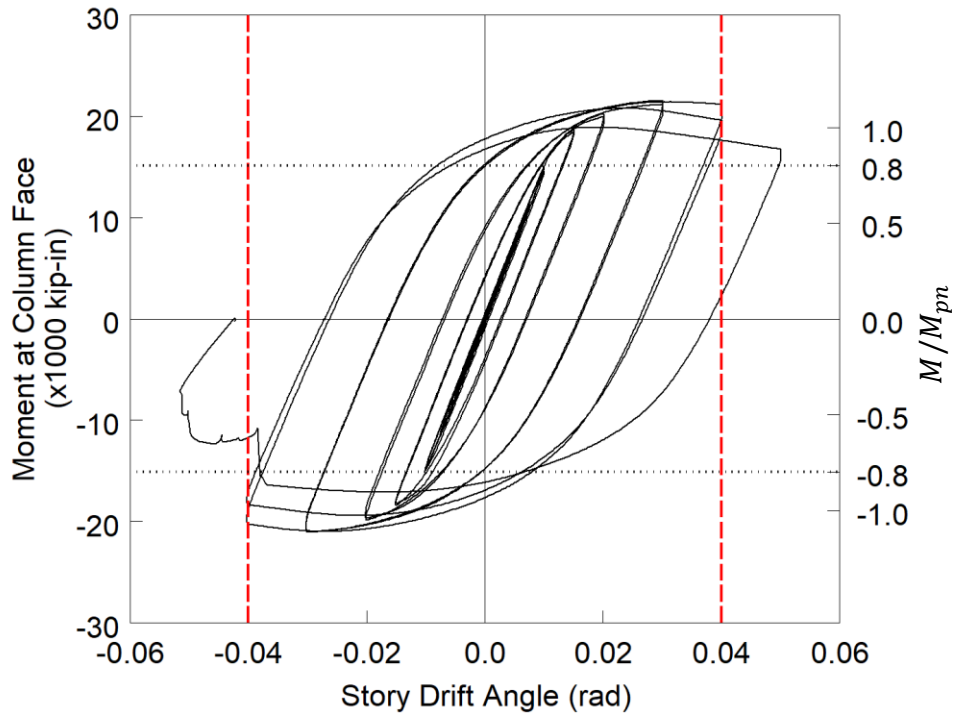


Figure 4.81 Specimen C6: Moment at Column Face versus Story Drift Response

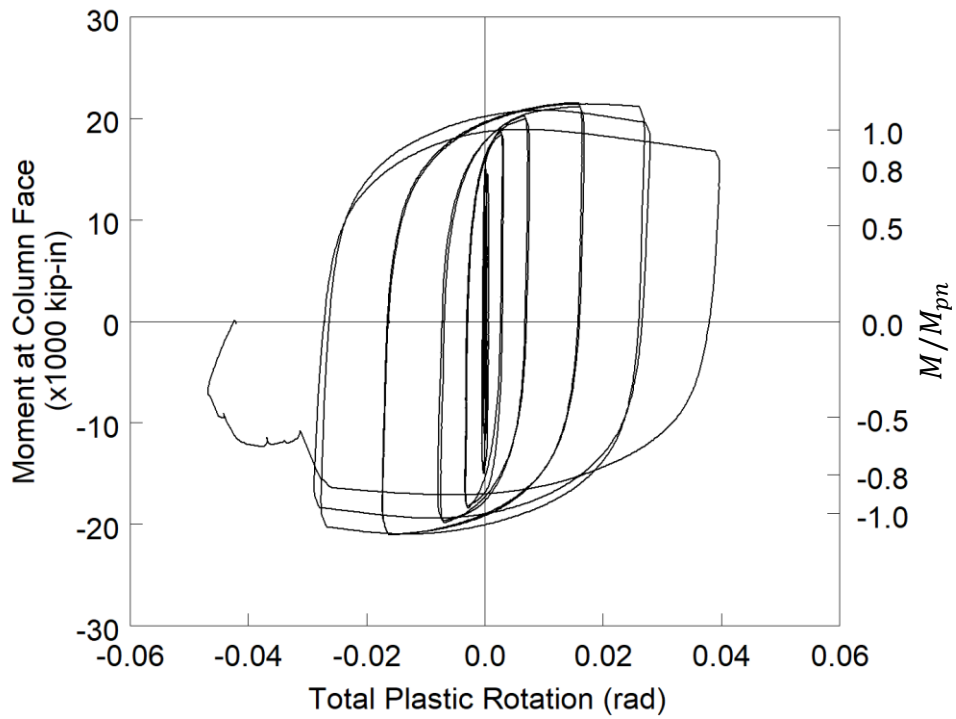


Figure 4.82 Specimen C6: Moment at Column Face versus Plastic Rotation

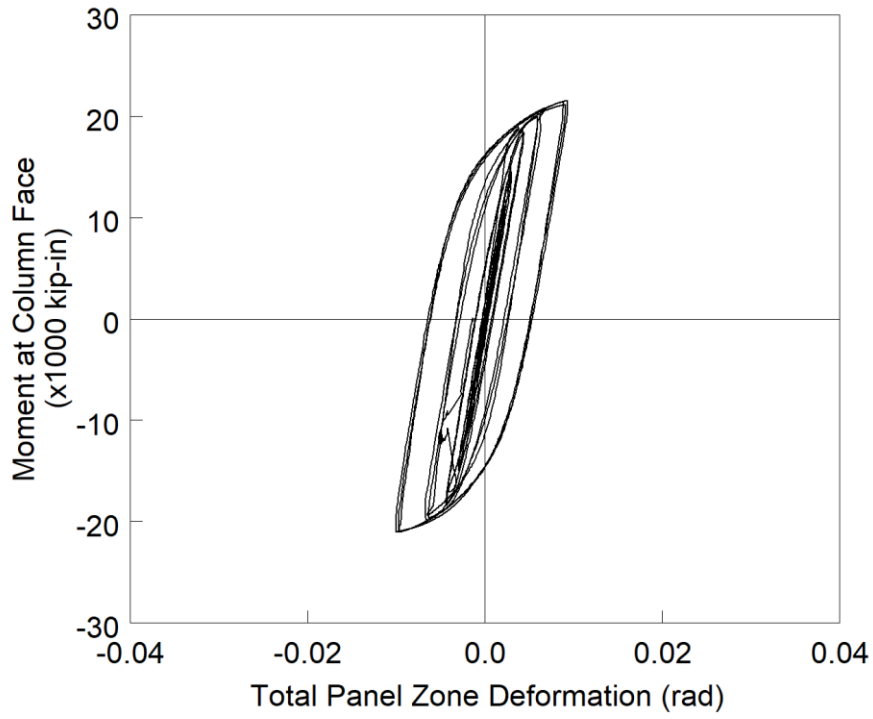


Figure 4.83 Specimen C6: Panel Zone Shear Deformation

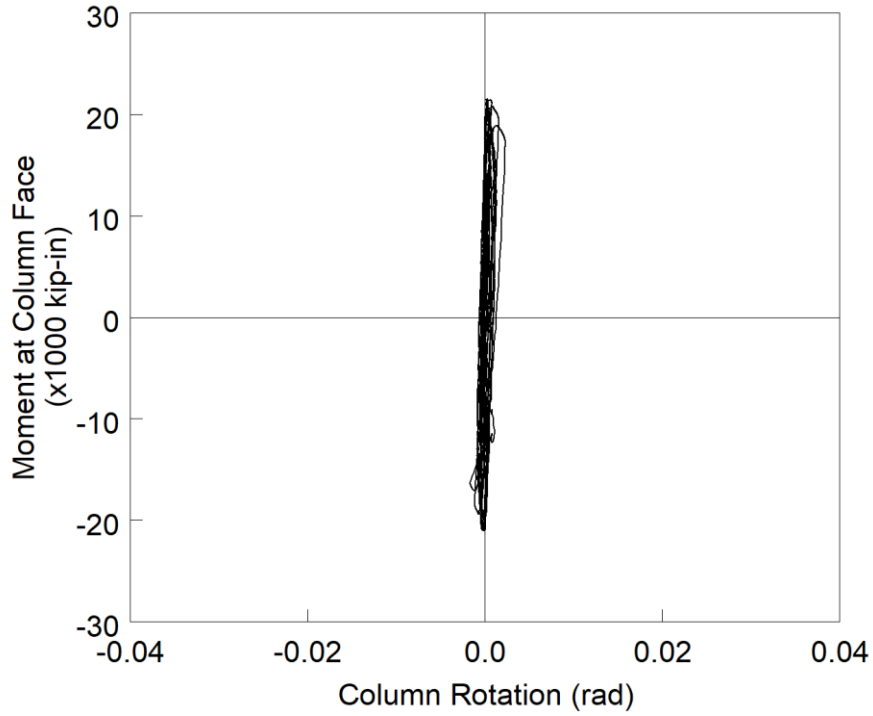


Figure 4.84 Specimen C6: Column Rotation

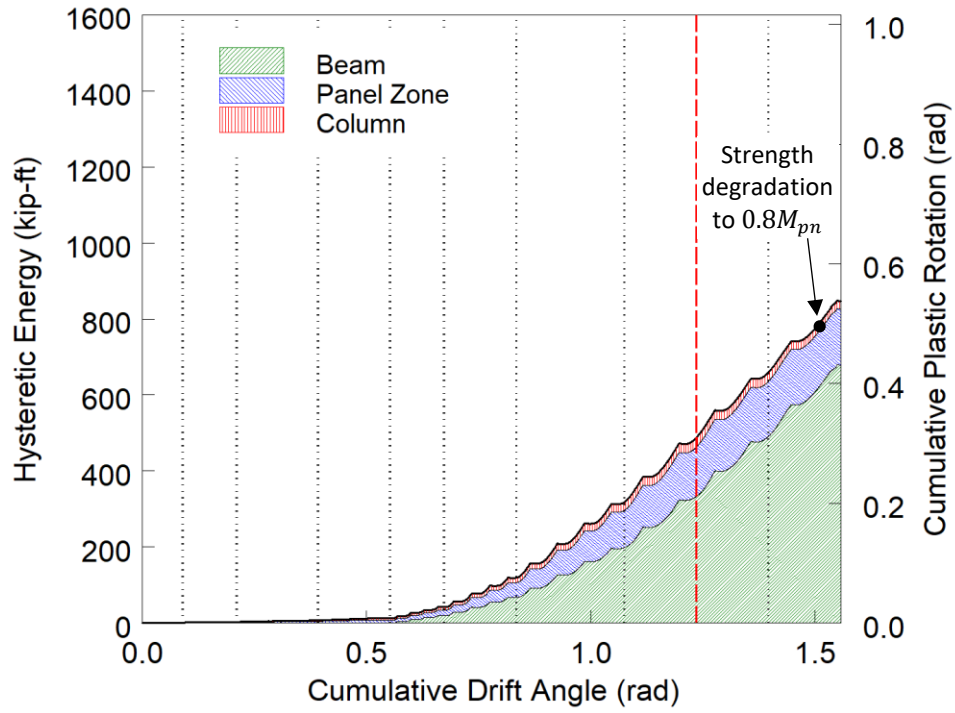
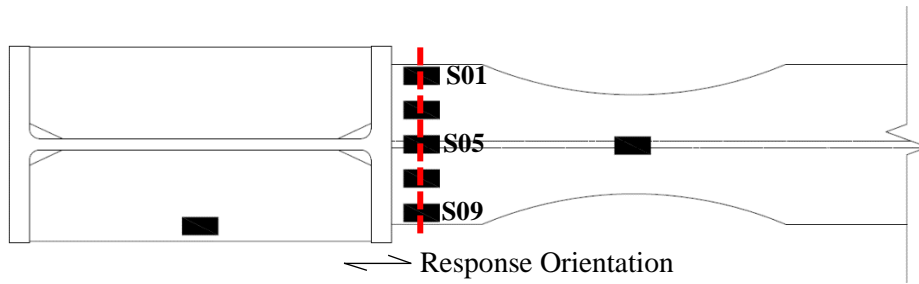
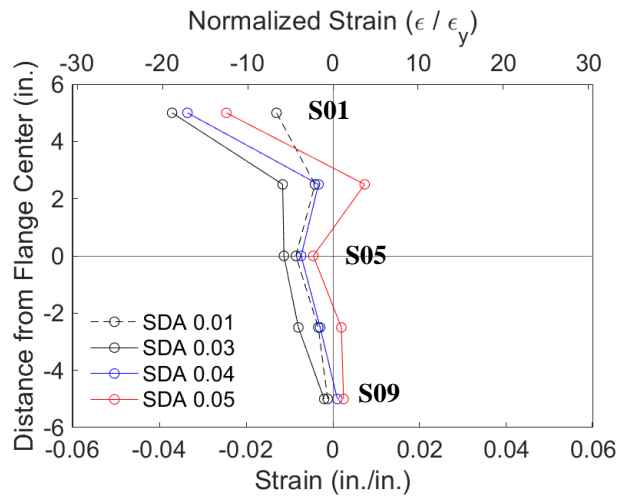


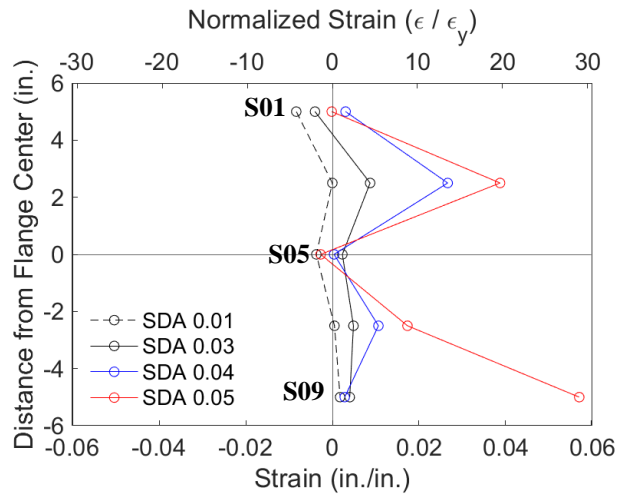
Figure 4.85 Specimen C6: Energy Dissipation



(a) Section

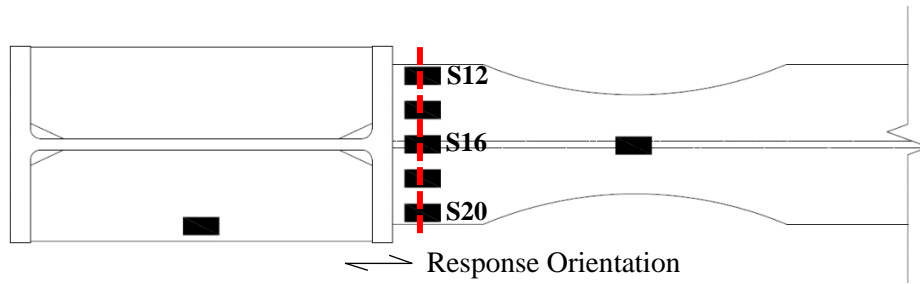


(b) Positive Drift

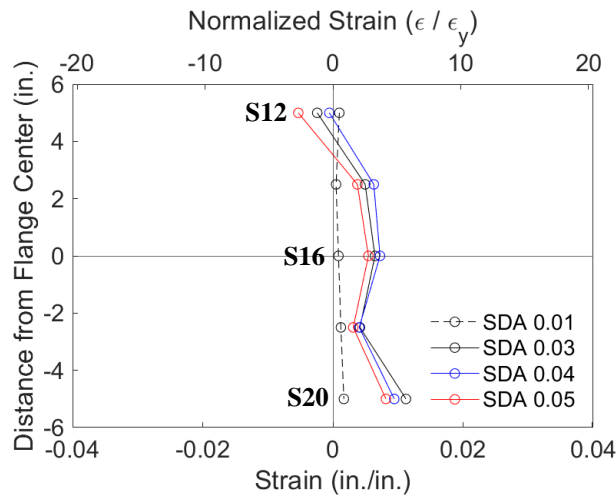


(c) Negative Drift

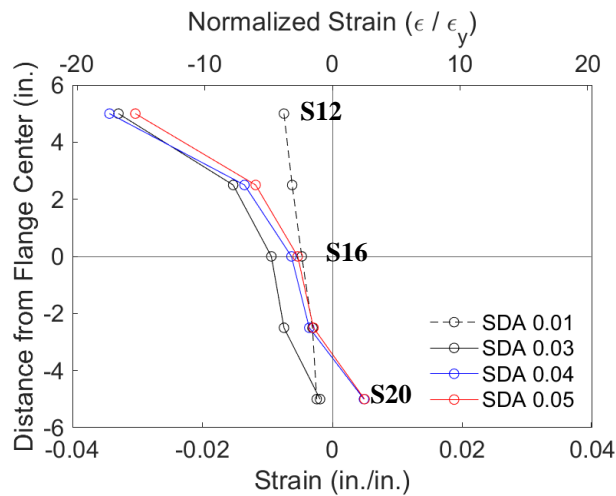
Figure 4.86 Specimen C6: Topside of Beam Top Flange Strain Profile



(a) Section

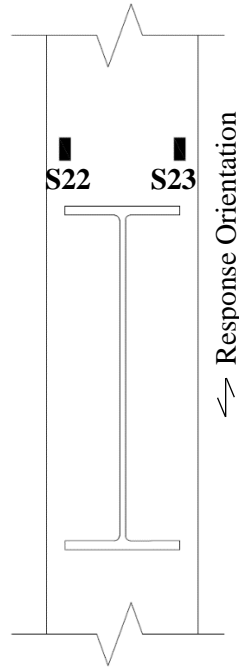


(b) Positive Drift

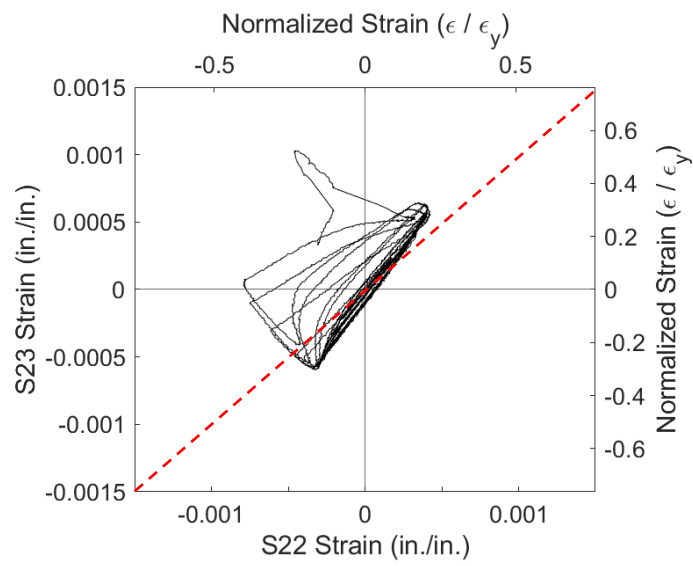


(c) Negative Drift

Figure 4.87 Specimen C6: Underside of Beam Bottom Flange Strain Profile

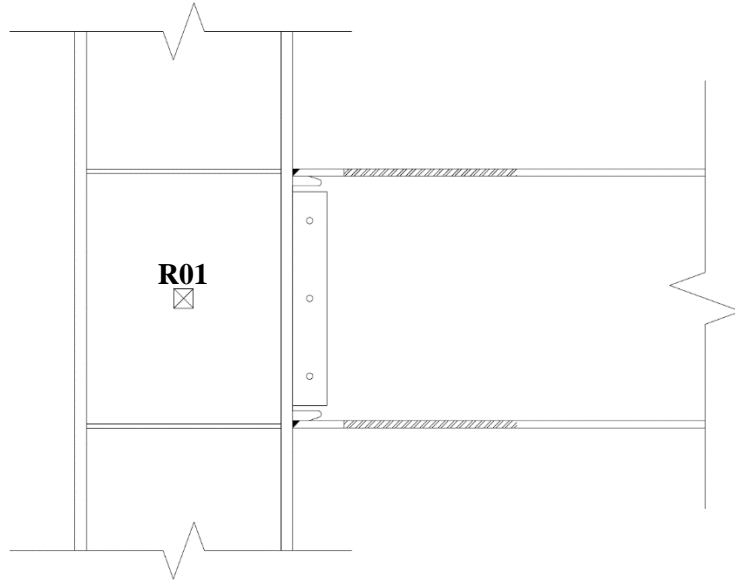


(a) Gauge Layout

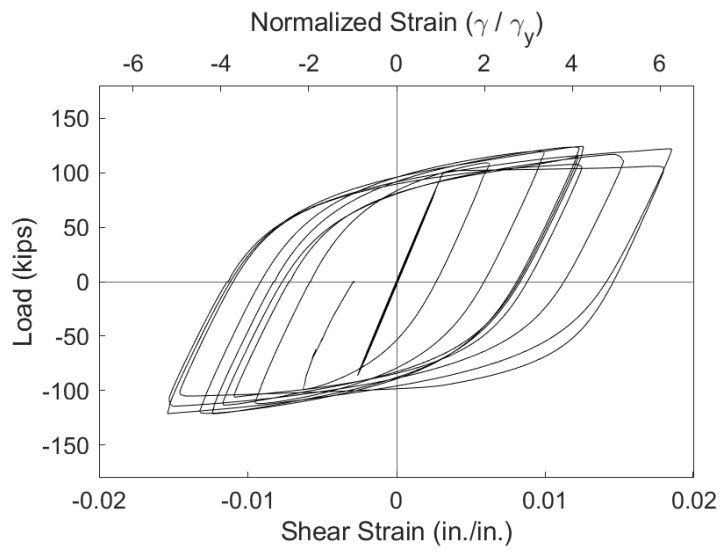


(b) Response

Figure 4.88 Specimen C6: Column Flange Warping

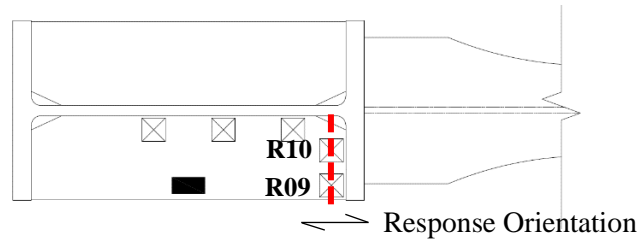


(a) Gauge Layout

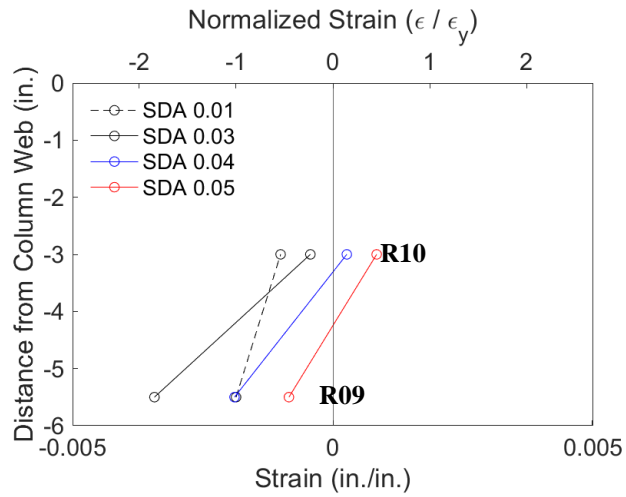


(b) Strain Rosette Gauge R01

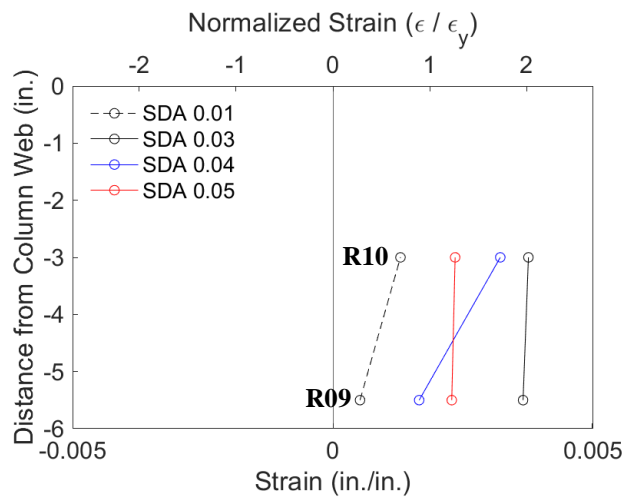
Figure 4.89 Specimen C6: Panel Zone Response



(a) Section

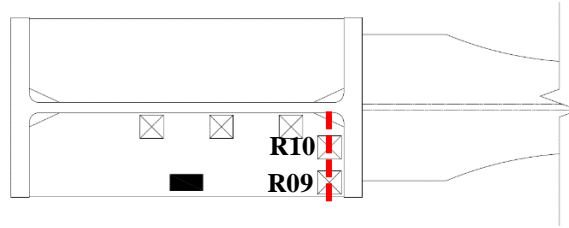


(b) Positive Drift

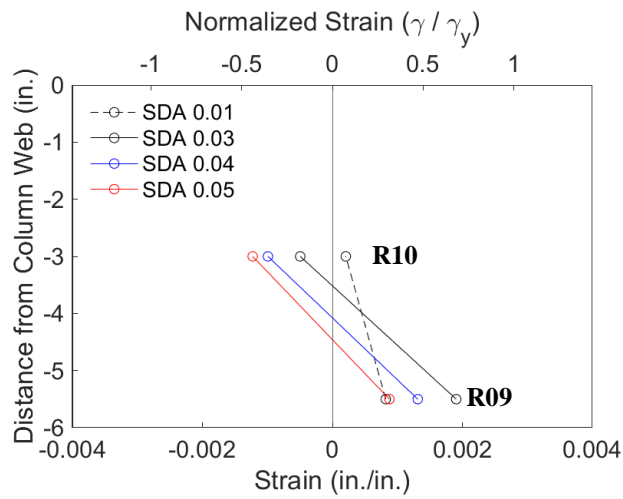


(c) Negative Drift

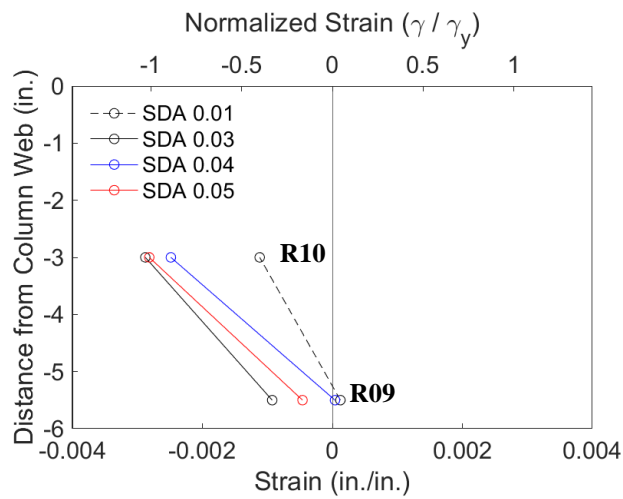
Figure 4.90 Specimen C6: Continuity Plate at Column Flange Edge Strain Profile



(a) Section

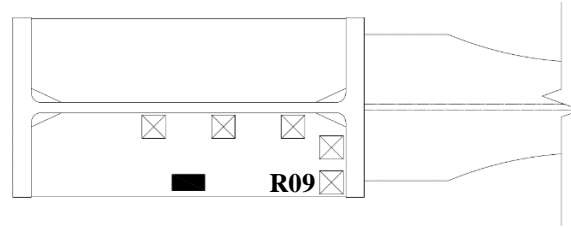


(b) Positive Drift

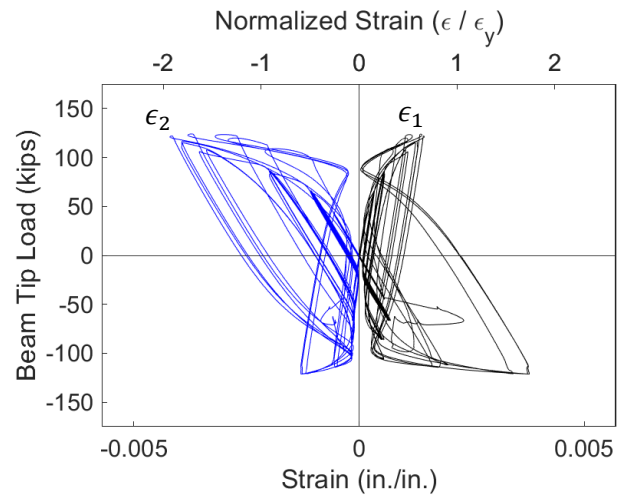


(c) Negative Drift

Figure 4.91 Specimen C6: Continuity Plate at Column Flange Edge Shear Strain Profile

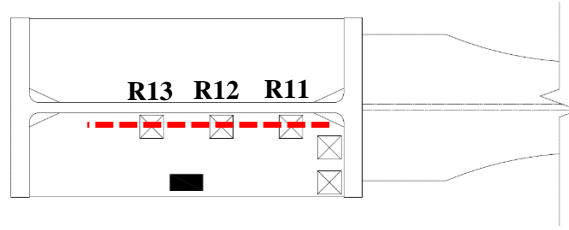


(a) Layout

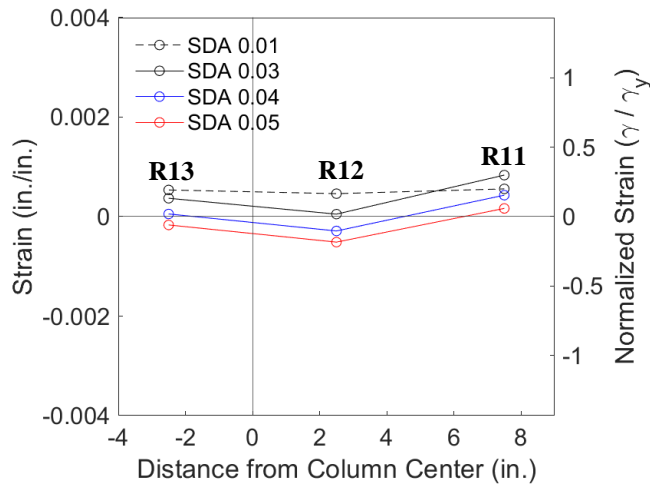


(b) Principal Strains

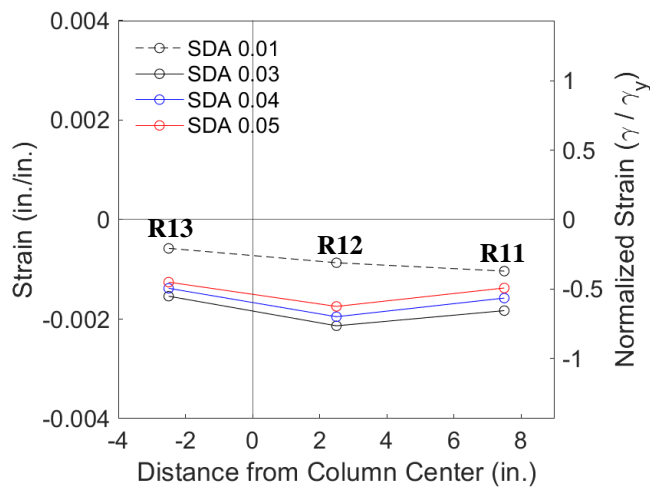
Figure 4.92 Specimen C6: Continuity Plate Strain Gauge Rosette R09 Response



(a) Section

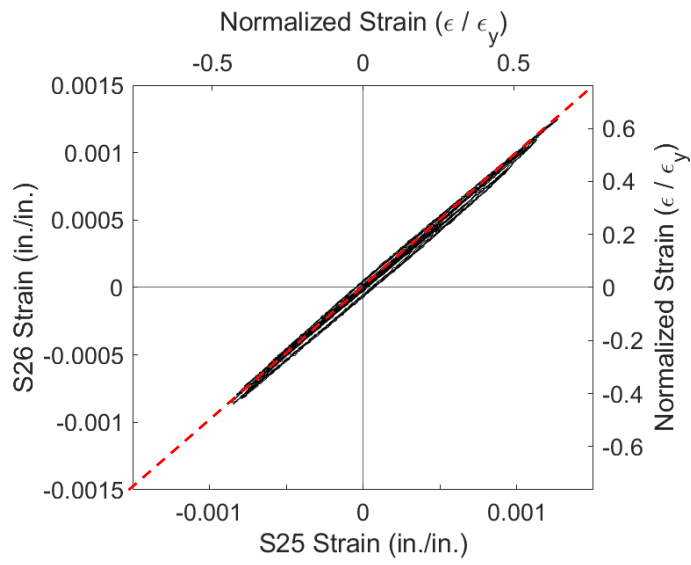
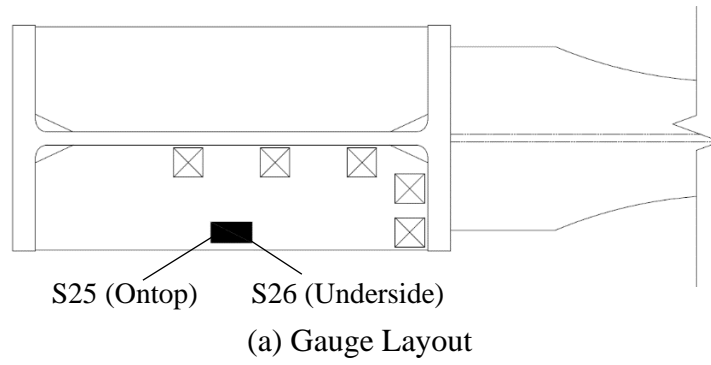


(b) Positive Drift



(c) Negative Drift

Figure 4.93 Specimen C6: Continuity Plate at Column Web Edge Shear Strain Profile



(b) Response

Figure 4.94 Specimen C6: Bottom Continuity Plate Bending

4.6 Specimen C6-G

4.6.1 General

Specimen C6-G was nominally identical to Specimen C6 except that the specimen was hot-dip galvanized prior to welding such that the effects of galvanization can be investigated. Figure 4.95 shows the specimen before testing. The specimen suffered a complete beam top flange fracture during the negative excursion of the first 0.05 rad drift.

4.6.2 Observed Performance

The observed response for Specimen C6-G is described below.

- Figure 4.96 shows the east side of the specimen at the peak excursions during the later cycles of the loading protocol. The specimen met the AISC acceptance criteria. It was observed that beam web buckling initiated during the first cycle of 0.04 rad drift. Flange local buckling initiated at the beam bottom flange within the RBS cut during the first cycle of 0.04 rad drift.
- Figure 4.97 shows cracking in the galvanization coating that first occurred at the RBS location during the second cycle of 0.02 rad drift. Once the cracked coating was brushed the bare pickled steel was left before the surface.
- A hairline crack was observed at the beam top flange CJP weld at the negative excursion of 0.03 rad drift (see Figure 4.98). This crack did not progress significantly during testing [see Figure 4.98(c)].
- Figure 4.99 shows the initiation of flange local buckling during the first negative excursion of 0.04 rad drift. Also demonstrated in this figure was flaking of the galvanization in the beam web in the regions of higher curvature due to beam web buckling. The shedding of the galvanization in sheets during yielding was observed in Figure 4.99(b).
- Beam web buckling was first observed during the 0.04 rad cycles. During the second cycle at -0.05 rad drift web buckling was pronounced and interacting with beam lateral-torsional buckling to create a step in the web (see Figure 4.100).
- During the first negative excursion of 0.06 rad drift the beam web k-area fractured in a region of high local curvature due to beam web buckling (see Figure 4.101). This fracture propagated to the top surface of the beam top flange [see Figure 4.101(c)]. The remainder of the top flange fractured once the negative excursion was resumed

(see Figure 4.102). The surface of the fracture reveals that the partial fracture consisted of mainly cleavage fracture. Shear fracture dominated the secondary fracture which completed separation of the flange.

- Figure 4.103 shows the east side of the specimen at the end of testing. No damage was observed to the continuity plate fillet welds at the end of testing (see Figure 4.104).

4.6.3 Recorded Response

4.6.3.1 Global Response

- Figure 4.105 shows the recorded displacement response of the beam tip measured with transducer L1. At 0.036 rad drift during the first negative excursion of 0.06 rad drift a partial fracture occurred in the k-area of the beam top flange. This fracture extended outward to the top surface of the beam top flange. Upon resuming negative excursion, the remainder of the top flange ruptured at 0.018 rad drift.
- Figure 4.106 shows the load-displacement response of the beam.
- Figure 4.107 shows the computed moment at the column face (M_f) versus the story drift angle. Two horizontal axes at 80% of the nominal plastic moment (M_{pn}) of the beam section are also added. In addition, two vertical axes at ± 0.04 rad story drift show the drift required for SMF connections per AISC 341. It is observed that the beam developed 1.1 times its nominal plastic bending moment. If the moment is computed at the plastic hinge location and compared to the expected plastic moment, then the peak connection strength factor (C_{pr}) is 1.18.
- Figure 4.108 shows the plastic response of the specimen. The plastic response is computed using the procedure outlined in Section 3.7. The computed elastic stiffness of the specimen was determined to be 46.9 kips/in.
- Figure 4.109 shows modest inelastic behavior of the panel zone.
- Figure 4.110 shows that minimal hysteretic behavior was observed in the column rotation.
- Figure 4.111 shows the dissipated energy of Specimen C6-G. Dotted vertical lines on the graph demonstrate the completion of each group of cycles, and the dashed red vertical line shows the completion of the first cycle of 0.04 rad in the AISC loading.

It is observed that the completion of the first drift cycle of 0.04 rad (the requirement for SMF connections per AISC 341) occurs after 492 kip-ft of energy has been dissipated. The connection did not degrade below $0.8M_{pn}$ until 1,104 kip-ft of energy had been dissipated. Therefore only 44% of the energy dissipation capacity was utilized after the completion of SMF requirement. It is observed that most (90%) of the energy dissipation capacity occurred in the beam.

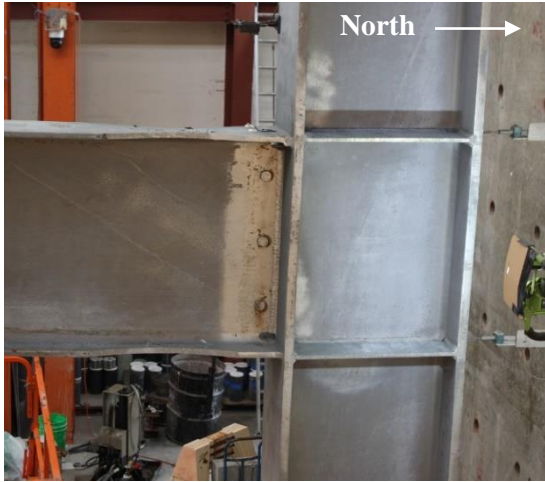


(a) West Side



(b) East Side

Figure 4.95 Specimen C6-G: Specimen before Testing



(a) +0.03 rad (2nd Cycle)



(b) -0.03 rad (2nd Cycle)



(c) +0.04 rad (2nd Cycle)



(d) -0.04 rad (2nd Cycle)



(e) +0.05 rad (1st Cycle)



(f) -0.05 rad (1st Cycle)

Figure 4.96 Specimen C6-G: East Side of Connection



Figure 4.97 Specimen C6-G: Cracks in Galvanization Coating



(a) Overview



(b) -0.03 rad (1st Cycle)



(c) End of Test

Figure 4.98 Specimen C6-G: Hairline Crack at Beam Top Flange CJP Weld



(a) -0.04 rad (1st Cycle)

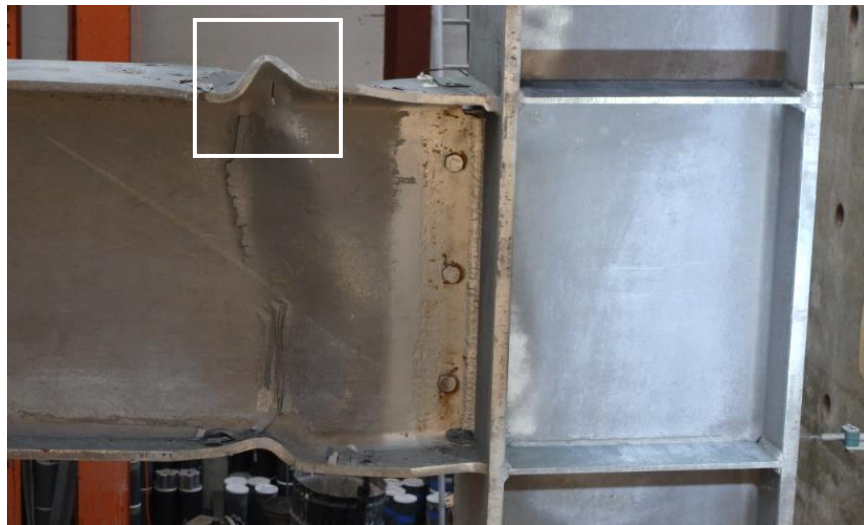


(b) -0.04 rad (2nd Cycle)

Figure 4.99 Specimen C6-G: Flange Local Buckling



Figure 4.100 Specimen C6-G: Web Local Buckling



(a) Overview



(b) East Side

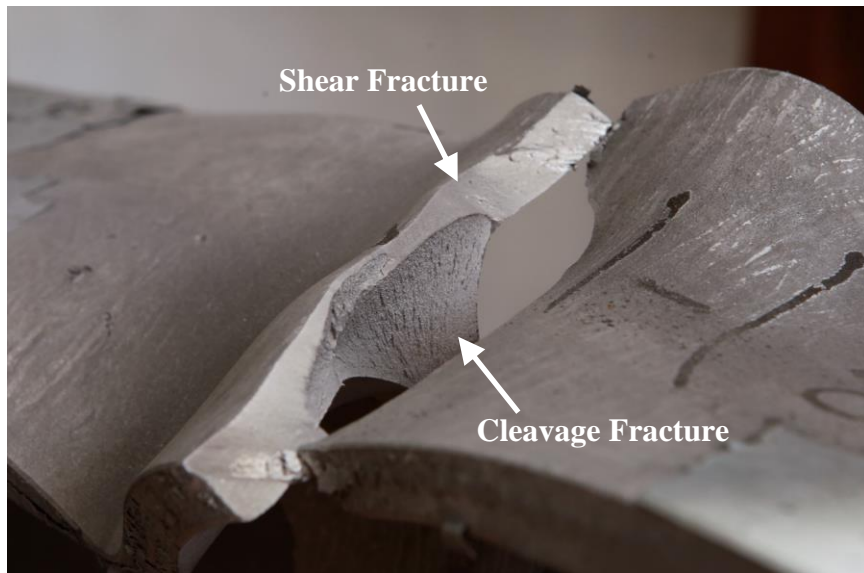


(c) Top Flange

Figure 4.101 Specimen C6-G: Beam Flange Partial Fracture at -0.06 rad (1st Cycle)



(a) West Side



(b) Fracture Surface

Figure 4.102 Specimen C6-G: Complete Beam Fracture at -0.06 rad (1st Cycle)

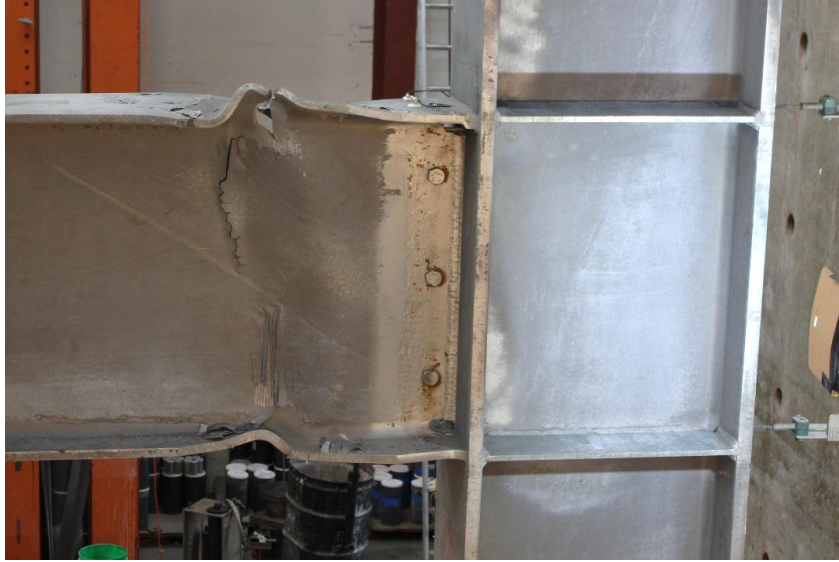


Figure 4.103 Specimen C6-G: East Side of Connection at End of Test



(a) West Top Flange



(b) East Top Flange

Figure 4.104 Specimen C6-G: Continuity Plate Welds at End of Test

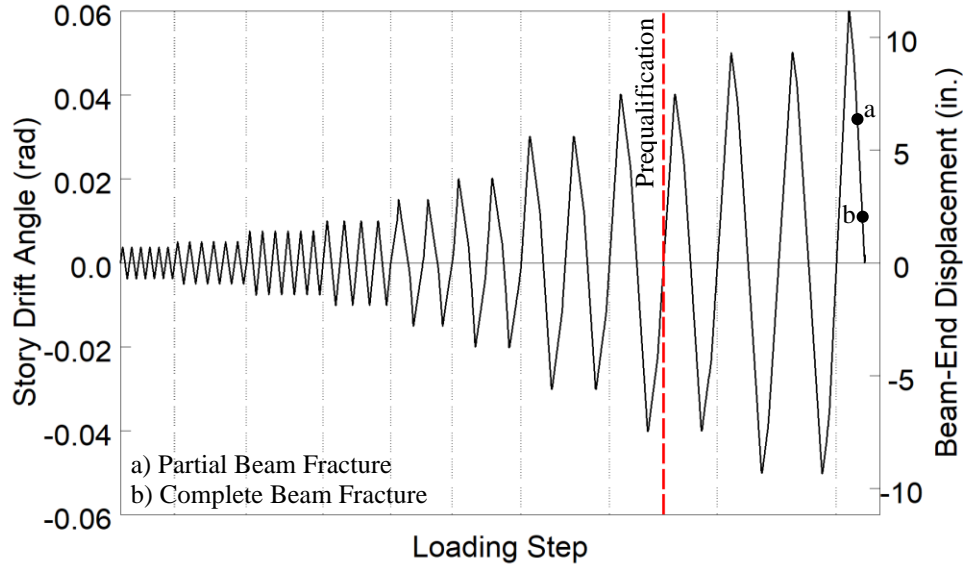


Figure 4.105 Specimen C6-G: Recorded Loading Sequence

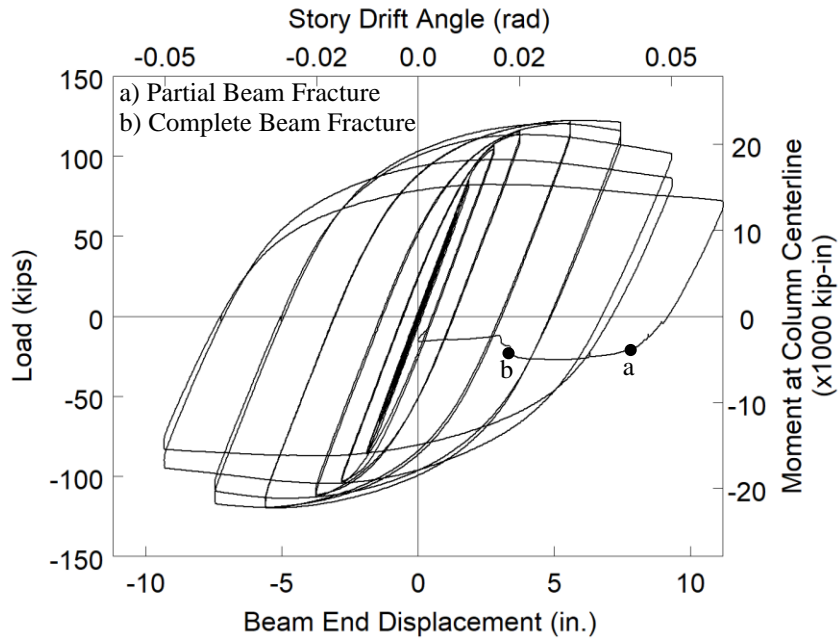


Figure 4.106 Specimen C6-G: Applied Load versus Beam End Displacement Response

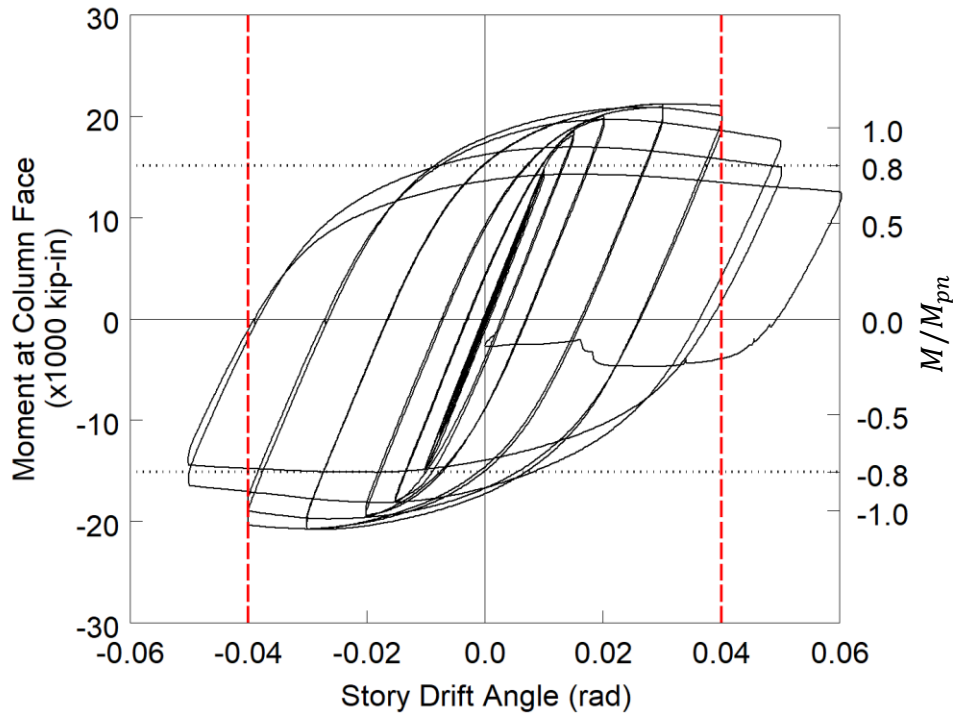


Figure 4.107 Specimen C6-G: Moment at Column Face versus Story Drift Response

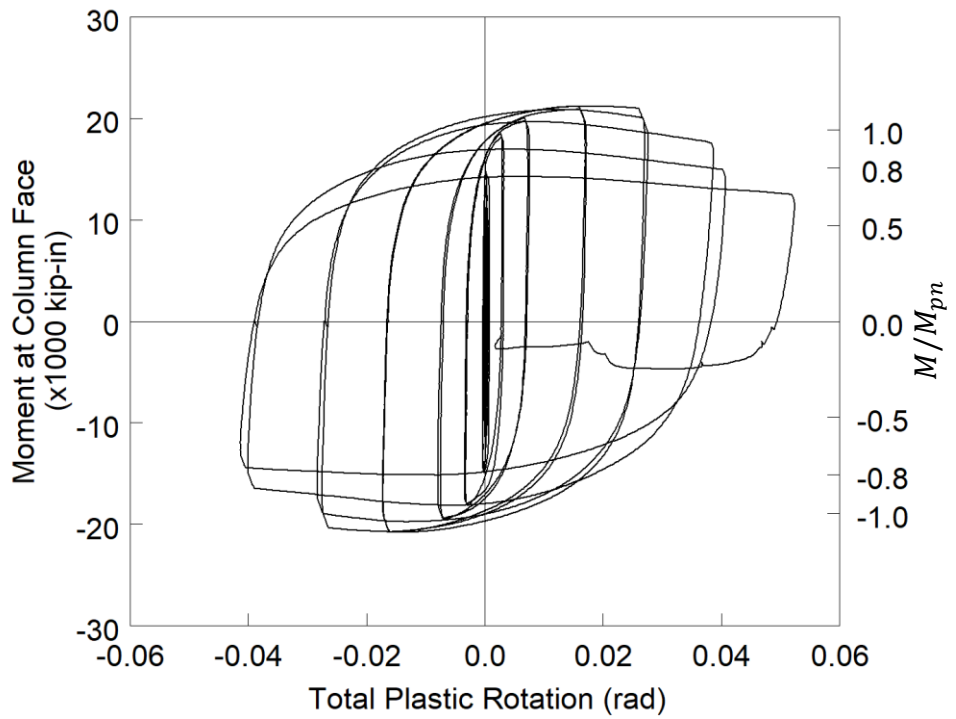


Figure 4.108 Specimen C6-G: Moment at Column Face versus Plastic Rotation

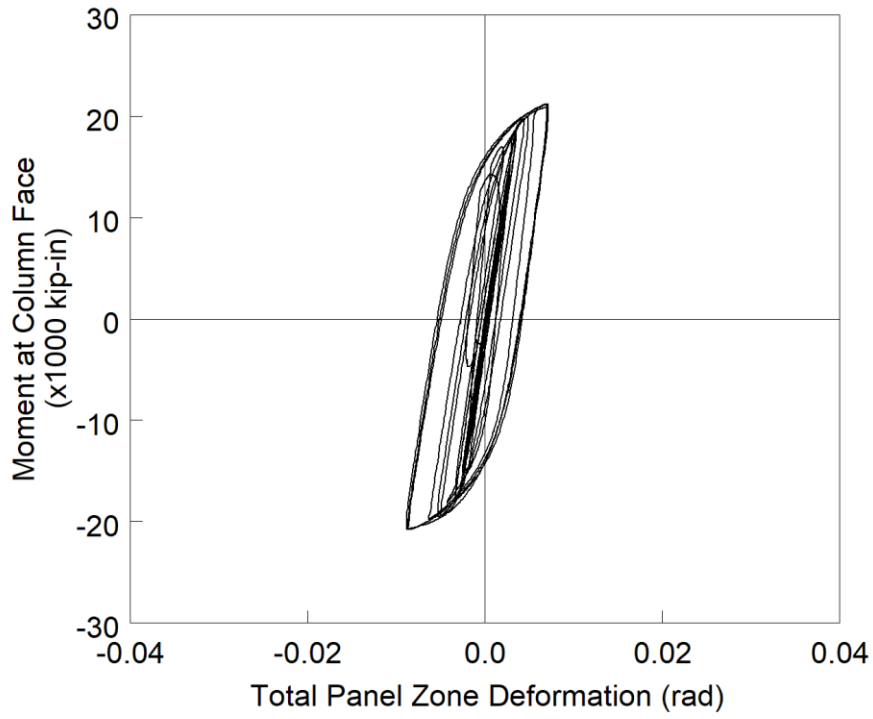


Figure 4.109 Specimen C6-G: Panel Zone Shear Deformation

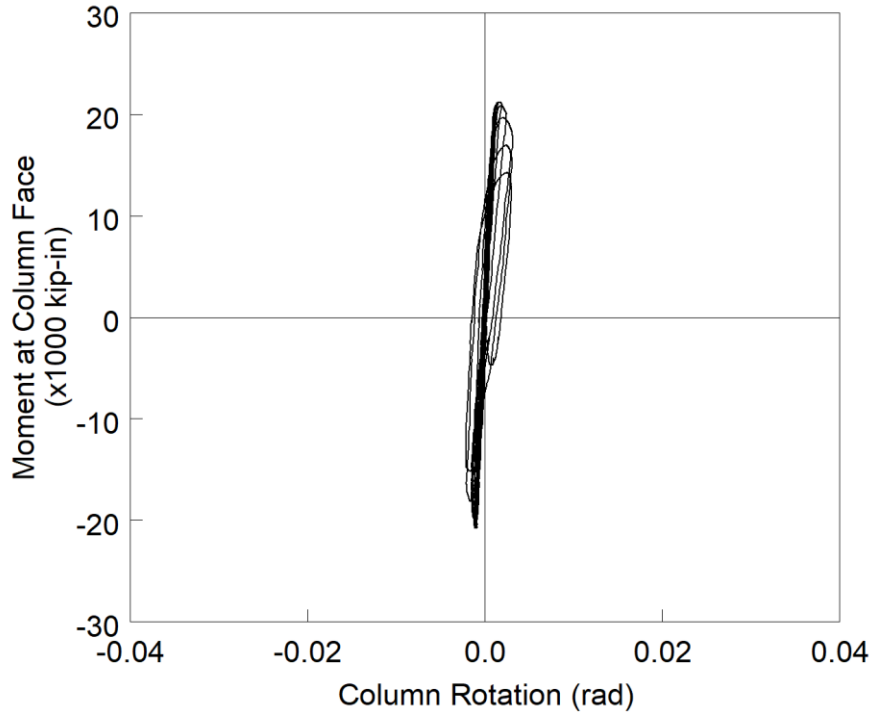


Figure 4.110 Specimen C6-G: Column Rotation

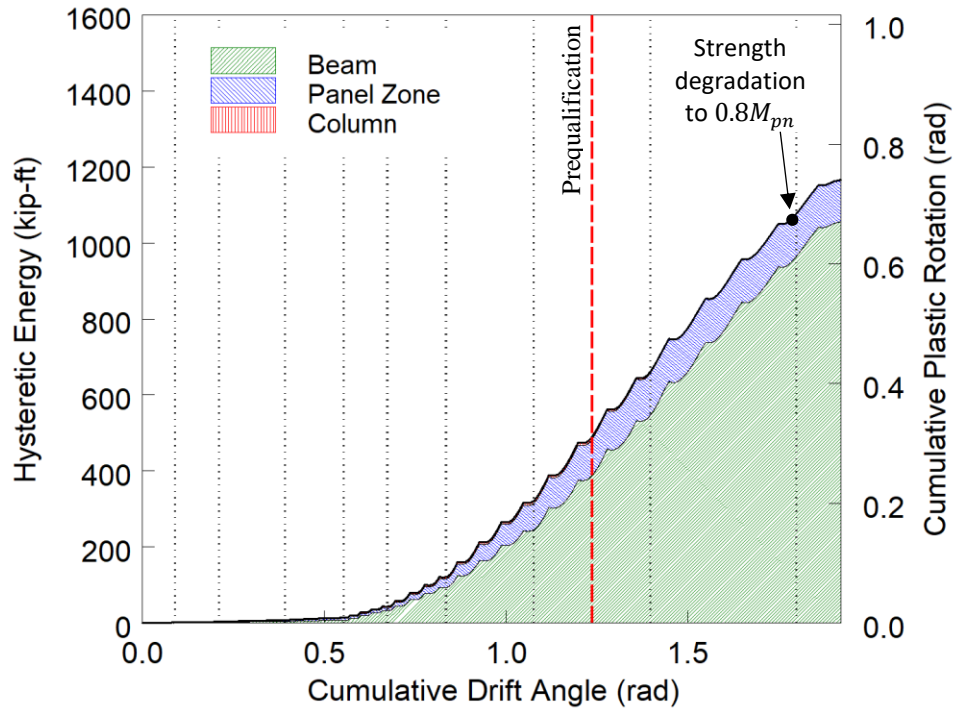


Figure 4.111 Specimen C6-G: Energy Dissipation

4.7 Specimen C7

4.7.1 General

Specimen C7 was designed to investigate the validity of using the plastic distribution to estimate the required strength of the continuity plate while violating the Lehigh Criterion. The continuity plates were designed to satisfy the governing AISC 360 §J10 concentrated force column limit state; WLY was the governing limit state that dictates the need of a continuity plate in this specimen. Instead of using a continuity plate to reinforce the column web, since it was found that the FLB limit state does not require reinforcement, a doubler plate was added to the east side of the specimen. The doubler plate was a minimum size such that the stability of the doubler plate was achieved without using plug welds within the doubler plate. The vertical welds fastening the doubler plate to the column were designed based on the distribution of shear force in the panel zone, which violates the current AISC 341 Provisions requiring vertical welds to develop the strength of the doubler plate. Horizontal welds were not used across the top and bottom edge of the extended doubler plate, which conforms to the current Provisions. Figure 4.112 shows the specimen before testing. The specimen developed a partial rupture of the beam bottom flange during the unloading portion of the second cycle of 0.05 rad drift; loading was not continued.

4.7.2 Observed Performance

The observed response for Specimen C7 is described below.

- Figure 4.113 shows the east side of the specimen at the peak excursions during the later cycles of the loading protocol. The specimen met the AISC acceptance criteria. It was observed that beam web buckling and beam flange local buckling both initiated during the first cycle of 0.04 rad drift. Flange local buckling initiated at the beam bottom flange within the RBS cut during the second cycle of 0.03 rad drift. Web local buckling started during the 0.03 rad drift cycles. The beam bottom flange developed a partial rupture during the unloading portion of the second cycle of 0.05 rad drift.
- Beam bottom flange yielding initiated at 0.005 rad drift cycles two inches from the column flange [see Figure 4.114(a)]. At 0.01 rad drift this yielding had spread outward and into the reduced beam section [see Figure 4.114(b)]. Figure 4.114(c) shows that the yielding had distributed through most of the reduced beam section by 0.04 rad drift. Similar yielding observations occurred on the beam top flange (see

Figure 4.115). By 0.02 rad drift the yielding had spread through the flange, showing yield lines on the underside of beam top flange (see Figure 4.116).

- Figure 4.117 shows web local yielding at the beam top flange location. The WLY was first observed at 0.02 rad drift and progressed slightly with each drift level. Figure 4.118 shows the WLY patterns at the end of testing. It was observed that the yielding was localized at the elevation just outside of the beam flange. Yielding was only observed on the side of the column which did not have a doubler plate.
- Web and flange local buckling started during the 0.03 rad drift cycles (see Figure 4.119). The flange local buckling continued to amplify during later cycles. A partial beam bottom flange occurred during the negative excursion of the second cycle of 0.05 rad.
- Figure 4.120 shows the condition of the connection at the end of testing.
- The partial beam flange tear was observed in Figure 4.121.
- The west side of the column demonstrated a yielding along a vertical line that runs the length of the beam web. This yield line was 2.5 in. from the beam web (see Figure 4.122).
- No damage was observed in the doubler plate fillet welds at the end of testing (see Figure 4.123).

4.7.3 Recorded Response

4.7.3.1 Global Response

- Figure 4.124 shows the recorded displacement response of the beam tip measured with transducer L1. The beam bottom flange partially fractured during the unloading portion of the second 0.05 rad drift cycles; loading was not continued after developing the partial fracture.
- Figure 4.125 shows the load-displacement response of the beam.
- Figure 4.126 shows the computed moment at the column face (M_f) versus the story drift angle. Two horizontal axes at 80% of the nominal plastic moment (M_{pn}) of the beam section are also added. In addition, two vertical axes at ± 0.04 rad story drift show the drift required for SMF connections per AISC 341. It is observed that the beam developed 1.1 times its nominal plastic bending moment. If the moment is

computed at the plastic hinge location and compared to the expected plastic moment, then the peak connection strength factor (C_{pr}) is 1.20.

- Figure 4.127 shows the plastic response of the specimen. The plastic response is computed using the procedure outlined in Section 3.7. The computed elastic stiffness of the specimen was determined to be 49.0 kips/in.
- Figure 4.128 shows negligible inelastic behavior of the panel zone. The black and blue lines are the measured panel zone deformations from the transducers placed on the column web and doubler plate, respectively. Little difference is observed between these two sides of the specimen.
- Figure 4.129 shows that negligible hysteretic behavior was observed in the column rotation.
- Figure 4.130 shows the dissipated energy of Specimen C7. Dotted vertical lines on the graph demonstrate the completion of each group of cycles, and the dashed red vertical line shows the completion of the first cycle of 0.04 rad in the AISC loading. It is observed that the completion of the first drift cycle of 0.04 rad (the requirement for SMF connections per AISC 341) occurs after 495 kip-ft of energy has been dissipated. The connection did not degrade below $0.8M_{pn}$ until 754 kip-ft of energy had been dissipated. Therefore only 65% of the energy dissipation capacity was utilized after the completion of SMF requirement. It is observed that most (93%) of the energy dissipation capacity occurred in the beam.

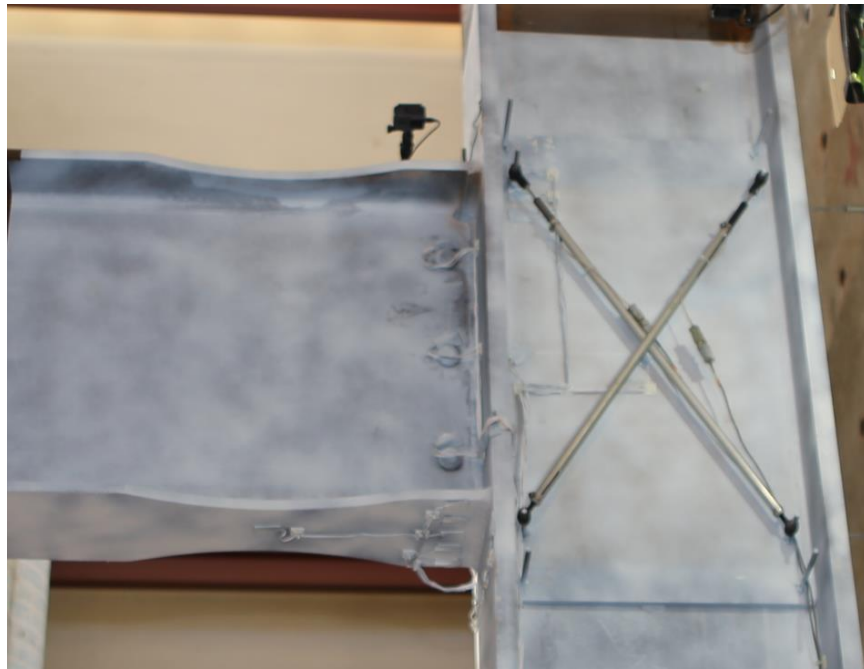
4.7.3.2 Local Response

- Figure 4.131 and Figure 4.132 show the strain gauge response from the extreme fiber of the beam top and beam bottom flange during the testing. Weak axis flexural response of the beam is observed across the flange consistent with the observed lateral-torsional buckling of the beam.
- Figure 4.133 shows the strain gauge response of the column flange which affixes the beam. It is observed that the column flange did not yield, but deviation from a 1:1 response demonstrates the torsional demand imposed on the column due to the lateral-torsional buckling of the beam.

- Figure 4.134 shows the shear strain response of the panel zone. Low levels of shear strain were anticipated due to the low utilization of the panel zone in resisting the panel zone shear ($DCR = 0.43$). A rosette placed on the doubler plate shows less shear response in the doubler plate than in the web.
- Figure 4.135 shows the response of the column directly behind the beam flange. Despite the doubler plate reinforcing, yielding level strains were reached in the column web for most of the width marked as $5k$. The strains between the column web and doubler plate are attributed to an out-of-plane flexural response due to warping of the column. The corresponding effect is more pronounced on the doubler plate side (Figure 4.136) due to the increased offset of the gauges from the axis of bending of the column web. Additionally, the fillet weld fastening the doubler plate the column flange is eccentric to the axis of the doubler plate, resulting in additional curvature.
- Figure 4.137 shows significant yielding of the column flange behind the beam flange. More strain is realized during the positive drift excursions, which is attributed to the lateral-torsional response of the beam.

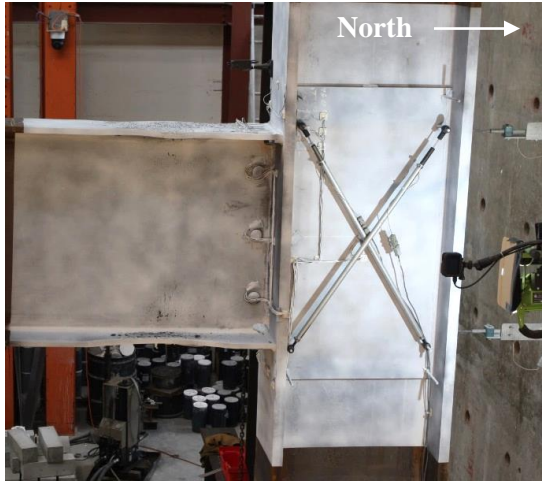


(a) West Side



(b) East Side

Figure 4.112 Specimen C7: Specimen before Testing



(a) +0.03 rad (2nd Cycle)



(b) -0.03 rad (2nd Cycle)



(c) +0.04 rad (2nd Cycle)



(d) -0.04 rad (2nd Cycle)

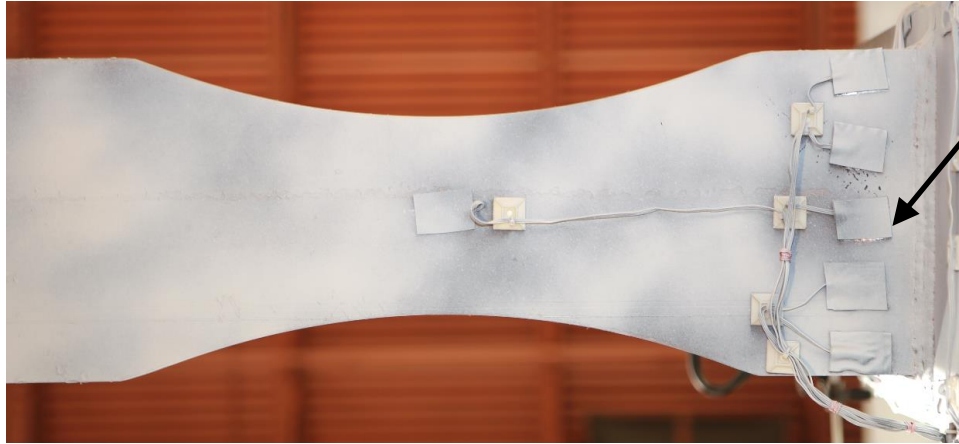


(e) +0.05 rad (1st Cycle)

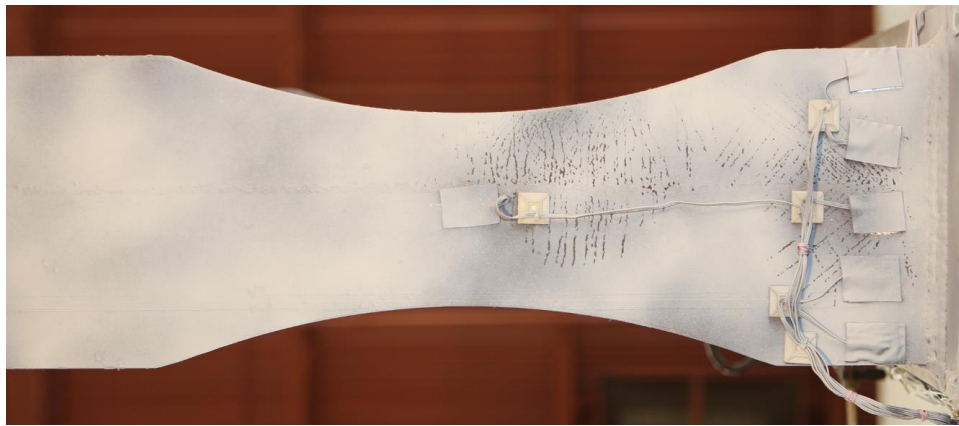


(f) -0.05 rad (1st Cycle)

Figure 4.113 Specimen C7: East Side of Connection



(a) -0.0005 rad (6th Cycle)



(b) -0.01 rad (2nd Cycle)



(c) +0.04 rad (1st Cycle)

Figure 4.114 Specimen C7: Beam Bottom Flange Yielding



Figure 4.115 Specimen C7: Beam Top Flange Yielding at -0.015 rad (2nd Cycle)

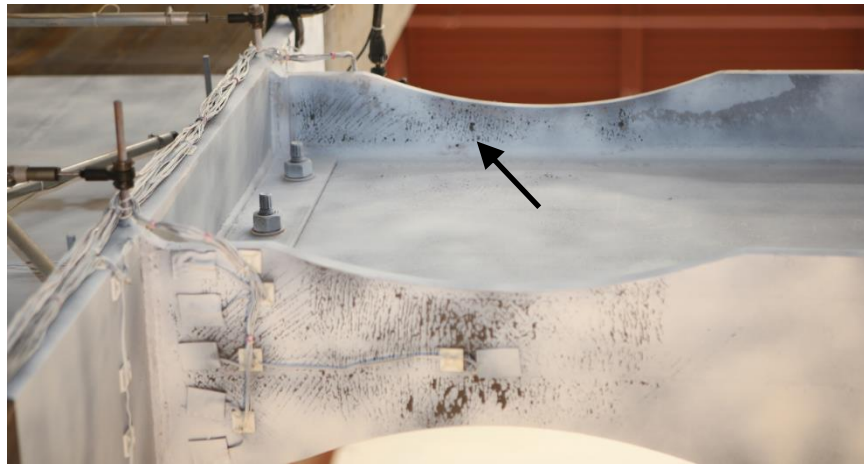


Figure 4.116 Specimen C7: Beam Top Flange Yielding at -0.02 rad (2nd Cycle)



(a) -0.03 rad (2nd Cycle)



(b) -0.04 rad (1st Cycle)

Figure 4.117 Specimen C7: Colum WLY at Beam Top Flange Level



(a) Beam Top Flange Level



(b) Beam Bottom Flange Level

Figure 4.118 Specimen C7: Colum WLY at End of Test



(a) -0.03 rad (1st Cycle)



(b) -0.04 rad (1st Cycle)

Figure 4.119 Specimen C7: Beam Flange Local Bucking



(a) West Side



(b) East Side

Figure 4.120 Specimen C7: Connection at End of Test



(a) Overview



(a) Fracture

Figure 4.121 Specimen C7: Beam Flange Partial Fracture



(a) Overview



(b) Column Yielding

Figure 4.122 Specimen C7: Column Yielding (End of Test)



Figure 4.123 Specimen C7: Doubler Plate at End of Test

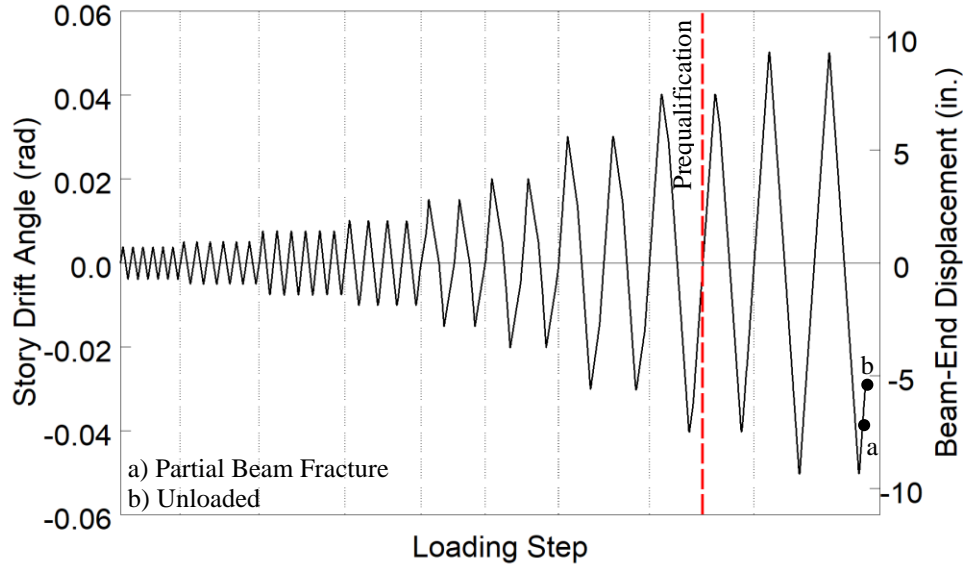


Figure 4.124 Specimen C7: Recorded Loading Sequence

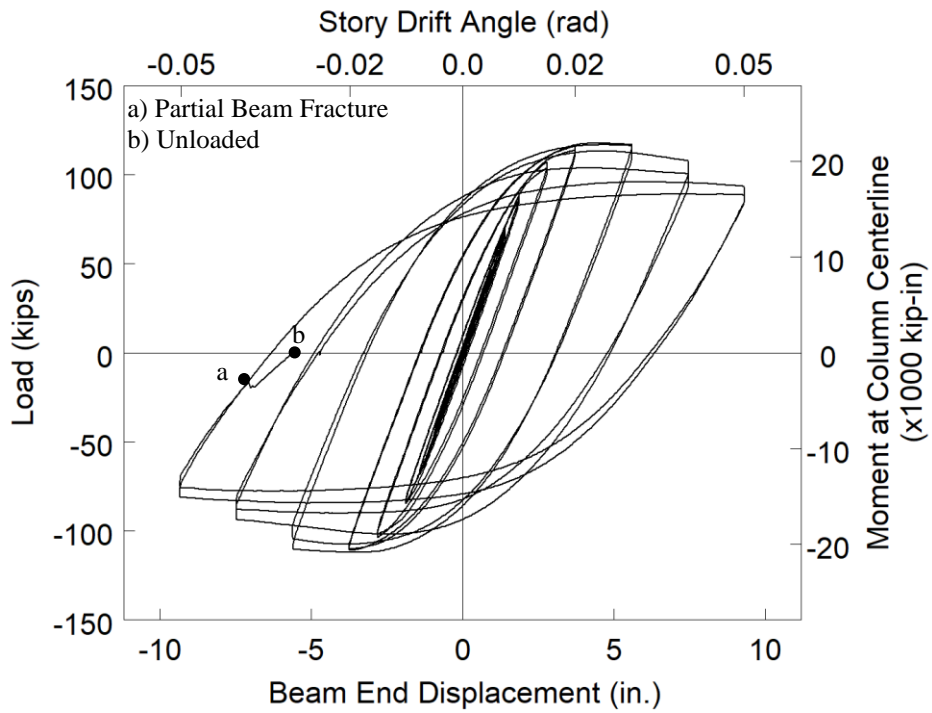


Figure 4.125 Specimen C7: Applied Load versus Beam End Displacement Response

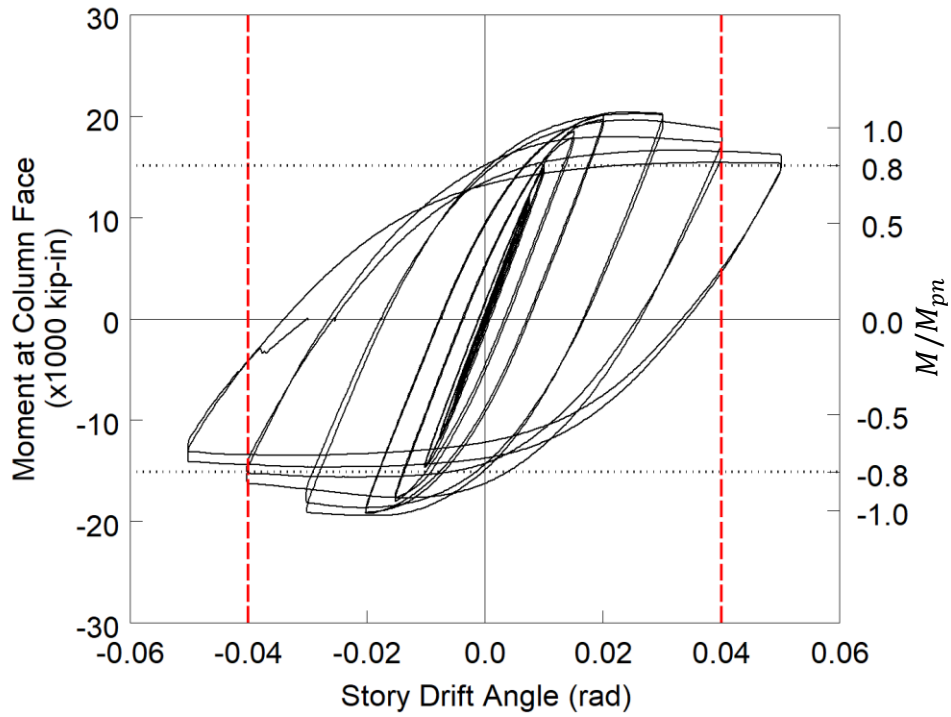


Figure 4.126 Specimen C7: Moment at Column Face versus Story Drift Response

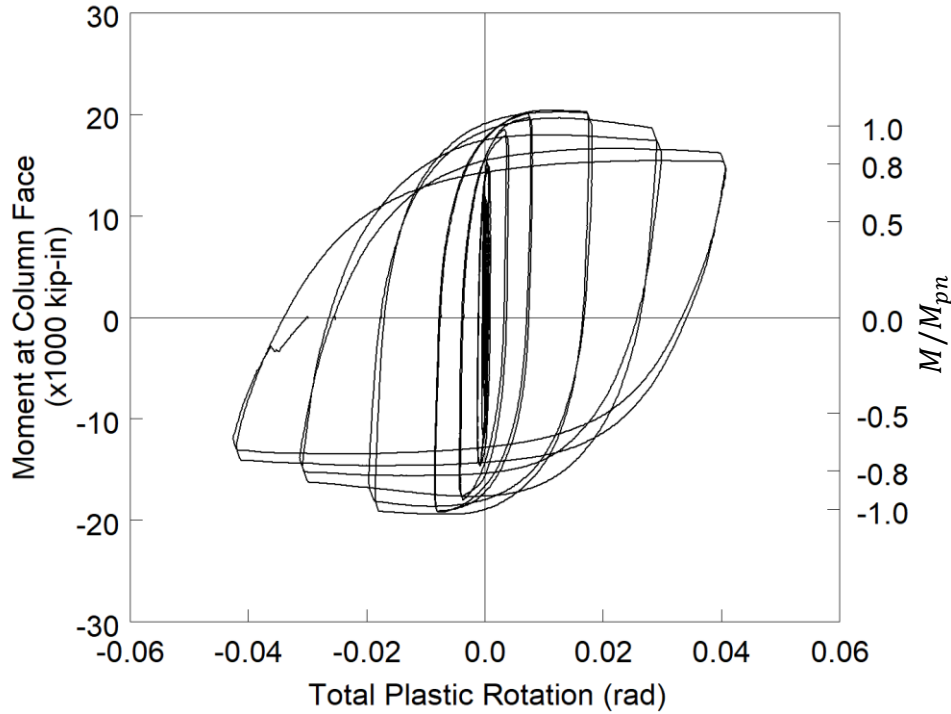


Figure 4.127 Specimen C7: Moment at Column Face versus Plastic Rotation

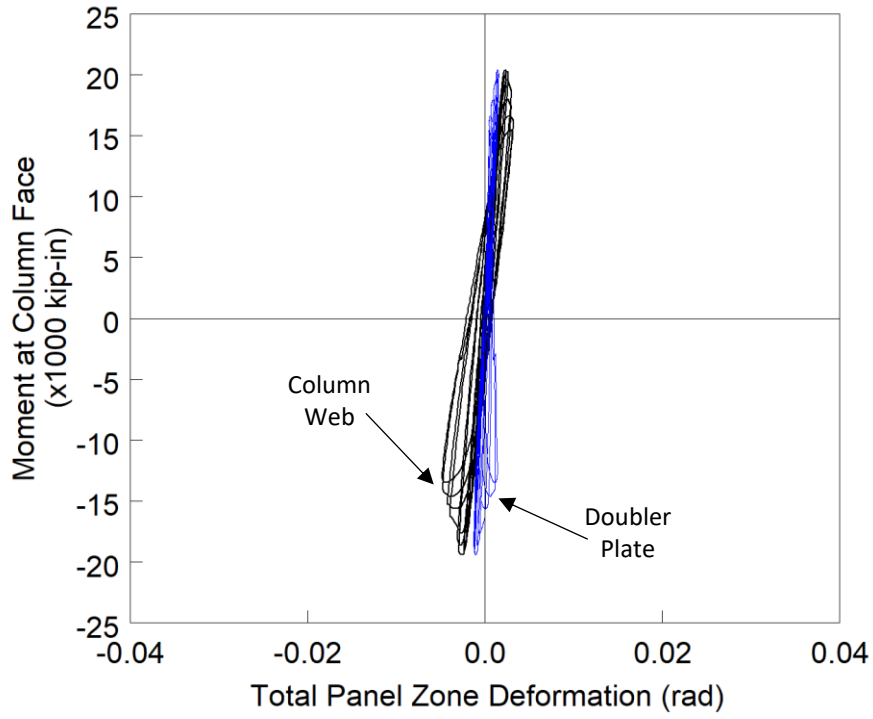


Figure 4.128 Specimen C7: Panel Zone Shear Deformation

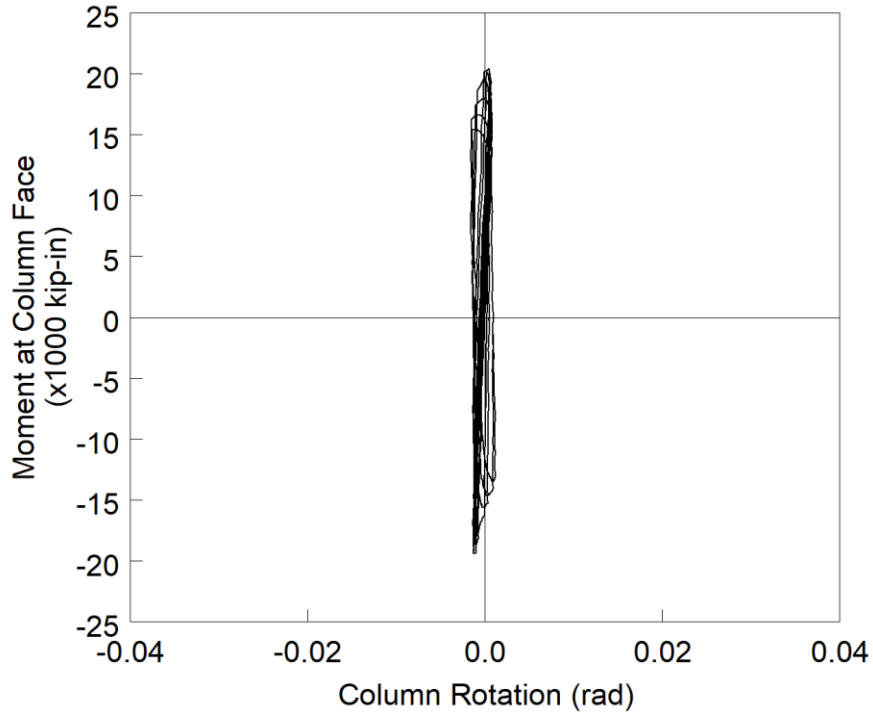


Figure 4.129 Specimen C7: Column Rotation

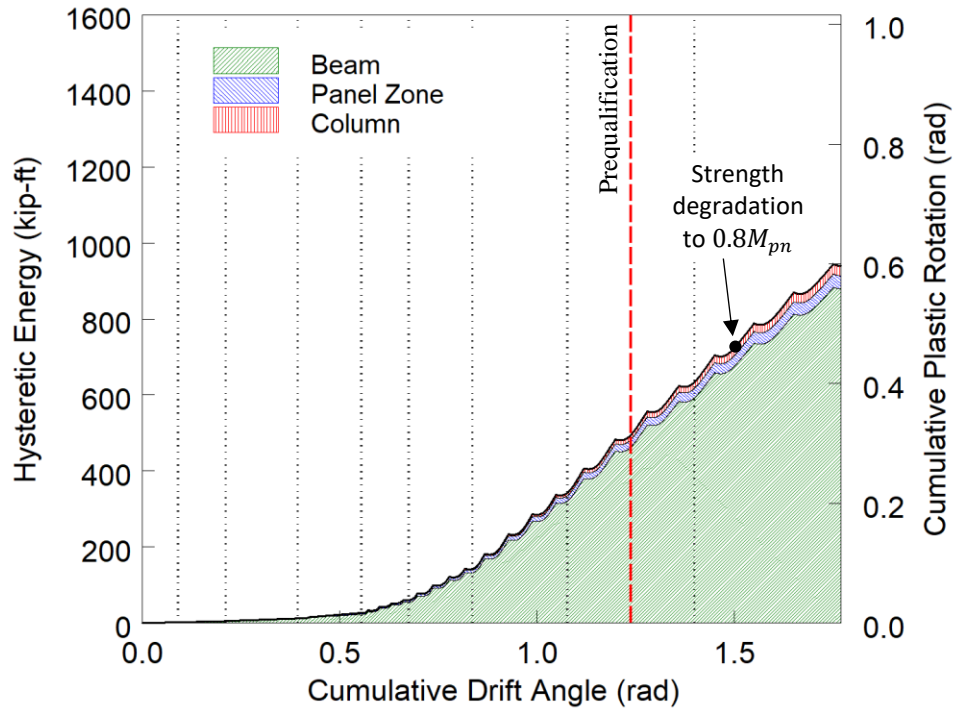
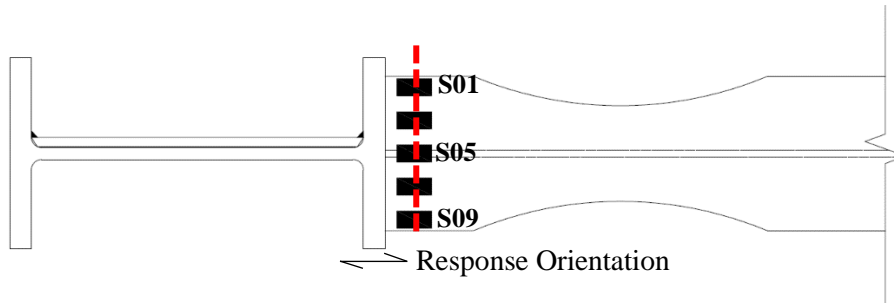
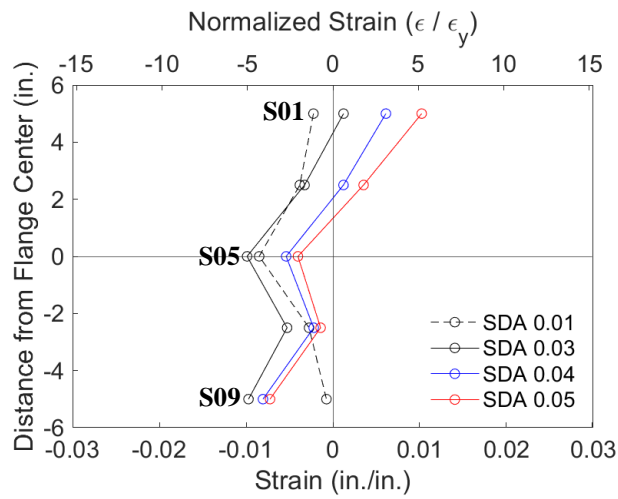


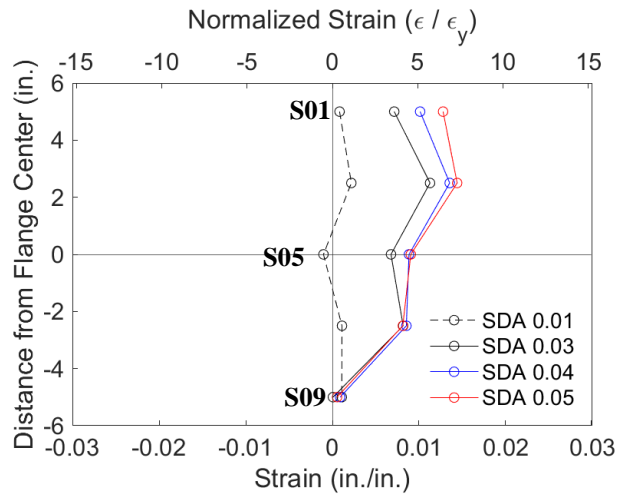
Figure 4.130 Specimen C7: Energy Dissipation



(a) Section

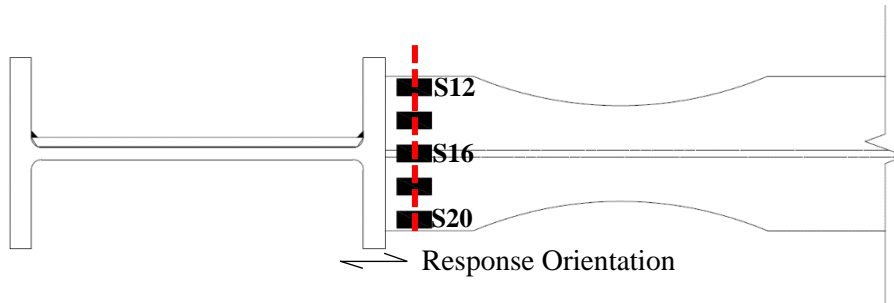


(b) Positive Drift

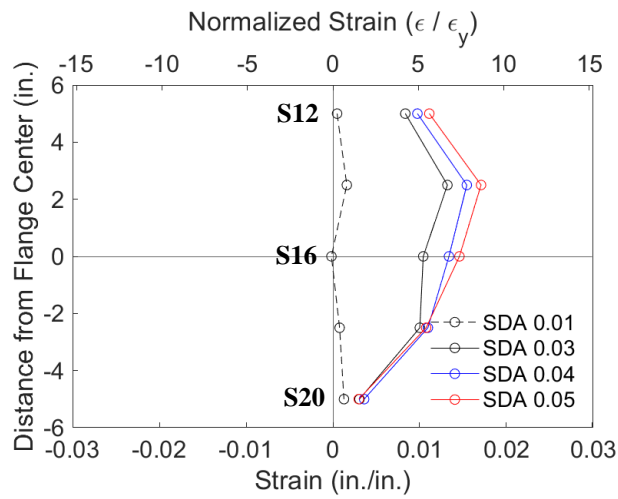


(c) Negative Drift

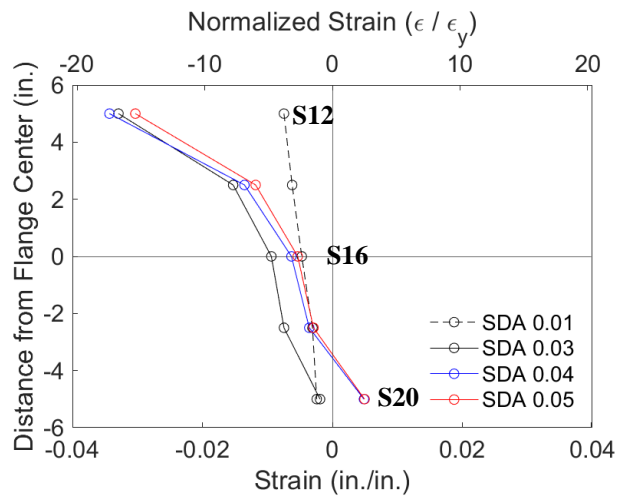
Figure 4.131 Specimen C7: Topside of Beam Top Flange Strain Profile



(a) Section

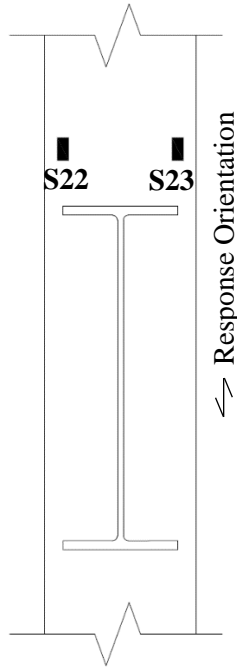


(b) Positive Drift

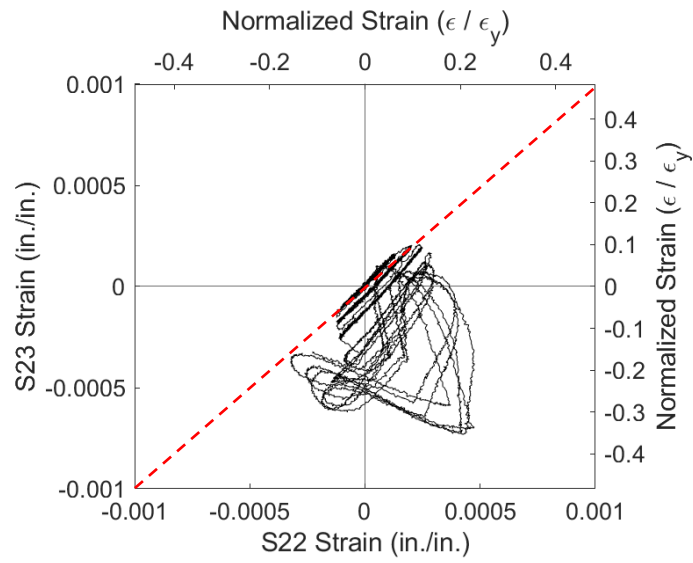


(c) Negative Drift

Figure 4.132 Specimen C7: Underside of Beam Bottom Flange Strain Profile

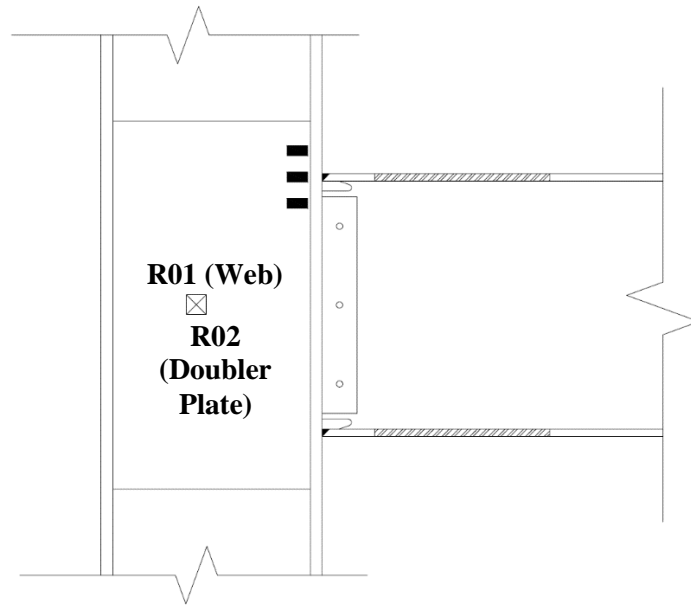


(a) Gauge Layout

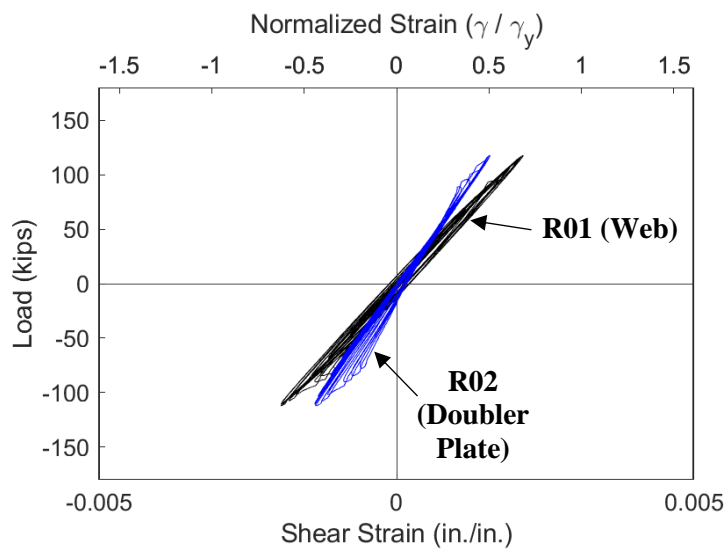


(b) Response

Figure 4.133 Specimen C7: Column Flange Warping

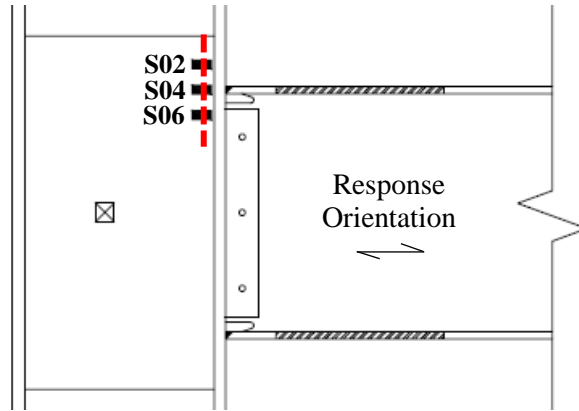


(a) Gauge Layout

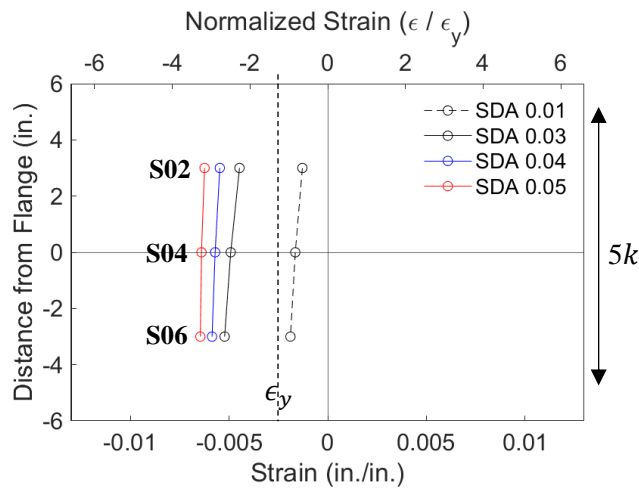


(b) Strain Rosette Gauges R01 and R02

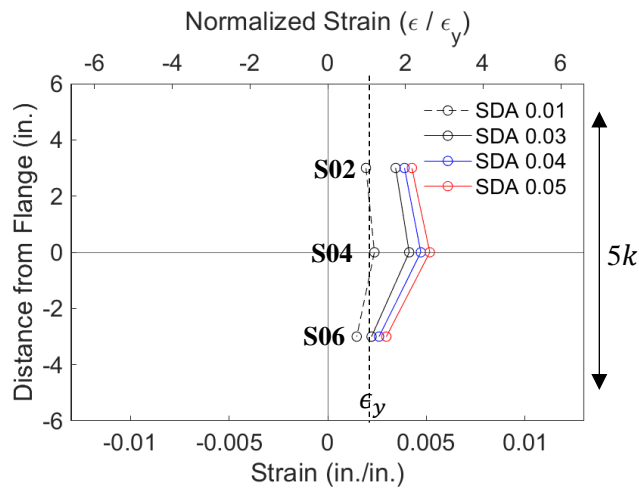
Figure 4.134 Specimen C7: Panel Zone Response



(a) Gauge Layout

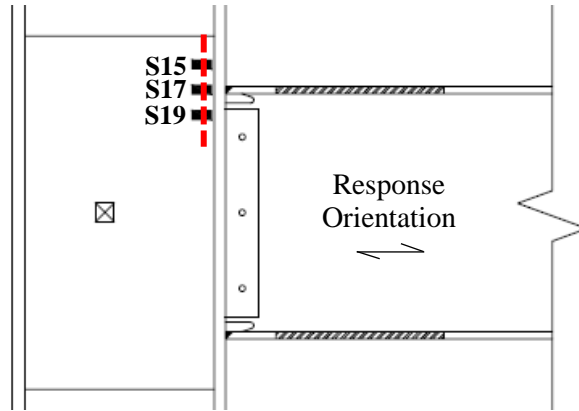


(b) Positive Drift

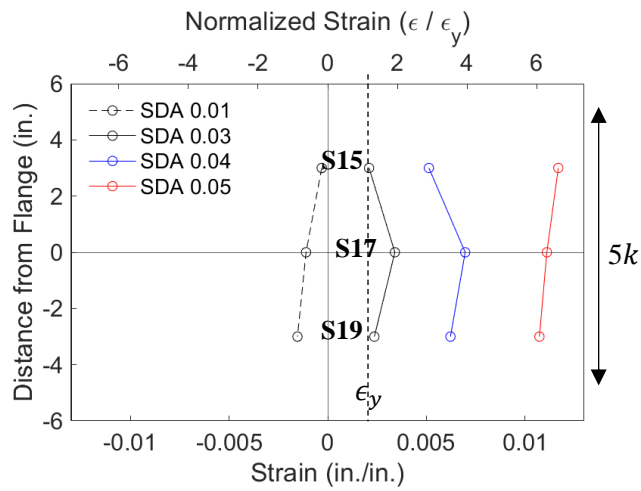


(c) Negative Drift

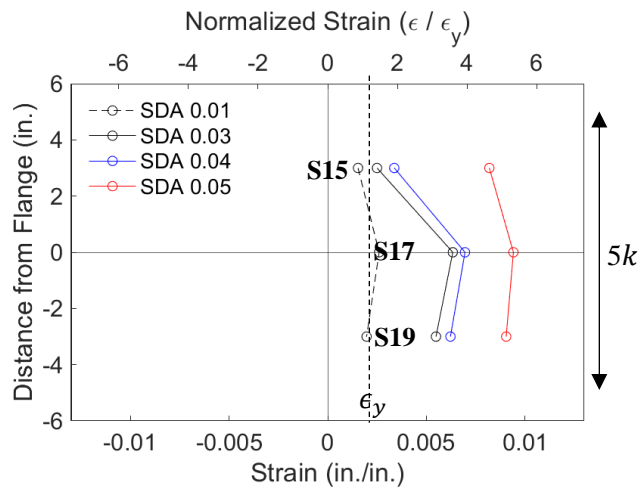
Figure 4.135 Specimen C7: Column Web Strain Profiles



(a) Gauge Layout

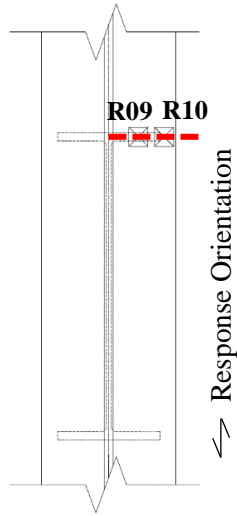


(b) Positive Drift

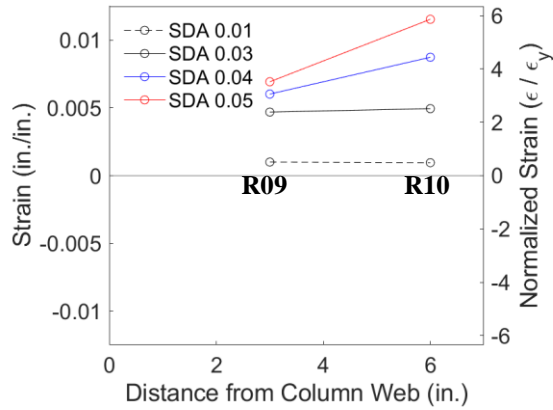


(c) Negative Drift

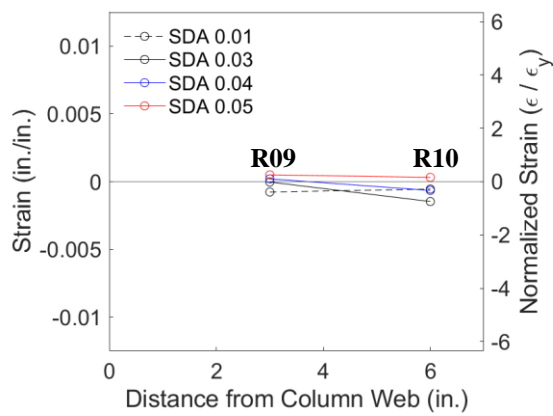
Figure 4.136 Specimen C7: Doubler Plate Response



(a) Section



(b) Positive Drift



(c) Negative Drift

Figure 4.137 Specimen C7: Column Flange Response

4.8 Specimen W1

4.8.1 General

Specimen W1 was designed to investigate use of the plastic methodology to design continuity plates. The resulting continuity plates were thinner than required by the current AISC 341 Provisions. Continuity plate double-sided fillet welds were sized such that $w = 0.75t_{cp}$. A pair of doubler plates stiffen the web of the column for panel zone yielding—these plates were extended 6 in. above and below the beam flange elevations. The doubler plate vertical welds use a PJP groove weld, and no horizontal welds were used in accordance with the current Provisions. Specimen W1 failed by a fracture of the east beam top flange CJP weld during the second cycle of 0.04 rad drift. Figure 4.138 shows the specimen before testing.

4.8.2 Observed Performance

The observed response for Specimen W1 is described below.

- Figure 4.139 shows the connection during testing. The loading protocol was applied symmetrically such that a clockwise rotation is a positive excursion on the east beam and a negative excursion on the west beam. The response is described such that a positive excursion refers to a clockwise rotation of the joint. The specimen met the AISC acceptance criteria by completing one complete cycle at 0.04 rad drift while the flexural strength at either column face did not degrade below 80% of the beam nominal flexural strength. Beam flange and web local buckling initiated at 0.03 rad drift and progressed throughout testing.
- Figure 4.140 and Figure 4.141 show the progressive beam yielding during testing. Yielding starts adjacent to the column flange and propagates outward, concentrating down the center of the beam.
- Figure 4.142 shows the progression of flange local buckling that developed in the east beam bottom flange. The local buckling develops in a opposite sense between the east and west beams depending on which flange of the beam was in compression.
- Figure 4.143 shows yielding in the panel zone observed at a at 0.03 rad drift. The yielding did not progress significantly further by the end of testing.

- Figure 4.144 shows the minor lateral-torsional buckling that developed in beam top flanges during the 0.04 rad drift cycles. The buckling was mirrored between positive and negative joint rotations, reflecting when the top flange experienced compression.
- Figure 4.145 shows the fractured east beam top flange CJP weld at -0.03 rad during the second negative excursion to 0.04 rad drift. The fracture started at the CJP Weld root on the underside of the specimen, on the tension side of the lateral-torsional buckling and propagated along the beam flange following the 30° bevel of the CJP weld. The progression of the fracture was observed in Figure 4.146. After initiating in the weld metal as a ductile tear the fracture transitioned to the bevel of the CJP weld after 0.75 in. The fracture continued its tearing in a ductile fashion until 50% of the flange was fractured when a secondary ductile fracture appeared in the reentrant corner in the center of the flange. The remainder of the fracture propagated due to cleavage through the flange (see Figure 4.147).
- Figure 4.148 shows the connection at the end of testing. Modest amounts of flange local bending and web local buckling were present. Additionally, modest levels of panel zone yielding were observed. Minor shear tab yielding was also observed.
- Continuity plates did not demonstrate yielding nor damage to any of the fillet welds during testing (see Figure 4.149 to Figure 4.151). A slight bow present in the continuity plates occurred before testing of the specimen and was not due to local buckling of the plate.

4.8.3 Recorded Response

4.8.3.1 Global Response

- Figure 4.152 shows the recorded displacement response of the beam tip measured with transducer L1 for the east beam and L2 for the west beam. The response from the east and west beams are shown in black and blue, respectively. The east beam CJP weld fractured at -0.03 rad drift during the second negative excursion of 0.04 rad drift. Figure 4.153 shows the column shear versus the applied story drift response.
- Figure 4.154 shows the load-displacement response of the beams.

- Figure 4.155 shows the computed moment at the column face (M_f) versus the story drift angle. Two horizontal axes at 80% of the nominal plastic moment (M_{pn}) of the beam section are also added. In addition, two vertical axes at ± 0.04 rad story drift show the drift required for SMF connections per AISC 341. It is observed that the beams developed about 1.5 times its nominal plastic bending moment. If the moment is computed at the plastic hinge location and compared to the expected plastic moment, then the peak connection strength factor (C_{pr}) is 1.41 and 1.40 for the east and west beams respectively.
- Figure 4.156 shows the plastic response of the specimen. The plastic response is computed using the procedure outlined in Section 3.7. The computed elastic stiffness of the specimen was determined to be 172.6 kips/in.
- Figure 4.157 shows modest hysteretic behavior in the panel zone.
- Figure 4.158 shows negligible hysteretic behavior in the column.
- Figure 4.159 shows the dissipated energy of Specimen W1. Dotted vertical lines on the graph demonstrate the completion of each group of cycles, and the dashed red vertical line shows the completion of the first cycle of 0.04 rad in the AISC loading. It is observed that the completion of the first drift cycle of 0.04 rad (the requirement for SMF connections per AISC 341) occurs after 1,952 kip-ft of energy has been dissipated. The connection did not degrade below $0.8M_{pn}$ until fracture of the east beam top flange occurred and 2,501 kip-ft of energy had been dissipated. Therefore 78% of the energy dissipation capacity was utilized after the completion of the SMF requirement. It is observed that most (82%) of the energy dissipation capacity occurred in the beam.

4.8.3.2 Local Response

- Figure 4.160 and Figure 4.161 shows the extreme fiber response of the east beam top and bottom flanges. Strains on the order of 6% ($30\epsilon_y$) are observed in the flanges which are exacerbated by high local curvatures and weak axis bending. Figure 4.162 and Figure 4.163 show the extreme fiber response of the west beam top and bottom flanges.

- Figure 4.164 shows the strain gauge response of the west column flange above the beam top flange. It is observed that the column flange did not yield, and little deviation from a 1:1 line demonstrates negligible column flange warping.
- Figure 4.165 shows the horizontal strain pattern on the doubler plate through two sections. The highest strain develops at the location of the beam flange and continuity plate. Horizontal strains in the center of the doubler plate are mostly balanced. Figure 4.166 shows the shear stress distribution in the doubler plate. The center of the doubler plate sees the most significant strains ($2\gamma_y$).
- Figure 4.167 shows the horizontal shear distribution of the top flange continuity plate. At lower drifts the strain response is mostly equal and opposite across the continuity plate. At higher levels of drift during the east negative excursion, the tension on the west edge of the plate develops more bending—an effect attributed to the development of the plastic hinge in the west beam bottom flange. It is observed that the continuity plate develops yielding level strains in the horizontal direction. Moderate shear strains are present at the edges of the continuity plate in contact with the column flange (see Figure 4.168). The principal strains of the outermost strain gauge rosettes demonstrate cyclic strains between $-3\epsilon_y$ and ϵ_y on the west side of the continuity plate and between $-\epsilon_y$ and $1.5\epsilon_y$ on the east side of the continuity plate. The compression bias of the west outmost strain gauge (R16) is congruent with the observed lateral-torsional buckling of the west beam. A similar conclusion is observed with the tension bias of the east outermost strain gauge (R22).
- Figure 4.170 shows the shear response of the continuity plate on the edge fillet welded with the doubler plate.
- Figure 4.171 shows the shear response of the west beam adjacent to the column. It is observed that the shear tab develops higher shear strains than the beam web.

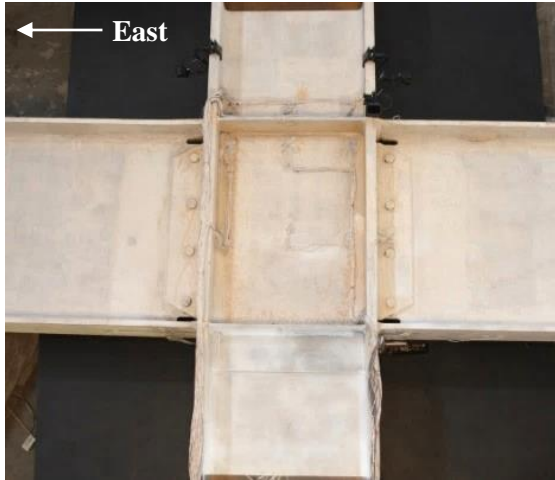


(a) Overview



(b) Connection Region

Figure 4.138 Specimen W1: Connection before Testing



(a) +0.02 rad (2nd Cycle)



(b) -0.02 rad (2nd Cycle)



(c) +0.03 rad (2nd Cycle)



(d) -0.03 rad (2nd Cycle)



(e) +0.04 rad (2nd Cycle)

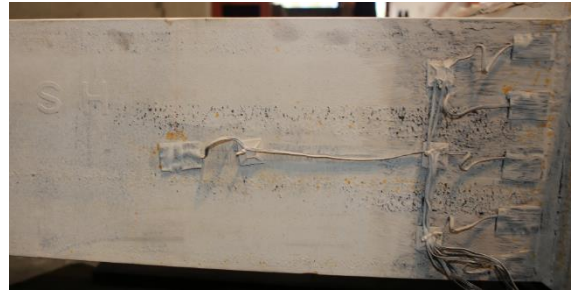


(f) -0.04 rad (2nd Cycle)

Figure 4.139 Specimen W1: Connection during Testing



(a) -0.015 rad (2nd Cycle)



(b) -0.02 rad (2nd Cycle)



(c) -0.03 rad (2nd Cycle)



(d) -0.04 rad (1st Cycle)

Figure 4.140 Specimen W1: East Beam Bottom Flange Yielding



(a) -0.015 rad (2nd Cycle)



(b) -0.02 rad (2nd Cycle)



(c) -0.03 rad (2nd Cycle)



(d) -0.04 rad (1st Cycle)

Figure 4.141 Specimen W1: West Beam Bottom Flange Yielding



(a) -0.03 rad (2nd Cycle)



(b) -0.04 rad (1st Cycle)

Figure 4.142 Specimen W1: East Beam Bottom Flange Local Buckling

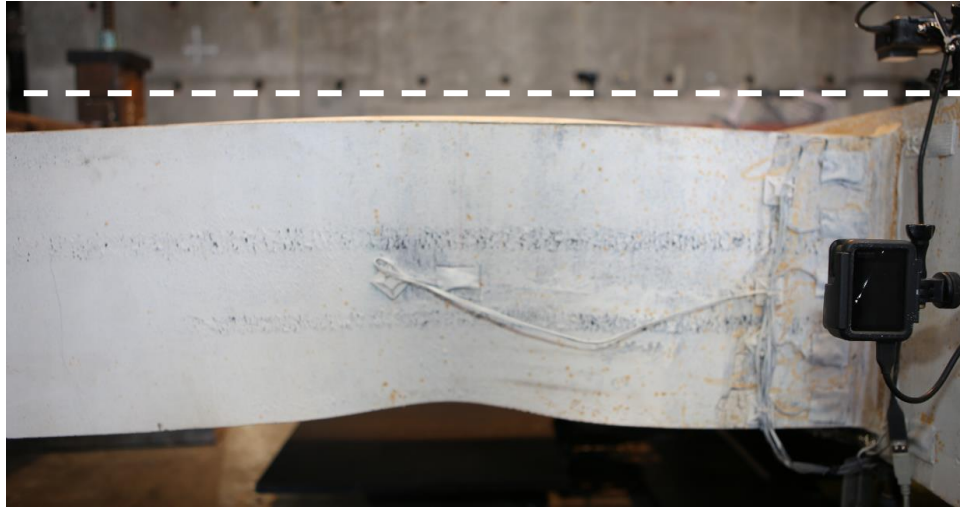


(a) Overview



(b) Yielding

Figure 4.143 Specimen W1: Panel Zone Yielding at +0.03 rad (2nd Cycle)



(a) West Beam Top Flange at +0.04 rad (1st Cycle)



(a) East Beam Top Flange at +0.04 rad (2nd Cycle)

Figure 4.144 Specimen W1: Lateral-Torsional Buckling



(a) Overview



(b) Fracture

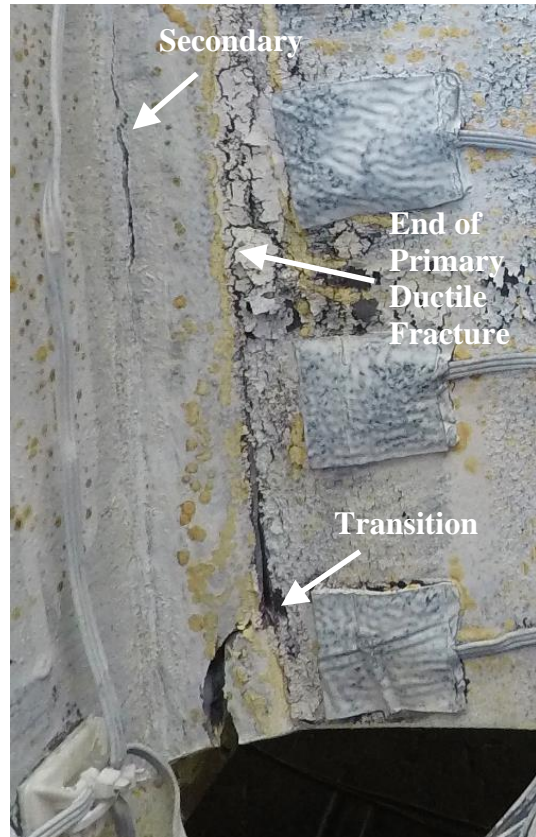
Figure 4.145 Specimen W1: East Beam Top Flange CJP Weld Fracture at -0.04 rad (2nd Cycle)



(a) Fracture Initiation



(c) after Fracture



(b) during Propagation

Figure 4.146 Specimen W1: East Beam Top Flange CJP Weld Fracture Progression

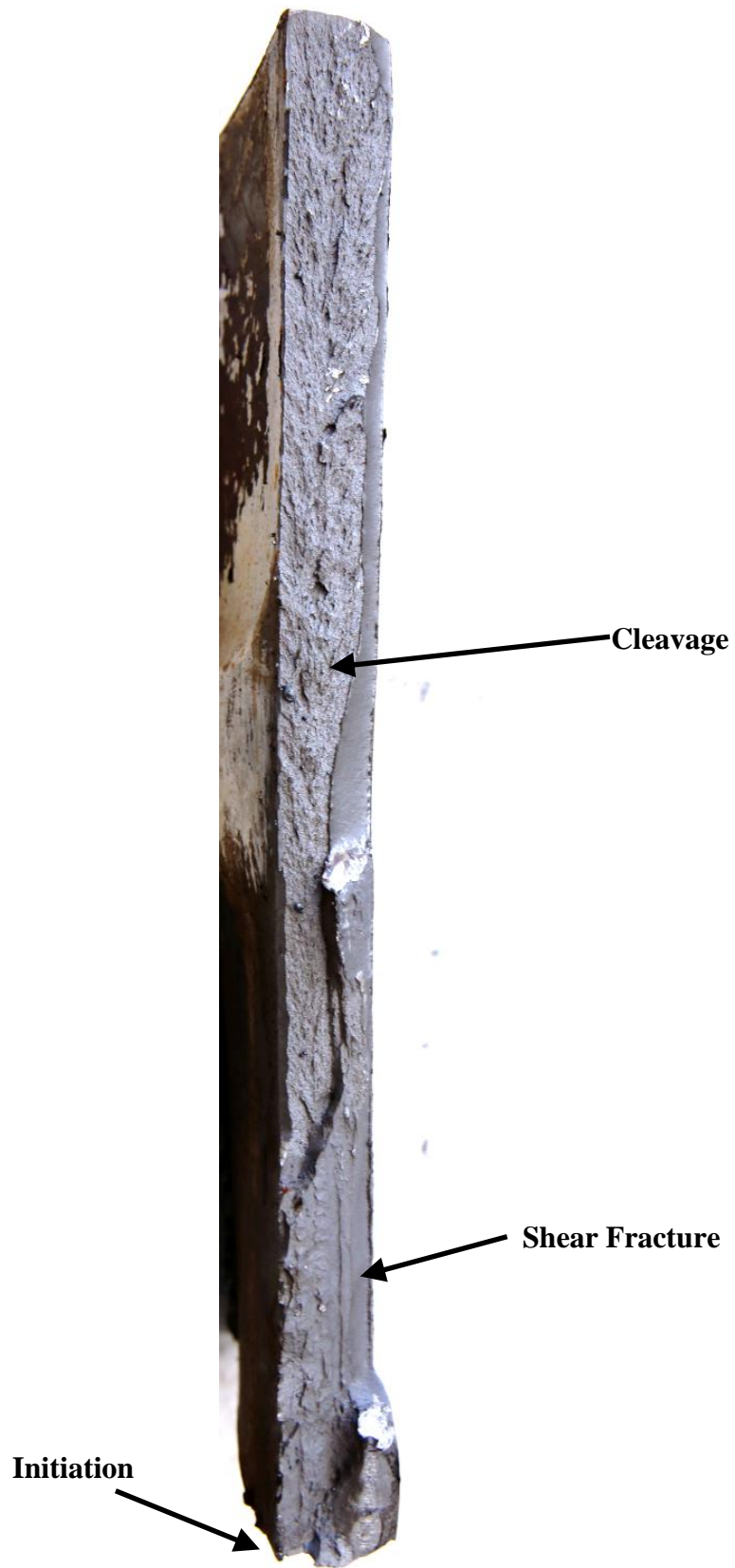


Figure 4.147 Specimen W1: East Beam Top Flange CJP Weld Fracture Surface

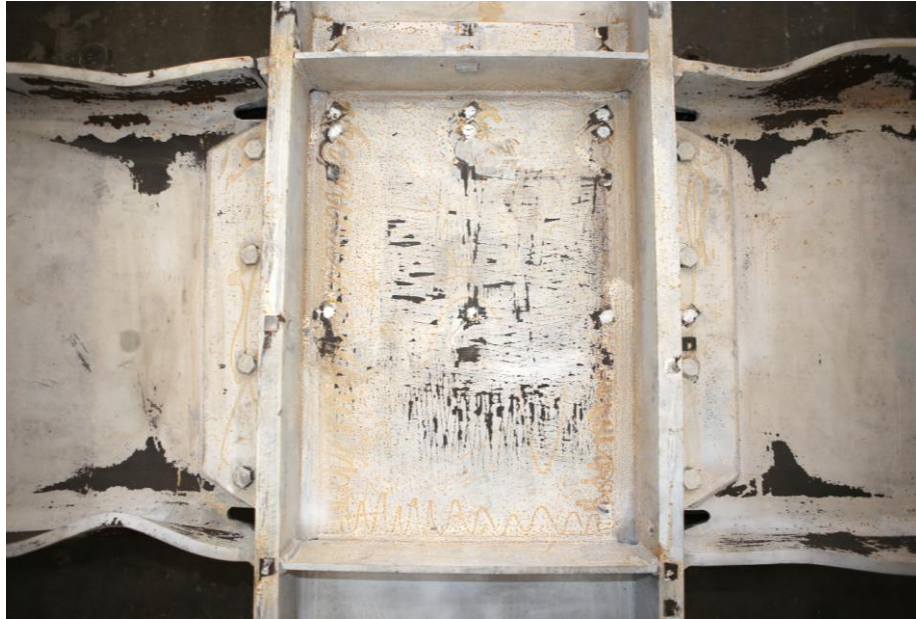


Figure 4.148 Specimen W1: Connection at End of Test



(a) Underside of Continuity Plate



(b) Edge of Continuity Plate

Figure 4.149 Specimen W1: Top Flange Continuity Plate (End of Test)



(a) Topside of Continuity Plate



(b) Underside of Continuity Plate

Figure 4.150 Specimen W1: Bottom Flange Continuity Plate (End of Test)



(a) Top Flange Continuity Plate



(b) Bottom Flange Continuity Plate

Figure 4.151 Specimen W1: Underside Continuity Plates (End of Test)

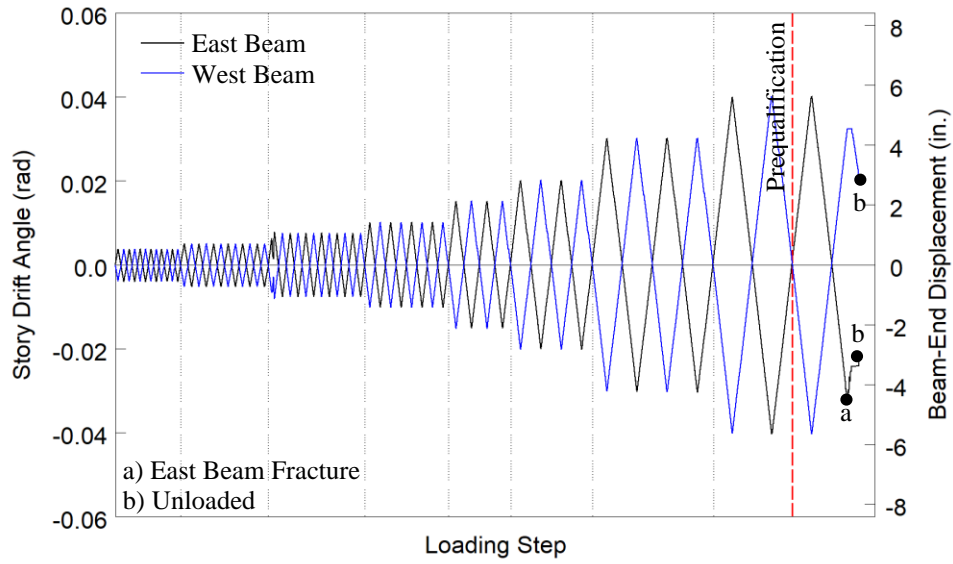


Figure 4.152 Specimen W1: Recorded Loading Sequence

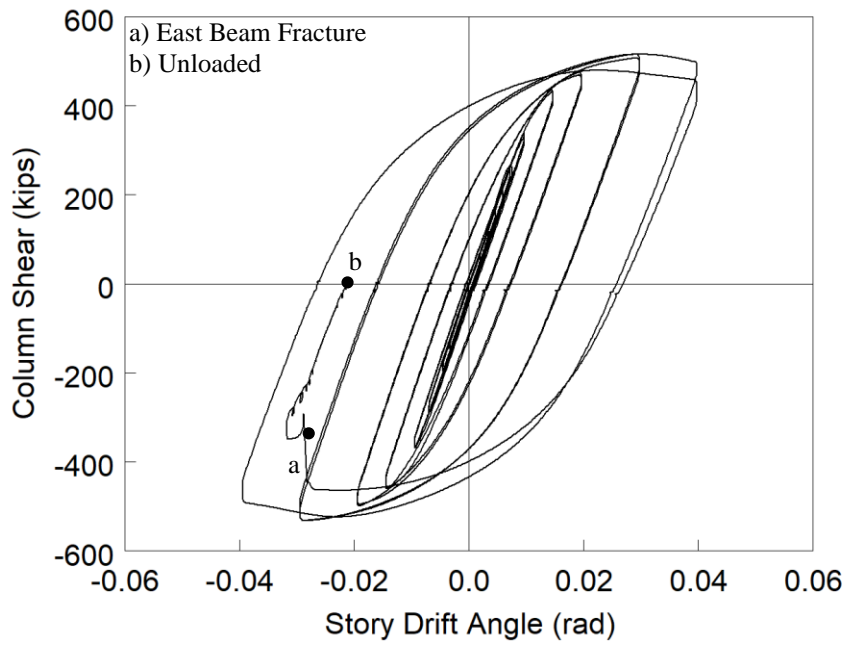
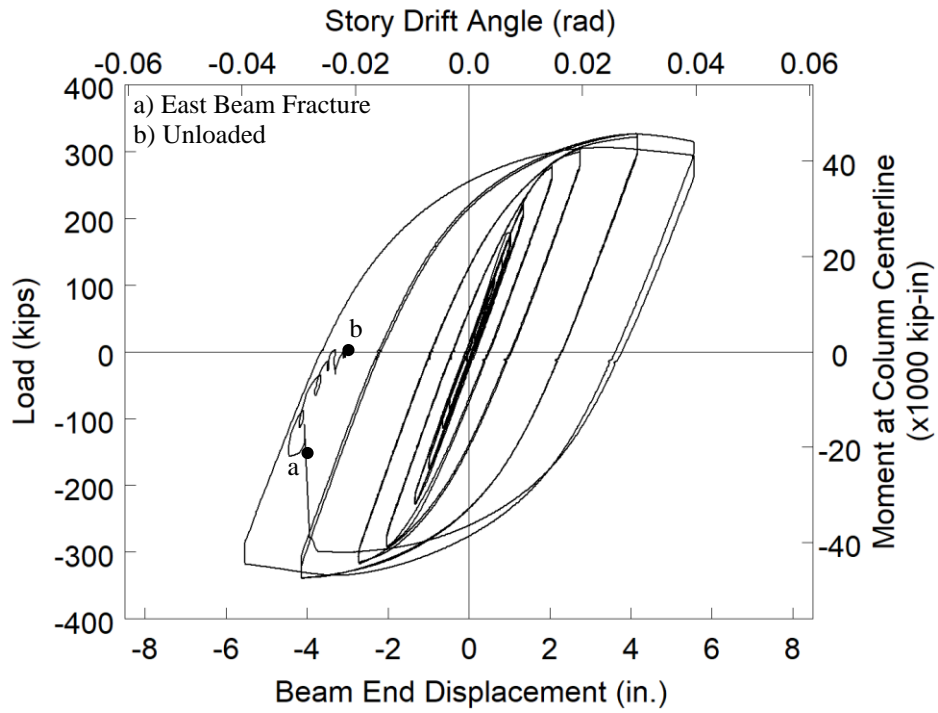
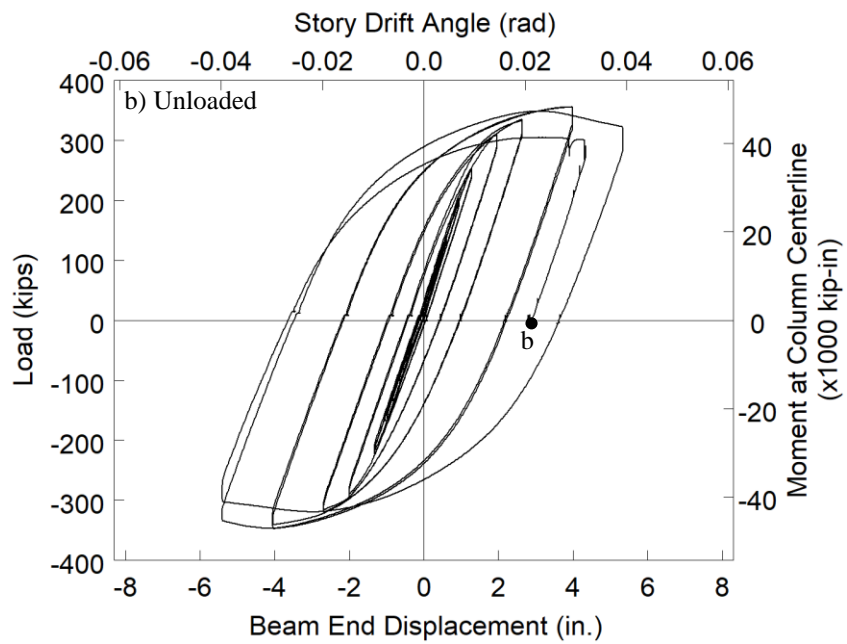


Figure 4.153 Specimen W1: Column Shear versus Story Drift Angle

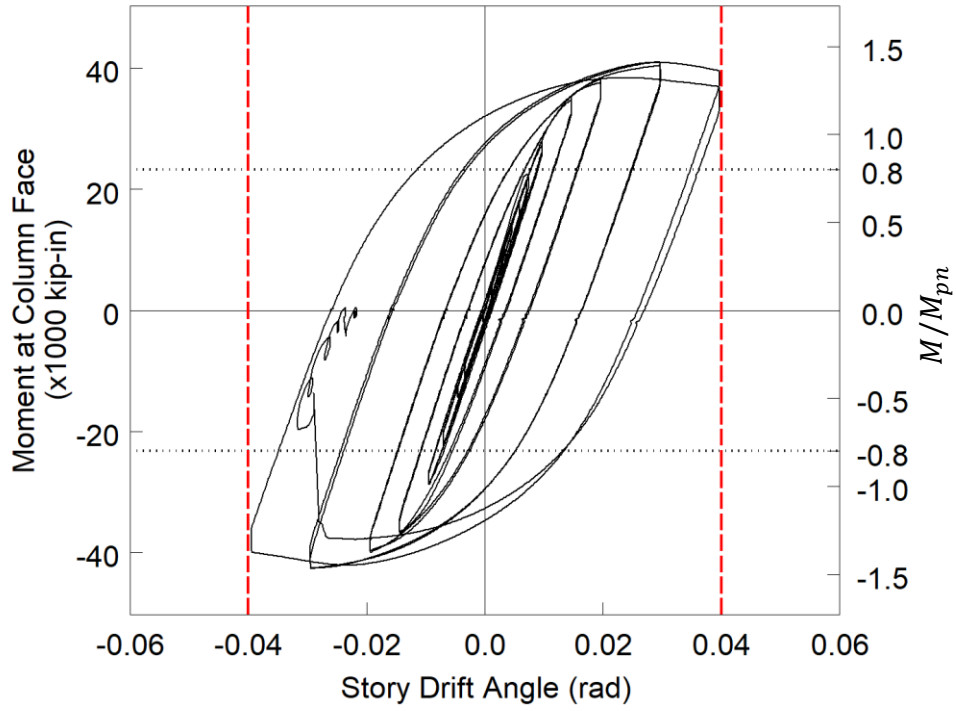


(a) East Beam

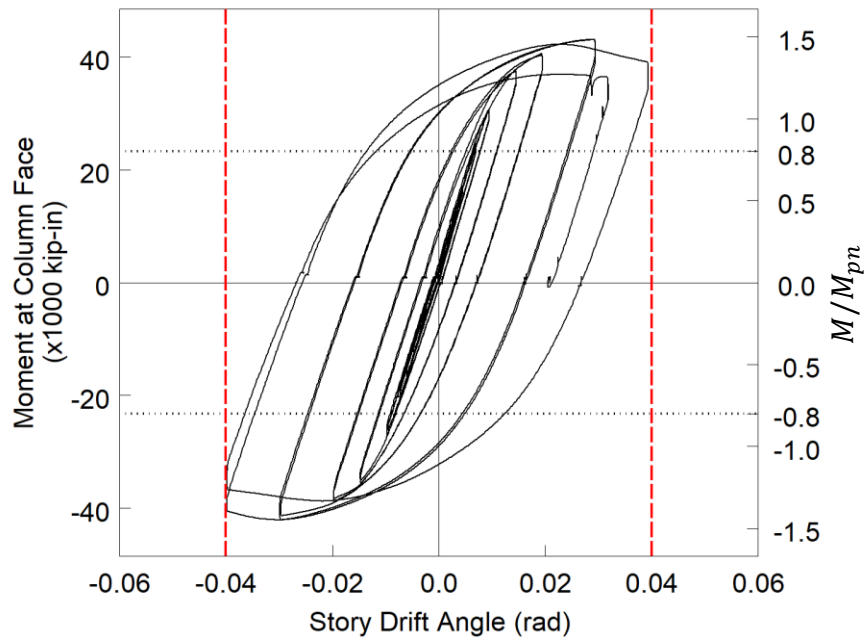


(b) West Beam

Figure 4.154 Specimen W1: Applied Load versus Beam End Displacement Response

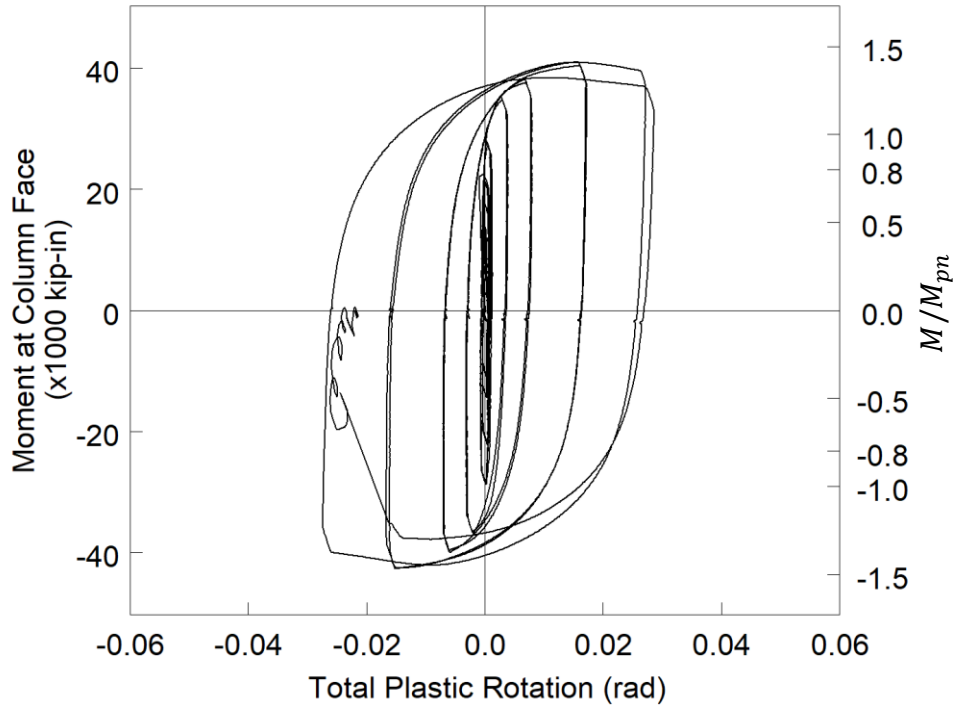


(a) East Beam

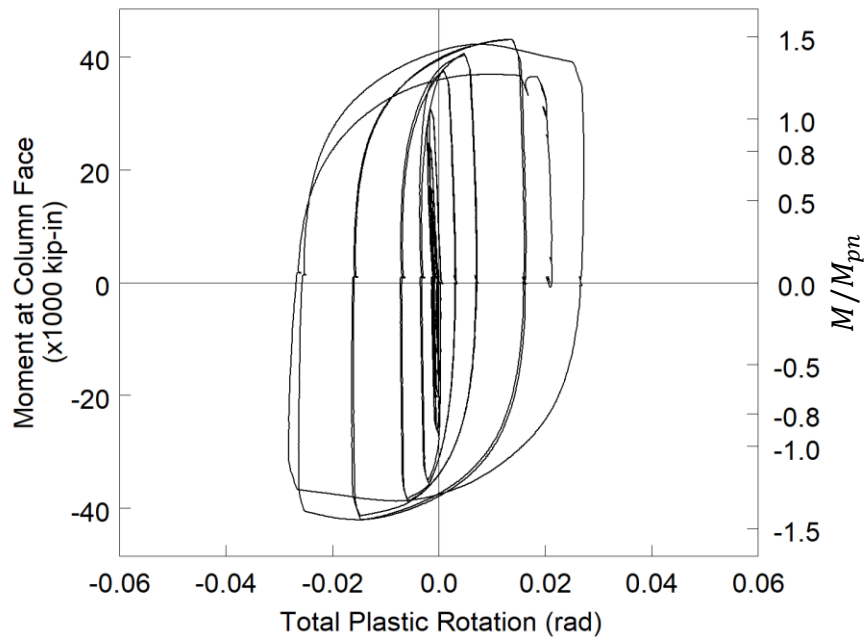


(b) West Beam

Figure 4.155 Specimen W1: Moment at Column Face versus Story Drift Response



(a) East Beam



(b) West Beam

Figure 4.156 Specimen W1: Moment at Column Face versus Plastic Rotation

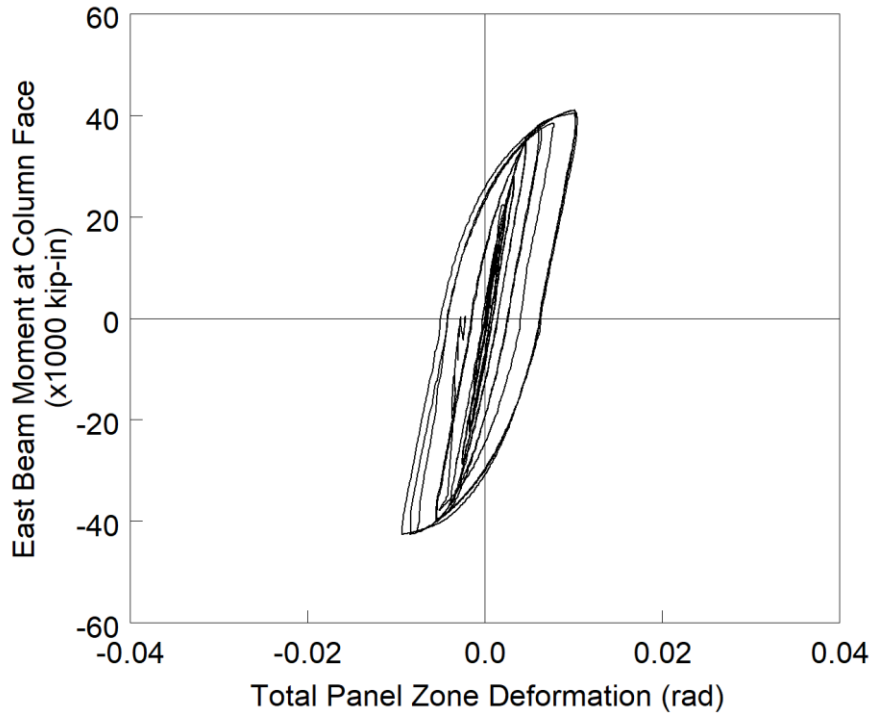


Figure 4.157 Specimen W1: Panel Zone Shear Deformation

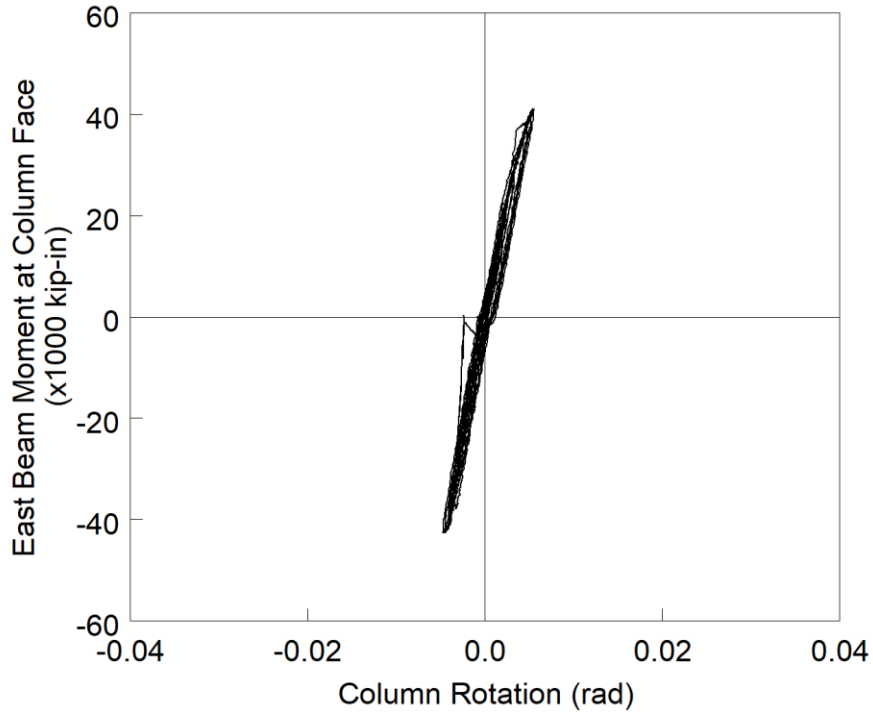


Figure 4.158 Specimen W1: Column Rotation

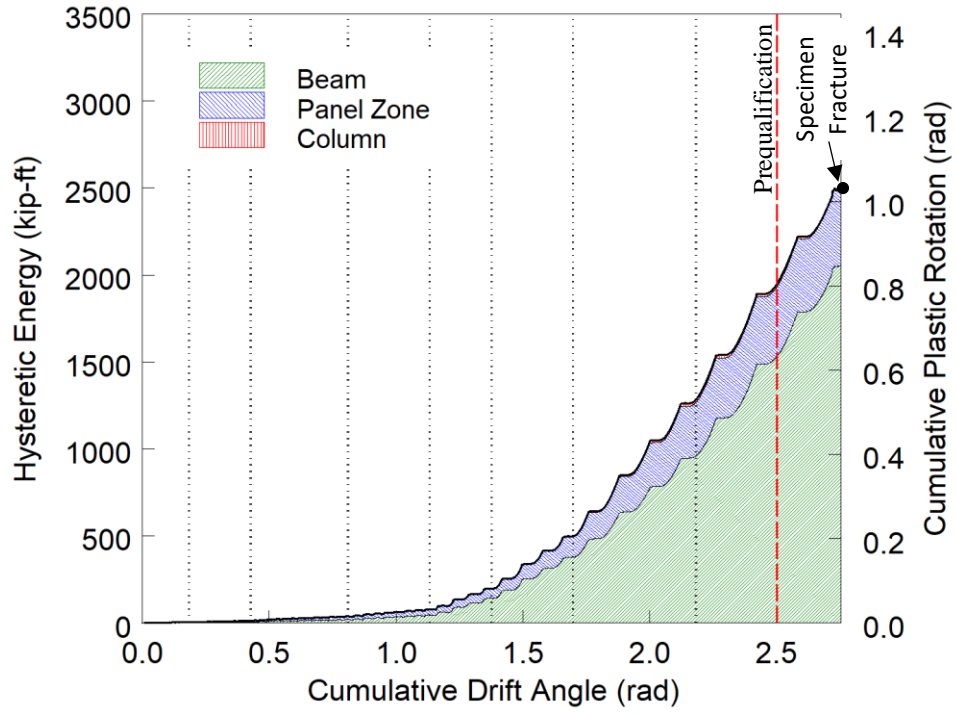
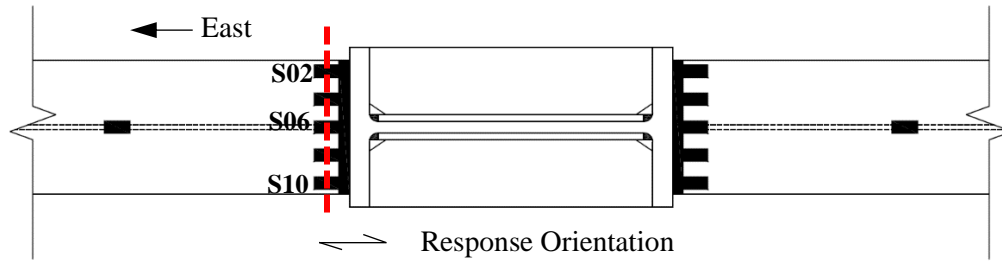
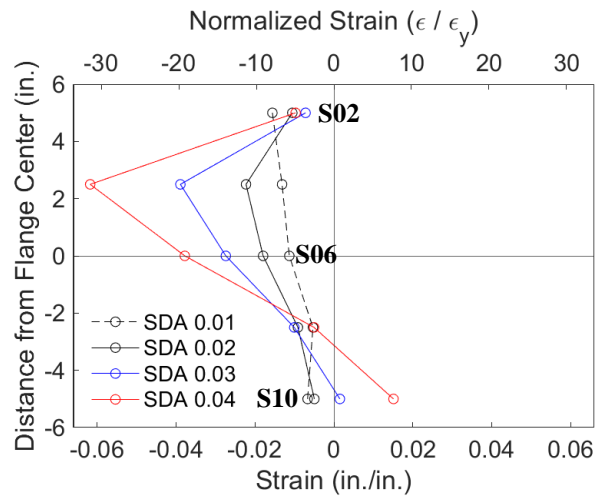


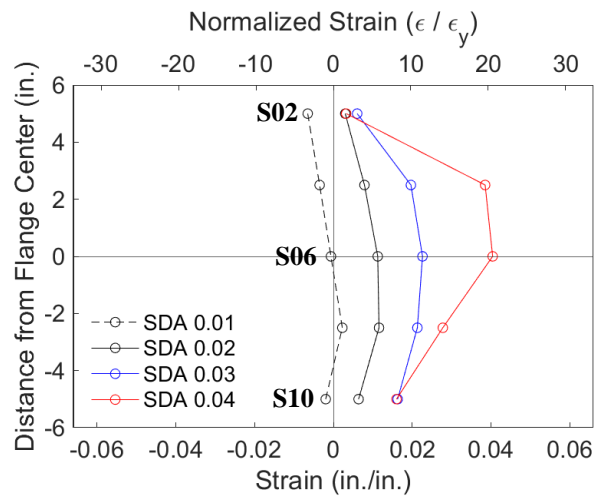
Figure 4.159 Specimen W1: Energy Dissipation



(a) Section

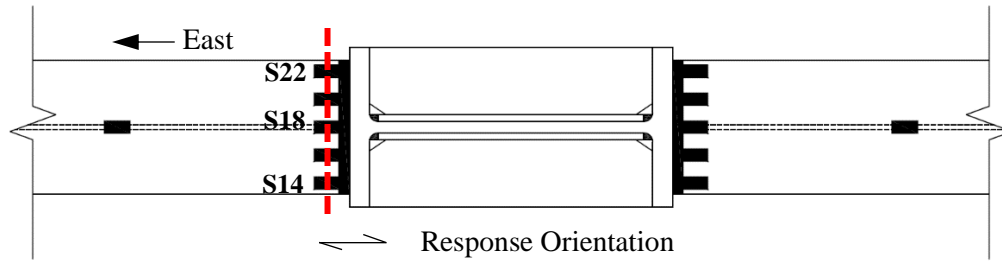


(b) Positive Drift

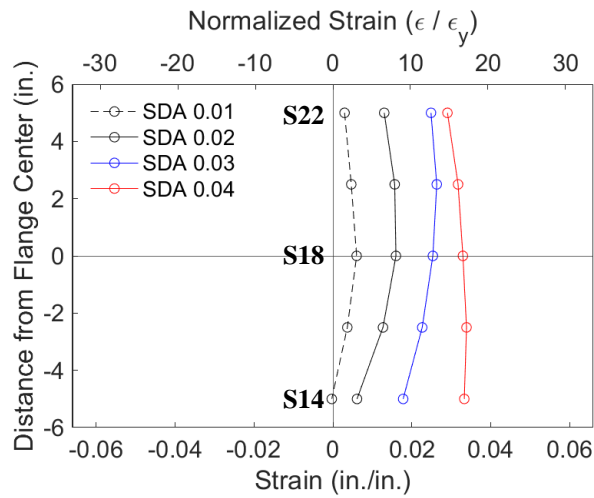


(c) Negative Drift

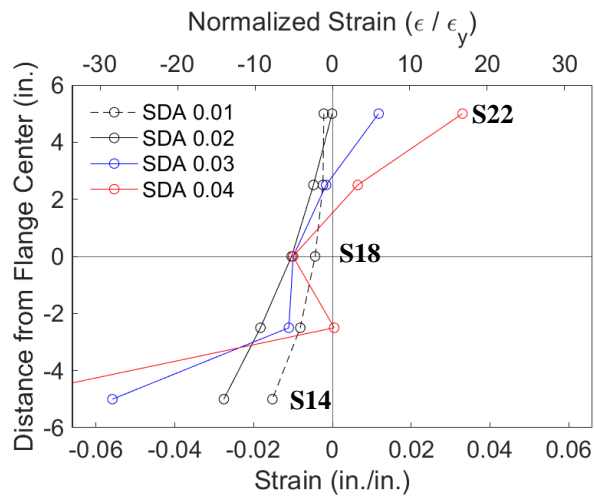
Figure 4.160 Specimen W1: Topside of East Beam Top Flange Strain Profile



(a) Section

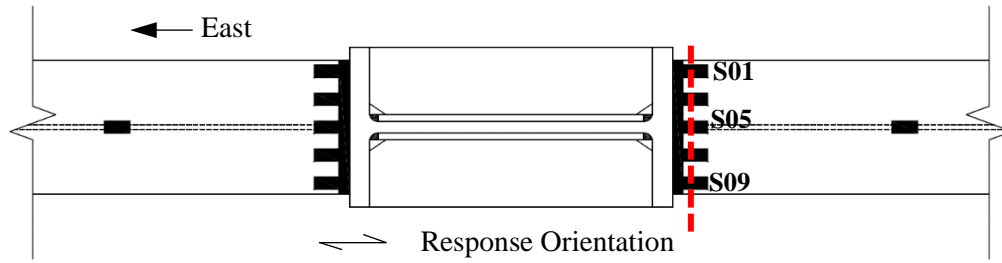


(b) Positive Drift

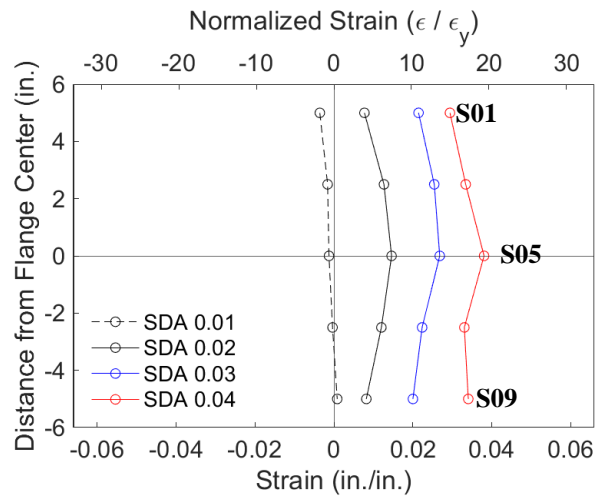


(c) Negative Drift

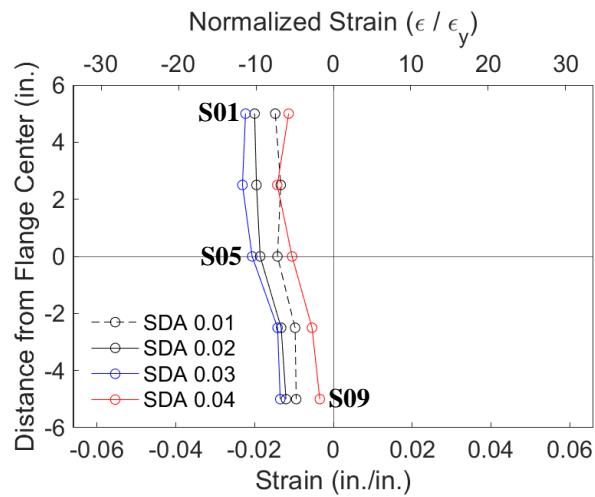
Figure 4.161 Specimen W1: Underside of East Beam Bottom Flange Strain Profile



(a) Section

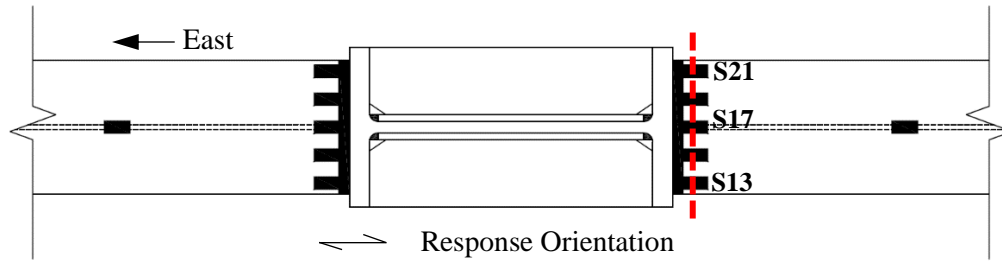


(b) Positive Drift

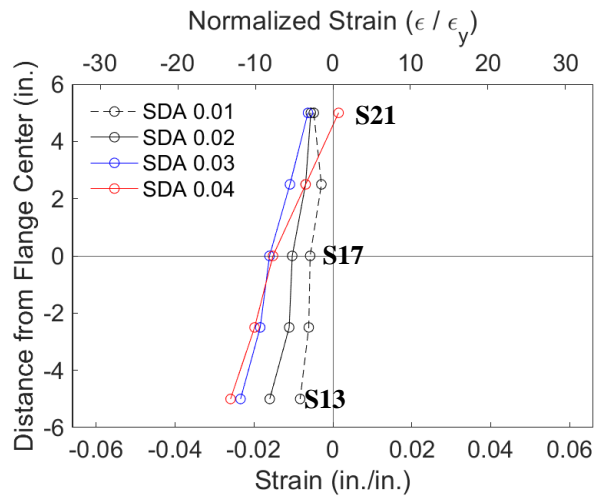


(c) Negative Drift

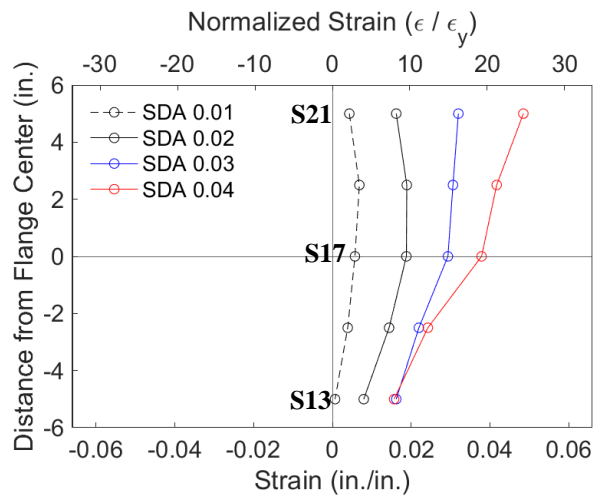
Figure 4.162 Specimen W1: Topside of West Beam Top Flange Strain Profile



(a) Section

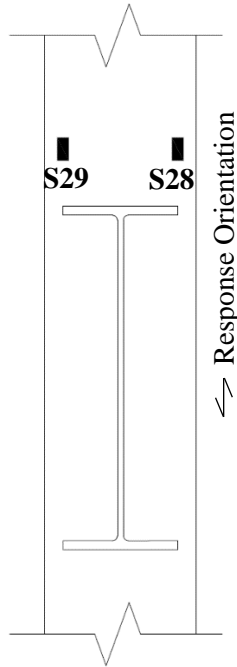


(b) Positive Drift

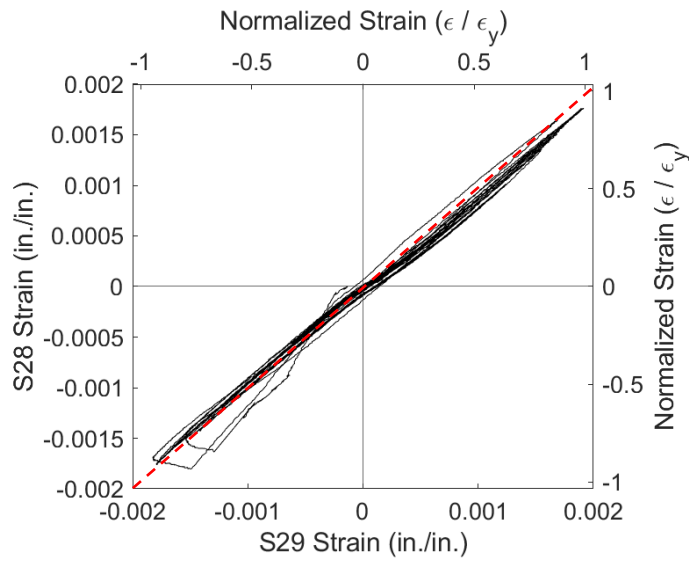


(c) Negative Drift

Figure 4.163 Specimen W1: Underside of West Beam Bottom Flange Strain Profile

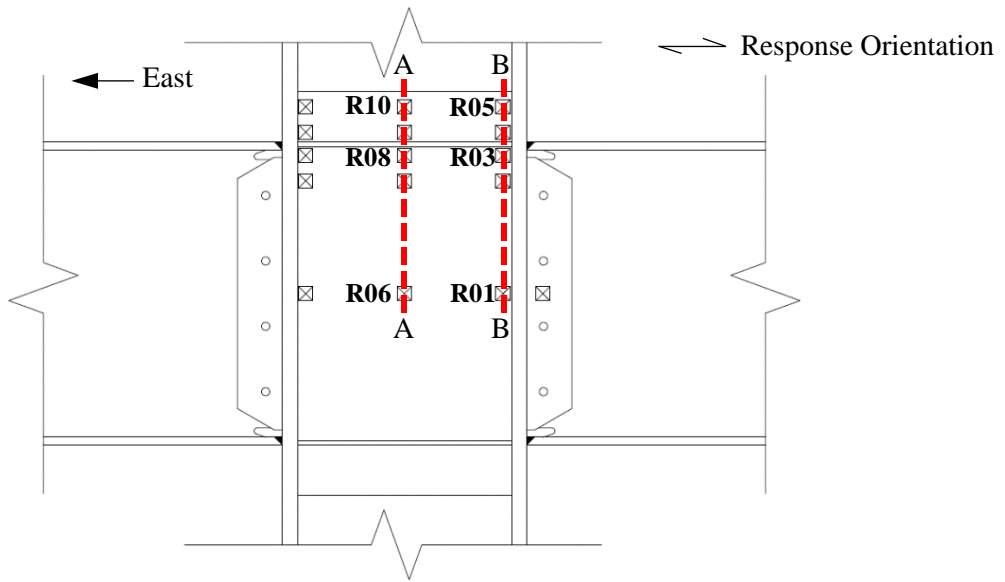


(a) Gauge Layout

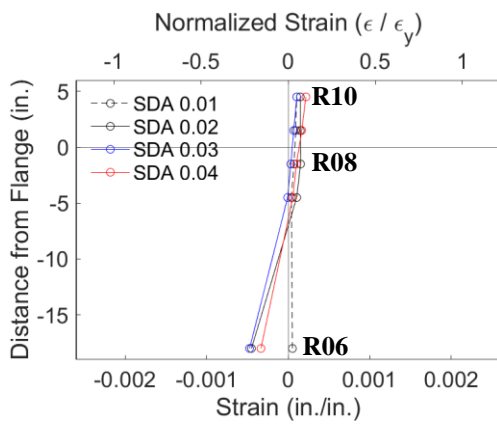


(b) Response

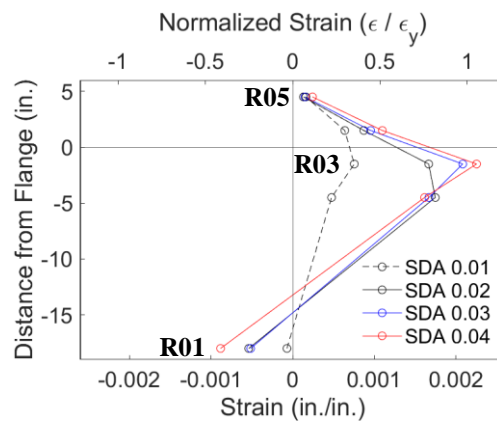
Figure 4.164 Specimen W1: Column Flange Warping



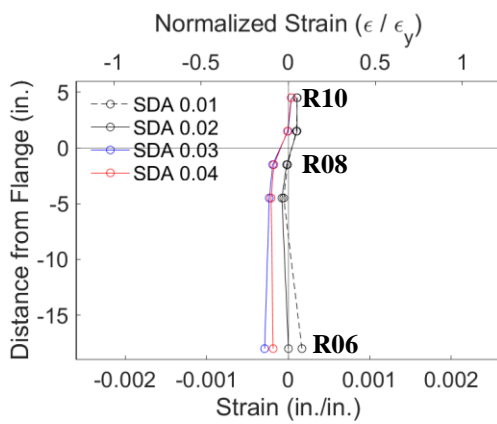
(a) Section Layout



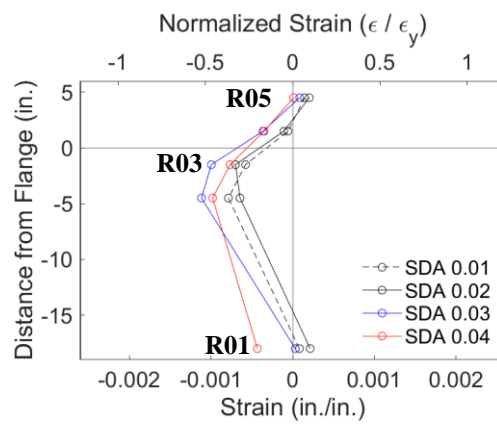
(b) Section A-A: Positive Drift



(c) Section B-B: Positive Drift

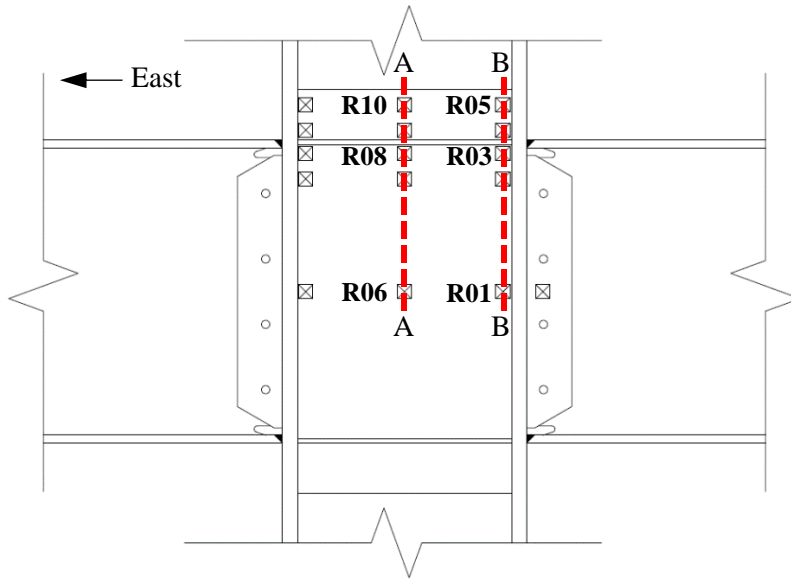


(d) Section A-A: Negative Drift

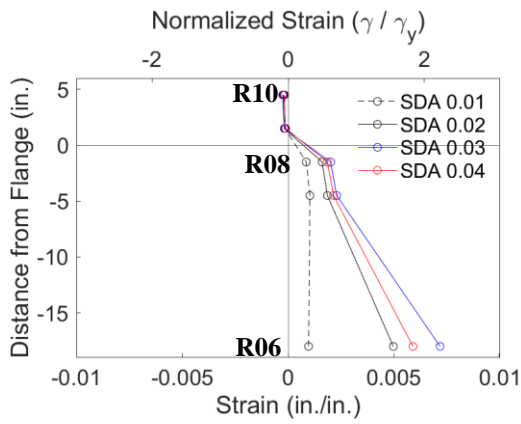


(e) Section B-B: Negative Drift

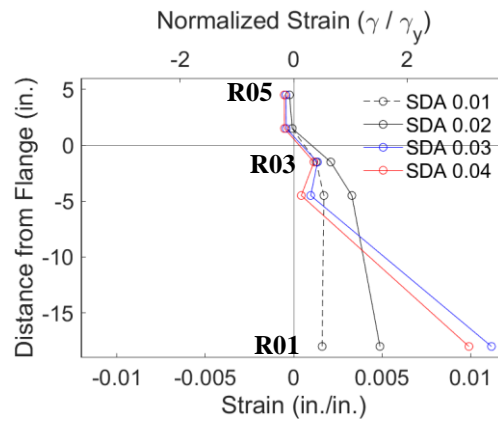
Figure 4.165 Specimen W1: Panel Zone Strain Profile



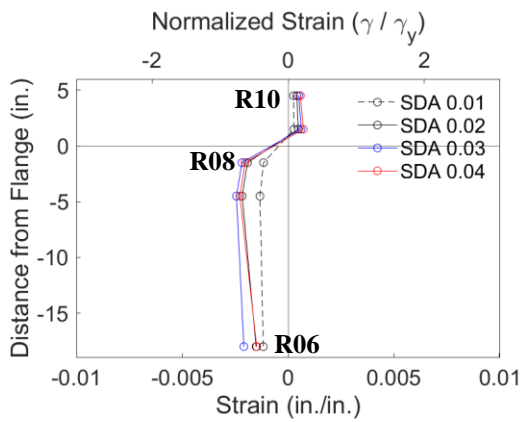
(a) Section Layout



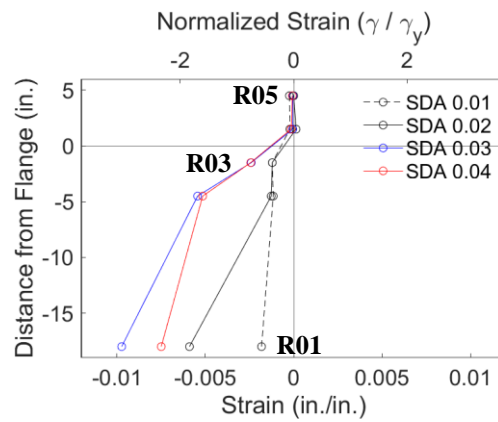
(b) Section A-A: Positive Drift



(c) Section B-B: Positive Drift



(d) Section A-A: Negative Drift



(e) Section B-B: Negative Drift

Figure 4.166 Specimen W1: Panel Zone Shear Strain Profile

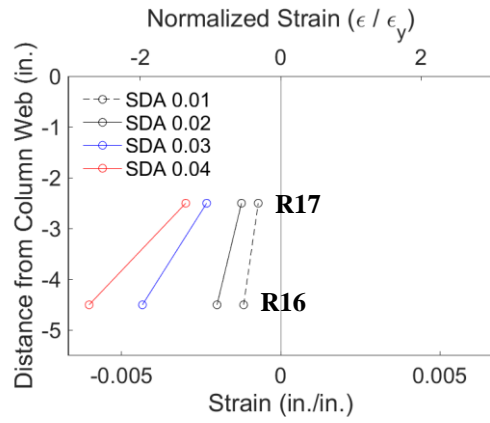
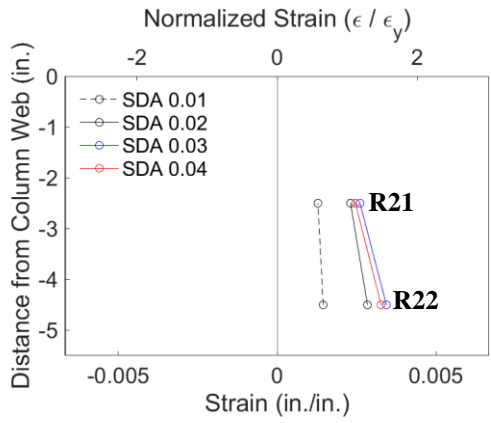
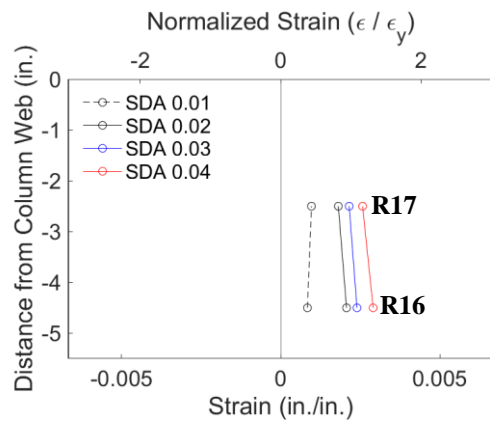
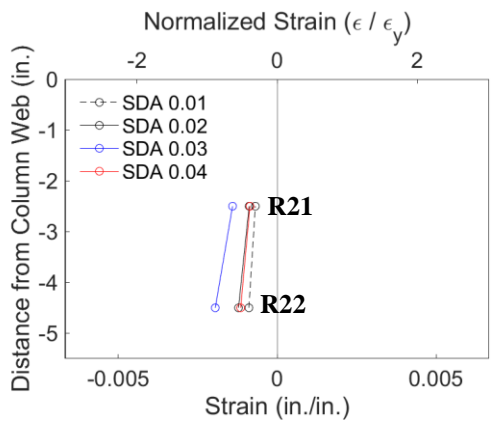
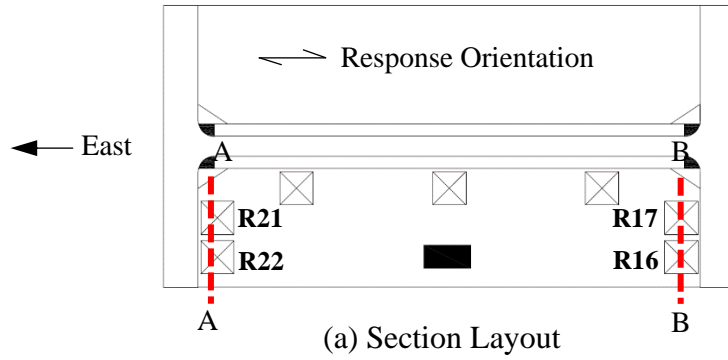


Figure 4.167 Specimen W1: Continuity Plate at Column Flange Edge Strain Profile

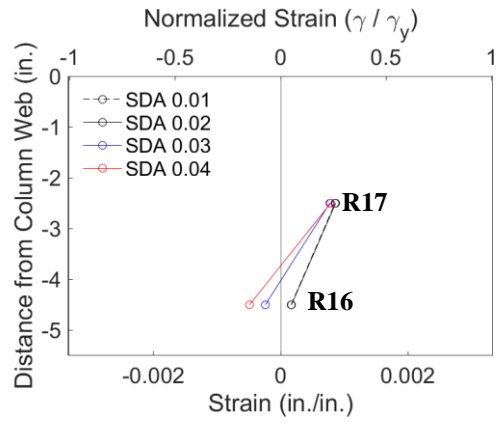
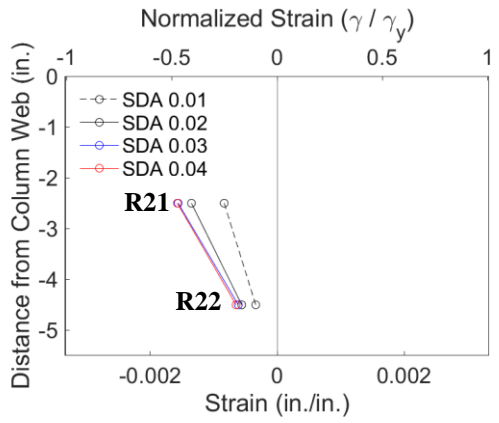
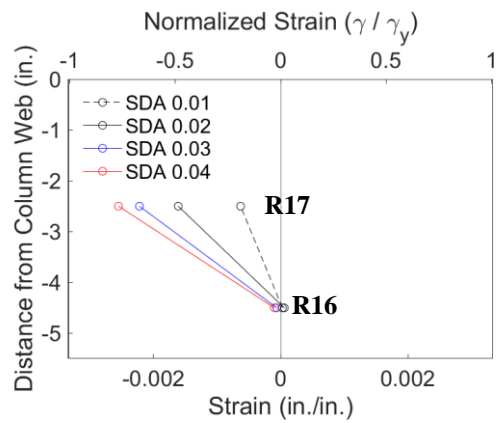
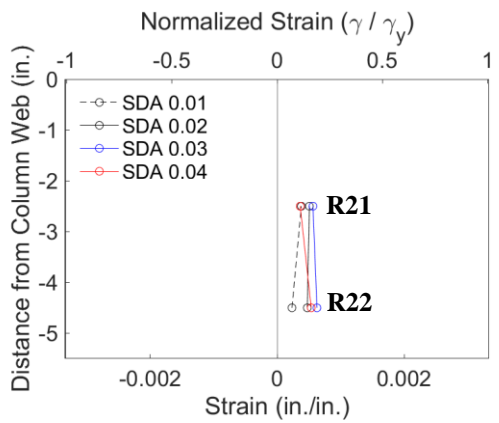
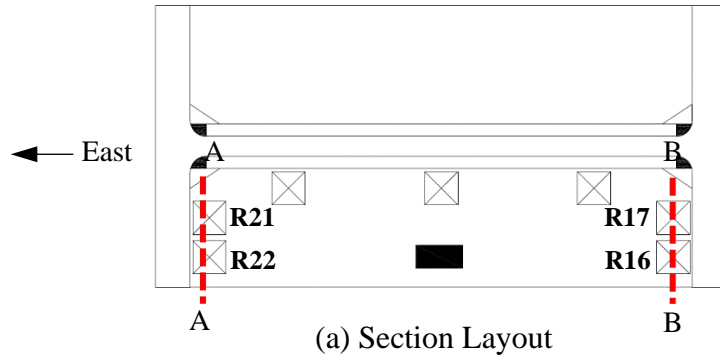
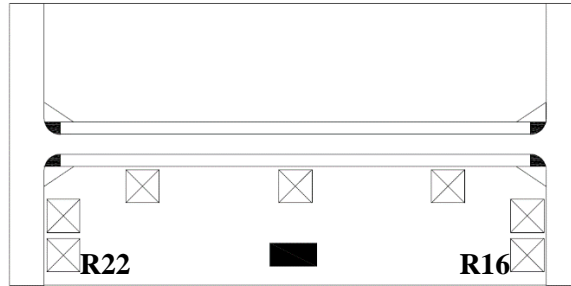
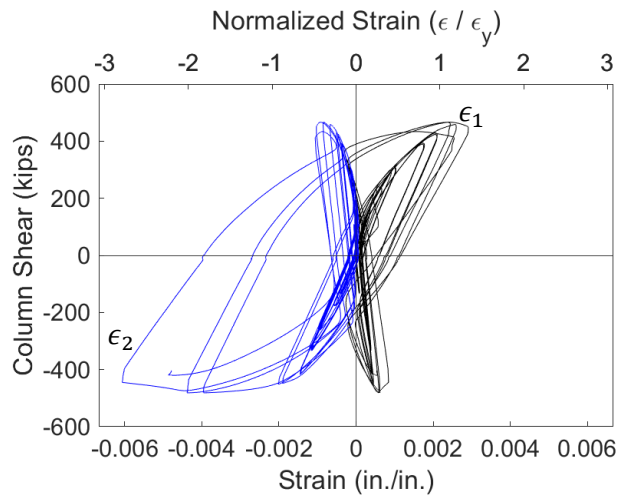


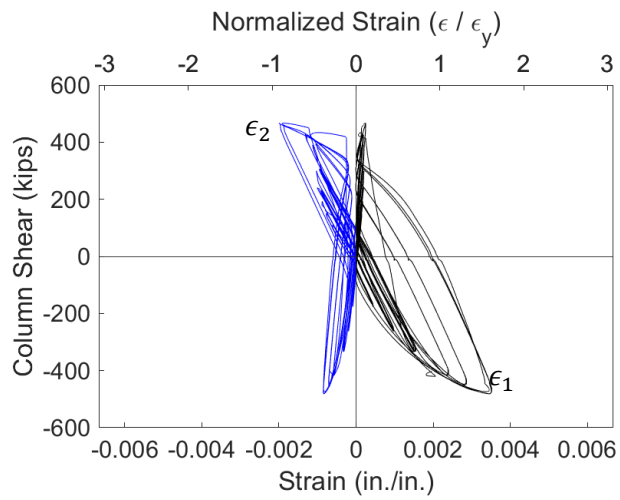
Figure 4.168 Specimen W1: Continuity Plate at Column Flange Edge Shear Strain Profile



(a) Layout

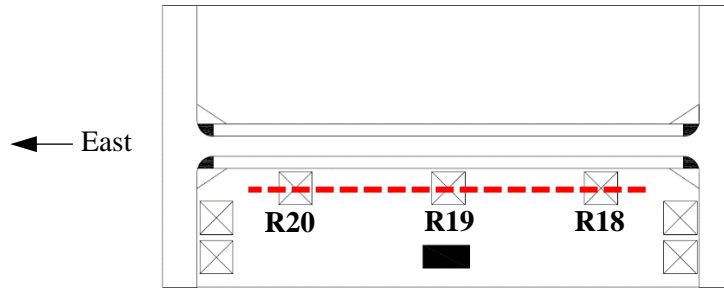


(b) Strain Gauge R16 Principal Strains

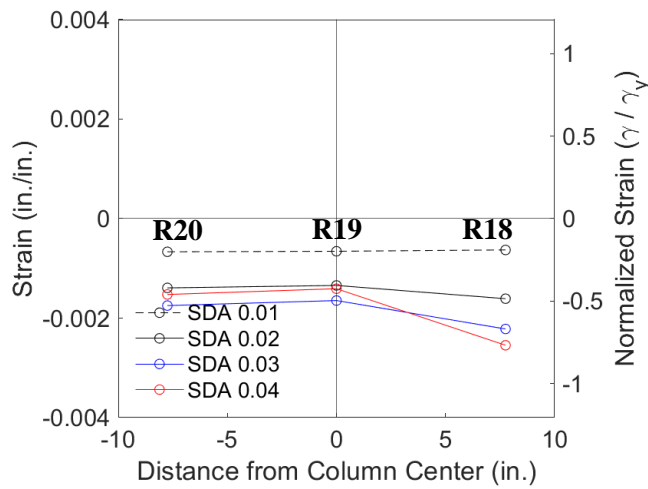


(b) Strain Gauge R22 Principal Strains

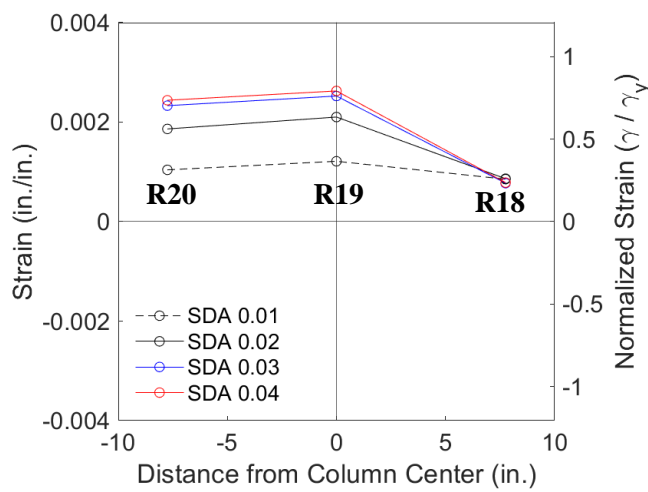
Figure 4.169 Specimen W1: Continuity Plate Strain Gauge Rosette Response



(a) Section Layout

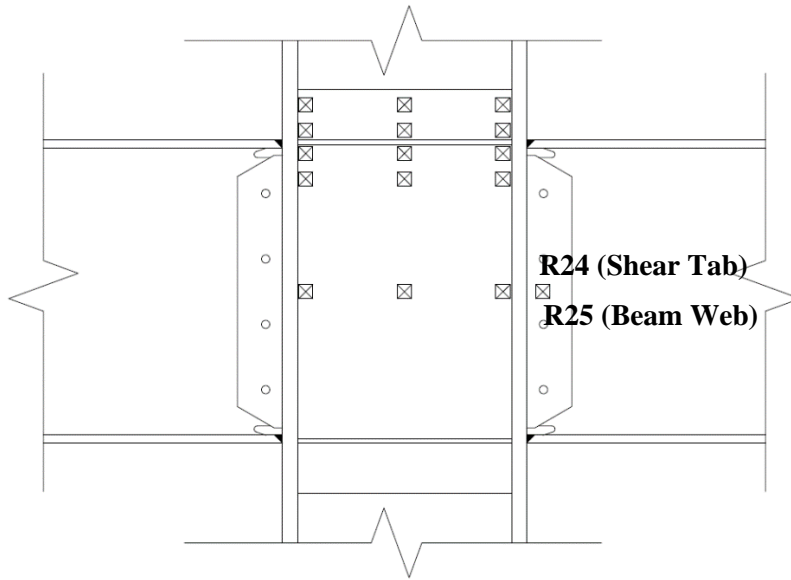


(b) Positive Drift

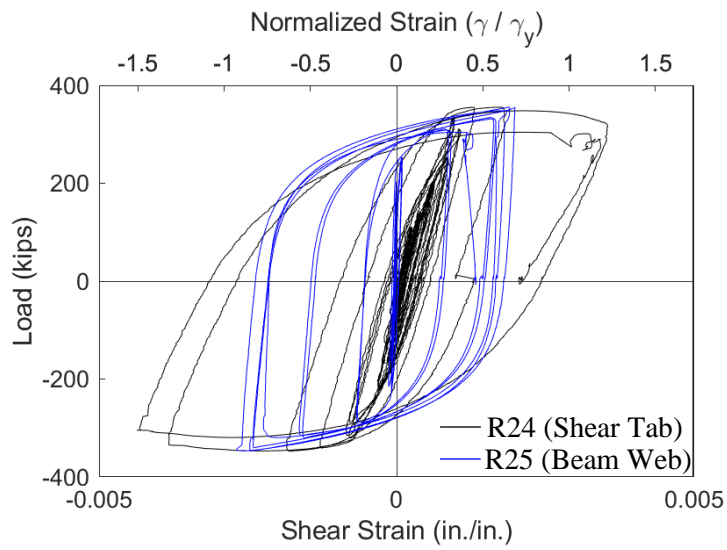


(c) Negative Drift

Figure 4.170 Specimen W1: Continuity Plate at Column Web Edge Shear Strain Profile



(a) Gauge Layout



(b) Strain Rosette Gauges R24 and R25

Figure 4.171 Specimen W1: Beam Shear Response

4.9 Specimen W2

4.9.1 General

Specimen W2 was designed to investigate use of the plastic methodology to design continuity plates. The continuity plate thickness was chosen to match the minimum thickness requirement of AISC 341, for which the plastic methodology results in an undersized continuity plate with a DCR of 1.43. Continuity plate double-sided fillet welds were sized such that $w = 0.75t_{cp}$. A pair of doubler plates stiffen the web of the column for panel zone yielding—these plates were extended 6 in. above and below the beam flange elevations. The doubler plate vertical welds use a PJP groove weld, and no horizontal welds were used in accordance with the current Provisions. Specimen W2 failed by a fracture of the east top and west bottom beam flange CJP weld during the second cycle of 0.06 rad drift. Figure 4.172 shows the specimen before testing.

4.9.2 Observed Performance

The observed response for Specimen W2 is described below.

- Figure 4.173 shows the connection during testing. The specimen met the AISC acceptance criteria by completing one complete cycle at 0.04 rad drift while the flexural strength at either column face did not degrade below 80% of the beam nominal flexural strength. Beam flange and web local buckling initiated at 0.03 rad drift and progressed throughout testing.
- Figure 4.174 and Figure 4.175 shows the bottom flange yielding and buckling of the east and west beams. The yielding of the flanges initiated during the 0.0075 rad drift cycles. It was observed that significant lateral-torsional buckling initiates at 0.04 rad drift and progresses in the later drift cycles.
- Figure 4.176 shows the progression of flange local buckling that developed in the east beam top flange. The local buckling develops in the flange of the beam in compression during that excursion and then is pulled relatively straight during the tension excursions.
- Figure 4.177 shows the initiation of a weld fracture during the second cycle of 0.03 rad drift. The fracture originates at the fusion face of the CJP weld and backing bar on the flange bevel side. Figure 4.178 shows the progression of this tear during the 0.04 rad and 0.05 rad drift cycles. At 0.05 rad drift cycles a weld tear on the top side

of the west beam bottom flange CJP weld was observed (see Figure 4.179). A similar fracture was observed in the east beam bottom flange CJP weld at 0.06 rad drift (see Figure 4.180).

- Figure 4.181 shows the severe lateral-torsional buckling, flange local buckling, and web local buckling of the east beam during the 0.06 rad drift cycles. The west beam has a similar profile with flanges arching up. Significant lateral bracing forces restraining the beams result in localized yielding at the restraint points.
- At -0.018 rad during the negative excursion of the east beam to 0.06 rad drift (2nd Cycle) the east beam top flange partially fractured (see Figure 4.182). This fracture extends from the top edge of the beam flange to about the centerline. The fracture initiated at the CJP weld root and deviated into the beam flange after traversing the CJP weld bevel for several inches. This weld fracture was accompanied by a tear at the far radius of the weld access hole (see Figure 4.183). Shortly after resuming load the west beam bottom flange experienced a similar fracture, propagating through 80% of the beam flange (see Figure 4.184).
- Figure 4.185 shows the connection after testing. Minor panel zone yielding was observed in the doubler plate after testing (see Figure 4.186). This picture also demonstrates that no continuity plate yielding was evident.
- No damage to the continuity plate fillet welds was observed during the testing or after test visual inspection (see Figure 4.187).

4.9.3 Recorded Response

4.9.3.1 Global Response

- Figure 4.188 shows the recorded displacement response of the beam tip measured with transducer L1 for the east beam and L2 for the west beam. The response from the east and west beams are shown in black and blue, respectively. The east beam top flange partially fractured at 0.018 rad during the second negative excursion to 0.06 rad drift. The west beam bottom flange fractured slightly past neutral during the positive excursion to 0.06 rad drift. Figure 4.189 shows the column shear versus the applied story drift response.
- Figure 4.190 shows the load-displacement response of the beams.

- Figure 4.191 shows the computed moment at the column face (M_f) versus the story drift angle. Two horizontal axes at 80% of the nominal plastic moment (M_{pn}) of the beam section are also added. In addition, two vertical axes at ± 0.04 rad story drift show the drift required for SMF connections per AISC 341. It is observed that the beams developed about 1.4 times its nominal plastic bending moment. If the moment is computed at the plastic hinge location and compared to the expected plastic moment, then the peak connection strength factor (C_{pr}) is 1.23 and 1.23 for the east and west beams respectively.
- Figure 4.192 shows the plastic response of the specimen. The plastic response is computed using the procedure outlined in Section 3.7. The computed elastic stiffness of the specimen was determined to be 144.8 kips/in.
- Figure 4.193 shows minor hysteretic behavior in the panel zone.
- Figure 4.194 shows zero hysteretic behavior in the column.
- Figure 4.195 shows the dissipated energy of Specimen W2. Dotted vertical lines on the graph demonstrate the completion of each group of cycles, and the dashed red vertical line shows the completion of the first cycle of 0.04 rad in the AISC loading. It is observed that the completion of the first drift cycle of 0.04 rad (the requirement for SMF connections per AISC 341) occurs after 1,755 kip-ft of energy has been dissipated. The connection did not degrade below $0.8M_{pn}$ until fracture of the east beam top flange occurred and 4,000 kip-ft of energy had been dissipated. Therefore only 44% of the energy dissipation capacity was utilized after the completion of the SMF requirement. It is observed that nearly all (96%) of the energy dissipation capacity occurred in the beam.

4.9.3.2 Local Response

- Figure 4.196 and Figure 4.197 shows the extreme fiber response of the east beam top and bottom flanges. Strains on the order of 4% ($20\epsilon_y$) are observed in the flanges which are exacerbated by high local curvatures and weak axis bending. Figure 4.198 and Figure 4.199 show the extreme fiber response of the west beam top and bottom flanges.

- Figure 4.200 shows the strain gauge response of the west column flange above the beam top flange. It is observed that the column flange did not yield but moderate levels of warping occurred during the latter part of the loading protocol.
- Figure 4.201 shows the horizontal strain pattern on the doubler plate through two sections. Horizontal strains in the center of the doubler plate are mostly balanced. Figure 4.202 shows the shear stress distribution in the doubler plate. The center of the doubler plate sees the most significant strains ($2\gamma_y$). Yielding of the doubler plate was anticipated.
- Figure 4.203 shows the horizontal shear distribution of the top flange continuity plate. The strain response is equal and opposite across the continuity plate. The continuity plate reaches yielding levels of horizontal strain. Moderate shear strains are present at the edges of the continuity plate in contact with the column flange (see Figure 4.204). Figure 4.205 shows the principal strains of strain gauge rosette R16 and R22, the outermost strain gauges, during testing. It is observed that the cyclic strains are limited to $\pm\epsilon_y$.
- Figure 4.206 shows the shear response of the continuity plate on the edge fillet welded with the doubler plate.
- Figure 4.207 shows the shear response of the west beam adjacent to the column.

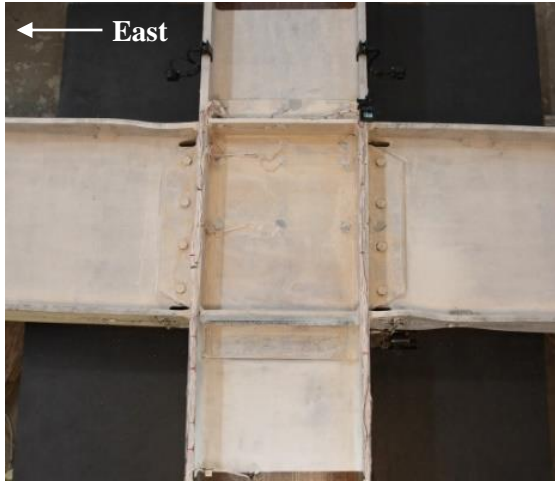


(a) Overview

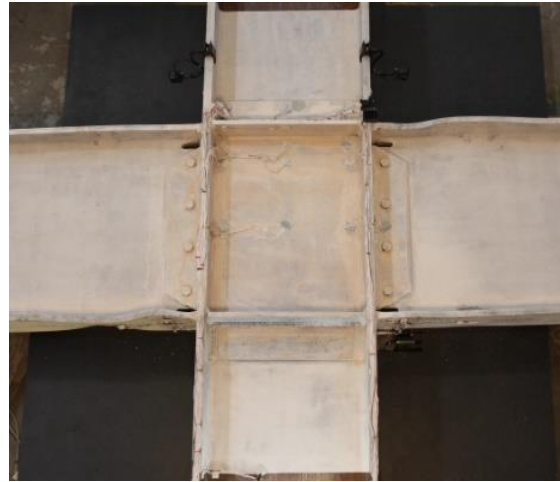


(b) Connection Region

Figure 4.172 Specimen W2: Connection before Testing



(a) +0.03 rad (2nd Cycle)



(b) -0.03 rad (2nd Cycle)



(c) +0.04 rad (2nd Cycle)



(d) -0.04 rad (2nd Cycle)



(e) +0.05 rad (1st Cycle)



(f) -0.05 rad (1st Cycle)

Figure 4.173 Specimen W2: Connection during Testing



(a) -0.02 rad (2nd Cycle)



(b) -0.03 rad (2nd Cycle)



(c) +0.04 rad (2nd Cycle)

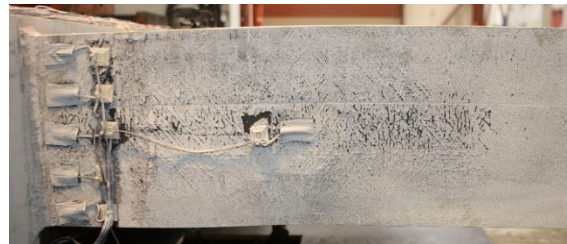


(d) -0.05 rad (2nd Cycle)

Figure 4.174 Specimen W2: East Beam Bottom Flange Yielding



(a) -0.02 rad (2nd Cycle)



(b) -0.03 rad (2nd Cycle)



(c) +0.04 rad (2nd Cycle)



(d) -0.05 rad (2nd Cycle)

Figure 4.175 Specimen W2: West Beam Bottom Flange Yielding



(a) +0.03 rad (2nd Cycle)



(b) +0.04 rad (2nd Cycle)

Figure 4.176 Specimen W2: East Beam Top Flange Local Buckling



(a) Overview



(b) Weld Fracture

Figure 4.177 Specimen W2: East Beam Top Flange CJP Weld Tear at -0.03 rad (2nd Cycle)



(a) -0.04 rad (2nd Cycle)



(b) -0.05 rad (2nd Cycle)

Figure 4.178 Specimen W2: East Beam Top Flange CJP Weld Tear Progression



(a) Overview



(b) Weld Fracture

Figure 4.179 Specimen W2: West Beam Bottom Flange CJP Weld Fracture at: -0.05 rad (2nd Cycle)



(a) Overview



(b) Weld Fracture

Figure 4.180 Specimen W2: East Beam Bottom Flange CJP Weld Fracture at: +0.06 rad (1st Cycle)



Figure 4.181 Specimen W2: East Beam Bottom Flange Lateral-Torsional Buckling at: -0.06 rad (1st Cycle)



Figure 4.182 Specimen W2: East Beam Top Flange Partial Fracture during Excursion to -0.06 rad (2nd Cycle)



(a) Overview



(b) Weld Fracture

Figure 4.183 Specimen W2: East Beam Top Flange Weld Access Hole Tear at -0.06 rad



Figure 4.184 Specimen W2: West Beam Bottom Flange Fracture during Excursion to -0.06 rad (2nd Cycle)



Figure 4.185 Specimen W2: Connection at End of Test



Figure 4.186 Specimen W2: Panel Zone (End of Test)



(a) East Beam Top Flange



(b) West Beam Top Flange



(c) East Beam Bottom Flange



(d) West Beam Bottom Flange

Figure 4.187 Specimen W2: Continuity Plate Fillet Welds (End of Test)

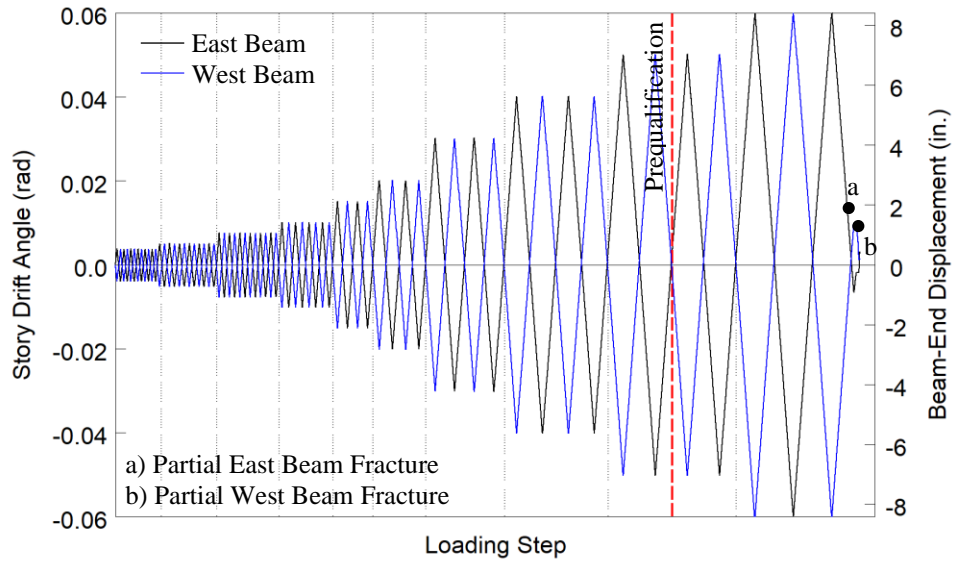


Figure 4.188 Specimen W2: Recorded Loading Sequence

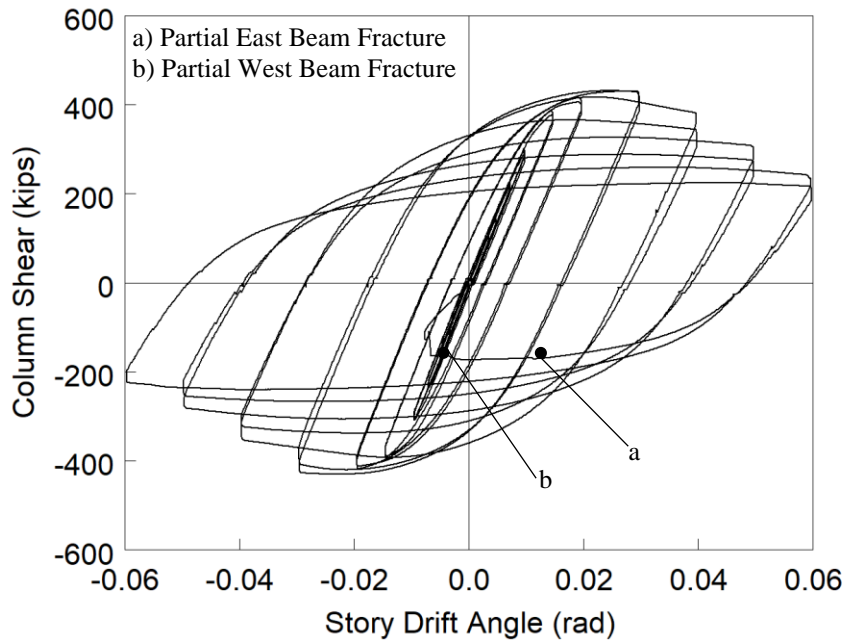
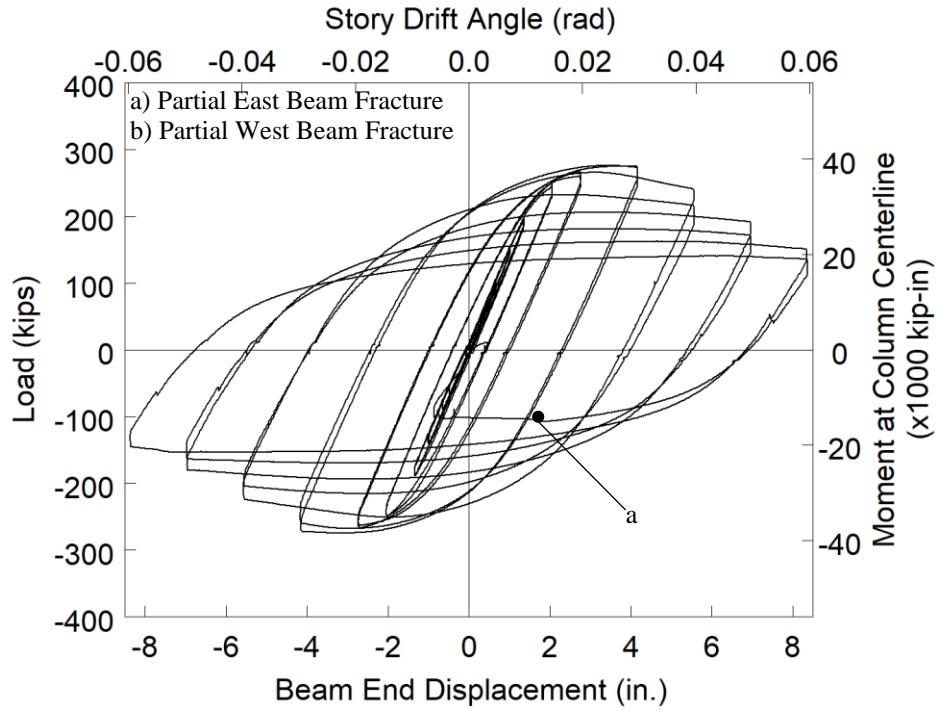
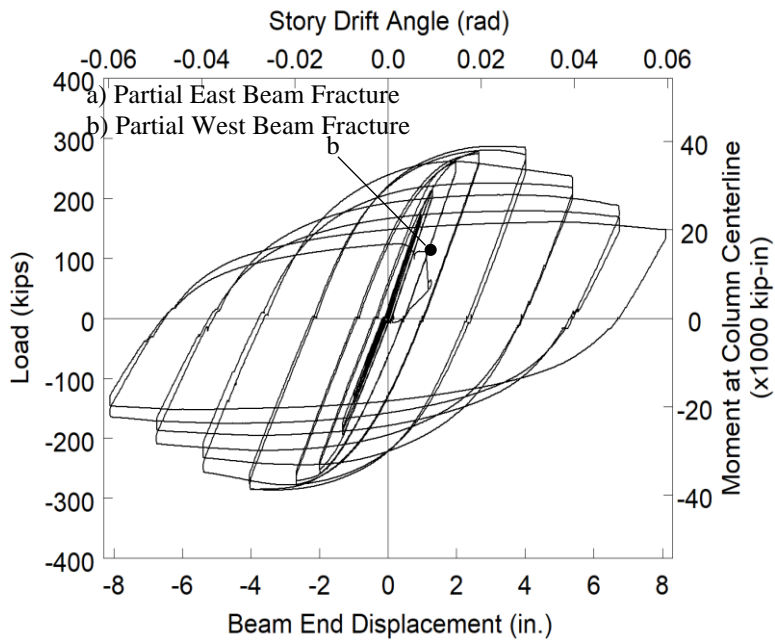


Figure 4.189 Specimen W2: Column Shear versus Story Drift Angle

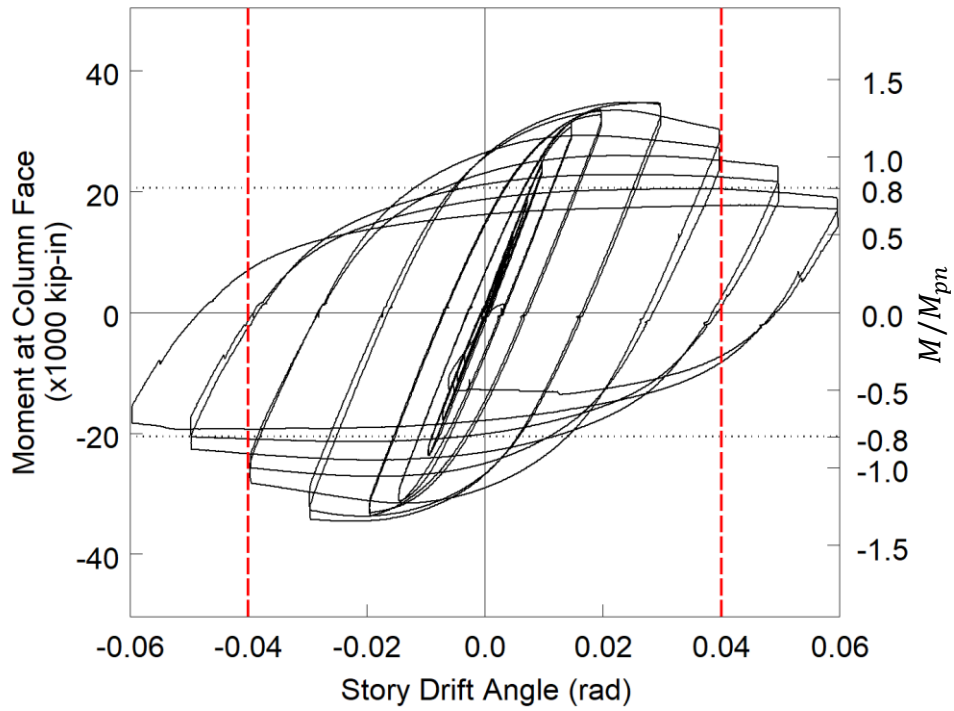


(a) East Beam

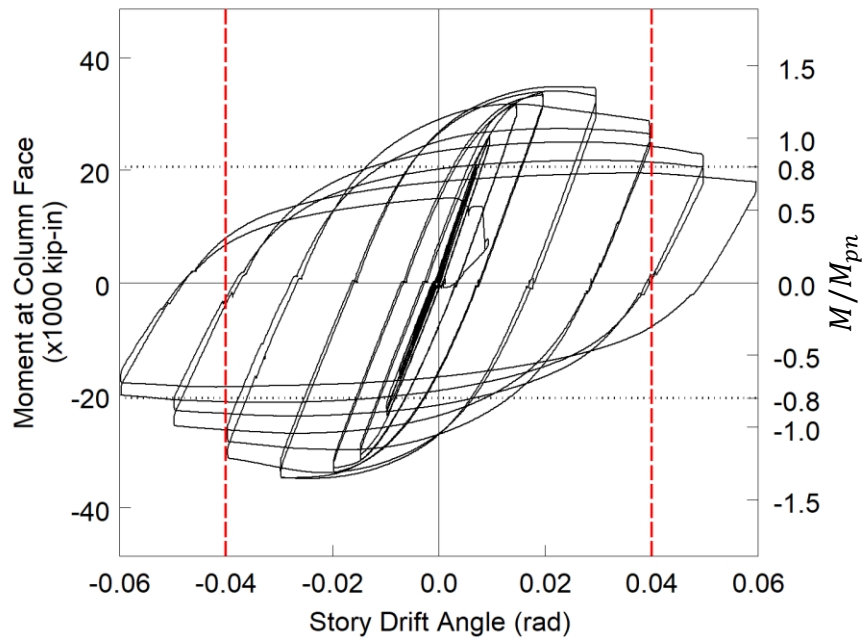


(b) West Beam

Figure 4.190 Specimen W2: Applied Load versus Beam End Displacement Response

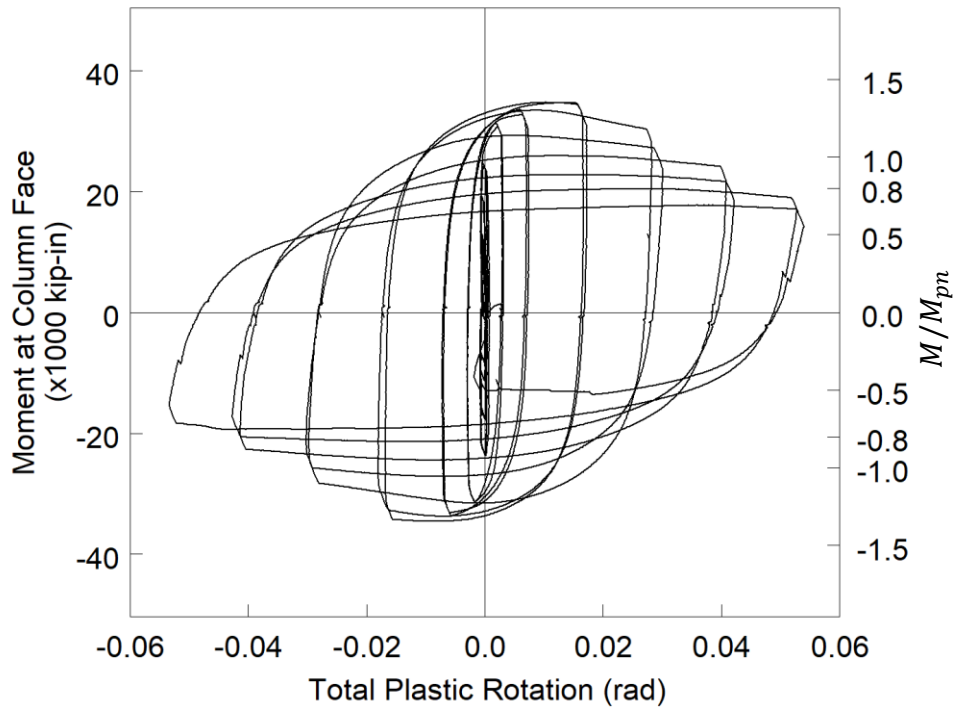


(a) East Beam

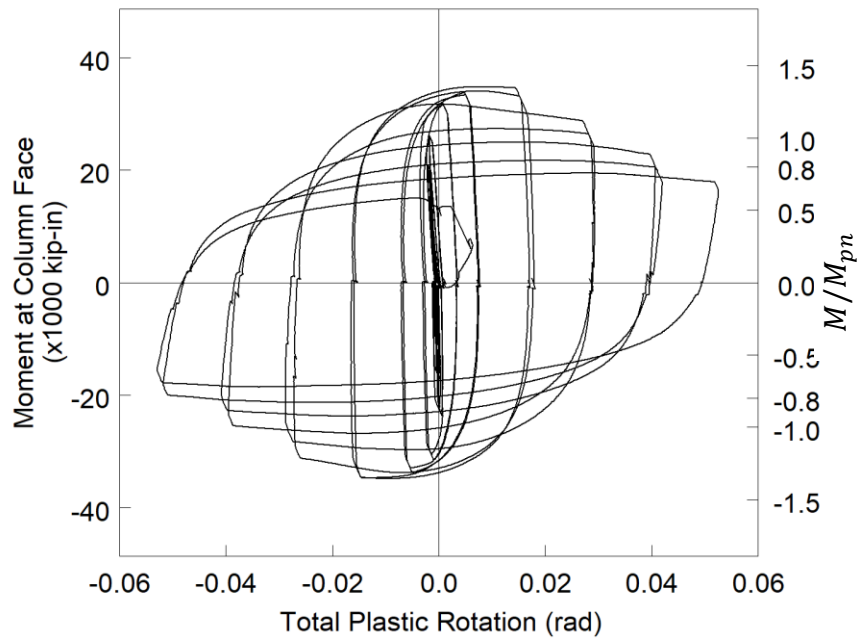


(b) West Beam

Figure 4.191 Specimen W2: Moment at Column Face versus Story Drift Response



(a) East Beam



(b) West Beam

Figure 4.192 Specimen W2: Moment at Column Face versus Plastic Rotation

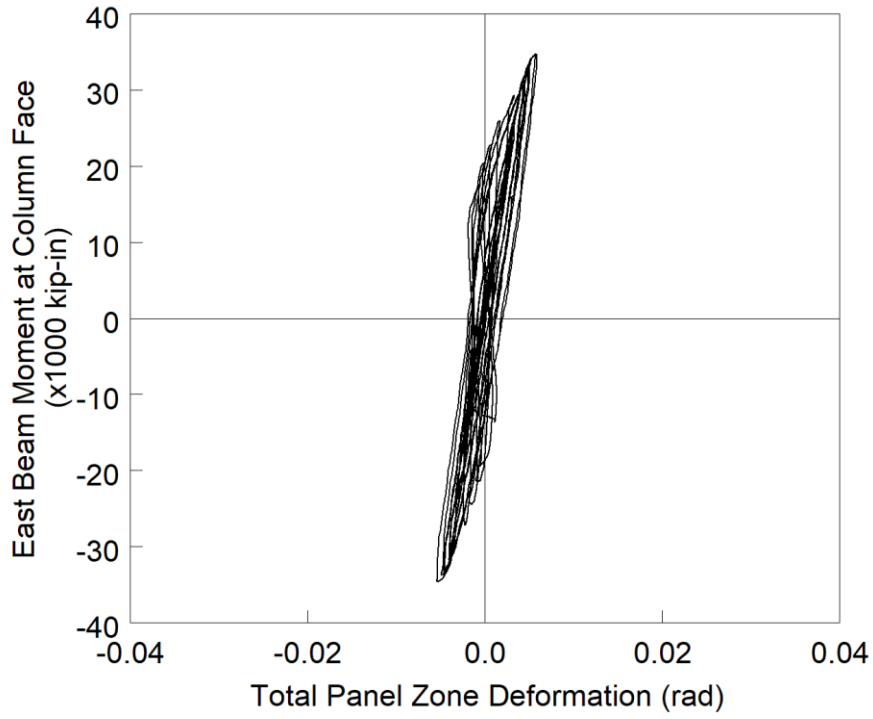


Figure 4.193 Specimen W2: Panel Zone Shear Deformation

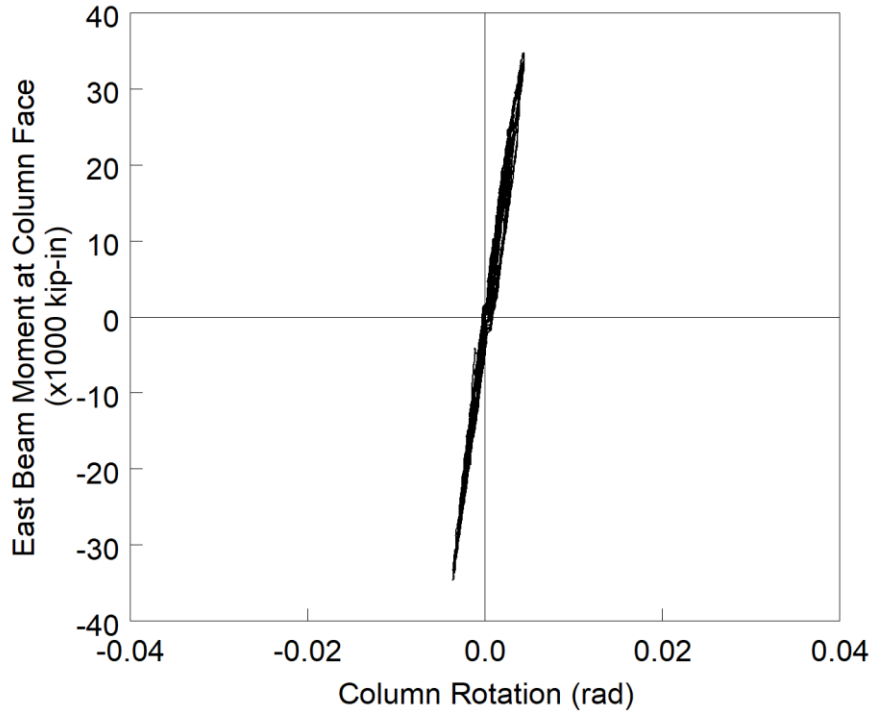


Figure 4.194 Specimen W2: Column Rotation

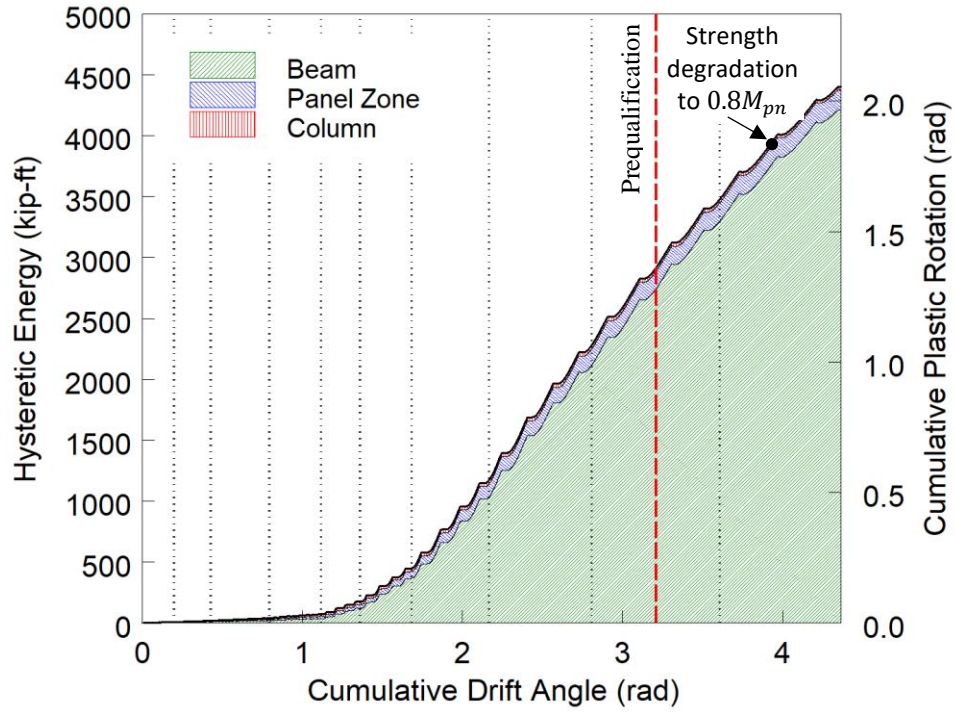
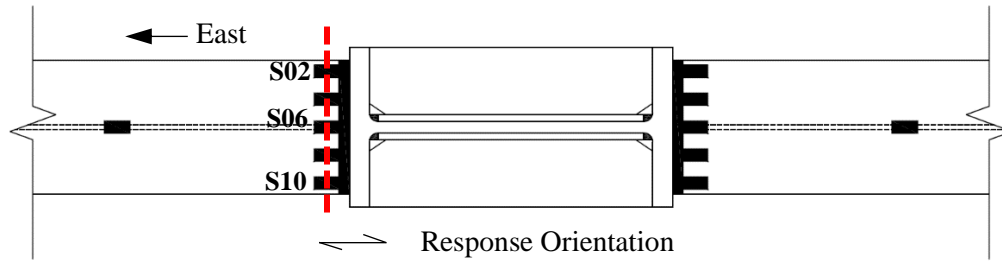
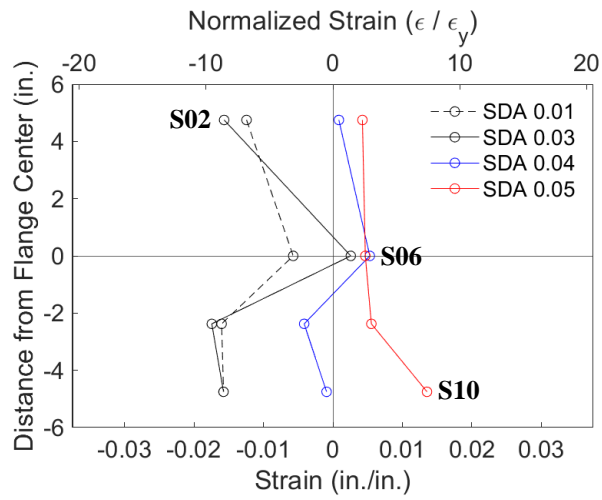


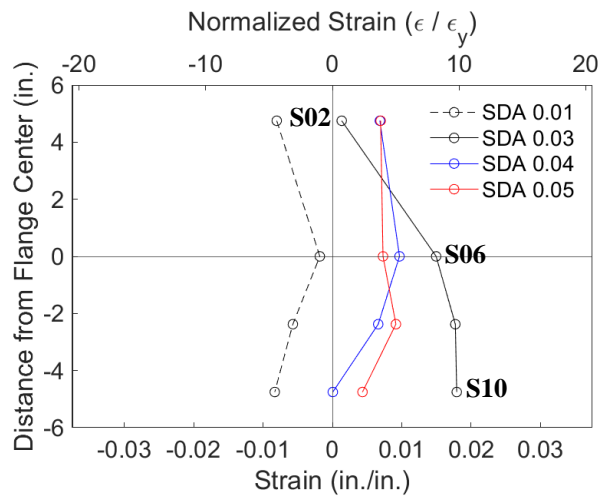
Figure 4.195 Specimen W2: Energy Dissipation



(a) Section

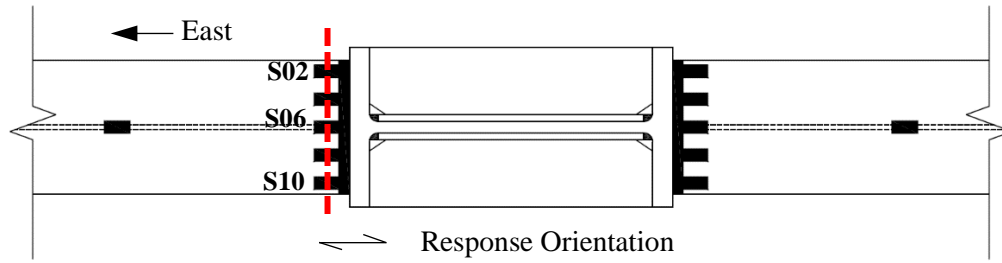


(b) Positive Drift

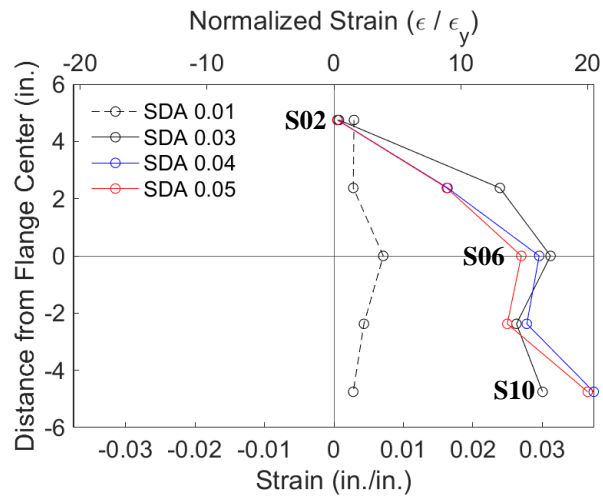


(c) Negative Drift

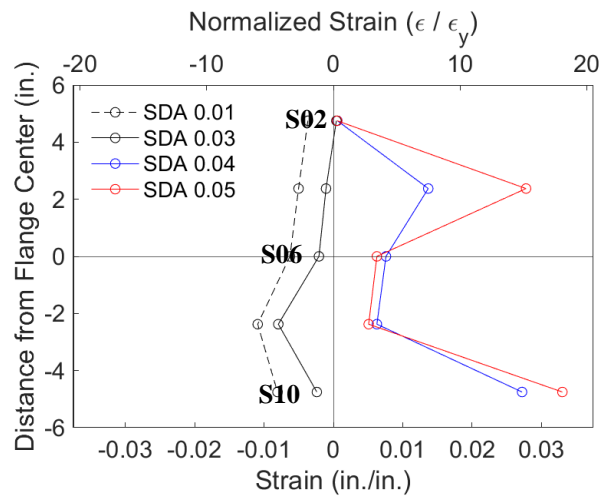
Figure 4.196 Specimen W2: Topside of East Beam Top Flange Strain Profile



(a) Section

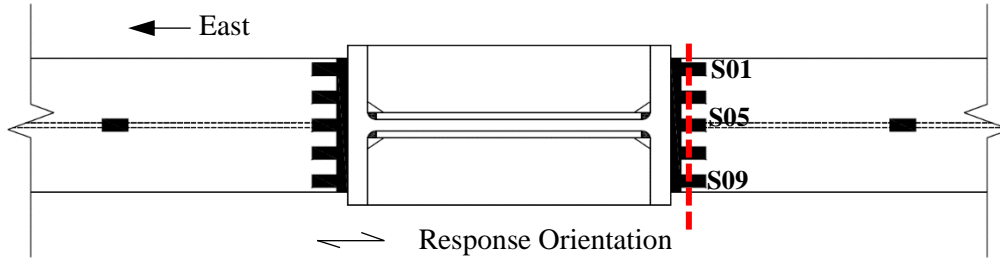


(b) Positive Drift

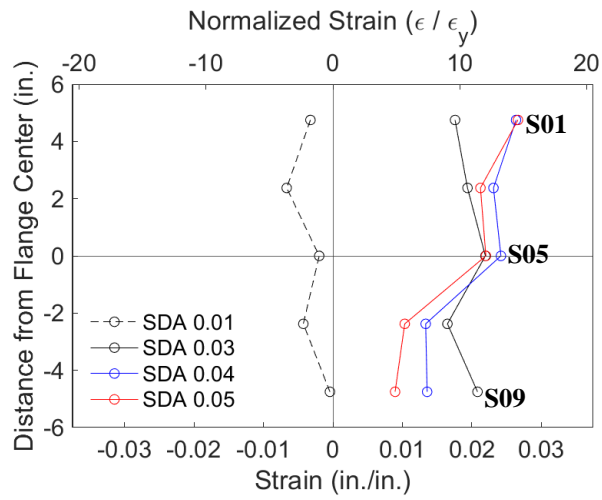


(c) Negative Drift

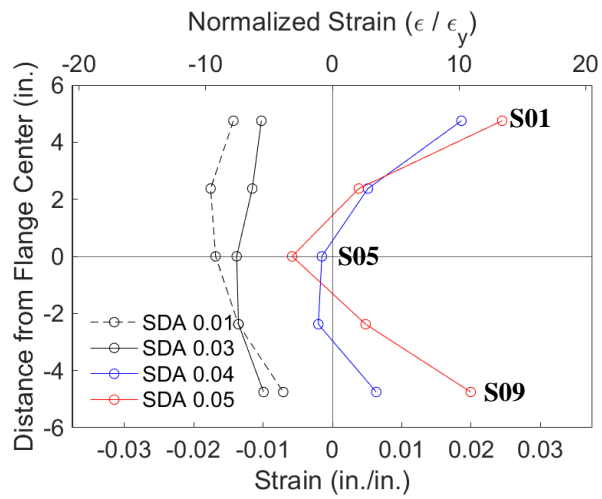
Figure 4.197 Specimen W2: Underside of East Beam Bottom Flange Strain Profile



(a) Section

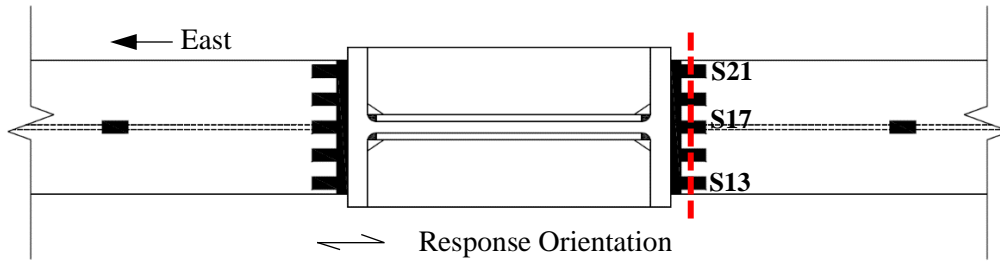


(b) Positive Drift

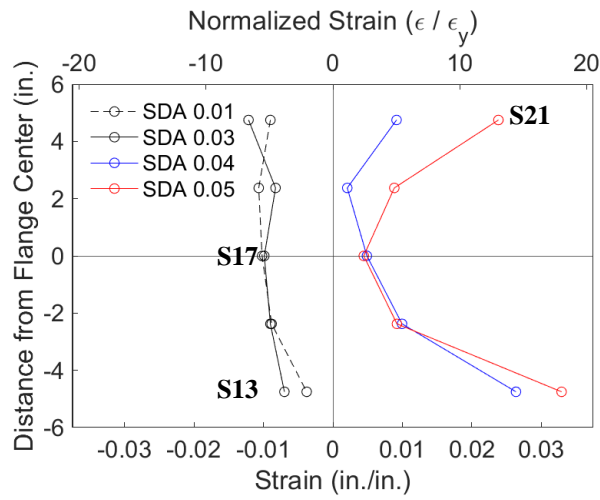


(c) Negative Drift

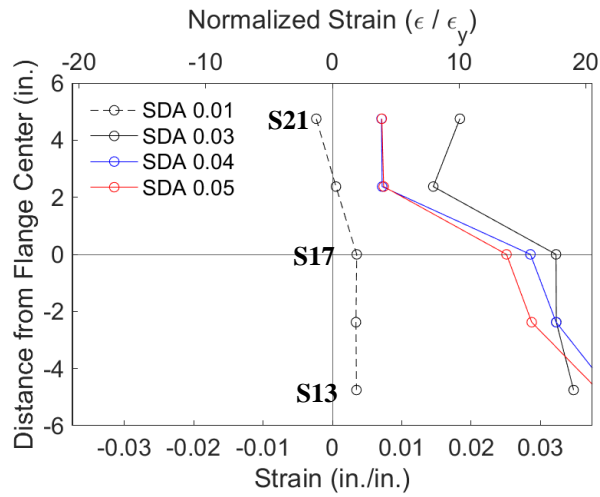
Figure 4.198 Specimen W2: Topside of West Beam Top Flange Strain Profile



(a) Section

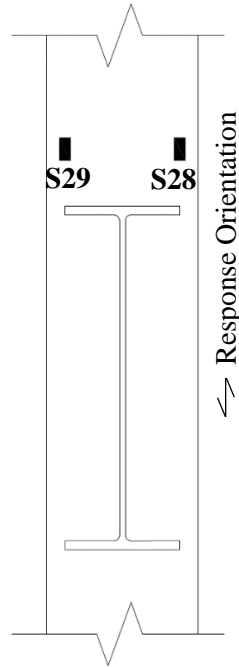


(b) Positive Drift

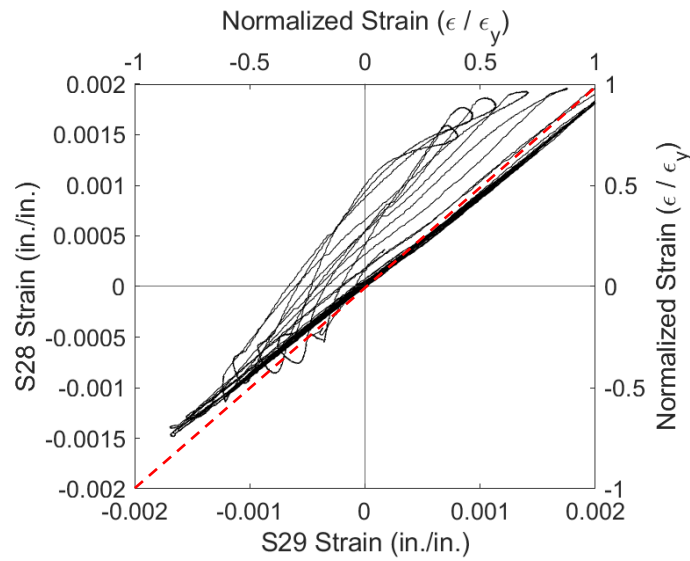


(c) Negative Drift

Figure 4.199 Specimen W2: Underside of West Beam Bottom Flange Strain Profile

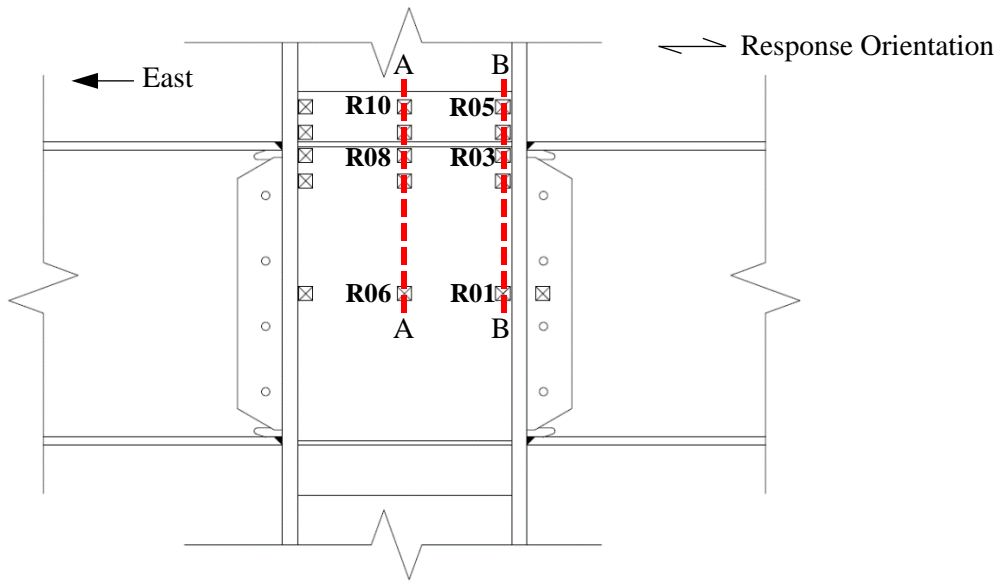


(a) Gauge Layout

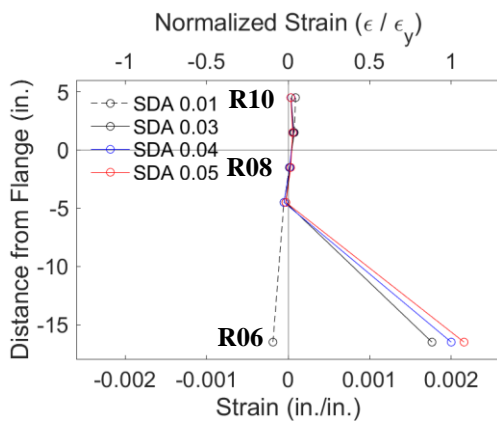


(b) Response

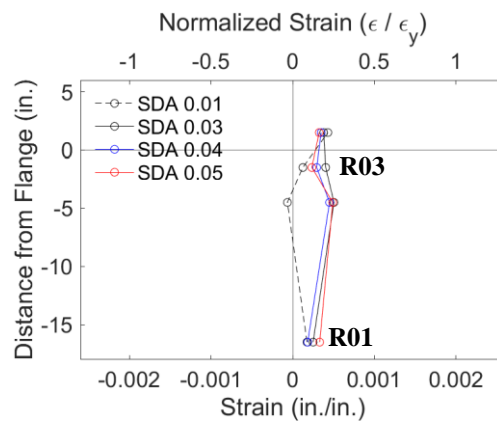
Figure 4.200 Specimen W2: Column Flange Warping



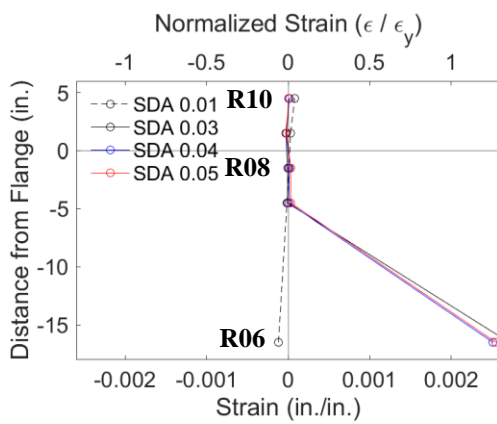
(a) Section Layout



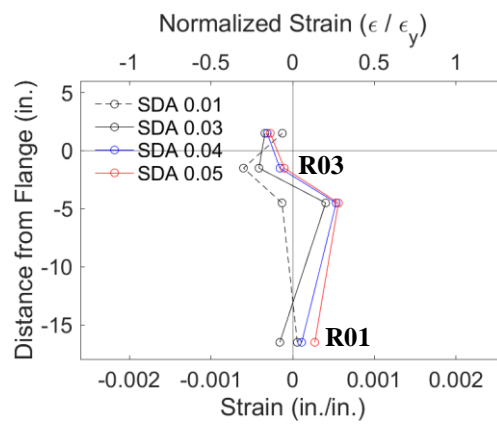
(b) Section A-A: Positive Drift



(c) Section B-B: Positive Drift

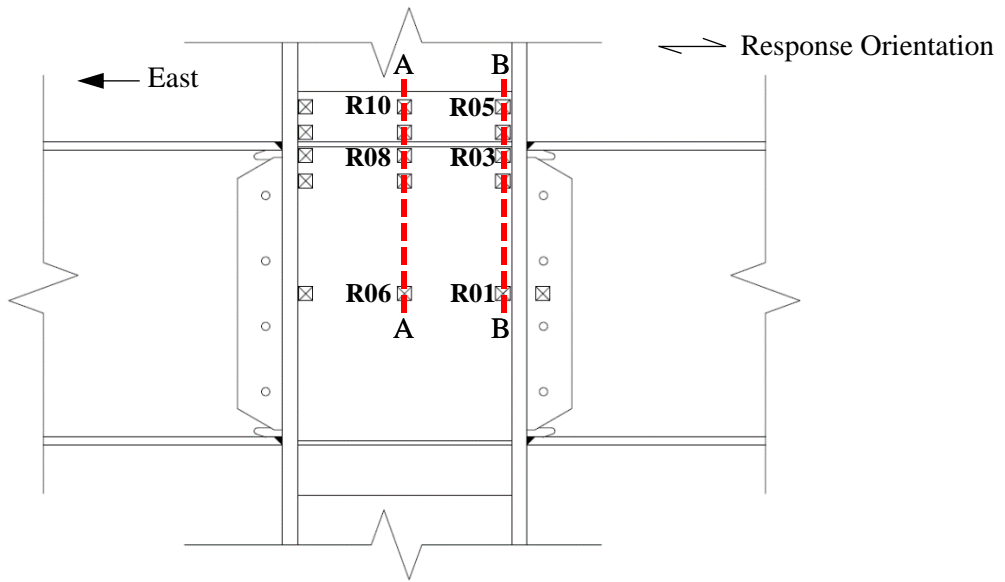


(d) Section A-A: Negative Drift

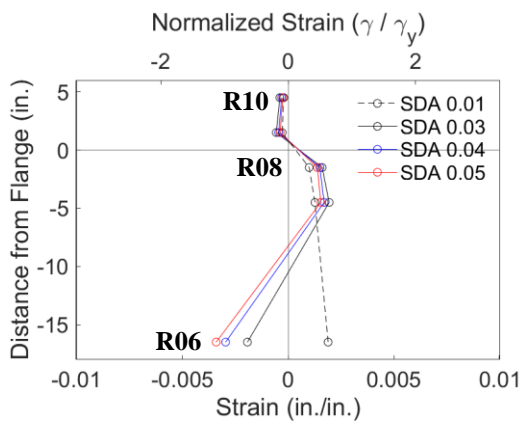


(e) Section B-B: Negative Drift

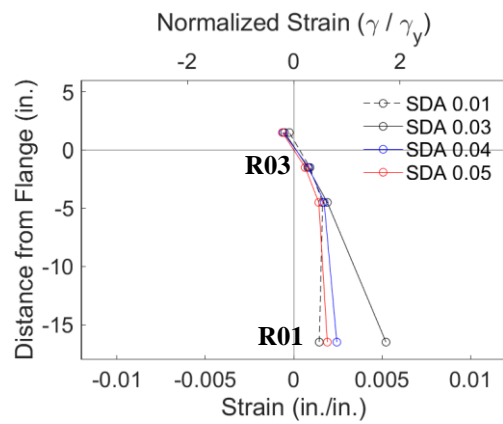
Figure 4.201 Specimen W2: Panel Zone Strain Profile



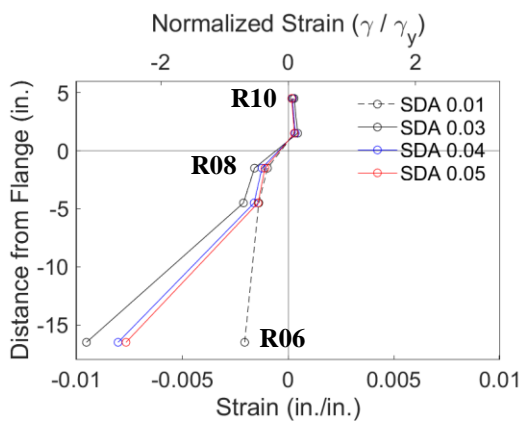
(a) Section Layout



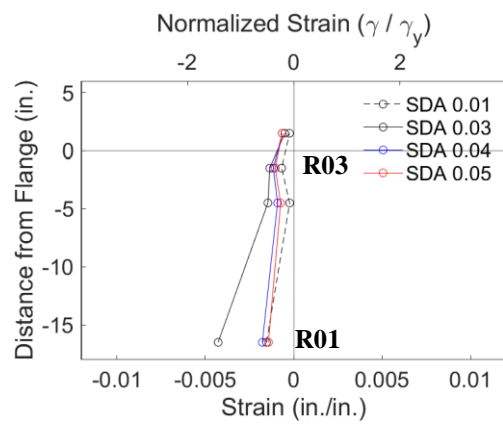
(b) Section A-A: Positive Drift



(c) Section B-B: Positive Drift



(d) Section A-A: Negative Drift



(e) Section B-B: Negative Drift

Figure 4.202 Specimen W2: Panel Zone Shear Strain Profile

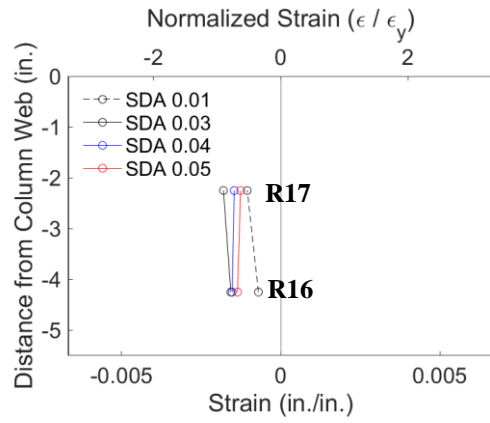
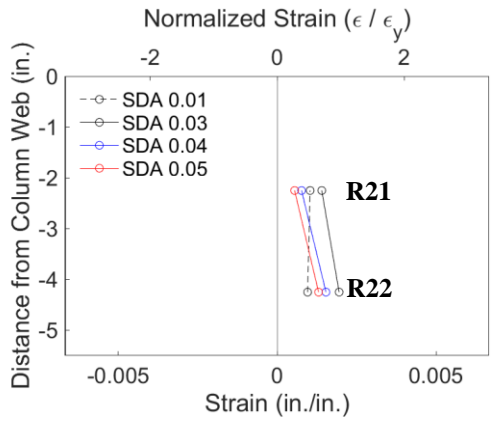
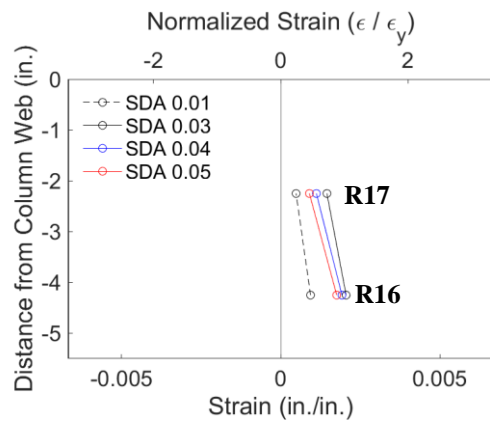
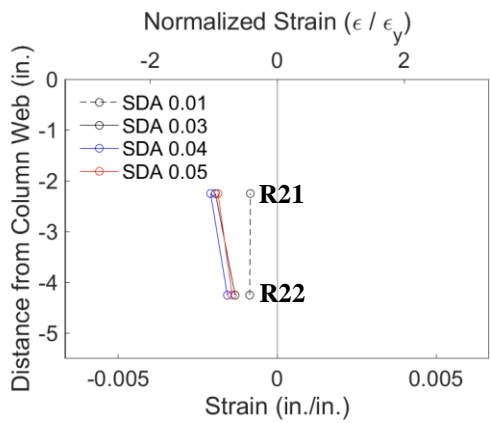
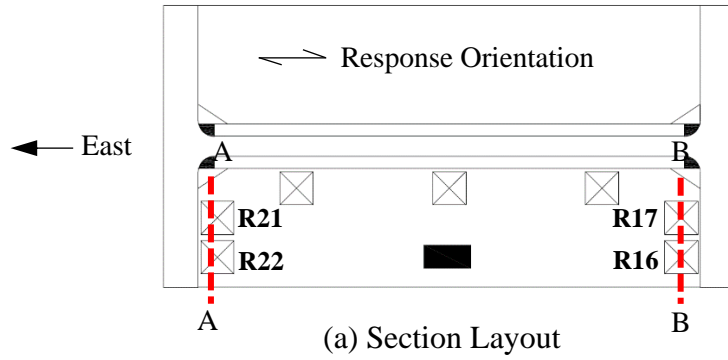


Figure 4.203 Specimen W2: Continuity Plate at Column Flange Edge Strain Profile

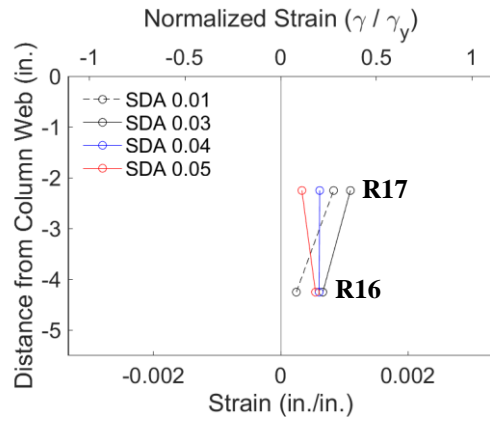
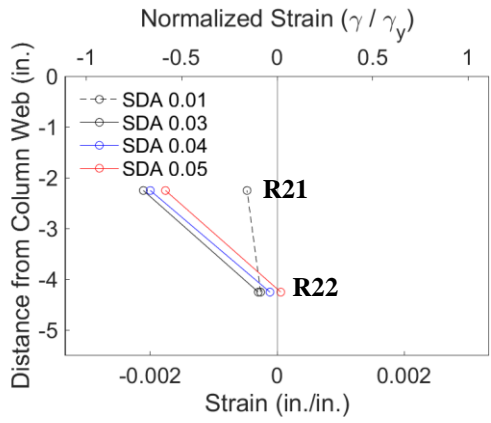
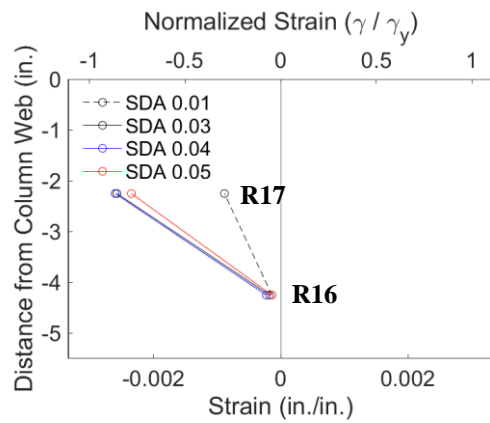
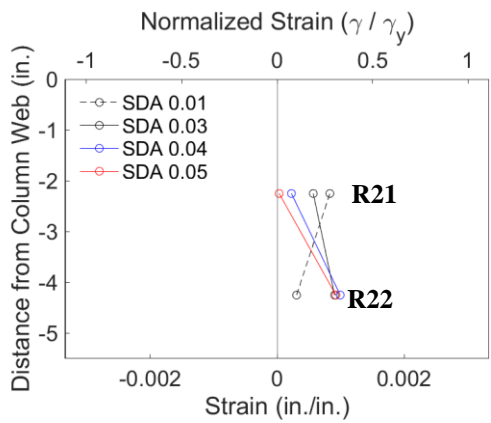
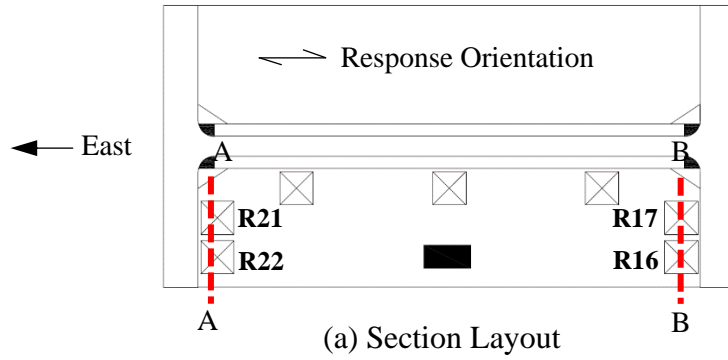
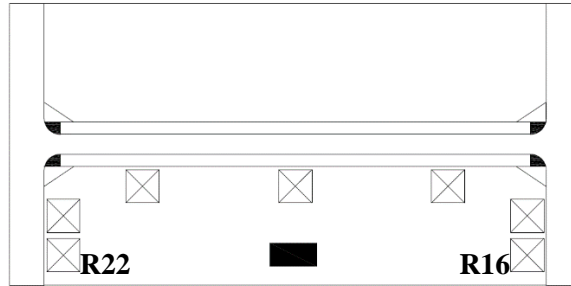
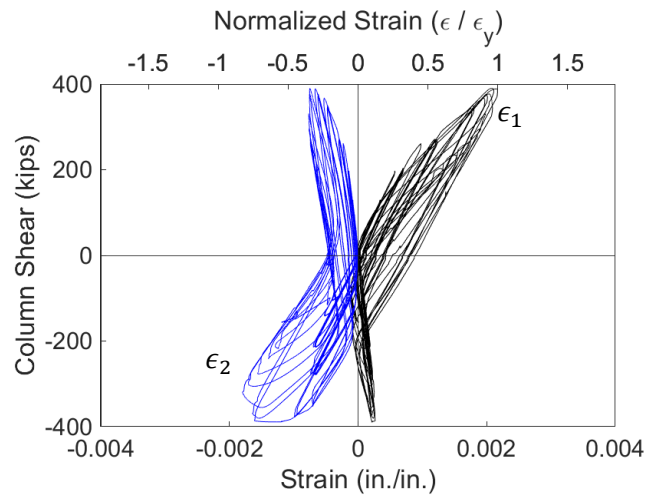


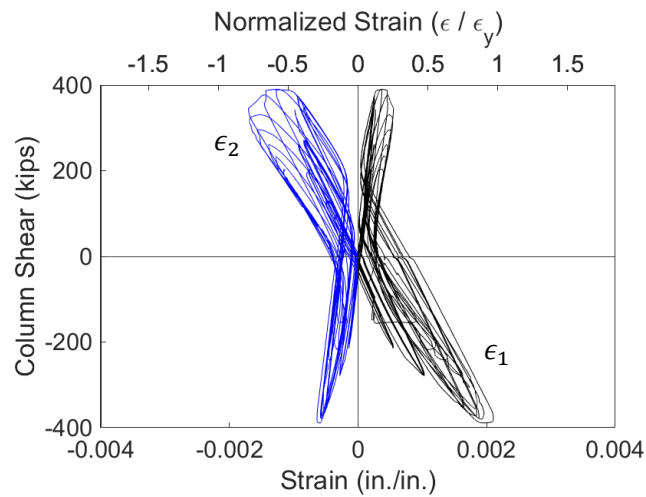
Figure 4.204 Specimen W2: Continuity Plate at Column Flange Edge Shear Strain Profile



(a) Layout

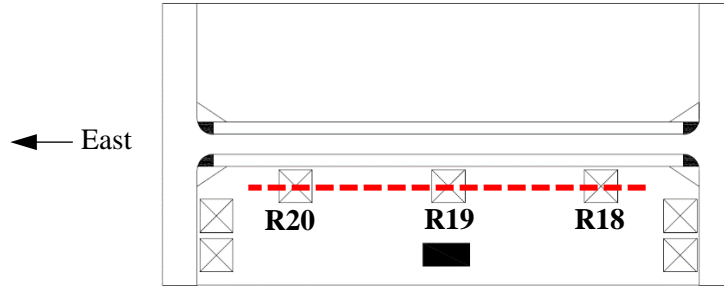


(b) Strain Gauge R16 Principal Strains

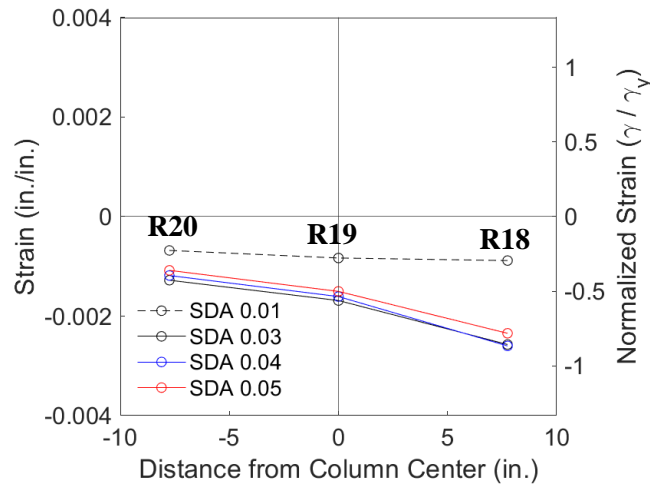


(b) Strain Gauge R22 Principal Strains

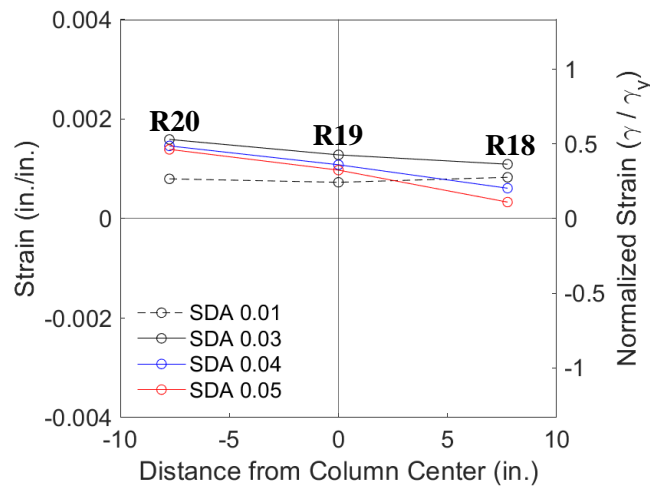
Figure 4.205 Specimen W2: Continuity Plate Strain Gauge Rosette Response



(a) Section Layout

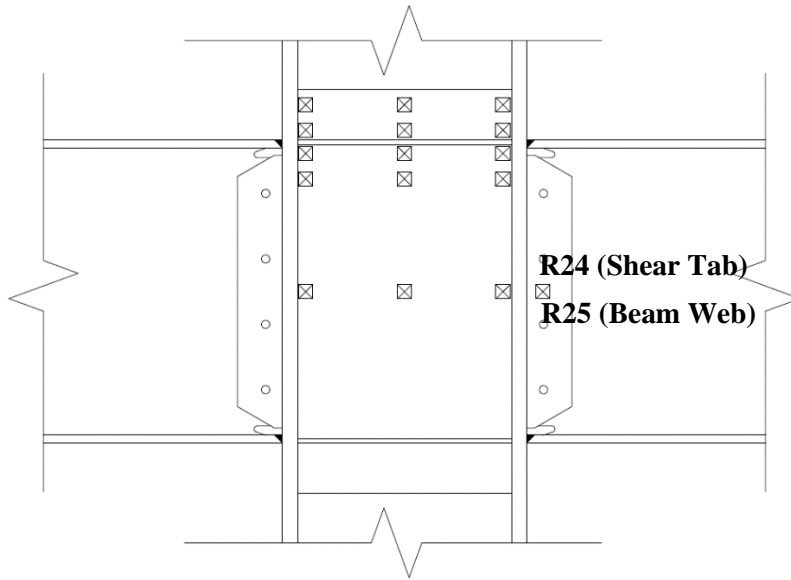


(b) Positive Drift

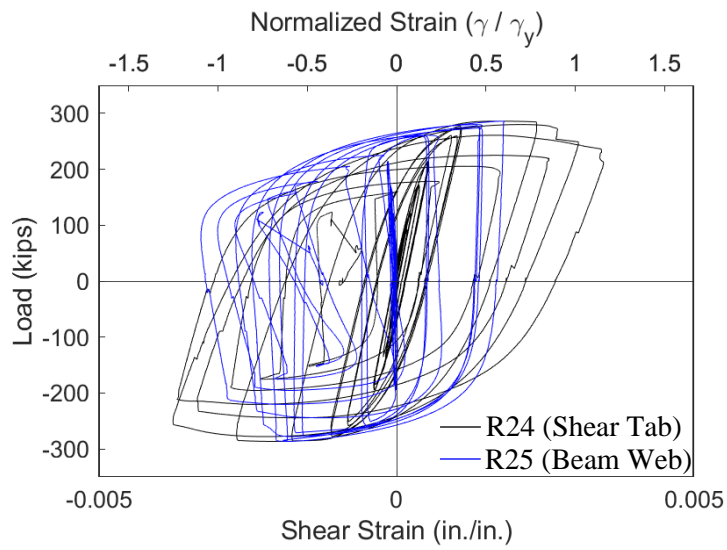


(c) Negative Drift

Figure 4.206 Specimen W2: Continuity Plate at Column Web Edge Shear Strain Profile



(a) Gauge Layout



(b) Strain Rosette Gauges R24 and R25

Figure 4.207 Specimen W2: Beam Shear Response

4.10 Specimen W3

4.10.1 General

Specimen W3 was designed to investigate use of the plastic methodology to design continuity plates. The resulting continuity plates were thinner than the current AISC 341 Provisions. Continuity plate double-sided fillet welds were sized such that $w = 0.75t_{cp}$. A pair of doubler plates stiffen the web of the column for panel zone yielding—these plates were extended 6 in. above and below the beam flange elevations. The doubler plates were designed to result in a weak panel zone, with a resulting DCR of 1.07; additionally, the stability criteria of the doubler plates were violated. The doubler plate vertical welds use a fillet weld sized to develop the shear strength of the plate, and no horizontal welds were used in accordance with the current Provisions. Specimen W3 failed by a fracture of the east beam top flange CJP weld during the second cycle of 0.06 rad drift. Figure 4.208 shows the specimen before testing.

4.10.2 Observed Performance

The observed response for Specimen W3 is described below.

- Figure 4.209 shows the connection during testing. The specimen met the AISC acceptance criteria by completing one complete cycle at 0.04 rad drift while the flexural strength at either column face did not degrade below 80% of the beam nominal flexural strength. Beam flange and web local buckling initiated at 0.03 rad drift and progressed throughout testing.
- Figure 4.210 and Figure 4.211 show the east beam bottom flange and west beam bottom flange during testing. The gradual progression of yielding, flange local buckling, and lateral-torsional buckling is observed. The progression of flange local buckling between the second cycle of 0.03 rad and the first cycle of 0.04 rad is shown in Figure 4.212.
- Figure 4.213 shows the initiation of tearing in the weld access holes. All four weld access holes show a similar behavior.
- Severe web buckling develops in both beams during the 0.05 rad drift cycles (see Figure 4.214). Figure 4.215 shows a similar severity of flange local buckling during the 0.05 rad drift cycles.

- Figure 4.216 shows the gradual progression of tearing in the east beam top flange CJP weld. The tear initiated at the CJP weld root during the second cycle of 0.04 rad drift. A similar tear was observed in the west beam top flange CJP weld (not pictured). During the first negative excursion to 0.06 rad drift the east beam top flange fractured through 60% of the width of the flange. The tear of the top flange was accompanied with a 5-in. tear of the beam web extending outward from the radius of the weld access hole (see Figure 4.217).
- Although the root of the CJP weld started to tear during earlier cycles the propagation of the tear to the top surface of the CJP weld occurred when the beam was under global compression during the first positive excursion of 0.06 rad drift (see Figure 4.218). This occurs due to the high local curvature of the flange local buckling. During the first negative excursion of 0.06 rad drift the fracture propagates to 60% of the beam flange width (see Figure 4.219). During the second negative excursion of 0.06 rad drift the east beam top flange fractures completely.
- Figure 4.220 shows the connection at the end of testing.
- Figure 4.221 shows a partial fracture of the west beam top flange at the end of testing. Also observed in this photo is minor column yielding above the beam flange.
- No yielding or damage to the continuity plate fillet welds was observed during testing (see Figure 4.222 and Figure 4.223). A detailed view of four of the continuity plate fillet welds is shown in Figure 4.224. Similarly, no damage was observed to the doubler plate fillet weld.

4.10.3 Recorded Response

4.10.3.1 Global Response

- Figure 4.225 shows the recorded displacement response of the beam tip measured with transducer L1 for the east beam and L2 for the west beam. The response from the east and west beams are shown in black and blue, respectively. The east beam top flange partially fractured at -0.038 rad during the first negative excursion to 0.06 rad drift. The remainder of the east beam top flange fractured during at 0.01 rad during the second negative excursion of 0.06 rad drift.
- Figure 4.227 shows the load-displacement response of the beams.

- Figure 4.228 shows the computed moment at the column face (M_f) versus the story drift angle. Two horizontal axes at 80% of the nominal plastic moment (M_{pn}) of the beam section are also added. In addition, two vertical axes at ± 0.04 rad story drift show the drift required for SMF connections per AISC 341. It is observed that the beams developed about 1.4 times its nominal plastic bending moment. If the moment is computed at the plastic hinge location and compared to the expected plastic moment, then the peak connection strength factor (C_{pr}) is 1.18 and 1.22 for the east and west beams respectively.
- Figure 4.229 shows the plastic response of the specimen. The plastic response is computed using the procedure outlined in Section 3.7. The computed elastic stiffness of the specimen was determined to be 100.8 kips/in.
- Figure 4.230 shows minor hysteretic behavior in the panel zone.
- Figure 4.231 shows minor hysteretic behavior from the column.
- Figure 4.232 shows the dissipated energy of Specimen W3. Dotted vertical lines on the graph demonstrate the completion of each group of cycles, and the dashed red vertical line shows the completion of the first cycle of 0.04 rad in the AISC loading. It is observed that the completion of the first drift cycle of 0.04 rad (the requirement for SMF connections per AISC 341) occurs after 1,255 kip-ft of energy has been dissipated. The connection did not degrade below $0.8M_{pn}$ until fracture of the east beam top flange occurred and 2,793 kip-ft of energy had been dissipated. Therefore only 45% of the energy dissipation capacity was utilized after the completion of the SMF requirement. It is observed that nearly all (94%) of the energy dissipation capacity occurred in the beam.

4.10.3.2 Local Response

- Figure 4.233 and Figure 4.234 show the extreme fiber response of the east beam top and bottom flanges. Strains on the order of 4% ($20\epsilon_y$) are observed in the flanges which are exacerbated by high local curvatures and weak axis bending. Figure 4.235 and Figure 4.236 show the extreme fiber response of the west beam top and bottom flanges.

- Figure 4.237 shows the strain gauge response of the west column flange above the beam top flange. It is observed that the column flange did not yield but moderate levels of warping occurred during the latter part of the loading protocol.
- Figure 4.238 shows the horizontal strain pattern on the doubler plate through two sections. Horizontal strains in the center of the doubler plate are mostly balanced. Figure 4.239 shows the shear stress distribution in the doubler plate. The center of the doubler plate sees the most significant strains (γ_y). Yielding of the doubler plate was anticipated.
- Figure 4.240 shows the horizontal shear distribution of the top flange continuity plate. The continuity plate reaches yielding levels of horizontal strain. Moderate shear strains are present at the edges of the continuity plate in contact with the column flange (see Figure 4.241). Figure 4.242 shows the principal strains of strain gauge rosette R16 and R22, the outermost strain gauges, during testing. It is observed that the cyclic strains are generally limited to $\pm\epsilon_y$ with a minor ratcheting of R16 to $2.5\epsilon_y$ during the compression excursions.
- Figure 4.243 shows the shear response of the continuity plate on the edge fillet welded with the doubler plate.
- Figure 4.244 shows the shear response of the west beam adjacent to the column. A significant ratcheting of the shear tab strain gauge was observed.

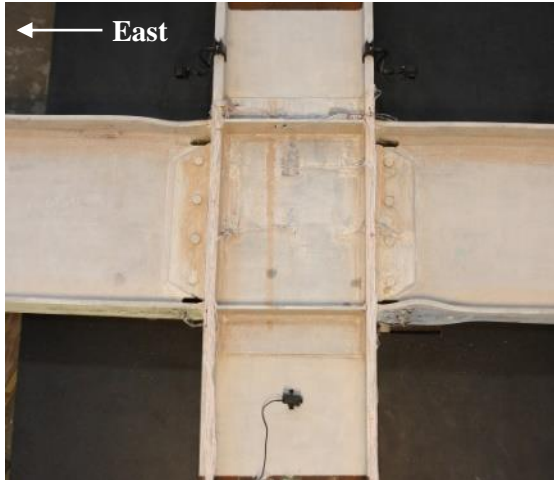


(a) Overview



(b) Connection Region

Figure 4.208 Specimen W3: Connection before Testing



(a) +0.03 rad (2nd Cycle)



(b) -0.03 rad (2nd Cycle)



(c) +0.04 rad (2nd Cycle)



(d) -0.04 rad (2nd Cycle)



(e) +0.05 rad (1st Cycle)



(f) -0.05 rad (1st Cycle)

Figure 4.209 Specimen W3: Connection during Testing



(a) -0.02 rad (2nd Cycle)



(b) -0.03 rad (2nd Cycle)



(c) -0.04 rad (2nd Cycle)



(d) -0.05 rad (1st Cycle)

Figure 4.210 Specimen W3: East Beam Bottom Flange Yielding



(a) -0.02 rad (2nd Cycle)



(b) -0.03 rad (2nd Cycle)



(c) -0.04 rad (2nd Cycle)



(d) -0.05 rad (1st Cycle)

Figure 4.211 Specimen W3: West Beam Bottom Flange Yielding



(a) +0.03 rad (2nd Cycle)

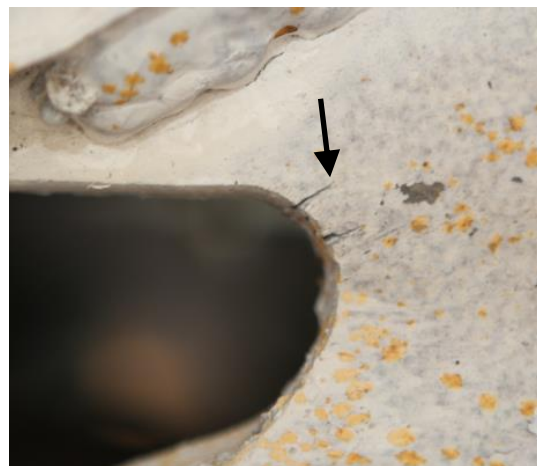


(b) +0.04 rad (1st Cycle)

Figure 4.212 Specimen W3: East Beam Top Flange Local Buckling



(a) Overview



(b) Weld Access Hole

Figure 4.213 Specimen W3: East Beam Top Flange Weld Access Hole Tearing at -0.05 rad (1st Cycle)



Figure 4.214 Specimen W3: Web Local Buckling at +0.05 rad (1st Cycle)



Figure 4.215 Specimen W3: Flange Local Buckling at -0.05 rad (1st Cycle)



(a) Overview



(b) -0.04 rad (2nd Cycle)



(c) -0.05 rad (1st Cycle)



(d) -0.06 rad (1st Cycle)

Figure 4.216 Specimen W3: East Beam Top Flange CJP Weld Tear Progression



Figure 4.217 Specimen W3: East Beam Top Flange Weld Access Hole Tear



(a) Overview



(b) Weld Tear

Figure 4.218 Specimen W3: East Beam Top Flange Fracture at +0.06 rad (1st Cycle)



(a) -0.06 rad (1st Cycle)



(b) -0.06 rad (2nd Cycle)

Figure 4.219 Specimen W3: East Beam Top Flange Fracture



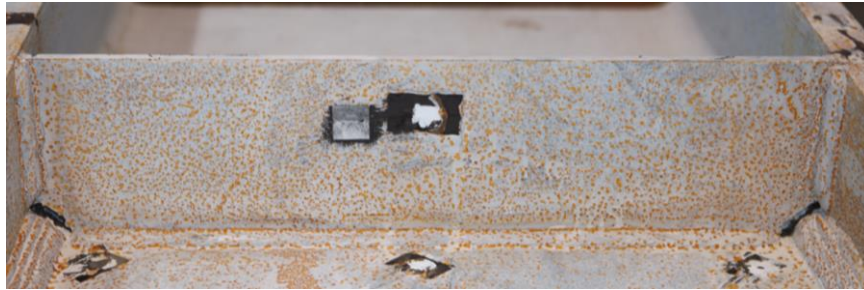
Figure 4.220 Specimen W3: Connection at End of Test



Figure 4.221 Specimen W3: West Beam Top Flange (End of Test)



(a) Topside



(b) Underside

Figure 4.222 Specimen W3: Top Flange Continuity Plate (End of Test)



(a) Topside



(b) Underside

Figure 4.223 Specimen W3: Bottom Flange Continuity Plate (End of Test)



(a) West Top Flange



(b) East Top Flange



(c) West Bottom Flange



(d) East Bottom Flange

Figure 4.224 Specimen W3: Continuity Plate Fillet Welds (End of Test)

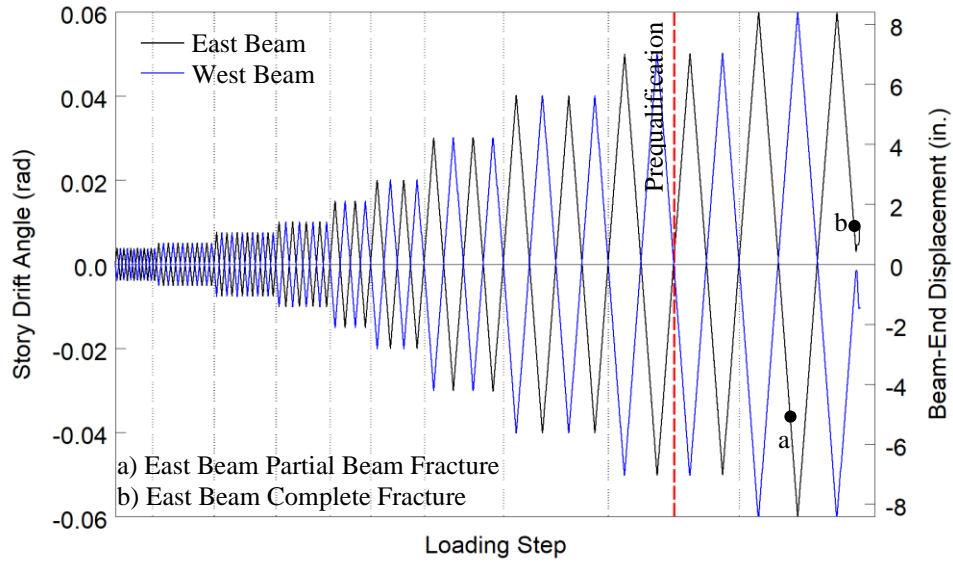


Figure 4.225 Specimen W3: Recorded Loading Sequence

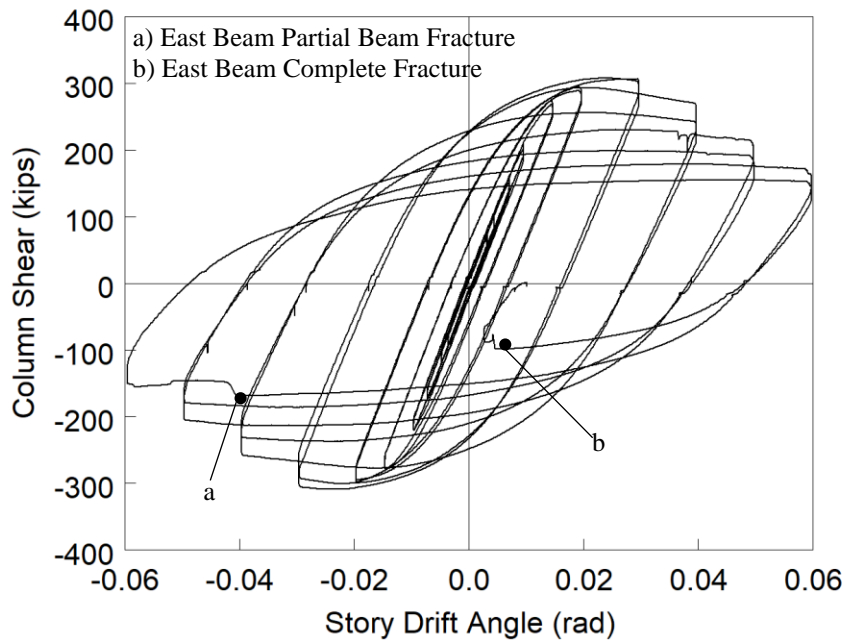
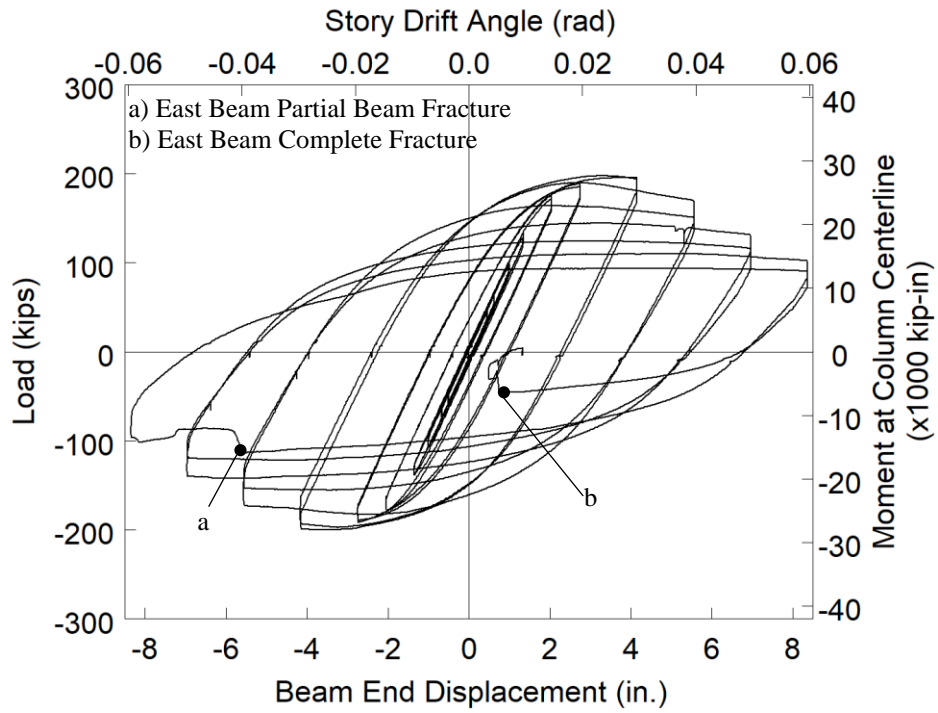
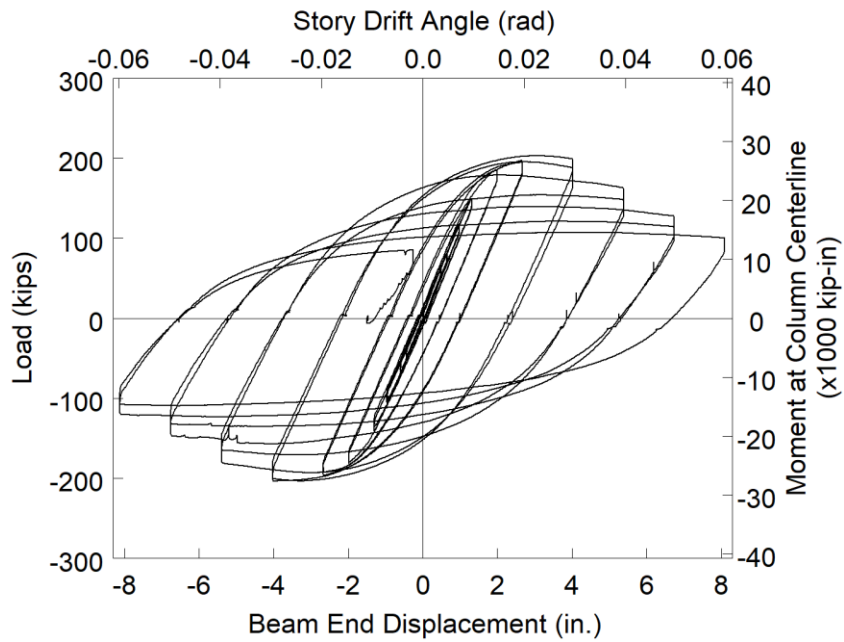


Figure 4.226 Specimen W3: Column Shear versus Story Drift Angle

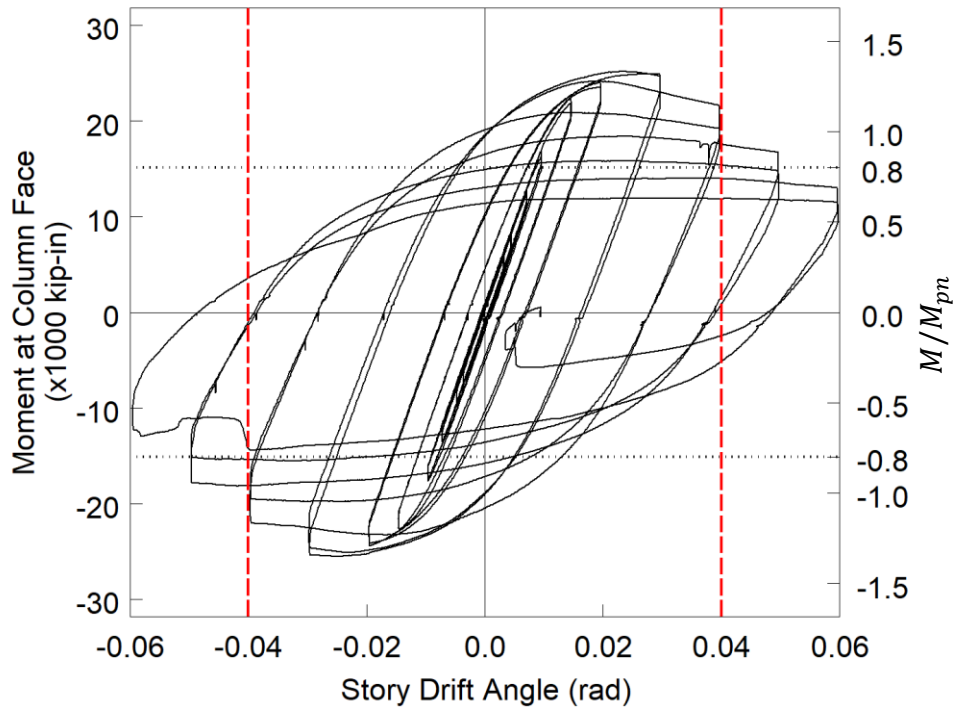


(a) East Beam

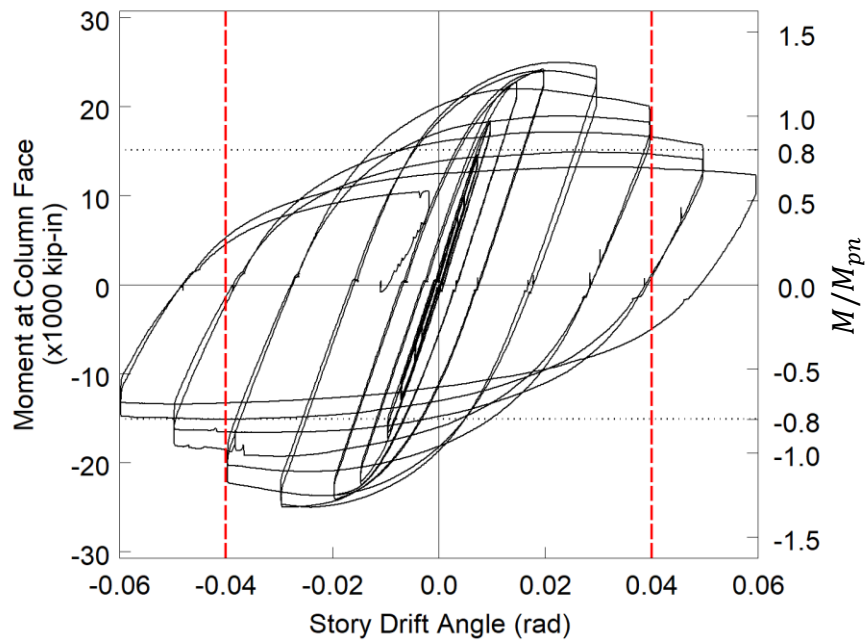


(b) West Beam

Figure 4.227 Specimen W3: Applied Load versus Beam End Displacement Response

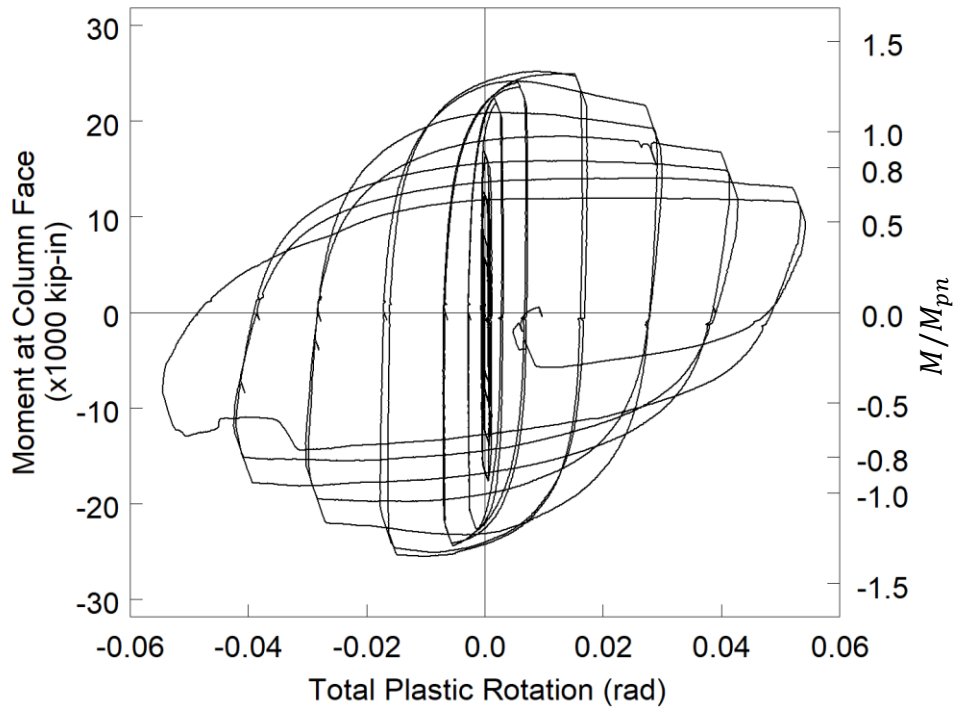


(a) East Beam

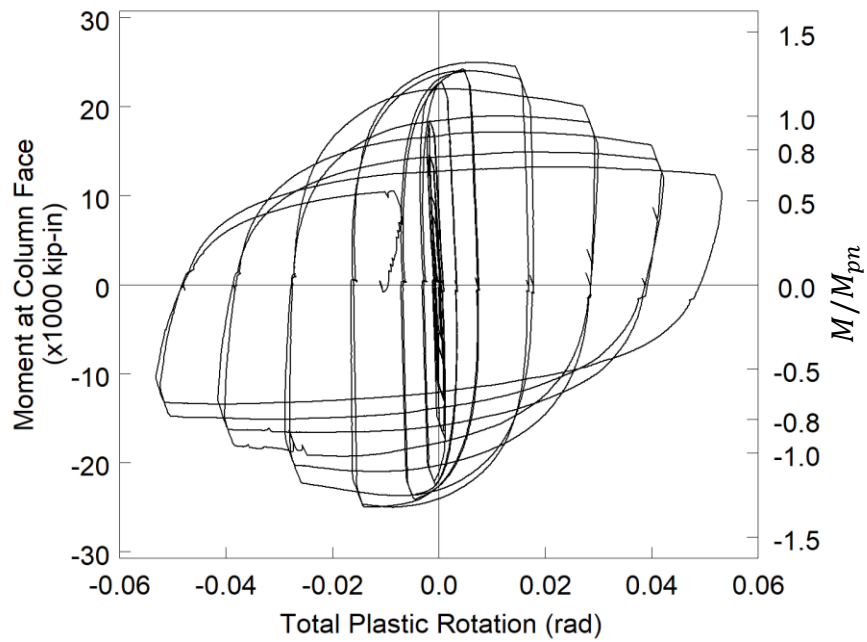


(b) West Beam

Figure 4.228 Specimen W3: Moment at Column Face versus Story Drift Response



(a) East Beam



(b) West Beam

Figure 4.229 Specimen W3: Moment at Column Face versus Plastic Rotation

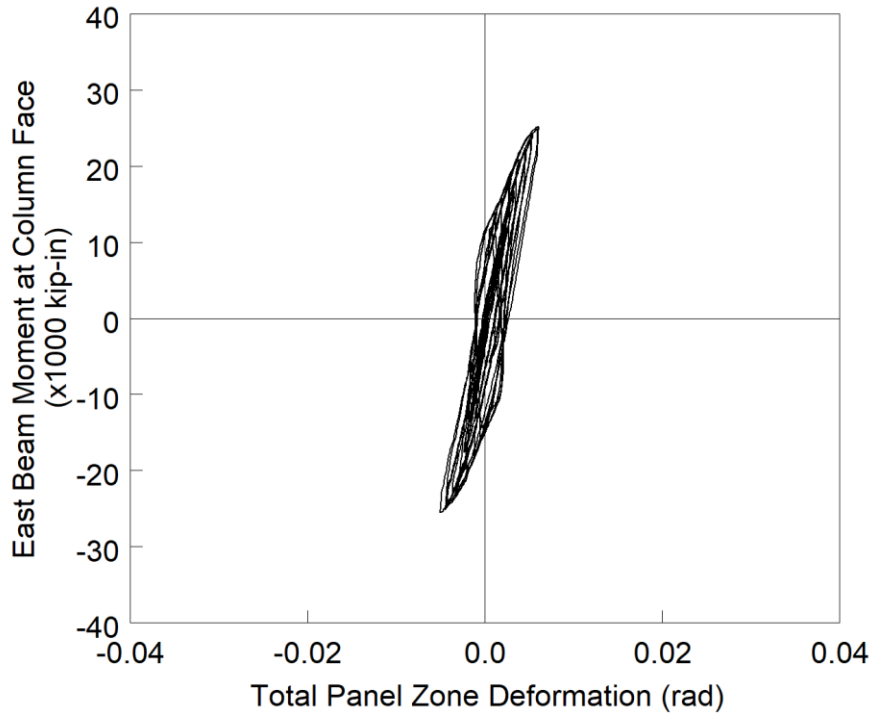


Figure 4.230 Specimen W3: Panel Zone Shear Deformation

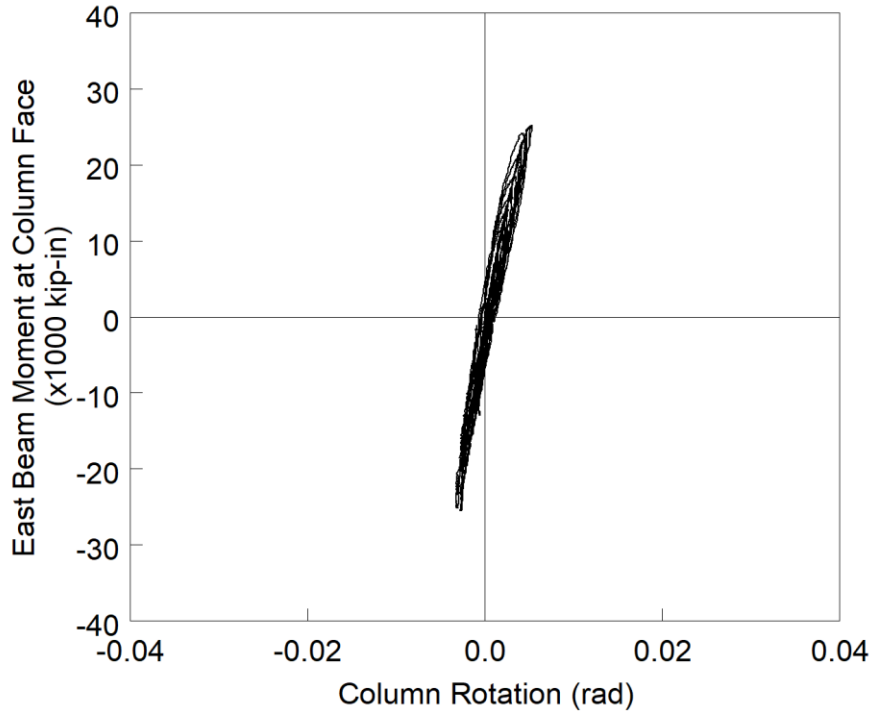


Figure 4.231 Specimen W3: Column Rotation

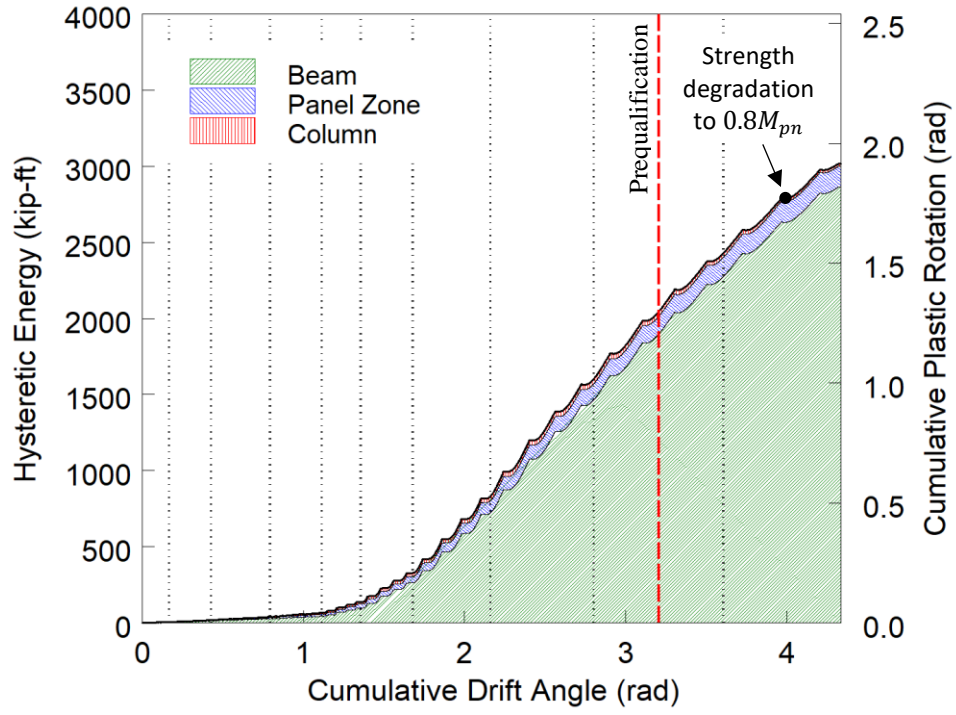
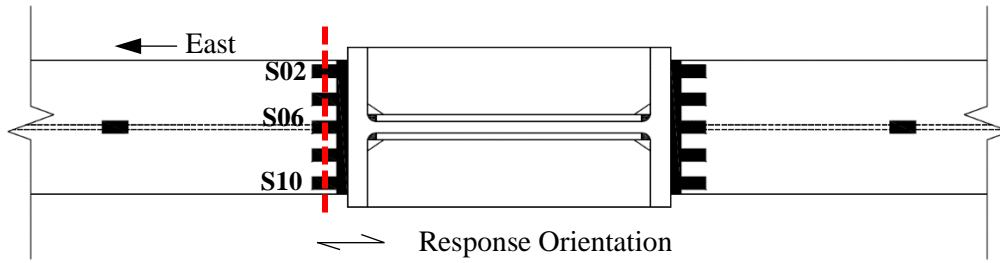
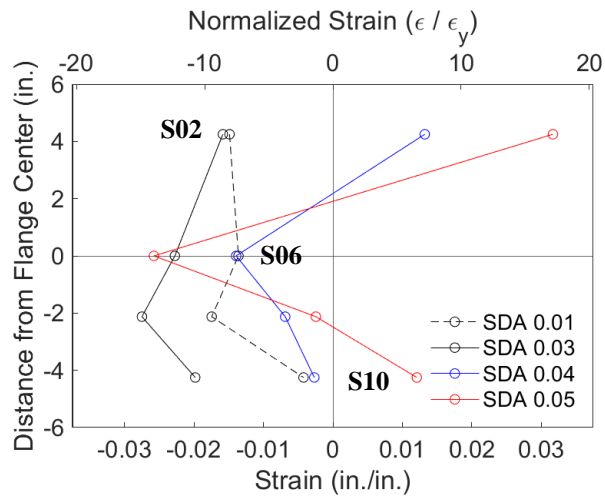


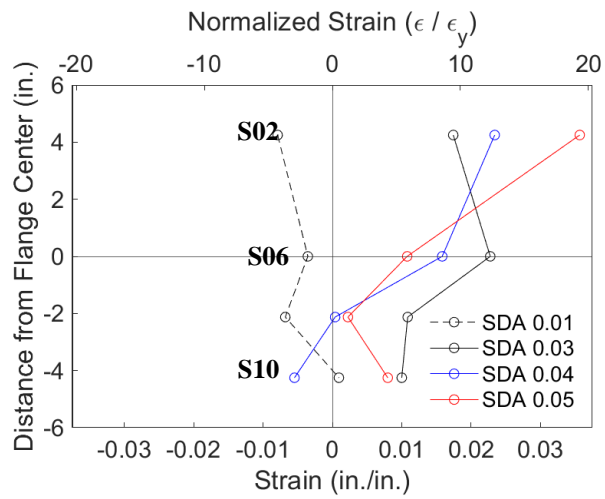
Figure 4.232 Specimen W3: Energy Dissipation



(a) Section

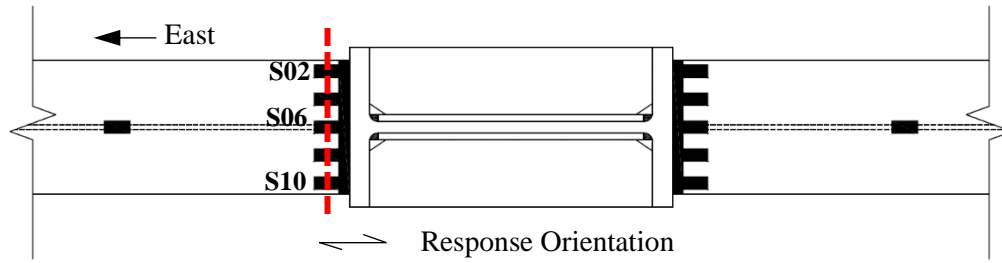


(b) Positive Drift

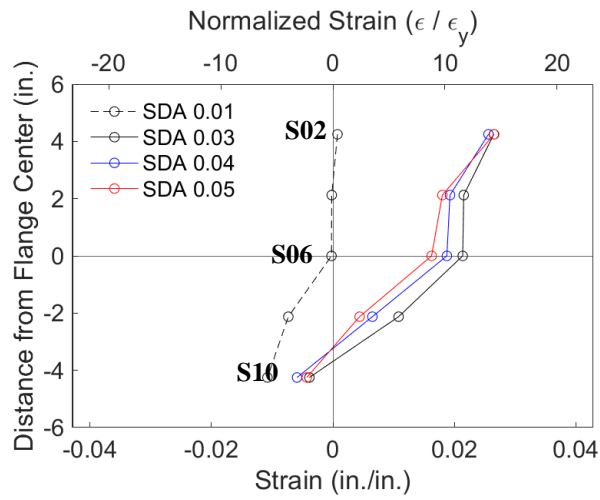


(c) Negative Drift

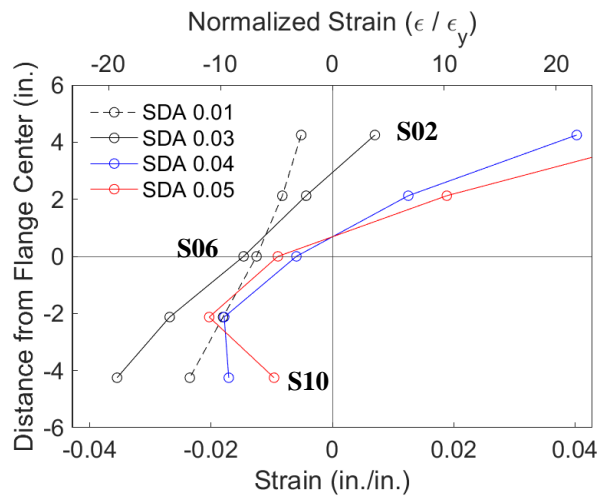
Figure 4.233 Specimen W3: Topside of East Beam Top Flange Strain Profile



(a) Section

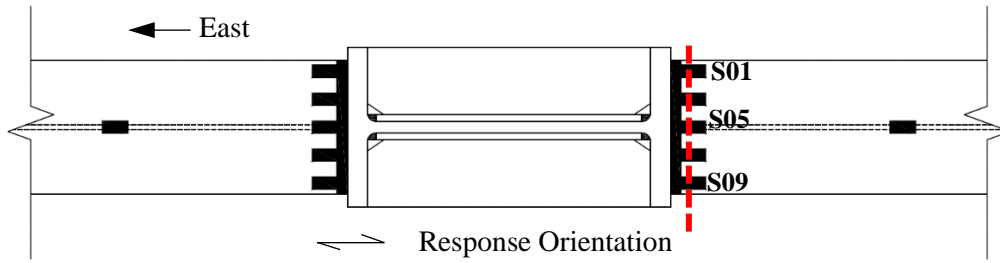


(b) Positive Drift

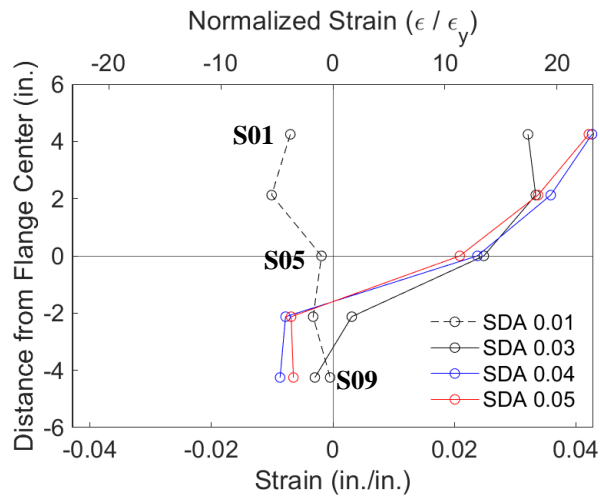


(c) Negative Drift

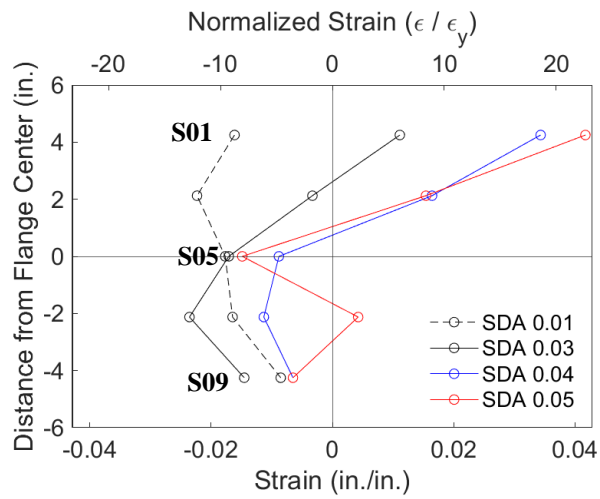
Figure 4.234 Specimen W3: Underside of East Beam Bottom Flange Strain Profile



(a) Section

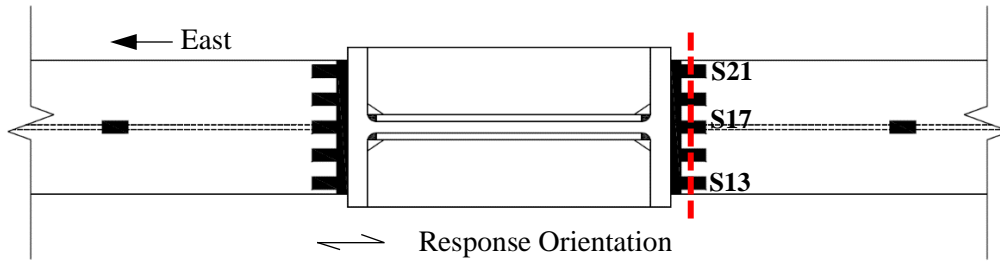


(b) Positive Drift

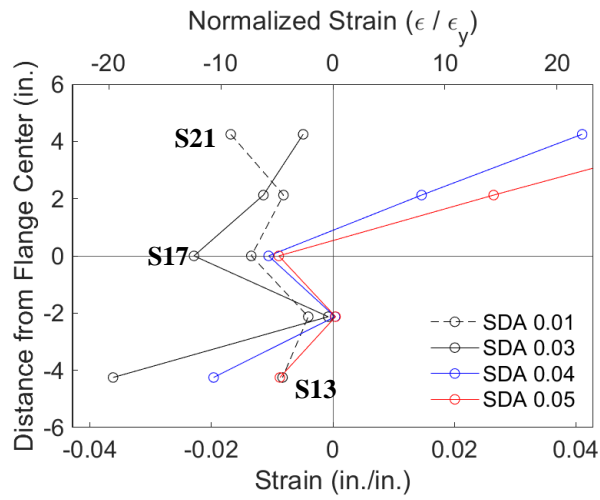


(c) Negative Drift

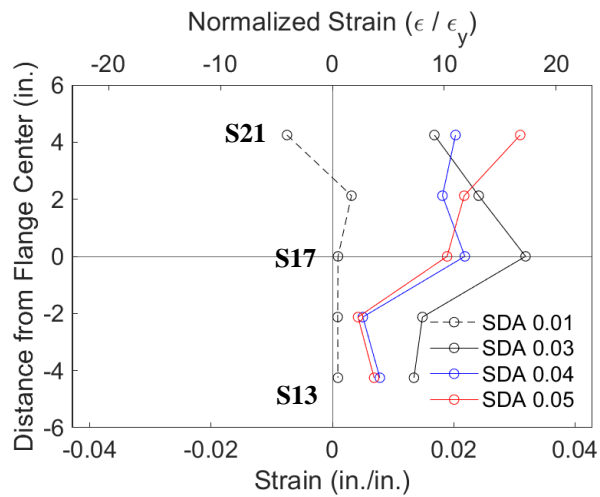
Figure 4.235 Specimen W3: Topside of West Beam Top Flange Strain Profile



(a) Section

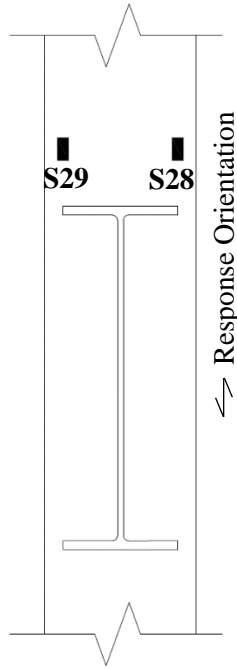


(b) Positive Drift

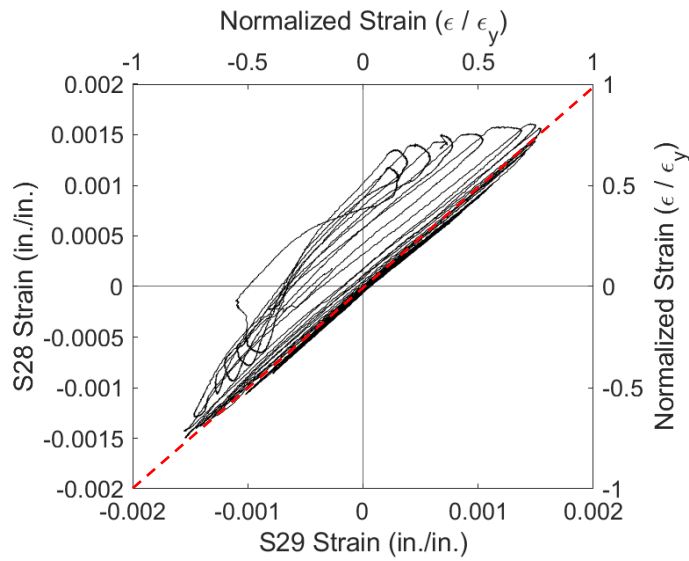


(c) Negative Drift

Figure 4.236 Specimen W3: Underside of West Beam Bottom Flange Strain Profile

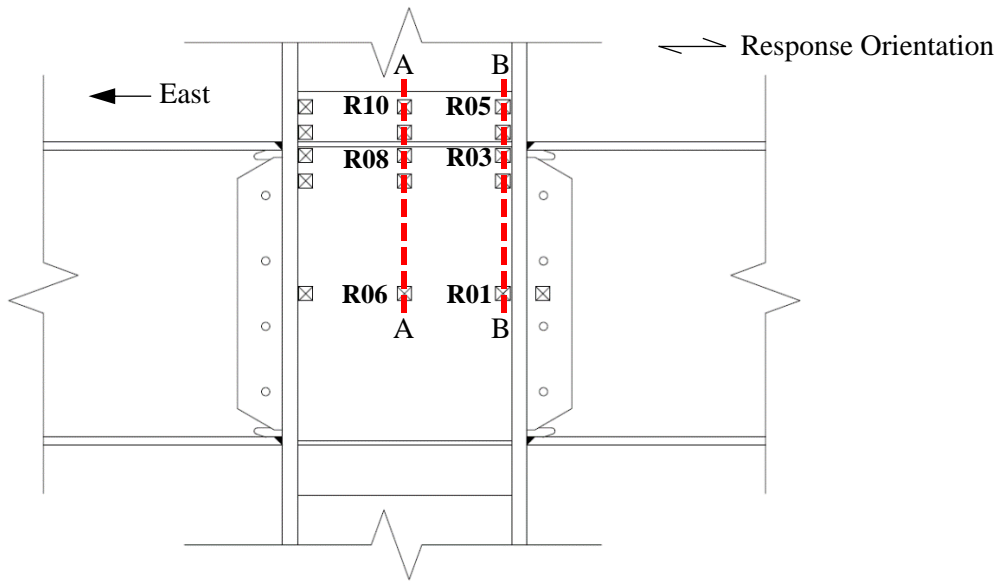


(a) Gauge Layout

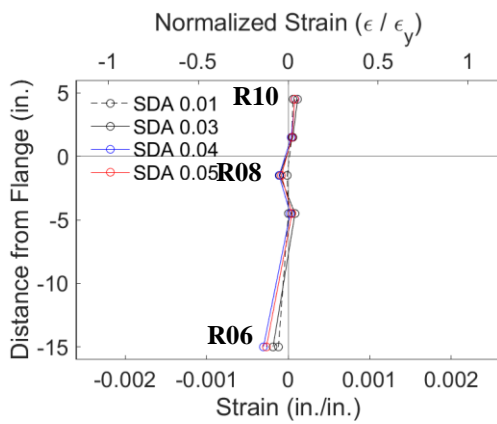


(b) Response

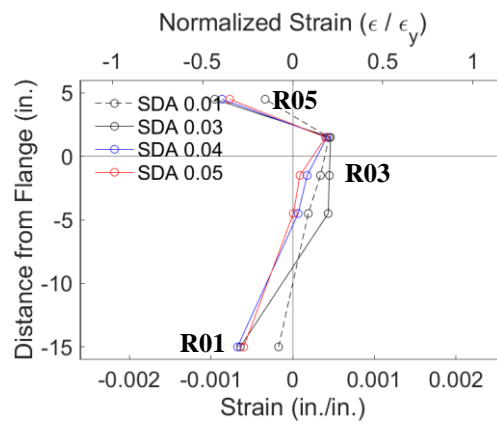
Figure 4.237 Specimen W3: Column Flange Warping



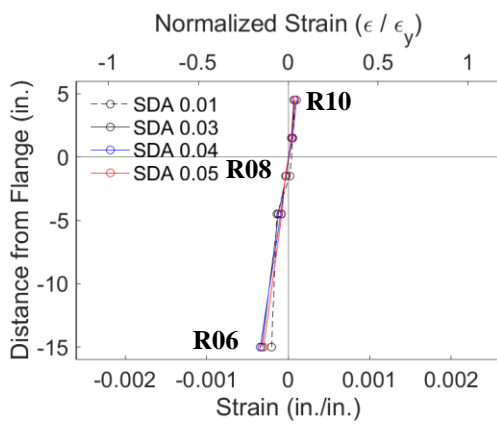
(a) Section Layout



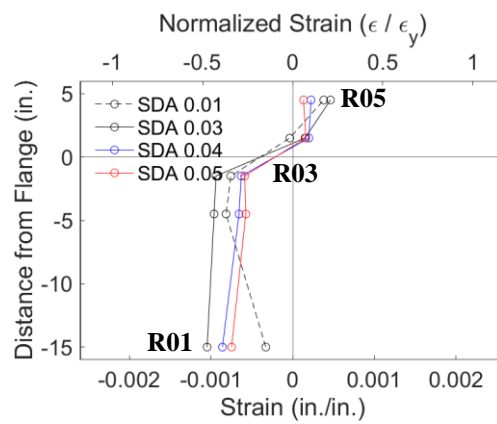
(b) Section A-A: Positive Drift



(c) Section B-B: Positive Drift

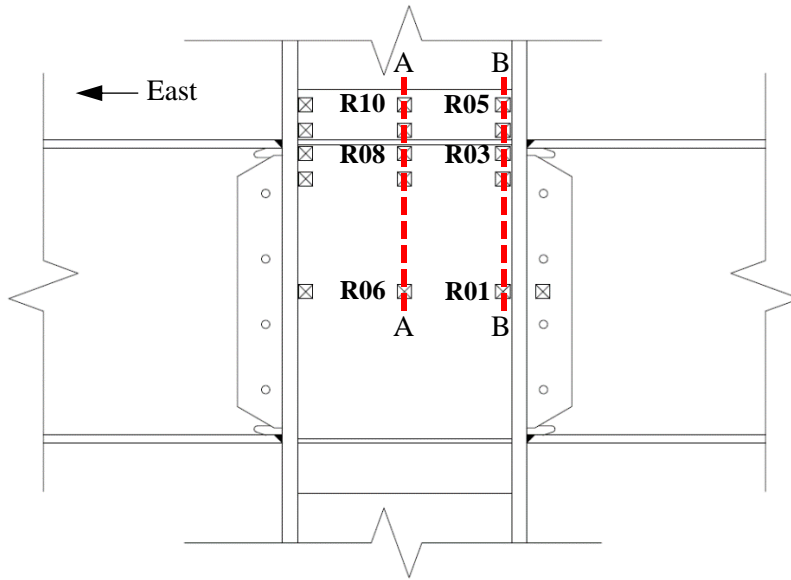


(d) Section A-A: Negative Drift

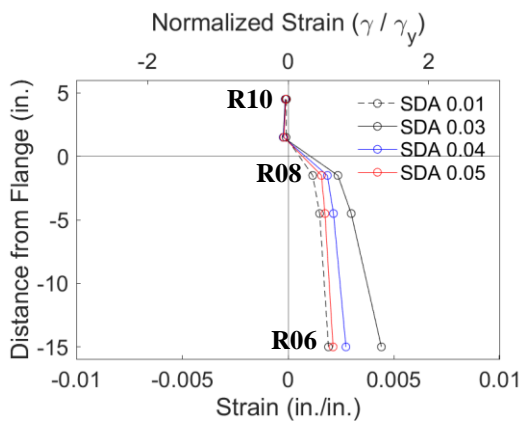


(e) Section B-B: Negative Drift

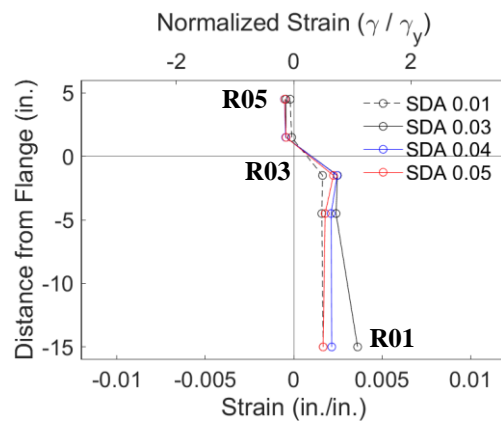
Figure 4.238 Specimen W3: Panel Zone Strain Profile



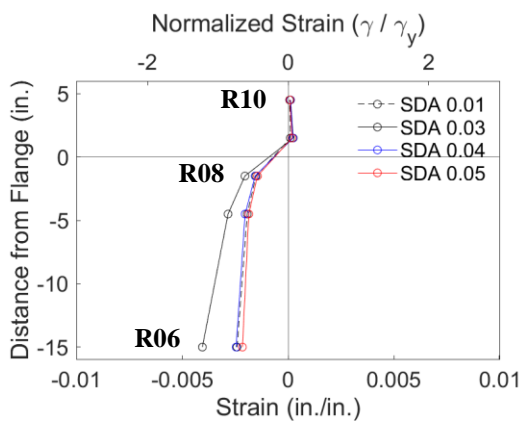
(a) Section Layout



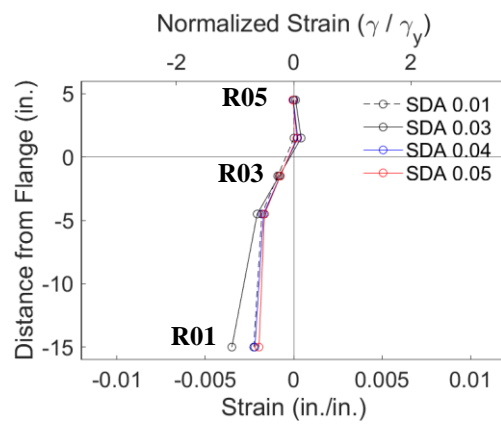
(b) Section A-A: Positive Drift



(c) Section B-B: Positive Drift



(d) Section A-A: Negative Drift



(e) Section B-B: Negative Drift

Figure 4.239 Specimen W3: Panel Zone Shear Strain Profile

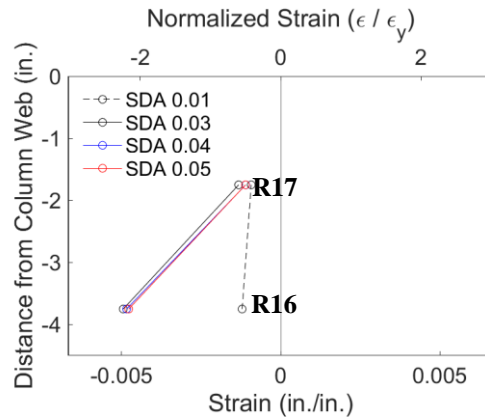
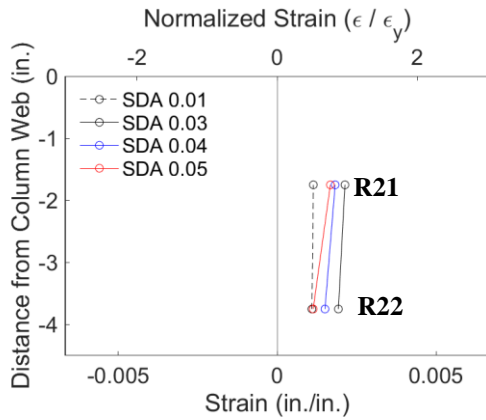
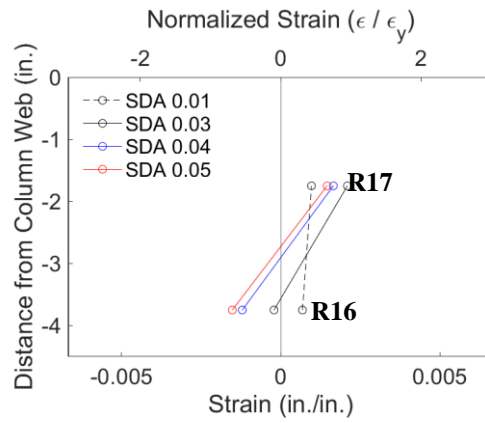
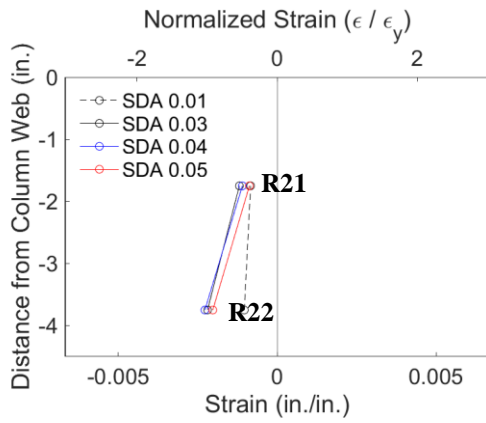
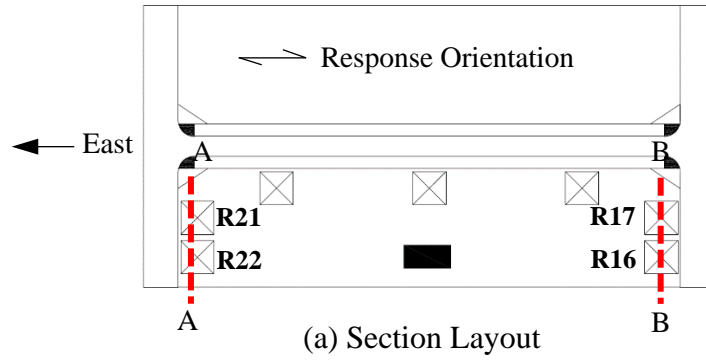
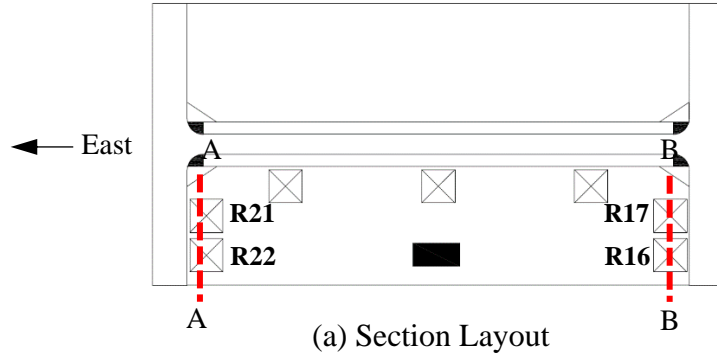
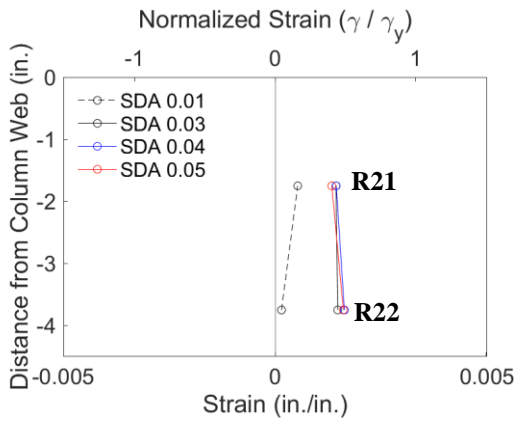


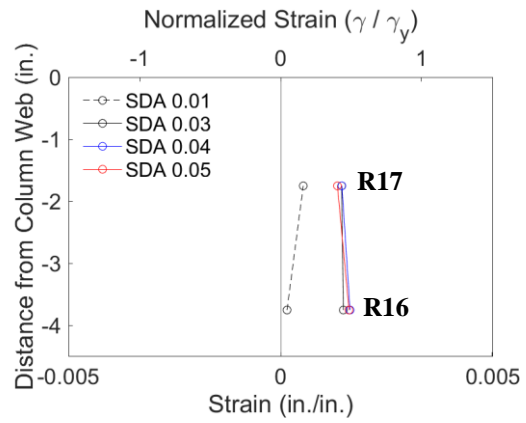
Figure 4.240 Specimen W3: Continuity Plate at Column Flange Edge Strain Profile



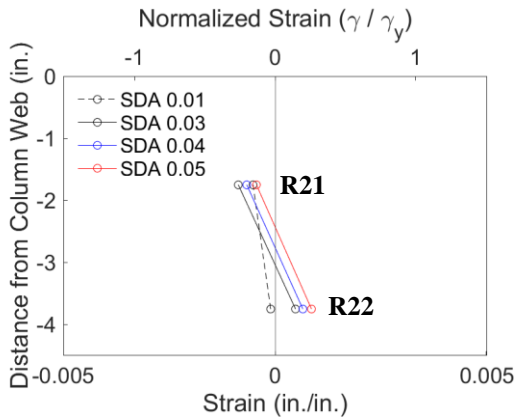
(a) Section Layout



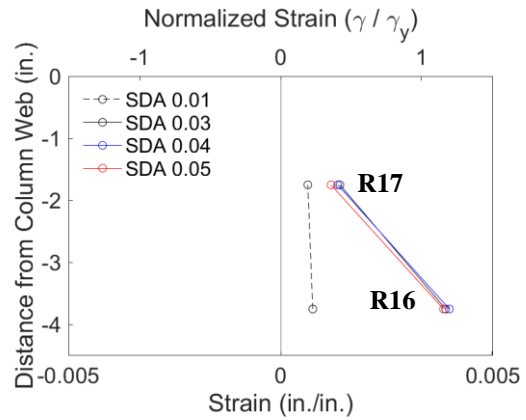
(b) Section A-A: Positive Drift



(c) Section B-B: Positive Drift

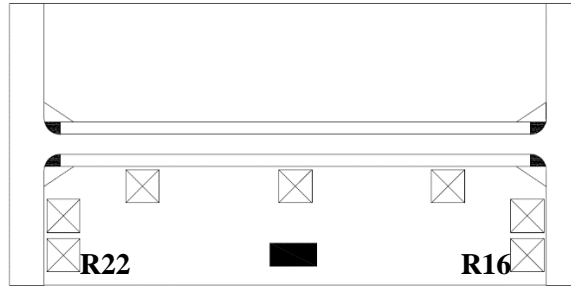


(d) Section A-A: Negative Drift

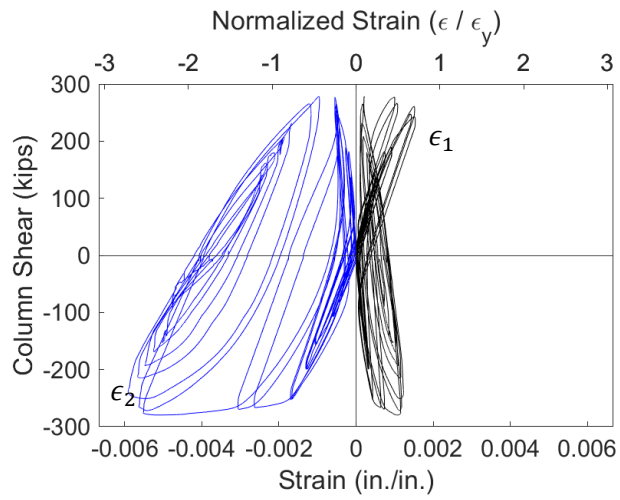


(e) Section B-B: Negative Drift

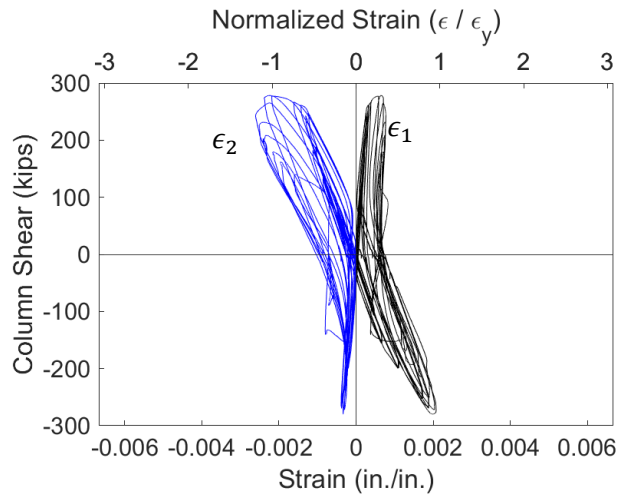
Figure 4.241 Specimen W3: Continuity Plate at Column Flange Edge Shear Strain Profile



(a) Layout

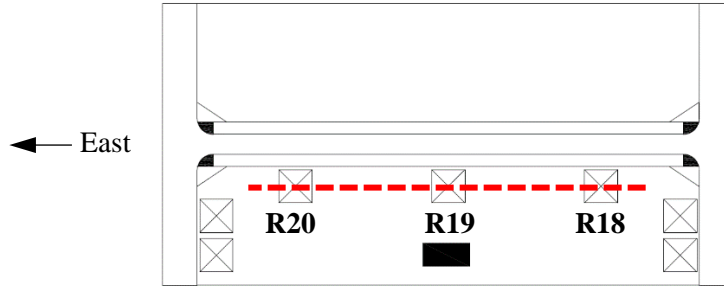


(b) Strain Gauge R16 Principal Strains

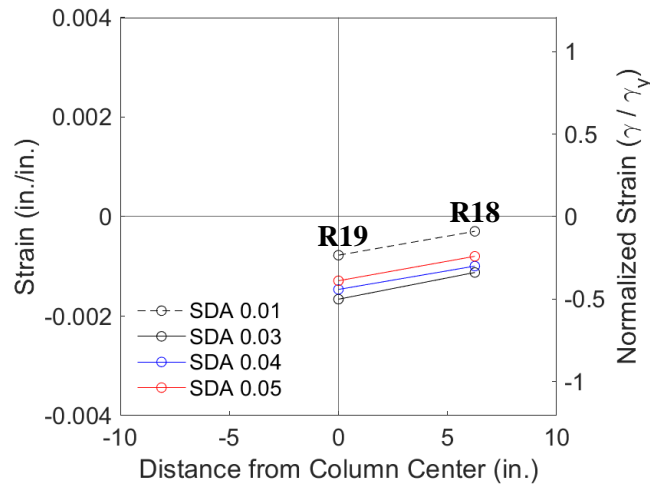


(b) Strain Gauge R22 Principal Strains

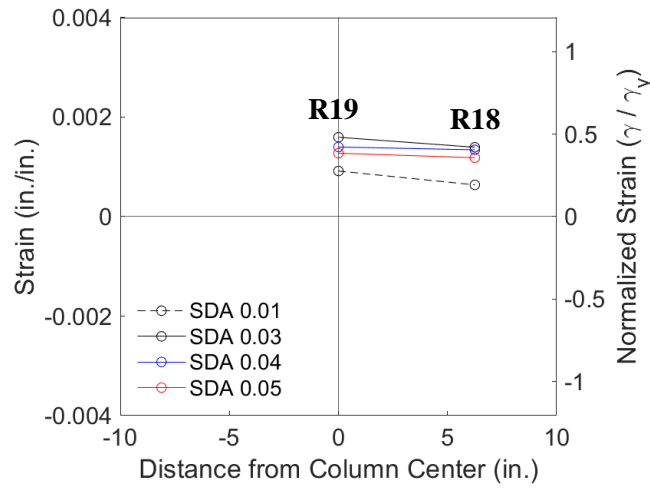
Figure 4.242 Specimen W3: Continuity Plate Strain Gauge Rosette Response



(a) Section Layout

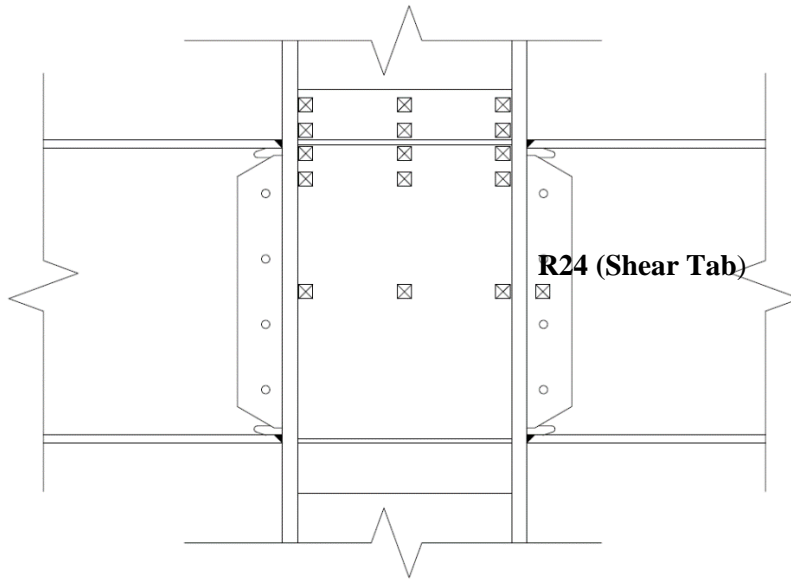


(b) Positive Drift

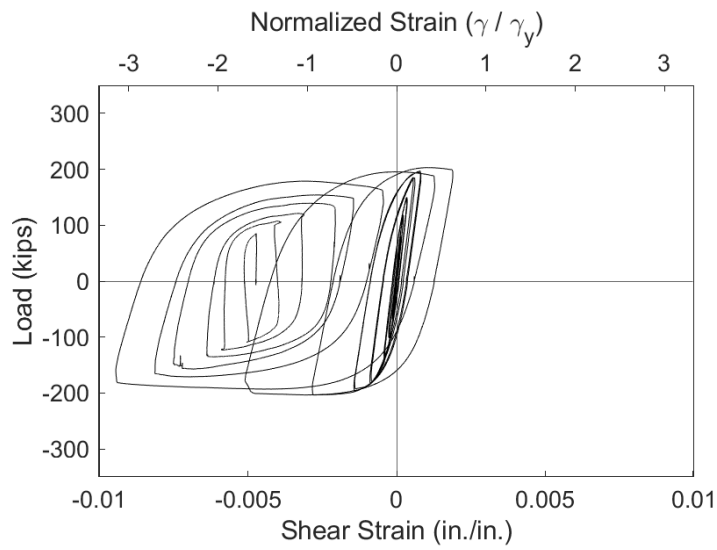


(c) Negative Drift

Figure 4.243 Specimen W3: Continuity Plate at Column Web Edge Shear Strain Profile



(a) Gauge Layout



(b) Strain Rosette Gauges R24

Figure 4.244 Specimen W3: Beam Shear Response

4.11 Specimen W4

4.11.1 General

Specimen W4 was designed to investigate use of the plastic methodology to design continuity plates. The resulting continuity plates satisfy the current minimum thickness requirements as per the AISC 341 Provisions. Continuity plate double-sided fillet welds were sized such that $w = 0.75t_{cp}$. A pair of doubler plates stiffen the web of the column for panel zone yielding. The doubler plate is placed within the panel zone and is welded to the continuity plates on the top and bottom edges. The doubler plate vertical welds use a fillet weld sized to develop the strength of the doubler plate. Horizontal fillet welds between the doubler plate and continuity plate were sized to develop 75% of the doubler plate shear capacity as per the current Provisions. Specimen W4 failed by a fracture of the east and west beam top beam flange CJP weld during the first cycle of 0.05 rad drift. Figure 4.245 shows the specimen before testing.

4.11.2 Observed Performance

The observed response for Specimen W4 is described below.

- Figure 4.246 shows the connection during testing. The specimen met the AISC acceptance criteria by completing one complete cycle at 0.04 rad drift while the flexural strength at either column face did not degrade below 80% of the beam nominal flexural strength.
- Figure 4.247 and Figure 4.248 show the east beam bottom flange and west beam bottom flange during testing. The progression of flange local buckling between the second cycle of 0.04 rad and the first cycle of 0.05 rad is shown in Figure 4.249.
- Figure 4.250 shows the initiation of web buckling during the first negative excursion of 0.04 rad drift.
- During the second negative excursion of 0.04 rad drift the east beam top flange partially fractured through 50% of the flange at the CJP weld (see Figure 4.251).
- During the first negative excursion of 0.05 rad drift the west beam top flange developed a partial fracture through 20% of the beam flange (see Figure 4.252).
- Severe lateral-torsional buckling developed in the east beam during the 0.05 rad drift cycles (see Figure 4.253).

- During the first negative excursion of 0.05 rad drift the east beam top flange completely fractured through the CJP weld (see Figure 4.254). This fracture propagated down the CJP weld bevel. Accompanying this fracture, the web of the east beam fractured (see Figure 4.255). This fracture propagated 5 in. from the radius of the weld access hole. Continuing the 0.05 rad drift cycles resulted in the complete fracture of the west beam top flange (see Figure 4.256). A close up of the east beam top flange fracture is shown in Figure 4.257.
- Figure 4.258 shows the connection at the end of testing. Continued negative excursion of the east beam resulted in the web continuing to fracture following a few inches outboard of the fillet welded shear tab.
- No yielding of the continuity plates was observed during testing (see Figure 4.259). Furthermore, no damage was observed in the continuity plate fillet welds. Minor yielding of the inside face of the column flange, above the top flange continuity plates, is shown in Figure 4.259(b).
- The top and bottom edge of the doubler plate of this specimen was welded to the continuity plate using a 5/8-in. fillet weld based on the Provisions. This weld was the sole attachment of the inside face of the continuity plate to the panel zone. The termination of the doubler plate vertical welds was held back from the continuity plate by 1 in. as per the Provisions. No damage was observed in any of these welds (see Figure 4.260).

4.11.3 Recorded Response

4.11.3.1 Global Response

- Figure 4.261 shows the recorded displacement response of the beam tip measured with transducer L1 for the east beam and L2 for the west beam. The response from the east and west beams are shown in black and blue, respectively. The east beam top flange fractured during the second negative excursion of 0.03 rad drift. Complete fracture occurred at a neutral position during the first negative excursion of 0.05 rad drift. Complete fracture of the west beam top flange occurred at 0.015 rad during the first negative excursion of 0.05 rad drift.
- Figure 4.263 shows the load-displacement response of the beams.

- Figure 4.264 shows the computed moment at the column face (M_f) versus the story drift angle. Two horizontal axes at 80% of the nominal plastic moment (M_{pn}) of the beam section are also added. In addition, two vertical axes at ± 0.04 rad story drift show the drift required for SMF connections per AISC 341. It is observed that the beams developed 1.5 times its nominal plastic bending moment. If the moment is computed at the plastic hinge location and compared to the expected plastic moment, then the peak connection strength factor (C_{pr}) is 1.39 and 1.34 for the east and west beams respectively.
- Figure 4.265 shows the plastic response of the specimen. The plastic response is computed using the procedure outlined in Section 3.7. The computed elastic stiffness of the specimen was determined to be 54.9 kips/in.
- Figure 4.266 shows minor hysteretic behavior in the panel zone.
- Figure 4.267 shows negligible hysteretic behavior from the column.
- Figure 4.268 shows the dissipated energy of Specimen W4. Dotted vertical lines on the graph demonstrate the completion of each group of cycles, and the dashed red vertical line shows the completion of the first cycle of 0.04 rad in the AISC loading. It is observed that the completion of the first drift cycle of 0.04 rad (the requirement for SMF connections per AISC 341) occurs after 852 kip-ft of energy has been dissipated. The connection did not degrade below $0.8M_{pn}$ until fracture of the east beam top flange occurred and 1,427 kip-ft of energy had been dissipated. Therefore only 60% of the energy dissipation capacity was utilized after the completion of the SMF requirement. It is observed that nearly all (96%) of the energy dissipation capacity occurred in the beam.

4.11.3.2 Local Response

- Figure 4.269 and Figure 4.270 show the extreme fiber response of the east beam top and bottom flanges. Strains on the order of 7% ($40\epsilon_y$) are observed in the flanges which are exacerbated by high local curvatures and weak axis bending. Figure 4.271 and Figure 4.272 show the extreme fiber response of the west beam top and bottom flanges.

- Figure 4.273 shows the strain gauge response of the west column flange above the beam top flange. It is observed that the column flange did not yield but minor levels of warping occurred during the last few cycles of the loading protocol.
- Figure 4.274 shows the horizontal strain pattern on the doubler plate through two sections. Figure 4.275 shows the shear stress distribution in the doubler plate. The center of the doubler plate sees the most significant strains (γ_y). Yielding of the doubler plate was anticipated.
- Figure 4.276 shows the horizontal shear distribution of the top flange continuity plate. The continuity plate reaches yielding levels of horizontal strain. Moderate shear strains are present at the edges of the continuity plate in contact with the column flange (see Figure 4.277). Figure 4.278 shows the principal strains of strain gauge rosette R16 and R22, the outermost strain gauges, during testing. It is observed that the cyclic strains are generally limited to $\pm 0.75\epsilon_y$.
- Figure 4.279 shows the shear response of the continuity plate on the edge fillet welded with the doubler plate.
- Figure 4.280 shows the shear response of the west beam adjacent to the column. A significant ratcheting of the shear tab strain gauge was observed.

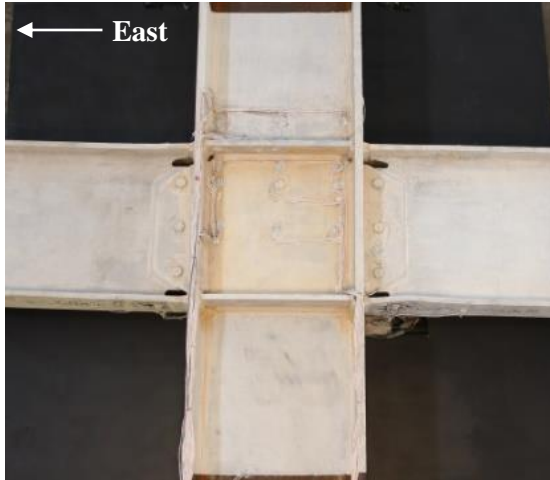


(a) Overview



(b) Connection Region

Figure 4.245 Specimen W4: Connection before Testing



(a) +0.03 rad (2nd Cycle)



(b) -0.03 rad (2nd Cycle)



(c) +0.04 rad (2nd Cycle)



(d) -0.04 rad (2nd Cycle)



(e) +0.05 rad (1st Cycle)



(f) -0.05 rad (1st Cycle)

Figure 4.246 Specimen W4: Connection during Testing



(a) +0.015 rad (1st Cycle)



(b) -0.02 rad (2nd Cycle)



(c) +0.03 rad (2nd Cycle)



(d) -0.04 rad (2nd Cycle)

Figure 4.247 Specimen W4: East Beam Bottom Flange Yielding



(a) +0.015 rad (1st Cycle)



(b) -0.02 rad (2nd Cycle)



(c) +0.03 rad (2nd Cycle)



(d) -0.04 rad (2nd Cycle)

Figure 4.248 Specimen W4: West Beam Bottom Flange Yielding



(a) +0.04 rad (2nd Cycle)



(b) +0.05 rad (1st Cycle)

Figure 4.249 Specimen W4: West Beam Bottom Flange Local Buckling



Figure 4.250 Specimen W4: West Beam Web Buckling at +0.04 rad (1st Cycle)

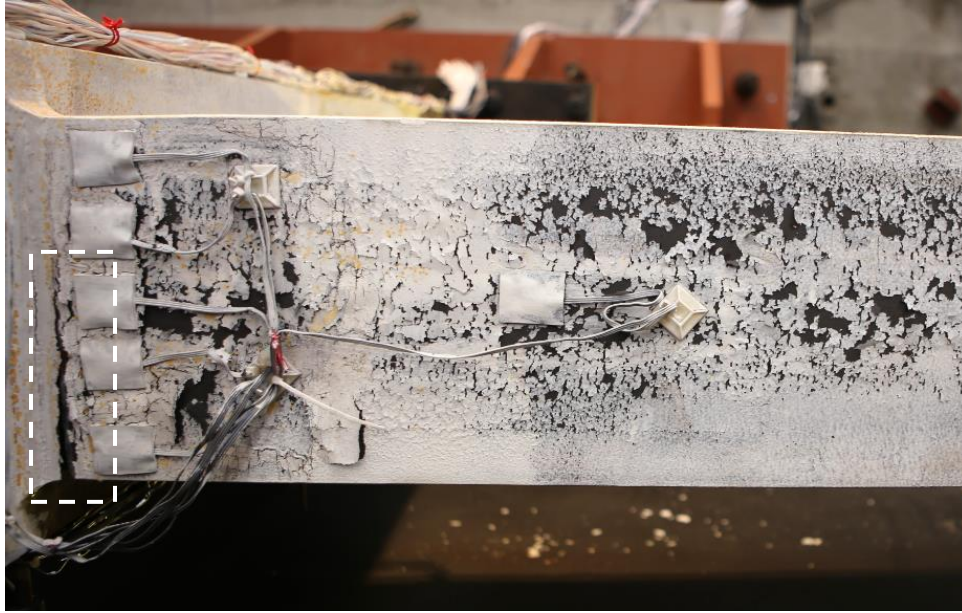
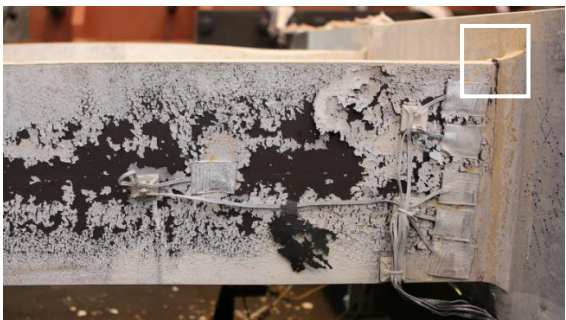


Figure 4.251 Specimen W4: East Beam Top Flange CJP Weld Fracture at -0.04 rad (2^{nd} Cycle)



(a) Overview



(b) Weld Tear

Figure 4.252 Specimen W4: West Beam Top Flange CJP Weld Tear at $+0.05$ rad (1^{st} Cycle)

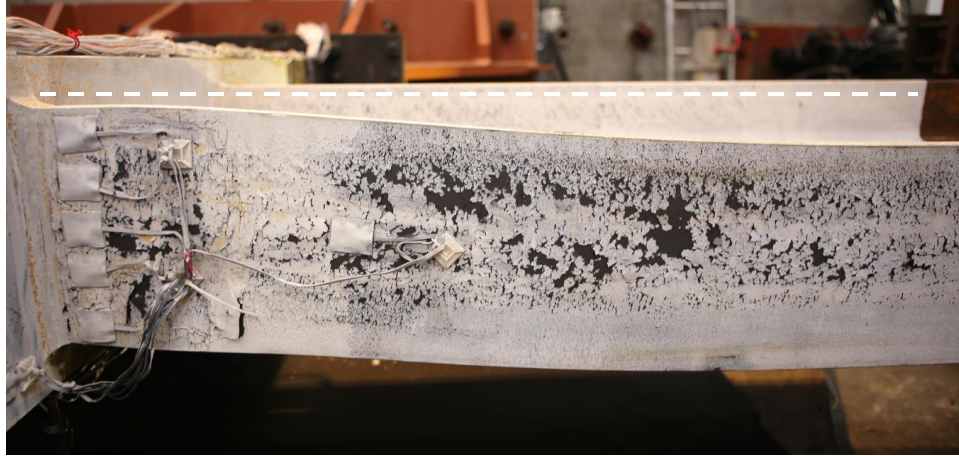


Figure 4.253 Specimen W4: East Beam Lateral-Torsional Buckling at +0.05 rad (1st Cycle)

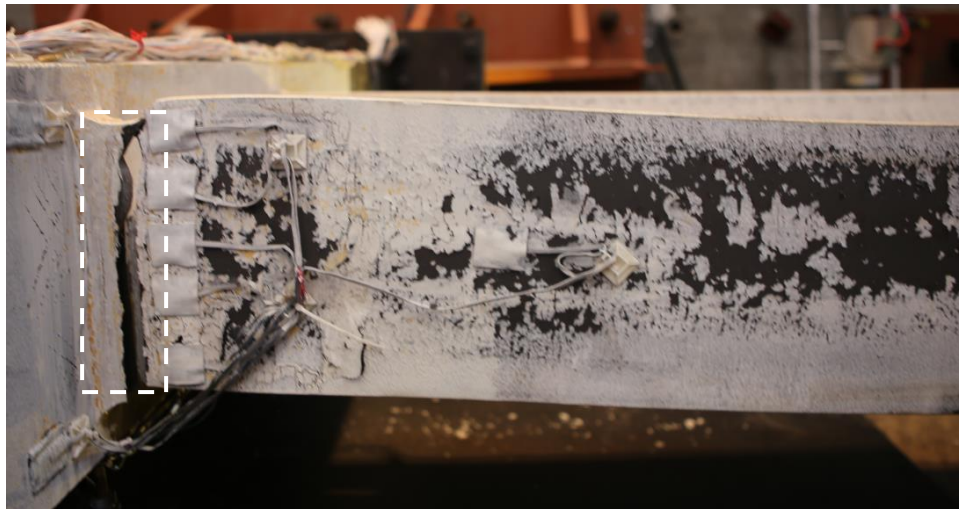
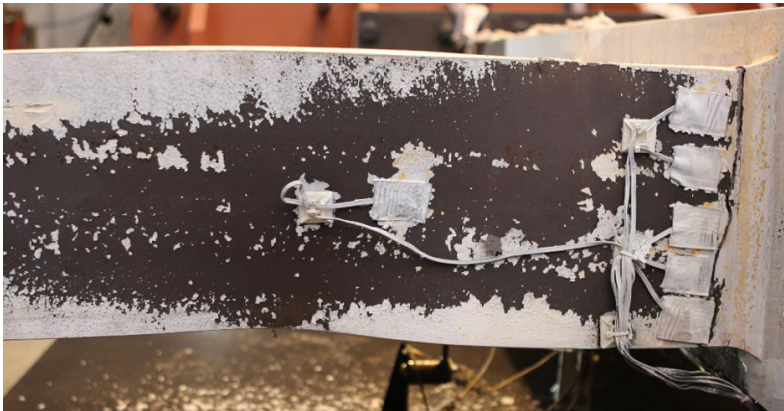


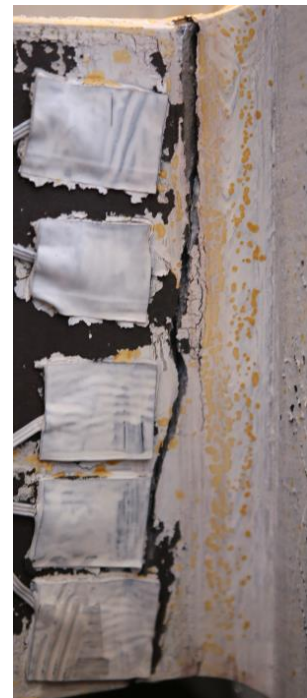
Figure 4.254 Specimen W4: East Beam Top Flange Fracture during First Excursion of -0.05 rad



Figure 4.255 Specimen W4: East Beam Top Flange Weld Access Hole Fracture during First of -0.05 rad



(a) Overview



(b) Fracture

Figure 4.256 Specimen W4: West Beam Top Flange Fracture (End of Test)

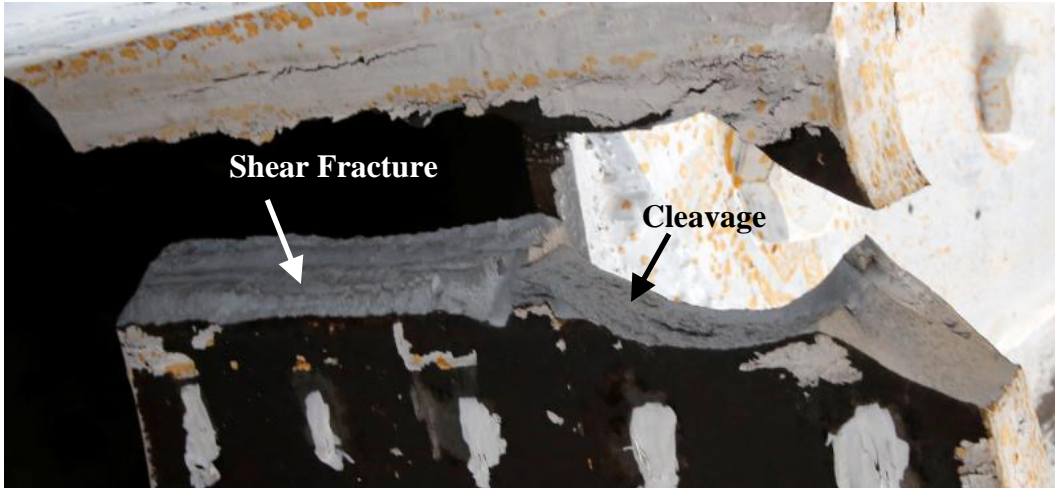


Figure 4.257 Specimen W4: East Beam Top Flange Fracture



Figure 4.258 Specimen W4: Connection at End of Testing



(a) Bottom Flange



(b) Top Flange

Figure 4.259 Specimen W4: Continuity Plates (End of Test)

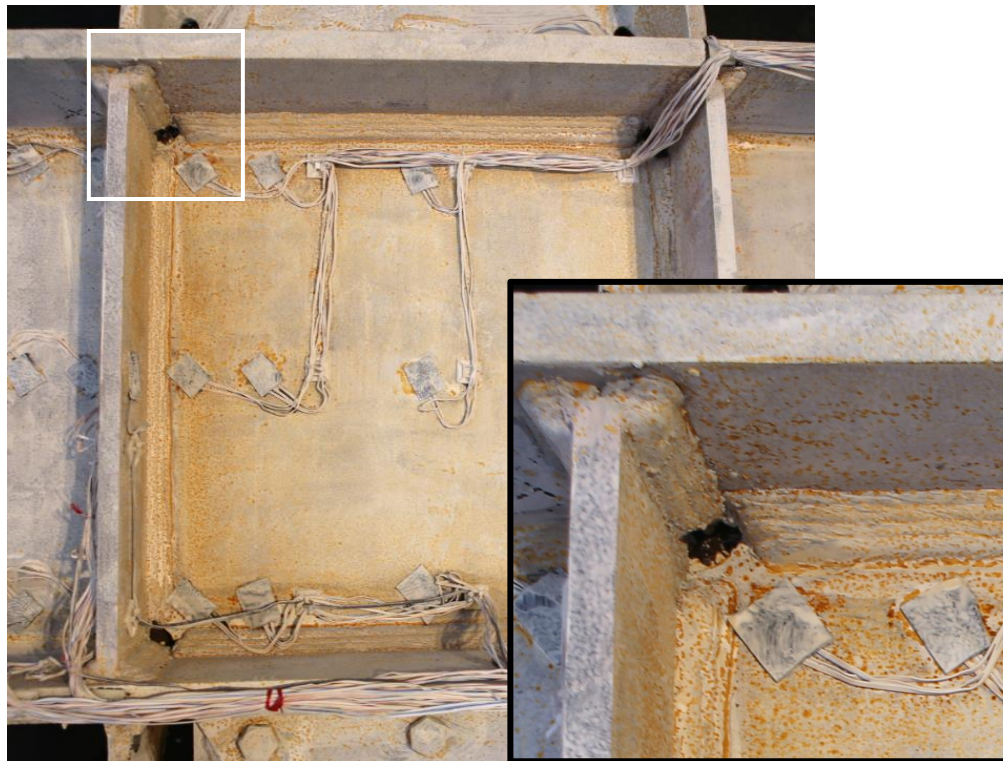


Figure 4.260 Specimen W4: Panel Zone (End of Test)

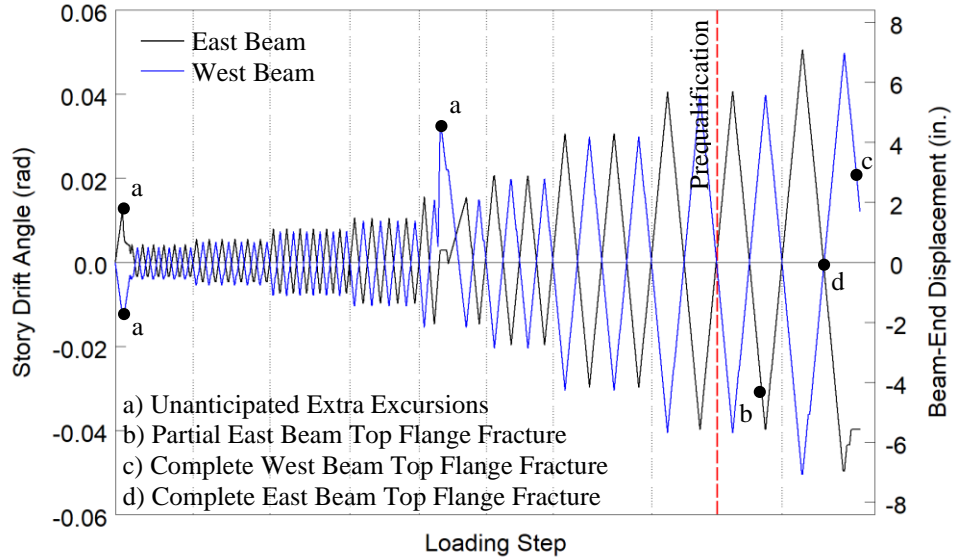


Figure 4.261 Specimen W4: Recorded Loading Sequence

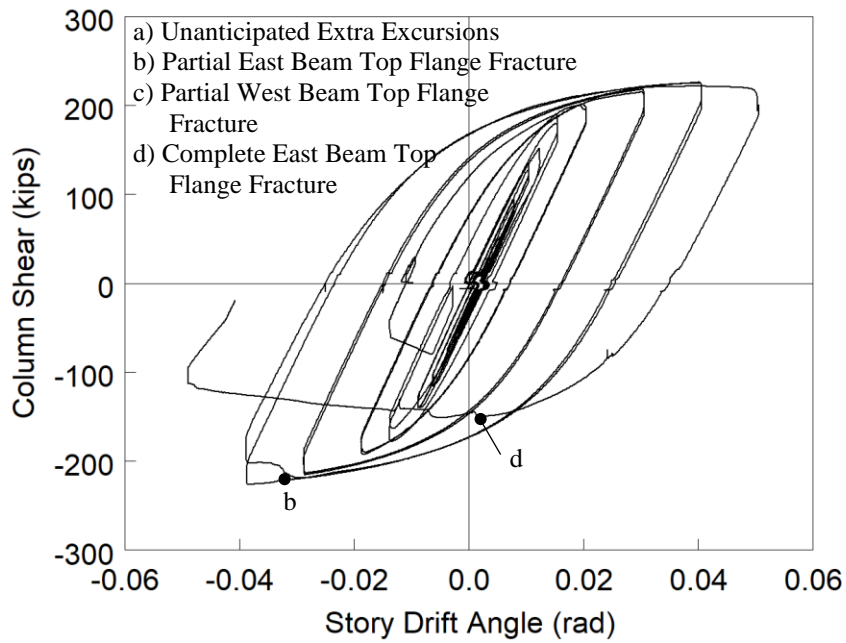
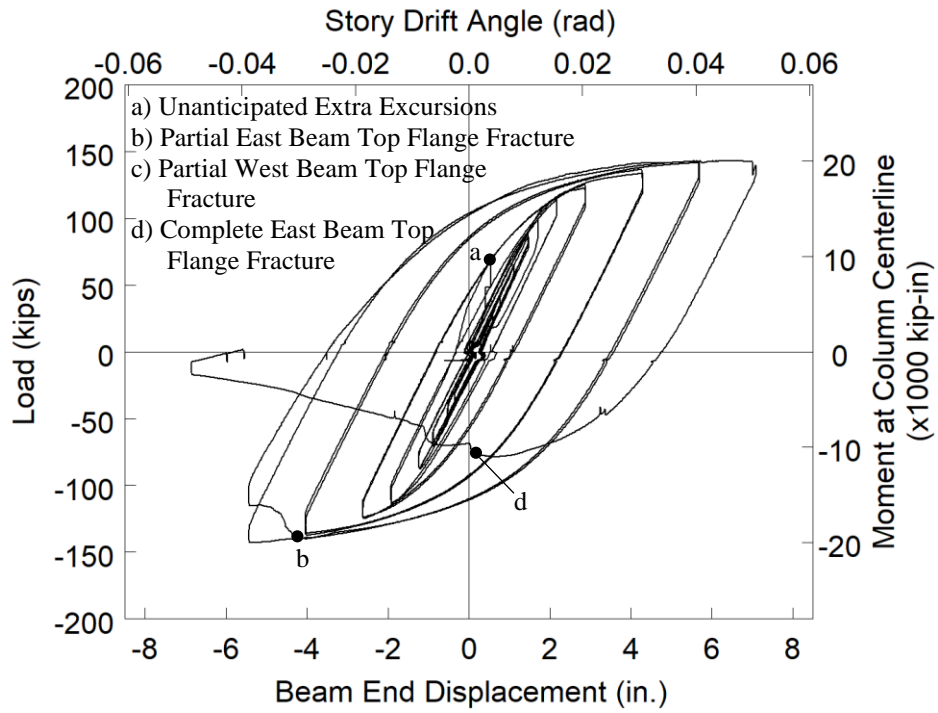
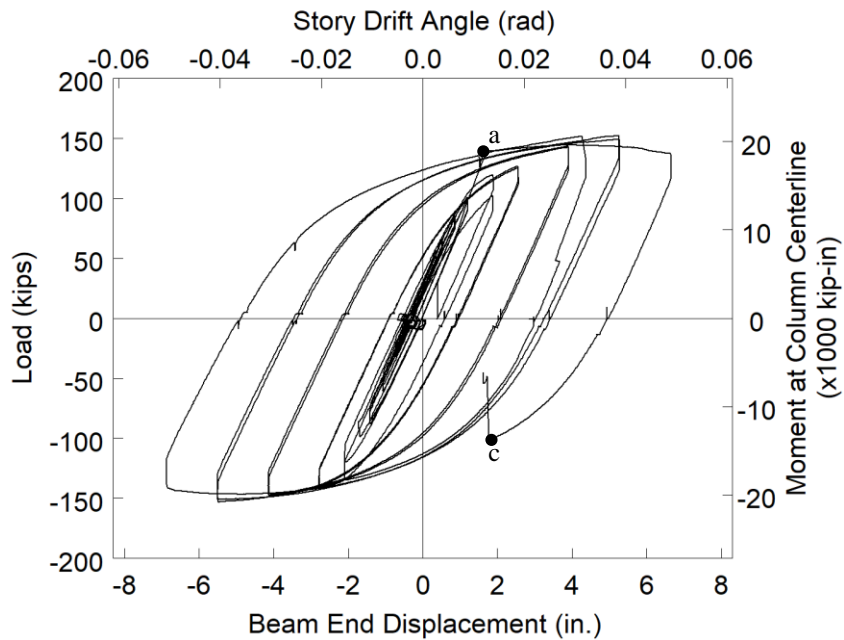


Figure 4.262 Specimen W4: Column Shear versus Story Drift Angle

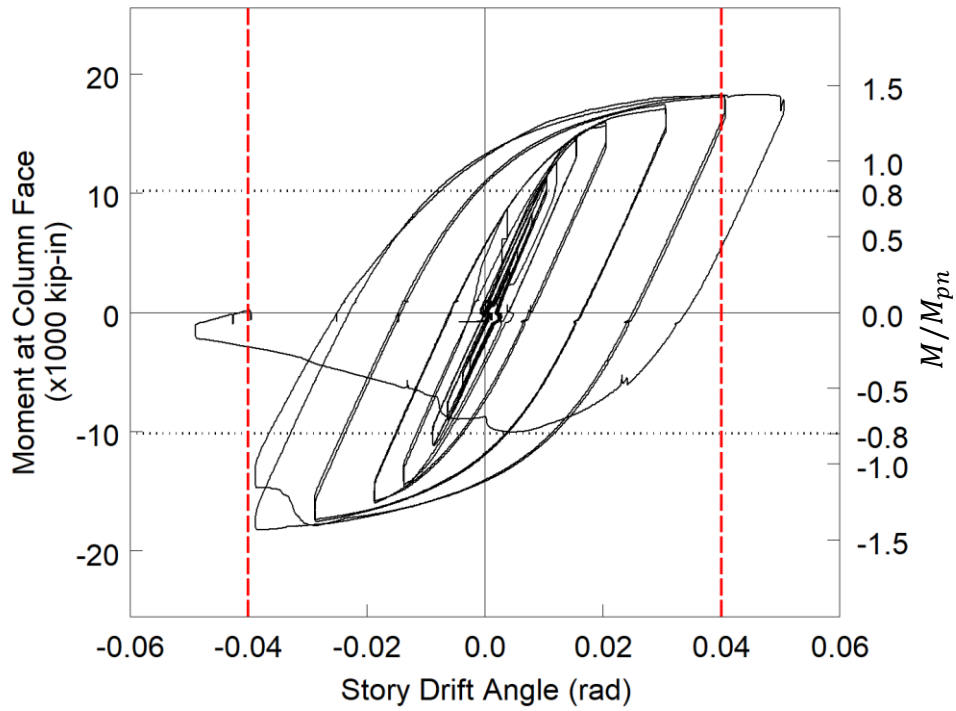


(a) East Beam

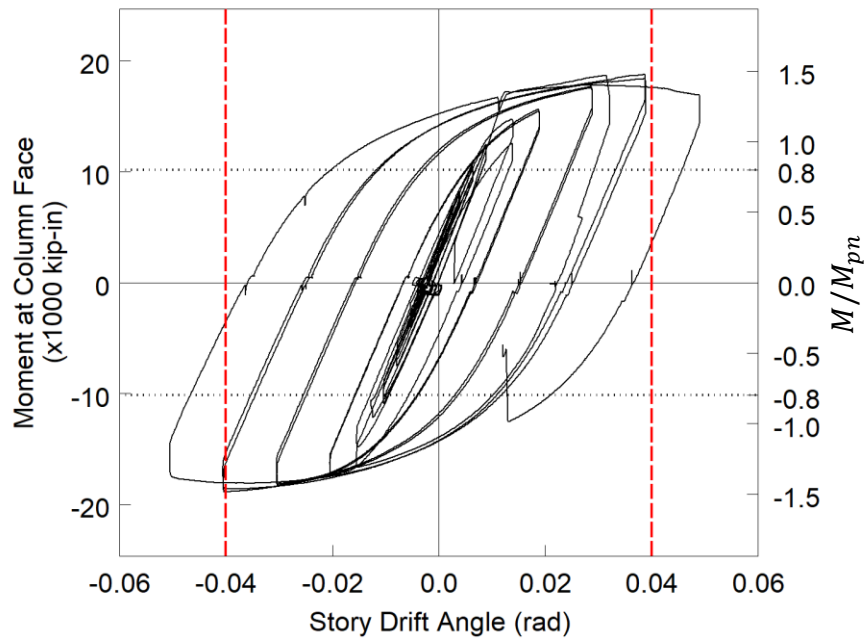


(b) West Beam

Figure 4.263 Specimen W4: Applied Load versus Beam End Displacement Response

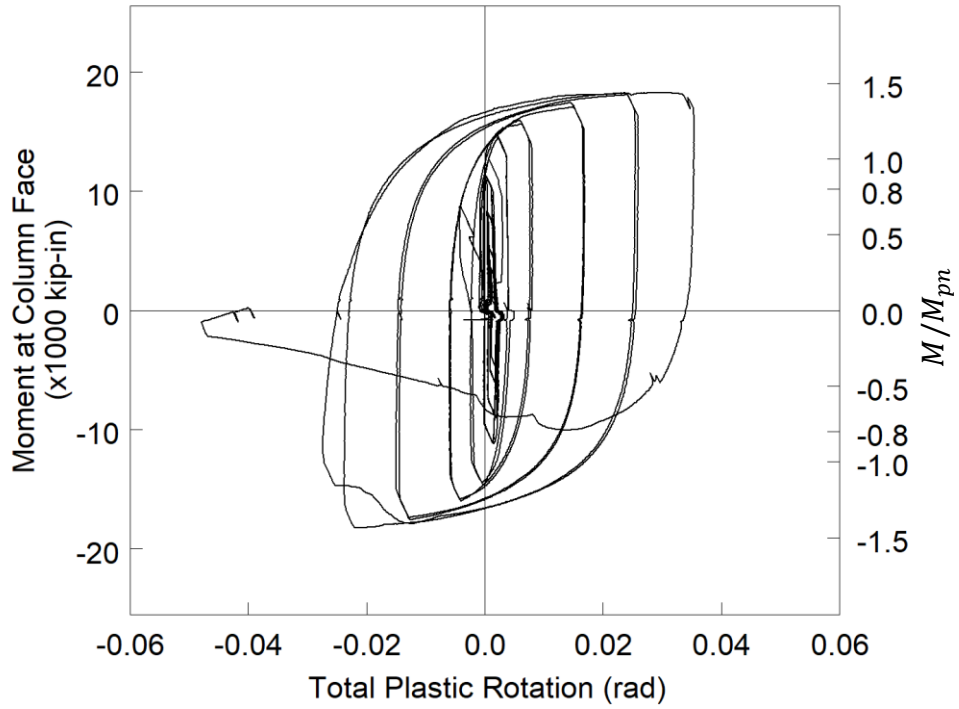


(a) East Beam

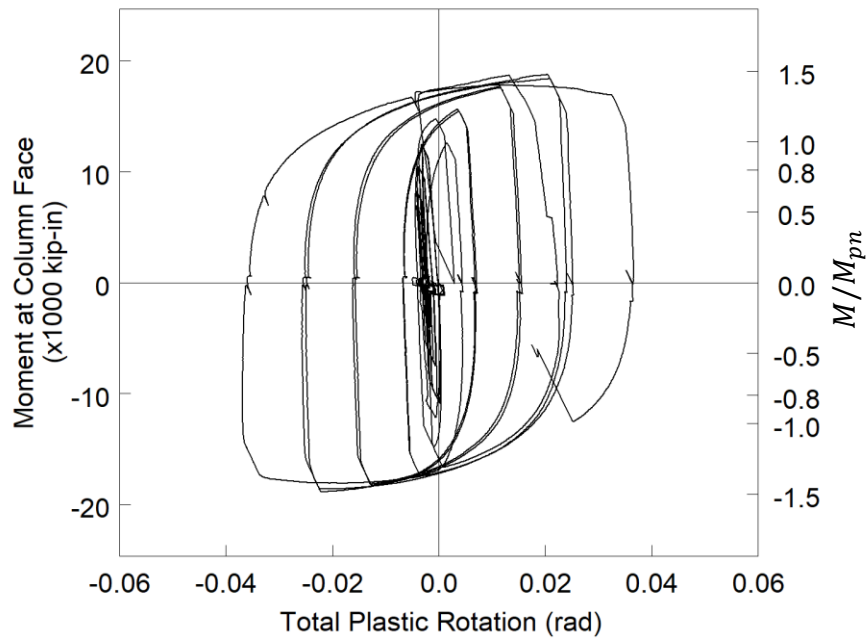


(b) West Beam

Figure 4.264 Specimen W4: Moment at Column Face versus Story Drift Response



(a) East Beam



(b) West Beam

Figure 4.265 Specimen W4: Moment at Column Face versus Plastic Rotation

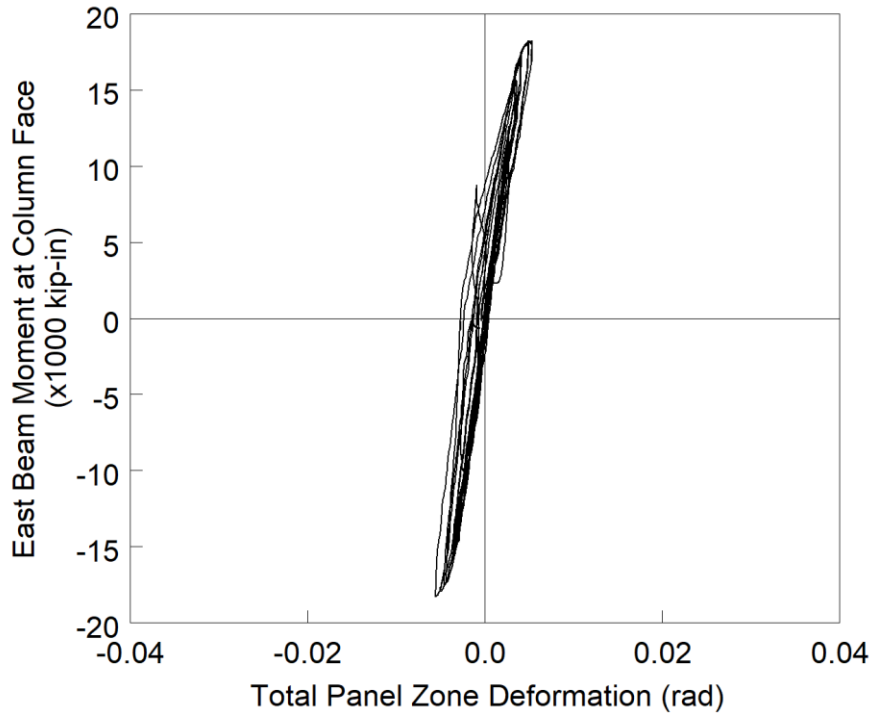


Figure 4.266 Specimen W4: Panel Zone Shear Deformation

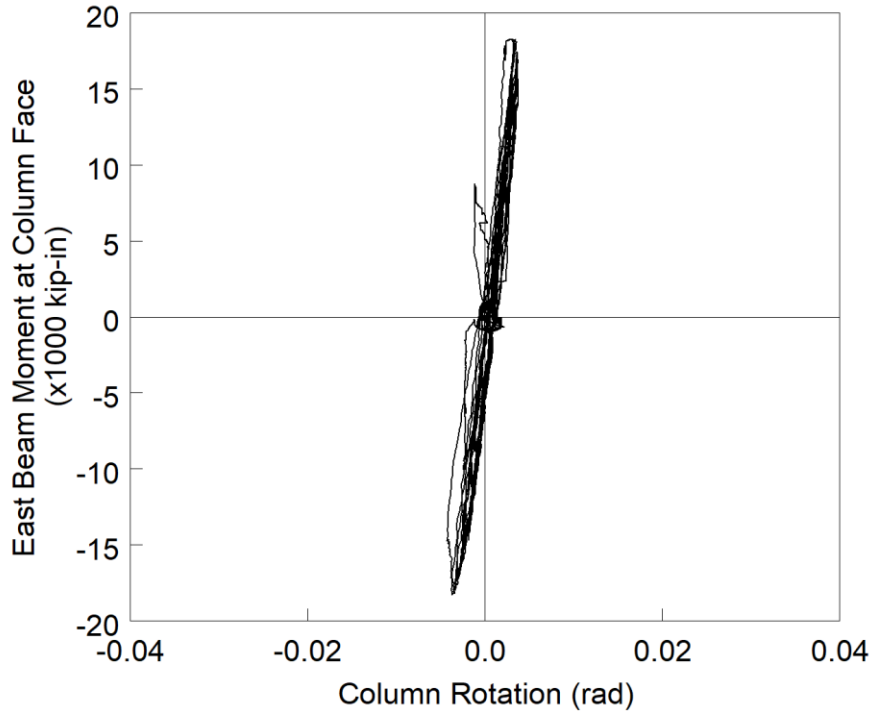


Figure 4.267 Specimen W4: Column Rotation

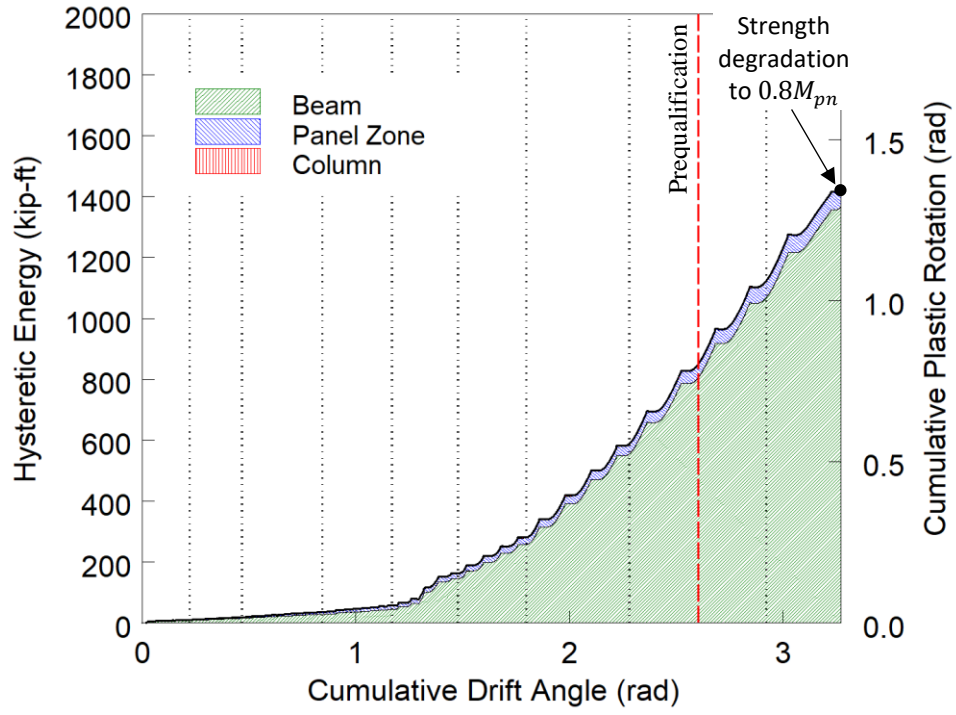
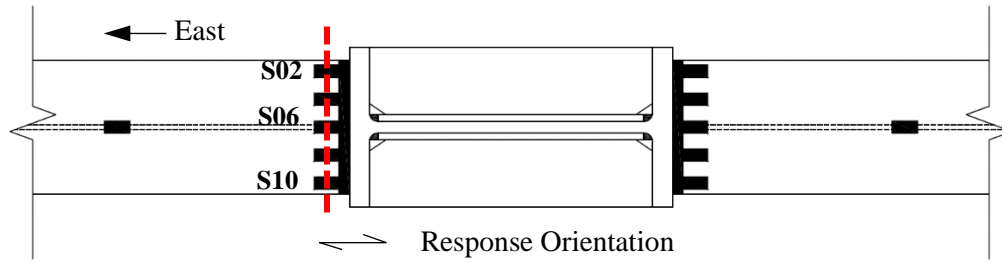
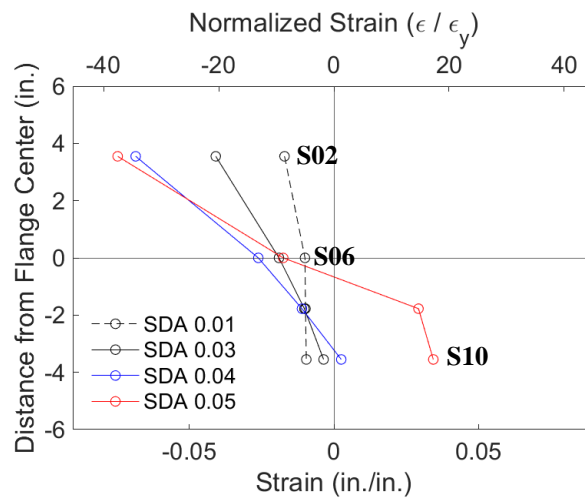


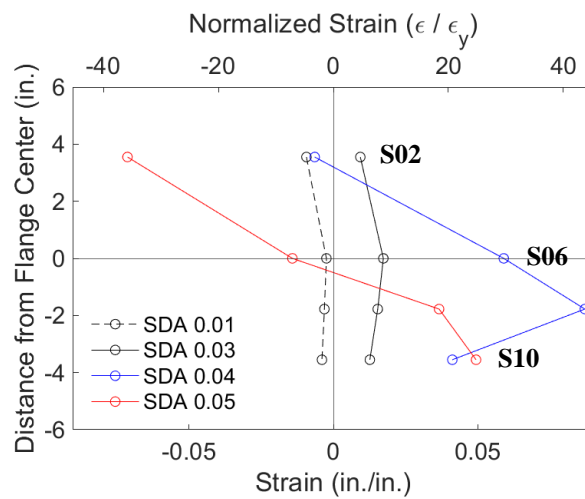
Figure 4.268 Specimen W4: Energy Dissipation



(a) Section

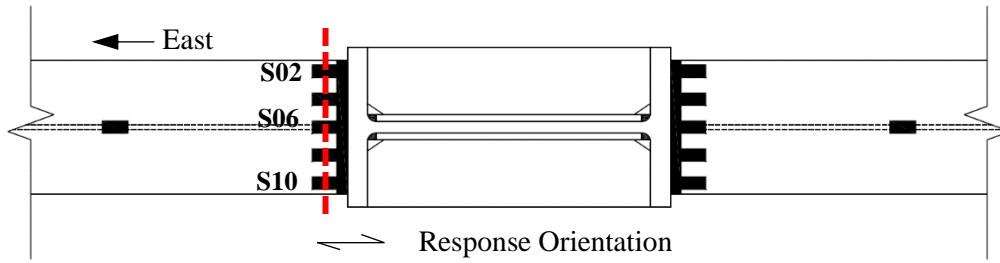


(b) Positive Drift

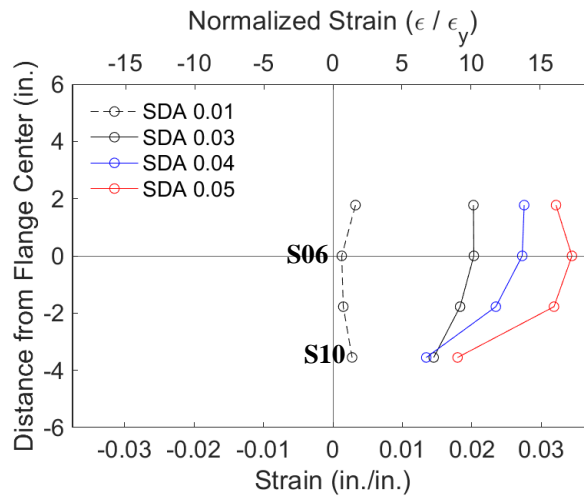


(c) Negative Drift

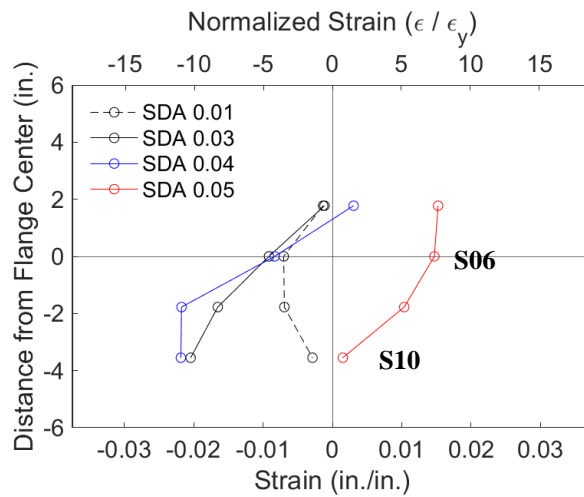
Figure 4.269 Specimen W4: Topside of East Beam Top Flange Strain Profile



(a) Section

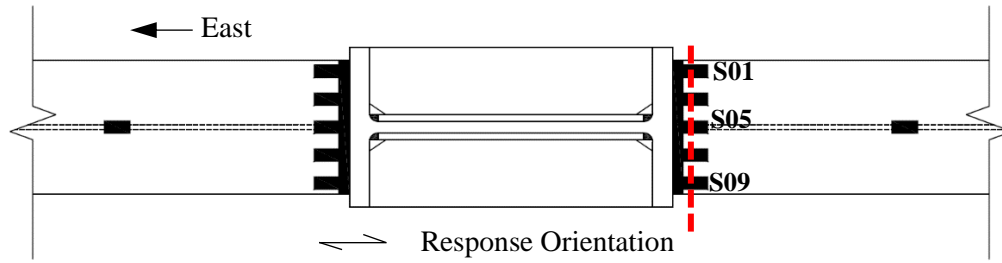


(b) Positive Drift

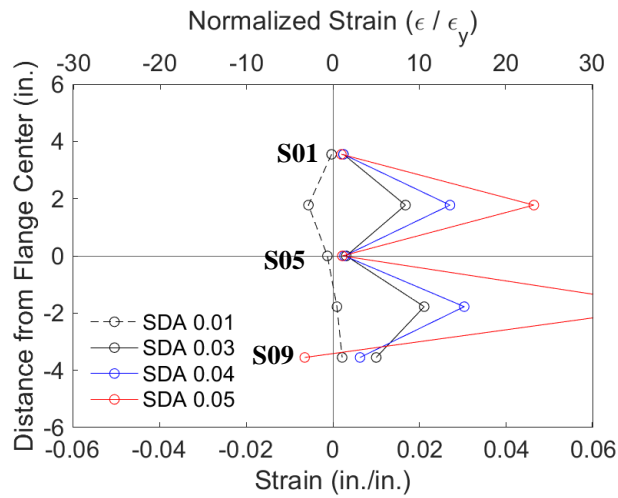


(c) Negative Drift

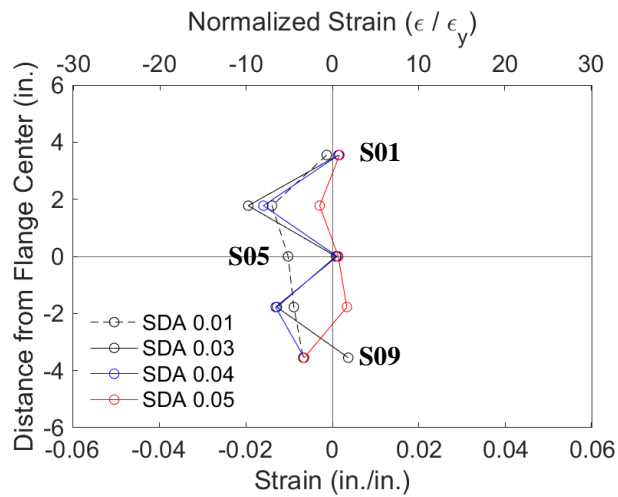
Figure 4.270 Specimen W4: Underside of East Beam Bottom Flange Strain Profile



(a) Section

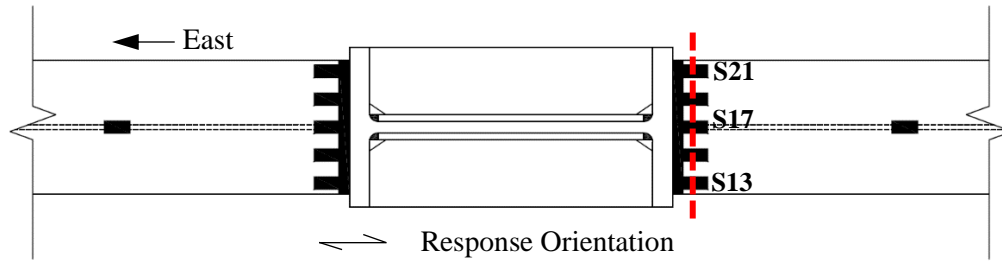


(b) Positive Drift

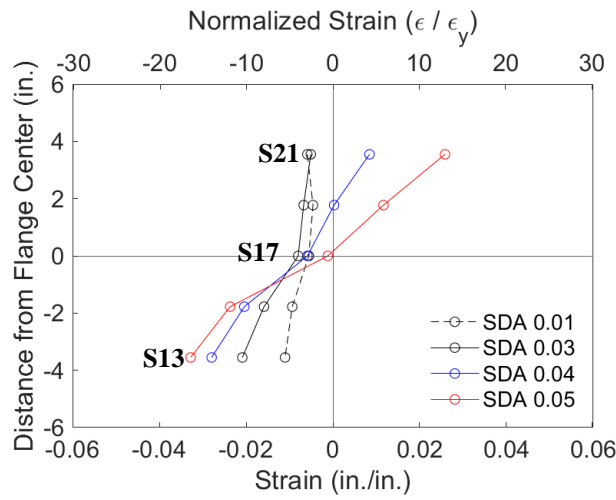


(c) Negative Drift

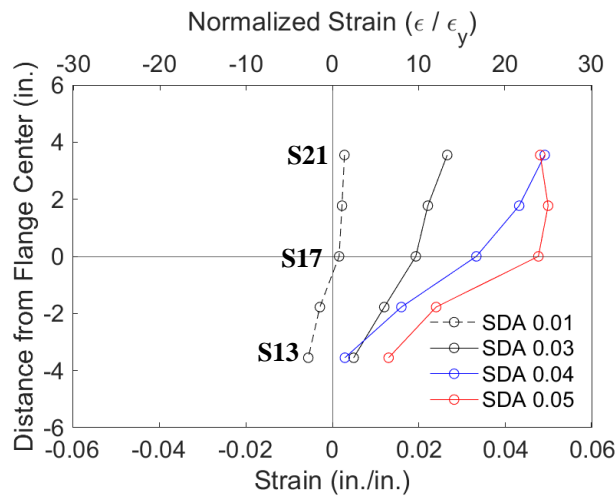
Figure 4.271 Specimen W4: Topside of West Beam Top Flange Strain Profile



(a) Section

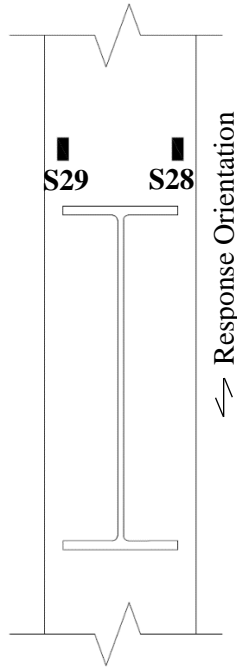


(b) Positive Drift

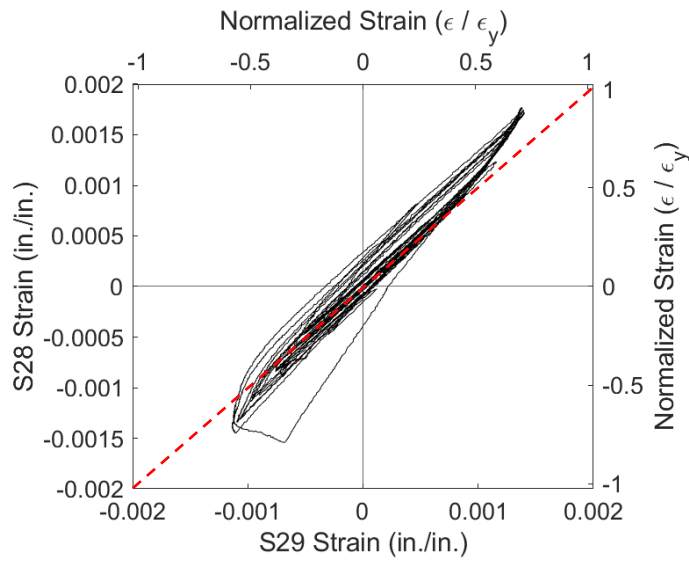


(c) Negative Drift

Figure 4.272 Specimen W4: Underside of West Beam Bottom Flange Strain Profile

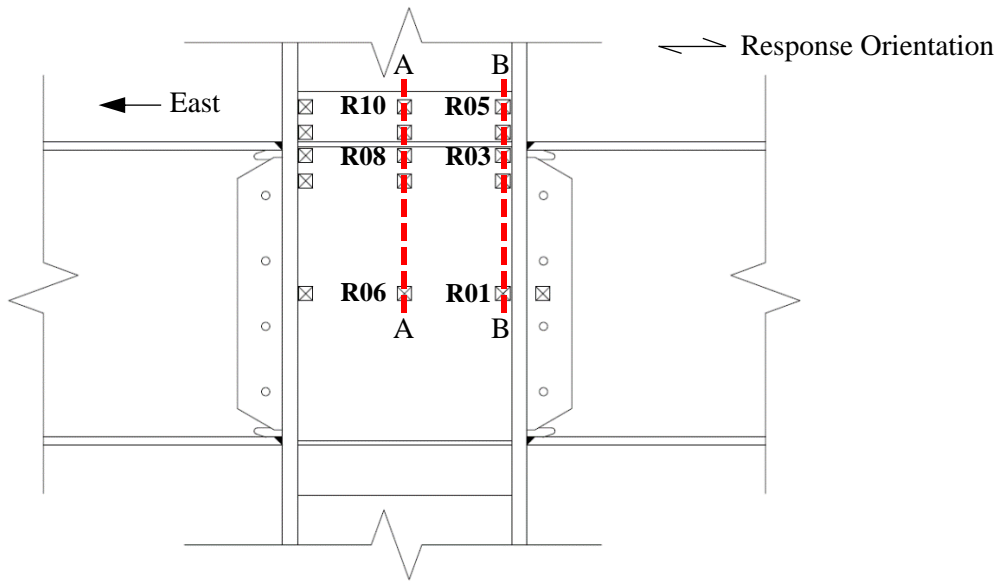


(a) Gauge Layout

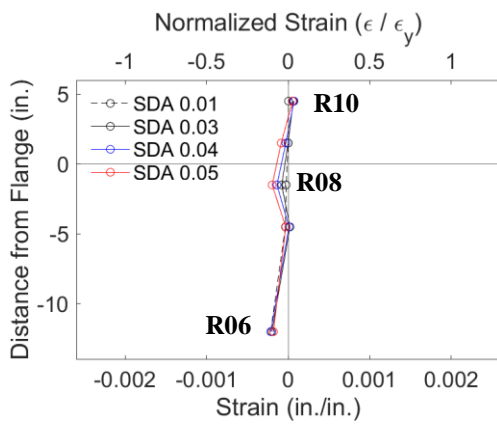


(b) Response

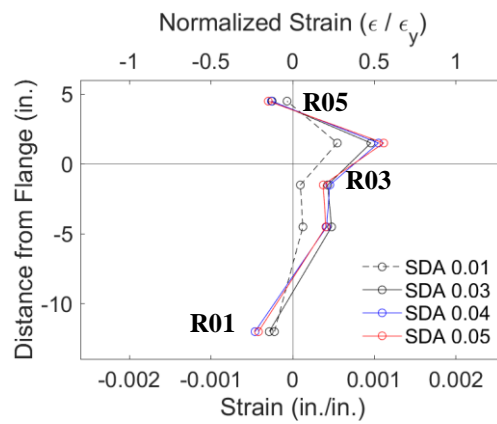
Figure 4.273 Specimen W4: Column Flange Warping



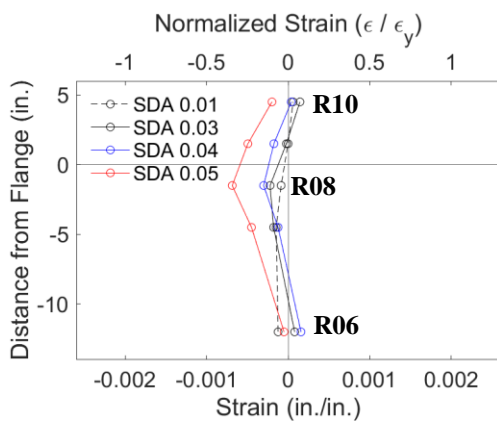
(a) Section Layout



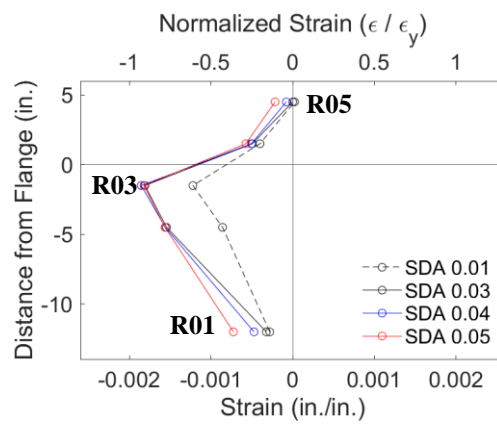
(b) Section A-A: Positive Drift



(c) Section B-B: Positive Drift

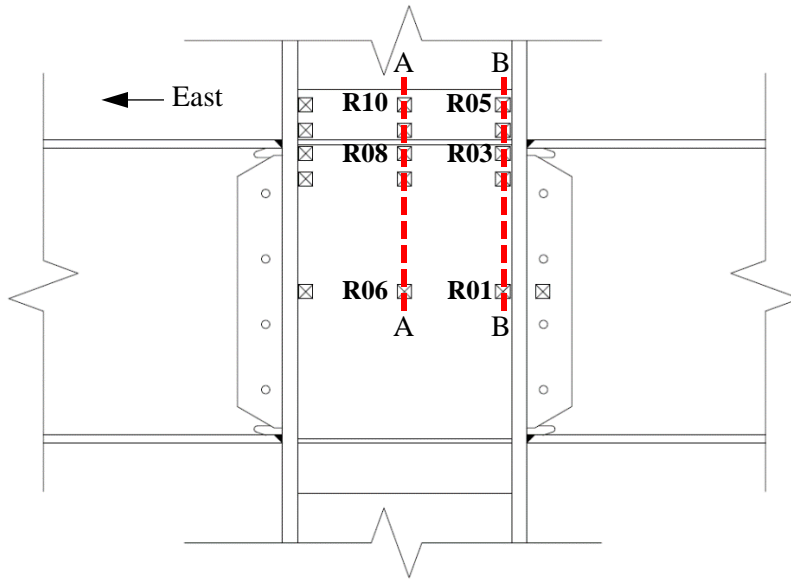


(d) Section A-A: Negative Drift

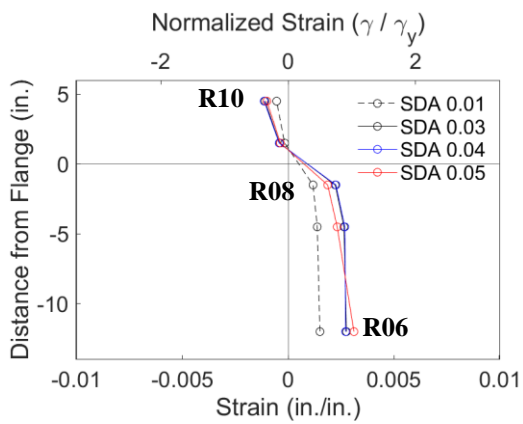


(e) Section B-B: Negative Drift

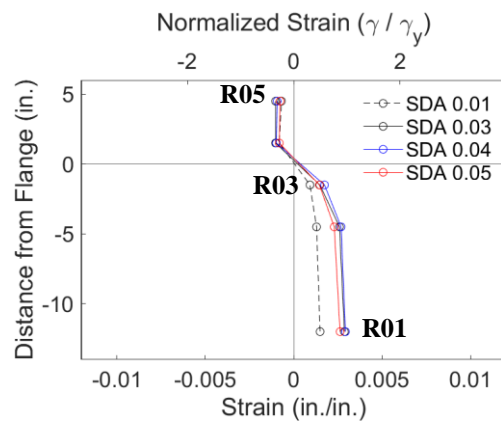
Figure 4.274 Specimen W4: Panel Zone Strain Profile



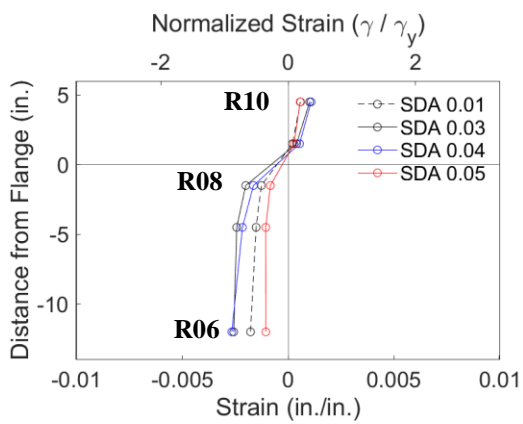
(a) Section Layout



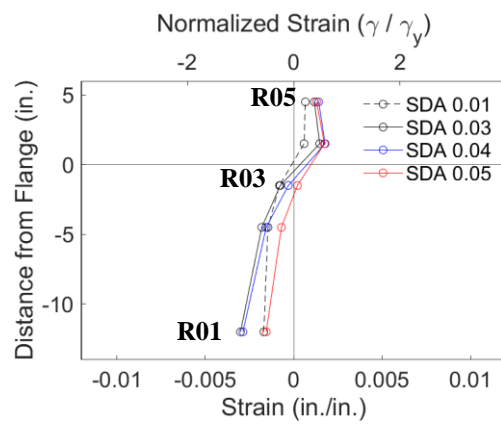
(b) Section A-A: Positive Drift



(c) Section B-B: Positive Drift

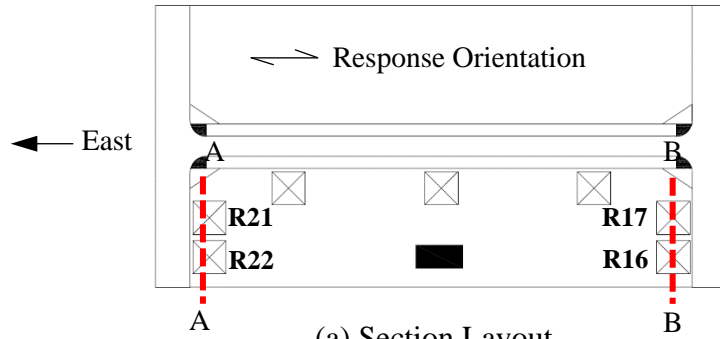


(d) Section A-A: Negative Drift

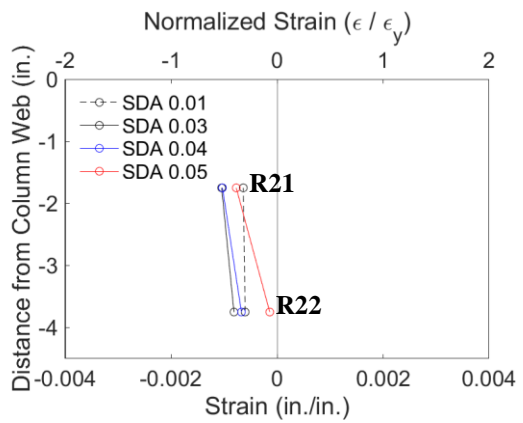


(e) Section B-B: Negative Drift

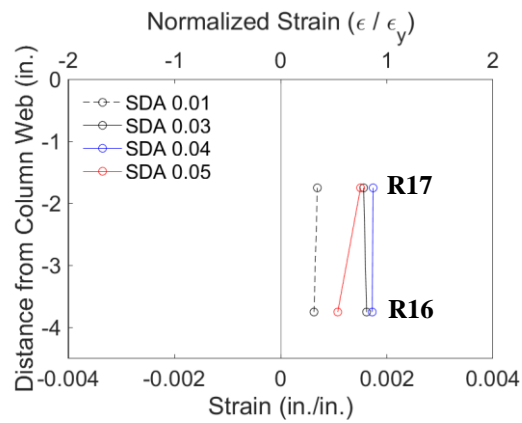
Figure 4.275 Specimen W4: Panel Zone Shear Strain Profile



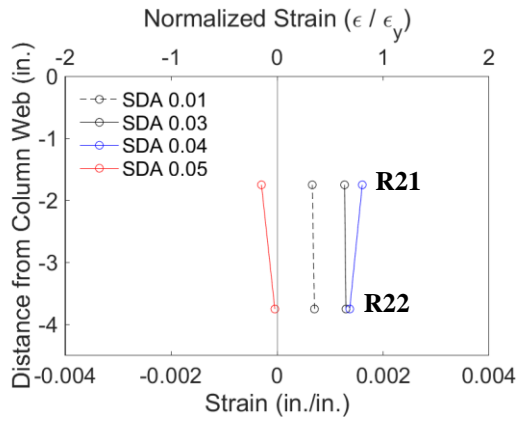
(a) Section Layout



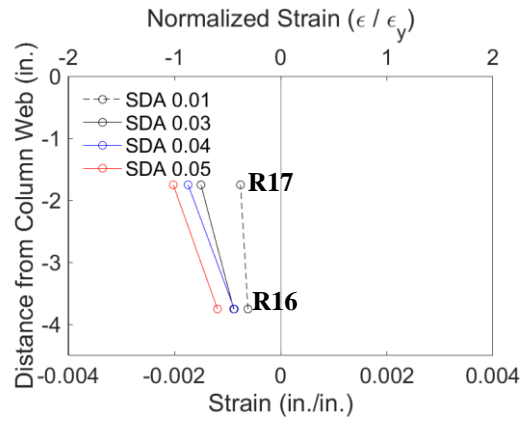
(b) Section A-A: Positive Drift



(c) Section B-B: Positive Drift

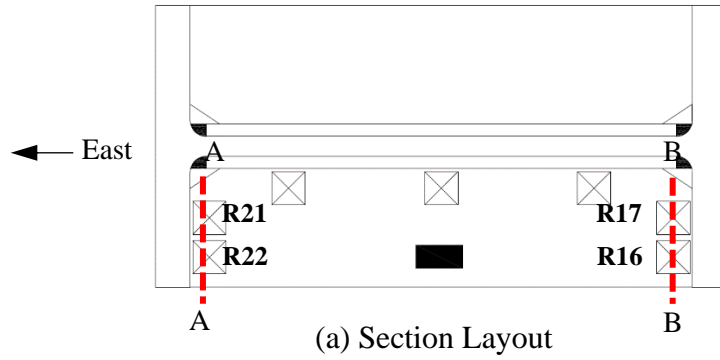


(d) Section A-A: Negative Drift

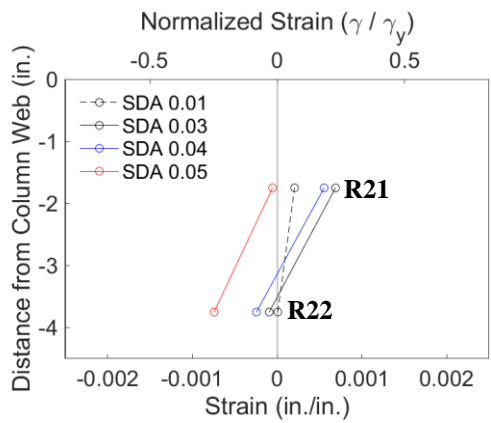


(e) Section B-B: Negative Drift

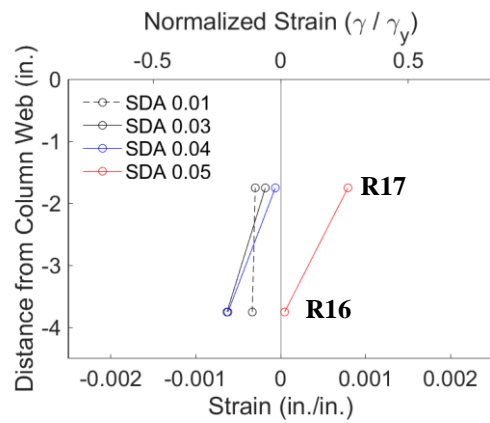
Figure 4.276 Specimen W4: Continuity Plate at Column Flange Edge Strain Profile



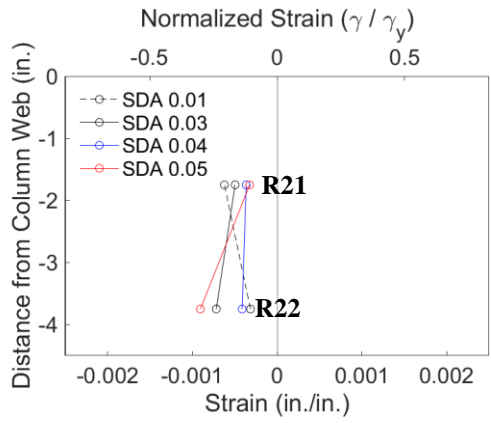
(a) Section Layout



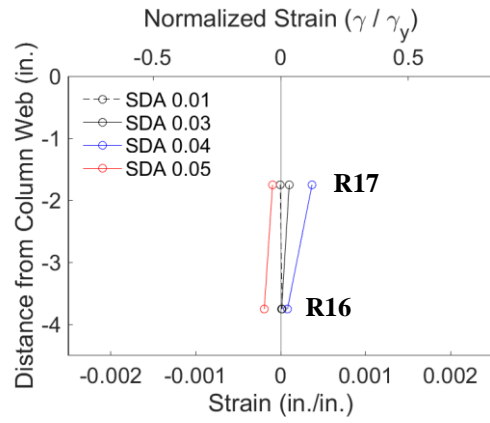
(b) Section A-A: Positive Drift



(c) Section B-B: Positive Drift

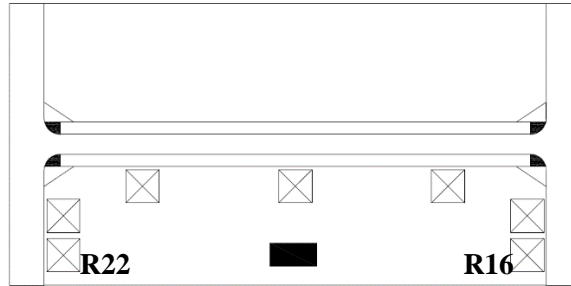


(d) Section A-A: Negative Drift

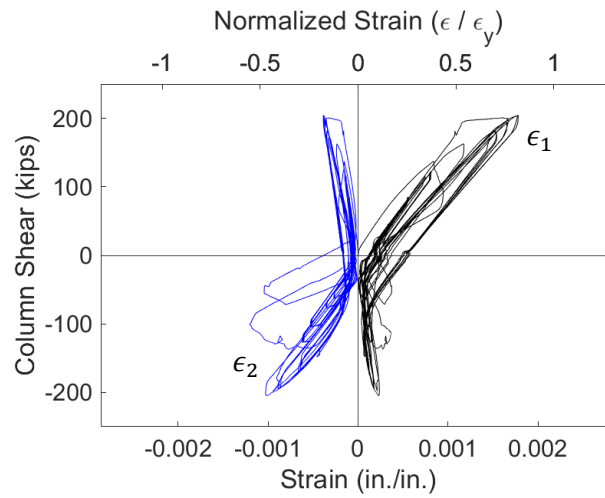


(e) Section B-B: Negative Drift

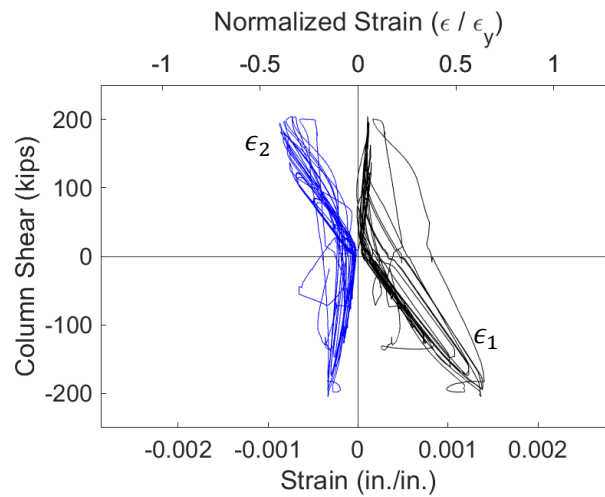
Figure 4.277 Specimen W4: Continuity Plate at Column Flange Edge Shear Strain Profile



(a) Layout

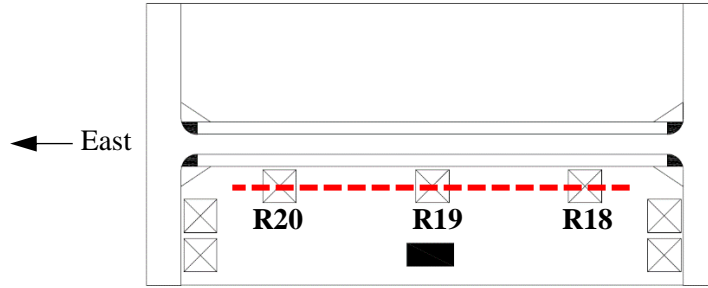


(b) Strain Gauge R16 Principal Strains

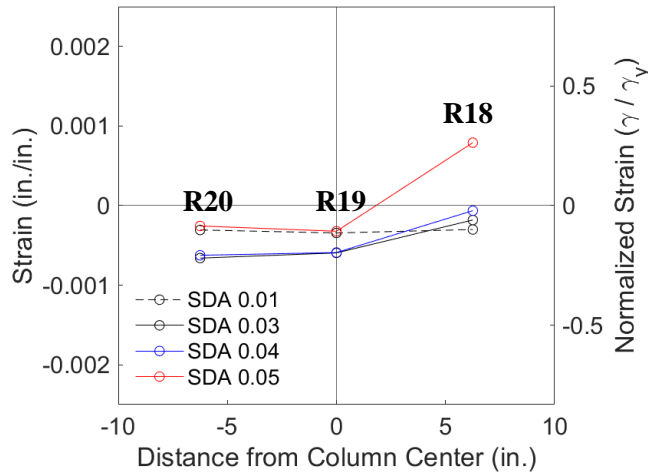


(b) Strain Gauge R22 Principal Strains

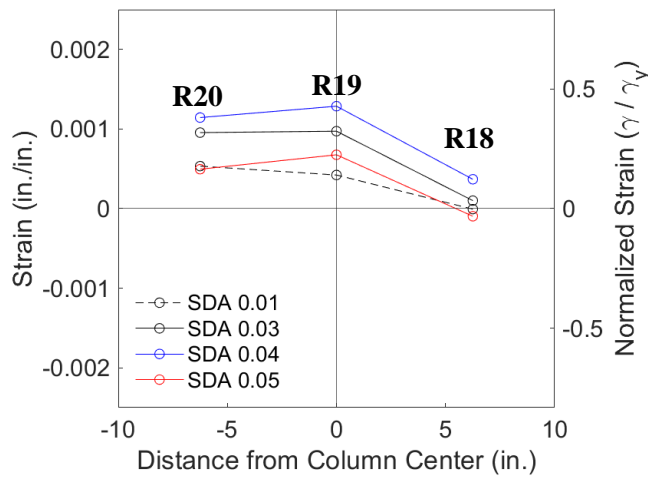
Figure 4.278 Specimen W4: Continuity Plate Strain Gauge Rosette Response



(a) Section Layout

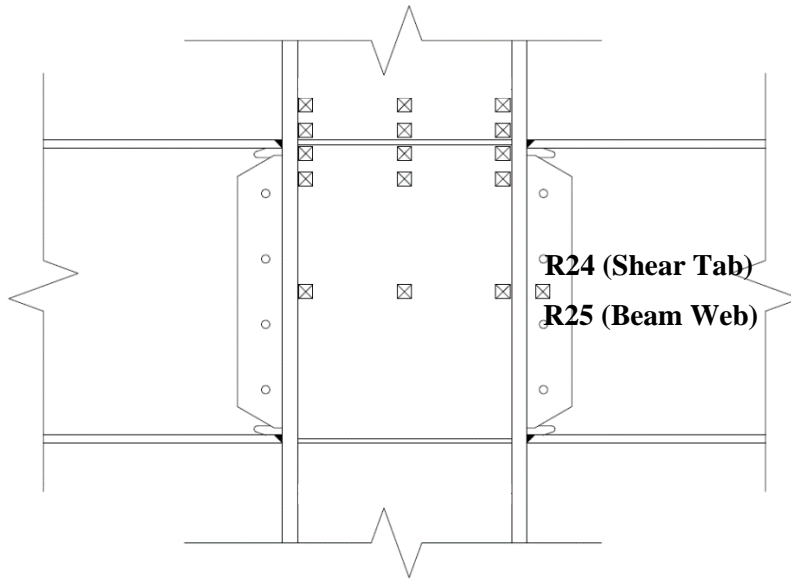


(b) Positive Drift

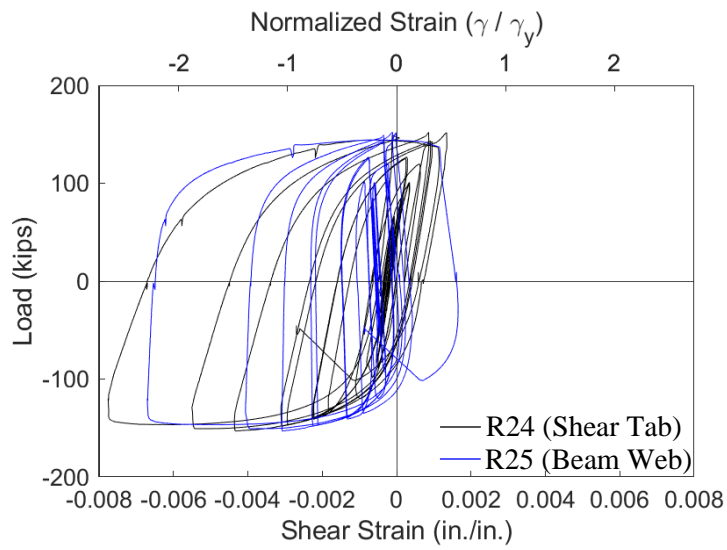


(c) Negative Drift

Figure 4.279 Specimen W4: Continuity Plate at Column Web Edge Shear Strain Profile



(a) Gauge Layout



(b) Strain Rosette Gauges R24 and R25

Figure 4.280 Specimen W4: Beam Shear Response

4.12 Specimen Macroetching

After testing, several sections of the specimens were cut out and sectioned using a cold saw. The surfaces of the sections were then polished and etched using a 5% Nital acid to reveal the formation of the welds. Figure 4.281 shows a macroetch of the beam bottom flange weld of Specimen C3; the beam bottom flange CJP weld did not fracture during testing. Evident in this figure is the beam flange CJP weld performed from the horizontal position and the reinforcing fillet placed on the underside of the beam in the overhead position after the backing bar is removed. Figure 4.282 shows the beam bottom and top flange welds of Specimen C5. The fractured top flange CJP weld is observed to propagate at a 35-degree angle through the weld metal, initiating at the reentrant corner formed between the weld and the column flange. Also shown in this figure are the continuity plate fillet welds, which show no indications of damage. A similar macroetch is performed on Specimen C6 (see Figure 4.283). In this case the beam top flange CJP weld fracture has two shear lips because the etching was taken closer to the edge of the beam flange. No damage to the fillet welds is observed. Figure 4.284 shows a similar section of the east beam flange welds from Specimen W1. The beam top flange CJP weld fracture is observed to follow the 30-degree bevel of the CJP weld.

Figure 4.285(a) shows a section through the doubler plate at an elevation which includes the beam web. This section shows the beam web CJP weld using the shear tab as a backing bar. The one-sided fillet weld fastening the shear tab to the column flange is also shown in the figure. The doubler plate fillet weld and bevel are shown in Figure 4.285(a) and (b).

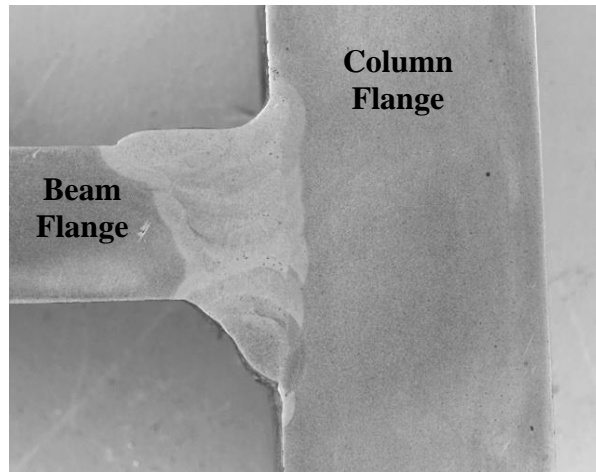
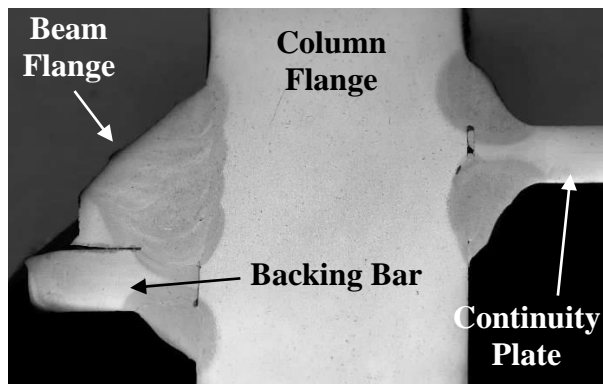
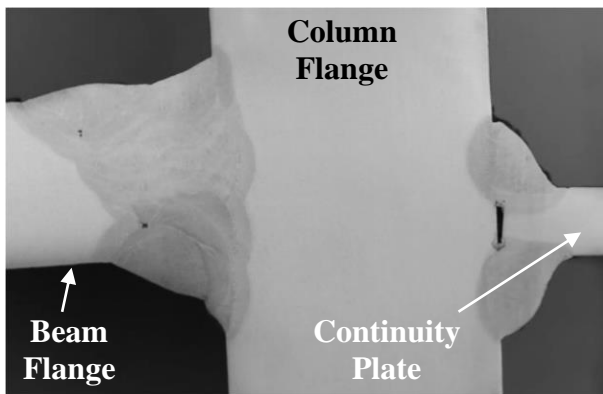


Figure 4.281 Macroetch of Specimen C3 Beam Bottom Flange CJP Weld

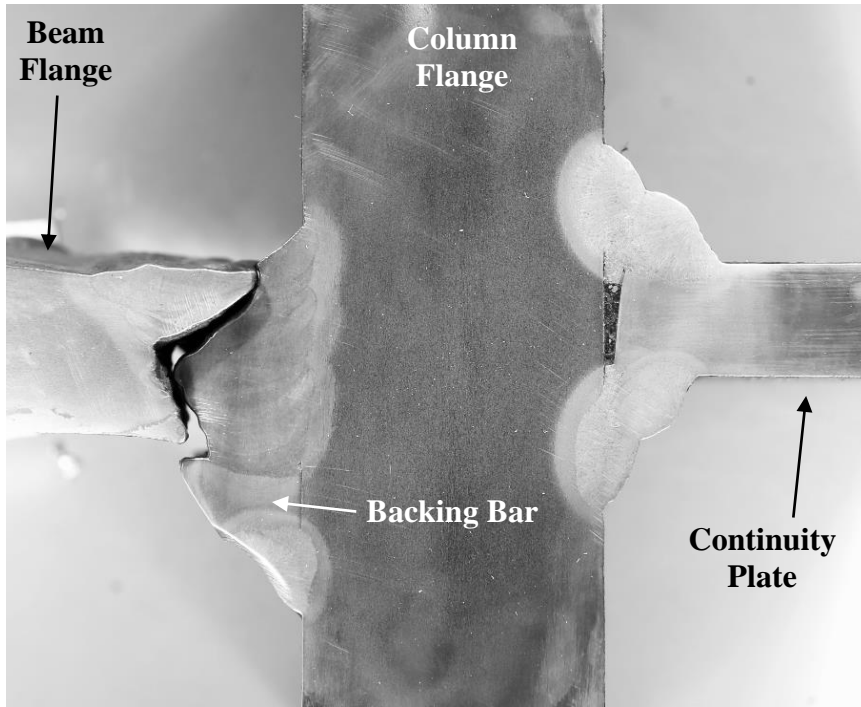


(a) Beam Top Flange

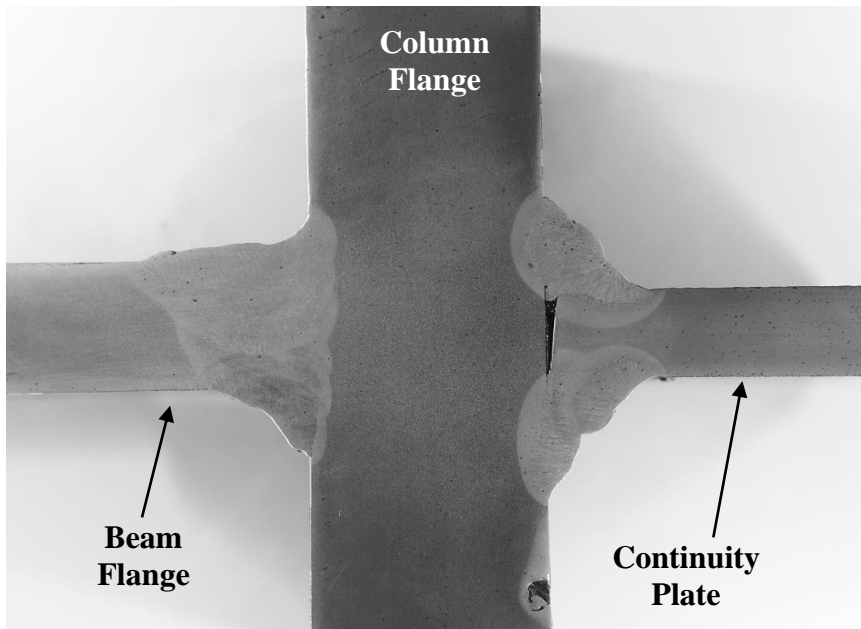


(b) Beam Bottom Flange

Figure 4.282 Macroetch of Specimen C5 Welds

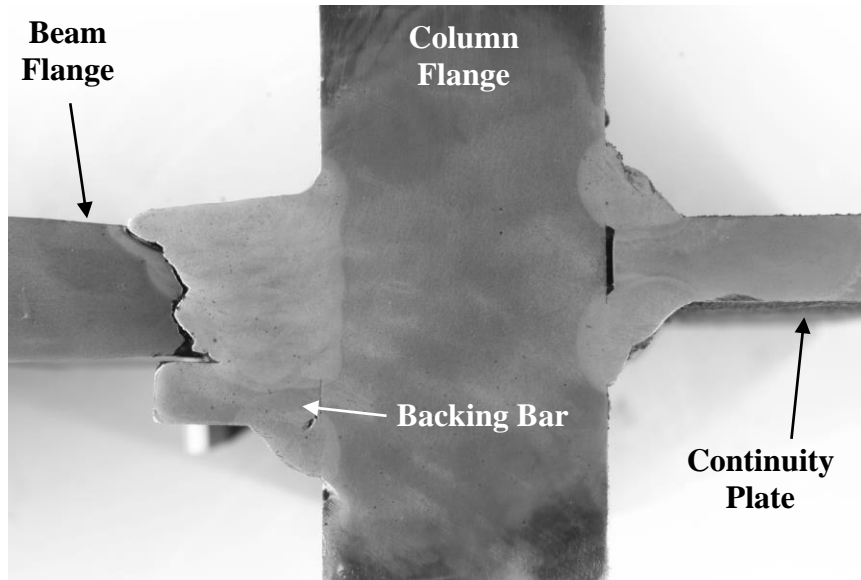


(a) Beam Top Flange

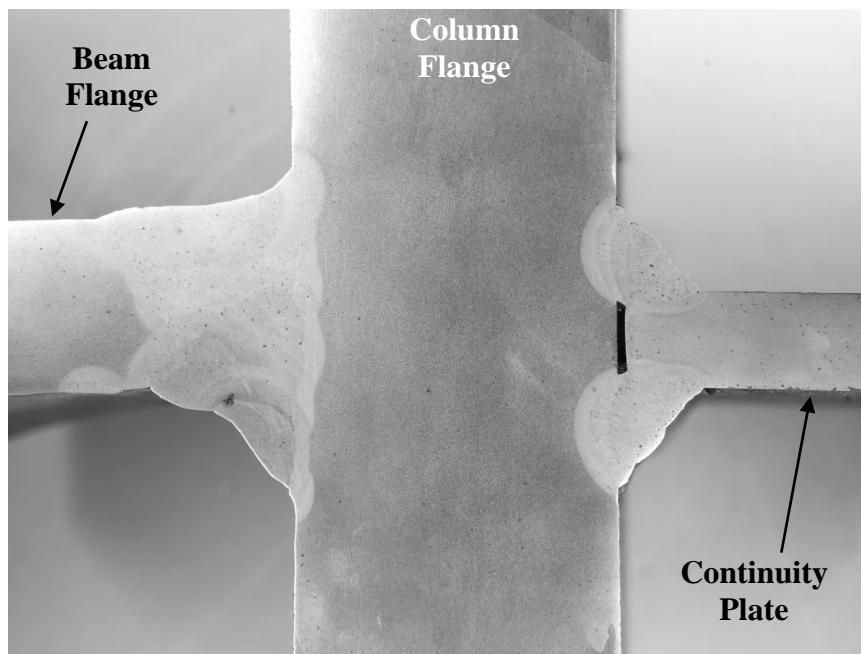


(b) Beam Bottom Flange

Figure 4.283 Macroetch of Specimen C6 Welds

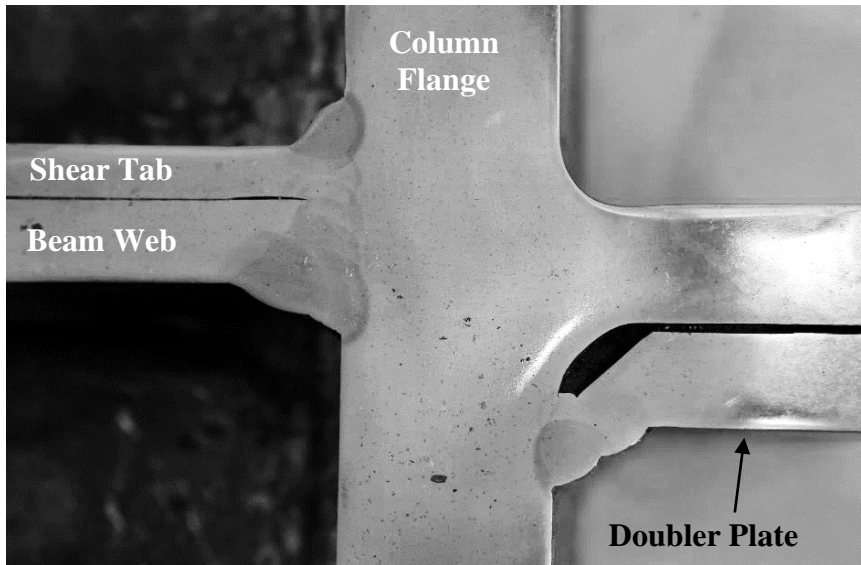


(a) Top Flange

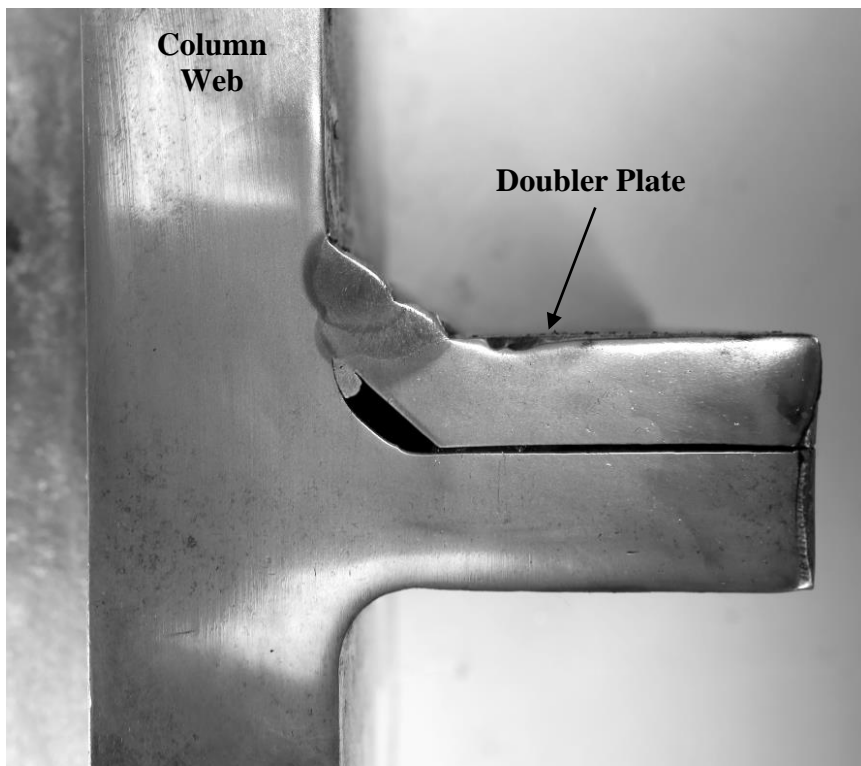


(b) Bottom Flange

Figure 4.284 Macroetch of Specimen W1 Welds (East Beam)



(a) Doubler Plate at Web



(b) Doubler Plate Above Beam Top Flange

Figure 4.285 Macroetch of Specimen C7 Welds

4.13 Lateral Bracing Force

During testing of the Phase 1 specimens the lateral bracing force was monitored using a set of strain gauge rosettes placed on each lateral brace column. The lateral braces were placed approximately $d_b/2$ away from the end of the RBS. The response of each of the specimens is tabulated in Table 4.1 through Table 4.5. The table shows the expected flange force of the specimen as per AISC 341 and the computed flange force determined from the peak load during each cycle. Specimen C3, Specimen C5, and Specimen C6 develop about 2.0% of the flange force at the brace location at the end of testing. All three of these specimens failed during the 0.05 rad cycles. Specimen C4 develops about 5.0% of the flange force during the 1st cycle of 0.05 rad cycles. Specimen C6-G saw the most significant flange force equal to 6.0% of the expected flange force or 7.6% of the measured force. The bracing force of Specimen C7 was not measured during testing.

The measured flange force was determined by dividing the measured moment at the brace location by the centroid between flanges. This procedure is consistent with AISC 341 (2016) §D1.2b stipulating the required force of the lateral bracing for highly ductile members.

Table 4.1 Specimen C3: Lateral Bracing Force

Drift (rad)	Cycle	Flange Force at Brace Location (kips)		Measured Brace Force (kips)	Normalized Brace Force	
		Expected	Measured		by Expected Flange Force (%)	by Measured Flange Force (%)
0.02	1	542	494	1.35	0.24	0.27
0.02	2		510	1.42	0.26	0.28
0.03	1		560	1.50	0.27	0.27
0.03	2		573	1.73	0.31	0.30
0.04	1		602	4.07	0.73	0.68
0.04	2		599	7.25	1.30	1.21
0.05	1		595	13.32	2.38	2.23

Table 4.2 Specimen C4: Lateral Bracing Force

Drift (rad)	Cycle	Flange Force at Brace Location (kips)		Measured Brace Force (kips)	Normalized Brace Force	
		Expected	Measured		by Expected Flange Force (%)	by Measured Flange Force (%)
0.02	1	486	521	2.05	0.42	0.39
0.02	2		522	2.10	0.43	0.40
0.03	1		567	1.81	0.37	0.32
0.03	2		574	1.84	0.38	0.32
0.04	1		565	2.42	0.50	0.43
0.04	2		537	2.83	0.58	0.53
0.05	1		492	4.55	0.94	0.92
0.05	2		448	11.33	2.33	2.53
0.06	1		405	22.17	4.56	5.47

Table 4.3 Specimen C5: Lateral Bracing Force

Drift (rad)	Cycle	Flange Force at Brace Location (kips)		Measured Brace Force (kips)	Normalized Brace Force	
		Expected	Measured		by Expected Flange Force (%)	by Measured Flange Force (%)
0.02	1	542	454	2.32	0.43	0.51
0.02	2		470	2.36	0.44	0.50
0.03	1		510	2.31	0.43	0.45
0.03	2		528	2.32	0.43	0.44
0.04	1		546	2.84	0.52	0.52
0.04	2		566	2.80	0.52	0.49
0.05	1		575	3.12	0.58	0.54
0.05	2		548	7.50	1.38	1.37

Table 4.4 Specimen C6: Lateral Bracing Force

Drift (rad)	Cycle	Flange Force at Brace Location (kips)		Measured Brace Force (kips)	Normalized Brace Force	
		Expected	Measured		by Expected Flange Force (%)	by Measured Flange Force (%)
0.02	1	448	490	0.80	0.18	0.16
0.02	2		498	1.17	0.26	0.23
0.03	1		524	1.86	0.42	0.35
0.03	2		533	2.42	0.54	0.45
0.04	1		530	3.23	0.72	0.61
0.04	2		518	3.11	0.69	0.60
0.05	1		468	9.56	2.13	2.04

Table 4.5 Specimen C6-G: Lateral Bracing Force

Drift (rad)	Cycle	Flange Force at Brace Location (kips)		Measured Brace Force (kips)	Normalized Brace Force	
		Expected	Measured		by Expected Flange Force (%)	by Measured Flange Force (%)
0.02	1	448	490	1.56	0.35	0.32
0.02	2		497	2.00	0.45	0.40
0.03	1		514	4.79	1.07	0.93
0.03	2		524	5.66	1.26	1.08
0.04	1		525	8.72	1.95	1.66
0.04	2		518	10.03	2.24	1.94
0.05	1		487	12.70	2.83	2.61
0.05	2		420	20.84	4.65	4.96
0.06	1		351	26.77	5.98	7.63

5 DISCUSSION OF TEST RESULTS

5.1 General

This chapter presents the comparison of the performance of specimens from Phase 1 (Specimens C3, C4, C6, C6-G, and C7), Phase 2 (Specimens W1, W2, W3, and W4), and the pilot study completed in 2016 (Specimens C1 and C2). All the specimens with a ‘C’ prefix were one-sided, simulating an exterior RBS moment connection with or without continuity plates. The careful design of these specimens for testing resulted in the ability to investigate the existing code criteria regarding the implementation of continuity plates in SMFs. Three of these specimens (Specimens C3, C4, and C7) directly challenge the Lehigh Criterion (Eq. 1.16) by omitting continuity plates, despite the ratio of beam flange width to column thickness being greater than 6.0. The one-sided specimens used either a W36×150 beam or a W30×116 beam. The tested columns consisted of two different shallow column shapes (W14×211 and W14×257) and several deeper column shapes (W24×176, W24×192, and W27×235). Specimens C1, C2, C5, C6, and C6-G used continuity plates. Only one specimen used a doubler plate (Specimen C7) consisting of a single-sided plate to reinforce the column web.

Specimens with a ‘W’ prefix were two-sided, simulating an interior WUF-W connection with continuity plates. Specimen W1 used two W36×150 beams, the largest beam size permitted by AISC 358-16, adjoined to a W27×258 column. Specimen W2 used two W33×141 beams fastened to a W27×217 column. Specimen W3 used two W30×116 beams connected to a W24×207 column. Finally, Specimen W4 used two W24×94 beams connected to a W24×182 column. All of the two-sided specimens used a pair of symmetric doubler plates with either a PJP or fillet weld attachment to the column flange. One specimen, Specimen W4, used a doubler plate that was terminated inside the continuity plates, while the other three specimens used a typical extended doubler plate detail.

All of the specimens with a continuity plate used 2-sided fillet welds to attach the continuity plate to the column flange and column web. Except for Specimens C6 and C6-G, the size of these fillet welds satisfy the proposed design rule of $w = (3/4)t_{cp}$, where w is the specified weld size, and t_{cp} is the thickness of the continuity plate. The doubler plate in Specimen C7 is designed using the assumed shear flow (Eq. 2.25) derived from the equilibrium of the plate instead of, as required by AISC 341-16, developing the shear

strength of the plate. Doubler plate welds for Phase 2 specimens develop the shear strength of the plate. Because the doubler plates of Specimen W4 do not extend beyond the continuity plates, this specimen uses a weld to attach the horizontal edge of the doubler plate, a requirement of AISC 341-16. This horizontal fillet weld is designed as per requirements to develop 75% of the shear strength of the doubler plate.

5.2 Observed Response and Governing Failure Modes

All of the specimens completed the AISC prequalification for SMF. Specifically, all the specimens completed at least one cycle of 0.04 rad drift without the strength of the connection degrading below $0.8M_{pn}$. The one-sided connections failed either by fracture of the beam flange within the reduced beam section or failure of the top flange CJP weld. Specimens, including those with and without continuity plates, which ultimately failed due to weld fracture demonstrated early signs of ductile weld tearing during the initial 0.03 rad cycle drifts. During each negative excursion where the top flange was in tension, the weld tear progressed until the complete fracture of the weld. The weld tears started in the center of the beam flange at the toe of a prominent weld pass in the reentrant corner. The typical fracture was a ductile shear fracture that propagated at a 35-degree angle through the weld metal until a fracture occurred perpendicular to the direction of loading (e.g., see Figure 4.49). The specimens which ruptured through the beam flange at the reduced beam section developed fractures in the vicinity of the largest local buckling amplitudes. Specimen C7 had a multi-stage fracture, which originated with a cleavage fracture in the k-area of the beam adjacent to severe web local buckling of the beam. The final stage of the fracture resulted in a ductile fracture of the entire beam top flange. Specimen C1 from the pilot study was the only specimen not loaded to failure. Instead, loading of this specimen stopped once the strength of the connection had degraded below $0.8M_{pn}$. Finally, a single cycle of 0.07 rad was imposed on Specimen C2 after completing two cycles of 0.05 rad of the AISC loading protocol.

Phase 2 specimens all fractured through the beam top flange CJP weld (e.g., see Figure 4.182). This fracture developed at the CJP weld root at the notch at the junction between weld metal and steel backing. The initiation of this fracture was during the 0.03 rad drift cycles, and its gradual progression occurred through the weld metal along the CJP weld bevel. Final fracture surfaces resulted in a mixture of shear fracture and cleavage.

Extreme local curvatures influenced the fractures by providing secondary initiation sites at other locations in the CJP weld. Several partial tears of the beam bottom flange CJP weld extending downward from the inside face of the flange was observed. In one specimen, Specimen W2, this resulted in a partial fracture of the beam bottom flange (see Figure 4.184). Table 5.1 compares the story drift capacities of all 12 specimens. (The drift capacity of two-sided specimens is the lowest obtained drift from either beam.) Figure 4.108 summarizes the completed drifts and the distribution of elastic and inelastic drift components. The expected and experimentally determined continuity plate and doubler plate forces are tabulated in Table 5.2 and Table 5.3.

The peak connection strength factor, C_{pr} , as determined by comparing the experimentally determined moment at the AISC 358-16 assumed plastic hinge location to the actual plastic moment, M_{pa} , of the beam is shown in Figure 5.2. (The computed C_{pr} for the two-sided specimens is the average of the two beams.) The average C_{pr} for the eight RBS connections is 1.19, which is similar to the value of 1.15 assumed in AISC 341-16. The average C_{pr} for the four WUF-W connections (eight beams total) is 1.30, less than the value of 1.4 stipulated in AISC 358-16. Figure 5.3 shows the normalized dissipated energy of each specimen and the distribution of energy dissipation between the column, panel zone, and beams. The energy is normalized by the summation of the actual plastic moment, M_{pa} , of the beams at the connection (i.e., for the two-sided connections the energy is normalized by $2M_{pa}$). The distribution shows that Specimens C2 and C5 demonstrated significant panel zone yielding, while Specimen C3 showed moderate panel zone yielding. This conclusion is reinforced by comparing the measured panel zone shear force, V_{pZ} , to the shear yielding strength of the panel zone (see Table 5.3). As predicted by the AISC 360-16 panel zone shear strength (Eq. 1.19), Specimens C4 and C7 did not dissipate energy through inelastic panel zone deformation.

Figure 5.4 shows the reserve energy ratio for each specimen. The reserve energy ratio is a metric that demonstrates a connection energy dissipation capacity beyond the single cycle of 0.04 rad drift as required by AISC 341-16. A value of 1 indicates no energy dissipation capacity after satisfying the minimum AISC qualification cycles. A value of 2, which was substantially achieved by Specimens C2, C4, C5, C6-G, W2, and W3, demonstrates that a connection has double the minimum required energy dissipation

capacity. The tested clear span-to-depth ratios are shown in Figure 5.5. Only Specimen W1 violated the AISC 358-16 minimum ratio of 7 for either RBS or WUF-W connections; this may explain the lowest reserve energy ratio by this specimen.

5.3 Effect of Galvanization

Specimen C6-G was nominally identical to Specimen C6, except the specimen was hot-dip galvanized before shop welding. Removal of the galvanization in the area of the connection was required to perform the simulated field welding. Zinc paint was then applied to the welded area to simulate standard practice. The load-displacement response of the two specimens was identical until the beam flange CJP weld fractured during 0.05 rad drift of Specimen C6 (see Figure 5.6). The discrepancy in cyclic performance between the two specimens is attributed to variability in toughness and geometry of the beam flange CJP welds. Therefore, for the specimens tested it appears that the galvanization did not affect the strength or the ductility capacity.

5.4 Continuity Plate Response

The specimens with continuity plates did not demonstrate any damage to the fillet weldments between the continuity plates and the column flanges or column webs. Except for Specimens C6 and C6-G, the continuity plate-to-column flange weld used a proposed weld size of $(3/4)t_{cp}$. Specimens C2 and C5 used the closest weld size that would develop at least $(3/4)t_{cp}$ (see Table 2.3).

According to the recorded strain gauge response of the continuity plates, all specimens, including Specimens C1 and C2, realized yielding or nearly yielding levels of strain (Mashayekh 2017). The limited amount of cyclic strain precludes significant hysteresis and strain hardening of the continuity plate. The yielding of Specimen C1, which is designed to remain elastic according to the flexibility design method, is explained through high levels of residual stresses in the continuity plates due to the welding of the plates. With the exception of Specimen C5, the strains in the continuity plates were limited to $2.5\epsilon_y$ (see Figure 5.7). The addition of cyclic buckling of the continuity plate used in Specimen C5 contributed to the recorded strain approaching $12\epsilon_y$ in tension; however, prior to buckling the strains were limited to $1.5\epsilon_y$ [see Figure 5.7(c)]. Therefore, most of the high strain response in C5 is attributed to the flexural buckling of the plate and not high membrane strains in the continuity plate. It is noted that the continuity plates of Specimen

C2, which used a continuity plate despite not requiring stiffening to satisfy FLB or WLY, still demonstrated yielding. This is attributed to the relative stiffness of the continuity plate.

Specimens W1 and W3 also show an asymmetric strain response; however, in this case, it is attributed to the lateral-torsional buckling of the adjacent beam [see Figure 5.7(e) and (g)]. The lateral-torsional buckling of the beam imposes an in-plane flexural demand to the continuity plate that exaggerates the compressive strains in the plate. Specimen W2 was the only specimen designed with an intentionally undersized continuity plate with a *DCR* of 1.43 (see Table 2.3). Instead of satisfying the governing column limit state, this continuity plate was sized based on matching 75% of the adjacent beam flange thickness as per AISC 341-16. Despite being undersized, the principal strains in the plate were limited to ϵ_y . This is attributed to a combination of two factors: (1) the measured peak flange force was 0.88 times the expected, and (2) the measured F_y value of the continuity plate material was 58.0 ksi. There appears to be no detrimental effect of two-sided connections on continuity plates. Before any lateral-torsional response of the beams, the axial response in the continuity plate near the column flange approximates equal and opposite pairs (e.g., see Figure 4.203). The shear response along the column web is substantially uniform (e.g., see Figure 4.206).

Specimen C5 was the only specimen that demonstrated buckling of the continuity plate. This buckling initiated at 0.04 rad drift during the peak beam flange force; local continuity plate curvature was straightened out during the tension excursions of the adjacent beam flange. Specimen C5 was designed with a width-to-thickness ratio of a continuity plate of 16. Three specimens were designed with a width-to-thickness ratio of 12—these specimens did not develop an instability during testing (see Table 5.2).

5.5 Doubler Plate Response

Only the design of the vertical welds adjoining the doubler plate to the column flange of Specimen C7 deviated from the provisions of AISC 341-16. This specimen and the four specimens with doubler plate weldments conforming to AISC 341 did not demonstrate any damage to the weldments. Specimen W4 utilized a doubler plate that was terminated within the continuity plates. The top and bottom edges of the doubler plate of this specimen was welded to the continuity plate using a fillet weld. This weld was the sole attachment of the

inside face of the continuity plate to the panel zone. No damage was observed in any of the weldments of this specimen.

Table 5.3 shows that the measured panel zone shear exceeded the yield strength of the plate in Specimen W1. This specimen observes the largest recorded strain in the center of the doubler plate (see Figure 5.8). Specimens W2, W3, and W4 have strains approaching the yielding strain in the middle of the doubler plate—consistent with the predicted behavior from Table 5.3. The edge of the doubler plate demonstrated higher shear strains, above $2\gamma_y$, as shown in Chapter 4. These locations experience local loading effects and high levels of residual stress. Figure 5.8 shows that the extended portion of the doubler plate shows negligible shear stress. Specimen W4, without the extended doubler plate, demonstrates a minor shear response corresponding to the shear of the column.

Specimen W3 used a doubler plate with a ratio of $(d_z + w_z)/t_{dp}$ of 102, which violates the AISC 341-16, limiting width-to-thickness ratio to 90. Despite the violation, doubler plate instability was not observed.

5.6 Column Limit States

Although the limit states of column flanges and webs under concentrated loads are implicitly investigated by all specimens in this test program, Specimens C3, C4, and C7 without continuity plates provide a unique opportunity to isolate the limit states.

5.6.1 Web Local Yielding (WLY)

Specimens C4 and C7 challenged the Lehigh Criterion by omitting continuity plates. The expected flange force of Specimen C4 was 611 kips, while the expected strength of the WLY limit state was 620 kips, resulting in a *DCR* of 0.99. Instrumentation of this specimen illustrated the WLY limit state by distributing five uniaxial strain gauges over a distance of $5k$ behind the beam flange at the toe of the column flange-to-column web radius. As discussed in Section 1.5.2, the distance of $5k$ was derived from experimental results, which confirmed a 2.5:1 diffusion of the beam flange force in the column web. The experimentally determined flange force of Specimen C4 was 667 kips—1.09 times higher than the expected flange force. The peak force occurred during the second cycle of 0.03 rad drift. The resulting peak flange force exceeds the estimated strength of the WLY limit state of 620 kips based on the actual yield stress (see Table 5.2). The local response of Specimen C4 demonstrates that, during the 0.03 rad drift cycles, yielding had distributed

over the $5k$ distance during the positive drift cycles. Negative excursions do not demonstrate yielding extending beyond $5k$ during the testing (see Figure 5.9). Continued positive excursions saw uniform incremental growth of the web strains. The difference between the positive and negative excursions is attributed to column warping producing an out-of-plane flexure of the column web during positive excursions when the beam top flange was in compression (see Figure 4.44). Therefore, despite the experimentally determined flange force exceeding the WLY limit state of the column by 8%, the limit state was not violated until 0.03 rad. The local response indicates peak cyclic strains of 0.01 in./in. ($5\epsilon_y$) directly behind the beam flange. The specimen failed by ductile tearing through the reduced beam section and not because the WLY was exceeded.

Specimen C7 was reinforced with a web doubler plate to satisfy the WLY limit state. The experimentally determined flange force of 594 kips is significantly lower than the actual WLY limit state of 917 kips. Despite this level of robustness, the local response of Specimen C7 demonstrated significant yielding in the column web and doubler plate over a distance of $5k$ (see Figure 5.10). This is attributed to the combined effect of warping of the column flange producing out-of-plane flexure of the column web and doubler plate. Additionally, the eccentric weldments of the doubler plate produce additional curvature, which exacerbates the extreme fiber measured strain response. Despite the additional flexural demands imposed on the column web and doubler plate, the specimen failed by ductile tearing through the reduced beam section.

Figure 5.11 shows that column web strains of Specimen W4 approached $1\epsilon_y$ adjacent to the continuity plate as the continuity plate yielded across its breadth (see Figure 5.12). This indicates that although the WLY limit state may be applicable to unreinforced columns that the significant plasticification that must occur to mobilize its full strength.

5.6.2 Flange Local Bending (FLB)

Localized yielding of the inside face of the column flange at the beam flange level was only observed in Specimen C4 (see Figure 5.13). Recorded strains in that region demonstrate strains of $4\epsilon_y$ at the edge of the column flange, diminishing to $2.5\epsilon_y$ several inches away [see Figure 5.14(a)]. Specimen C4 demonstrated strains on average of $3\epsilon_y$ with little gradient across the column flange [see Figure 5.14(b)]. Specimen C7 developed strains of $6\epsilon_y$, diminishing to $3.5\epsilon_y$ at the other gauge location [see Figure 5.14(c)]. It is

noted that the recorded strains are influenced by the lateral-torsional response of the beam, which superimposes a weak-axis flexure on the beam flanges. Weak-axis flexure of the beams changes the distribution of the flange forces between sides of the column while keeping the net flange force unchanged. For the specimens tested, at the gauge location, the positive excursion demonstrated the highest peak strain.

The moderate levels of strains recorded behind the beam flange suggest the initiation of a FLB yield line mechanism; however, the inclined yield line that would be expected to extend (Prochnow et al. 2000) from the radius of the column outward at an inclination away from the beam flange was not observed.

5.7 RBS Lateral Bracing Force

During the Phase 1 testing program, the lateral bracing force of the lateral bracing at approximately $d_b/2$ away from the end of the RBS was monitored. The bracing force is normalized by the measured instantaneous beam flange force as determined from static equilibrium. Table 5.4 shows the computed normalized maximum bracing force recorded during testing. It is observed that the lateral bracing force of the specimens that terminated at 0.05 rad developed approximately 2% of the beam flange force. Specimen C6-G developed 5% of the measured flange force during the 0.05 rad drift cycles. Specimens C4 and C6-G developed 5.5% and 7.7%, respectively, of the measured flange force during the 0.06 rad drift cycles. The bracing force is compared to the required bracing force as per §D1.2b of AISC 341-16 for highly ductile members. This provision requires 6% of the expected beam flange force to be used when designing lateral bracing.

Table 5.1 Specimen Performance Comparison

Spec. No.	Beam	Column	Continuity Plate (in.)	Doubler Plate	Cycle at Failure	Failure Mode
C1 ^a	W30×116	W24×176	3/4	-	-	Not Tested to Failure (Stopped at 0.05 rad)
C2 ^a	W36×150	W14×257	5/8	-	1 st of 0.07 rad after 0.05 rad	RBS Fracture
C3	W36×150	W14×257	-	-	1 st of 0.05 rad	Beam Top Flange CJP Weld
C4	W30×116	W27×235	-		1 st of 0.06 rad	RBS Fracture
C5	W36×150	W14×211	3/8		2 nd of 0.05 rad	Beam Top Flange CJP Weld
C6	W30×116	W24×176	1/2		1 st of 0.05 rad	Beam Top Flange CJP Weld
C6-G	W30×116	W24×176	1/2		1 st of 0.06 rad	RBS Fracture
C7	W30×116	W24×192	-	1 × 5/8"	2 nd of 0.05 rad	RBS Fracture
W1	W36×150	W27×258	1/2	2 × 5/8"	2 nd of 0.04 rad	Beam Top Flange CJP Weld
W2	W33×141	W27×217	3/4	2 × 3/4"	2 nd of 0.06 rad	Beam Top Flange CJP Weld
W3	W30×116	W24×207	1/2	2 × 1/2"	2 nd of 0.06 rad	Beam Top Flange CJP Weld
W4	W24×94	W24×182	3/4	2 × 5/8"	1 st of 0.05 rad	Beam Top Flange CJP Weld

a) Specimens tested and reported in Mashayekh and Uang (2018).

Table 5.2 Continuity Plate Design and Experimentally Determined Forces

Spec. No.	Expected per Design ^a					Experimental Results		
	Expected P_f (kips)	Cont. Plate b/t	w^b/t_{cp}	FLB (kips)	WLY (kips)	Measured P_f^c (kips)	$\frac{\text{Measured } P_f}{\text{Expected } P_f}$	Local Buckling
C1	597	8.0	0.75	642	431	629	1.05	No
C2	745	9.6	0.80	1168	826	790	1.06	No
C3	738	-	-	1317	932	725	0.98	-
C4	611	-	-	859	620	667	1.09	-
C5	765	16.0	0.83	897	679	693	0.91	Yes
C6	582	12.0	1.00	640	430	627	1.08	No
C6-G	582	12.0	1.00	640	430	618	1.06	No
C7	558	-	-	799	917	594	1.07	-
W1	1127	12.0	0.75	1097	1716	997	0.88	No
W2	1002	7.8	0.75	816	1677	913	0.91	No
W3	826	11.0	0.75	894	1215	734	0.89	No
W4	745	7.3	0.75	527	1048	662	0.89	No

a) Values tabulated for F_{ya} and $\phi = 1$, FLB and WLY calculated as per AISC 360 §J10.1 and §J10.2.

b) Weld size, w , tabulated for continuity plate-to-column flange fillet weld.

c) Measured P_f derived by assuming 85% of the beam moment at the column face is resolved in the flanges.

Table 5.3 Doubler Plate Design and Experimentally Determined Forces

Spec.	Expected per Design							Experimental Results		
	t_{dp} (in.)	Expected V_{pz} (kips)	Panel Zone ϕR_n^a (kips)	$0.6F_y d_c t_{pz}$ (kips)	$\frac{d_z + w_z}{t_{cw}}$	$\frac{d_z + w_z}{t_{dp}}$	Doubler Plate Vertical Weld	Measured V_{pz}^b (kips)	$\frac{\text{Measured } V_{pz}}{\text{Expected } V_{pz}}$	Instability?
C1	-	596	745	664	68	-	-	620	1.04	No
C2	-	717	825	662	40	-	-	752	1.05	No
C3	-	710	761	611	40	-	-	691	0.97	No
C4	-	610	948	831	59	-	-	656	1.08	No
C5	-	678	626	518	48	-	-	661	0.97	No
C6	-	581	777	692	68	-	-	618	1.06	No
C6-G	-	581	777	692	68	-	-	609	1.05	No
C7	0.63	557	1494	1317	63	81	7/16 in. Fillet	585	1.05	No
W1	0.63	2040	2299	2173	61	95	PJP	1951	0.96	No
W2	0.75	2063	2402	2303	68	76	PJP	1747	0.85	No
W3	0.50	1729	1784	1672	58	102	11/16 in.	1439	0.83	No
W4	0.63	1472	1741	1661	64	72	7/8 in.	1367	0.93	No

a) Values tabulated for F_{ya} and $\phi = 1$; panel zone strength determined as per AISC 360 Eq. J10-11.

b) Panel zone shear, V_{pz} , determined from equilibrium.

Table 5.4 Specimen Lateral Bracing Force Comparison

Spec. No.	Beam	Column	Connection	Failure of Specimen	Maximum Normalized Lateral Bracing Force (%)
C3	W36×150	W14×257	RBS	1 st of 0.05 rad	2.2
C4	W30×116	W27×235	RBS	1 st of 0.06 rad	5.5
C5	W36×150	W14×211	RBS	2 nd of 0.05 rad	1.4
C6	W30×116	W24×176	RBS	1 st of 0.05 rad	2.0
C6-G	W30×116	W24×176	RBS	1 st of 0.06 rad	7.6

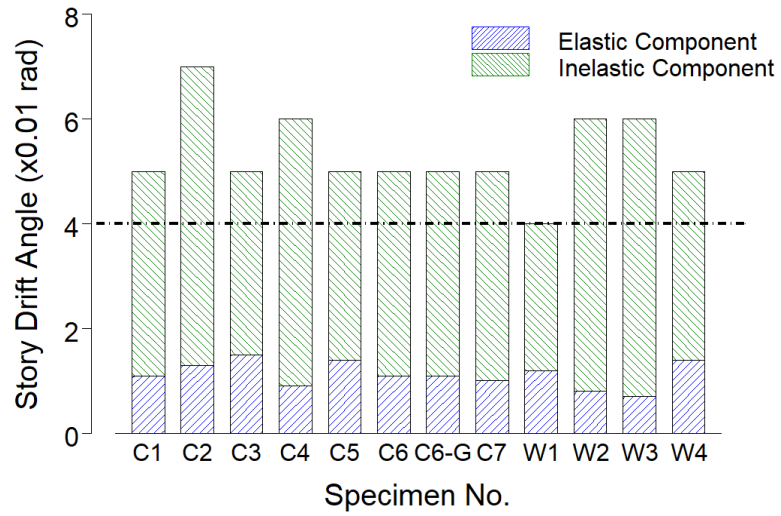


Figure 5.1 Summary of Specimen Story Drift Capacity

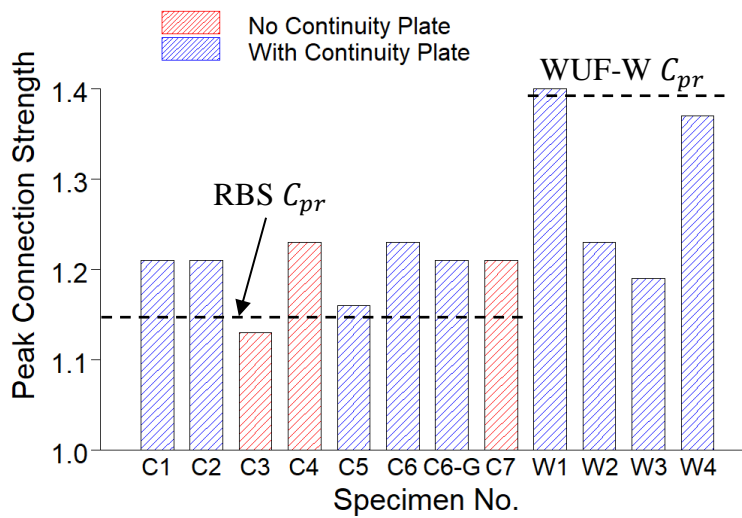


Figure 5.2 Summary of Measured Peak Connection Strength Factor, C_{pr}

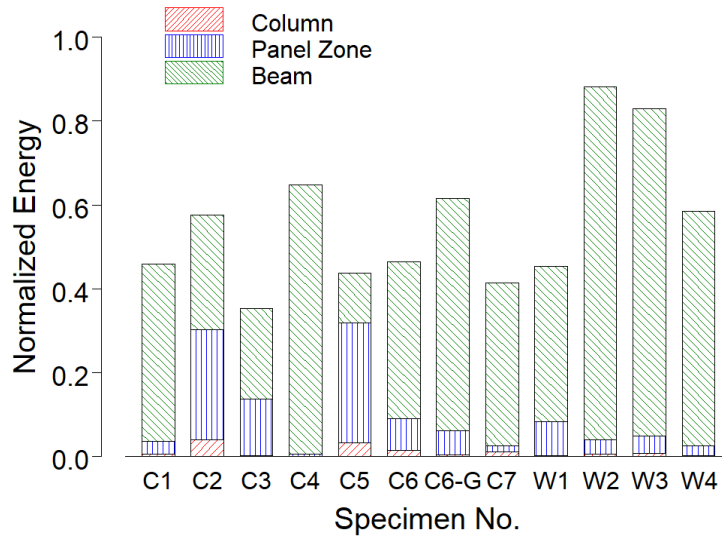


Figure 5.3 Summary of Normalized Energy Dissipation Capacity

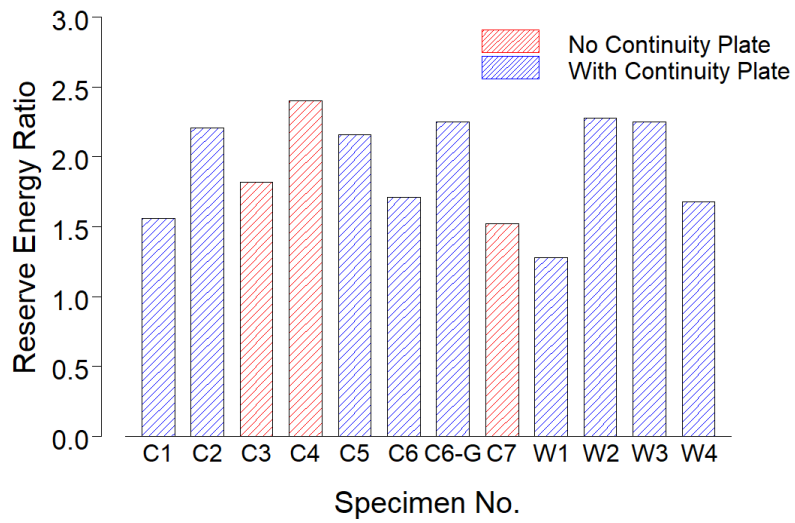


Figure 5.4 Summary of Reserve Energy Ratio

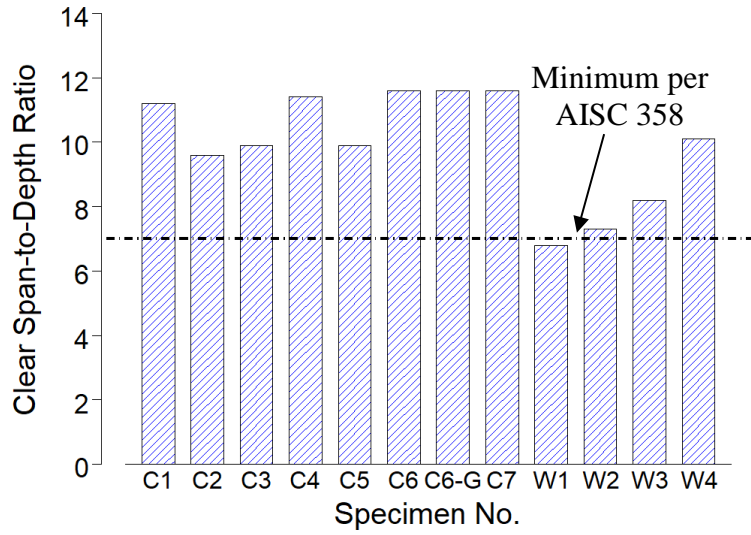


Figure 5.5 Summary of Beam Clear Span-to-Depth Ratio

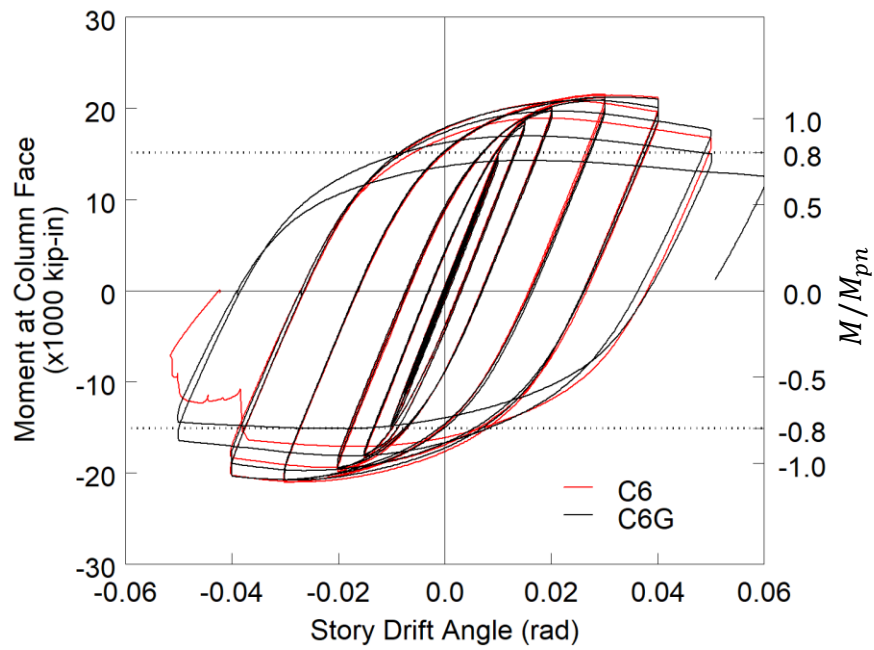
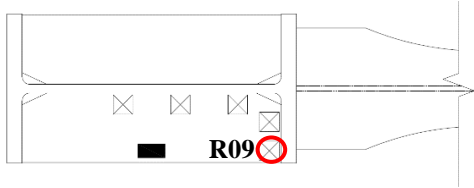
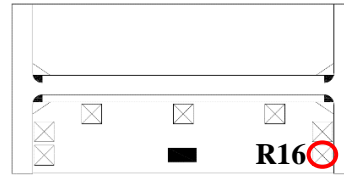


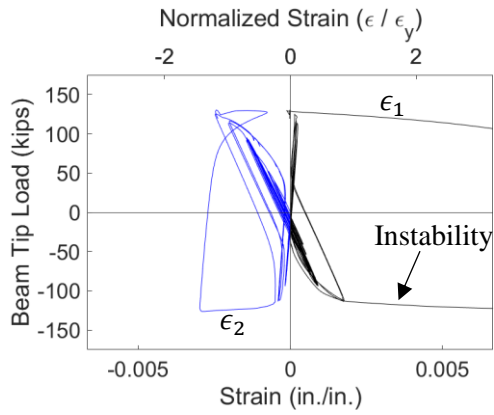
Figure 5.6 Comparison of Specimens C6 and C6-G Responses



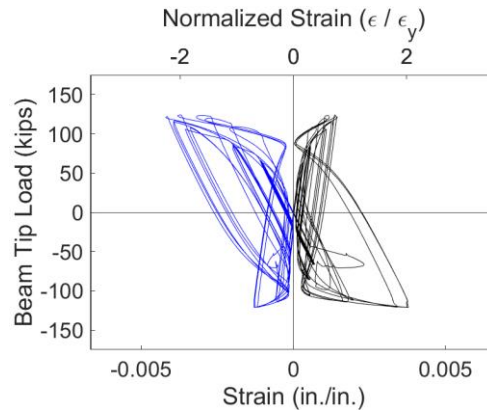
(a) One-Sided Gauge Position



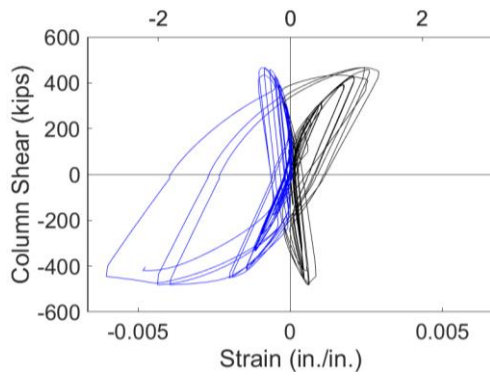
(b) Two-Sided Gauge Position



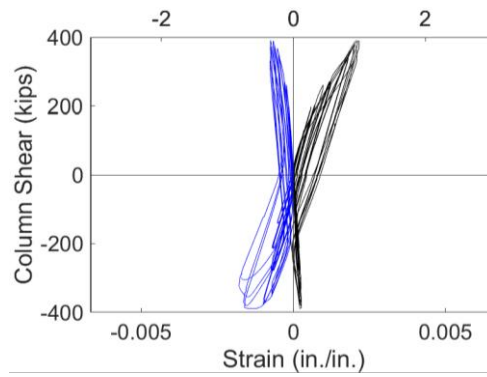
(c) Spec. C5 to (up to +0.04 rad, 1st Cycle)



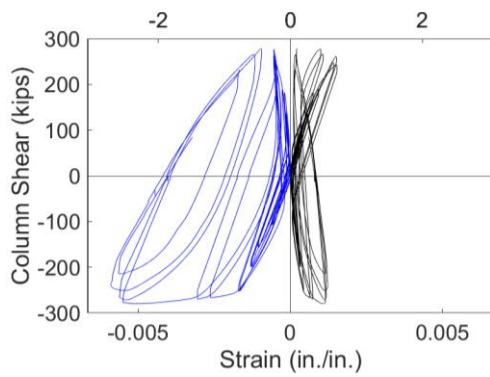
(d) Specimen C6



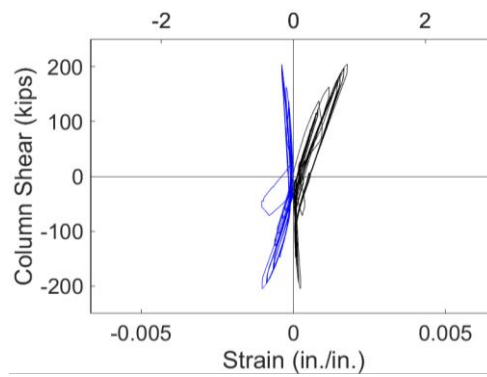
(e) Specimen W1



(f) Specimen W2

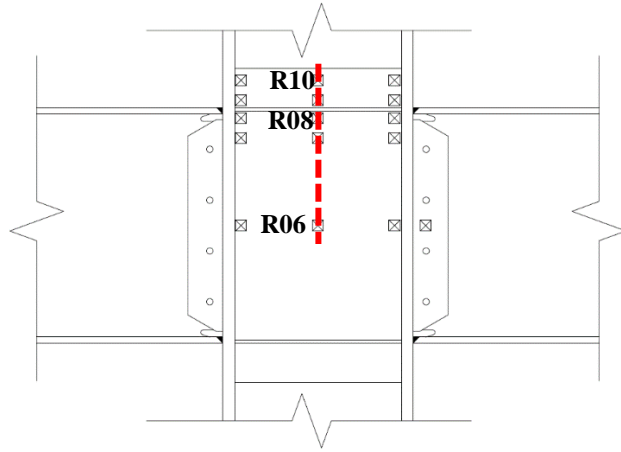


(g) Specimen W3

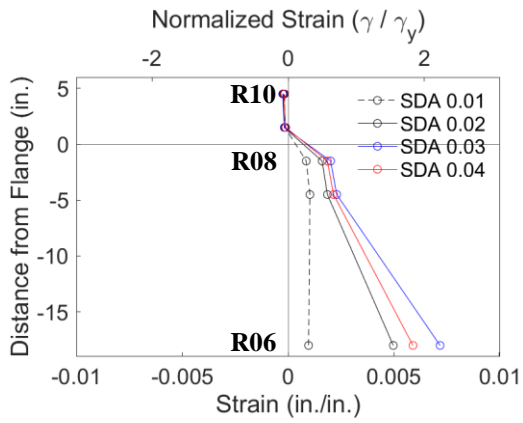


(h) Specimen W4

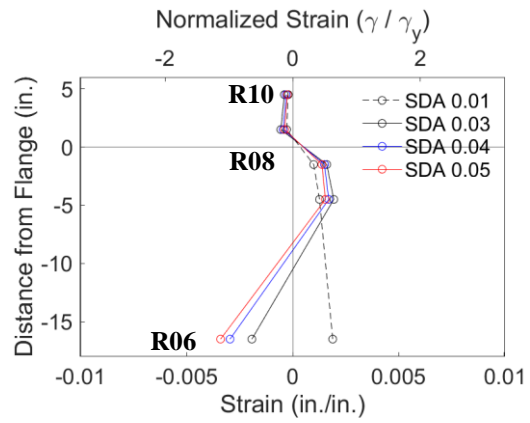
Figure 5.7 Continuity Plate Principal Strains



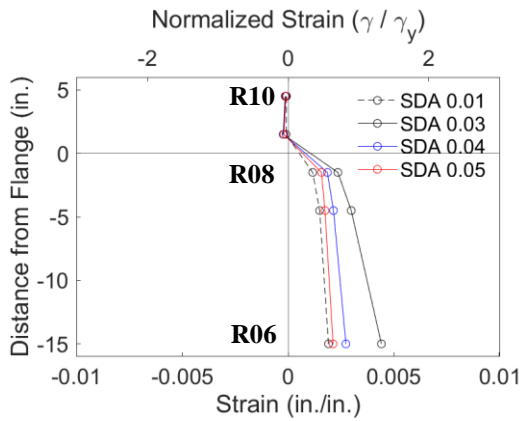
(a) Section Layout



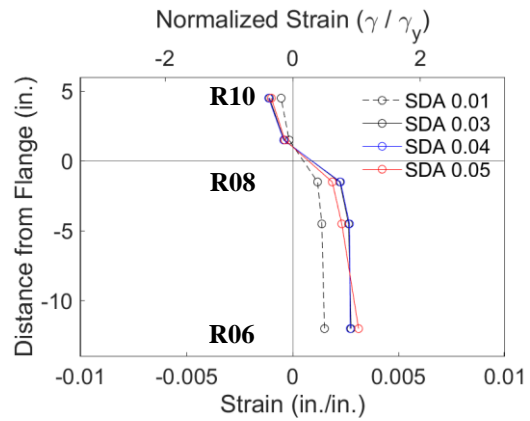
(b) Specimen W1



(c) Specimen W2

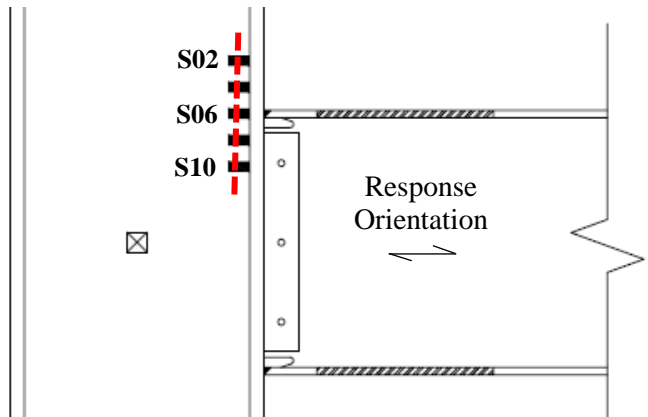


(d) Specimen W3

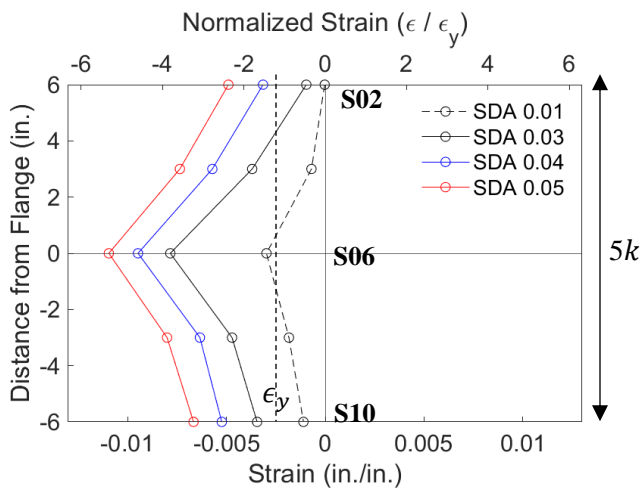


(e) Specimen W4

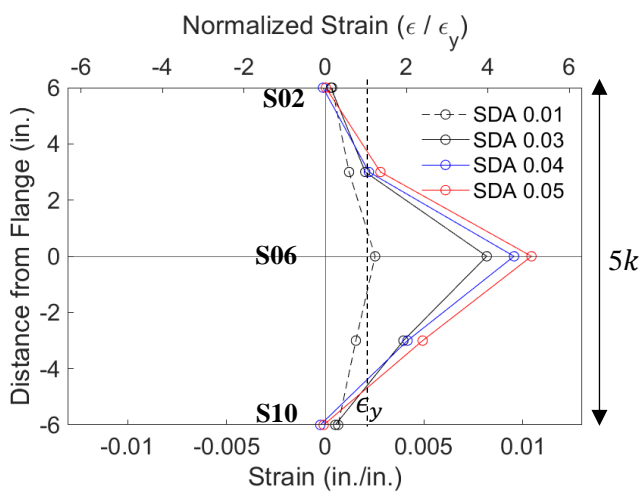
Figure 5.8 Doubler Plate Shear Strain Profiles (Positive Drift)



(a) Gauge Layout

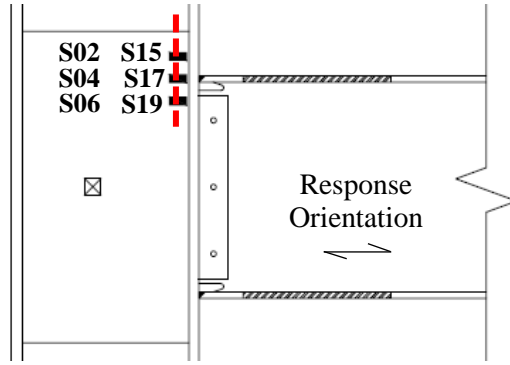


(b) Positive Drift

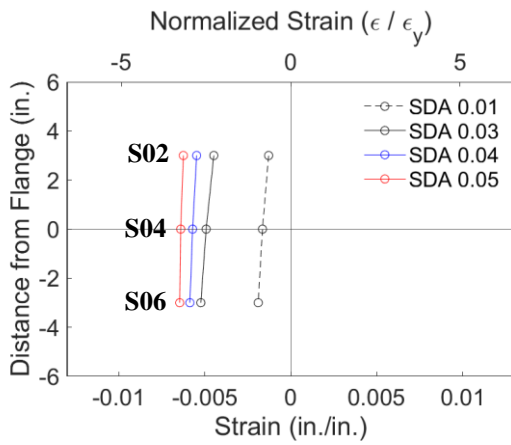


(c) Negative Drift

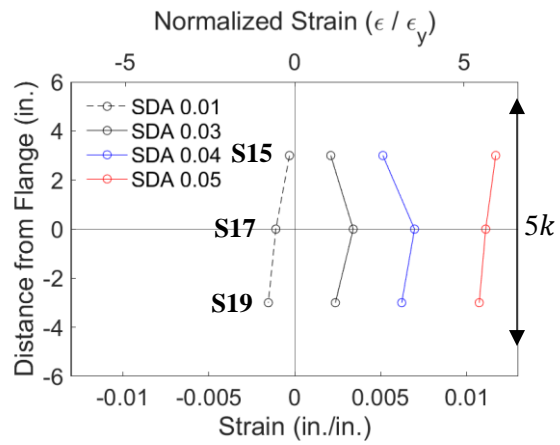
Figure 5.9 Specimen C4: Column Web Strain Profiles



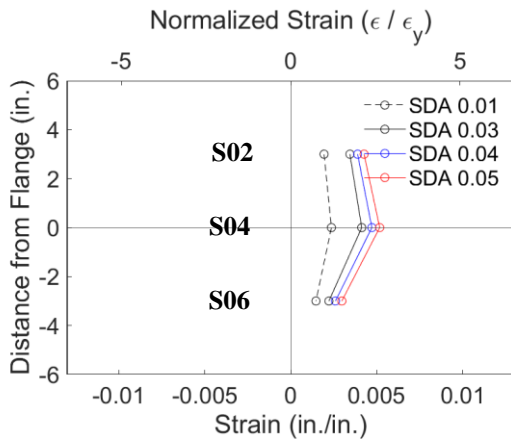
(a) Gauge Layout



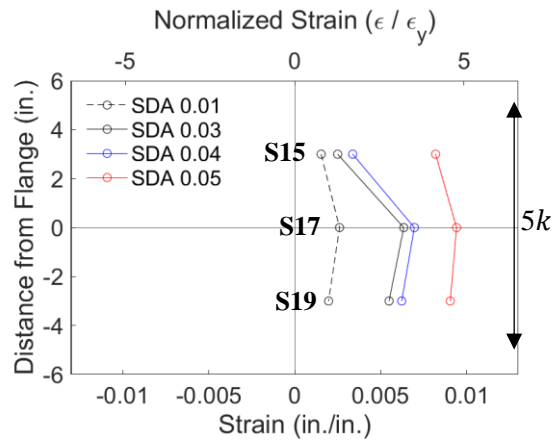
(b) Column Web (Positive Drift)



(c) Doubler Plate (Positive Drift)

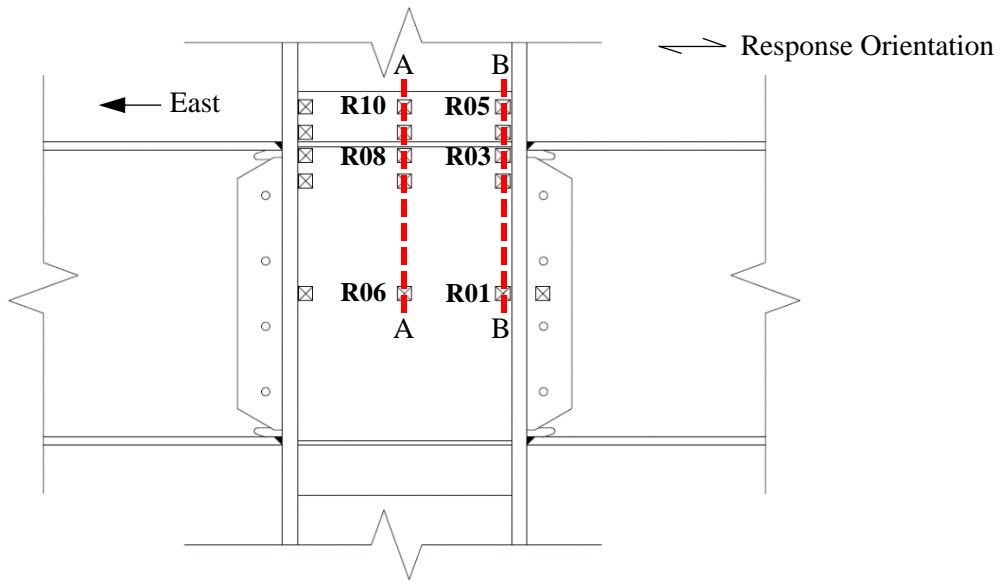


(d) Column Web (Negative Drift)

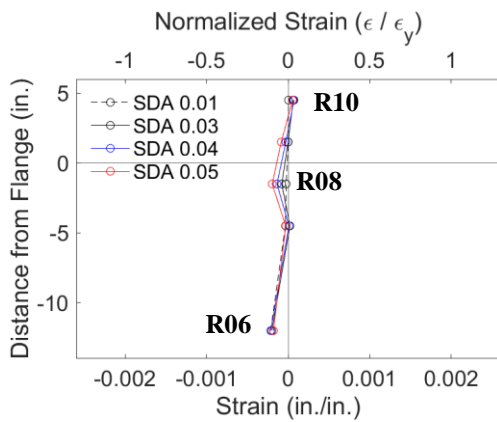


(e) Doubler Plate (Negative Drift)

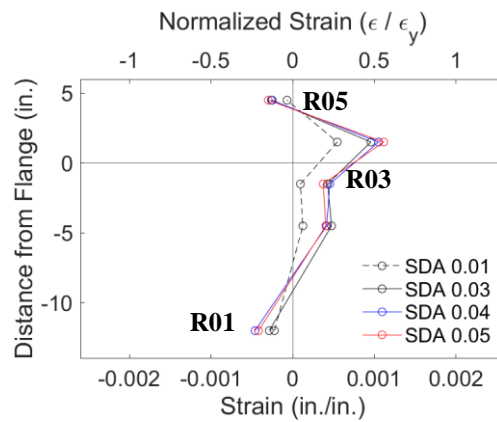
Figure 5.10 Specimen C7: Comparison of Column Web and Doubler Plate Strains



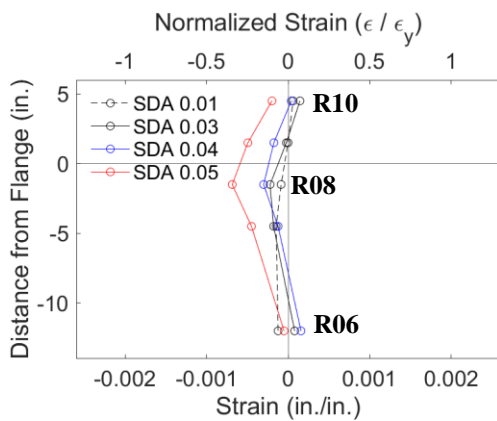
(a) Section Layout



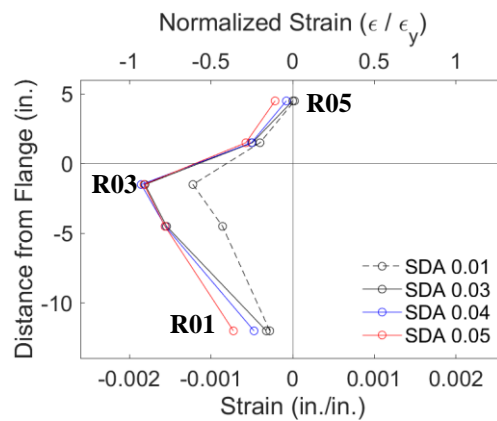
(b) Section A-A: Positive Drift



(c) Section B-B: Positive Drift



(d) Section A-A: Negative Drift



(e) Section B-B: Negative Drift

Figure 5.11 Specimen W4: Panel Zone Strain Profile

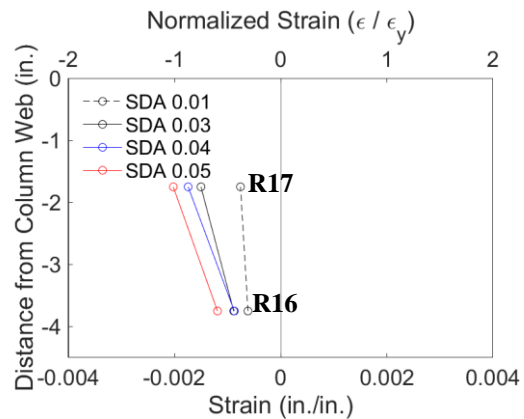
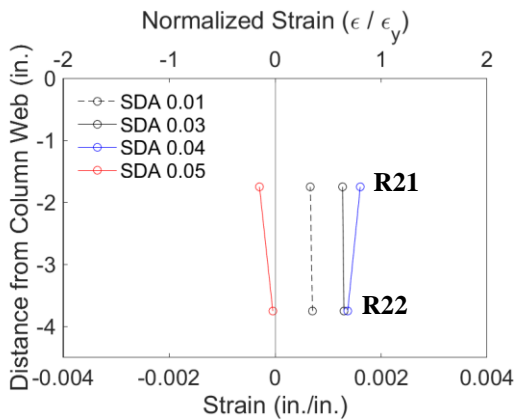
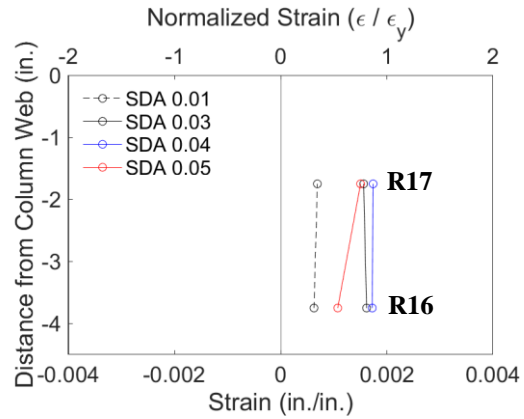
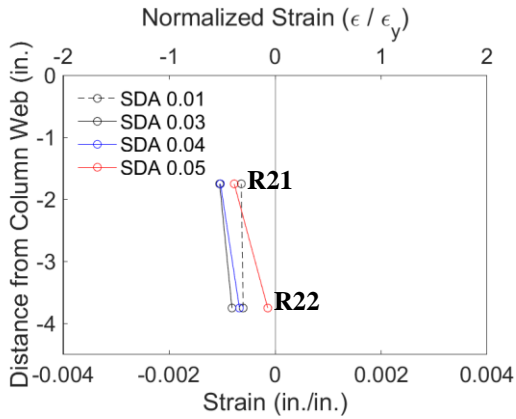
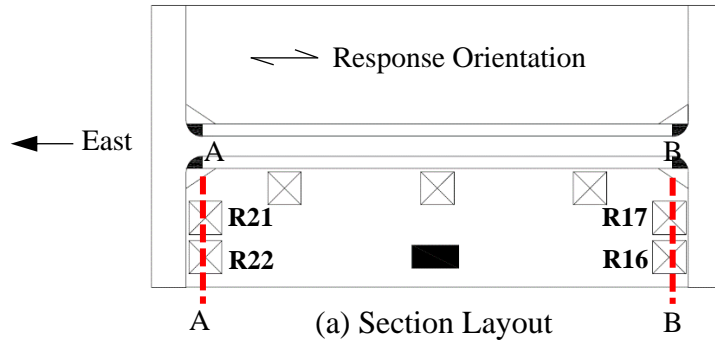


Figure 5.12 Specimen W4: Continuity Plate at Column Flange Edge Strain Profile

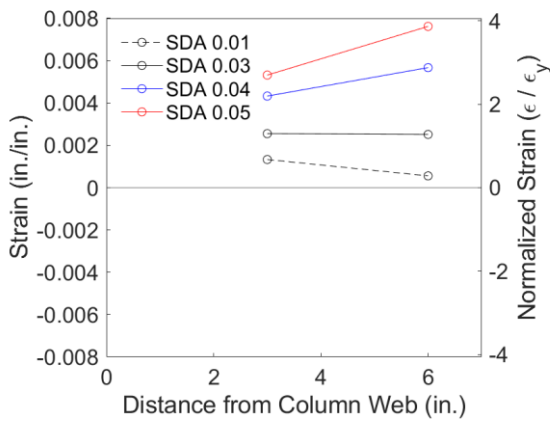


(a) Overview

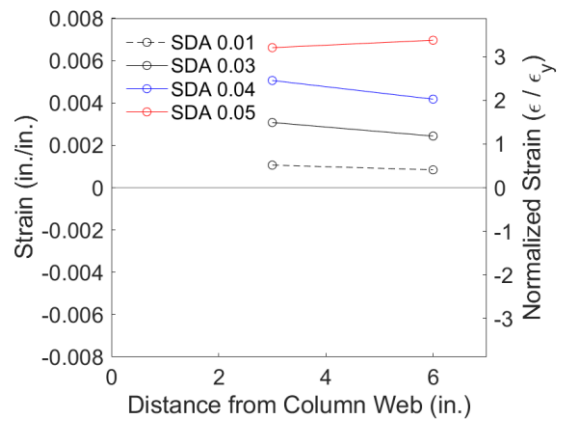


(b) Yielding

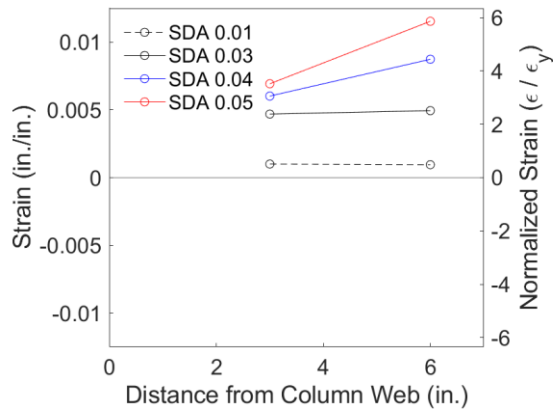
Figure 5.13 Specimen C4: Observed Column Flange Localized Yielding (End of Test)



(a) Specimen C3



(b) Specimen C4



(c) Specimen C7

Figure 5.14 Recorded Column Flange Response (Positive Drift)

6 SUMMARY AND CONCLUSIONS

6.1 Summary

Cyclic testing of ten full-scale steel moment frame connections was conducted to evaluate the efficacy of economized continuity plate and doubler plate weld details. Phase 1 of the testing included Specimens C3, C4, C5, C6, C6-G, and C7. The Phase 1 specimens were one-sided RBS connections tested in the upright position with a single 220-kip hydraulic actuator. Phase 2 of the testing included Specimens W1, W2, W3, and W4. The Phase 2 specimens were two-sided WUF-W connections tested in the horizontal position with two 500-kip hydraulic actuators. The testing was performed in displacement control to impose a prescribed drift according to the standard AISC cyclic loading sequence, as specified in the 2016 Seismic Provisions (AISC 341-16). In the case of the two-sided specimens, imposed drifts were applied equal and opposite on either side of the connection. These ten specimens are accompanied by Specimens C1 and C2, which were tested previously as part of a pilot project (Mashayekh and Uang 2018).

The Phase 1 specimens were carefully designed to investigate the applicable column limit states of Flange Local Bending (FLB) and Web Local Yielding (WLY). The omission of Web Local Crippling (WLC) from the investigation was because it is found to seldom govern the design of column stiffening of Special Moment Frames (SMFs). Three of these specimens were designed to directly challenge a criterion in AISC 341-16, which imposes a minimum thickness of an unstiffened column flange to be equal to the adjacent beam flange width divided by 6. This criterion is named as the Lehigh Criterion in this study after the institution of the founding study (Ricles et al. 2000). Specimen C7 challenged this criterion by reinforcing the governing column limit state, WLY, by the addition of a column web doubler plate. Since this doubler plate was not required based on the shear strength requirement of the panel zone, a new design methodology to design the vertical welds was applied in lieu of the stringent requirements imposed by the provisions in AISC 341-16.

The Phase 2 specimens were designed to subject the continuity plates to a higher level of force that is realized by the WUF-W connection and investigate the effect of a continuity plate stiffening of two-sided connections. Since a relatively high panel zone shear force was anticipated in the Phase 2 specimens, the doubler plate weldments were designed as

per AISC 341-16 to develop the shear strength of the plate. Specimen W4 used a doubler plate that was terminated inside the continuity plates, while the other three specimens used an extended doubler plate detail.

All of the specimens that had continuity plates used two-sided fillet welds to attach the continuity plate to the column flange and column web. Except for Specimens C6 and C6-G, the size of these fillet welds satisfy the proposed design rule of $w = (3/4)t_{cp}$, where w is the specified weld size, and t_{cp} is the thickness of the continuity plate. All of the W-shaped beams and columns were fabricated from ASTM A992 steel, while the continuity and doubler plates were fabricated from ASTM A572 Gr. 50 steel. Simulated field welding of the beam top and bottom flange CJP welds were performed in the shop with the frame standing in the upright position. Beam flange CJP welds used an E70T-6 (Lincoln Electric NR-305) electrode in the flat position. The beam web, the reinforcing fillet on the beam top flange backing, and the reinforcing fillet on the beam bottom flange were welded with an E71T-8 (Lincoln Electric NR-232) electrode in the vertical and overhead positions. The continuity plate and doubler plate welds were shop welded with an E70T-9C (Lincoln Electric OSXLH-70) electrode. The electrodes used for the continuity plate and doubler plate welding satisfy the notch-toughness requirements of AWS D1.8 (2016) for Demand Critical welds. Specifically, they have a minimum notch-toughness of 20 ft-lb at 0°F and 40 ft-lb at 70°F.

All of the specimens passed the AISC Acceptance Criteria for SMF applications, i.e., all specimens achieved at least one cycle of 0.04 rad story drift angle while not experiencing a strength degradation resulting in a moment capacity less than 80% of the beam nominal plastic moment at the column face. After passing the Acceptance Criteria, the Phase 1 specimens eventually failed either through low-cycle fatigue of the beam in the reduced beam section (Specimens C4, C6-G, and C7) or through fracture of the beam top flange CJP weld (Specimens C3, C5, and C6). Specimens that failed through fracture of the beam top flange demonstrated initial tearing of the beam top flange CJP weld during the 0.03 rad drift cycles. The tearing initiated at the toe of a prominent weld pass on the top surface of the CJP weld slightly outward of the re-entrant corner formed by the beam top flange and column flange. Continued ductile tearing of the weld occurred during each negative excursion when the beam top flange was loaded in tension. The fracture

propagated through the weld metal at an angle of about 35°. Eventual fracture of the beam top flange CJP weld occurred primarily through cleavage and ductile fracture once the remaining material was overloaded.

The Phase 2 specimens all failed eventually through fracture of the beam top flange CJP weld. This fracture primarily initiated at the beam flange CJP weld root, where the root of the weld met the backing bar. Secondary initiation sites developed in the CJP weld from extreme local curvatures that developed due to the flange local buckling at the plastic hinge near the face of the column. Ductile tearing of the weld was observed during excursions which put the affected flange in tension. Tearing of the weld tended to propagate outward along the CJP weld bevel until a cleavage fracture occurred. No damage was observed to any of the continuity plates or doubler plate welds. Except for the continuity plate of Specimen C5, yielding of the continuity plate was limited to $2.5\epsilon_y$ according to measurements of principal strains near the column flange edge. Specimen C5 was the only specimen that showed buckling of the continuity plate. The high strains observed in the continuity plate of Specimen C5 were due to local buckling of the plate.

Except for Specimens C2 and C5, the primary mechanism for energy dissipation was the plastic hinging of the beam. Instead, these two specimens developed significant energy dissipation in the panel zones. All of the specimens presented reserve energy ratios above 1.3, demonstrating that significant reserve energy dissipation potential exists beyond the AISC minimum criteria (including one cycle of 0.04 rad drift) for connection prequalification. The specimen which realized the least reserve energy capacity had a clear span-to-depth ratio of 6.8, slightly violating the limit imposed by the AISC 358-16 requirement of 7.0. The relatively poor performance of this specimen might be partially attributed to the relatively high beam moment gradient (i.e., high shear) of this specimen.

6.2 Conclusions

The following conclusions can be made:

- (1) All of the specimens tested in this program passed the AISC Acceptance Criteria for Special Moment Frames.
- (2) Three of eight RBS connections failed through ductile tearing of the beam top flange CJP weld. The tear propagated for several tension excursions in a ductile manner through the weld metal until a brittle overload of the remaining flange material

occurred. The propensity to fracture is attributed to variability in weld surface topology (i.e., how sharp the re-entrant corner is formed between the beam flange and column flange) and variability in weld notch toughness. This assertion is confirmed by the observation that the two nominally identical specimens (Specimens C6 and C6-G) failed through different mechanisms.

- (3) Including the pilot program (Specimens C1 and C2), a total of nine specimens were tested with fillet welds fastening the continuity plate to the column flange. Most of these specimens (seven) used a proposed fillet weld size, w , of $(3/4)t_{cp}$. The remaining two specimens were conservatively designed with $w = t_{cp}$. No damage was observed in any fillet welds. Therefore, the AISC 341-16 requirement to connect the continuity plate to the column flange with CJP groove welds may be unnecessary.
- (4) The continuity plate of Specimen C5 developed local buckling during the 0.04 rad drift cycles. The width-to-thickness ratio of this plate was 16. Three specimens (Specimens C6, C6-G, and W1) used a width-to-thickness ratio of 12 and did not develop any instability. A width-to-thickness ratio equal to $0.56\sqrt{E/F_y}$, which limits the width-to-thickness of continuity plates fabricated with Grade 50 material to 13.5, is recommended.
- (5) Except for the continuity plate of Specimen C5, recorded principal strains were limited to $2.5\epsilon_y$. The recorded strains of Specimen C5 were limited to ϵ_y prior to flexural buckling of the continuity plate during the first 0.04 rad drift cycle. The limited amount of cyclic strain precludes significant hysteresis and strain hardening of the continuity plate. Except for the continuity plate of Specimen W2, all of the continuity plates satisfied the column strength limit states of §J10 in AISC 360-16. Specimen W2 used an undersized continuity plate that instead satisfied the thickness requirement of 75% of the adjacent beam flange for a two-sided connection. Therefore, sizing a continuity plate for the column strength limit states of §J10 in AISC 360-16 appears to limit inelastic strains preventing strain hardening from occurring.
- (6) A detailed review of the limiting column flange thickness of $b_{bf}/6$ given by §E3.6f.1(b) in AISC 341-16 provided in Chapter 1 of this report reveals consecutive simplification of the limit from a low-cycle fatigue analysis performed on WUF-W

connections. The violation of this criterion for three RBS specimens of Phase 1 (Specimens C3, C4, and C7) indicates that this criterion may be unnecessarily applied to RBS connections. As discussed in Chapter 1, this criterion triggers the mandatory use of continuity plates in a significant number of RBS connections, which may be relatively lightly loaded when compared to a typical WUF-W connection.

- (7) The Web Local Yielding (WLY) limit state in AISC 360-16 §J10.2 appears to correspond well with the prediction despite the application of cyclic loading. It is noted that column warping produces out-of-plane flexural strains in the column web, which are superimposed on the predicted web strains.
- (8) The Flange Local Bending (FLB) limit state AISC 360-16 §J10.1 was found to be developed in a conservative way by selectively limiting parameters to conservative values. The level of conservatism that was enjoyed by the original derivation (Graham et al. 1960) is expected to drop off as heavier sections are selected. Although localized column flange yielding was observed on the inside face of the column flange at the beam flange level, a complete yield line mechanism was not anticipated or observed.
- (9) Specimen C7 used a relatively lightly loaded doubler plate such that inelastic behavior of the plate was not anticipated. The vertical weldments attaching this plate to the inside faces of the column flanges were designed for the computed shear flow on the edge of the doubler plate based on the relative elastic stiffness. This fillet weld was undersized by a factor of 2, according to AISC 341-16, but did not demonstrate any damage during testing. The fillet weld throat was maintained through the doubler plate bevel by specifying that the bevel angle shall be 45°.
- (10) One specimen, Specimen W3, used a doubler plate with a $(w_z + d_z)/t_{dp}$ ratio of 102, which violated the AISC 341-16 width-to-thickness limit of 90. No instability of this doubler occurred during testing.
- (11) The lateral bracing force of a lateral brace placed approximately $d/2$ away from the end of the RBS was limited to 5% of the flange force during the 0.05 rad drift cycles. During the 0.06 rad drift cycles, one specimen, Specimen C6-G, saw a lateral bracing force equal to 7.6% of the flange force. This column was a W24×176 shape, representing a deeper column section. Another specimen, Specimen C4, developed

lateral bracing forces of 5.5% during the 0.06 rad drift cycles. In general, the deeper column sections require higher bracing forces, but the force requirements are bounded within the AISC 341-16 requirements during the cycles up to 0.05 rad drift.

- (12) The average peak connection strength factor for the eight one-sided RBS connections of Phase 1 was determined to be 1.19. This is slightly higher than the recommended value of 1.15 as per AISC 341-16.
- (13) The average peak connection strength factor for the four two-sided WUF-W connections of Phase 2 was determined to be 1.30. This results in a 10% reduction in estimated flange force when compared to the recommended value of 1.4 as per AISC 341-16.
- (14) A duplicate RBS specimen that used the same design details and metallurgical properties was hot-dip galvanized before simulated field welding. This specimen performed better, completing one additional cycle of 0.05 rad drift and one additional cycle of 0.06 rad drift. The better performance is not attributed to the effect of galvanization. Therefore, for the one specimen tested, it appears that the galvanization did not affect the strength or the ductility capacity of the connection.

REFERENCES

- Abbas, E.K., (2015). “A low Cycle Fatigue Testing Framework for Evaluating the Effect of Artifacts on the Seismic Behavior of Moment Frames.” *Ph.D Dissertation*, Virginia Polytechnic Institute, Blacksburg, VI.
- American Institute of Steel Construction (1992). “Seismic Provisions for Structural Steel Buildings.” *ANSI/AISC 341*, Chicago, IL.
- American Institute of Steel Construction (1997). “Seismic Provisions for Structural Steel Buildings.” *ANSI/AISC 341*, Chicago, IL.
- American Institute of Steel Construction (2005). “Seismic Provisions for Structural Steel Buildings.” *ANSI/AISC 341-05*, Chicago, IL.
- American Institute of Steel Construction (2010). “Seismic Provisions for Structural Steel Buildings.” *ANSI/AISC 341-10*, Chicago, IL.
- American Institute of Steel Construction (2016). “Specifications for Structural Steel Buildings.” *ANSI/AISC 360-16*, Chicago, IL.
- American Institute of Steel Construction (2016b). “Seismic Provisions for Structural Steel Buildings.” *ANSI/AISC 341-16*, Chicago, IL.
- American Institute of Steel Construction (2016c). “Prequalified Connections for Special and Intermediate Steel Moment Frames for Seismic Applications, including Supplement No. 2.” *ANSI/AISC 358*, Chicago, IL.
- American Institute of Steel Construction (1997). “AISC Advisory Statement on Mechanical Properties Near the Fillet of Wide Flange Shapes and Interim Recommendations January 10, 1997.” *Modern Steel Construction*, Vol. 37, No. 2, pp. 18.
- American Society of Civil Engineers 7 (2016). “Minimum Design Loads and Associated Criteria for Buildings and Other Structures.” *ASCE/SEI 7-16*, Reston, VA.
- American Welding Society (2016). “Structural Welding Code–Seismic Supplement.” *AWS D1.8*, Miami, FL.
- Anderson, T.L. (2017). “Fracture Mechanics: Fundamentals and Applications.” *CRC Press*, Boca Raton, FL.
- Bjorhovde, R., Golland, L J., Benac, D. J. (1999). “Tests of Full-Scale Beam-to-Column Connections.” *Internal Report*, Southwest Research Institute, San Antonio, Texas.
- Carter, C. J. (1999). “Stiffening of Wide-Flange Columns at Moment Connections: Wind and Seismic Applications.” *Design Guide 13*, AISC, Chicago, IL.

- Chi, W.-M., Deirerlein G.G., Ingraffea, A. (1997). "Finite Element Fracture Mechanics Investigation of Welded Beam-Column Connections." *Report No. SAC/BD -97/05*, SAC Joint Venture, Sacramento, CA.
- Chi, W.-M., Kanvinde, A.M., Deirelein, G.G. (2006). "Prediction of Ductile Fracture in Steel Connections using SMSC Criterion." *Journal of Structural Engineering*, ASCE Vol. 132, No. 2, pp. 171-181.
- Chi, B., and Uang, C-M. (2002). "Cyclic Response and Design Recommendations of Reduced Beam Section Moment Connections with Deep Columns." *Journal of Structural Engineering*, ASCE, Vol. 128, No. 4, pp. 464-473.
- Deierlein, G. G., Chi W. M. (1999). "Integrative Analytical Investigation on the Fracture Behavior of Welded Moment Resisting Connections." *Report No. SAC/BD -99/15*, SAC Joint Venture, Sacramento, CA.
- Dexter, R. J., Prochnow, S. D., Perez, M. I. (2001), "Constrained Through-Thickness Strength of Column Flanges of Various Grades and Chemistries." *Engineering Journal*, AISC, Vol. 38, No. 4, pp. 181-189.
- Doswell, B. (2015) "Plastic Strength of Connection Elements." *Engineering Journal*, AISC, Vol 52, No. 1, pp. 47-66.
- El-Tawil, S., Mikesell, T., Kunnath, S. K. (2000) "Effect of Local Details and Yield Ratio on Behavior of FR Steel Connections." *Journal of Structural Engineering*, ASCE, Vol. 126, No. 1, pp. 79-87.
- El-Tawil, S., Vidarsson, E., Mikesell, T., Kunnath, S. (1999), "Inelastic Behavior and Design of Steel Panel Zones." *Journal of Structural Engineering*, ASCE, Vol 125, No. 2, pp. 183-193.
- Engelhardt, M. D. (1999), "Design of Reduced Beam Section Moment Connections." *Proceedings, North American Steel Construction Conference*, Toronto, Ontario, May 19-21, 1999, AISC, Chicago, IL.
- Engelhardt, M. D., Husain, A. S., (1993). "Cyclic-Loading Performance of Welded Flange-Bolted Web Connections." *Journal of Structural Engineering*, ASCE, Vol. 19, No. 12, pp. 3537-2550.
- Engelhardt, M. D., Venti, M.J., Fry, G.T., Jones, S.L., Holliday, S.D. (2000), "Behavior and Design of Radius Cut Reduced Beam Section Connections." *Report No. SAC/BD-00/17*, SAC Joint Venture, Sacramento, CA.
- Engelhardt, M. D., Sabol, T.A. (1997). "Seismic-resistant steel moment connections: developments since the 1994 Northridge earthquake." *Earthquake Engineering and Structural Dynamics*, Vol. 1, No.1, pp. 68-76.

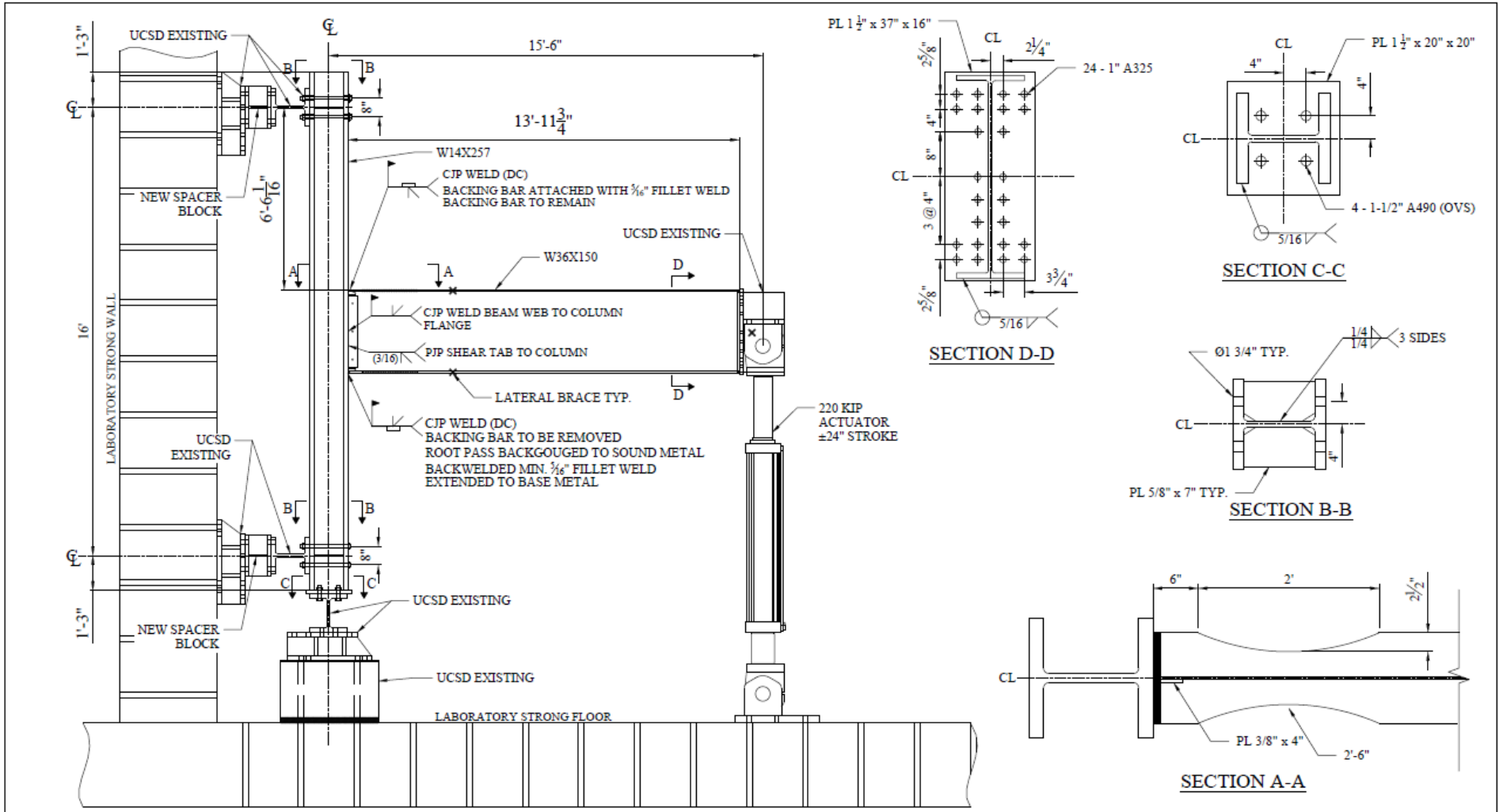
- Engelhardt, M. D., Winneberger, T., Zekany, A. J., Potyraj, T. J. (1998), "Experimental Investigation of Dogbone Moment Connections." *Engineering Journal*, AISC, Vol. 35, No. 4, pp. 128-139.
- Federal Emergency Management Agency (2000a). "Recommended Seismic Design Criteria for New Steel Moment Frame Buildings." *FEMA 350*, Washington, DC.
- Federal Emergency Management Agency (2000b). "Recommended Seismic Evaluation and Upgrade Criteria for Existing Welded Steel Moment Frame Buildings." *FEMA 351*, Washington, DC.
- Federal Emergency Management Agency (2000c). "Recommended Postearthquake Evaluation and Repair Criteria for Welded Steel Moment-Frame Buildings." *FEMA 352*, Washington, DC.
- Federal Emergency Management Agency (2000d). "Recommended Specifications and Quality Assurance for Steel Moment Frame Construction for Seismic Applications." *FEMA 353*, Washington, DC.
- Federal Emergency Management Agency (2000e). "A Policy Guide to Steel Moment Frame Construction." *FEMA 354*, Washington, DC.
- Federal Emergency Management Agency (2000f). "State of Art Reports on Steel Moment Frame Structures." *FEMA 355A through FEMA 355F*, Washington, DC.
- Goel, S. C., Stojadinvic, B., Lee, K-H. (1997), "Truss Analogy for Steel Moment Connections." *Engineering Journal*, AISC, Vol. 34, No. 2, pp. 43-53.
- Graham, J. D., Sherbourne, A.N., Khabaz, R. N., Jensen, C. D. (1960). "Welded Interior Beam-to-Column Connections." *Welding Research Council*, No. 63, pp. 1-28.
- Gupta, U. (2013), "Cyclic Loading Analysis of Doubler Plate Attachment Details for Steel Moment Resisting Frames." *Masters Thesis*, University of Texas at Austin.
- Hamburger, R. O. (2006). "Prequalified Connections for Special and Intermediate Steel Moment Frames for Seismic Applications." *Structures Congress*, ASCE.
- Hamburger, R. O., and Malley, J.O. (2016), "Seismic Design of Steel Special Moment Frames: A Guide for Practicing Engineers." *Seismic Design Technical Brief No. 2*, National Institute of Standard and Technology, Gaithersburg, MD.
- Hancock, J. W., Cowling, M. J. (1980). "Role of State of Stress in Crack-tip Failure Processes." *Metal Science*, Vol. 14, No. 8, pp. 234-304.
- Hancock, J. W., Mackenzie, A. C. (1976), "On the Mechanisms of Ductile Failure in High-Strength Steels Subjected to Multi-Axial Stress-States." *Journal of the Mechanics and Physics of Solids*, Vol. 24, pp. 147-169.

- Han, S. W., Moon, K.H., Jung, J. (2014), "Cyclic Performance of Welded Unreinforced Flange-Welded Web Moment Connections." *Earthquake Spectra*, Vol. 30, No. 4, pp. 1663-1681.
- Han, S. W., Jung, J., Ha S. J. (2016), "Seismic Performance of WUF-W Moment Connections According to Access Hole Geometries." *Earthquake Spectra*, Vol. 32, No. 2, pp. 909-926.
- Han, S. W., Kim, N., H, (2017), "Permissible Parameter Ranges of Access Hole Geometries for WUF-W Connections." *Earthquake Spectra*, Vol. 33, No. 2, pp. 687-707.
- Hajjar, J. F, Dexter, R.J., Ojard, S.D., Ye, Y., Cotton S.C. (2003). "Continuity Plate Detailing for Steel Moment-Resisting Connections." *Engineering Journal*, AISC, Vol. 40, No. 4, pp. 189-211.
- Hajjar, J. F., Leon, R. T., Gustafson, M. A., Shield, C. K. (1998). "Seismic Response of Composite Moment-Resisting Connections. II: Behavior." *Journal of Structural Engineering*, ASCE, Vol. 124, No. 8, pp. 877-885.
- Johnson, M. Q., Mohr, B., Barsom, J. (2000). "Evaluation of Mechanical Properties in Full-Scale Connections and Recommended Minimum Weld Toughness for Moment Resisting Frames." *Report No. SAC/BD 00/14*, SAC Joint Venture, Sacramento, CA.
- Kanvinde, A. M., Deierlein, G.G. (2004). "Micromechanical Simulation of Earthquake Induced Fracture in Steel Structures." *Report No. TR. 145*, Blume Earthquake Engineering Center, Stanford University, Stanford, CA.
- Kanvinde, A. M. (2017). "Predicting Fractures in Civil Engineering Steel Structures: State of the Art." *Journal of Structural Engineering*, ASCE, Vol. 143, No. 3.
- Kaufman, E. J, Xue, M., Lu, K-W., Fisher, J.W. (1996a). "Achieving Ductile Behavior of Moment Connections." *Modern Steel Construction*, AISC, Vol. 36, No. 1, pp. 30-39.
- Lee, C-H., Jeon, S-W., Kim, J-H., Uang, C-U. (2005), "Effects of Panel Zone Strength and Beam Web Connection Method on Seismic Performance of Reduced Beam Section Steel Moment Connections." *Journal of Structural Engineering*, ASCE, Vol. 131, No. 2, pp. 1854-1865.
- Lee, C-H., Cotton. S. C, Hajjar, J. F., Dexter, R. J. (2005a), "Cyclic Behavior of Steel Moment-Resisting Connections Reinforced by Alternative Column Stiffener Details I. Connection Performance and Continuity Plate Detailing." *Engineering Journal*, AISC, Vol. 42, No. 4, pp. 189-214.
- Lee, C-H., Cotton. S. C, Hajjar, J. F., Dexter, R. J. (2005b), "Cyclic Behavior of Steel Moment-Resisting Connections Reinforced by Alternative Column Stiffener Details II. Panel Zone Behavior and Doubler Plate Detailing." *Engineering Journal*, ASCE, Vol. 42, No. 4, pp. 189-214.

- Malley, J. O., Frank, K. (2000), "Materials and Fracture Investigations in the FEMA/SAC Phase 2 Steel Project." *Proceedings, 12th World Conference on Earthquake Engineering*, Auckland, New Zealand.
- Mashayekh, A. (2017). "Sloped Connections and Connections with Fillet Welded Continuity Plates for Seismic Design of Special Moment Frames." *Ph.D Dissertation*, Department of Structural Engineering, University of California, San Diego, CA.
- Mashayekh, A., Uang, C-M. (2018). "Experimental Evaluation of a Procedure for SMF Continuity Plate and Weld Design." *Engineering Journal*, AISC, Vol 55, No. 2, pp. 109-122.
- Matos C. G., Dodds, R.H. (2000). "Modelling the Effects of Residual Stresses on Defects in Welds of Steel Frame Connections." *Engineering Structures*, Vol. 22, No. 9, pp. 1103-1120.
- Mao, C., Ricles, J., Lu, L-W., Fisher, J. (2000). "Effect of Local Details on Ductility of Welded Moment Connections." *Journal of Structural Engineering*, ASCE, Vol. 127, No. 9, pp. 1036-1044.
- Paret, T. F, (2000), "The W1 Issue. I: Extent of Weld Fracturing During Northridge Earthquake." *Journal of Structural Engineering*, ASCE, Vol .126, No. 1, pp. 10-18.
- Popov, E. P., Amin, N.R., Louie, J.C., Stephen, R.M. (1986). "Cyclic Behavior of Large Beam-Column Assemblies." *Engineering Journal*, AISC, Vol. 23, No. 1, pp. 9-23.
- Popov, E. P., Pinkney, B., (1971). "Cyclic Yield Reversals in Steel Building Connections." *Engineering Journal*, AISC, Vol. 8, No. 3, pp. 66-79.
- Popov, E. P., Blondet, M., Stepanov, L., Stojadinovic, B. (1996). "Full-Scale Beam-Column Connection Tests." *Experimental Investigations of Beam-Column Subassemblages, Report No. SAC 96-01, Part 2*, Applied Technology Council, Redwood City, CA.
- Prochnow, S. D., Dexter, R. J., Hajjar, J. F., Ye, Y., Cotton, S. C. (2000). "Local Flange Bending and Local Web Yielding Limit States in Steel Moment Resisting Connections." *Structural Engineering Report No. ST-00-4*, University of Minnesota, Minneapolis, MN.
- Rice, J. R., Tracey, D. M. (1969), "On the Ductile Enlargement of Voids in Triaxial Stress Fields." *Journal of the Mechanics and Physics of Solids*, Vol. 17, pp. 201-217.
- Ricles, J. M, Mao, C., Lu, L-W., Fisher, J.W. (2000). "Development and Evaluation of Improved Details for Ductile Welded Unreinforced Flange Connections." *Report No. SAC/BD-00/24*, SAC Joint Venture, Sacramento, CA.
- Ricles, J. M., Mao, C., Lu, L-W., Fisher, J. M. (2002), "Inelastic Cyclic Testing of Welded Unreinforced Moment Connections." *Journal of Structural Engineering*, ASCE, Vol. 128, No. 4, pp. 429-440.

- Ricles, J. M., Mao, C., Lu, L-W., Fisher, J. M. (2003), "Ductile Details for Welded Unreinforced Moment Connections Subjected to Inelastic Cyclic Loading." *Engineering Structures*, Vol. 25, No. 5, pp. 667-680.
- Sherbourne, A. N., Jensen C. D. (1957). "Direct Welded Beam Column Connections." *Report No. 233.12*, Fritz Laboratory, Lehigh University, Bethlehem, PA.
- Shirsat, P. S., Engelhardt, M. D. (2012), "Preliminary Analysis of Doubler Plate Attachment Details for Steel Moment Frames." *Proceedings, 15th World Conference on Earthquake Engineering*, Lisbon, Portugal.
- Smith, C. M., Deierlein, G. G., Kanvinde, A. M. (2014). "A Stress-Weighted Damage Model for Ductile Fracture Initiation in Structural Steel Under cyclic Loading and Generalized Stress States." *Report No. TR. 187*. Blume Earthquake Engineering Center, Stanford University, Stanford, CA.
- Tide, R. H. R. (2000). "Evaluation of Steel Properties and Cracking in the "k"-Area of W Shapes." *Engineering Structures*, Vol. 22, No. 2, pp. 128-134.
- Tran, T. T., Hasset, P.M., Uang, C-M. (2013). "A Flexibility-Based Formulation for the Design of Continuity Plates in Steel Special Moment Frames." *Engineering Journal*, AISC, Vol. 50, No. 3, pp. 181-200.
- Tremblay, R., Timler, P., Bruneau, M., Filiatrault, A. (1998). "Performance of Steel Structures during the 1994 Northridge Earthquake." *Canadian Journal of Civil Engineering*, Vol. 22, No. 2, pp. 338-360.
- Uniform Building Code (1988). *International Conference of Building Officials*, Whittier, CA.
- Uang, C.-M., Yu, Q.-S., Noel, S., Gross, J. (2000). "Cyclic Testing of Steel Moment Connections Rehabilitated with RBS of Welded Haunch." *Journal of Structural Engineering*, Vol. 126, No. 1, pp. 57-68.
- Uang, C.-M., Bondad, D. (1996). "Static cyclic Testing of pre-Northridge and Haunch Repaired Steel Moment Connections." *Rep. No. SSRP-96/02*, SAC, Sacramento, CA.
- Yee, R. K., Paterson, S. R., Egan, G. R. (1998), "Engineering Evaluations of Column Continuity Plate Detail Design and Welding Issues in Welded Steel Moment Frame Connections." *Welding for Seismic Zones in New Zealand*, Aptech Engineering Services, Inc., Sunnyvale, CA.

APPENDIX A: DESIGN DRAWINGS



ELEVATION

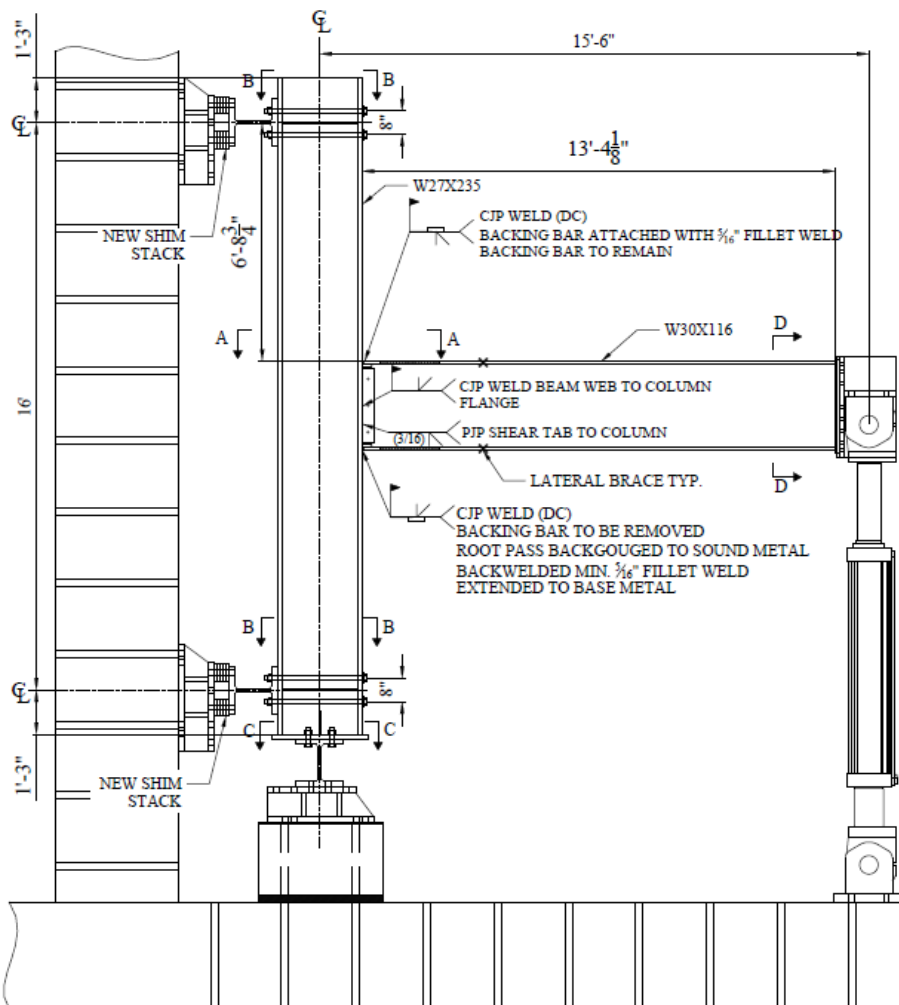
NOTES:

ALL ROLLED SHAPES SHALL BE A992
 ALL PLATES SHALL BE A572 U.N.O
 ELECTRODES SHALL COMPLY WITH AWS D1.8 FOR DEMAND CRITICAL (DC) WELDS AS INDICATED
 ALL HOLES ARE 1-3/4" U.N.O BY BOLT DESIGNATION

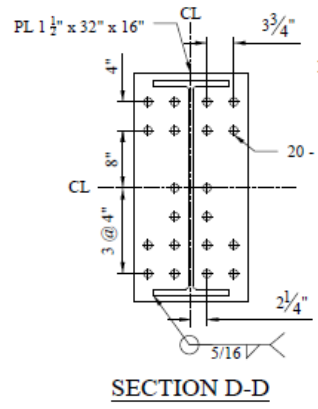
**AISC SMF RESEARCH PROJECT
 SPECIMEN C3**

UCSD DEPARTMENT OF STRUCTURAL ENGINEERING

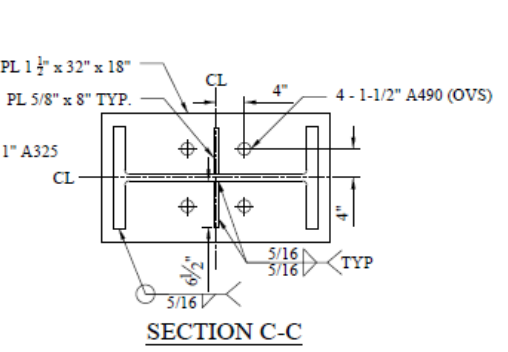
DESIGNER:	DATE:	DRAWING NO.:	REV NO.:
MARS	2018.08.23	C3-A	1



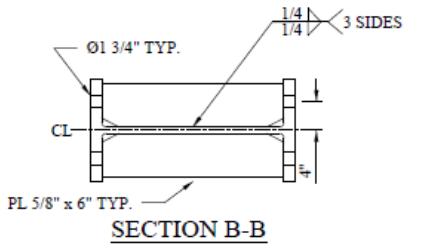
ELEVATION



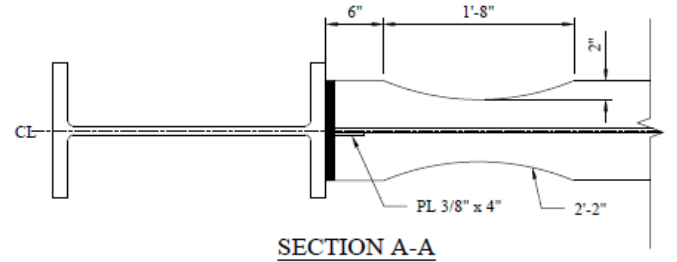
SECTION D-D



SECTION C-C



SECTION B-B



SECTION A-A

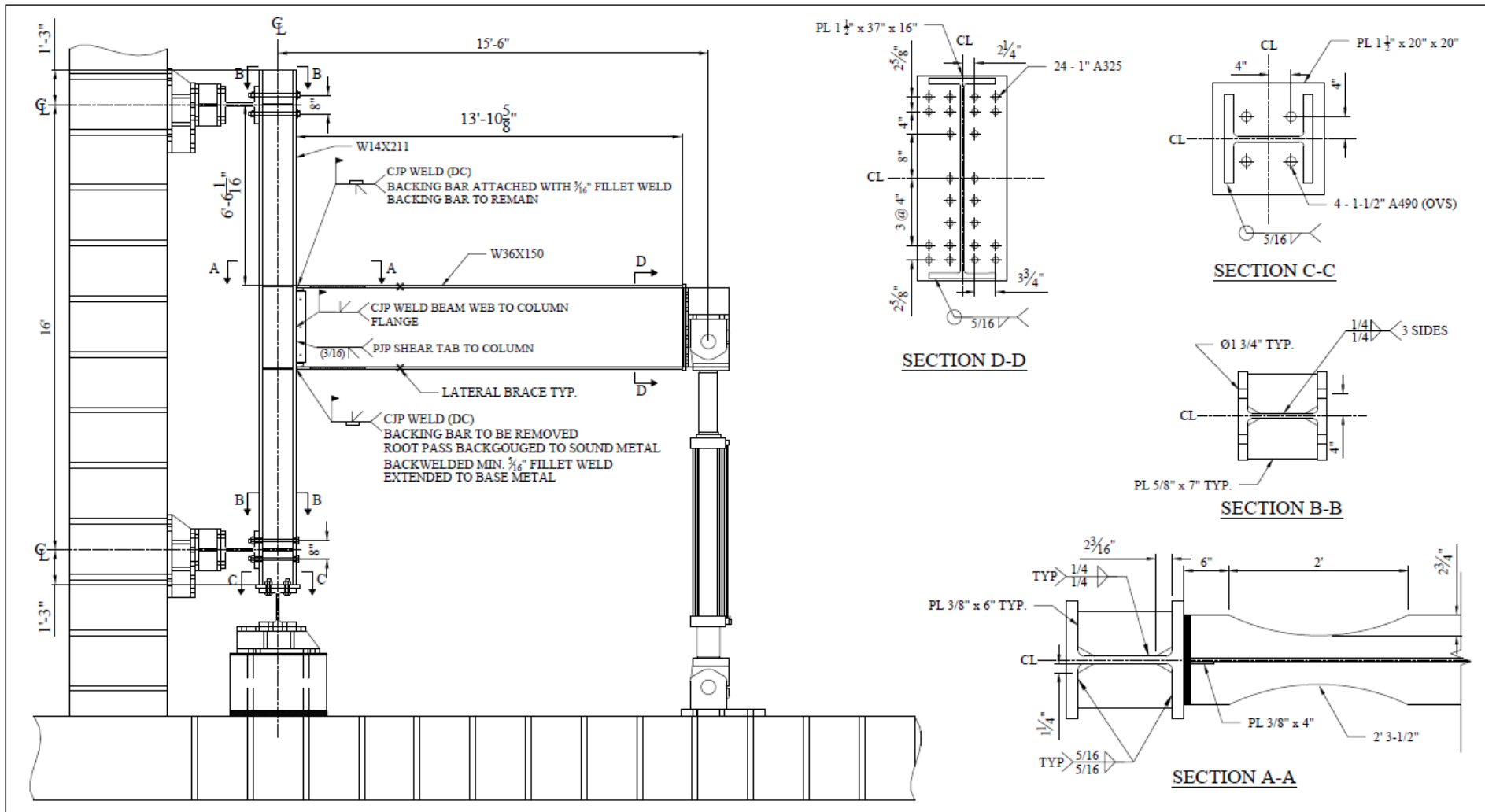
NOTES:

- ALL ROLLED SHAPES SHALL BE A992
- ALL PLATES SHALL BE A572 U.N.O
- ELECTRODES SHALL COMPLY WITH AWS D1.8 FOR DEMAND CRITICAL (DC) WELDS AS INDICATED
- ALL HOLES ARE 1-3/4" U.N.O BY BOLT DESIGNATION

**AISC SMF RESEARCH PROJECT
SPECIMEN C4**

UCSD DEPARTMENT OF STRUCTURAL ENGINEERING

DESIGNER:	DATE:	DRAWING NO.:	REV NO.:
MARS	2018.08.23	C4-A	1



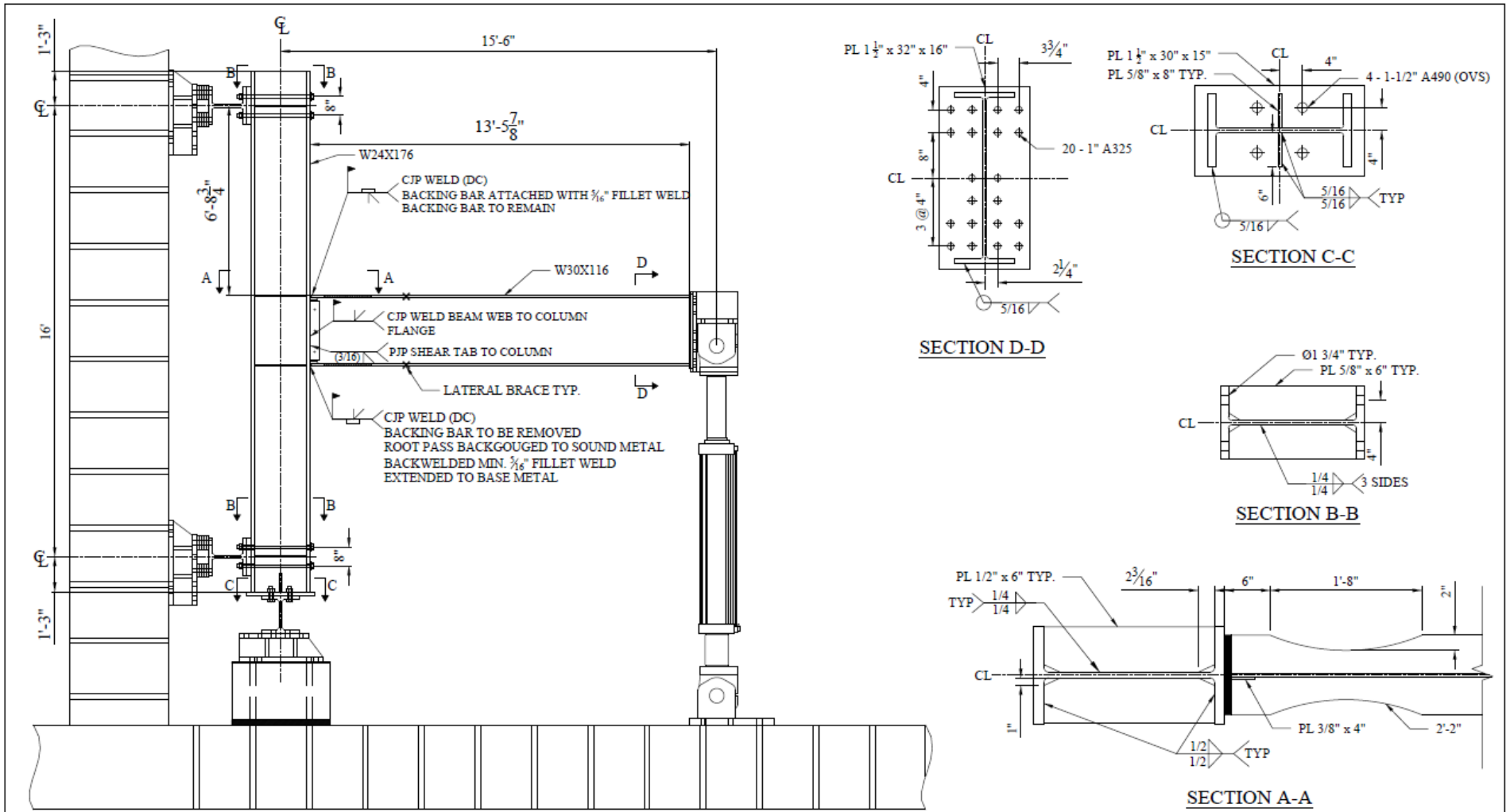
ELEVATION

NOTES:

ALL ROLLED SHAPES SHALL BE A992
 ALL PLATES SHALL BE A572 U.N.O
 ELECTRODES SHALL COMPLY WITH AWS D1.8 FOR DEMAND CRITICAL (DC) WELDS AS INDICATED
 ALL HOLES ARE 1-3/4" U.N.O BY BOLT DESIGNATION

**AISC SMF RESEARCH PROJECT
 SPECIMEN C5
 UCSD DEPARTMENT OF STRUCTURAL ENGINEERING**

DESIGNER: MARS	DATE: 2018.08.23	DRAWING NO.: C5-A	REV NO.: 1
--------------------------	----------------------------	-----------------------------	----------------------

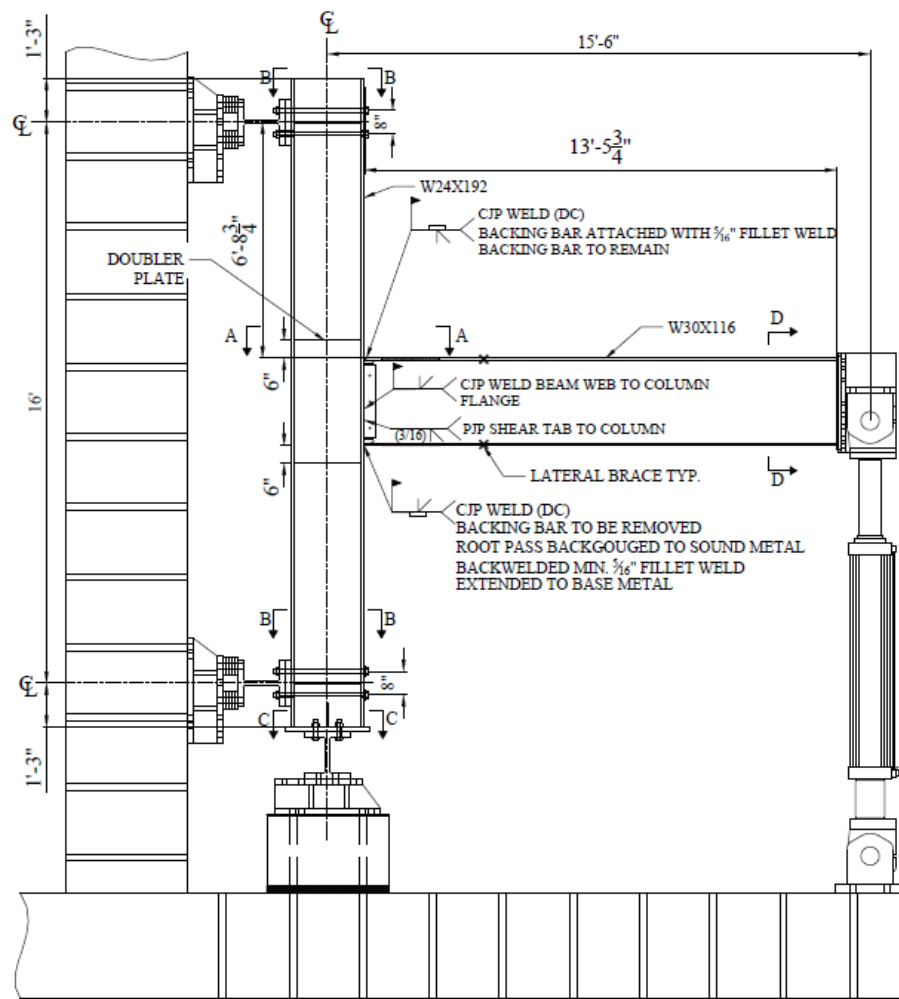


ELEVATION

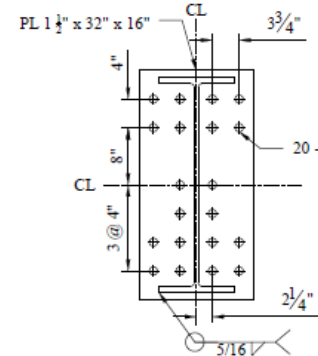
AISC SMF RESEARCH PROJECT
SPECIMEN C6
UCSD DEPARTMENT OF STRUCTURAL ENGINEERING

NOTES:
 ALL ROLLED SHAPES SHALL BE A992
 ALL PLATES SHALL BE A572 U.N.O
 ELECTRODES SHALL COMPLY WITH AWS D1.8 FOR DEMAND CRITICAL (DC) WELDS AS INDICATED
 ALL HOLES ARE 1-3/4" U.N.O BY BOLT DESIGNATION

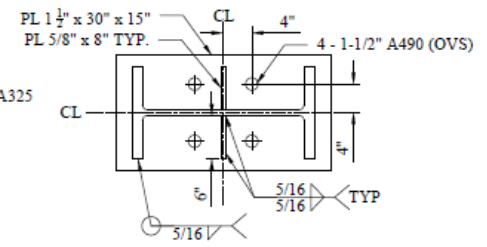
DESIGNER:	DATE:	DRAWING NO.:	REV NO.:
MARS	2018.08.23	C6-A	1



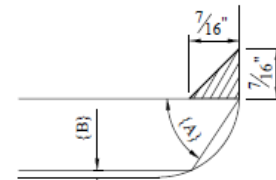
ELEVATION



SECTION D-D

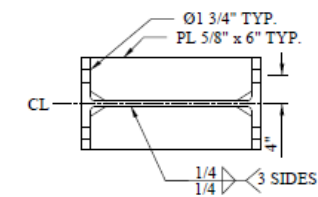


SECTION C-C

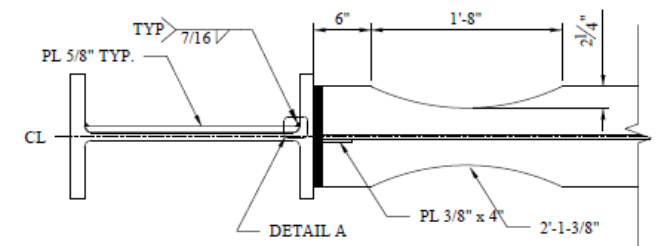


DETAIL A

DETAIL A NOTES:
 BEVEL (A) SHALL BE AT LEAST 45°
 DOUBLER PLATE MAY ENCR OACH FILLET
 GAP (B) SHALL BE NO LARGER THAN 1/16"



SECTION B-B



SECTION A-A

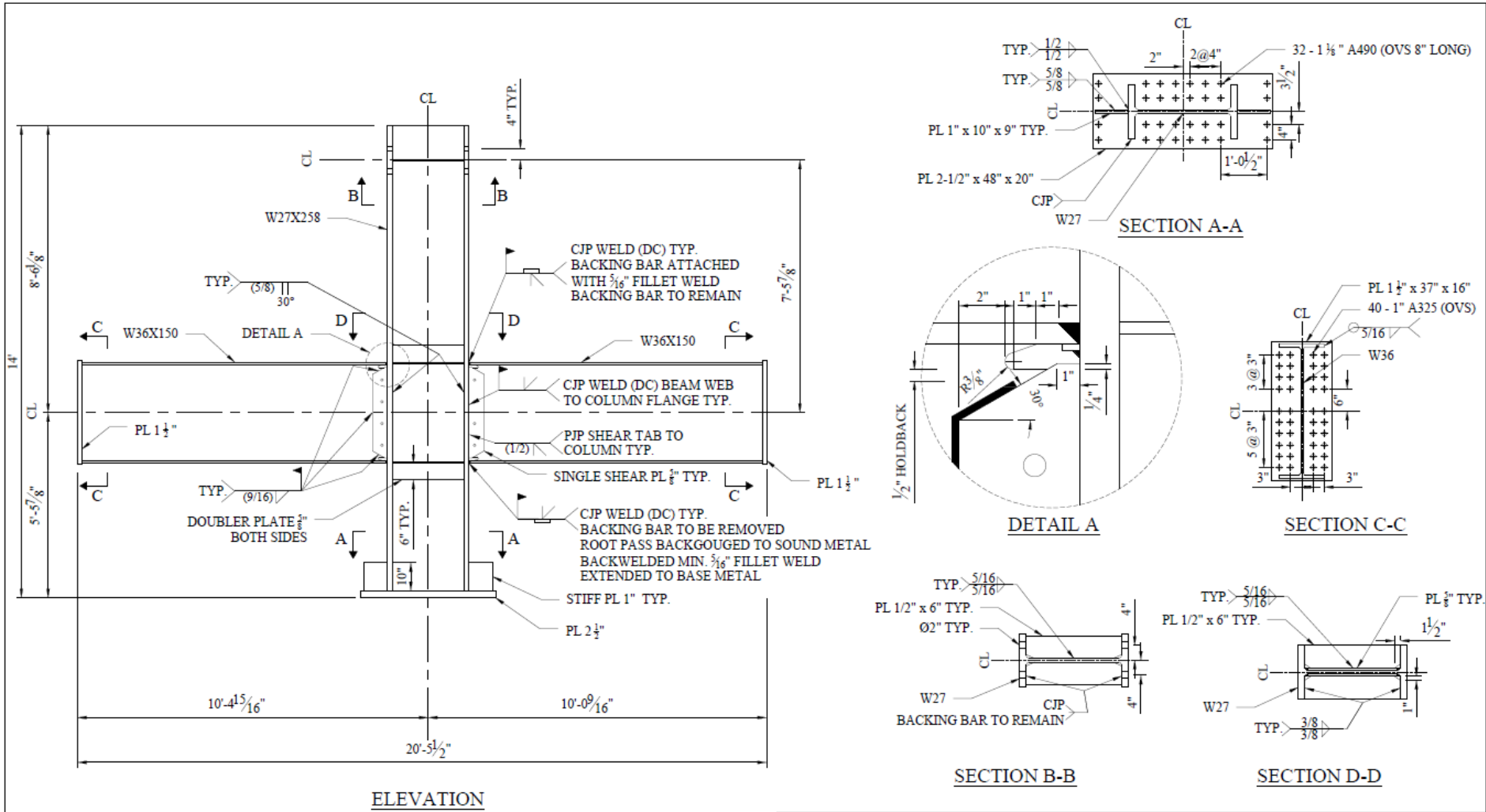
NOTES:

ALL ROLLED SHAPES SHALL BE A992
 ALL PLATES SHALL BE A572 U.N.O
 ELECTRODES SHALL COMPLY WITH AWS D1.8 FOR DEMAND CRITICAL (DC) WELDS AS INDICATED
 ALL HOLES ARE 1-3/4" U.N.O BY BOLT DESIGNATION

**AISC SMF RESEARCH PROJECT
 SPECIMEN C7**

UCSD DEPARTMENT OF STRUCTURAL ENGINEERING

DESIGNER:	DATE:	DRAWING NO.:	REV NO.:
MARS	2018.08.23	C7-A	1



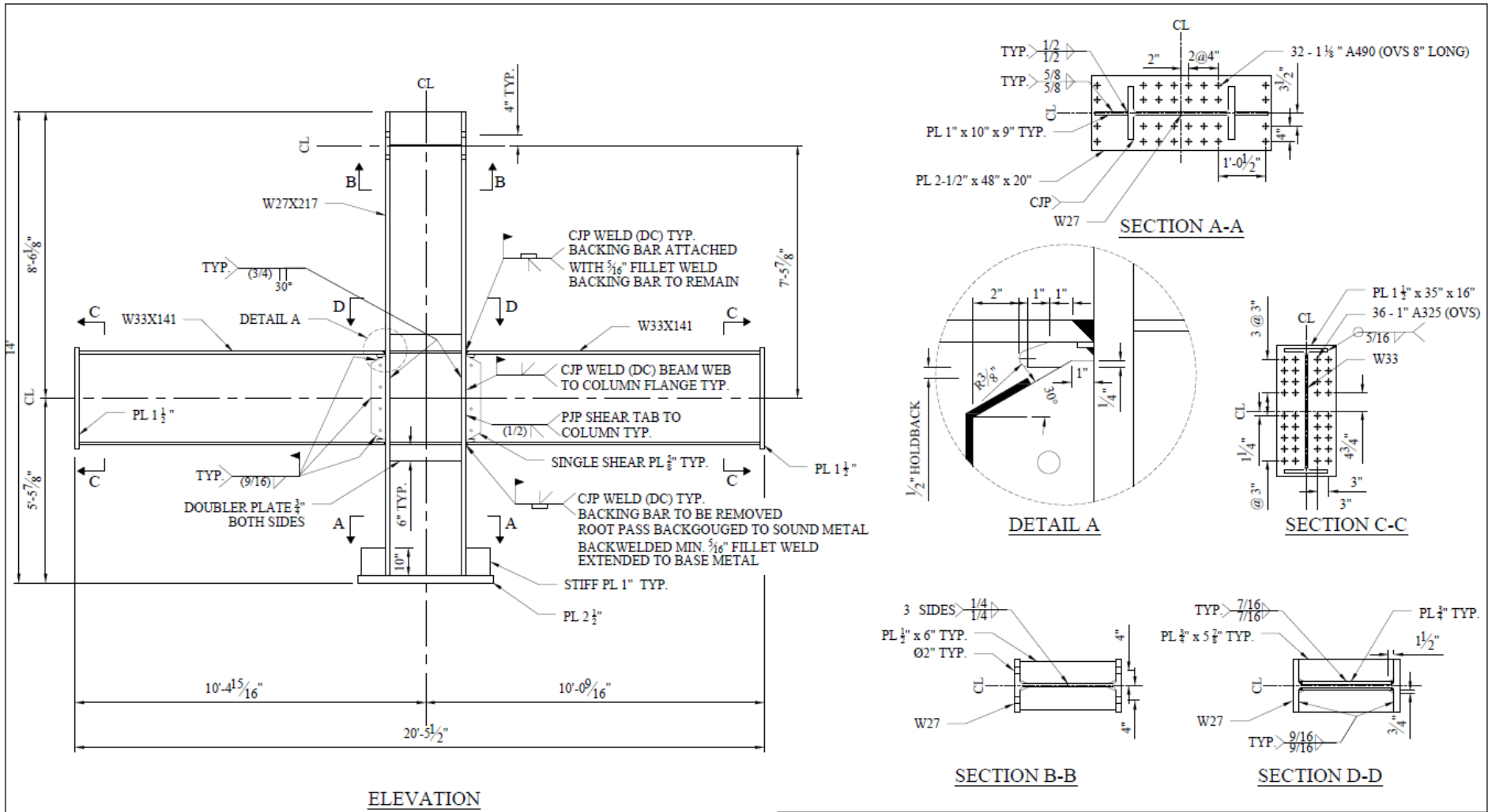
NOTES:

ALL ROLLED SHAPES SHALL BE A992
 ALL PLATES SHALL BE A572 U.N.O
 ELECTRODES SHALL COMPLY WITH AWS D1.8 FOR DEMAND CRITICAL (DC) WELDS AS INDICATED

SECTION D-D

**AISC SMF RESEARCH PROJECT PHASE 2
 SPECIMEN W1
 UCSD DEPARTMENT OF STRUCTURAL ENGINEERING**

DESIGNER: MARS	DATE: 2019.04.20	DRAWING NO.: W1-A	REV NO.: 0
-------------------	---------------------	----------------------	---------------



NOTES:

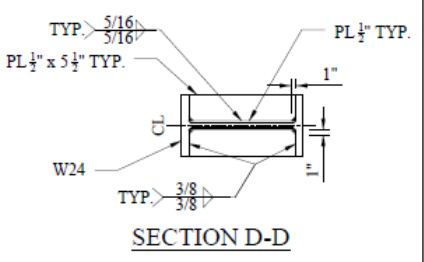
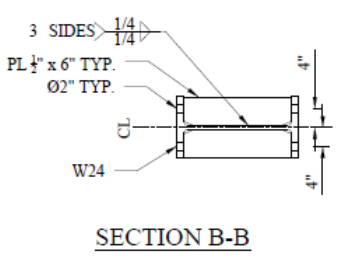
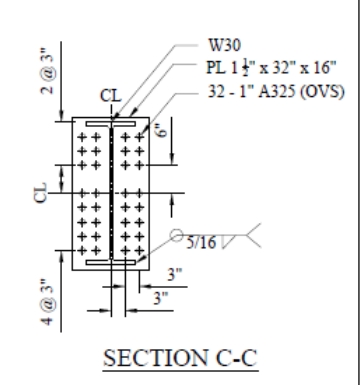
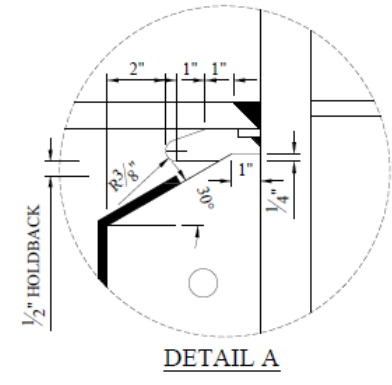
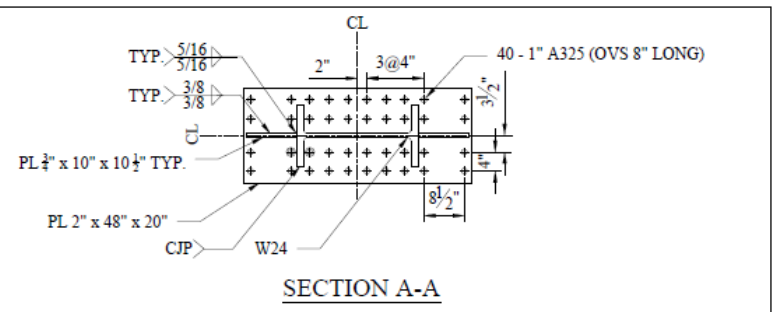
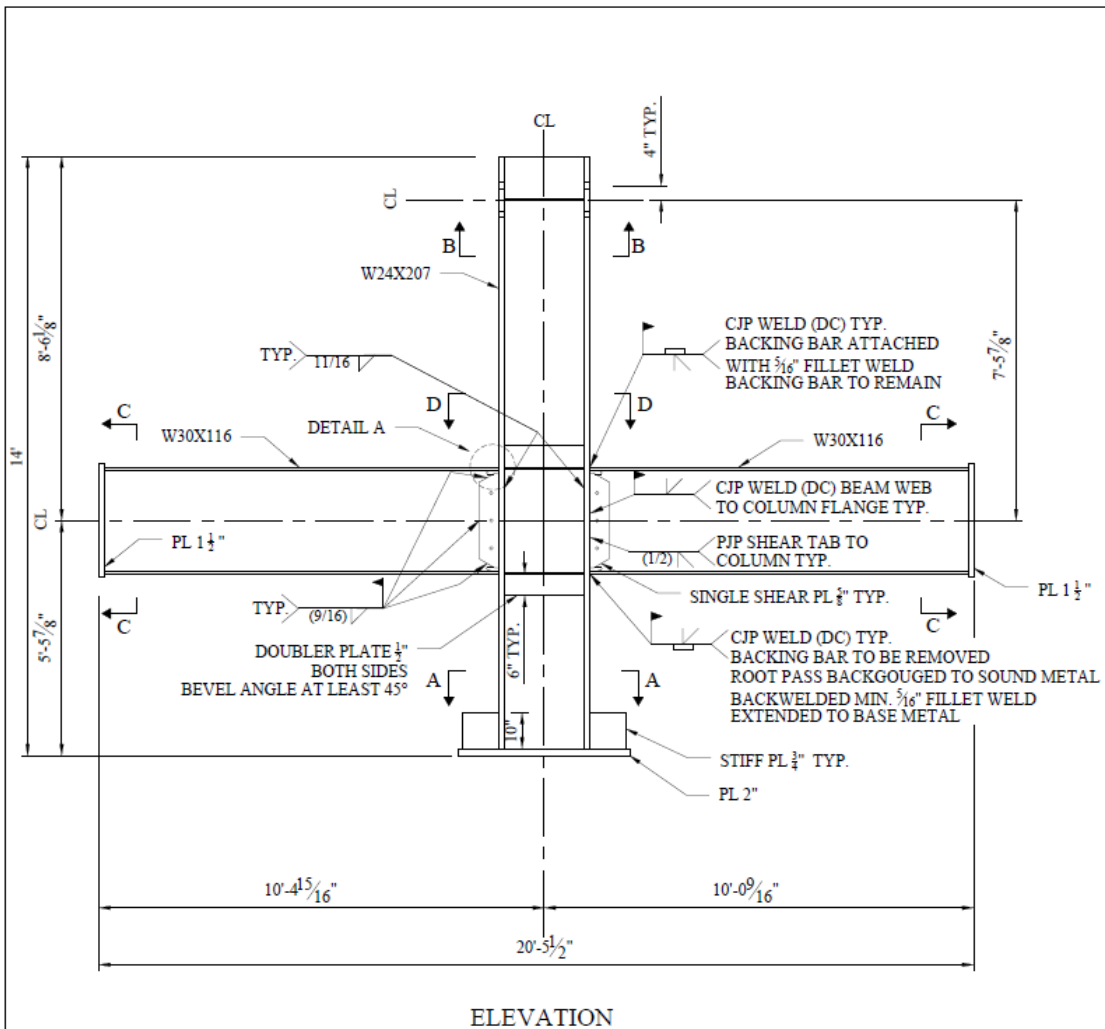
ALL ROLLED SHAPES SHALL BE A992
 ALL PLATES SHALL BE A572 U.N.O
 ELECTRODES SHALL COMPLY WITH AWS D1.8 FOR DEMAND CRITICAL (DC) WELDS AS INDICATED

SECTION D-D

**AISC SMF RESEARCH PROJECT PHASE 2
 SPECIMEN W2**

UCSD DEPARTMENT OF STRUCTURAL ENGINEERING

DESIGNER:	DATE:	DRAWING NO.:	REV NO.:
MARS	2019.04.21	W2-A	0

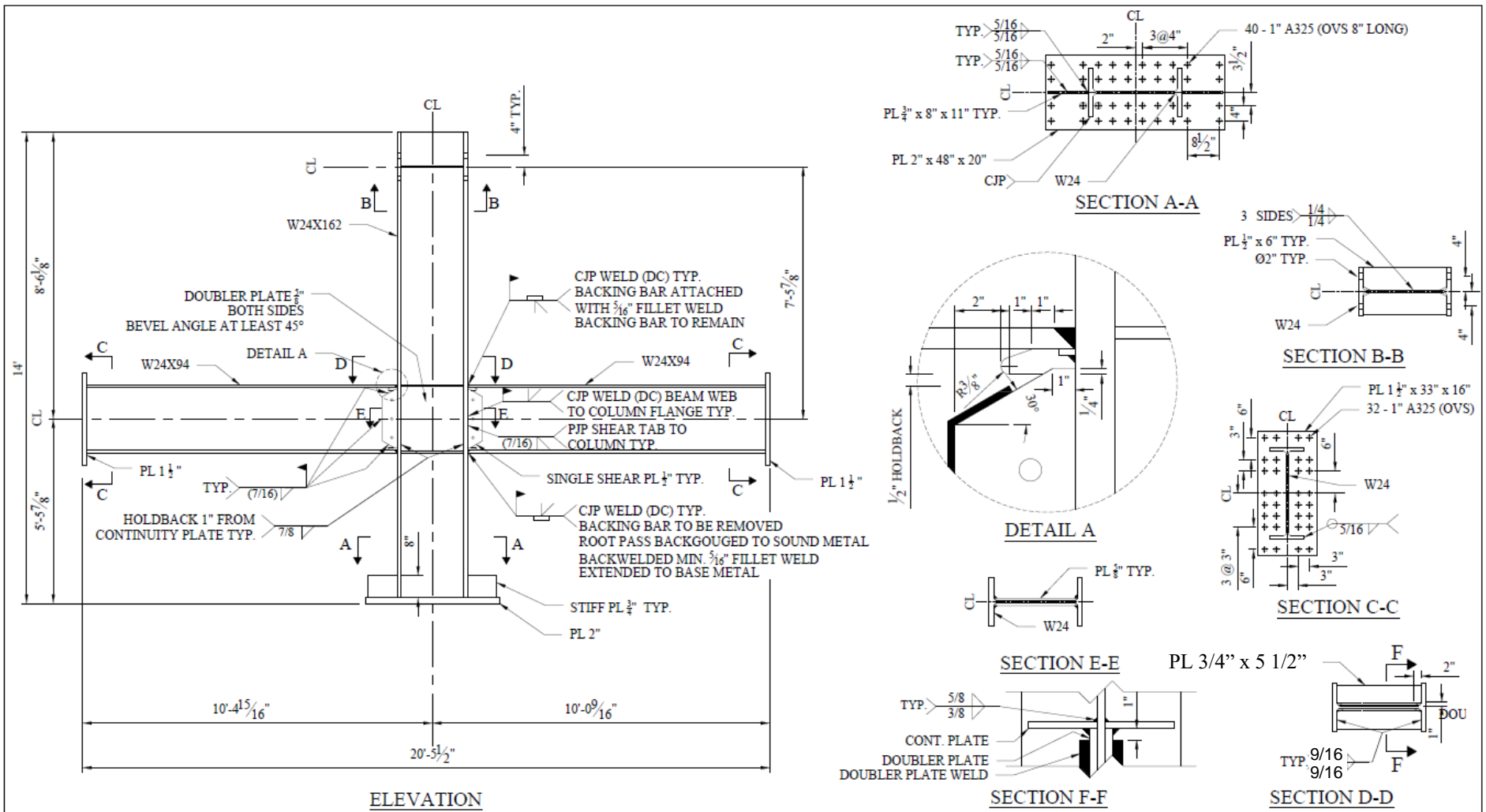


NOTES:
 ALL ROLLED SHAPES SHALL BE A992
 ALL PLATES SHALL BE A572 U.N.O
 ELECTRODES SHALL COMPLY WITH AWS D1.8 FOR DEMAND CRITICAL (DC) WELDS AS INDICATED

SECTION D-D

AISC SMF RESEARCH PROJECT PHASE 2
 SPECIMEN W3
 UCSD DEPARTMENT OF STRUCTURAL ENGINEERING

DESIGNER:	DATE:	DRAWING NO.:	REV NO.:
MARS	2019.04.22	W3-A	0



**AISC SMF RESEARCH PROJECT PHASE 2
 SPECIMEN W4
 UCSD DEPARTMENT OF STRUCTURAL ENGINEERING**

DESIGNER:	DATE:	DRAWING NO.:	REV NO.:
MARS	2019.04.22	W4-A	0

APPENDIX B: WELD INSPECTION REPORTS



WCIS
2500 Hoover Ave. Suite D San Diego CA 91950
O: 619.326.4405 F: 619.430.2453
www.wcinspection.com

TESTING & INSPECTION REPORT

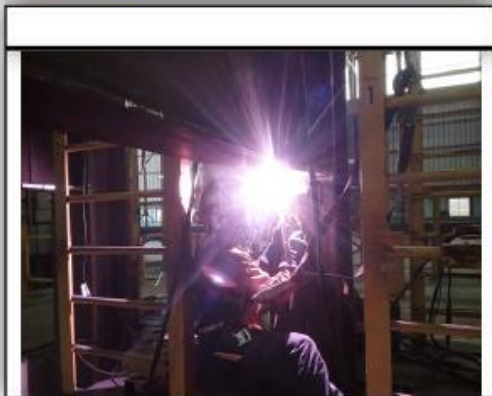
PAGE: 1 of 2

INSPECTOR NAME: Ryan E. Bordenkecher		JOB NUMBER: 9870	DATE: 9/26/18
JOB NAME: AISC Mock-up		DSA FILE # / OSHPD INC. #: NA	
ADDRESS: 5454 Industrial Pkwy, San Bernardino, CA 92407		DSA APPL # / OSHPD PERMIT #: NA	
GENERAL CONTRACTOR: NA		JURISDICTION: AISC	
ARCHITECT: NA	ENGINEER: NA	SUBCONTRACTOR/FABRICATOR: San Bernadino Steel/Herrick	
<small>REQUIREMENTS: Limit one job number, one permit number per sheet. Identify all work by type and SPECIFIC location. Each joint must be specifically identified for BSWHS bolt inspection. Non-compliant work must be specifically identified. Communication (RFI, Sketch etc.) voiding previous non-compliant items must be filed, record conversations and communications with project designers, building and permit granting authority officials.</small>			
HOURS			
REGULAR 8	1.5X	2X	MEAL PERIOD 30 Min.
TIME IN 5:45 AM		TIME OUT 2:15 PM	
Shop <input checked="" type="checkbox"/>	Field <input type="checkbox"/>	UT <input type="checkbox"/>	MT <input type="checkbox"/>
PT <input type="checkbox"/>	Material ID <input type="checkbox"/>	Welding <input checked="" type="checkbox"/>	Bolting <input type="checkbox"/>
Fireproofing <input type="checkbox"/>	Phased Array <input type="checkbox"/>		
DESCRIPTION OF WORK INSPECTED			
<p>Arrived on location at San Bernadino Steel/Herrick to provide continuous visual inspection and perform non-destructive testing of the modified re-design of moment frame welded connections to be destructively tested at UCSD Seismic Testing Facility in San Diego, CA.</p> <p>Verified welding performed by certified personnel using approved materials, consumables, and weld procedures for steel moment frame seismic resistant design per AWS D1.8 and AISC 341 Seismic Provision.</p> <p>Reviewed mock-up drawings to include welded joint configuration, fit-up tolerances, weld types, and backing.</p> <p>Verified proper fit-up, pre-heat, welding sequence, equipment parameters, workmanship and technique are in compliance with approved mock-up drawings and current code requirements for seismic design.</p> <p>Welding of piece marks identified as 30001/1A (RBS WF beam) to 10001/1A (WF column): -30001/1A HT#440889 (A992) -10001/1A HT#N039862 (A992)</p> <p>Visually inspected/accepted complete joint penetration groove welds at top/bottom flanges and web per AWS D1.1 Section 6, Part C 6.9, Table 6.1.</p> <p>Visually inspected/accepted fillet welded reinforcing fillet welds at top flange backing bar left in place and bottom flange removed backing bar per AWS D1.1 Section 6, Part C 6.9, Table 6.1.</p> <p>Non-destructive ultrasonic flaw detection of CJP groove welds and magnetic particle examination of run-off tab removal/reinforcing fillet welds to be performed after a 24-hour cooling period has been reached.</p> <p>169-001-18</p>			
CERTIFICATE OF COMPLIANCE			
The work was inspected in accordance with the approved documents <input checked="" type="checkbox"/> Yes <input type="checkbox"/> No		I hereby declare that, to the best of my personal knowledge, the work performed and the materials used and installed covered by this report, are in compliance with the approved documents and any approved Post Approval Documents/Amended Construction Documents, unless otherwise noted in this report.	
The work inspected met the requirement of the approved documents <input checked="" type="checkbox"/> Yes <input type="checkbox"/> No			
<small>*See additional comments for information regarding non-compliant inspection results.</small>		Inspector Initials: <u>REE</u>	
ADDITIONAL COMMENTS / NON-COMPLIANCE ITEMS / DEVIATIONS / EXCEPTIONS			
Inspector Signature: <u><i>REE</i></u> Inspector Name Print: <u>Ryan E. Bordenkecher</u> Inspector certification: <u>AWS/CWI 05101101</u>			
<small>All Inspections based on minimum of 4 hours and over 4 hours-8 hours minimum. If Inspector is called to a project and no work is performed a 2 hour show up charge will be applied This report will be distributed to the architect, engineer, client and governing jurisdiction (e.g. DSA) as required by applicable codes and project documents CC: Project Architect; Structural Engineer; Project Inspector; DSA Regional Office; School District</small>			

PROJECT: AISC Mock-up

CONTRACTOR: San Bernadino Steel/Herrick

ADDRESS: 5454 Industrial Pkwy., San Bernadino, CA 92407



Certification of Compliance: All work, unless otherwise noted, complies with the approved documents.

NAME: Ryan E. Bordenkecher

CERTIFICATION NO: AWS CWI # AWS/CWI 05101101

TESTING & INSPECTION REPORT

PAGE: 1 of 2

INSPECTOR NAME: Ryan E. Bordenkecher		JOB NUMBER: 9870	DATE: 9/25/18
JOB NAME: AISC Mock-up		DSA FILE # / OSHPD INC. #: NA	
ADDRESS: 5454 Industrial Pkwy, San Bernadino, CA 92407		DSA APPL # / OSHPD PERMIT #: NA	
GENERAL CONTRACTOR: NA		JURISDICTION: AISC	
ARCHITECT: NA	ENGINEER: NA	SUBCONTRACTOR/FABRICATOR: San Bernadino Steel/Herrick	

REQUIREMENTS: Limit one job number, one permit number per sheet. Identify all work by type and SPECIFIC location. Each joint must be specifically identified for SSWHS bolt inspection. Non-compliant work must be specifically identified. Communication (RFI, Sketch etc.) voiding previous non-compliant items must be listed, record conversations and communications with project designers, building and permit granting authority officials.

HOURS					
REGULAR	1.5X	2X	TIME IN	TIME OUT	MEAL PERIOD
8			5:45 AM	2:15 PM	30 Min.

Shop Field UT MT PT Material ID Welding Bolting Fireproofing Phased Array

DESCRIPTION OF WORK INSPECTED

Arrived on location at San Bernadino Steel/Herrick to provide continuous visual inspection and perform non-destructive testing of the modified re-design of moment frame welded connections to be destructively tested at UCSD Seismic Testing Facility in San Diego, CA.

Verified welding performed by certified personnel using approved materials, consumables, and weld procedures for steel moment frame seismic resistant design per AWS D1.8 and AISC 341 Seismic Provision

Reviewed mock-up drawings to include welded joint configuration, fit-up tolerances, weld types, and backing

Verified proper fit-up, pre-heat, welding sequence, equipment parameters, workmanship and technique are in compliance with approved mock-up drawings and current code requirements for seismic design

Welding of piece marks identified as 30003/1A (RBS WF beam) to 10003/1A (WF column)
 -30003/1A HT#421418 (A992)
 -10003/1A HT#452444 (A992)

Visually inspected/accepted complete joint penetration groove welds at top/bottom flanges and web per AWS D1.1 Section 6, Part C 6.9, Table 6.1

Visually inspected/accepted fillet welded reinforcing fillet welds at top flange backing bar left in place and bottom flange removed backing bar per AWS D1.1 Section 6, Part C 6.9, Table 6.1

Non-destructive ultrasonic flaw detection of CJP groove welds and magnetic particle examination of run-off tab removal/reinforcing fillet welds to be performed after a 24-hour cooling period has been reached.

169-001-18

WELDER NAME	FILLER METAL / ELECTRODE	ELECTRODE DIAMETER	AVERAGE AMPS / VOLTS / TRAVEL SPEED / JOINT CONFIGURATION	REMARKS
Salvador Ramirez	E70T-6 (Lincoln NR-305)	.093	425/25/12 IPM/BTC-U4a-F	
	E71T-8 (Lincoln NR-232)	.072	255/21/7 IPM/BTC-U4a-F	

CERTIFICATE OF COMPLIANCE

The work was inspected in accordance with the approved documents Yes No

The work inspected met the requirement of the approved documents Yes No

I hereby declare that, to the best of my personal knowledge, the work performed and the materials used and installed covered by this report, are in compliance with the approved documents and any approved Post Approval Documents/Amended Construction Documents, unless otherwise noted in this report.

Inspector Initials: REB

ADDITIONAL COMMENTS / NON-COMPLIANCE ITEMS / DEVIATIONS / EXCEPTIONS

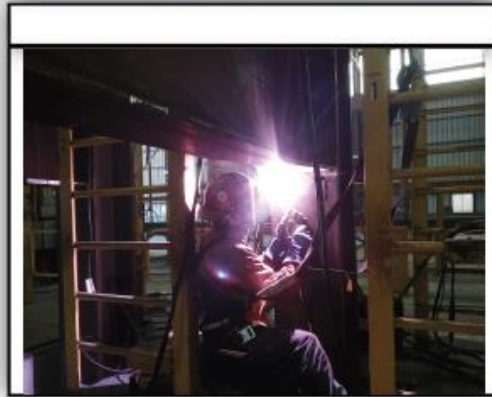
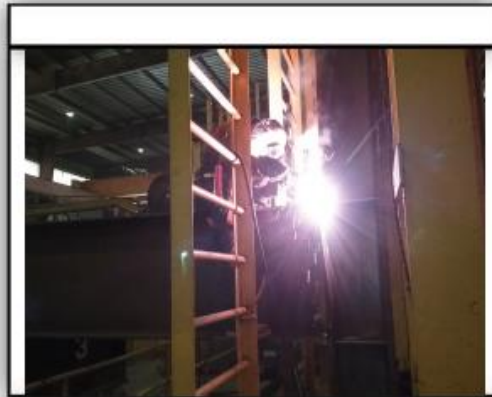
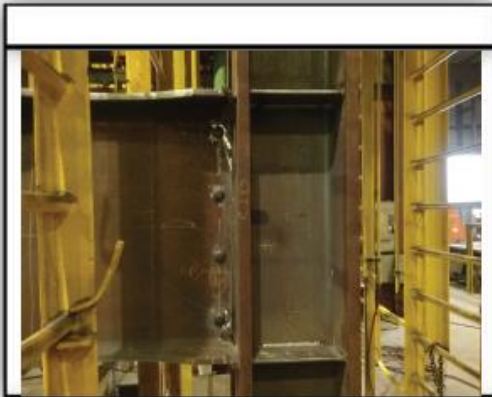
Inspector Signature: *R. Bordenkecher*
 Inspector Name Print: Ryan E. Bordenkecher
 Inspector certification: AWS/CWI 05101101

All Inspections based on minimum of 4 hours and over 4 hours-8 hours minimum. If Inspector is called to a project and no work is performed a 2 hour show up charge will be applied. This report will be distributed to the architect, engineer, client and governing jurisdiction (e.g. DSA) as required by applicable codes and project documents.
 CC: Project Architect, Structural Engineer, Project Inspector, DSA Regional Office, School District

PROJECT: AISC Mock-up

CONTRACTOR: San Bernadino Steel/Herrick

ADDRESS: 5454 Industrial Pkwy., San Bernadino, CA 92407



Certification of Compliance: All work, unless otherwise noted, complies with the approved documents.

NAME: Ryan E. Bordenkecher

CERTIFICATION NO: AWS CWI # AWS/CWI 05101101



TESTING & INSPECTION REPORT

INSPECTOR NAME: Ryan E. Bordenkecher		JOB NUMBER: 9870	DATE: 9/27/18
JOB NAME: AISC Mock-up		DBA FILE # / OSHPD INC. #: NA	
ADDRESS: 5454 Industrial Pkwy, San Bernadino, CA 92407		DBA APPL # / OSHPD PERMIT #: NA	
GENERAL CONTRACTOR: NA		JURISDICTION: AISC	
ARCHITECT: NA	ENGINEER: NA	SUBCONTRACTOR/FABRICATOR: San Bernadino Steel/Herrick	

REQUIREMENTS: Limit one job number, one permit number per sheet. Identify all work by type and SPECIFIC location. Each joint must be specifically identified for BSWSIS bolt inspection. Non-compliant work must be specifically identified. Communication (RFI, Sketch etc.) voiding previous non-compliant items must be listed, record conversations and communications with project designers, building and permit granting authority officials.

HOURS					
REGULAR	1.5X	2X	TIME IN	TIME OUT	MEAL PERIOD
4			5:45 AM	9:45 AM	
Shop <input checked="" type="checkbox"/>	Field <input type="checkbox"/>	UT <input checked="" type="checkbox"/> MT <input checked="" type="checkbox"/> PT <input type="checkbox"/>	Material ID <input type="checkbox"/>	Welding <input type="checkbox"/> Bolting <input type="checkbox"/>	Fireproofing <input type="checkbox"/> Phased Array <input type="checkbox"/>

DESCRIPTION OF WORK INSPECTED

Arrived on location at San Bernadino Steel/Herrick to perform non-destructive ultrasonic flaw detection and magnetic particle testing of the modified re-design of moment frame welded connections to be destructively tested at UCSD Seismic Testing Facility in San Diego, CA.

Calibrations on non-destructive testing equipment were performed prior to, during, and after testing to ensure proper functioning of equipment throughout the entire examination process in accordance with applicable code requirements.

Performed non-destructive ultrasonic shearwave testing of moment frame complete joint penetration groove welds located at WF beam to column top/bottom flanges and web on piece marks identified as 30003/1A and 10003/1A and 30001/1A to 10001/1A. Ultrasonic testing was unremarkable with no defects noted at the time of testing. See attached UT report for further information.

Performed non-destructive magnetic particle testing of moment frame complete joint penetration groove weld run off tabs located at WF beam to column top/bottom flanges and at bottom flange 5/16" reingorcing fillet weld upon backing bar removal on piece marks identified as 30003/1A to 10003/1A and 30001/1A to 10001/1A. Magnetic particle testing was unremarkable with no defects noted at the time of testing. See attached MT report for further information

169-001-18

WELDER NAME	FILLER METAL / ELECTRODE	ELECTRODE DIAMETER	AVERAGE AMPS / VOLTS / TRAVEL SPEED / JOINT CONFIGURATION	REMARKS
Salvador Ramirez	E70T-8 (Lincoln NR-305)	.083	425/25/12 IPM/BTC-U4a-F	
	E71T-8 (Lincoln NR-232)	.072	255/21/7 IPM/BTC-U4a-F	

CERTIFICATE OF COMPLIANCE	
The work was inspected in accordance with the approved documents <input checked="" type="checkbox"/> Yes <input type="checkbox"/> No	I hereby declare that, to the best of my personal knowledge, the work performed and the materials used and installed covered by this report, are in compliance with the approved documents and any approved Post Approval Documents/Amended Construction Documents, unless otherwise noted in this report.
The work inspected met the requirement of the approved documents <input checked="" type="checkbox"/> Yes <input type="checkbox"/> No	
Inspector Initials: <u>REE</u>	

ADDITIONAL COMMENTS / NON-COMPLIANCE ITEMS / DEVIATIONS / EXCEPTIONS

Inspector Signature: REE
 Inspector Name Print: Ryan E Bordenkecher
 Inspector certification: AWS/CWI 05101101

All inspections based on minimum of 4 hours and over 4 hours-8 hours minimum. If Inspector is called to a project and no work is performed a 2 hour show up charge will be applied. This report will be distributed to the architect, engineer, client and governing jurisdiction (e.g. DSA) as required by applicable codes and project documents.
 CC: Project Architect; Structural Engineer; Project Inspector; DSA Regional Office; School District



ULTRASONIC TEST REPORT

Job Identification: AISC Mock-up	Address: 5454 Industrial Pkwy.	Date: 9/27/18
City of: San Bernardino	Building Permit No.: N/A	Report: 2 of 4
General Contractor: NA	Sub Contractor: San Bernardino Steel/Herrick	
Architect: NA	Engineer: NA	

Quality Requirements-Section No. AWS D1.1 Table 6.2

ULTRASONIC EQUIPMENT							
Instrument	Manufacturer			Transducers			
		TW-DUFD	SUB140	9016208	Mitech	0	NDT Systems
Reference Blocks	Model / Type			Crystal Serial No.			
	IIW Type I	1018	E2742	120875	AWW070		
Couplant	Manufacturer		Batch Series No.		Size		
	Sonotech	UTX Powder	12HD47	N/A	AWS-0268		
				Ref. Level	52		

ULTRASONIC TESTING OF MATERIALS						
Surface Condition	Thickness	Joint Type	Welding Process	Exam from Face	Volumetric Exam in Leg	Scanning Level
Clean/Dry	5/8-1"	T	FCAW	A & B	1 & 2	Per AWS D1.1 Table 6.2

ITEMS EXAMINED/TESTED

Line	Piece Mark/Weld ID	Description	Interpretation				Remarks
			# weld(s)	Accepted	Rejected	Repaired	
	10001/1A	CJP at top/bottom flanges and web	3	3	N/A	N/A	
	10003/1A	CJP at top/bottom flanges and web	3	3	N/A	N/A	
Total Welds			6	6	N/A	N/A	

Comments:

INDICATION(S) FOUND IN REJECTED WELDS

Line	Indication #	Transducer Angle (°)	From Face	App (S, H, B, ...)	DECIBELS (dB)				DISCONTINUITY (in.)				Discontinuity Classification	REMARKS (Discontinuity Evaluation)	
					Ind Level	Ref	Att	Ind	Length	Angular Distance (Sound Path)	Depth from "A" Surface	DISTANCE (in.)			
					a	b	c	d				From X			From Y

I, the undersigned, certify that the statements in this record are correct and that the test welds were prepared and tested in conformance with the requirements of Clause 5, Part F of AWS D1.1/D1.1M: 2015 Structural Welding Code-Steel and the Project Specifications.

Instrument Calibration has been performed for horizontal and vertical linearity, shear wave and longitudinal. In accordance with WCIS-UT-101	Inspector	
	Inspector: Ryan E. Bordenkecher	Level: II
	Signature:	



REPORT OF MAGNETIC PARTICLE TESTING OF WELDS

Project Name: AISC Mock-up Client Project number 9870
 Quality Requirements-Section No. AWS D1.1 Section 6, Table 6.1 WCIS Project Number 169-001-18
 Items Examined/Tested: Moment frame CJP groove weld R/O tabs and bottom flange 5/16" reinf. fillets

LINE	Piece Mark Grid Line	DESCRIPTION	Area Examined		Interpretation		Repairs		REMARKS
			Entire	Specific	Accepted	Rejected	Accepted	Rejected	
1	10001/1A	MF beam to column		X	X				4-R/O tabs & 1-reinf. fit.
2	10003/1A	MF beam to column		X	X				4-R/O tabs & 1-reinf. fit.
3									
4									
5									
6									
7									
8									
9									
10									
11									
12									
13									
14									
15									
16									
17									
18									
19									
20									

Quantity: 10 Total Accepted: 10 Total Rejected: 0

Comments: _____

PRE-EXAMINATION
 Surface Preparation: Clean/Dry

EQUIPMENT
 Instrument Make: Parker Model: DA-400 S/N Number: 24363

METHOD OF INSPECTION
 Dry Wet Visible Fluorescent How Media Applied: Blower
 AC DC Residual Continuous Yoke Prods Other _____
 Direction for Field: Circular Longitudinal Strength of Field: Known indications

POST EXAMINATION
 Demagnetizing Technique (if required): NA Cleaning (if required): NA Marking Method: NA

I, the undersigned, certify that the statements in this record are correct and that the test welds were prepared and tested in conformance with the requirements of AWS D1.1/D1.1M: 2003, Structural Welding Code - Steel

Inspector Ryan E. Bordenkecher SNT-TC-1A Lev. II MT Date 9/27/18



Project #: 9870
Bldg. Permit #:
Date of Report: 9/27/18

PROJECT: AISC Mock-up

CONTRACTOR: San Bernadino Steel/Herrick

ADDRESS: 5454 Industrial Pkwy., San Bernadino, CA 92407



Certification of Compliance: All work, unless otherwise noted, complies with the approved documents.

NAME: Ryan E. Bordenkecher



SMITH-EMERY COMPANY

Daily Inspection Report

Project Name: AISC/UCSD SMF Project		SE Job #	New Job
Address:		Jurisdiction:	
Off-Site		Permit #	
Shop Name: Work performed at San Bernadino Steel	Date:	Jurisdiction, spoke to:	
Shop Address: 5454 Industrial Pkwy San Bernardino, Ca	Start Time: _____ AM	Page: 1 of	
	End Time: _____ PM		
<input type="checkbox"/> Concrete <input type="checkbox"/> Fireproofing <input type="checkbox"/> Masonry <input checked="" type="checkbox"/> Steel Field <input type="checkbox"/> Steel Shop <input type="checkbox"/> Other			

Description of Work Inspected

Performed ultrasound testing of complete joint penetration groove welds, see attached reports.
 Performed mag-particle testing of weld tab removal, see attached reports.

Inspector: Julian Razo
 AWS/CWI #03120501
 ICC Structural Steel & Bolting #5232503
 ICC Structural Steel Welding #5232503
 ICC Fireproofing #5232503
 L.A. City Steel Construction, Drilled In Anchors
 & Fireproofing #P018657
 L.A. County Structural Steel & Welding #01735
 U.T. Level II /SNT-TC-1A
 M.T. Level II/SNT-TC-1A

Work Not In Compliance

The work was WAS NOT inspected
 Material sampling was WAS NOT N/A performed
 The work inspected met DID NOT meet the requirements
 with the requirements of the approved documents.

CC: Project Architect, Structural Engineer, Project Inspector

Date	Signature
Employee ID	Name

ALL REPORTS ARE SUBMITTED AS THE CONFIDENTIAL PROPERTY OF CLIENTS. AUTHORIZATION FOR PUBLICATION OF OUR REPORT, CONCLUSIONS, OR EXTRACTS FROM OR REGARDING THEM IS RESERVED PENDING OUR WRITTEN APPROVAL AS A MUTUAL PROTECTION TO CLIENTS, THE PUBLIC AND OURSELVES. © Smith Emery Company 2.0b
 SECO 101A

SMITH-EMERY COMPANY

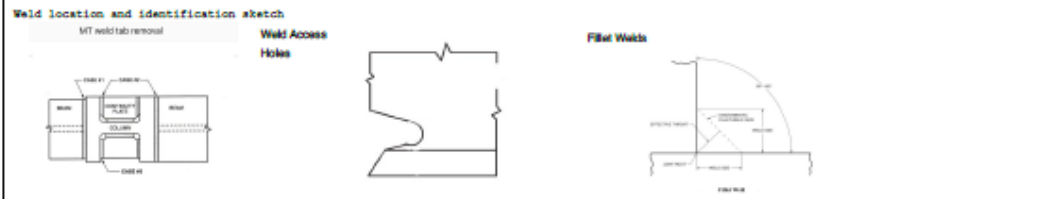
DSA
OSHPD
SE Job No. **New Job**
Permit No.

REPORT OF MAGNETIC PARTICLE SHOP EXAMINATION

Job Name
AISC/UCSD

Job Address
Worked performed at San Bernardino Steel 5454 Industrial Pkwy San Bernardino

Jobsite Location (area/floor)



Piece Work	Location	ACCEPT	REJECT	ACCEPT REPAIR	REJECT REPAIR	Remarks
10001 1/A	Case 1 A side	✓				MT Weld tab removal 4 locations
10001 1/A	Case 1 B side	✓				MT Weld tab removal 4 locations

Equipment (brand) Magnaflux	Model Y7 AC/DC	Output 4 amps	Current 120 vol	Particle type Red Particle
Material Carbon Steel	Surface Clean	Test Temp. Ambient	Spacing 4-6 inches	Quality Requirement-section AWS D1.1 Sec 6
Direction <input type="checkbox"/> Circular <input type="checkbox"/> Long <input checked="" type="checkbox"/> Both		Method of inspection <input type="checkbox"/> Prod <input checked="" type="checkbox"/> Yoke <input type="checkbox"/> Coil <input checked="" type="checkbox"/> AC <input type="checkbox"/> DC <input type="checkbox"/> Wet <input checked="" type="checkbox"/> Dry <input checked="" type="checkbox"/> Visible <input type="checkbox"/> Fluorescent		

6/26/19 2673 Julian Razo
Dated Employee ID Name

ALL REPORTS ARE SUBMITTED AS THE CONFIDENTIAL PROPERTY OF CLIENTS. AUTHORIZATION FOR PUBLICATION OF OUR REPORT, CONCLUSIONS, OR EXTRACTS FROM OR REGARDING THEM IS RESERVED PENDING OUR WRITTEN APPROVAL AS A MUTUAL PROTECTION TO CLIENTS, THE PUBLIC AND OURSELVES.
© 2004 Smith Emery Company

SMITH-EMERY COMPANY

SE Job No.

Permit No.

REPORT OF ULTRASONIC SHOP WELD TESTING

Job Name AISC/UCSD SMF Project		Work at performed at San Bernadino Steel				
Job Address 5454 Industrial Pkwy San Bernardino, Ca						
Place Work	Location	ACCEPT	REJECT	ACCEPT REPAIR	REJECT REPAIR	Remarks
Col 10001 1/A	Moment Conn	✓				CJP A) Side T/B Flgs & Web
Col 10001 1/A	Moment Conn	✓				CJP B) Side T/B Flgs & Web
Equipment (brand) Sonatest	Model D-20	Serial No. I011912		Angle(s) <input checked="" type="checkbox"/> 70 <input type="checkbox"/> 60 <input type="checkbox"/> 45		
Transducer (brand) GE Gamma	Size .75 x .625	Frequency 2.25		Reference Level 40	Scanning Level 60	
Quality Requirements AWS D1.1 Clause 6 Table 6.2						
Remarks						

6/26/19 2673 Julian Razo
 Dated Employee ID Name

ALL REPORTS ARE SUBMITTED AS THE CONFIDENTIAL PROPERTY OF CLIENTS. AUTHORIZATION FOR PUBLICATION OF OUR REPORT, CONCLUSIONS, OR EXTRACTS FROM OR REGARDING THEM IS RESERVED PENDING OUR WRITTEN APPROVAL AS A MUTUAL PROTECTION TO CLIENTS, THE PUBLIC AND OURSELVES.
 © 2004 Smith Emery Company

SMITH-EMERY COMPANY

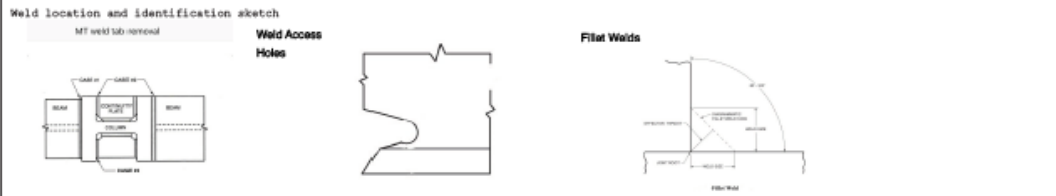
DSA
OSHPD
SE Job No. **New Job**
Permit No.

REPORT OF MAGNETIC PARTICLE SHOP EXAMINATION

Job Name
AISC/UCSD

Job Address
Worked performed at San Bernardino Steel 5454 Industrial Pkwy San Bernardino

Jobsite Location (area/floor)



Piece Work	Location	ACCEPT	REJECT	ACCEPT REPAIR	REJECT REPAIR	Remarks
10004 1/A	Case 1 A side	✓				MT Weld tab removal 4 locations
10004 1/A	Case 1 B side	✓				MT Weld tab removal 4 locations

Equipment (brand) Magnaflux	Model Y7 AC/DC	Output 4 amps	Current 120 vol	Particle type Red Particle
Material Carbon Steel	Surface Clean	Test Temp. Ambient	Spacing 4-6 inches	Quality Requirement-section AWS D1.1 Sec 6
Direction <input type="checkbox"/> Circular <input type="checkbox"/> Long <input checked="" type="checkbox"/> Both		Method of inspection <input type="checkbox"/> Prod <input checked="" type="checkbox"/> Yoke <input type="checkbox"/> Coil <input checked="" type="checkbox"/> AC <input type="checkbox"/> DC <input type="checkbox"/> Wet <input checked="" type="checkbox"/> Dry <input checked="" type="checkbox"/> Visible <input type="checkbox"/> Fluorescent		

6/27/19 2673 Julian Razo
Dated Employee ID Name

ALL REPORTS ARE SUBMITTED AS THE CONFIDENTIAL PROPERTY OF CLIENTS. AUTHORIZATION FOR PUBLICATION OF OUR REPORT, CONCLUSIONS, OR EXTRACTS FROM OR REGARDING THEM IS RESERVED PENDING OUR WRITTEN APPROVAL AS A MUTUAL PROTECTION TO CLIENTS, THE PUBLIC AND OURSELVES.
© 2004 Smith Emery Company

SMITH-EMERY COMPANY

SE Job No. _____

Permit No. _____

REPORT OF ULTRASONIC SHOP WELD TESTING

Job Name AISC/UCSD SMF Project		Work at performed at San Bernadino Steel				
Job Address 5454 Industrial Pkwy San Bernardino, Ca						
Piece Work	Location	ACCEPT	REJECT	ACCEPT REPAIR	REJECT REPAIR	Remarks
Col 10004 1/A	Moment Conn	✓				CJP A) Side T/B Flgs & Web
Col 10004 1/A	Moment Conn	✓				CJP B) Side T/B Flgs & Web
Equipment (brand) Sonatest	Model D-20	Serial No. I011912		Angle(s) <input checked="" type="checkbox"/> 70 <input type="checkbox"/> 60 <input type="checkbox"/> 45		
Transducer (brand) GE Gamma	Size .75 x .625	Frequency 2.25		Reference Level 40	Scanning Level 60	
Quality Requirements AWS D1.1 Clause 6 Table 6.2						
Remarks						

6/27/19 2673 Julian Razo
Dated Employee ID Name

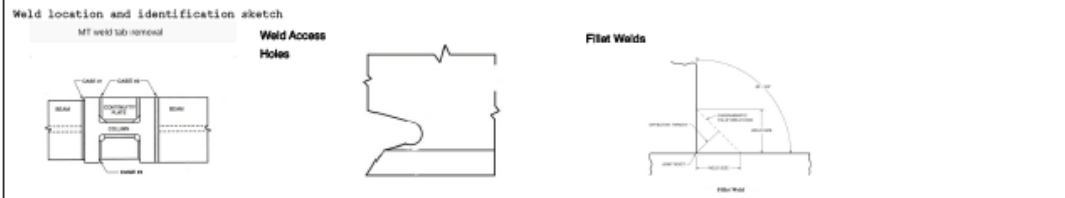
ALL REPORTS ARE SUBMITTED AS THE CONFIDENTIAL PROPERTY OF CLIENTS. AUTHORIZATION FOR PUBLICATION OF OUR REPORT, CONCLUSIONS, OR EXTRACTS FROM OR REGARDING THEM IS RESERVED PENDING OUR WRITTEN APPROVAL AS A MUTUAL PROTECTION TO CLIENTS, THE PUBLIC AND OURSELVES.
© 2004 Smith Emery Company

SMITH-EMERY COMPANY

DSA
 OSHFPD
 SE Job No. **New Job**
 Permit No. _____

REPORT OF MAGNETIC PARTICLE SHOP EXAMINATION

Job Name
AISC/UCSD
 Job Address
Worked performed at San Bernardino Steel 5454 Industrial Pkwy San Bernardino
 Jobsite Location (area/floor)



Piece Work	Location	ACCEPT	REJECT	ACCEPT	REJECT	Remarks
				REPAIR	REPAIR	
10002 1/A	Case 1 A side	✓				MT Weld tab removal 4 locations
10002 1/A	Case 1 B side	✓				MT Weld tab removal 4 locations
10003 1/A	Case 1 A side	✓				MT Weld tab removal 4 locations
10003 1/A	Case 1 B side	✓				MT Weld tab removal 4 locations
A5K1011	Case 1 A side	✓				MT Weld tab removal 4 locations

Equipment (brand) Magnaflux		Model Y7 AC/DC	Output 4 amps	Current 120 vol	Particle type Red Particle
Material Carbon Steel	Surface Clean	Test Temp. Ambient	Spacing 4-6 inches	Quality Requirement-section AWS D1.1 Sec 6	
Direction <input type="checkbox"/> Circular <input type="checkbox"/> Long <input checked="" type="checkbox"/> Both		Method of inspection <input type="checkbox"/> Prod <input checked="" type="checkbox"/> Yoke <input type="checkbox"/> Coil <input checked="" type="checkbox"/> AC <input type="checkbox"/> DC <input type="checkbox"/> Wet <input checked="" type="checkbox"/> Dry <input checked="" type="checkbox"/> Visible <input type="checkbox"/> Fluorescent			

7/1/19 2673 Julian Razo
 Dated Employee ID Name

ALL REPORTS ARE SUBMITTED AS THE CONFIDENTIAL PROPERTY OF CLIENTS. AUTHORIZATION FOR PUBLICATION OF OUR REPORT, CONCLUSIONS, OR EXTRACTS FROM OR REGARDING THEM IS RESERVED PENDING OUR WRITTEN APPROVAL AS A MUTUAL PROTECTION TO CLIENTS, THE PUBLIC AND OURSELVES.
 © 2014 Smith Emery Company

SMITH-EMERY COMPANY

SE Job No. _____

Permit No. _____

REPORT OF ULTRASONIC SHOP WELD TESTING

Job Name AISC/UCSD SMF Project		Work at performed at San Bernadino Steel				
Job Address 5454 Industrial Pkwy San Bernardino, Ca						
Piece Work	Location	ACCEPT	REJECT	ACCEPT REPAIR	REJECT REPAIR	Remarks
Col 10002 1/A	Moment Conn	✓				CJP A) Side T/B Flgs & Web
Col 10002 1/A	Moment Conn	✓				CJP B) Side T/B Flgs & Web
Col 10003 1/A	Moment Conn	✓				CJP B) Side T/B Flgs & Web
Col 10003 1/A	Moment Conn	✓				CJP B) Side T/B Flgs & Web
Assy A5K1011	Moment Conn	✓				CJP B) Side T/B Flgs & Web
Equipment (brand) Sonatest	Model D-20	Serial No. I011912		Angle(s) <input checked="" type="checkbox"/> 70 <input type="checkbox"/> 60 <input type="checkbox"/> 45		
Transducer (brand) GE Gamma	Size .75 x .625	Frequency 2.25		Reference Level 40	Scanning Level 60	
Quality Requirements AWS D1.1 Clause 6 Table 6.2						
Remarks						

7/1/19 2673 Julian Razo
 Dated Employee ID Name

ALL REPORTS ARE SUBMITTED AS THE CONFIDENTIAL PROPERTY OF CLIENTS. AUTHORIZATION FOR PUBLICATION OF OUR REPORT, CONCLUSIONS, OR EXTRACTS FROM OR REGARDING THEM IS RESERVED PENDING OUR WRITTEN APPROVAL AS A MUTUAL PROTECTION TO CLIENTS, THE PUBLIC AND OURSELVES.

APPENDIX C: CERTIFIED MILL TEST REPORTS

Specimen C5 Column

Invoice No. 749265
Bill of Lading 233608
Customer No. 7950
Customer P.O. 020255

NUCOR-YAMATO STEEL CO.
 P.O. BOX 1228; BLYTHEVILLE, AR 72316

CERTIFIED MILL TEST REPORT
100% Melted and Manufactured in U.S.A
 All Shapes produced by Nucor-Yamato Steel are cast and rolled to a fully-killed and fine grain practice.

Date: 2016-04-01

HERRICK CORPORATION
 BOX 8429
 STOCKTON CA 95208
 USA

SAN BERNARDINO STEEL
 C/O KEEP ON TRUCKING
 RANCHO CUCAMONGA, CA FOR TRK DEL TO
 SAN BERNARDINO CA 92295
 USA

ASTM A992/A992M-11 A572/A572M GR50-15
 ASTM A709/A709M-15 GR50T (345T)
 ASTM A709/A709M-15 GR50ST (345ST)
 CSA G40.21-13 50WMT (345WMT)
 ASTM A6/A6M-14

Item	Item Description	QTY	Heat#	Mechanical Properties										Chemical Properties (wt %)													
				Yield to Tensile Ratio	Yield Strength KSI	Yield Strength MPa	Tensile Strength KSI	Tensile Strength MPa	ELONG %	Charpy Impact			C	Mn	P	S	SI	Cu	Ni	Cr	Mo	V	Cb	CE	Sn	Pcm	CI
										Temp °F	Temp °C	Impact Energy ft-lbf															
1	W14X211.0 38 ft 0 in W360X314 (11.58 m)	1	452443	0.77 0.77	57 393	74 510	28 27	70 21	70 21	90 96	100 122	136	C	.08	1.31	.016	.021	.26	.27	.16	.14	.04	.04	.001	.37	.01	.18
2	W14X211.0 38 ft 0 in W360X314 (11.58 m)	4	452444	0.77 0.80	56 61	73 503	28 29	70 21	70 21	261 354	261 354	271 367	C	.08	1.31	.016	.019	.24	.28	.14	.14	.04	.05	.001	.37	.01	.18

ELONGATION BASED ON 8.00 INCH GAUGE LENGTH
 $P_{cm} = C + S/30 + Mn/20 + Cu/20 + Ni/60 + Cr/20 + Mo/15 + V/10 + Sb/10 + 5B$ (B=Approx .0005)
 Corrosion Index = $26.01(\%Cu) + 3.28(\%Ni) + 1.2(\%Cr) + 1.49(\%Si) + 17.28(\%P) - 7.29(\%Cu)(\%Ni) - 9.10(\%Ni)(\%P) - 33.39(\%Cu)^2$
 ISO 9001:2008 certified (Registration #0985-07)
 All mechanical testing is performed by the Quality Testing Lab, which is independent of the production departments.

CARBON EQUIVALENT CE = $C + Mn/6 + (Cr + Mo + V)/5 + (Ni + Cu)/15$
 Mercury has not been used in the direct manufacturing of this material.
 This material was produced in accordance with the Nucor-Yamato Steel Quality Manual.


I hereby certify that the contents of this report are accurate and correct. All test results and operations performed by this material manufacturer are in compliance with the requirements of the material specifications, and when designated by the purchaser, meet the applicable specifications.


 Doug Lennell
 Chief Metallurgist

State of Arkansas
 County of Mississippi
 Sworn to and subscribed before me
 on 2016-04-01
 My commission expires on 07/17/2023.



Specimen C3 Column

Contract No.				 INSPECTION CERTIFICATE EN 10204(2004) TYPE 3.1 ORIGINAL																PAGE: 1 / 31			
Customer		GS GLOBAL																		Factory		63, Jungbong-Daero, Dong-gu, Incheon, S. Korea	
PO No.		46201708AG11																		Certificate No.		IH20171203158-1	
L/C No.																				Class certificate No.			
Commodity		H-BEAM																		Issue date		2017-12-15	
Specification		ASTM A572 (50)/A992/CSA G40.21-13 50W/M(345W/M)																					

Dimensions	Length	Heat No.	Qty	Weight (kg)	Chemical Composition											Tensile Test			Yield Ratio	BEND TEST	Impact Test (J)			Remarks (Impact Specimen Size)		
					C	Si	Mn	P	S	Cr	Ni	Mo	Co	Al	N	Nb	Sn	CEq			Tensile Strength	Yield Strength	Elongation		V-Notch	2
14X16X257	45.00 FT	N 039862	1	5,246	33	19	139	8	2	15	5	1	7	4	40	3	9	40	587 532	410 407	27.5 28.0	0.764 0.766				
14X16X257	55.00 FT	N 039861	1	6,412	33	17	144	8	2	12	5	1	8	3	41	4	6	41	545 532	400 397	26.0 26.5	0.794 0.747				
14X16X257	55.00 FT	N 039862	3	19,236	33	19	139	8	2	15	5	1	7	4	40	3	9	40	537 532	410 407	27.5 28.0	0.764 0.766				
18X6X35	40.00 FT	E 201163	19	12,065	33	15	52	21	7	26	8	2	16	4	13	2	9	28	505 497	380 385	27.0 28.0	0.753 0.775				
18X6X35	40.00 FT	E 201164	8	5,080	35	16	52	28	3	27	9	2	22	5	14	2	10	31	508 502	388 382	27.0 27.5	0.764 0.761				
18X6X35	40.00 FT	E 201166	5	3,175	33	17	52	19	10	29	9	2	15	4	13	2	9	27	498 505	420 429	24.5 24.0	0.844 0.850				
18X6X35	45.00 FT	E 201165	3	2,142	33	14	51	19	7	25	9	2	15	4	11	2	9	27	495 490	413 404	27.0 28.0	0.835 0.825				
18X6X35	45.00 FT	E 201177	6	4,284	33	16	53	15	7	28	8	2	14	4	11	1	11	28	487 491	408 414	27.5 26.0	0.838 0.844				
18X6X35	45.00 FT	E 201178	6	4,284	33	18	57	12	9	19	6	1	11	4	12	2	8	27	468 472	371 374	29.5 29.0	0.793 0.793				
18X6X35	50.00 FT	E 201169	4	3,176	33	15	52	21	7	26	8	2	16	4	13	2	9	28	505 497	380 385	27.0 26.0	0.753 0.775				
SUB TOTAL			56	65,100																						

Note

(1) Ceq: (C+Mn/6+Cr/5+V/5+Mo/5+N/15+Cu/15)

(2) Gauge length : 200 mm

(3) Y.R = Y.S/T.S

WE HEREBY CERTIFY THAT THE MATERIAL HAS BEEN MADE AND TESTED IN ACCORDANCE WITH THE ABOVE SPECIFICATION AND ALSO WITH THE REQUIREMENTS CALLED FOR THE ABOVE ORDER.

J. C. Ahn
General Manager of QA Team

This test report can be verified the authenticity to scan the top-right QR code via 'Qreal' mobile app. 2017.12.18.10:28:17 2123266 2017.12.18.10:28:17

Job # 9870
PO # 987-L

Specimen C4, C6 or C7 Beam (for 2 Pieces)

NUCOR - YAMATO STEEL COMPANY

NUCOR - YAMATO STEEL COMPANY
 PO Box 1228
 Blytheville AR 72316
 USA

Date
2014-08-01

CERTIFIED MILL TEST REPORT
100% Melted and Manufactured in U.S.A
 All Shapes produced by Nucor-Yamato Steel are cast and rolled to a fully killed and fine grain practice

SOLD TO

SHIP TO

HERRICK CORPORATION BOX 8429 STOCKTON CA 95208 USA	STOCKTON STEEL C/O KEEP ON TRUCKING BNSF R/R STOCKTON, CA FOR TRK DEL TO STOCKTON CA 95212 USA	Invoice	Bill Of Lading
		646116	162479
		Customer No.	Customer P.O.
		1382	354-3
Specifications: ASTM A992/A992M-11 A572/A572M GR50-13a, ASTM A709/A709M-13a GR50 (345) , ASTM A709/A709M-13a GR50S (345S) , CSA G40.21-13 50WM (345WM) , ASTM A6/A6M-13a			

Product Description	Heat Quantity	Heat Number	Length
* W30X116.0 (W760X173)	8	426935	50 ft 4 in(15.34 m)

Mechanical Properties								
Yield To Tensile Ratio	UOM	Yield Strength	Tensile Strength	Elong %	Temp F/C	Impact Energy	Freq	Loc
0.79	KSI	57	72	28				
0.79	KSI	58	73	29				
	MPa	393	496	28				
	MPa	400	503	29				

Chemical Properties															
C	Mn	P	S	Si	Cu	Ni	Cr	Mo	V	Cb	Sn	CE	Pcm	Cl	
.08	1.10	.013	.023	.25	.23	.09	.12	.04	.00	.024	.01	.32	.16	.0	

ELONGATION BASED ON 8.00 INCH GAUGE LENGTH
 CARBON EQUIVALENT CE= C+Mn/6+(Cr+Mo+V)/5+(Ni+Cu)/15
 Pcm= C+Si/30+Mn/20+Cu/20+Ni/60+Cr/20+Mo/15+V/10+5B(B=Approx .0005)
 Mercury has not been used in the direct manufacturing of this material
 Corrosion Index= 26.01(%Cu)+3.88(%Ni)+1.2(%Cr)+1.49(%Si)+17.28(%P)-7.29(%Cu)(%Ni)-9.10(%Ni)(%P)-33.39(%Cu)^2

I hereby certify that the contents of this report are accurate and correct. All test results and operations performed by this material manufacturer are in compliance with the requirements of the material specifications, and when designated by the purchaser, meet the applicable specifications.

Doug Lennell
 Chief Metallurgist

State of Arkansas
 County of Mississippi
 Sworn to and subscribed before me

on 2014-08-01 *Deborah Ann Rhoads*
 My commission expires on 07/17/2023



Invoice No.	796989
Bill of Lading	267158
Customer No.	7873
Customer P.O.	877-7

NUCOR-YAMATO STEEL CO.
P.O. BOX 1228: BLYTHEVILLE, AR 72316

CERTIFIED MILL TEST REPORT	
100% Melted and Manufactured in U.S.A All Shapes produced by Nucor-Yamato Steel are cast and rolled to a fully killed and fine grain practice	
Date	2017-01-20

Specimen C6 Column

HERRICK CORPORATION
BOX 8429
STOCKTON CA 95208
USA

STOCKTON STEEL CO
KEEP ON TRUCKING BNSF R/R
STOCKTON, CA FOR TRK
DEL TO STOCKTON CA 95212
USA

ASTM A992/A992M-11 A572/A572M GR50-15
ASTM A709/A709M-15 GR50 (345)
ASTM A709/A709M-15 GR50S (345S)
CSA G40.21-13 50WM (345WM)
ASTM A6/A6M-14

Item#	Item Description	QTY	Heat#	Mechanical Properties							Chemical Properties																
				Yield to Tensile Ratio	Yield Strength		Tensile Strength	ELONG	Charpy Impact			C	Mn	P	S	Si	Cu	Ni	Cr	Mo	V	Cb	CE	Sn	Pcm	Cl	
					KSI	MPa			KSI	MPa	%																Temp
1	W24X131.0 58 ft 8 in W610X195 (17.88 m)	1	463933	0.76 0.79	55 57 379 393	72 72 496 496	28 27							.07	1.10	.016	.027	.23	.28	.11	.16	.03	.01	.020	.32	.01	.16
* 2	W24X176.0 40 ft 0 in W610X262 (12.19 m)	3	463912	0.74 0.75	55 57 379 393	74 76 510 524	26 27							.08	1.36	.018	.022	.21	.25	.12	.14	.05	.05	.000	.37	.01	.18

ELONGATION BASED ON 8.00 INCH GAUGE LENGTH
 $P_{cm} = C + Si/30 + Mn/20 + Cu/20 + Ni/60 + Cr/20 + Mo/15 + V/10 + S/8 (B = Approx .0005)$
 Corrosion Index = $26.01(\%Cu) + 3.88(\%Ni) + 1.2(\%Cr) + 1.49(\%Si) + 17.28(\%P) - 7.29(\%Cu)(\%Ni) - 9.10(\%Ni)(\%P) - 33.39(\%Cu)^2$
 ISO 9001:2008 certified (Registration # 0985-07).
 All mechanical testing is performed by the Quality Testing Lab, which is independent of the production departments.

I hereby certify that the contents of this report are accurate and correct. All test results and operations performed by this material manufacturer are in compliance with the requirements of the material specifications, and when designated by the purchaser, meet the applicable specifications.

Doug Lonnell
Chief Metallurgist

State of Arkansas
County of Mississippi
Sworn to and subscribed before me
on 2017-01-20
My commission expires on 07/17/2023



Specimen C7 Column



台安路104-1, 桃園市八德區
6F, No. 104, Sec. 1, Chung-an E.Rd., Taipai City 104-1, Taiwan
Tel: 886-2-2551-1100 Fax: 886-2-2552-6520

Mild Works
No. 22, Pingding, Wuu Village,
Sihu Township, Miaoli County 36842, Taiwan

材質證明書 (出廠證明書)

MILL TEST CERTIFICATE
In accordance with ASTM A992

發證日期 DATE OF ISSUE	Aug-31-2016
證書編號 CERTIFICATE NO.	H07815

客戶名稱 CUSTOMER	THYSSENKRUPP STEEL SERVICES		出貨日期 SHIPPING DATE	Aug. 30, 2016																		
合約號碼 CONTRACT NO.	U51607 (ORDER NO.:H318030)		貨品名稱 COMMODITY	WIDE FLANGE BEAMS																		
專案工程號碼 PROJECT NO.	500811		總重量 TOTAL WEIGHT	*1,170,785 (kg)																		
標準 STANDARD	ASTM A992-11		捆包(英)數 BUNDLES (PIECES)	**0 捆 (**902 磅)																		
備註 REMARKS	CREDIT NO. (ISSUING BANK):																					
產品尺寸 PRODUCT DIMENSIONS		機械性能 MECHANICAL PROPERTY				化學成份 CHEMICAL COMPOSITION (%)						型式	試驗									
規格 SPECIFICATION	重量 WEIGHT	長度 LENGTH	厚度 HEAT NO.	屈服 YIELD	抗拉 TENSILE	伸長 EL.	斷面收縮 RA.	C	Mn	P	S	CU	NI	CR	MO	V	Nb	TI	Co	其他	試驗	
單位 UNIT	mm	mm		MPa	MPa	%	%	%	%	%	%	%	%	%	%	%	%	%	%	%	OK	TEST
W 24x127x1750	35.00	8,381	H03341	345	450	23.0	13	0.025	0.005	0.005	0.005	0.005	0.005	0.005	0.005	0.005	0.005	0.005	0.005	0.005	OK	
W 24x127x1750	43.00	9,328	H03341	354	453	23.7	13	0.025	0.005	0.005	0.005	0.005	0.005	0.005	0.005	0.005	0.005	0.005	0.005	0.005	OK	
W 24x127x1830	40.00	8,640	H03307	358	455	23.3	13	0.025	0.005	0.005	0.005	0.005	0.005	0.005	0.005	0.005	0.005	0.005	0.005	0.005	OK	
W 24x127x1830	47.00	9,528	H03340	354	453	23.7	13	0.025	0.005	0.005	0.005	0.005	0.005	0.005	0.005	0.005	0.005	0.005	0.005	0.005	OK	
W 27x141x1830	50.00	10,810	H03362	372	472	24.5	14	0.025	0.005	0.005	0.005	0.005	0.005	0.005	0.005	0.005	0.005	0.005	0.005	0.005	OK	
				<p>此證明書係根據本廠之檢驗報告而發出。若需複核或更正，請向本廠索取。此證明書之內容不得作為任何法律之依據。本廠對本證明書之內容不負責任。</p> <p>This mill test certificate report covers only the material as it is shipped and is not intended for use as a substitute for the original test report. If duplicated, corrected, or omitted, all data and the certified material test report are thereby invalid.</p> <p>我們特此證明，本廠所生產之材料均符合本廠之規格。本廠對本證明書之內容不負責任。</p> <p>We hereby certify that the material herein described has been manufactured in accordance with the standards and specification specified by you and that it satisfies the requirements.</p> <p>本廠對本證明書之內容不負責任。</p> <p>The input of test values with underline are invalid.</p>				<p>東和鋼鐵 企業股份 有限公司 材質證明書</p>				<p>品質管理 品質控制經理</p> <p>鄧凱晶</p>										

San Doc: 201603001
JIT # 9870
PO # 987-2

Invoice No.	805912
Bill of Lading	273183
Customer No.	7950
Customer P.O.	381-26

NUCOR-YAMATO STEEL CO.
P.O. BOX 1228: BLYTHEVILLE, AR 72316

CERTIFIED MILL TEST REPORT
100% Melted and Manufactured in U.S.A
All Shapes produced by Nucor-Yamato Steel are cast and rolled to a fully killed and fine grain practice

Date	2017-02-20
------	------------

Specimen C6-G
Column 10006

HERRICK CORPORATION
BOX 8429
STOCKTON CA 95208
USA

SAN BERNARDINO STEEL
C/O KEEP ON TRUCKING
RANCHO CUCAMONGA, CA FOR TRK DEL TO
SAN BERNARDINO CA 92235
USA

ASTM A992/A992M-11 A572/A572M GR50-15
ASTM A709/A709M-15 GR50 (345)
ASTM A709/A709M-15 GR50S (345S)
CSA G40.21-13 50WM (345WM)
ASTM A6/A6M-14

Item#	Item Description	QTY	Heat#	Mechanical Properties							Chemical Properties																	
				Yield to Tensile Ratio	Yield Strength	Tensile Strength	ELONG	Charpy Impact			C	Mn	P	S	Si	Cu	Ni	Cr	Mo	V	Cb	CE	Sn	Pcm	Cl			
					KSI	KSI		%	Temp	Impact Energy																Loc		
1	W24X176.0 29 ft 0 in W610X262 (8.84 m)	1	460158	0.77 0.76	57 57 393 393	74 75 510 517	27 26								.08	1.35	.016	.018	.27	.26	.11	.16	.04	.05	.001	.38	.01	.19
2	W24X176.0 29 ft 0 in W610X262 (8.84 m)	9	465327	0.77 0.77	57 56 393 386	74 73 510 503	28 28								.07	1.35	.015	.020	.25	.26	.10	.09	.03	.05	.001	.35	.01	.17
3	W24X176.0 58 ft 4 in W610X262 (17.78 m)	4	465327	0.77 0.77	57 56 393 386	74 73 510 503	28 28								.07	1.35	.015	.020	.25	.26	.10	.09	.03	.05	.001	.35	.01	.17
4	W24X176.0 29 ft 0 in W610X262 (8.84 m)	2	465328	0.77 0.77	56 56 386 386	73 73 503 503	28 28								.07	1.35	.014	.020	.24	.25	.12	.11	.03	.05	.001	.36	.01	.18

ELONGATION BASED ON 8.00 INCH GAUGE LENGTH
 Pcm= C+Si/30+Mn/20+Cu/20+Ni/60+Cr/20+Mo/15+V/10+5B(B=Approx .0005)
 Corrosion Index= 25.01(%Cu)+3.88(%Ni)+1.2(%Cr)+1.49(%Si)+17.28(%P)-7.29(%Cu)(%Ni)-9.10(%Ni)(%P)-33.39(%Cu)^2
 ISO 9001:2008 certified (Registration # 0985-07).
 All mechanical testing is performed by the Quality Testing Lab, which is independent of the production departments.

I hereby certify that the contents of this report are accurate and correct. All test results and operations performed by this material manufacturer are in compliance with the requirements of the material specifications, and when designated by the purchaser, meet the applicable specifications.

Doug Linnell
Chief Metallurgist

State of Arkansas
County of Mississippi
Sworn to and subscribed before me
on 2017-02-20
My commission expires on 07/17/2023



Specimen C4, C6 or C7 Beam



CERTIFIED MILL TEST REPORT

Customer # 000442

Printed: 10 / 09 / 2016
Produced: 09 / 25 / 2016

(260) 625-8100 (260) 625-8950 FAX
Quality Steel 100% EAF Melted
and Manufactured in the USA
Recycled content: PC = 77.0%, PI = 19.4%
ISO 9001:2009 and ABS Certified

GENERAL INFORMATION		SPECIFICATIONS		SHIPMENT DETAILS		BOL # 0000426810 - 41006.00 lbs	
Product	Wide Flange Beam	Standards	Grades	Bundle / ASN #	Length	pcs	Cust PO Recv PO Job
* Size	W30X116	ASTM A6/A6M - 16	A992 / A992M	022298029	50' 6"	1	A3482-00013 Project Sarah
Heat Number	A127163	ASTM A992/A992M - 11	A709 gr50/gr345	022298031	50' 6"	1	A3482-00019 Project Sarah
Condition(s)	As-Rolled Fine Grained Fully Killed No Weld Repair	ASTM A709/A709M - 16a ASTM A572/A572M - 15 AASHTO M270M/M270 - 12 ASTM A36/A36M - 14 CSA G40.21-13	A572 gr50/gr345 M270 gr345/gr50 A36 / A36M 50W/350W	022298037	50' 6"	1	A3482-00019 Project Sarah
				022298034	50' 6"	1	A3482-00019 Project Sarah
				022298035	50' 6"	1	A3482-00019 Project Sarah
				022298036	50' 6"	1	A3482-00019 Project Sarah
				022298032	50' 6"	1	A3482-00019 Project Sarah

CHEMICAL ANALYSIS (weight percent)

C	Mn	P	S	Si	Cu	Ni	Cr	Mo	Sn	V	Nb/Cb	Al	N	B	*C1	*C2	*C3	*PC	*I	Analysis Type
.07	1.23	.014	.025	.23	.30	.10	.10	.031	.011	.035	.001	.001	.0142	.0003	.33	.37	.31	.16	5.64	Heat

MECHANICAL TESTING

Test	Yield (fy) Strength ksi / MPa	Tensile (fu) Strength ksi / MPa	fy / fu ratio	% Elong. (8" gage)
1	57 / 392	71 / 489	.80	30
2	58 / 403	72 / 494	.81	27
3				
4				

CHARPY IMPACT TESTS (available only when specified at time of order)

Test	Temp		Absorbed Energy		Specimen 3	Average	Minimum
	F / C		Specimen 1	Specimen 2			
1							
2							
3							
4							
5							
6							
7							

Notes: *Calculated Chemistry Values: Carbon Equivalents (C1, C2, C3, PC), Corrosion Index (I) 1 (ASTM G101) = 23.01[Cu] + 3.85[Ni] + 1.23[Cr] + 1.49[S] + 17.29[P] + 7.25[Cu] + 9.16[Ni] + 33.23[Cu]
CE1 (IV) = C + Mn/8 + (Cr+Mo+V)/5 + (Ni+Cu)/15 CE2 (AWS) = C + (Mn+Si)/8 + (Cr+Mo+V)/5 + (Ni+Cu)/15 CE3 (CET) = C + (Mn/6) + (Si/24) + (Cr/5) + (Ni/40) + (Mo/9) + (V/14) Pcm (AWS) = C + Si/30 + Mn/20 + Cu/20 + Ni/60 + Cr/10 + Mo/15 + V/10 + S

I hereby certify that the material described herein has been made to the applicable specification by the electric arc furnace/continuous cast process and tested in accordance with the requirements of American Bureau of Shipping Rules with satisfactory results.

ABS CERTIFICATION

Signed: _____
I hereby certify that the content of this report are accurate and correct. All tests and operations performed by this material manufacturer are in compliance with the requirements of the material specifications and applicable purchaser designated requirements.
Signed: **Jeremy Cronkhite**
Quality Manager

State of Indiana, County of Whitley Sworn to and subscribed before me
this _____ day of _____
Signed: _____ My commission expires: _____
Notary Public

ASTM A6 - 14.6: A signature is not required on the test report; however, the document shall clearly identify the organization submitting the report. Notwithstanding the absence of a signature, the organization submitting the report is responsible for the content of the report. **San Diego Steel**
Job # 9870
PO # 987-2

Specimen C4 Beam 30006

Contract No.	
Customer	GS GLOBAL
PO No.	46201706A802
I/C No.	
Commodity	H-BEAM
Specification	ASTM A572 GR50/A992/CSA G40.21-13 50MM(345MM)

INSPECTION CERTIFICATE

EN 10204(2004) TYPE 3.1

ORIGINAL



PAGE: 13/91

Factory	6363,Donghaean-ro,Nam-gu,Pohang-si,Gyeongsangbuk-do,Korea
Certificate No.	IH20170908315-3
Class certificate No.	
Issue date	2017-09-23

Dimensions	Length	Heat No.	Quantity (PCS)	Weight (kg)	Chemical Composition															Tensile Test			Yield Ratio (%)	BEND TEST	Impact Test(L)			Remarks (Impact Specimen Size)		
					C	Si	Mn	P	S	Cu	Ni	Mo	Cr	Al	V	Nb	Sn	CEq	Tensile Strength	Yield Strength	Elongation (%)	V-Notch			1	2	3			
					x100					x1000					x100					x1000					x100					N/mm2
30X10-1/2X99	60.00 FT	3G7359	11	29,634	17	16	102	23	9	24	8	2	16	4	29	1	12	40	546	405	27.5									
30X10-1/2X99	65.00 FT	3G6997	4	11,672	18	15	103	17	9	20	8	2	12	3	32	2	9	40	536	403	26.5									
30X10-1/2X116	35.00 FT	3G6076	3	5,523	17	15	104	15	7	17	8	2	10	4	30	2	7	39	557	401	24.1									
30X10-1/2X116	45.00 FT	3G7361	1	2,367	17	13	103	21	10	23	10	2	15	3	28	2	12	40	570	416	25.0									
30X10-1/2X116	45.00 FT	3G7362	3	7,101	18	15	103	18	10	22	9	2	14	3	54	2	11	42	574	425	23.4									
30X10-1/2X116	50.00 FT	3G7001	1	2,630	17	15	101	19	9	18	8	2	11	3	30	2	8	39	555	423	25.3									
30X10-1/2X116	50.00 FT	3G7002	2	5,260	17	16	102	24	9	22	9	2	15	3	30	2	9	40	551	416	25.0									
30X10-1/2X116	50.00 FT	3G7003	1	2,630	18	15	103	21	13	21	9	2	11	3	29	2	9	40	554	428	25.1									
30X10-1/2X116	55.00 FT	3G7361	4	11,572	17	13	103	21	10	23	10	2	15	3	28	2	12	40	570	416	25.0									
30X10-1/2X116	60.00 FT	3G7361	15	47,340	17	13	103	21	10	23	10	2	15	3	28	2	12	40	570	416	25.0									
SUB TOTAL			45	125,729																										

Conditions of supply : As Rolled
 (1) Ceq : (C+Mn/6+Cr/5+V/5+Mo/5+Ni/15+Cu/15)
 (2) Gauge length : 200 mm
 (3) YR = Y.S/1.5

Note

WE HEREBY CERTIFY THAT THE MATERIAL HAS BEEN MADE AND TESTED IN ACCORDANCE WITH THE ABOVE SPECIFICATION AND ALSO WITH THE REQUIREMENTS CALLED FOR THE ABOVE ORDER.

[Signature]
 General Manager of QA Team.

Specimen C3 or C5 Beam

(.4)

NUCOR - YAMATO STEEL COMPANY
 PO Box 1228
 Blytheville AR 72316
 USA

NUCOR - YAMATO STEEL COMPANY

Date
 2014-03-31

CERTIFIED MILL TEST REPORT
100% Melted and Manufactured in U.S.A
 All Shapes produced by Nucor-Yamato Steel are cast and rolled to a fully killed and fine grain practice

SOLD TO

SHIP TO

HERRICK CORPORATION BOX 8429 STOCKTON CA 95208 USA	SAN BERNARDINO STEEL C/O KEEP ON TRUCKING RANCHO CUCAMONGA, CA FOR TRK DEL TO SAN BERNARDINO CA 92235 USA	Invoice	Bill Of Lading
		621653	148116
		Customer No.	Customer P.O.
		1382	349-3

Specifications: ASTM A992/A992M-11 A572/A572M GR50-13a, ASTM A709/A709M-13a GR50 (345), ASTM A709/A709M-13a GR50S (345S), CSA G40.21-13 50WM (345WM), ASTM A6/A6M-13a

Product Description	Heat Quantity	Heat Number	Length
* W36X150.0 (W920X223)	5	421418	62 ft 0 in(18.90 m)

Mechanical Properties								
Yield To Tensile Ratio	UOM	Yield Strength	Tensile Strength	Elong %	Temp F/C	Impact Energy	Freq	Loc
0.79	KSI	57	72	28				
0.77	KSI	55	71	24				
	MPa	393	496	28				
	MPa	379	490	24				

Chemical Properties															
C	Mn	P	S	SI	Cu	NI	Cr	Mo	V	Cb	Sn	CE	Pcm	CI	
.08	1.10	.019	.028	.25	.24	.08	.12	.03	.01	.019	.01	.32	.17	.0	

ELONGATION BASED ON 8.00 INCH GAUGE LENGTH
 Pcm= C+Si/30+Mn/20+Cu+Ni/60+Cr/20+Mo/15+V/10+5B[B=Approx .0005]
 Corrosion Index= 26.01(%Cu)+3.88(%Ni)+1.2(%Cr)+1.49(%S)+17.28(%P)-7.29(%Cu)(%Ni)-9.10(%Ni)(%P)-33.39(%Cu)^2
 CARBON EQUIVALENT CE= C+Mn/6+(Cr+Mo+V)/5+(Ni+Cu)/15
 Mercury has not been used in the direct manufacturing of this material

I hereby certify that the contents of this report are accurate and correct. All test results and operations performed by this material manufacturer are in compliance with the requirements of the material specifications, and when designated by the purchaser, meet the applicable specifications.

Ray Linnell
 Chief Metallurgist

State of Arkansas
 County of Mississippi
 Sworn to and subscribed before me
 on 2014-03-31
 My commission expires on 07/17/2023



Specimen C3 or C5 Beam

Invoice No.	702784
Bill of Lading	200367
Customer No.	7873
Customer P.O.	357-3

NUCOR-YAMATO STEEL CO.
P.O. BOX 1226 BLYTHEVILLE, AR 72316

(C7)

CERTIFIED MILL TEST REPORT
100% Melted and Manufactured in U.S.A
All Shapes produced by Nucor-Yamato Steel are cast and rolled to a fully killed and fine grain practice

Date: 2015-07-01

SP 5.30

HERRICK CORPORATION
BOX 8429
STOCKTON CA 95208
USA

183

STOCKTON STEEL CO
KEEP ON TRUCKING BNSF R/R
STOCKTON, CA FOR TRK
DEL TO STOCKTON CA 95212
USA

ASTM A992/A992M-11 A572/A572M GR50-13a
ASTM A709/A709M-13a GR50 (345)
ASTM A709/A709M-13a GR50S (345S)
CSA G40.21-13 50WM (345WM)
ASTM A6/ABM-14

Item	Item Description	Qty	Heat#	Mechanical Properties						Chemical Properties (wt %)																		
				Yield to Tensile Ratio	Yield Strength		Tensile Strength	ELONG	Charpy Impact			C	Mn	P	S	Si	Cu	Ni	Cr	Mo	V	Cb	CE	Sn	Pcm	Ct		
					KSI	KSI			%	Temp	Impact Energy																Loc	
1	W36X150.0 39 ft 4 in W920X223 (11.99 m)	1	440886	0.77	54	70	28								.08	1.17	.017	.027	.20	.26	.11	.17	.04	.00	.019	.34	.01	.17
2	W36X150.0 54 ft 8 in W920X223 (16.66 m)	1	440886	0.77	55	71	27								.08	1.17	.017	.027	.20	.26	.11	.17	.04	.00	.019	.34	.01	.17
3	W36X150.0 61 ft 8 in W920X223 (18.80 m)	2	440889	0.77	55	71	28								.07	1.12	.011	.022	.22	.29	.09	.11	.02	.00	.019	.31	.01	.16
4	W36X150.0 64 ft 0 in W920X223 (19.51 m)	1	440893	0.77	55	71	28								.07	1.10	.014	.027	.19	.29	.12	.13	.04	.01	.021	.32	.01	.16
5	W36X150.0 54 ft 0 in W920X223 (16.46 m)	2	440895	0.76	55	72	29								.08	1.10	.013	.022	.21	.25	.12	.12	.04	.00	.019	.32	.01	.16
6	W36X160.0 56 ft 4 in W920X238 (17.17 m)	1	440911	0.77	55	71	28								.08	1.10	.010	.024	.22	.27	.11	.10	.03	.00	.029	.31	.01	.16

ELONGATION BASED ON 8.00 INCH GAUGE LENGTH
 $Pcm = C + S(30 + Mn/20 + Cu/20 + Ni/60 + Cr/20 + Mo/15 + V/10 + 5B) \approx .0005$
 CARBON EQUIVALENT $CE = C + Mn/6 - (Cr + Mo + V)/5 + (Ni + Cu)/15$
 Mercury has not been used in the direct manufacturing of this material.
 Corrosion Index = $26.01(\%Cu) + 3.88(\%Ni) + 1.2(\%Cr) + 1.49(\%Si) + 17.28(\%P) - 7.29(\%Cu)(\%Ni) - 9.10(\%Ni)(\%P) - 33.39(\%Cu)^2$
 ISO 9001:2008 certified (Registration # 0985-07).
 All mechanical testing is performed by the Quality Testing Lab, which is independent of the production departments.

I hereby certify that the contents of this report are accurate and correct. All test results and operations performed by this material manufacturer are in compliance with the requirements of the material specifications, and when designated by the purchaser, meet the applicable specifications.

Doug Linnell
Chief Metallurgist

State of Arkansas
County of Mississippi
Sworn to and subscribed before me
on 2015-07-01
My commission expires on 07/17/2023



Invoice No.	913776
Bill of Lading	347625
Customer No.	7950
Customer P.O.	987-1

NUCOR-YAMATO STEEL CO.
P.O. BOX 1228: BLYTHEVILLE, AR 72316

CERTIFIED MILL TEST REPORT	
100% Melted and Manufactured in U.S.A	
All Shapes produced by Nucor-Yamato Steel are cast and rolled to a fully killed and fine grain practice	
Date	2018-09-24

S
O
L
D
T
O
HERRICK CORPORATION
BOX 8429
STOCKTON CA 95208
USA

S
H
I
P
T
O
SAN BERNARDINO STEEL
C/O KEEP ON TRUCKING
RANCHO CUCAMONGA, CA FOR TRK DEL TO
SAN BERNARDINO CA 92235
USA

ASTM A992/A992M-11 A572/A572M GR50-15
ASTM A709/A709M-15 GR50T (345T)
ASTM A709/A709M-15 GR50ST (345ST)
CSA G40.21-13 50WMT (345WMT)
ASTM A6/A6M-14

Item#	Item Description	QTY	Heat#	Mechanical Properties										Chemical Properties															
				Yield to Tensile Ratio	Yield Strength		Tensile Strength	ELONG	Charpy Impact			C	Mn	P	S	Si	Cu	Ni	Cr	Mo	V	Cb	CE	Sn	Pcm	Cl			
					KSI	MPa			KSI	MPa	%																Temp	Impact Energy	Loc
																											* F	ft* lbf	
1	W27X235.0 27 ft 4 in W690X350 (8.33 m)	1	488640	0.73 0.76	52 54 356 370	71 71 490 490	28 26	70 21	99 134	141 191	114 155	Cor	.08	1.31	.013	.022	.20	.27	.13	.19	.05	.04	.001	.38	.01	.19			

ELONGATION BASED ON 8.00 INCH GAUGE LENGTH
 $Pcm = C + Si/30 + Mn/20 + Cu/20 + Ni/60 + Cr/20 + Mo/15 + V/10 + 5B$ (B=Approx. .0005)
Corrosion Index = $25.01(\%Cu) + 3.88(\%Ni) + 1.2(\%Cr) + 1.49(\%Si) + 17.28(\%P) - 7.29(\%Cu)^2 - 9.10(\%Ni)(\%P) - 33.39(\%Cu)^2$
 ISO 9001:2015 certified (Registration # 0985-07).
 All mechanical testing is performed by the Quality Testing Lab, which is independent of the production departments.
 The Charpy machine striker geometry used by Nucor-Yamato Steel is the 8 mm (0.315")striker (KVg) per ASTM A370 Section 22.1.2 and ISO 148-1 Section 7.3.

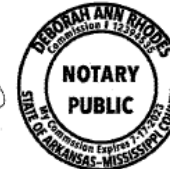
CARBON EQUIVALENT CE = $C + Mn/6 + (Cr + Mo + V)/5 + (Ni + Cu)/15$
 Mercury has not been used in the direct manufacturing of this material.
 This material was produced in accordance with the Nucor-Yamato Steel Quality Manual.

I hereby certify that the contents of this report are accurate and correct. All test results and operations performed by this material manufacturer are in compliance with the requirements of the material specifications, and when designated by the purchaser, meet the applicable specifications.

Doug Lennell
Chief Metallurgist


State of Arkansas
County of Mississippi
Sworn to and subscribed before me

on 2018-09-24
My commission expires on 07/17/2023



REPORT OF CHEMICAL/PHYSICAL TESTS

CERTIFICATE NO.	DATE	PAGE
1595258	Mar 07, 2018	1
MILL ORDER NO.	DATE	
319495		
CUSTOMER ORDER NO.		
20018-013		
JOB/REQ. NO.		
SHIPPING NO.	DATE	
1595258	03/07/2018	
CARRIER		
BURLINGTON NORTHERN		
CAR/TRUCK NO.		
PINK		

	SOLD TO	HERRICK CORPORATION [SAN BERNARDINO] PO BOX 8429 ATTN: ERIN BILLINGSLEY STOCKTON, CA 95208 USA	THE HERRICK CORPORATION PO BOX 8429 (95208) 3003 E. HAMMER LANE STOCKTON, CA 95212 USA
		THIS MATERIAL HAS BEEN MANUFACTURED, TESTED AND FOUND TO MEET THE SPECIFICATIONS AND PURCHASE ORDER REQUIREMENTS HSLA STRUCTURAL QUALITY PLATE ASTM A572-15 GRADE 50 ASME SA572 GRADE 50 2017 ASTM A709-17 GRADE 50 - KILLED FINE GRAIN PRACTICE.	

PHYSICAL PROPERTIES											
ITEM NO.	DESCRIPTION	HEAT NO.	SLAB	YIELD PSI X 100	TENSILE PSI X 100	% ELONG 8" 2"	% RA	HARDNESS BHN	BEND TEST	IMPACTS	
1	0.3750 X 96.000ME X 360.000										
	6 PCS 22050 LBS *	N17266		625	815	31		(OUTER)			
				640	825	19		(INNER)			
	3 PCS 11025 LBS	N17268		630	805	28		(OUTER)			
				640	805	18		(INNER)			
2	0.5000 X 96.000ME X 360.000										
	2 PCS 9802 LBS	N16987		740	910	23		(OUTER)			
				700	815	18		(INNER)			
	11 PCS 42877 LBS TOTALS										

CHEMICAL ANALYSIS																		
HEAT NO.	C	Mn	P	S	Si	Cu	Ni	V	Co	Al	Cr	Mo	Ti	B	N	Ca	CE	McQuaid Grain Size
N17266	.14	1.08	.011	.004	22	.01	.05	.016	.017	.044	.02	.00	.000		.0042			
N17268	.14	1.07	.014	.004	24	.01	.05	.020	.018	.039	.02	.00	.000		.0053			
N16987	.14	1.10	.015	.004	22	.01	.06	.021	.016	.031	.02	.00	.000		.0075			
HEATS INDICATED WITH (+) WERE MELTED & MANUFACTURED IN THE USA. HEATS INDICATED WITH (^) WERE ROLLED IN THE USA.																		
..... END OF REPORT																		

I certify the above to be correct as contained in the records of EVRAZ INC. NA By _____

Charles R. [Signature]
 Quality Coordinator

N17707

EVRAZ EVRAZ INC. NA
Evraz Oregon Steel 14400 N. Rivergate Blvd., Portland, Oregon 97203

REPORT OF CHEMICAL/PHYSICAL TESTS

CERTIFICATE NO.	DATE	PAGE
1606207	May 15, 2018	1
MILL ORDER NO.	DATE	
294363		
CUSTOMER ORDER NO.		
LSI JOBBER		
FORMEL NO.		
1048		
SHIPPING NO.	DATE	
1606207	05/15/2018	
CARRIER	BURLINGTON NORTHERN	
CARTRUCK NO.	TTPXB2205	

ISO 9001 REGISTERED CERTIFIED ORGANIZATION	SOLD TO	OREGON STEEL MILL OSH JOBBER 14400 N. RIVERGATE BLVD PORTLAND, OR 97203
		LSI PLATE W.O.# <u>252-16280</u> CUSTOMER <u>San Bernardino</u> P.O.# <u>20018049</u> DATE <u>05/10/18</u>

THIS MATERIAL HAS BEEN MANUFACTURED, TESTED AND FOUND TO MEET THE SPECIFICATIONS AND PURCHASE ORDER REQUIREMENTS
 A572 STRUCTURAL QUALITY PLATE ASTM A572-13A GRADE 50 ASME SA572 GRADE 50 2013.
 KILLED FINE GRAIN PRACTICES.

PHYSICAL PROPERTIES

ITEM	DESCRIPTION	HEAT NO.	SLAB	YIELD PSI X 100	TENSILE PSI X 100	% ELONG 8" 2"	% RA	HARDNESS BHN	BEND TEST	IMPACTS
1	0.6250 X 96.0000 X 360.000									
	4 PCS 24504 LBS	N17355		640	815	29				
				575	765	20				
	4 PCS 24504 LBS	N17707		510	705	29				
				525	718	27				
	8 PCS 49008 LBS TOTALS									

CHEMICAL ANALYSIS

HEAT NO.	C	Mn	P	S	Si	Cr	Ni	V	Co	Al	Ca	Mo	Ti	B	N	CE	Max
N17355	.16	1.10	.013	.006	.21	.01	.05	.052	.000	.032	.03	.00	.000		.0150		
N17707	.14	1.03	.010	.006	.22	.01	.05	.016	.013	.048	.02	.00	.002		.0041		

HEATS INDICATED WITH (+) WERE MELTED & MANUFACTURED IN THE USA. HEATS INDICATED WITH (*) WERE ROLLED IN THE USA.

END OF REPORT

I certify the above to be correct as contained in the records of EVRAZ INC. NA By San Bernardino Steel

Job # STK
 PO # 20018049

Specimen C6-G Stiffener Plate p116

NUCOR
NUCOR CORPORATION
NUCOR STEEL UTAH

Mill Certification

10/11/2018

MTR#:96146-
Lot #:120200556720
W CEMETERY ROAD
PLYMOUTH, UT 84330 US
800-453-2686
Fax: 435-458-2309

Sold To: INTSEL STEEL WEST LLC
PO BOX 21119
HOUSTON, TX 77226 US

Ship To: INTSEL STEEL WEST - SALT LAKE
1887 S 700 W
SALT LAKE CITY, UT 84104 US

Customer PO	SLC-14255	Sales Order #	12010074 - 9.1
Product Group	Hot Roll - Merchant Bar Quality	Product #	3017258
Grade	Nucor Multigrade	Lot #	120200556720
Size	0.5" x 6"	Heat #	1202005567
BOL #	BOL-190444	Load #	96146
Description	Hot Roll - Merchant Bar Quality Flat 1/2" x 6" Nucor Multigrade 20' 0" [240"] 2001-6000 lbs	Customer Part #	
Production Date	06/16/2018	Qty Shipped LBS	16332
Product Country Of Origin	United States	Qty Shipped EA	80
Original Item Description		Original Item Number	

I hereby certify that the material described herein has been manufactured in accordance with the specifications and standards listed above and that it satisfies those requirements.

Melt Country of Origin : United States

Melting Date: 06/13/2018

C (%)	Mn (%)	P (%)	S (%)	Si (%)	Ni (%)	Cr (%)	Mo (%)	Cu (%)	Ti (%)	V (%)	Nb (%)
0.18	0.69	0.006	0.026	0.23	0.08	0.09	0.02	0.30	0.001	0.023	0.000
Sn (%)	0.010										
ASTM A529 S78.2 CE (%) : 0.38											
ASTM A992 5.4 CE (%) : 0.35											
Other Test Results											
Yield (PSI) : 54900				Yield (PSI) : 55000				Tensile (PSI) : 75300			
Tensile (PSI) : 75200				Elongation in 8" (%) : 34.0				Elongation in 8" (%) : 33.0			


Comments:

NUCOR MULTIGRADE MEETS THE REQUIREMENTS OF:
ASTM A36/A36M-14, A529/A529M-14 GR50,
A572/A572M-18 GR50, A709/A709M-11e1 GR36/50 NO CVN,
CSA G40.21-13 GR44W(300W)/GR50W(350W),
AASHTO M270/M270M-15 GR36/GR50, ASME SA36/SA36M-13

Nucor-Plymouth is an ISO-9001 and an ABS certified mill. CMTR complies with DIN EN 10204 - 3.1 All manufacturing processes of the steel materials in this product, including melting, casting, and hot rolling have occurred in the United States. All products produced are weld free. Mercury, in any form, has not been used in the production or testing of this material.

REPORT OF CHEMICAL/PHYSICAL TESTS

CERTIFICATE NO.	DATE	PAGE
1603151	Apr 26, 2018	1
MILL ORDER NO.	DATE	
321637		
CUSTOMER ORDER NO.	20018-012	
JOB/REQ. NO.		
SHIPPING NO.	DATE	
1603151	04/26/2018	
CARRIER	UNION PACIFIC	
CAR/TRUCK NO.	TFPX8111010R	

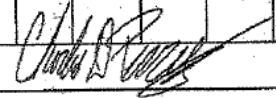
	SOLD TO	HERRICK CORPORATION [SAN BERNARDINO] PO BOX 8429 ATTN: ERIN BILLINGSLEY STOCKTON, CA 95208 USA	THE HERRICK CORPORATION PO BOX 8429 (95208) 3003 E. HAMMER LANE STOCKTON, CA 95212 USA
		THIS MATERIAL HAS BEEN MANUFACTURED, TESTED AND FOUND TO MEET THE SPECIFICATIONS AND PURCHASE ORDER REQUIREMENTS HSLA STRUCTURAL QUALITY PLATE ASTM A572-15 GRADE 50 ASME SA572 GRADE 50 2017 ASTM A709-17 GRADE 50. KILLED FINE GRAIN PRACTICE.	

PHYSICAL PROPERTIES

ITEM NO.	DESCRIPTION	HEAT NO.	SLAB	YIELD PSI X 100	TENSILE PSI X 100	% ELONG 8" 2"	% RA	HARDNESS BHN	BEND TEST	IMPACTS
1	0.3750 X 96.000ME X 360.000 2 PCS 7350 LBS	N17704		585 665	770 810	28 18		(OUTER) (INNER)		
* 2	0.5000 X 96.000ME X 360.000 7 PCS 34307 LBS	N17704		640 650	780 790	32 17		(OUTER) (INNER)		
9 PCS 41657 LBS TOTALS										

CHEMICAL ANALYSIS

HEAT NO.	C	Mn	P	S	Si	Cu	Ni	V	Cb	Al	Cr	Mo	Ti	B	N	Ca	CE	McQuaid Ebn Grain Size
N17704	.14	1.07	.011	.004	.25	.01	.05	.018	.014	.048	.02	.00	.002		.0049			
N17704	.14	1.07	.011	.004	.25	.01	.05	.018	.014	.048	.02	.00	.002		.0049			
HEATS INDICATED WITH (+) WERE MELTED & MANUFACTURED IN THE USA. HEATS INDICATED WITH (^) WERE ROLLED IN THE USA.																		
..... END OF REPORT																		

I certify the above to be correct as contained in the records of EVRAZ INC. NA By  Quality Coordinator

9960

Contract No.	
Customer	GS GLOBAL
PO No.	46201711AB16
L/C No.	
Commodity	H-BEAM
Specification	ASTM A572 G50/A992/CSA G40.21-13 50MM(345MM)

INSPECTION CERTIFICATE

EN 10204(2004) TYPE 3.1

PAGE: 17/71	
Factory	G363,Donghaean-ro,Nam-gu,Pohang-si,Gyeongsangbuk-do,S.Korea
Certificate No.	JH20180205012-7
Class certificate No.	
Issue date	2018-02-23

Dimensions	Length	Heat No.	Quantity (PCS)	Weight (kg)	Chemical Composition															Tensile Strength (N/mm ²)	Yield Strength (N/mm ²)	Elongation (%)	Impact Test (J/cm)	BEND TEST	Remarks
					C	Si	Mn	P	S	Cu	Ni	Mo	Cr	Al	V	Nb	Sn	As	Sb						
36X12X135	60.00 FT	3H0557	3	11,022	17	15	103	22	13	24	9	2	7	3	31	2	12	39	549 553	422 424	24.6 24.3	0.760 0.760			
36X12X150	35.00 FT	3H0558	3	7,143	17	14	102	72	11	24	8	2	13	4	32	2	11	40	539 543	392 395	26.2 25.9	0.720 0.720			
36X12X160	35.00 FT	JH0560	4	10,160	17	13	100	17	10	17	10	3	11	3	30	1	8	39	556 560	418 421	27.8 27.3	0.750 0.750			
36X12X160	50.00 FT	3H0550	3	10,887	17	13	100	17	10	17	10	3	11	3	30	1	8	39	556 560	418 421	27.8 27.3	0.750 0.750			
36X12X160	60.00 FT	3H0550	3	13,062	17	13	100	17	10	17	10	3	11	3	30	1	8	39	556 560	418 421	27.8 27.3	0.750 0.750			
36X12X170	40.00 FT	3H0554	3	9,255	17	14	99	20	10	14	6	1	10	3	55	2	6	38	558 563	400 405	25.0 24.7	0.710 0.710			
36X12X170	50.00 FT	3GS666	1	3,856	18	16	103	13	9	15	7	3	10	4	56	2	7	40	548 551	391 393	24.5 24.0	0.710 0.710			
36X12X210	40.00 FT	3H0563	2	7,620	18	14	101	23	16	23	11	2	14	4	55	2	10	41	566 569	415 417	24.5 24.2	0.730 0.730			
TOTAL			204	576,363																***** END *****					

<p>Conditions of supply : As Rolled (1) Ceq: (C+Mn/6+Cr/5+V/5+Mo/5+Ni/15+Cu/15) (2) Gauge length : 200 mm (3) Y.R = Y S/T.S</p>	Note	<p>WE HEREBY CERTIFY THAT THE MATERIAL HAS BEEN MADE AND TESTED IN ACCORDANCE WITH THE ABOVE SPECIFICATION AND ALSO WITH THE REQUIREMENTS CALLED FOR THE ABOVE ORDER.</p> <p style="text-align: right;"><i>[Signature]</i> General Manager of QA Team</p>
--	------	---

This test report can be verified the authenticity to scan the top-right QR code via "Qreal" mobile app. 2018.02.27.10:24:46 2121266 HMS 1102(A)-3a , A4(210:297)

9960/9970
PO # 2100523197
R M T N

Invoice No.	951295
Bill of Lading	374540
Customer No.	7603
Customer P.O.	45166

NUCOR-YAMATO STEEL CO.
P.O. BOX 1228; BLYTHEVILLE, AR 72316

CERTIFIED MILL TEST REPORT
100% Melted and Manufactured in U.S.A
All Shapes produced by Nucor-Yamato Steel are cast and rolled to a fully killed and fine grain practice

Date	2019-04-17
------	------------

9960

BROWN STRAUSS STEEL CO.
2495 URAVAN ST
AURORA CO 80011
USA

BROWN STRAUSS-FONTANA
C/O MHX FONTANA - NAPA
13600 NAPA STREET
FONTANA CA 92335
USA

ASTM A992/A992M-11 A572/A572M GR50-15
ASTM A709/A709M-15 GR50 (345)
ASTM A709/A709M-15 GR50S (345S)
CSA G40.21-13 50WM (345WM)
ASTM A6/A6M-14

Item	Item Description	QTY	Heat#	Mechanical Properties								Chemical Properties (wt %)														
				Yield to Tensile Ratio	Yield Strength	Tensile Strength	ELONG	Charpy Impact			C	Mn	P	S	Si	Cu	Ni	Cr	Mo	V	Cb	CE	Sn	Pcm	CI	
					KSI	KSI		%	Temp	Impact Energy																Loc
					MPa	MPa		%	* F	ft+lbF																
1	W33X141.0 60 ft 0 in W840X210 (18.29 m)	2	498876	0.77 0.76	55 53 379 364	71 69 492 477	24 29					.08	1.10	.012	.028	.18	.26	.09	.13	.04	.01	.019	.32	.01	.16	
2	W33X141.0 50 ft 0 in W840X210 (15.24 m)	1	501579	0.81 0.81	59 60 405 414	73 74 503 510	27 26					.08	1.10	.012	.025	.23	.34	.12	.10	.04	.01	.019	.32	.01	.17	
3	W33X141.0 50 ft 0 in W840X210 (15.24 m)	1	502481	0.78 0.76	57 56 395 386	74 74 509 510	26 26					.08	1.14	.012	.025	.24	.30	.13	.13	.04	.01	.018	.33	.01	.17	
4	W33X141.0 40 ft 0 in W840X210 (12.19 m)	3	506190	0.77 0.77	53 53 364 363	68 69 470 473	30 29					.07	1.01	.011	.024	.21	.30	10	.12	.02	01	022	.29	.01	.15	

ELONGATION BASED ON 8.00 INCH GAUGE LENGTH
 $Pcm = C + Si/30 + Mn/20 + Cu/20 + Ni/60 + Cr/20 + Mo/15 + V/10 + 5B$ (B=Approx. .0005)
 CARBON EQUIVALENT CE = $C + Mn/6 + (Cr + Mo + V)/5 + (Ni + Cu)/15$
 Mercury has not been used in the direct manufacturing of this material.
 Corrosion Index = $26.01(\%Cu) + 3.88(\%Ni) + 1.2(\%Cr) + 1.49(\%Si) + 17.28(\%P) - 7.29(\%Cu)(\%Ni) - 9.10(\%Ni)(\%P) - 33.39(\%Cu)^2$
 ISO 9001:2008 certified (Registration # 0985-07).
 All mechanical testing is performed by the Quality Testing Lab, which is independent of the production departments.

I hereby certify that the contents of this report are accurate and correct. All test results and operations performed by this material manufacturer are in compliance with the requirements of the material specifications, and when designated by the purchaser, meet the applicable specifications.

Doug Linnell
Chief Metallurgist

State of Arkansas
County of Mississippi
Sworn to and subscribed before me
on 2019-04-17
My commission expires on 07/17/2023

SQ J H
Delores H. Hinde
NOTARY PUBLIC

Invoice No.	951300
Bill of Lading	374546
Customer No.	7603
Customer P.O.	45166

NUCOR-YAMATO STEEL CO.
P.O. BOX 1228: BLYTHEVILLE, AR 72316

CERTIFIED MILL TEST REPORT
100% Melted and Manufactured in U.S.A
All Shapes produced by Nucor-Yamato Steel are cast and rolled to a fully killed and fine grain practice

Date 2019-04-17

9960

BROWN STRAUSS STEEL CO.
2495 URAVAN ST
AURORA CO 80011
USA

BROWN STRAUSS-FONTANA
C/O MHX FONTANA - NAPA
13600 NAPA STREET
FONTANA CA 92335
USA

ASTM A992/A992M-11 A572/A572M GR50-15
ASTM A709/A709M-15 GR50 (345)
ASTM A709/A709M-15 GR50S (345S)
CSA G40.21-13 50WM (345WM)
ASTM A6/A6M-14

Item	Item Description	QTY	Heat#	Mechanical Properties							Chemical Properties (wt %)														
				Yield to Tensile Ratio	Yield Strength KSI	Tensile Strength KSI	ELONG %	Charpy Impact			C	Mn	P	S	Si	Cu	Ni	Cr	Mo	V	Cb	CE	Sn	Pcm	CI
								Temp	Impact Energy	Loc															
								* F	ft*lbft																
				MPa	MPa	%	* C	J																	
1	W30X116.0 50 ft 0 in W760X173 [18.29 m]	6	504994	0.78 0.78	53 366 373	68 469 480	27 28																		
2	W30X116.0 55 ft 0 in W760X173 [16.76 m]	1	506364	0.77 0.77	54 375 379	71 490 492	28 28																		
3	W30X116.0 55 ft 0 in W760X173 [16.76 m]	2	506366	0.77 0.78	54 55 372 381	70 71 483 487	28 27																		

ELONGATION BASED ON 8.00 INCH GAUGE LENGTH
 $Pcm = C + Si/30 + Mn/20 + Cu/20 + Ni/60 + Cr/20 + Mo/15 + V/10 + 5B(B = Approx .0005)$
 Carbon Equivalent CE = $C + Mn/6 + (Cr + Mo + V)/5 + (Ni + Cu)/15$
 Mercury has not been used in the direct manufacturing of this material.
 Corrosion Index = $26.01(\%Cu) + 3.88(\%Ni) + 1.2(\%Cr) + 1.49(\%S) + 17.28(\%P) - 7.29(\%Cu)(\%Ni) - 9.10(\%Ni)(\%P) - 33.39(\%Cu)^2$
 ISO 9001:2008 certified (Registration # 0985-07).
 All mechanical testing is performed by the Quality Testing Lab, which is independent of the production departments.

I hereby certify that the contents of this report are accurate and correct. All test results and operations performed by this material manufacturer are in compliance with the requirements of the material specifications, and when designated by the purchaser, meet the applicable specifications.

Doug Linnell
Chief Metallurgist

State of Arkansas
County of Mississippi
Sworn to and subscribed before me

on 2019-04-17
My commission expires on 07/17/2023


SQH 2



9960

Contract No.	
Customer	GS GLOBAL
PO No.	46201804A803
L/C No.	
Commodity	H-BEAM
Specification	ASTM A572 G50/A992/CSA G40.21-13 50WM(245WM)

INSPECTION CERTIFICATE
EN 10204(2004) TYPE 3.1

		PAGE [4 / 17]
Factory	63, Jungbong-Daero, Dong-gu, Incheon, S Korea	
Certificate No.	IH20180606058-4	
Class certificate No.		
Issue date	2018-06-29	

Dimensions	Length	Heat No.	Quantity (PCS)	Weight (kg)	Chemical Composition															Tensile Test			Yield Ratio(%)	BEND TEST	Impact Test(L)			Remarks (Impact Specimen Size)
					×100					×1000					×100					Tensile Strength	Yield Strength	Elongation (%)			V-Notch			
					C	Si	Mn	P	S	Cu	Ni	Mo	Cr	Al	V	Nb	Sn	CEq	N/mm2						%	AVG	1	
24X9X94	50.00 FT	N 042175	1	2,132	19	17	95	17	8	17	13	4	11	4	13	4	8	40	528	398	27.5	0.754						
24X9X94	50.00 FT	N 042176	1	2,132	18	15	94	20	8	21	8	2	12	5	13	3	16	39	523	406	27.5	0.777						
24X9X94	50.00 FT	N 042938	7	14,924	18	12	102	19	13	26	11	1	14	2	13	3	9	41	560	412	27.0	0.736						
24X9X94	50.00 FT	N 042939	5	10,660	19	16	94	22	7	26	9	1	11	4	13	4	9	40	541	380	26.5	0.703						
24X9X94	60.00 FT	N 042937	1	2,558	18	14	95	22	11	24	10	1	14	3	15	4	10	39	558	401	28.0	0.719						
24X9X94	60.00 FT	N 042938	3	7,674	18	12	102	19	13	26	11	1	14	2	13	3	9	41	560	412	27.0	0.736						
24X9X94	65.00 FT	N 042938	5	13,860	18	12	102	19	13	26	11	1	14	2	13	3	9	41	560	412	27.0	0.736						
24X9X94	65.00 FT	N 042939	1	2,772	19	16	94	22	7	26	9	1	11	4	13	4	9	40	541	380	26.5	0.703						
24X9X103	45.00 FT	N 042935	4	8,392	18	15	95	26	4	25	10	2	12	4	14	4	12	39	548	402	29.0	0.734						
24X9X103	45.00 FT	N 042936	2	4,196	18	14	96	27	7	25	9	1	16	3	14	3	8	40	564	393	30.0	0.697						
SUB TOTAL			30	69,300																								

Note
(1) Ceq: (CE=C+Mn/6+Cr/5+V/5+Mo/5+Ni/15+Cu/15)
(2) Gauge length: 200 mm
(3) YR = Y.S/T.S

***** NEXT *****

WE HEREBY CERTIFY THAT THE MATERIAL HAS BEEN MADE AND TESTED IN ACCORDANCE WITH THE ABOVE SPECIFICATION AND ALSO WITH THE REQUIREMENTS CALLED FOR THE ABOVE ORDER.

J. E. Han
General Manager of QA Team

This test report can be verified the authenticity to scan the top-right QR code via "Qreal" mobile app. 2018.06.29 14:10:21 2121266 HMS L102(A)-3a A4(210x297)

RWAB

MT-1188 9960

DATE	6/28/08
INVOICE NO.	240687
BILL OF LADING	916373
CUSTOMER NO.	7950
CUSTOMER P.O.	# 25312-2536

NUCOR-YAMATO STEEL CO.
P.O. BOX 1228 • BLYTHEVILLE AR 72316

SAN BERNARDINO STEEL
C/O KREP ON TRUCKING
RANCHO CUCAMONGA, CA FOR TRK DEL TO
SAN BERNARDINO, CA 92235

CERTIFIED MILL TEST REPORT

100% MELTED AND MANUFACTURED IN U.S.A.
All shapes produced by Nucor-Yamato Steel are cast and rolled to a fully killed and fine grain practice.

ASTM A992/A992M-06a A572/A572M GR50-06
ASTM A709/A709M-07 GR50 (345)
ASTM A709/A709M-07 GR508 (345B)
ASTM A6/AS6-07

HERRICK CORPORATION
PO BOX 8429
STOCKTON, CA 95208

80 81 82

9960
W1 - 10001

ITEM #	ITEM DESCRIPTION	QTY	HEAT #	MECHANICAL PROPERTIES							CHEMICAL PROPERTIES															
				YIELD TO TENSILE RATIO	YIELD STRENGTH PSI	TENSILE STRENGTH PSI	ELONG %	CHARPY TEMP * F	IMPACT ENERGY FT-LBS	C	Mn	P	S	SI	Cu	Ni	Cr	Mo	V	Cb	CE					
1	W27 -258.0 34' 8" W690 x384.0 10.566 M	1	321559	.75	57000	76000	26	+70	38	42	43	.08	1.36	.016	.017	.27	.28	.09	.09	.02	.05	.001	.36			
				.75	57000	76000	26																			
					393	524	26	+21	52	57	58	(CORE)														
2	W27 -258.0 39' 4" W690 x384.0 11.989 M	1	321557	.76	58000	76000	26	+70	70	88	96	.08	1.38	.015	.019	.27	.27	.10	.09	.03	.05	.001	.36			
				.76	59000	78000	26	+70	70	116	102															
					400	524	26	+21	95	119	130	(CORE)														
3	W27 -258.0 42' W690 x384.0 .802 M	3	321553	.76	56000	74000	28	+70	74	60	57	.07	1.38	.022	.020	.24	.30	.09	.11	.03	.05	.001	.37			
				.76	56000	74000	28	+70	129	110	155															
					386	510	28	+21	100	81	77	(CORE)														
4	W27 -258.0 43' W690 x384.0 13.106 M	2	321553	.76	56000	74000	28	+70	74	60	57	.07	1.38	.022	.020	.24	.30	.09	.11	.03	.05	.001	.37			
				.76	56000	74000	28	+70	129	110	155															
					386	510	28	+21	100	81	77	(CORE)														
5	W27 -258.0 44' W690 x384.0 13.411 M	2	321548	.75	57000	76000	25	+70	47	88	116	.08	1.36	.014	.016	.28	.27	.09	.07	.02	.05	.002	.36			
				.76	58000	76000	24																			
					393	524	25	+21	64	115	157	(CORE)														
6	W27 -258.0 44' W690 x384.0 13.411 M	2	321551	.76	57000	75000	26	+70	141	241	105	.08	1.37	.019	.019	.28	.27	.09	.10	.02	.05	.002	.36			
				.77	57000	76000	27	+70	79	100	106															
					393	517	26	+21	191	327	142	(CORE)														
7	W27 -258.0 45' W690 x384.0 13.716 M	4	321555	.75	55000	73000	29	+70	55	69	35	.08	1.36	.020	.020	.26	.26	.10	.11	.03	.05	.002	.37			
				.77	56000	73000	27	+70	55	46	52															
					379	503	29	+21	75	94	47	(CORE)														

ELONGATION BASED ON 8.00 INCH GAUGE LENGTH

we certify that the contents of this report are accurate and correct. All test results and operations performed by this material manufacturer are in compliance with the requirements of the material specifications listed in the Specifications Block above.

Day Linnell

QUALITY ASSURANCE

CUSTOMER COPY

STATE OF ARKANSAS COUNTY OF MISSISSIPPI
SWORN TO AND SUBSCRIBED BEFORE ME

30 Day of 06/08

Charlene Wallis NOTARY PUBLIC

MY COMMISSION EXPIRES 10/21/2013



9960 9960

NUCOR-YAMATO STEEL CO.
P O BOX 1228
BLYTHEVILLE AR 72316

DATE
2/02/13

CERTIFIED MILL TEST REPORT
100% MELTED AND MANUFACTURED IN U.S.A.

All shapes produced by Nucor-Yamato Steel are cast and rolled to a fully killed and fine grain practice.

SOLD TO HERRICK CORPORATION PO BOX 8429 STOCKTON, CA 95208		SHIP TO STOCKTON STEEL CO KEEP ON TRUCKING BNSF R/R STOCKTON, CA FOR TRK DEL TO STOCKTON, CA 95212		INVOICE 533660	CUSTOMER NO. 7873
				BILL OF LADING 97717	CUSTOMER P.O. 331-10
1 SPECIFICATIONS GRADE: A57H A709/A709H-11 GR50S (345S) A57H A6/A6M-12 A572/A572H GR50-07 A52M A709/A709H-11 GR50 (345)					

ITEM	ITEM DESCRIPTION	QTY	HEAT #	MECHANICAL PROPERTIES							CHEMICAL PROPERTIES													
				YIELD TO FRACTURE MPa	YIELD STRENGTH MPa	TENSILE STRENGTH MPa	ELONG %	TEMP °C	CHARPY IMPACT PEAK Joules	C	Mn	P	S	Si	Cu	Ni	Cr	Mo	V	Nb	CE			
1	W24 -207.0 49'	2	399025	.76	57000	75000	27	+70	133112135	.071	.35	.017	.021	.25	.27	.09	.14	.03	.05	.003	.36			
	.75			57000	76000	27	+21	180152183 (CORE)																
	W610 x307.0 14.935 M					393	517	27																
2	W24 -207.0 50'	1	399018	.77	59000	77000	27	+70	159199185	.071	.35	.012	.025	.29	.25	.11	.15	.04	.05	.003	.37			
	.75			57000	76000	26	+70	267221220																
	W610 x307.0 15.240 M					407	531	27	+21	216270251 (CORE)														
3	W24 -207.0 50'	5	399024	.78	56000	72000	28	+70	194104194	.081	.36	.014	.023	.20	.25	.11	.12	.04	.06	.003	.37			
	.76			56000	74000	28	+70	205208134																
	W610 x307.0 15.240 M					386	496	28	+21	263141263 (CORE)														
4	W24 -229.0 49'	1	399022	.76	56000	74000	26	+70	131 85154	.071	.35	.012	.025	.21	.25	.10	.12	.03	.05	.003	.36			
	.74			53000	72000	28	+70	93 77 79																
	W610 x341.0 14.935 M					386	510	26	+21	178115209 (CORE)														
5	W24 -229.0 50'	1	399029	.75	54000	72000	27	+70	189158205	.081	.36	.014	.023	.20	.25	.11	.12	.04	.06	.003	.37			
	.76			55000	72000	27																		
	W610 x341.0 15.240 M					372	496	27	+21	249214278 (CORE)														
6	W24 -229.0 60'	2	399022	.76	56000	74000	26	+70	131 85154	.071	.35	.012	.025	.21	.25	.10	.12	.03	.05	.003	.36			
	.74			53000	72000	28	+70	93 77 79																
	W610 x341.0 18.288 M					386	510	26	+21	178115209 (CORE)														
7	W24 -229.0 60'	2	399023	.75	53000	71000	27	+70	199149213	.071	.35	.013	.023	.24	.27	.10	.11	.04	.05	.003	.36			
	.75			53000	71000	28	+70	134143244																
	W610 x341.0 18.288 M					365	490	27	+21	270202289 (CORE)														

ELONGATION BASED ON 8.00 INCH GAUGE LENGTH
 $P_{cm} = C + Si / 30 + Mn / 20 + Cu / 20 + Ni / 60 + Cr / 20 + Mo / 15 + V / 10 + Nb / 10 + 5B / 10000$ (485)
 Corrosion Indwar: $CI = 26.01(\%Cu) + 3.38(\%Ni) + 1.2(\%Cr) + 1.49(\%S) + 17.23(\%P) - 7.29(\%Cu)(\%Ni) - 9.16(\%Ni)(\%P) - 33.39(\%Cu)^2$
 Carbon Equivalent CE = $C + Mn/6 + (Cr+Ni+V)/5 + (Nb+Cu)/15$
 Mercury has not been used in the direct manufacturing of this material.
 I hereby certify that the contents of this report are accurate and correct. All test results and questions performed by this laboratory shall conform with the requirements of the national specifications listed in the Specification Book sheet.
 GARY PENNELL
 QUALITY MANAGER
 STATE OF ARKANSAS
 COUNTY OF MISSISSIPPI
 SWORN TO AND SUBSCRIBED BEFORE ME THIS
 Day of _____ 2013

Invoice No.	922462
Bill of Lading	B53695
Customer No.	7670
Customer P.O.	PPO-002586-1

NUCOR-YAMATO STEEL CO.
P.O. BOX 1228 BLYTHEVILLE, AR 72316

CERTIFIED MILL TEST REPORT
100% Melted and Manufactured in U.S.A
All Shapes produced by Nucor-Yamato Steel are cast and rolled to a fully killed and fine grain practice

Date	2018-11-05
------	------------

9960

CCC STEEL, INC.
2576 E VICTORIA ST
RANCHO DOMINGUEZ CA 90220-0000
USA

CCC STEEL, INC. - C/O
ANCON TRANS BNSF R/R
VERNON, CA FOR TRK DEL TO
COMPTON CA 90224
USA

ASTM A992/A992M-11 A572/A572M GR50-15
ASTM A709/A709M-15 GR50 (345)
ASTM A709/A709M-15 GR50S (345S)
CSA G40.21-13 50WM (345WM)
ASTM A6/A6M-14

Item#	Item Description	QTY	Heat#	Mechanical Properties							Chemical Properties																	
				Yield to Tensile Ratio	Yield Strength		Tensile Strength		ELONG %	Charpy Impact			C	Mn	P	S	Si	Cu	Ni	Cr	Mo	V	Cb	CE	Sn	Pcm	CI	
					KSI	MPa	KSI	MPa		Temp ° F	Impact Energy ft-lbf	Loc																
1	W14X283.0 60 ft 0 in W360X421 (18.29 m)	1	492890	0.75 0.77	53 54 362 370	70 70 482 481	28 27								.06	1.35	.019	.022	.27	.23	.09	.13	.03	.05	.002	.34	.01	.16
2	W27X178.0 35 ft 0 in W690X265 (10.67 m)	1	496778	0.79 0.79	57 57 392 396	72 73 499 502	26 28								.07	1.20	.013	.028	.25	.28	.10	.11	.03	.02	.019	.33	.01	.17
3	W27X178.0 60 ft 0 in W690X265 (18.29 m)	1	496778	0.79 0.79	57 57 392 396	72 73 499 502	26 28								.07	1.20	.013	.028	.25	.28	.10	.11	.03	.02	.019	.33	.01	.17
4	W27X217.0 45 ft 0 in W690X323 (13.72 m)	1	494737	0.77 0.77	58 58 399 399	75 75 519 516	26 26								.07	1.35	.016	.020	.26	.29	.11	.13	.03	.05	.003	.36	.01	.17

ELONGATION BASED ON 8.00 INCH GAUGE LENGTH
 $Pcm = C + 5(30 + Mn/20 + Cu/20 + Ni/60 + Cr/20 + Mo/15 + V/10 + 5B) / (B \approx 0.0005)$
 Corrosion Index = $26.01(\%Cu) + 3.88(\%Ni) + 1.2(\%Cr) + 1.49(\%Si) + 17.28(\%P) - 7.29(\%Cu)(\%Ni) - 9.10(\%Ni)(\%P) - 33.39(\%Cu)^2$
 ISO 9001:2015 certified (Registration # 0985-07).
 All mechanical testing is performed by the Quality Testing Lab, which is independent of the production departments.
 The Charpy machine striker geometry used by Nucor-Yamato Steel is the 8 mm (0.315") striker (KV₂) per ASTM A370 Section 22.1.2 and ISO 148-1 Section 7.3.

CARBON EQUIVALENT CE = $C + Mn/6 + (Cr + Mo + V)/5 + (Ni + Cu)/15$
 Mercury has not been used in the direct manufacturing of this material.
 This material was produced in accordance with the Nucor-Yamato Steel Quality Manual.

I hereby certify that the contents of this report are accurate and correct. All test results and operations performed by this material manufacturer are in compliance with the requirements of the material specifications, and when designated by the purchaser, meet the applicable specifications.

Doug Linnell
Chief Metallurgist

State of Arkansas
County of Mississippi
Sworn to and subscribed before me
on 2018-11-05
My commission expires on 07/17/2023



材質證明書 (出廠證明書)
MILL TEST CERTIFICATE
In accordance with ASTM A992

開立日期 DATE OF ISSUE	Feb. 25, 2019
證明書編號 CERTIFICATE NO.	H09738

客戶名稱 CUSTOMER	BEST-STEEL TRADE CORP.	交貨日期 SHIPPING DATE	Feb. 23, 2019
訂貨編號 CONTRACT NO.	US1811 (ORDER NO.:H21840)	商品名稱 COMMODITY	WIDE FLANGE BEAMS
項目(工程)編號 PROJECT NO.	US-LA-L-357	合計重量 TOTAL WEIGHT	***691,716 (kg)
採用規格 STANDARD	ASTM A992-11	合計捆(支)數 BUNDLES (PIECES)	**0 捆 (**249 支)
備註 REMARKS	CREDIT NO.(ISSUING BANK):()		

產品尺寸 PRODUCT DIMENSIONS				機械性質 MECHANICAL PROPERTY				化學成份 CHEMICAL COMPOSITION (%)													TYPE: L	備註 RAD. TEST
規格 SPECIFICATION	長度 (總長) LENGTH (TOTAL PCS)	重量 WEIGHT kg	鋼號 HEAT NO.	屈服點 YIELD POINT	抗拉強度 TENSILE STRENGTH	伸長率 Elo in 200mm	斷裂 伸長率 ELONG. Y.R.	C	Si	Mn	P	S	Cu	Ni	Cr	Mo	V	Nb	Sn	Pb	Cev	
in.xm.(lbs/ft)	(ft)			N/mm ²	N/mm ²	%	%	100	100	1000	1000	100	100	1000	1000	1000	1000	1000	1000	1000	1000	
W 24.0x 12.75x 162.0	35.00	7,719	H77491	345	450	18.0	85	23	40	160	35	45	60	45	35	150	150	50	20	15	450	OK
W 24.0x 12.75x 162.0	40.00	8,820	H77491	400	544	26.7	73	15	19	110	12	6	22	7	9	20	12	10	17	12	381	OK
W 24.0x 12.75x 162.0	50.00	22,050	H77492	378	516	24.4	73	16	22	119	9	6	21	7	8	20	13	11	16	12	396	OK
W 24.0x 12.75x 162.0	55.00	12,129	H72821	411	546	24.0	75	15	21	116	18	2	24	9	10	23	16	11	11	10	397	OK
W 24.0x 12.75x 162.0	40.00	9,588	H77491	396	539	24.0	72	15	19	110	12	6	22	7	9	20	12	10	17	12	381	OK
W 24.0x 12.75x 176.0	40.00	9,588	H71104	4043	555	20.5	71	14	24	97	14	9	25	7	8	15	15	10	10	10	349	OK
W 24.0x 12.75x 176.0	40.00	9,588	H71104	396	539	24.0	72	14	24	97	14	9	25	7	8	15	15	10	10	10	349	OK

• 本材質證明書不得複印複製，對其更新內容。
This mill test certificate report contents neither can be duplicated nor extracted. If duplicated, amended, or extracted, all data and the certified material test report are therefore invalid.

• 茲證明本廠所列產品，均係按訂規檢驗製造及試驗，並符合規格要求。
We hereby certify that the material herein described has been manufactured in accordance with the standards and specifications specified by you and that it satisfies the requirements.

• 衝擊試驗值有底線者為非平均值。
The impact test values with underline are IDV.



品質管制人員 QUALITY CONTROL MANAGER
鄧凱明

本證明書須蓋本公司鋼印方為有效。客戶若複製本證明書，應加註「與正本相同」之文字並註明其公司大小。 This certificate is invalid without the steel seal of Tung Ho Steel Enterprise Corp.

S 鋼廠

Job # 9960/9970
PO # ENG05219A

7700 & 7700



EVRAZ INC. NA
Evraz Oregon Steel 14400 N. Rivergate Blvd., Portland, Oregon 97203

REPORT OF CHEMICAL/PHYSICAL TESTS

CERTIFICATE NO.	DATE	PAGE
1665990	May 04, 2019	1
MILL ORDER NO.	DATE	
336231		
CUSTOMER ORDER NO.	20019-021	
JOB/REQ. NO.		
SHIPPING NO.	DATE	
1665990	05/04/2019	
CARRIER	BURLINGTON NORTHERN	
CAR/TRUCK NO.	YELLOW	



HERRICK CORPORATION [SAN BERNARDINO]
PO BOX 8429
ATTN: ERIN BILLINGSLEY
STOCKTON, CA 95208
USA

THE HERRICK CORPORATION
PO BOX 8429 (95208)
3003 E. HAMMER LANE
STOCKTON, CA 95212
USA

THIS MATERIAL HAS BEEN MANUFACTURED, TESTED AND FOUND TO MEET THE SPECIFICATIONS AND PURCHASE ORDER REQUIREMENTS
HSLA STRUCTURAL QUALITY PLATE ASTM A572-18 GRADE 50 ASME SA572 GRADE 50 2017
ASTM A709-18 GRADE 50. KILLED FINE GRAIN PRACTICE.

PHYSICAL PROPERTIES

ITEM	DESCRIPTION	HEAT NO.	SLAB	YIELD PSI X 100	TENSILE PSI X 100	% ELONG 8" 2"	% RA	HARDNESS BHN	BEND TEST	IMPACTS
2	0.5000 X 96.000ME X 360.000 PT# 6251 2 PCS 9802 LBS	^ N21707		615 665	790 815	31 16		(OUTER) (INNER)		9960/9970 - Plate 1/2"
4	1.5000 X 96.000ME X 360.000 PT# 6266 2 PCS 29404 LBS	^ N20800		635 590	840 795	19 23				
	4 PCS 39206 LBS TOTALS									

CHEMICAL ANALYSIS

HEAT NO.	C	Mn	P	S	Si	Cu	Ni	V	Cb	Al	Cr	Mo	Ti	B	N	Ca	CE	Microalloy Element
N21707	14	1.06	.015	.007	.22	.01	.04	.018	.018	.035	.03	.00	.002		.0041			
N20800	16	1.12	.017	.006	.22	.01	.05	.055	.000	.031	.03	.00	.000		.0160			

HEATS INDICATED WITH (+) WERE MELTED & MANUFACTURED IN THE USA. HEATS INDICATED WITH (^) WERE ROLLED IN THE USA.

..... END OF REPORT

I certify the above to be correct as contained in the records of EVRAZ INC. NA By Aaron Capps
Quality Coordinator

N20741 9960



EVRAZ INC. NA
Evraz Oregon Steel 14400 N. Rivergate Blvd., Portland, Oregon 97203

REPORT OF CHEMICAL/PHYSICAL TESTS

CERTIFICATE NO.	DATE	PAGE
1654232	Feb 20, 2019	1
MILL ORDER NO.	DATE	
294363		
CUSTOMER ORDER NO.		
LSI JOBBER		
JOURNAL NO.		
048		
SHIPPING NO.	DATE	
1654232	02/20/2019	

	SOLD TO OREGON STEEL MILL OSM JOBBER 14400 N. RIVERGATE BLVD PORTLAND, OR 97203	LSI PLATE W.O.# 252-17702 CUSTOMER San Bernardino Steel P.O.# 2019-020 DATE 02/19/19

THIS MATERIAL HAS BEEN MANUFACTURED, TESTED AND FOUND TO MEET THE SPECIFICATIONS AND PURCHASE ORDER REQUIREMENTS
 HSLA STRUCTURAL QUALITY PLATE ASTM A572-13A GRADE 50 ASME SA572 GRADE 50 2013.
 KILLED FINE GRAIN PRACTICE.

CONVYER
 MITCHELL BROS
 CURTRUCK NO.
 13367

PHYSICAL PROPERTIES										
ITEM	DESCRIPTION	HEAT NO.	SLAB	YIELD PSI X 100	TENSILE PSI X 100	% ELONG F 2"	% RA	HARDNESS BHN	BEND TEST	IMPACTS
1	0.6250 X 96.0000 X 360.000 1 PC 6126 LBS 1 PC 6126 LBS TOTALS	N20741		620	805	21				9960-Plate 5/8"

CHEMICAL ANALYSIS																	
HEAT NO.	C	Mn	P	S	Si	Cu	Ni	V	Co	Al	Cr	Mo	Ti	B	N	Ce	Wooden Sample
N20741	.14	1.10	.017	.006	.23	.01	.05	.048	.000	.034	.02	.00	.000		.0110		
HEATS INDICATED WITH (+) WERE MELTED & MANUFACTURED IN THE USA. HEATS INDICATED WITH (^) WERE ROLLED IN THE USA.																	
----- END OF REPORT -----																	

I certify the above to be correct as contained in the records of EVRAZ INC. NA By Aaron Cappel
 Quality Coordinator
 JCS STK



JSW Steel (USA) INC.
5200, East McKinney Road,
BAYTOWN, TX 77523

METALLURGICAL TEST REPORT

MET - 04 Rev. No.: 3 Rev. Date: 02/27/2018

3/28/2019

Bulletin	Order Item	Heat	PO No.	Shipping Mode	Order Dimensions	Slab Origin	TC No.
R052303	JSW12177-04	S27292	20019-013	RAIL PTTX 136460	0.75x96x360		R052303-7292-1

			9960/9970- Plate 3/4"
--	--	--	--------------------------

Plates Certified for the Following grades	Specifications	Marking Instructions
ASTM-A572-50 AR		Stencil in 1 location(s); X Loc. 18 Y Loc. 30; CUST; MADEINUSA PN PO; DIM GRADE; FREIGHT ORDER ITEM PLATEID SHIPWEEK SLABID
Hot Rolled Carbon Steel Plates Plates Manufactured in the USA		TRANSMODE Stamp in 1 location(s); X Loc. 18 Y Loc. 12; Slab ID; Slab ID

Sold To: HERRICK CORPORATION P.O. BOX 8429 STOCKTON, CA 95208
Ship To: HERRICK CORP C/O MHX LLC 11355 ARROW RT. BNSF TRACK 1362 RANCHO CUCAMONGA, CA 91730

Test	C	Mn	P	S	Si	Cu	Ni	Cr	Mo	Sn	Al	N	V	B	Ti	Nb	Ca	CE
LADLE	0.14	1.34	0.012	0.003	0.31	0.010	0.010	0.020	0.000	0.000	0.033	0.0060	0.069	0.0001	0.001	0.002	0.0022	0.38

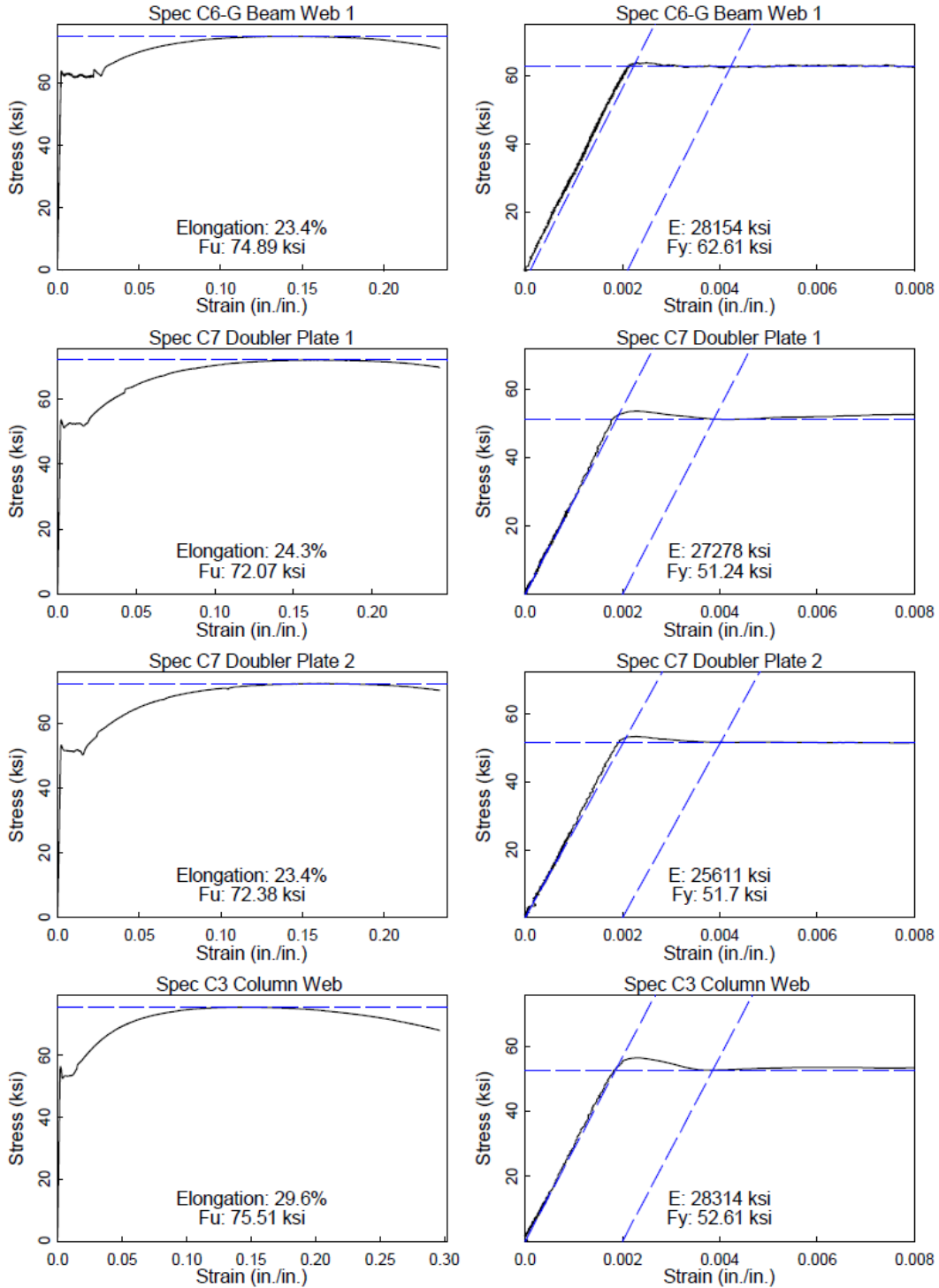
Carbon Equivalent CE = C + Mn/6 + (Cr + Mo + V)/5 + (Ni + Cu)/15
 PCM = C + Si/30 + Mn/20 + Cu/20 + Ni/60 + Cr/20 + Mo/15 + V/10 + 5B

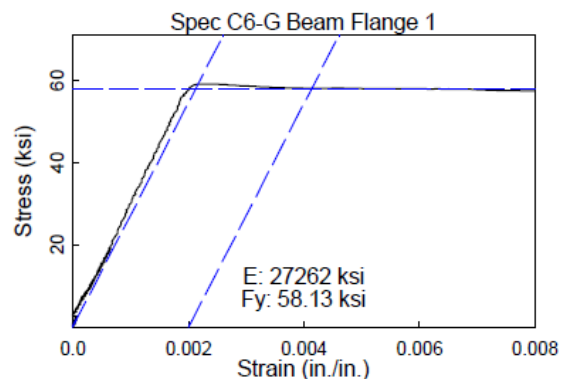
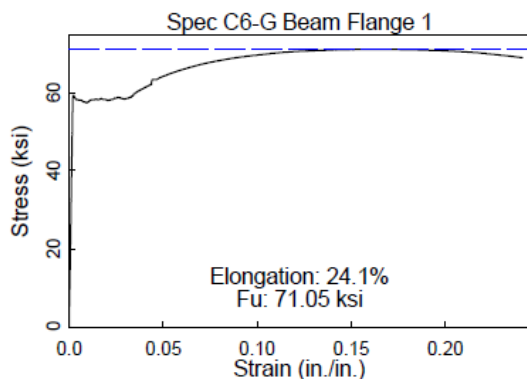
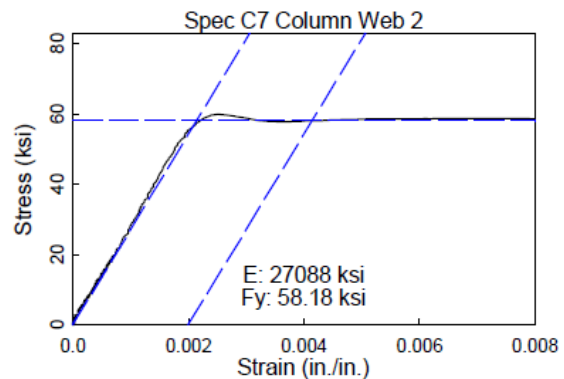
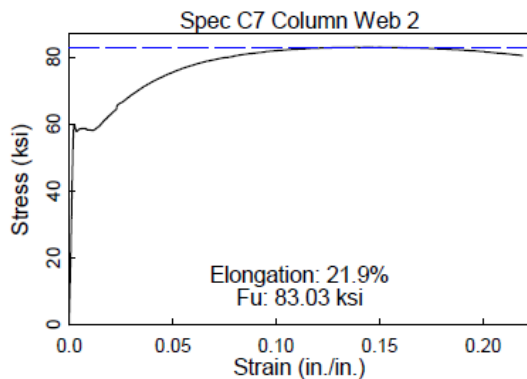
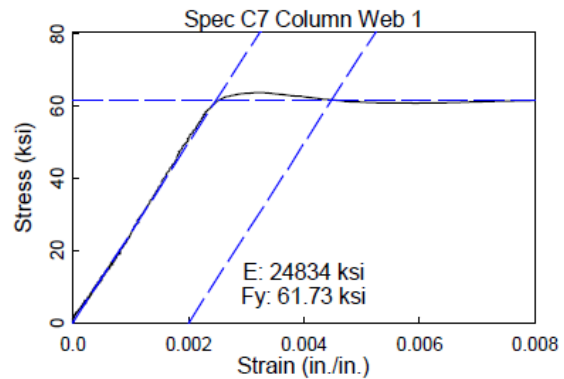
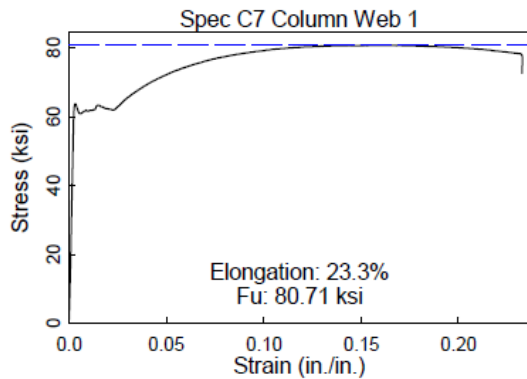
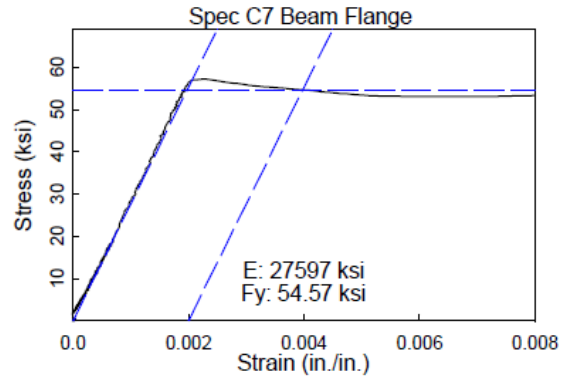
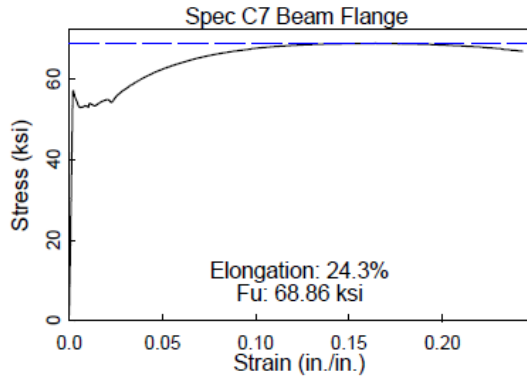
Plate Tested	Slab Identity	Gauge Tested	Test Cond	Test Dir.	Yield Point	Tensile Stgth.	Elong In 2"	YS/UTS Ratio	Yield Strength Determined At
1122857	02D	0.7500	AR	T	58	81	40.0%	0.72	0.2%

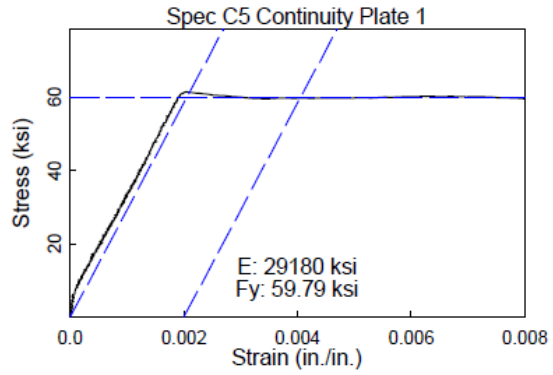
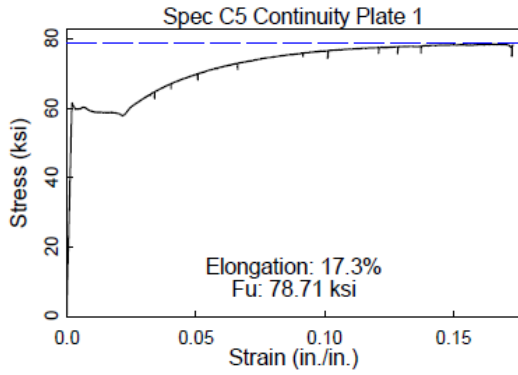
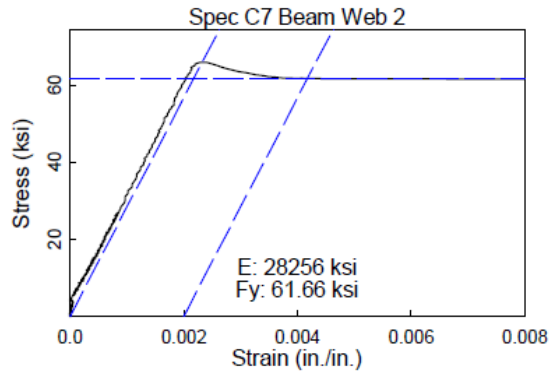
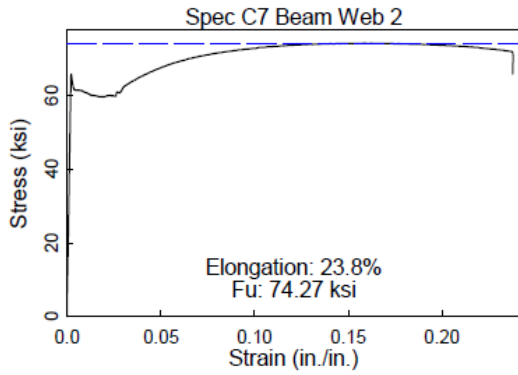
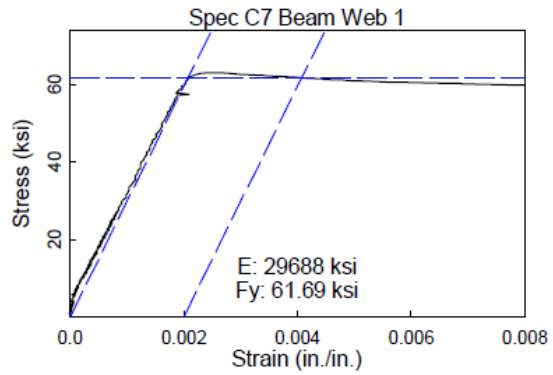
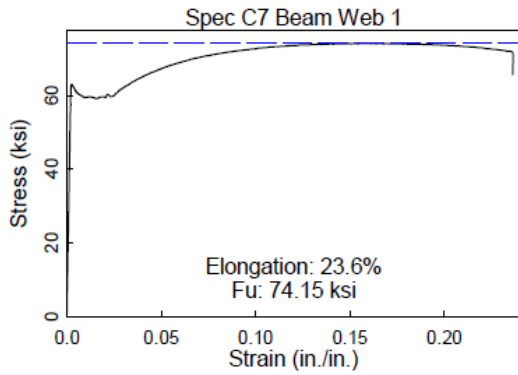
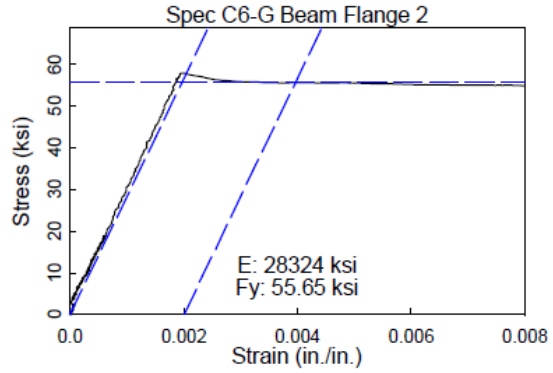
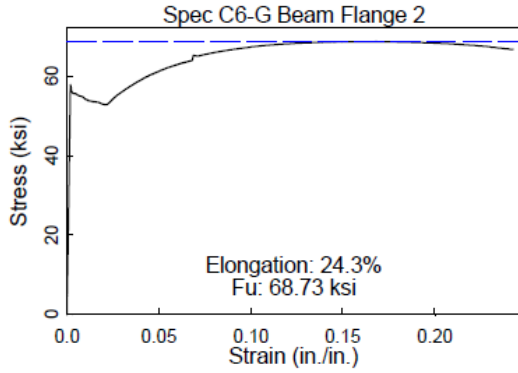
Plates Certified For The Above Tests

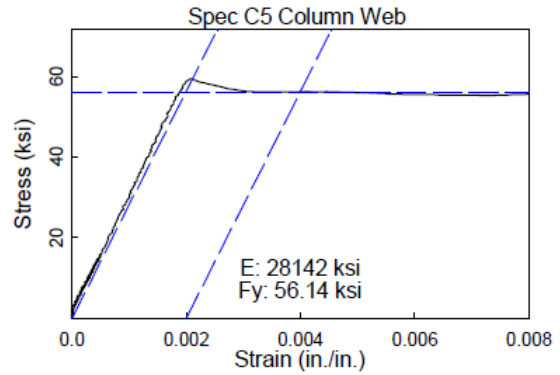
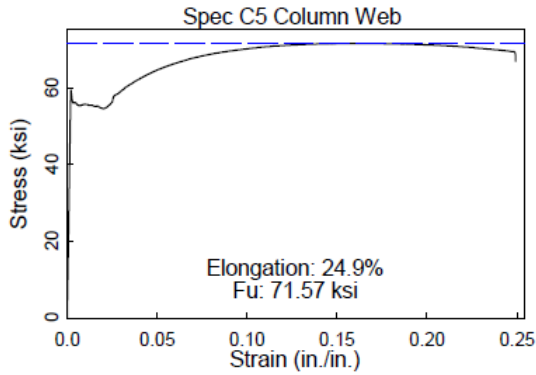
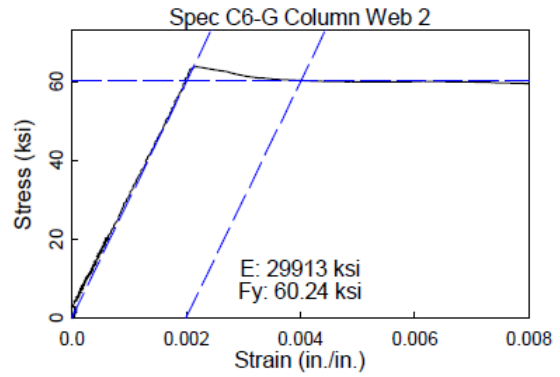
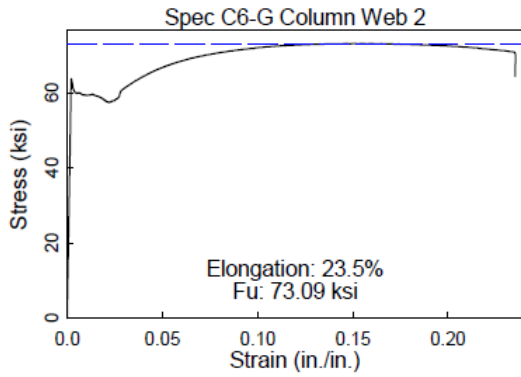
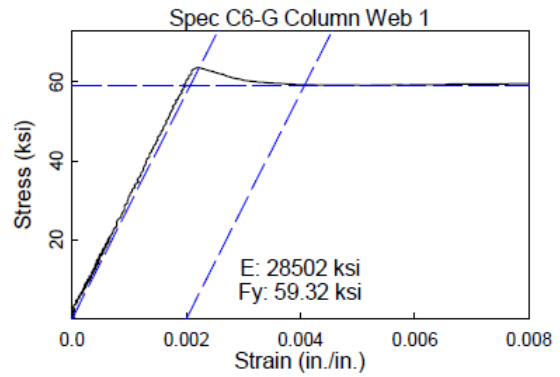
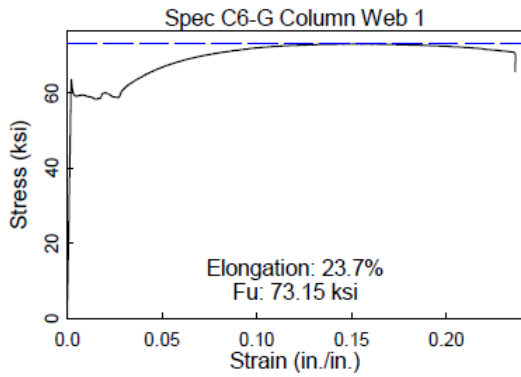
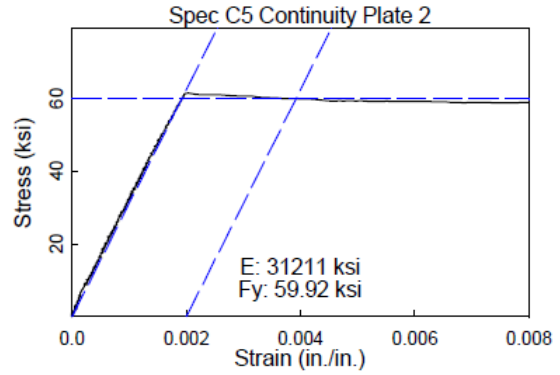
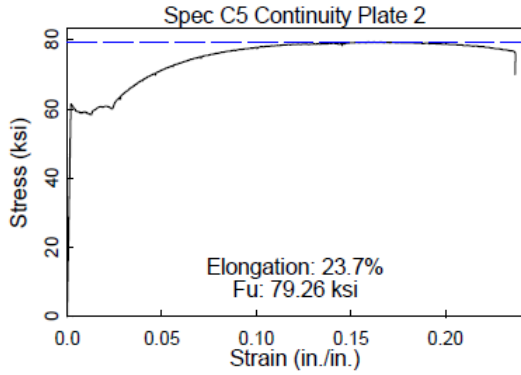
Material	Thick(IN)	Width(IN)	Len(IN)	Wgt(LB)	Material	Thick(IN)	Width(IN)	Len(IN)	Wgt(LB)	Material	Thick(IN)	Width(IN)	Len(IN)	Wgt(LB)
1122857A	0.7500	96.000	360.00	7350.912	1122857B	0.7500	96.000	360.00	7350.912					

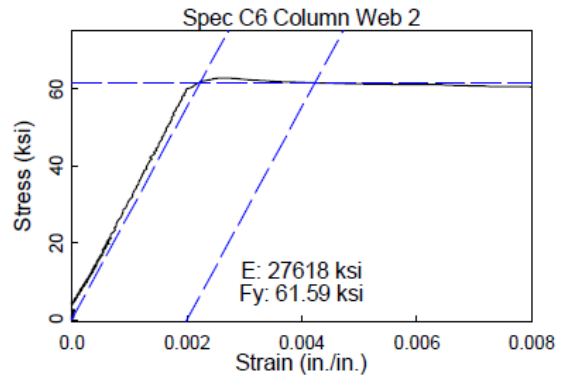
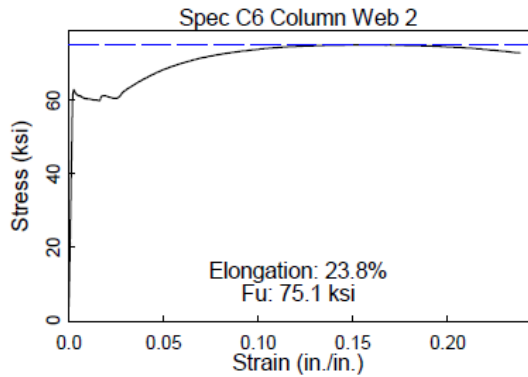
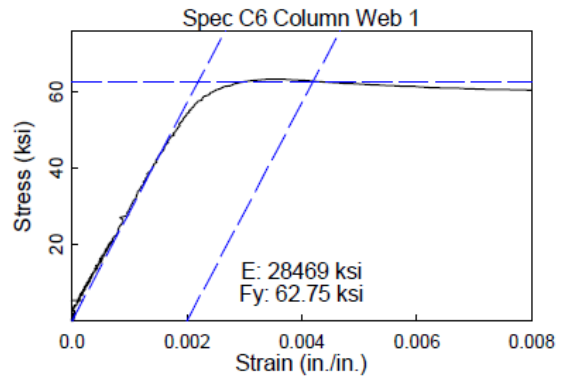
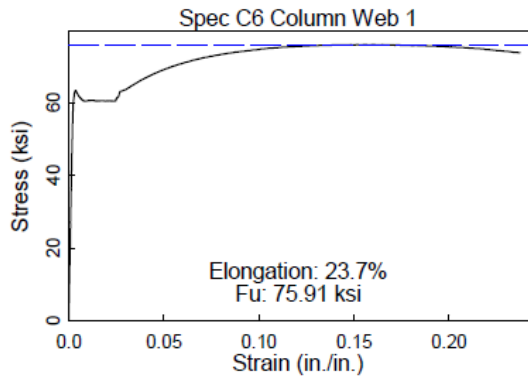
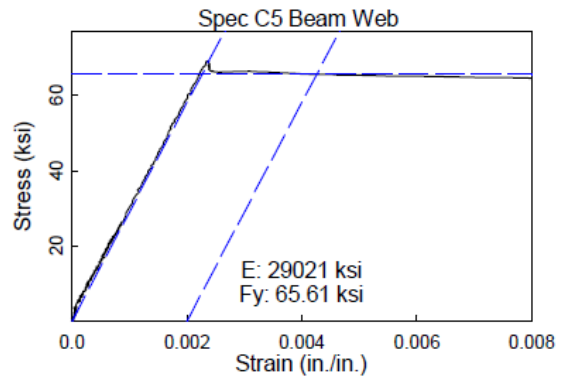
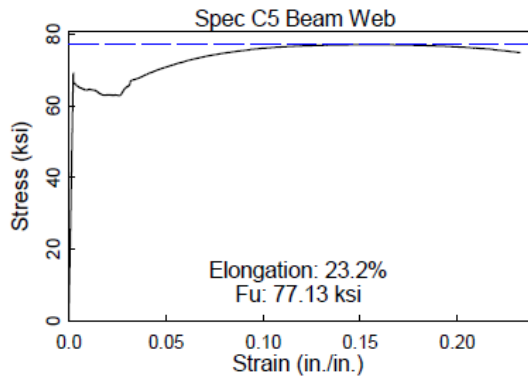
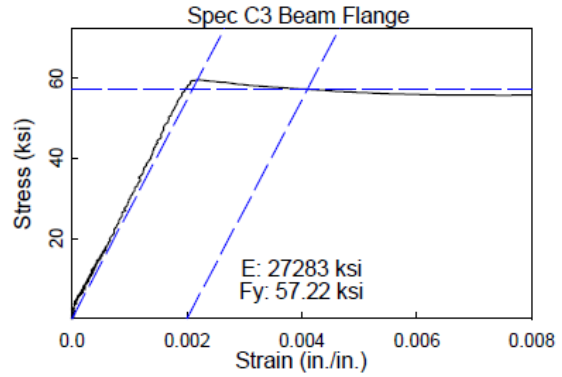
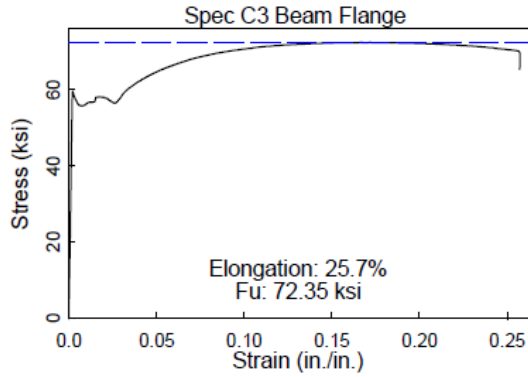
APPENDIX D: TENSION COUPON TESTING

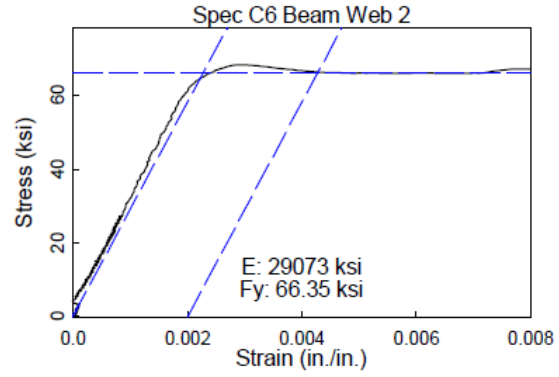
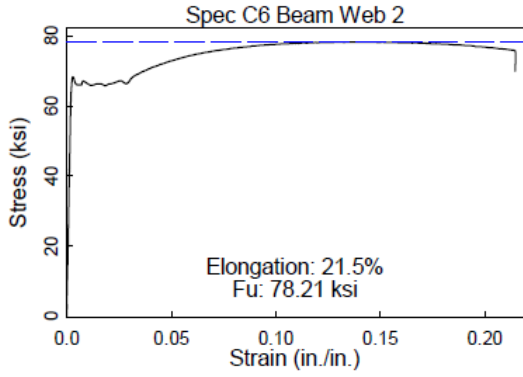
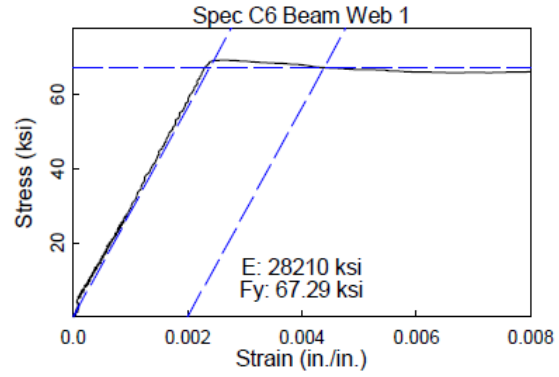
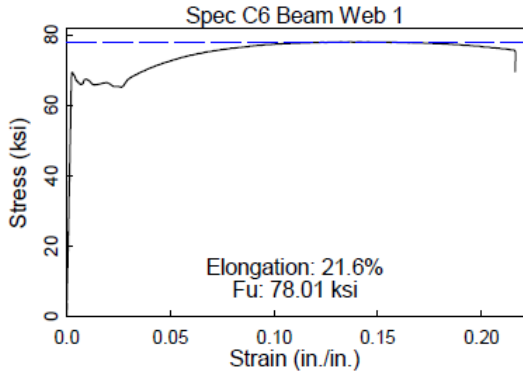
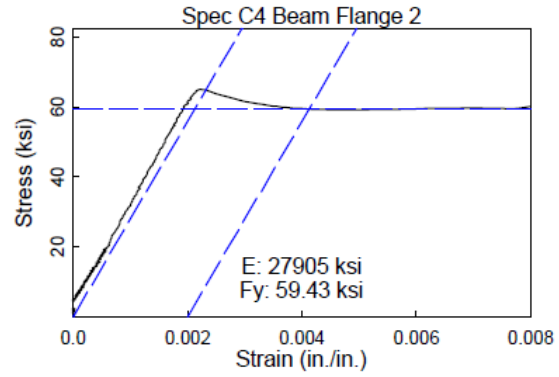
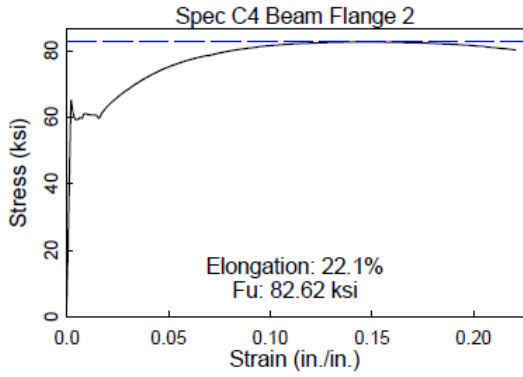
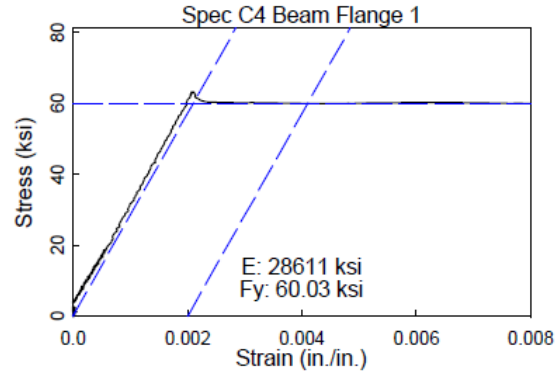
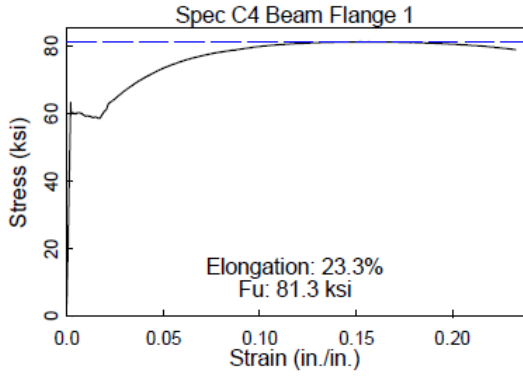


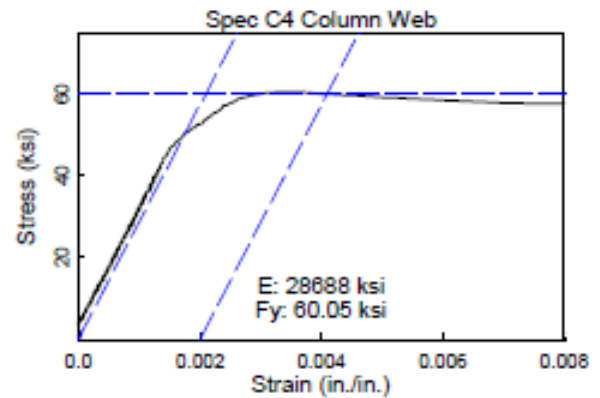
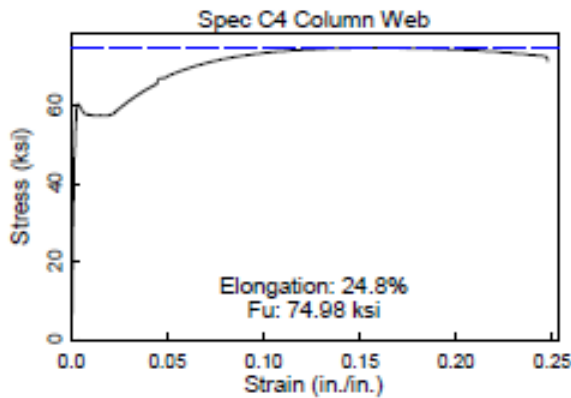
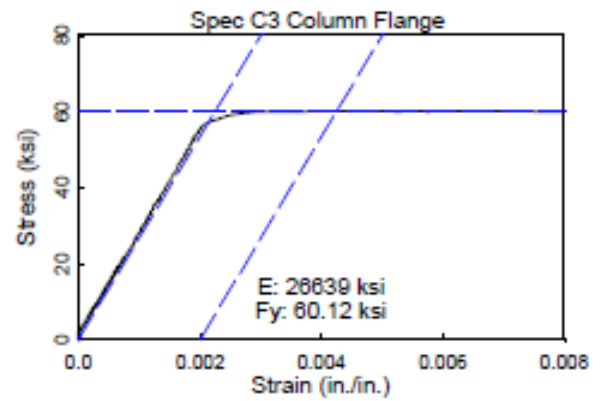
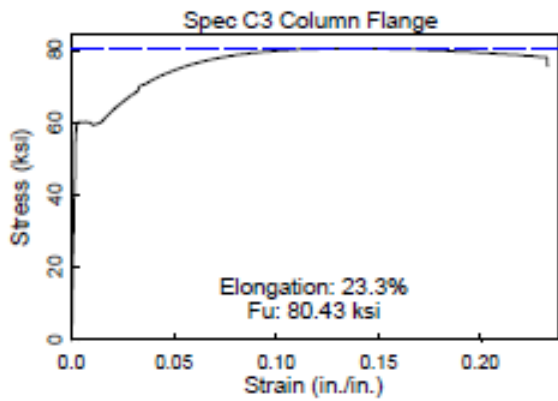
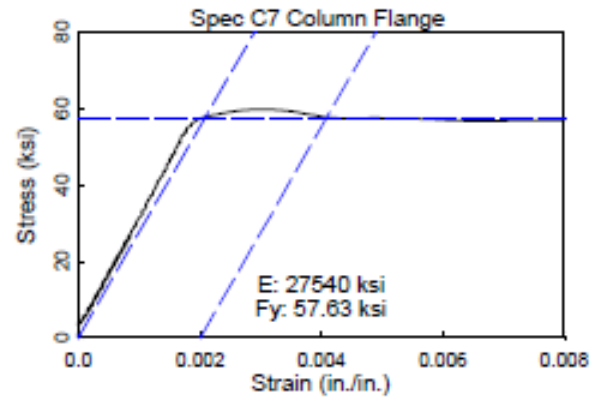
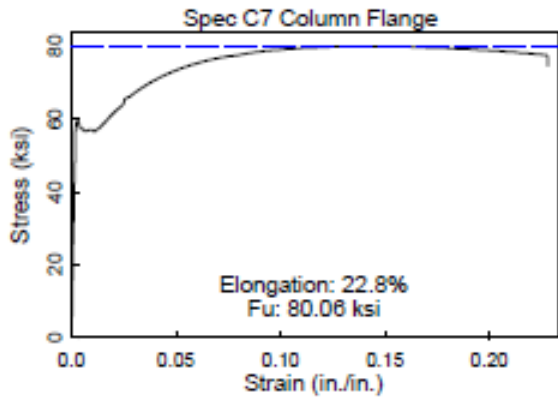
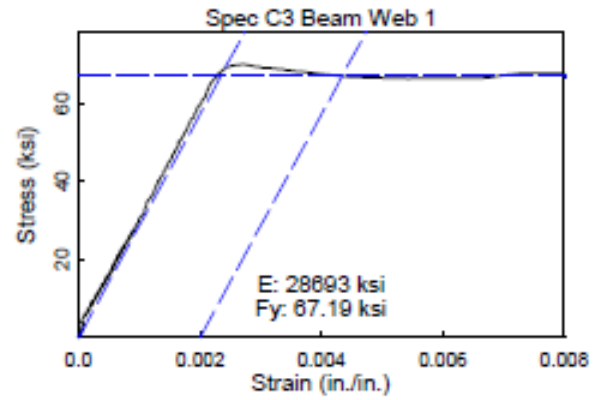
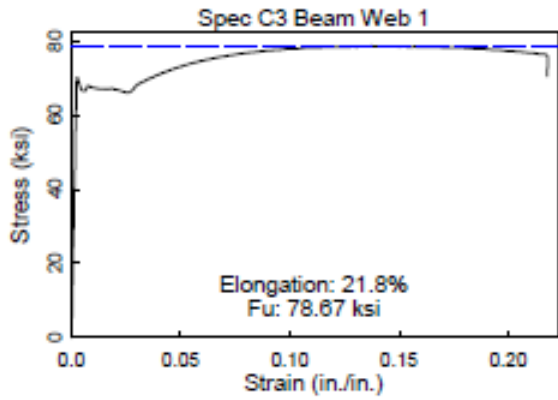


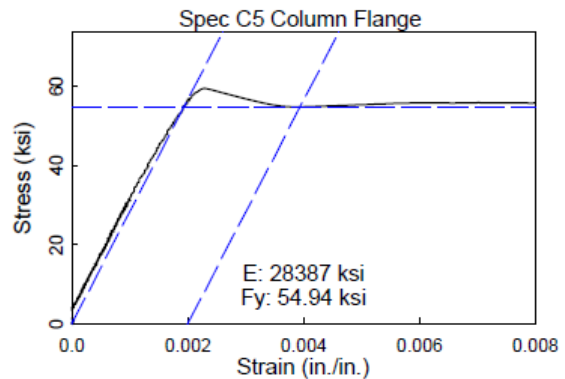
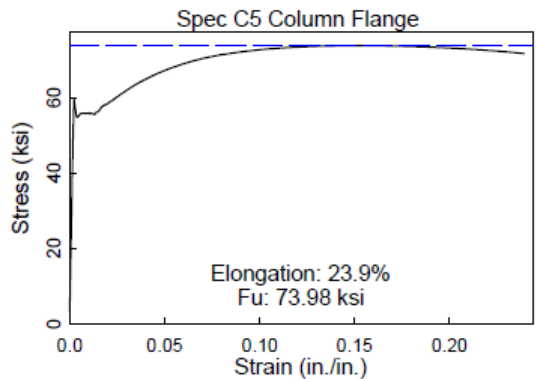
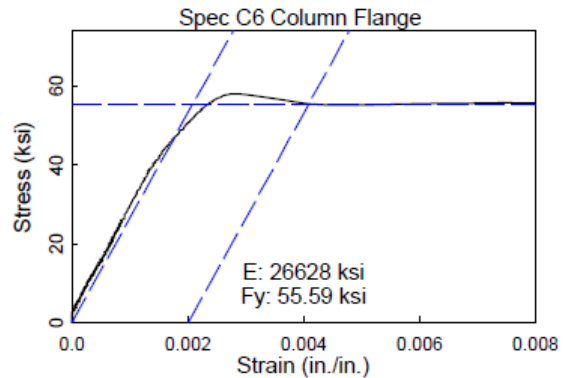
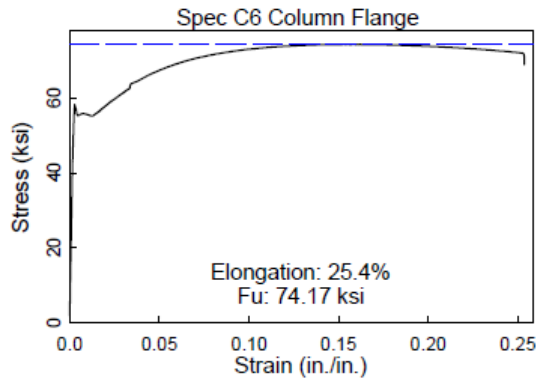
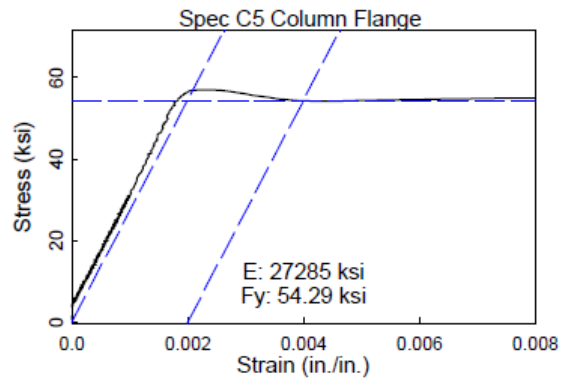
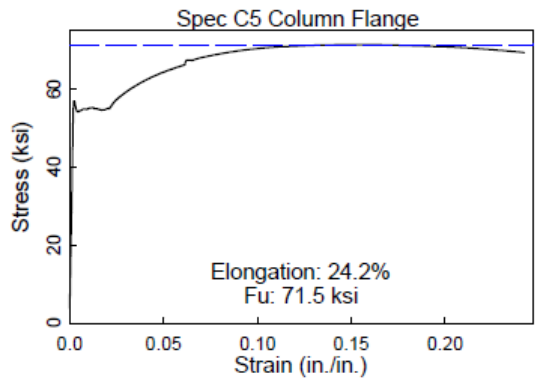
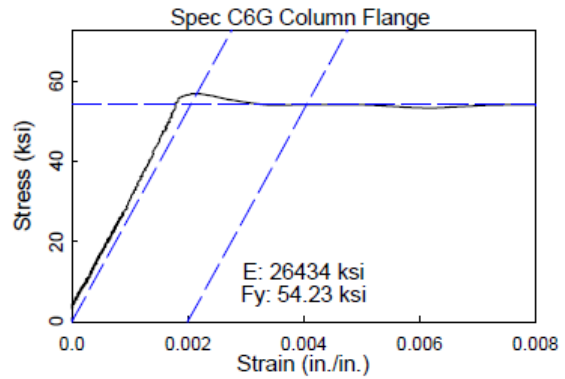
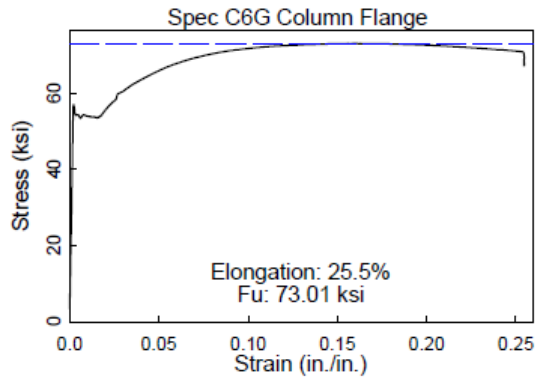


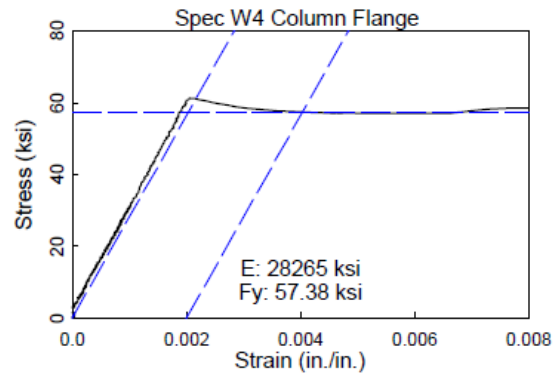
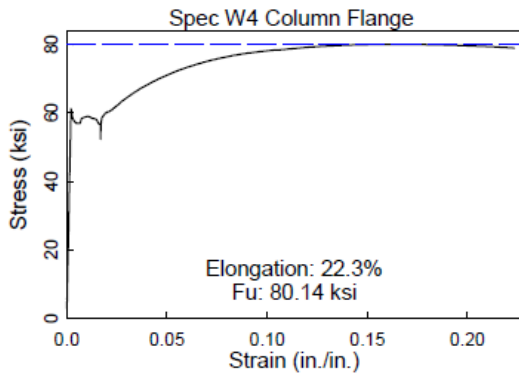
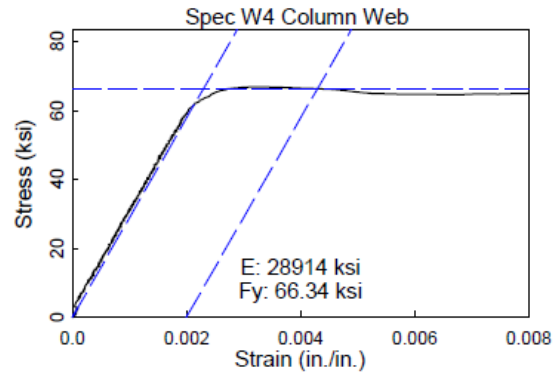
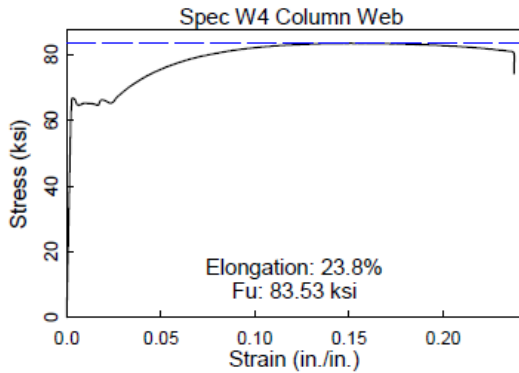
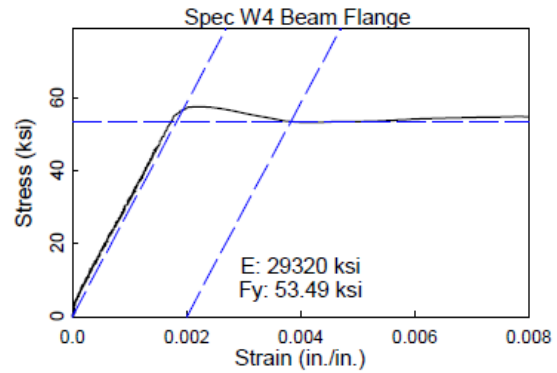
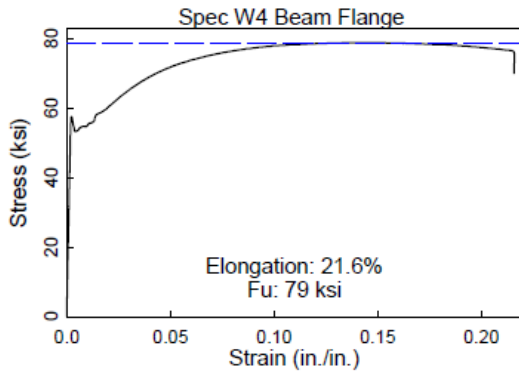
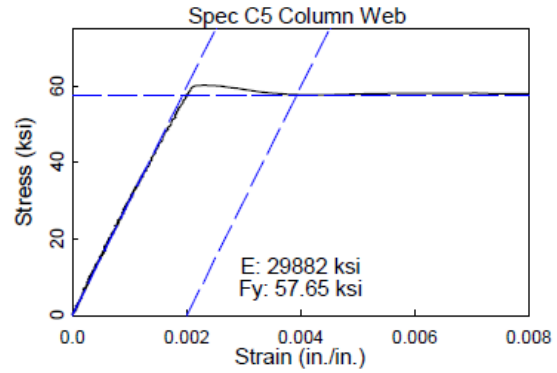
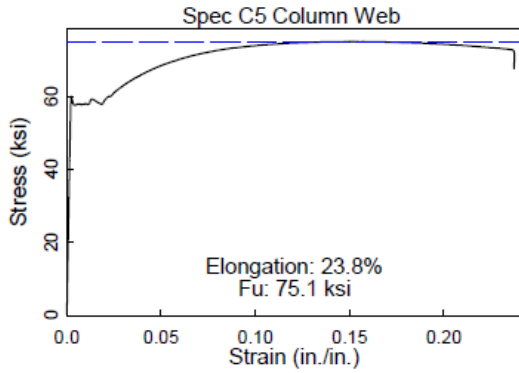


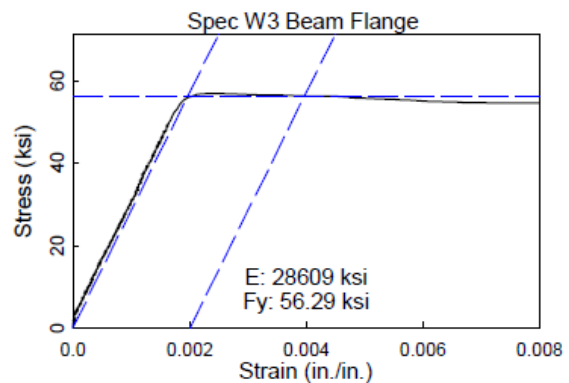
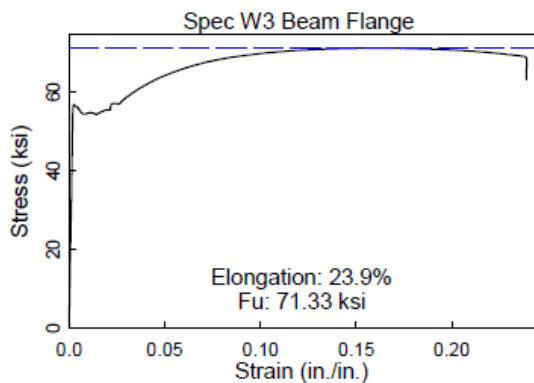
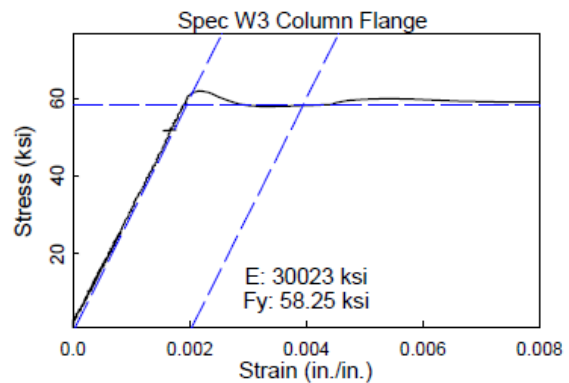
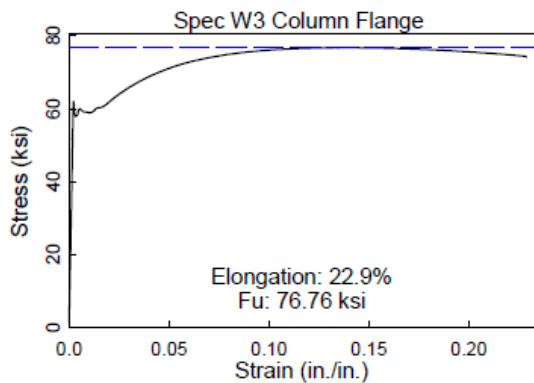
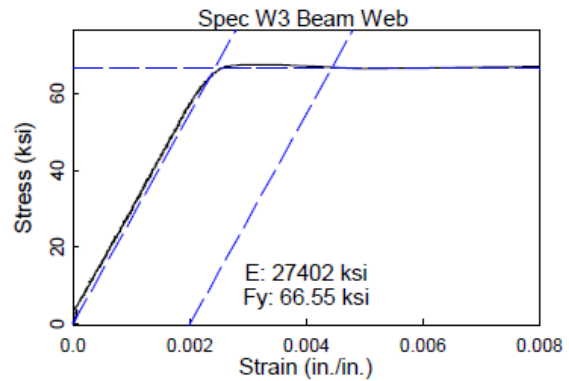
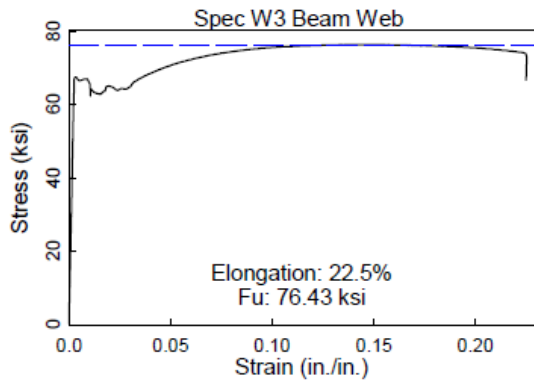
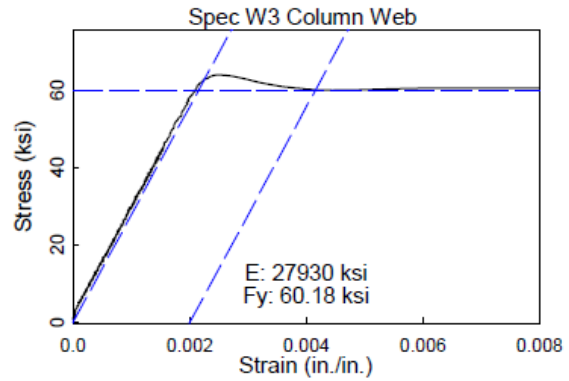
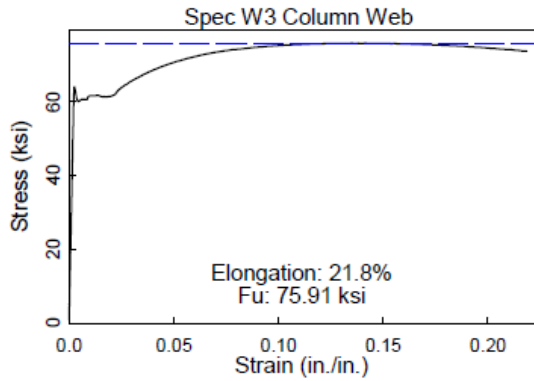


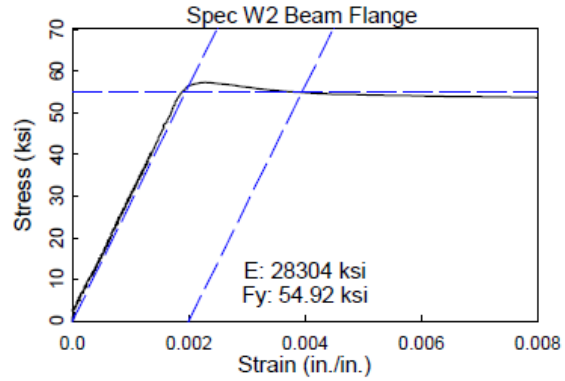
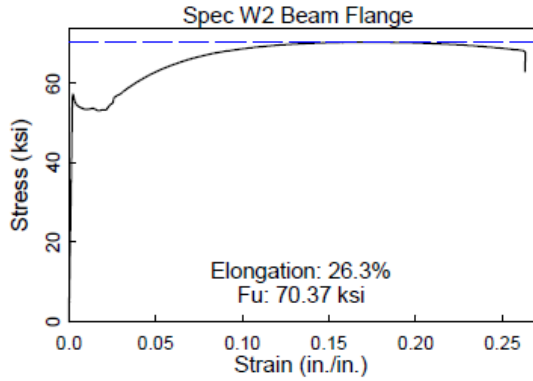
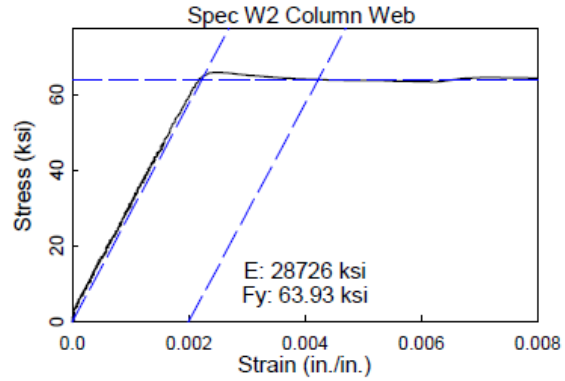
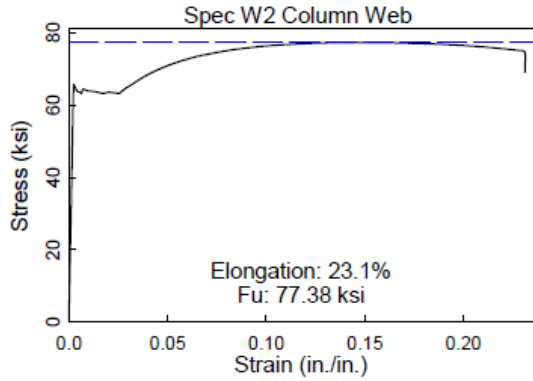
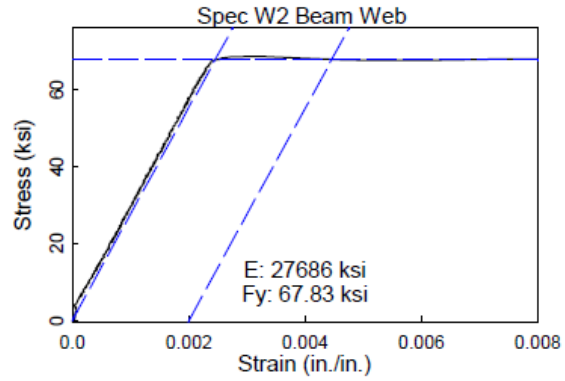
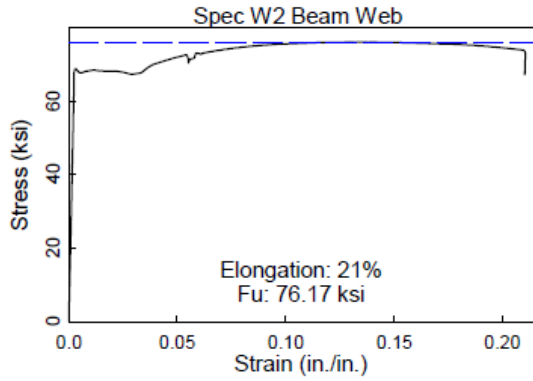
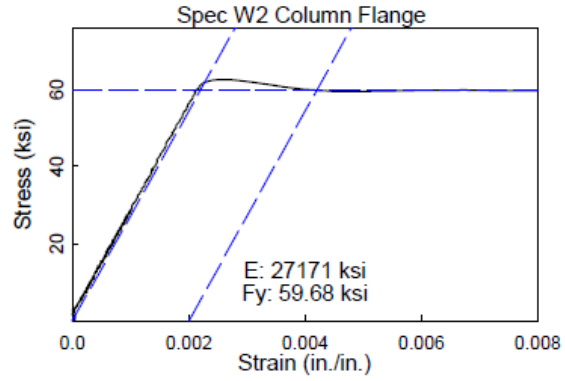
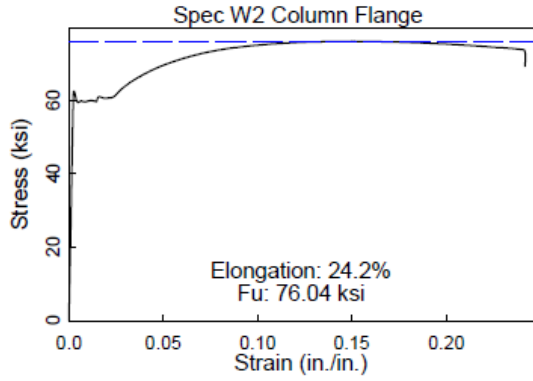


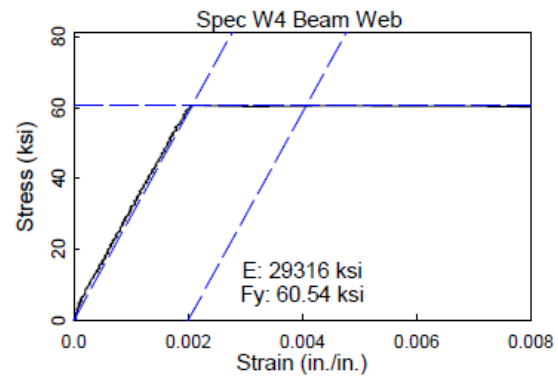
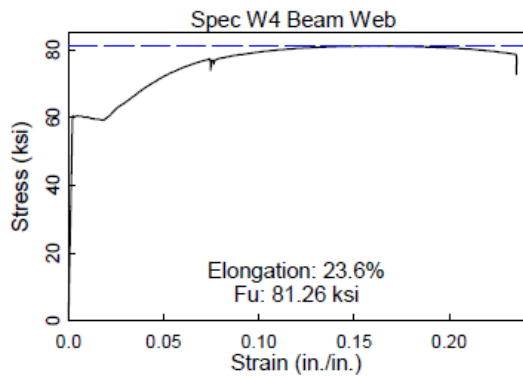
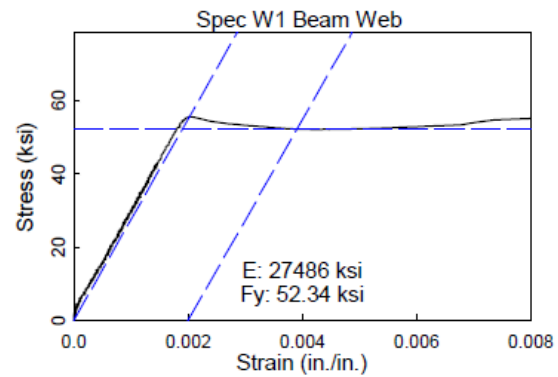
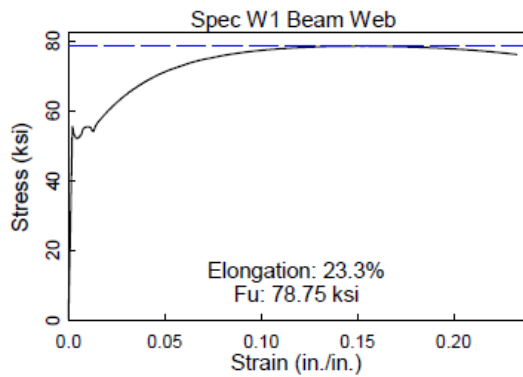
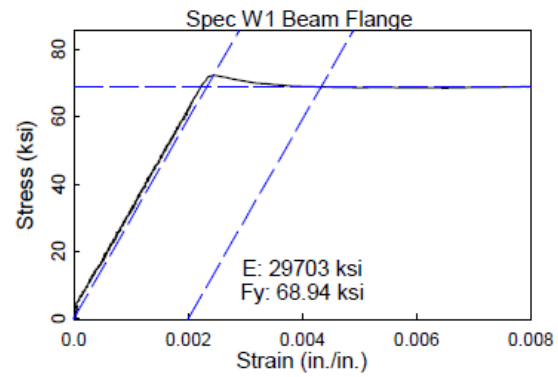
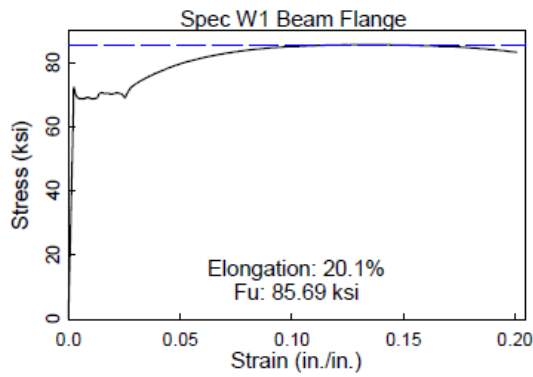
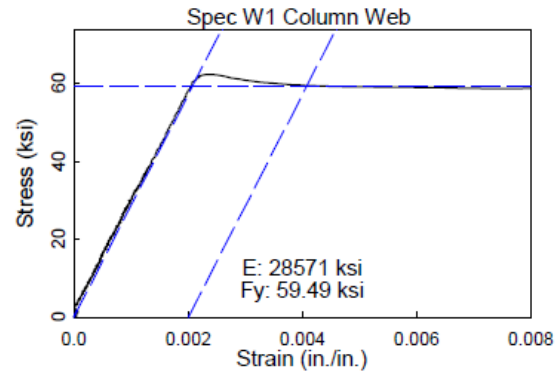
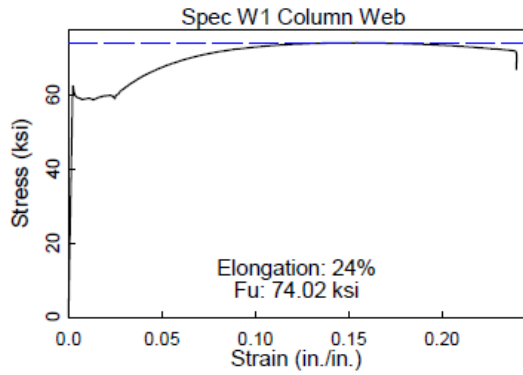


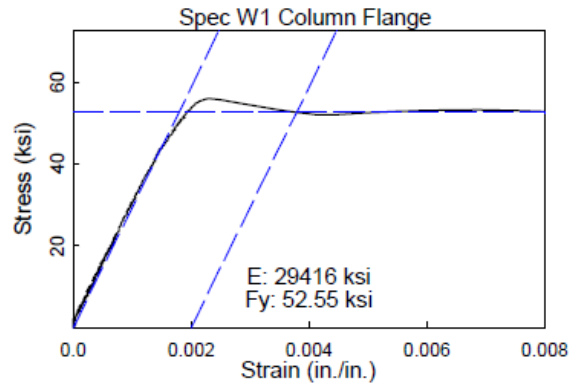
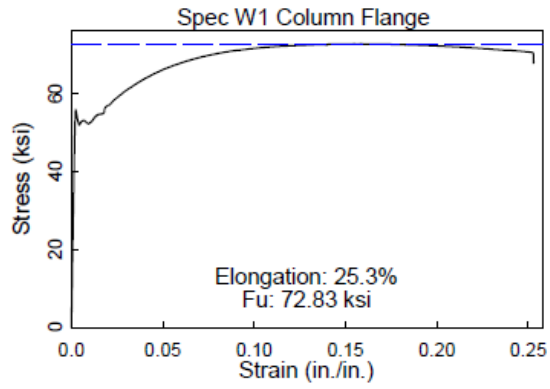












APPENDIX E: WELDING PROCEDURE SPECIFICATIONS

The Herrick Corporation FIELD Welding Procedure Specification Index Herrick Job #9870

WPS ID #	JOINT	ROOT/ANGLE	POSITION	ELECTRODE DIAMETER	LINCOLN ELECTRODE	CVN	PREQUALIFIED			DATE	REV #
							D1.8	YES	NO		
FCAW - Complete Penetration Welds											
FCAW CP-2	BTC-U4a-F	1/4" 45°	Vert (3G)	.072	NR-232	Yes	Yes	X		3/24/14	1
FCAW CP-22	BTC-U4a-F	3/8" 30°	Flat (1G)	3/32"	NR-305	Yes	Yes	X		3/24/14	1
FCAW - Fillet Welds											
FCAW F-3	Fillet	Fillet	OH (4F)	.072	NR-232	Yes	Yes	X		3/24/14	2
MIXED WELDS											
MIX-#2	Field	E71T-8 & E70T-6	1G	0.72 & 3/32"	NR-232 & NR-305	YES	YES		X	7/12/01	0


WELDING PROCEDURE SPECIFICATION (WPS) YES (X)

PREQUALIFIED X QUALIFIED BY TESTING _____

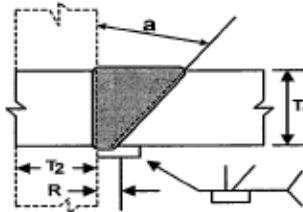
Company Name The Herrick Corporation
 Welding Process (es) FCAW
 Supporting PQR No. (s) N/A

Identification # FCAW CP - 2
 Revision # 1 Date 03/24/14 By JWG
 Authorized by _____ Date 07/25/13
 Type - Manual () Semi - Automatic (X)
 Machine () Automatic ()

JOINT DESIGN USED Type <u>BTC-U4a-F</u> Single (X) Double Weld () Backing Yes (X) No () Backing Material <u>A36 1/4" Min.</u> Root Opening <u>1/4"</u> Root Face Dimension <u>0</u> Groove Angle <u>45°</u> Radius (J - U) <u>N/A</u> Back Gouging Yes () No (X) Method <u>N/A</u>		POSITION Position of Groove <u>Vert (3G)</u> Fillet <u>N/A</u> Vertical Progression <u>Up (X)</u> Down ()	
BASE METALS Material Spec. <u>AWS D1.1 Table 3.1 Group 1, 2, 3</u> Type or Grade <u>(Except for Group 3 to Group 3)</u> Thickness Groove <u>Unlimited</u> Fillet <u>N/A</u> Diameter (Rebar) <u>N/A</u>		ELECTRICAL CHARACTERISTICS DC Transfer Mode (GMAW) Short - Circuiting () Globular () Spray () Current: AC () DCEP () DCEN (X) Pulsed () Power Source: CC () CV (X)	
FILLER METALS AWS Specification <u>A5.20</u> AWS Classification <u>E71T-8</u> <u>Lincoln's NR-232</u>		TECHNIQUE Stringer or Weave Bead <u>Stringer Bead</u> Multi - pass or Single Pass (per side) <u>Multi/Single</u> Number of electrodes <u>One</u> Longitudinal <u>N/A</u> Lateral <u>N/A</u> Angle <u>N/A</u>	
SHIELDING Flux <u>N/A</u> Gas <u>N/A</u> Composition <u>N/A</u> Electrode - Flux (Class) <u>N/A</u> Flow Rate <u>N/A</u> Gas Cup Size <u>N/A</u>		Contact Tube to Work Distance <u>3/4" - 1 1/4"</u> Peening: <u>None</u> Interpass Cleaning <u>Pneumatic Chipping Hammer or Brush</u>	
PREHEAT Preheat Temp., Min. <u>See below *</u> Interpass Temp., Min. <u>See below</u> Max <u>550° F</u>		POSTWELD HEAT TREATMENT Temp. <u>None*</u> Time <u>N/A</u>	


 Jose W Garcia
 CWI 98010941
 QC1 EXP. 12/1/2015

WELDING PROCEDURE

Pass or Weld Layer (s)	Process	Filler Metals		Current		In/Min Wire Feed Speed	Volts	In/Min Travel Speed	Joint Details								
		Class	Diam.	Type & Polarity	Amps												
ALL	FCAW	E71T-8	.072	DCEN	255 ±10%	170 ±10%	21 ±7%	7" ±15%									
Heat Input Range: 30 - 78 KJ/in																	
ALL	FCAW	E71T-8	.072	DCEN	315 ±10%	250 ±10%	24 ±7%	9" ±15%	<table border="1"> <thead> <tr> <th colspan="2">TOLERANCES</th> </tr> <tr> <th>AS DETAILED</th> <th>AS FIT UP</th> </tr> </thead> <tbody> <tr> <td>R = + 1/16, - 0</td> <td>+ 1/4, - 1/16</td> </tr> <tr> <td>a = + 10°, - 0°</td> <td>+ 10°, - 5°</td> </tr> </tbody> </table>	TOLERANCES		AS DETAILED	AS FIT UP	R = + 1/16, - 0	+ 1/4, - 1/16	a = + 10°, - 0°	+ 10°, - 5°
TOLERANCES																	
AS DETAILED	AS FIT UP																
R = + 1/16, - 0	+ 1/4, - 1/16																
a = + 10°, - 0°	+ 10°, - 5°																
Heat Input Range: 30 - 78 KJ/in																	

MINIMUM PREHEAT AND INTERPASS TEMPERATURE

UP TO 3/4"	OVER 3/4" - 1 1/2"	OVER 1 1/2" - 2 1/2"	OVER 2 1/2"
NONE *	50 °F	150 °F	225 °F

* When Base Metal is Below 32 °F, preheat to at least 70° and maintain during welding. For Material A913-65 use elevated preheat temperature as per AWS D1.1-(2010) Table 3.2 Category C. This procedure conforms to ANSI/AWS D1.1-(2010), see project specification for additional notes. The maximum pass width for 1G, 2G, and 4G, is 5/8" and 1" for 3G. Thickness of weld layer in groove weld, except surface layer, shall not exceed 1/4".

WELDING PROCEDURE SPECIFICATION (WPS) YES (X)

PREQUALIFIED X QUALIFIED BY TESTING _____

Company Name The Herrick Corporation
 Welding Process (es) FCAW
 Supporting PQR No. (s) N/A

Identification # FCAW CP - 22
 Revision #1 Date 03/24/14 By JWG
 Authorized by _____ Date 07/25/13
 Type - Manual () Semi - Automatic (X)
 Machine () Automatic ()

JOINT DESIGN USED Type <u>BTC-U4a-F</u> Single (X) Double Weld () Backing Yes (X) No () Backing Material <u>A36 1/4" Min.</u> Root Opening <u>3/8"</u> Root Face Dimension <u>0</u> Groove Angle <u>30°</u> Radius (J - U) <u>N/A</u> Back Gouging Yes () No (X) Method <u>N/A</u>		POSITION Position of Groove <u>Flat (1G)</u> Fillet <u>N/A</u> Vertical Progression Up () Down ()	
BASE METALS Material Spec. <u>AWS D1.1 Table 3.1 Group 1, 2, 3</u> Type or Grade <u>(Except for Group 3 to Group 3)</u> Thickness Groove <u>Unlimited</u> Fillet <u>N/A</u> Diameter (Rebar) <u>N/A</u>		ELECTRICAL CHARACTERISTICS DC Transfer Mode (GMAW) Short - Circuiting () Globular () Spray () Current AC () DCEP (X) DCEN () Pulsed () Power Source: CC () CV (X)	
FILLER METALS AWS Specification <u>A5.20</u> AWS Classification <u>E70T-6</u> <u>Lincoln's NR-305</u>		TECHNIQUE Stringer or Weave Bead <u>Stringer Bead</u> Multi - pass or Single Pass (per side) <u>Multi/Single</u> Number of electrodes <u>One</u> Longitudinal <u>N/A</u> Lateral <u>N/A</u> Angle <u>N/A</u>	
SHIELDING Flux <u>N/A</u> Gas <u>N/A</u> Composition <u>N/A</u> Electrode - Flux (Class) <u>N/A</u> Flow Rate <u>N/A</u> Gas Cup Size <u>N/A</u>		Contact Tube to Work Distance <u>1 5/8" - 2 1/4"</u> Peening: None Interpass Cleaning <u>Pneumatic Chipping Hammer or Brush</u>	
PREHEAT Preheat Temp., Min. See below * Interpass Temp., Min See below Max <u>550° F</u>		POSTWELD HEAT TREATMENT Temp. None* Time <u>N/A</u>	

Jose W Garcia
 CWI 98010941
 QC1 EXP. 12/1/2015

WELDING PROCEDURE

Pass or Weld Layer (s)	Process	Filler Metals		Current		In/Min Wire Feed Speed	Volts	In/Min Travel Speed	Joint Details								
		Class	Diam.	Type & Polarity	Amps												
ALL	FCAW	E70T-6	3/32"	DCEP	425 ±10%	240 ±10%	25 ±7%	13" ±10%	<table border="1"> <thead> <tr> <th colspan="2">TOLERANCES</th> </tr> <tr> <th>AS DETAILED</th> <th>AS FIT UP</th> </tr> </thead> <tbody> <tr> <td>R = + 1/16, - 0</td> <td>+ 1/4, - 1/16</td> </tr> <tr> <td>D = + 10°, - 0°</td> <td>+ 10°, - 5°</td> </tr> </tbody> </table>	TOLERANCES		AS DETAILED	AS FIT UP	R = + 1/16, - 0	+ 1/4, - 1/16	D = + 10°, - 0°	+ 10°, - 5°
TOLERANCES																	
AS DETAILED	AS FIT UP																
R = + 1/16, - 0	+ 1/4, - 1/16																
D = + 10°, - 0°	+ 10°, - 5°																
Heat input Range: 35 - 66 KJ/in																	
ALL	FCAW	E70T-6	3/32"	DCEP	475 ±10%	300 ±10%	28 ±7%	17" ±10%									
Heat Input Range: 35 - 66 KJ/in																	

MINIMUM PREHEAT AND INTERPASS TEMPERATURE

UP TO 3/4"	OVER 3/4" - 1 1/2"	OVER 1 1/2" - 2 1/2"	OVER 2 1/2"
NONE *	50 °F	150 °F	225 °F

* When Base Metal is Below 32 °F, preheat to at least 70° and maintain during welding. For Material A913-65 use elevated preheat temperature as per AWS D1.1-(2010) Table 3.2 Category C. This procedure conforms to ANSI/AWS D1.1-(2010), see project specification for additional notes. The maximum pass width for 1G, 2G, and 4G, is 5/8" and 1" for 3G. Thickness of weld layer in groove weld, except surface layer, shall not exceed 1/4".


Herrick

WELDING PROCEDURE SPECIFICATION (WPS) YES (X)
 PREQUALIFIED X QUALIFIED BY TESTING _____

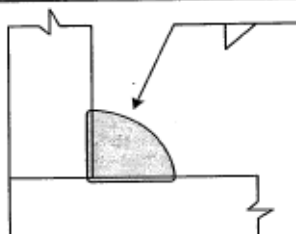
Company Name The Herrick Corporation
 Welding Process (es) FCAW
 Supporting PQR No. (s) N/A

Identification # FCAW F - 3
 Revision # 2 Date 03/24/14 By JWG
 Authorized by [Signature] Date 07/25/13
 Type - Manual () Semi - Automatic (X)
 Machine () Automatic ()

JOINT DESIGN USED Type <u>Fillet</u> Single (X) Double Weld () Backing Yes () No (X) Backing Material <u>N/A</u> Root Opening <u>N/A</u> Root Face Dimension <u>N/A</u> Groove Angle <u>N/A</u> Radius (J - U) <u>N/A</u> Back Gouging Yes () No (X) Method <u>N/A</u>		POSITION Position of Groove <u>N/A</u> Fillet <u>O.H (4F)</u> Vertical Progression Up () Down ()	
BASE METALS Material Spec. <u>AWS D1.1 Table 3.1 Group 1, 2, 3</u> Type or Grade <u>(Except for Group 3 to Group 3)</u> Thickness Groove <u>N/A</u> Fillet <u>Unlimited</u> Diameter (Rebar) <u>N/A</u>		ELECTRICAL CHARACTERISTICS DC Transfer Mode (GMAW) Short - Circuiting () Globular () Spray () Current: AC () DCEP () DCEN (X) Pulsed () Power Source: CC () CV (X)	
FILLER METALS AWS Specification <u>A5.20</u> AWS Classification <u>E71T-8 Lincoln's NR-232</u>		TECHNIQUE Stringer or Weave Bead <u>Stringer Bead</u> Multi - pass or Single Pass (per side) <u>Multi/Single</u> Number of electrodes <u>One</u> Longitudinal <u>N/A</u> Lateral <u>N/A</u> Angle <u>N/A</u>	
SHIELDING Flux <u>N/A</u> Gas <u>N/A</u> Composition <u>N/A</u> Electrode - Flux (Class) <u>N/A</u> Flow Rate <u>N/A</u> Gas Cup Size <u>N/A</u>		Contact Tube to Work Distance <u>3/4" - 1 1/4"</u> Peening: <u>None</u> Interpass Cleaning <u>Pneumatic Chipping Hammer or Brush</u>	
PREHEAT Preheat Temp., Min. <u>See below *</u> Interpass Temp., Min <u>See below</u> Max <u>550° F</u>		POSTWELD HEAT TREATMENT Temp. <u>None*</u> Time <u>N/A</u>	


 Jose W Garcia
 CWI 98010941
 QC1-EXP-12/1/2015

WELDING PROCEDURE

Pass or Weld Layer (s)	Process	Filler Metals		Current		In/Min Wire Feed Speed	Volts	In/Min Travel Speed	Joint Details	
		Class	Diam.	Type & Polarity	Amps					
ALL	FCAW	E71T-8	.072	DCEN	255 ±10%	170 ±10%	21 ±7%	7" ±15%	 FILLET Min. Weld Size See Table 5.8	
Heat Input Range: 30 - 78 KJ/in										
ALL	FCAW	E71T-8	.072	DCEN	315 ±10%	250 ±10%	24 ±7%	9" ±15%		
Heat Input Range: 30 - 78 KJ/in										

MINIMUM PREHEAT AND INTERPASS TEMPERATURE

UP TO 3/4"	OVER 3/4" - 1 1/2"	OVER 1 1/2" - 2 1/2"	OVER 2 1/2"
NONE *	50 °F	150 °F	225 °F

* When Base Metal is Below 32 °F, preheat to at least 70° and maintain during welding. For Material A913-65 use elevated preheat temperature as per AWS D1.1-(2010) Table 3.2 Category C. This procedure conforms to ANSI/AWS D1.1-(2010), see project specification for additional notes. The maximum single pass fillet weld size for 1F and 3F is 1/2", for 2F is 3/8", and for 4F is 5/16"

Herrick

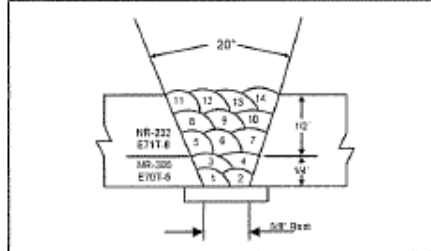
PROCEDURE QUALIFICATION RECORD (PQR)

Company Name The Herrick Corporation
 Welding Process (es) FCAW

Identification # MIX - #2
 Revision _____ Date _____ By _____
 Authorized by _____ Date 07/12/01
 Type - Manual () Semi - Automatic (X)
 Machine () Automatic ()

JOINT DESIGN USED Type <u>B-L2a-F</u> Single (X) Double Weld () Backing Yes (X) No () Backing Material <u>A36 1/2"</u> Root Opening <u>5/8"</u> Root Face Dimension <u>0</u> Groove Angle <u>20°</u> Radius (J - U) <u>N/A</u> Back Gouging Yes () No (X) Method <u>N/A</u>		POSITION Position of: Groove <u>Flat (1G)</u> Fillet <u>N/A</u> Vertical Progression Up () Down ()	
BASE METALS Material Spec <u>A572</u> Type or Grade <u>50</u> Thickness Groove <u>3/4"</u> Fillet <u>N/A</u> Diameter (Pipe) <u>N/A</u>		ELECTRICAL CHARACTERISTICS <u>DC</u> Transfer Mode (GMAW) Short - Circuiting () Globular () Spray () Current: AC () DCEP (X) DCEN (X) Pulsed () Other _____	
FILLER METALS AWS Specification <u>A5.20</u> AWS Classification <u>E70T-6</u> (Lincoln's <u>NR-305</u>) AWS Classification <u>E71T-8</u> (Lincoln's <u>NR-232</u>)		TECHNIQUE Stringer or Weave Bead <u>Stringer Bead</u> Multi - pass or Single Pass (per side) <u>Multiple</u> Number of electrodes <u>One</u> Electrode Spacing Longitudinal <u>N/A</u> Lateral <u>N/A</u> Angle <u>N/A</u>	
SHIELDING Flux <u>N/A</u> Gas <u>N/A</u> Electrode - Flux (Class) <u>N/A</u> Composition <u>N/A</u> Flow Rate <u>N/A</u> Gas Cup Size <u>N/A</u>		Contact Tube to Work Distance <u>1-1/2" and 3/4"</u> Peening <u>None</u> Interpass Cleaning <u>Pneumatic Chipping Hammer or Brush</u>	
PREHEAT Preheat Temp, Min <u>70°F</u> Interpass Temp, Min <u>70°F</u> Max <u>550°F</u>		POSTWELD HEAT TREATMENT Temp <u>None</u> Time <u>N/A</u>	

DETAIL



Pass or Weld Layer (s)	Process	Filler Metals		Current		Volts	In/Min Travel Speed
		Class	Diam.	Type & Polarity	Amps		
1-4	FCAW	E70T-6	3/32"	DCEP	425	28	15"
5-14	FCAW	E71T-8	072	DCEN	250	22	10"

Tested as per FEMA 353

ACCURATE WELD TESTING LAB

5223 TWEEDY BLVD., SOUTH GATE, CA 90280 PH(323)564-5879 FX(323)564-3843

Date: July 24, 2001

SAN BERNARDINO STEEL/HERRICK CORP.
5454 N. INDUSTRIAL PARKWAY
SAN BERNARDINO, CA 92427

Test Date: 07/24/01
WPS#: MIX#2
LAB# 776

CHARPY "V" NOTCH**TAKING SAMPLE OF THE WELD @ MID THICKNESS**

@THE WELD@ - 0°F.				
NOTCH LOCATION	IMPACT VALUE	% SHEAR	MILL. LAT. EXP	
1. WELD METAL	33	30	.034"	
2. WELD METAL	35	30	.030"	
3. *WELD METAL	35	30	.036"	
4. WELD METAL	33	30	.035"	
5. *WELD METAL	26	20	.026"	

AVG. FT. LBS.: 33.6

* LOW & HIGH READING, AVERAGE OF REMAINING THREE.



ACCURATE WELD TESTING LAB

Ronald S. Mobley 07/24/01
RONALD S. MOBLEY, LAB MANAGER

WE CERTIFY THAT THE ABOVE INFORMATION IS TRUE AND CORRECT

ACCURATE WELD TESTING LAB

5223 TWEEDY BLVD., SOUTH GATE, CA 90280 PH(323)564-5879 FX.(323)564-3843

SAN BERNARDINO STEEL/HERRICK.
5454 N. INDUSTRIAL PARKWAY
SAN BERNARDINO, CA 92427

Date: 07/17/01
Lab#: 675
WPS# MIX#2

CHARPY "V" NOTCH

SAMPLE WAS TAKEN FROM THE WELD @ MID THICKNESS

MATERIAL: A-572, GR. 50

CVN SIZE: 10 MM X 10 MM TEST TEMP: +70° F. MIN. ACCEPTABLE VALUE: 40 FT. LBS

	NOTCH LOCATION	IMPACT VALUE	% SHEAR	MILL. LAT. EXP
1.	BASE METAL	60	90	.063"
2.	*BASE METAL	64	90	.059"
3.	*BASE METAL	57	90	.056"
4.	BASE METAL	59	90	.059"
5.	BASE METAL	61	90	.060"

AVG. FT. LBS.: 60

* LOW & HIGH READING, AVERAGE OF REMAINING THREE.



ACCURATE WELD TESTING LAB

Ronald S. Mobley
07/17/01
RONALD S. MOBLEY, LAB-MANAGER

WE CERTIFY THAT THE ABOVE INFORMATION IS TRUE AND CORRECT



FLUX-CORED SELF-SHIELDED (FCAW-S) WIRE

INNERSHIELD® NR®-232

Mild Steel, All Position • AWS E71T-8, E71T8-A2-CS3-H16

KEY FEATURES

- High deposition rates for out-of-position welding
- Penetrating arc
- Fast freezing, easy to remove slag system
- Meets AWS D1.8 seismic lot waiver requirements

WELDING POSITIONS

All

TYPICAL APPLICATIONS

- Structural fabrication, including those subject to seismic requirements
- General plate fabrication
- Hull plate and stiffener welding on ships and barges
- Machinery parts, tanks, hoppers, racks and scaffolding

CONFORMANCES

AWS A5.20/A5.20M:	E71T-8-H16
AWS A5.36:	E71T8-A2-CS3-H16
ASME SFA-A5.20:	E71T-8-H16
ABS:	3YSA
Lloyd's Register:	3YS H15
DNV Grade:	III YMS H15
GL:	3YH10S
BV Grade:	SA3YMH
CWB/CSA W48-06:	E491T-8 H16
DB:	EN 758 T42 3 Y N 2
TUV:	EN 758 T42 3 Y N 2
MIL-E-24403/1*:	MIL-71T-BAS
FEMA 353	
AWS D1.8	
JIS Z 3313	T49T3B-1NA-H15

*Military Grade Classification of MIL-71T-BAS for 0.068 in (1.7 mm) and 0.072 in (1.8 mm) diameters only

DIAMETERS / PACKAGING

Diameter in (mm)	13.5 lb (6.1 kg) Coil 54 lb (24.5 kg) Master Carton	13.5 lb (6.1 kg) Coil 54 lb (24.5 kg) Hermetically Sealed Pail	25 lb (11.3 kg) Steel Spool
0.068 (1.7)	ED012518	ED030232	ED030643
0.072 (1.8)	ED012522		ED030644
5/64 (2.0)	ED012525		ED030647
Diameter in (mm)	25 lb (11.3 kg) Plastic Spool (Vacuum Sealed Foil Bag)		50 lb (22.7 kg) Coil
0.068 (1.7)	ED030948		ED012519
0.072 (1.8)			ED012523
5/64 (2.0)			ED012526

MECHANICAL PROPERTIES⁽¹⁾

	Yield Strength ⁽²⁾ MPa (ksi)	Tensile Strength MPa (ksi)	Elongation %	Hardness Rockwell B	Charpy V-Notch / (ft-lbf) @ -20°C (-20°F)
Requirements - AWS E71T-8	400 (58) min	480-655 (70-95)	22 min	-	27 (20) min
Typical Results⁽³⁾ - As-Welded	460-520 (66-75)	575-615 (83-89)	25-31	87-90	47-75 (35-55)

⁽¹⁾Typical of weld metal. ⁽²⁾Measured with 0.2% offset. ⁽³⁾See test results disclaimer.
NOTE: FEMA 353 and AWS D1.8 structural steel seismic supplement test data can be found on this product at www.lincolnelectric.com.

DEPOSIT COMPOSITION⁽¹⁾

	%C	%Mn	%Si	%S	%P	%Al
Requirements - AWS E71T-B	0.30 max	1.75 max	0.60 max	0.03 max	0.03 max	1.8 max
Typical Results⁽²⁾	0.16-0.18	0.61-0.72	0.26-0.33	≤0.01	≤0.01	0.5-0.8

TYPICAL OPERATING PROCEDURES

Diameter, Polarity	CTWD ⁽³⁾ mm (in)	Wire Feed Speed m/min (in/min)	Voltage ⁽⁴⁾ (volts)	Approx. Current (amps)	Melt-Off Rate kg/hr (lb/hr)	Deposition Rate kg/hr (lb/hr)	Efficiency (%)
0.069 in (1.7 mm), DC-	19-32 (3/4-1 1/4)	2.8 (110)	18-19	195	2.3 (5.0)	1.8 (3.9)	78
		3.3 (130)	19-21	225	2.8 (6.2)	2.0 (4.6)	74
		3.8 (150)	19-21	250	3.2 (7.1)	2.4 (5.3)	75
		4.3 (170)	20-22	270	3.5 (7.8)	2.8 (6.1)	78
		5.0 (195)	23-24	300	4.3 (9.4)	3.2 (7.0)	74
		6.4 (250)	23-24	350	5.4 (11.8)	4.0 (9.0)	76
		7.4 (320)	25-27	400	6.9 (15.2)	5.2 (11.4)	75
0.072 in (1.8 mm), DC-	19-32 (3/4-1 1/4)	2.0 (80)	16-18	130	1.8 (4.0)	1.5 (3.3)	83
		3.5 (140)	18-21	225	3.1 (6.8)	2.5 (5.5)	81
		3.9 (155)	19-22	240	3.3 (7.2)	2.7 (6.0)	83
		4.3 (170)	20-23	255	3.6 (8.0)	2.9 (6.5)	81
		6.4 (250)	22-24	315	5.3 (11.7)	4.3 (9.6)	82
		7.4 (290)	23-25	350	6.2 (13.6)	5.0 (11.0)	81
5/64 in (2.0 mm), DC-	19-32 (3/4-1 1/4)	1.5 (60)	16-17	145	1.7 (3.7)	1.2 (2.7)	73
		2.9 (115)	19-20	260	3.2 (7.0)	2.5 (5.5)	78
		3.0 (120)	19-20	270	3.3 (7.3)	2.6 (5.7)	78
		3.3 (130)	20-21	285	3.5 (7.8)	2.8 (6.2)	79
		4.6 (180)	22-23	365	5.0 (10.9)	3.9 (8.7)	80

⁽¹⁾Typical of weld metal. ⁽²⁾Measured with 0.2% offset. ⁽³⁾See test results disclaimer. ⁽⁴⁾NOTE: F344, 203 and AWS D1.8 structures steel fabricators supplement test data can be found on this product at www.lincolnelectric.com.

Material Safety Data Sheets (MSDS) and Certificates of Conformance are available on our website at www.lincolnelectric.com

TEST RESULTS
 Test results for mechanical properties, deposit or electrode composition and diffusible hydrogen levels were obtained from a weld produced and tested according to prescribed standards, and should not be assumed to be the expected results in a particular application or weldment. Actual results will vary depending on many factors, including, but not limited to, weld procedure, plate chemistry and temperature, weldment design and fabrication methods. Users are cautioned to confirm by qualification testing, or other appropriate means, the suitability of any welding consumable and procedure before use in the intended application.

CUSTOMER ASSISTANCE POLICY
 The Lincoln Electric Company is manufacturing and selling high quality welding equipment, consumables, and cutting equipment. Our challenge is to meet the needs of our customers and to exceed their expectations. On occasion, purchasers may ask Lincoln Electric for information or advice about their use of our products. Our employees respond to inquiries to the best of their ability based on information provided to them by the customer and the knowledge they may have concerning the application. Our employees, however, are not in a position to verify the information provided or to evaluate the engineering requirements for the particular weldment. Accordingly, Lincoln Electric does not warrant or guarantee or assume any liability with respect to such information or advice. Moreover, the provision of such information or advice does not create, expand, or alter any warranty on our products. Any express or implied warranty that might arise from the information or advice, including any implied warranty of merchantability or any warranty of fitness for any customer's particular purpose is specifically disclaimed.
 Lincoln Electric is a responsive manufacturer, but the selection and use of specific products sold by Lincoln Electric is solely within the control of, and remains the sole responsibility of the customer. Many variables beyond the control of Lincoln Electric affect the results obtained in applying these types of fabrication methods and service requirements.
 Subject to Change - This information is accurate to the best of our knowledge at the time of printing. Please refer to www.lincolnelectric.com for any updated information.



The Lincoln Electric Company
 23801 St. Clair Avenue
 Cleveland, Ohio 44111-1199

CERTIFICATE OF CONFORMANCE



Product: Innershield® NR®-232
 Classification: E71T-8-H16
 E71T8-A2-C83-H16
 Specification: AWS A5.20:2005, ASME SFA-5.20
 AWS A5.36:2012, ASME SFA-5.36
 Date: October 03, 2016

This is to certify that the product named above is of the same classification(s) and design as the material used for the tests reported herein. The material was tested according to the specification(s) indicated and met all requirements. It was manufactured and supplied according to a Quality System Program that meets the requirements of ISO9001 among others as documented on The Lincoln Electric web page (<http://www.lincolnelectric.com/en-us/company/certifications.aspx>).

Operating Settings		E71T8-A2-C83-H16 Requirements	E71T-8-H16 Requirements	RESULTS
Electrode Size			.068" (1.7 mm)	5/64" (2.0 mm)
Current Type/Polarity			DC-	DC-
Nominal Voltage, V			21	20
Wire Feed Speed, cm/min (in/min)			483 (190)	457 (180)
Nominal Current, A			230	325
Average Heat Input, kJ/in (kJ/in)			1.7 (43)	1.7 (42)
Contact Tip to Work Distance, mm (in)			25 (1)	25 (1)
Pass/Layers			13/6	13/6
Preheat Temperature, °C (°F)		(60 min.)		
Interpass Temperature, °C (°F)		(275 - 325)		
Postweld Heat Treatment		As-welded		
Mechanical properties of weld deposits				
Tensile Strength, MPa (ksi)		(70 - 95)	590 (86)	830 (91)
Yield Strength, 0.2% Offset, MPa (ksi)		(58 min.)	460 (67)	500 (72)
Elongation, %		22 min.	30	28
Average Impact Energy		(20 min.)	39 (29)	57 (42)
Joules @ -20 °C (ft.lbs @ -20 °F)			39,39,39 (28,28,29)	57,59,59 (42,42,43)
Average Hardness, HRB		Info. Only	90	91
Chemical composition of weld deposits (weight %)				
C		0.30 max.	0.18	0.13
Mn		1.75 max.	0.65	0.64
Si		0.60 max.	0.27	0.29
S		0.030 max.	0.009	0.00
P		0.030 max.	0.01	0.01
Al		1.8 max.	0.6	0.6
B		Not Specified	0.0015	0.0015
Diffusible Hydrogen (per AWS A4.3)				
Electrode Size			.068" (1.7 mm)	5/64" (2.0 mm)
Current Type/Polarity			DC-	DC-
Nominal Voltage, V			21	21
Nominal Current, A			339	286
Diffusible Hydrogen, mL/100g		16 max.	8.2	6.2
Abs. Humidity (gr moisture/lb dry air)			62	62

The Lincoln Electric Company
22301 St. Clair Avenue
Cleveland, Ohio 44117-1199

CERTIFICATE OF CONFORMANCE



Product: Innershield® NR®-332
Classification: E71T-B-H16
Specification: E71T-A2-C83-H16
AWS A5.20-2005, ASME SFA-5.20
AWS A5.36-2012, ASME SFA-5.36
Date: October 03, 2016

1. This document meets the requirements of EN 10204, type 2.2, when a specific lot or order number is referenced. It does not meet the requirements of type 3.1.
2. The electrode sizes required to be tested for this classification are 0.088 inch and 5/64 inch. All other sizes manufactured will also meet these requirements.
3. Fillet Weld Test (conditions as required): Met requirements.
4. Radiographic inspection: Met requirements.
5. The strength and elongation properties reported here were obtained from tensile specimens artificially aged at 105°C (220°F) for 48 hours.
6. Strength values in SI units are reported to the nearest 10 MPa converted from actual data. Preheat and interpass temperature values in SI units are reported to the nearest 5 degrees.

Toronto Cunningham
Toronto Cunningham, Certification Supervisor
October 03, 2016
Date

Jon Ogborn
Jon Ogborn, Manager, Consumable Compliance
October 03, 2016
Date



CERTIFICATE OF CONFORMANCE

The Lincoln Electric Company
 23001 St. Clair Avenue
 Cleveland, Ohio 44117-1199

Product: Innershield® NR-232
 Electrode Lot Number: 14610717
 Classification: E71T-B-H16
 Specification: AWS D1.8:2016
 Date: May 24, 2017

This is to certify that the above listed product was manufactured to meet the Class TQ requirement of AWS A5.01 as required by clause 6.3.8.1 of AWS D1.8:2016.

The product stated herein was manufactured and supplied in accordance with the Quality System Program of The Lincoln Electric Co., Cleveland, Ohio, U.S.A., as outlined in our Quality Assurance Manual. The Quality System Program of The Lincoln Electric Co. has been accepted by ASME, ABS and approved by VATTUV, and is certified to ISO 9001.

Operating Settings	AWS D1.8 Requirements	High Heat Input Results .072" (1.8 mm)	Low Heat Input Results .072" (1.8 mm)
Required Size for Classification			
Current Type/Polarity		DC-	DC-
Nominal Voltage, V		22	20
Wire Feed Speed, cm/min (ft/min)		394 (155)	457 (180)
Nominal Current, A		245	270
Average Heat Input, kJ/mm (kJ/in)		2.9 (73)	1.2 (30)
Contact Tip to Work Distance, mm (in)		25 (1)	22 (7/8)
Travel Speed, cm/min (ft/min)		11 (4.4)	27 (10.6)
Pass/Layers		8/5	18/7
Preheat Temperature, °C (°F)		135 (275)	20 (68)
Interpass Temperature, °C (°F)		230 (450)	120 (250)
Weld Position		3G	1G

Mechanical properties of weld deposits

Tensile Strength, MPa (ksi)	(70 min.) (58 min.) 22 min.	580 (84) 410 (59) 28	630 (92) 500 (72) 26
Average Impact Energy Joules @ 21 °C (ft-lbs @ 70 °F)	(40 min.)	112 (82)	107 (79)
Average Impact Energy Joules @ -18 °C (ft-lbs @ 0 °F)	(40 min.)	59 (43) 54,60,62 (40,44,46)	61 (45) 58,61,63 (43,46,46)

- This product satisfies the requirements of AWS D1.8:2016, Annex E, after exposure for 1 week at 80°F / 60% relative humidity.
- The Charpy V-notch impact values reported at -18 °C (0 °F) are required when the Lowest Anticipated Service Temperature (LAST) is -28 °C (-20 °F).
- The Charpy V-notch impact values reported at 21 °C (70 °F) are required when the Lowest Anticipated Service Temperature (LAST) is 10 °C (50 °F).
- The strength and elongation properties reported here were obtained from tensile specimens artificially aged at 105°C (220°F) for 48 hours.
- Strength values in SI units are reported to the nearest 10 MPa converted from actual data. Preheat and interpass temperature values in SI units are reported to the nearest 5 degrees.

May 24, 2017

Date

Toronto Cunningham
 Toronto Cunningham, Certification Supervisor

Jan Ogborn

May 24, 2017

Date

Jan Ogborn, Manager, Consumable Compliance



INNERSHIELD® NR®-305

Mild Steel, Flat & Horizontal • AWS E70T-6, E70T6-A2-CS3-H16

KEY FEATURES

- High deposition rates in the flat and horizontal positions
- Smooth arc and low spatter levels
- Capable of producing weld deposits with impact properties exceeding 27 J (20 ft•lb) at -29°C (-20°F)
- Welds on lightly rusted or primed plate
- Meets AWS D1.8 seismic lot waiver requirements

WELDING POSITIONS

Flat & Horizontal

CONFORMANCES

AWS A5.20/A5.20M:	E70T-6 H16
AWS A5.36:	E70T6-A2-CS3-H16
ASME SFA-A5.20:	E70T-6 H16
FEMA 353	
AWS D1.8	
JIS Z 3313	T 49 3 T6-0 N A-H15

TYPICAL APPLICATIONS

- General plate fabrication
- Structural fabrication, including those subject to seismic requirements
- Bridges and offshore rigs
- Shipyards, stiffener welding on barges
- Welding over tack welds made with stick electrode

DIAMETERS / PACKAGING

Diameter In (mm)	25 lb (11.3 kg) Steel Spool	25 lb (11.3 kg) Plastic Spool (Vacuum Sealed Foil Bag)	50 lb (22.7 kg) Coil	50 lb (22.7 kg) 50 lb Coil (Vacuum Sealed Foil Bag)
5/64 (2.0) 3/32 (2.4)	ED034185	ED030971	ED012593	ED030005

MECHANICAL PROPERTIES⁽¹⁾

	Yield Strength ⁽²⁾ MPa (ksi)	Tensile Strength MPa (ksi)	Elongation %	Hardness Rockwell B	Charpy V-Notch J (ft•lb) @ -29°C (-20°F)
Requirements - AWS E70T-6	400 (58) min	480-655 (70-95)	22 min	-	27 (20) min
Typical Results⁽³⁾ - As-Welded	465-535 (68-77)	565-620 (82-90)	24-28	88-93	27-41 (20-30)

DEPOSIT COMPOSITION⁽¹⁾

	%C	%Mn	%Si	%S	%P	%Al
Requirements - AWS E70T-6	0.30 max	1.75 max	0.60 max	0.03 max	0.03 max	1.8 max
Typical Results⁽³⁾	0.06-0.09	1.08-1.57	0.20-0.27	≤0.01	≤0.01	0.9-1.1

TYPICAL OPERATING PROCEDURES

Diameter, Polarity	CTWD mm (in)	Wire Feed Speed m/min (in/min)	Voltage (volts)	Approx. Current (amps)	Melt-Off Rate kg/hr (lb/hr)	Deposition Rate kg/hr (lb/hr)	Efficiency (%)
5/64 in (2.0 mm), DC+	35-51 (1 3/8-2)	4.4 (175)	20-22	300	8.5 (10.5)	4.0 (8.8)	84
		5.6 (220)	21-23	330	6.0 (13.3)	5.0 (11.1)	83
		6.8 (260)	23-24	360	7.1 (15.7)	5.0 (13.1)	83
		7.6 (300)	24-26	375	8.2 (18.1)	6.9 (15.2)	84
		8.3 (325)	25-27	400	8.9 (19.7)	7.4 (16.4)	83
		4.1 (160)	21-23	330	6.0 (13.3)	5.0 (11.0)	82
3/32 in (2.4 mm), DC+	41-54 (1 5/8-2 1/4) ⁽⁴⁾	6.1 (240)	24-26	425	9.1 (20.0)	7.6 (16.7)	83
		7.5 (300)	27-29	475	11.3 (25.0)	9.5 (21.0)	84
		10.2 (400)	33-35	525	15.2 (33.4)	12.7 (28.0)	83

⁽¹⁾Typical of weld metal. ⁽²⁾Measured with 0.2% offset. ⁽³⁾See test results disclaimer. ⁽⁴⁾Use CTWD of 2 1/4 in (54 mm) for wire feed speeds greater than 300 ipm.
NOTE: FEMA 353 and AWS D1.8 structural steel seismic supplement test data can be found on this product at www.lincolnelectric.com.



Material Safety Data Sheets (MSDS) and Certificates of Conformance are available on our website at www.lincolnelectric.com

TEST RESULTS

Test results for mechanical properties, deposit or electrode composition and diffusible hydrogen levels were obtained from a weld produced and tested according to prescribed standards, and should not be assumed to be the expected results in a particular application or weldment. Actual results will vary depending on many factors, including, but not limited to, weld procedure, plate chemistry and temperature, weldment design and fabrication methods. Users are cautioned to confirm by qualification testing or other appropriate means, the suitability of any welding consumable and procedure before use in the intended application.

CUSTOMER ASSISTANCE POLICY

The Lincoln Electric Company is manufacturing and selling high quality welding equipment, consumables, and cutting equipment. Our challenge is to meet the needs of our customers and to exceed their expectations. On occasion, purchasers may wish Lincoln Electric for information or advice about their use of our products. Our employees respond to inquiries to the best of their ability based on information provided to them by the customers and the knowledge they may have concerning the application. Our employees, however, are not in a position to verify the information provided or to evaluate the engineering requirements for the particular weldment. Accordingly, Lincoln Electric does not warrant or guarantee or assume any liability with respect to such information or advice. Moreover, the provision of such information or advice does not create, expand, or alter any warranty on our products. Any express or implied warranty that might arise from the information or advice, including any implied warranty of merchantability or any warranty of fitness for any customer's particular purpose is specifically disclaimed.

Lincoln Electric is a responsible manufacturer, but the selection and use of specific products sold by Lincoln Electric is solely within the control of, and remains the sole responsibility of the customer. Many variables beyond the control of Lincoln Electric affect the results obtained in applying these types of fabrication methods and service requirements.

Subject to Change – This information is accurate to the best of our knowledge at the time of printing. Please refer to www.lincolnelectric.com for any updated information.

Publication c32000/6 | Issue Date 07/15
© Lincoln Global, Inc. All Rights Reserved.

THE LINCOLN ELECTRIC COMPANY
22801 St. Clair Avenue • Cleveland, OH • 44117-1199 • U.S.A.
Phone: +1.216.481.8100 • www.lincolnelectric.com



The Lincoln Electric Company
 22801 St. Clair Avenue
 Cleveland, Ohio 44117-1199

CERTIFICATE OF CONFORMANCE



Product: **Innershield® NR®-305**
 Classification: **E70T-G-H16**
E70T6-A2-CS3-H16
 Specification: **AWS A5.20:2005, ASME SFA-5.20**
AWS A5.36:2012, ASME SFA-5.36
 Date: **July 07, 2016**

This is to certify that the product named above is of the same classification(s) and design as the material used for the tests reported herein. The material was tested according to the specification(s) indicated and met all requirements. It was manufactured and supplied according to a Quality System Program that meets the requirements of ISO9001 among others as documented on The Lincoln Electric web page (<http://www.lincolnelectric.com/en-us/company/Pages/certifications.aspx>).

Operating Settings	E70T-G-H16 Requirements	RESULTS
Electrode Size	5/64 inch	5/64 inch
Current Type/Polarity		DC+
Nominal Voltage, V		25
Wire Feed Speed, cm/min (in/min)		711 (280)
Nominal Current, A		360
Average Heat Input, kJ/mm (kJ/in)	(35 - 65)	2.0 (50)
Contact Tip to Work Distance, mm (in)		35 (1 3/8)
Pass/Layers		9/5
Preheat Temperature, °C (°F)	(60 min.)	20 (71)
Interpass Temperature, °C (°F)	(275 - 325)	165 (325)
Postweld Heat Treatment	As-welded	As-welded

Mechanical properties of weld deposits	E70T-G-H16 Requirements	RESULTS
Tensile Strength, MPa (ksi)	(70 - 95)	540 (79)
Yield Strength, 0.2% Offset, MPa (ksi)	(58 min.)	440 (64)
Elongation %	22 min.	29
Average Impact Energy Joules @ -29 °C (ft-lbs @ -20 °F)	(20 min.)	52 (38) 52,52,53 (38,38,39)
Average Hardness, HRB	Info. Only	85

Chemical composition of weld deposits (weight %)	E70T-G-H16 Requirements	RESULTS
C	0.30 max.	0.07
Mn	1.75 max.	1.37
Si	0.60 max.	0.23
S	0.03 max.	0.00
P	0.03 max.	0.01
Al	1.8 max.	0.8

Diffusible Hydrogen (per AWS A4.3)	E70T-G-H16 Requirements	RESULTS
Electrode Size		5/64 inch
Current Type/Polarity		DC+
Nominal Voltage, V		24
Nominal Current, A		358
Diffusible Hydrogen, mL/100g	16.0 max.	4.3
Abs. Humidity (gr moisture/lb dry air)		55

The Lincoln Electric Company
 22801 St. Clair Avenue
 Cleveland, Ohio 44117-1199

CERTIFICATE OF CONFORMANCE



Product: Innershield® NR®-305
 Classification: E70T-6-H16
 E70TB-A2-CS3-H16
 Specification: AWS A5.20:2005, ASME SFA-5.20
 AWS A5.36:2012, ASME SFA-5.36
 Date: July 07, 2016

Operating Settings	E70T-6-H16 Requirements	RESULTS
Electrode Size	3/32 inch	3/32 inch
Current Type/Polarity		DC+
Nominal Voltage, V		26
Wire Feed Speed, cm/min (in/min)		610 (240)
Nominal Current, A		385
Average Heat Input, kJ/mm (kJ/in)	(40 - 65)	2.0 (52)
Contact Tip to Work Distance, mm (in)		41 (1 5/8)
Pass/Layers		9/5
Preheat Temperature, °C (°F)	(60 min.)	20 (71)
Interpass Temperature, °C (°F)	(275 - 325)	165 (325)
Postweld Heat Treatment	As-welded	As-welded

Mechanical properties of weld deposits		
Tensile Strength, MPa (ksi)	(70 - 95)	550 (80)
Yield Strength, 0.2% Offset, MPa (ksi)	(58 min.)	450 (65)
Elongation %	22 min.	28
Average Impact Energy Joules @ -29 °C (ft-lbs @ -20 °F)	(20 min.)	49 (36) 47,48,52 (35,36,39)
Average Hardness, HRB	Info. Only	88

Chemical composition of weld deposits (weight %)		
C	0.30 max.	0.06
Mn	1.75 max.	1.41
Si	0.60 max.	0.22
S	0.03 max.	0.00
P	0.03 max.	0.01
Al	1.8 max.	0.9

Diffusible Hydrogen (per AWS A4.3)	E70T-6-H16 Requirements	RESULTS
Electrode Size		3/32 inch
Current Type/Polarity		DC+
Nominal Voltage, V		27
Nominal Current, A		431
Diffusible Hydrogen, mL/100g	16.0 max.	6.1
Abs. Humidity (gr moisture/lb dry air)		68

The Lincoln Electric Company
 22801 St. Clair Avenue
 Cleveland, Ohio 44117-1199

CERTIFICATE OF CONFORMANCE



Product: Innershield® NR®-305
 Classification: E70T6-H16
 E70T6-A2-CS3-H16
 Specification: AWS A5.20:2005, ASME SFA-5.20
 AWS A5.30:2012, ASME SFA-5.36
 Date: July 07, 2016

Operating Settings	E70T6-A2-CS3-H16 Requirements	RESULTS
Electrode Size	5/64 inch	5/64 inch
Current Type/Polarity		DC+
Nominal Voltage, V		25
Wire Feed Speed, cm/min (in/min)		711 (280)
Nominal Current, A		360
Average Heat Input, kJ/min (kJ/in)	(35 - 65)	2.0 (50)
Contact Tip to Work Distance, mm (in)		35 (1 3/8)
Pass/Layers		9/5
Preheat Temperature, °C (°F)	(60 min.)	20 (71)
Interpass Temperature, °C (°F)	(275 - 325)	165 (325)
Postweld Heat Treatment	As-welded	As-welded

Mechanical properties of weld deposits

Tensile Strength, MPa (ksi)	(70 - 95)	540 (79)
Yield Strength, 0.2% Offset, MPa (ksi)	(58 min.)	440 (64)
Elongation %	22 min.	29
Average Impact Energy Joules @ -29 °C (ft-lbs @ -20 °F)	(20 min.)	52 (38)
		52, 52, 53 (38, 38, 39)
Average Hardness, HRB	Info. Only	85

Chemical composition of weld deposits (weight %)

C	0.30 max.	0.07
Mn	1.75 max.	1.37
Si	0.60 max.	0.23
S	0.030 max.	0.004
P	0.030 max.	0.014
Al	1.8 max.	0.8
B	Not Specified	0.0014

Diffusible Hydrogen (per AWS A4.3)

	E70T6-A2-CS3-H16 Requirements	RESULTS
Electrode Size		5/64 inch
Current Type/Polarity		DC+
Nominal Voltage, V		24
Nominal Current, A		358
Diffusible Hydrogen, mL/100g	16 max.	4
Abs. Humidity (gr moisture/lb dry air)		55

The Lincoln Electric Company
 22801 St. Clair Avenue
 Cleveland, Ohio 44117-1199

CERTIFICATE OF CONFORMANCE



Product: Innershield® NR®-305
 Classification: E70T-6-H16
 E70T6-A2-CS3-H16
 Specification: AWS A5.20:2005, ASME SFA-5.20
 AWS A5.36:2012, ASME SFA-5.36
 Date: July 07, 2016

Operating Settings	E70T6-A2-CS3-H16 Requirements	RESULTS
Electrode Size	3/32 inch	3/32 inch
Current Type/Polarity		DC+
Nominal Voltage, V		26
Wire Feed Speed, cm/min (in/min)		610 (240)
Nominal Current, A		385
Average Heat Input, kJ/mm (kJ/in)	(40 - 65)	2.0 (52)
Contact Tip to Work Distance, mm (in)		41 (1 5/8)
Pass/Layers		9/5
Preheat Temperature, °C (°F)	(60 min.)	20 (71)
Interpass Temperature, °C (°F)	(275 - 325)	165 (325)
Postweld Heat Treatment	As-welded	As-welded

Mechanical properties of weld deposits

Tensile Strength, MPa (ksi)	(70 - 95)	550 (80)
Yield Strength, 0.2% Offset, MPa (ksi)	(58 min.)	450 (65)
Elongation %	22 min.	28
Average Impact Energy Joules @ -29 °C (ft-lbs @ -20 °F)	(20 min.)	49 (36) 47, 48, 52 (35, 36, 39)
Average Hardness, HRB	Info. Only	88

Chemical composition of weld deposits (weight %)

C	0.30 max.	0.06
Mn	1.75 max.	1.41
Si	0.60 max.	0.22
S	0.030 max.	0.003
P	0.030 max.	0.013
Al	1.8 max.	0.9

Diffusible Hydrogen (per AWS A4.3)

	E70T6-A2-CS3-H16 Requirements	RESULTS
Electrode Size		3/32 inch
Current Type/Polarity		DC+
Nominal Voltage, V		27
Nominal Current, A		431
Diffusible Hydrogen, mL/100g	16 max.	6
Abs. Humidity (gr moisture/lb dry air)		68

1. This document meets the requirements of EN10204, type 2.2, when a specific lot or order number is referenced. It does not meet the requirements of type 3.1.
2. Fillet Weld Test (positions as required): Met requirements.
3. Radiographic Inspection: Met requirements.
4. The strength and elongation properties reported here were obtained from tensile specimens artificially aged at 105°C (220°F) for 48 hours.
5. Strength values in SI units are reported to the nearest 10 MPa converted from actual data. Preheat and interpass temperature values in SI units are reported to the nearest 5 degrees.

Toronto Cunningham

July 07, 2016

Toronto Cunningham, Certification Supervisor

Date

Marie Quintana

July 07, 2016

Marie Quintana, Director, Consumable Compliance

Date

The Lincoln Electric Company
22801 S. Clair Avenue
Cleveland, Ohio 44117-1199

Product: Innershield® NR®-305
Electrode Lot Number: 14159485
Classification: E70T-6-H16
Specification: AWS D1.8:2009
Date: June 08, 2015

This is to certify that the above listed product was manufactured to meet the Class T4 requirement of AWS A5.01 as required by clause 6.3.8.1 of AWS D1.8:2009.

The product noted herein was manufactured and supplied in accordance with the Quality System Program of The Lincoln Electric Co., Cleveland, Ohio, U.S.A., as outlined in our Quality Assurance Manual. The Quality System Program of The Lincoln Electric Co. has been accepted by ASME, ABS and approved by VOTIV, and is certified to ISO 9001:2013

CERTIFICATE OF CONFORMANCE
(APPLIES ONLY TO U.S. PRODUCTS)



Operating Settings	AWS D1.8 Requirements	High Heat Input Results	Low Heat Input Results
Electrode Size Polarity Wire Feed Speed, cm/min (in/min) Voltage, V Current, A Average Heat Input, kJ/mm (kJ/in) Contact Tip to Work Distance, mm (in) Pass/Layers Preheat Temperature, °C (°F) Interpass Temperature, °C (°F) Postweld Heat Treatment Weld Position	As-welded	3/32 inch DC+ 762 (300) 29 520 2.5 (64) 44 (1.75) 3/8 120 (250) 230 (450) As-welded 1G	3/32 inch DC+ 457 (180) 24 360 1.5 (37) 44 (1.75) 1/4/5 20 (68) 120 (250) As-welded 1G
Mechanical properties of weld deposits			
Tensile Strength, MPa (ksi) Yield Strength, 0.2% Offset, MPa (ksi) Elongation %	(70 min.) (58 min.) 22 min.	560 (81) 450 (66) 25	610 (89) 540 (78) 24
Average Impact Energy Joules @ 21 °C (49 °F)	(40 min.)	72 (53)	61 (45)
Average Impact Energy Joules @ 10 °C (49 °F)	(40 min.)	71, 72, 72 (52, 53, 53) 64, 65, 66 (47, 48, 49)	57, 63, 64 (42, 46, 47) 54 (40)

- This product satisfies the requirements of AWS D1.8:2009, Annex E, after exposure for 2 weeks at 80°F / 80% relative humidity. (LAST) is -1 °C (30 °F).
- The Charpy V-notch impact values reported at 10 °C (50 °F) are required when the Lowest Anticipated Service Temperature (LAST) is 10 °C (50 °F).
- The Charpy V-notch impact values reported at 21 °C (70 °F) are required when the Lowest Anticipated Service Temperature (LAST) is 10 °C (50 °F).
- Test assembly constructed of ASTM A372 Grade 50 steel.
- The strength and elongation properties reported here were obtained from tensile specimens artificially aged at 119°C (250°F) for 48 hours.
- Strength values in SI units are reported to the nearest 10 MPa converted from actual data. Preheat and interpass temperature values in SI units are reported to the nearest 5 degrees.

Toronto Cunningham
Toronto Cunningham, Certification Supervisor
June 08, 2015
Date

David Fink
Dave Fink, Manager, Compliance
Engineering, Consumable R&D
June 08, 2015
Date

**The Herrick Corporation SHOP Welding Procedure Specifications Index
Herrick Job #9960**

WPS ID#	PROCESS	JOINT	TYPE WELD	POSITION	ELECT. DIA	ELECTRODE TYPE	CVN	PREQ	QUAL	D1.8	REV.	DATE
COMPLETE PENETRATION WELDS												
THC-CP7	FCAW-G	B-U4b	0-45 Deg CP	1G-2G	3/32"	OSXLH-70	YES	YES		YES	1	5/28/14
THC-CP8	FCAW-G	TC-U4b	0-45 Deg CP	1G-2G	3/32"	OSXLH-70	YES	YES		YES	1	5/28/14
THC-CP12	FCAW-G	B-U4b	0-30 Deg CP	1G-2G	3/32"	OSXLH-70	YES		YES	YES	2	5/28/14
THC-CP13	FCAW-G	TC-U4b	0-30 Deg CP	1G-2G	3/32"	OSXLH-70	YES		YES	YES	2	5/28/14
THC-CP43	FCAW-G	Dblr-F	5/8 - 30 Deg CP	FLAT	3/32"	OSXLH-70	YES	YES		YES	0	5/31/19
PARTIAL PENETRATION WELDS												
THC-PP1	FCAW-G	BTC-P4	0-45 Deg PP	1G-2G	3/32"	OSXLH-70	YES	YES		YES	1	5/28/14
FILLET WELDS												
THC-F1	FCAW-G	FILLET	FILLET	1F-2F	3/32"	OSXLH-70	YES	YES		YES	2	5/28/14


Herrick

WELDING PROCEDURE SPECIFICATION (WPS) YES (X)
 PREQUALIFIED X QUALIFIED BY TESTING _____

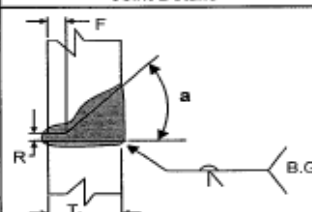
Company Name The Herrick Corporation
 Welding Process (es) FCAW-G
 Supporting PQR No. (s) N/A

Identification # THC-CP7
 Revision # 2 Date 5/28/14 By Joe Kraft
 Authorized by _____ Date 10/11/12
 Type Manual () Semi - Automatic (X)
 Machine () Automatic ()

JOINT DESIGN USED Type <u>B-U4b-F</u> Single (X) Double Weld () Backing Yes () No (X) Backing Material <u>N/A</u> Root Opening <u>0-1/8"</u> Root Face Dimension <u>0-1/8"</u> Groove Angle <u>45°</u> Radius (J - U) <u>N/A</u> Back Gouging Yes (X) No () Method <u>AIRARC</u>	POSITION Position of Groove <u>(1G) & (2G)</u> Fillet <u>N/A</u> Vertical Progression Up () Down ()
BASE METALS Material Spec. <u>AWS D1.1 Table 3.1 Group 1, 2, 3</u> Type or Grade <u>(Except for Group 3 to Group 3)</u> Thickness Groove <u>Unlimited</u> Fillet <u>N/A</u> Diameter (Rebar) <u>N/A</u>	ELECTRICAL CHARACTERISTICS DC Transfer Mode (GMAW) Short - Circuiting () Globular () Spray () Current: AC () DCEP (X) DCEN () Pulsed () Power Source: CC () CV (X)
FILLER METALS AWS Specification <u>A5.20</u> AWS Classification <u>E70T-9</u> (Lincoln's OSXLH-70)	TECHNIQUE Stringer or Weave Bead <u>Stringer Bead</u> Multi - pass or Single Pass (per side) <u>Multi/Single</u> Number of electrodes <u>One</u> Longitudinal <u>N/A</u> Lateral <u>N/A</u> Angle <u>N/A</u>
SHIELDING Flux <u>N/A</u> Gas <u>CO2</u> Composition <u>100%</u> Electrode - Flux (Class) <u>N/A</u> Flow Rate <u>50 CFH</u> Gas Cup Size <u>5/8"</u>	Contact Tube to Work Distance <u>1-1/8"</u> Peening: None Interpass Cleaning <u>Pneumatic Chipping Hammer or Brush</u>
PREHEAT Preheat Temp., Min. See below * Interpass Temp., Min See below Max <u>550° F</u>	POSTWELD HEAT TREATMENT Temp. <u>None**</u> Time <u>N/A</u>

 **Jose W Garcia**
 CWI 98010941
 QCT EXP. 12/1/2015

WELDING PROCEDURE

Pass or Weld Layer (s)	Process	Filler Metals		Current		In/Min Wire Feed Speed	Volts	In/Min Travel Speed	Joint Details	
		Class	Diam.	Type & Polarity	Amps					
ALL	FCAW-G	E70T-9	3/32"	DCEP	311-379	135-165	23-27	8"-14"		
Heat Input Range: 30 - 80 KJ/in										
ALL	FCAW-G	E70T-9	3/32"	DCEP	400-490	180-220	27-31	12"-20"		
Heat Input Range: 30 - 80 KJ/in										

TOLERANCES	
AS DETAILED	AS FIT UP
R = + 1/16, - 0	+ 1/16, - 1/8
F = + 1/16, - 0	NOT LIMITED
a = 10, - 0	10, - 5

MINIMUM PREHEAT AND INTERPASS TEMPERATURE

UP TO 3/4"	OVER 3/4" - 1 1/2"	OVER 1 1/2" - 2 1/2"	OVER 2 1/2"
NONE *	50 °F	150 °F	225 °F


* When Base Metal is Below 32° F, preheat to at least 70° and maintain during welding.
 **This procedure may vary due to fabrication sequence, fit-up, pass size, etc. within the limitation of variables given in the ANSI/AWS D1.1 (2010). See project welding specifications for additional notes.

Herrick

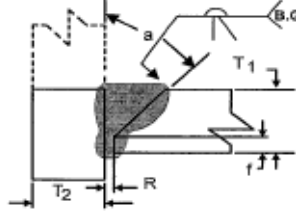
WELDING PROCEDURE SPECIFICATION (WPS) YES (X)
 PREQUALIFIED X QUALIFIED BY TESTING _____

Company Name The Herrick Corporation Identification # THC-CP8
 Revision # 2 Date 5/28/14 By Joe Kraft
 Authorized by [Signature] Date 10/11/12
 Type Manual () Semi - Automatic (X)
 Machine () Automatic ()

JOINT DESIGN USED Type <u>TC-U4b-F</u> Single (X) Double Weld () Backing Yes () No (X) Backing Material <u>N/A</u> Root Opening <u>0-1/8"</u> Root Face Dimension <u>0-1/8"</u> Groove Angle <u>45°</u> Radius (J - U) <u>N/A</u> Back Gouging Yes (X) No () Method <u>AIRARC</u>		POSITION Position of Groove <u>(1G) & (2G)</u> Fillet <u>N/A</u> Vertical Progression Up () Down ()	
BASE METALS Material Spec. <u>AWS D1.1 Table 3.1 Group 1, 2, 3</u> Type or Grade <u>(Except for Group 3 to Group 3)</u> Thickness Groove <u>Unlimited</u> Fillet <u>N/A</u> Diameter (Rebar) <u>N/A</u>		ELECTRICAL CHARACTERISTICS <u>DC</u> Transfer Mode (GMAW) Short - Circuiting () Globular () Spray () Current: AC () DCEP (X) DCEN () Pulsed () Power Source: CC () CV (X)	
FILLER METALS AWS Specification <u>A5.20</u> AWS Classification <u>E70T-9 (Lincoln's QSXLH-70)</u>		TECHNIQUE Stringer or Weave Bead <u>Stringer Bead</u> Multi - pass or Single Pass (per side) <u>Multi/Single</u> Number of electrodes <u>One</u> Longitudinal <u>N/A</u> Lateral <u>N/A</u> Angle <u>N/A</u>	
SHIELDING Flux <u>N/A</u> Gas <u>CO2</u> Composition <u>100%</u> Electrode - Flux (Class) <u>N/A</u> Flow Rate <u>50 CFH</u> Gas Cup Size <u>5/8"</u>		Contact Tube to Work Distance <u>1-1/8"</u> Peening <u>None</u> Interpass Cleaning <u>Pneumatic Chipping Hammer or Brush</u>	
PREHEAT Preheat Temp., Min. <u>See below *</u> Interpass Temp., Min <u>See below</u> Max <u>550° F</u>		POSTWELD HEAT TREATMENT Temp. <u>None**</u> Time <u>N/A</u>	

 **Jose W Garcia**
 CWI 98010941
 QC1 EXP. 12/1/2015

WELDING PROCEDURE

Pass or Weld Layer (s)	Process	Filler Metals		Current		In/Min Wire Feed Speed	Volts	In/Min Travel Speed	Joint Details										
		Class	Diam.	Type & Polarity	Amps														
ALL	FCAW-G	E70T-9	3/32"	DCEP	311-379	135-165	23-27	8"-14"											
Heat Input Range: 30 - 80 KJ/in																			
ALL	FCAW-G	E70T-9	3/32"	DCEP	400-490	180-220	27-31	12"-20"	<table border="1"> <thead> <tr> <th colspan="2">TOLERANCES</th> </tr> <tr> <th>AS DETAILED</th> <th>AS FIT UP</th> </tr> </thead> <tbody> <tr> <td>R = + 1/16, - 0</td> <td>+ 1/16, - 1/8</td> </tr> <tr> <td>t = + 1/16, - 0</td> <td>NOT LIMITED</td> </tr> <tr> <td>a = + 10, - 0</td> <td>+ 10, - 5</td> </tr> </tbody> </table>	TOLERANCES		AS DETAILED	AS FIT UP	R = + 1/16, - 0	+ 1/16, - 1/8	t = + 1/16, - 0	NOT LIMITED	a = + 10, - 0	+ 10, - 5
TOLERANCES																			
AS DETAILED	AS FIT UP																		
R = + 1/16, - 0	+ 1/16, - 1/8																		
t = + 1/16, - 0	NOT LIMITED																		
a = + 10, - 0	+ 10, - 5																		
Heat Input Range: 30 - 80 KJ/in																			

MINIMUM PREHEAT AND INTERPASS TEMPERATURE

UP TO 3/4"	OVER 3/4" - 1 1/2"	OVER 1 1/2" - 2 1/2"	OVER 2 1/2"
NONE *	50 °F	150 °F	225 °F

* When Base Metal is Below 32° F, preheat to at least 70° and maintain during welding.

**This procedure may vary due to fabrication sequence, fit-up, pass size, etc. within the limitation of variables given in the ANSI/AWS D1.1 (2010). See project welding specifications for additional notes.

Company Name The Herrick Corporation
 Welding Process (es) FCAW-G
 Supporting PQR No. (s) FCAW-CP-4b

Identification # THC-CP12
 Revision # 2 Date 5/28/14 By Joe Kraft
 Authorized by [Signature] Date 10/11/12
 Type - Manual () Semi - Automatic (X)
 Machine () Automatic ()

JOINT DESIGN USED Type <u>B-U4b-F</u> Single (X) Double Weld () Backing Yes () No (X) Backing Material <u>N/A</u> Root Opening <u>0-1/16"</u> Root Face Dimension <u>0-1/16"</u> Groove Angle <u>30°</u> Radius (J - U) <u>N/A</u> Back Gouging Yes (X) No () Method <u>AIRARC</u>		POSITION Position of Groove <u>(1G) & (2G)</u> Fillet <u>N/A</u> Vertical Progression Up () Down ()	
BASE METALS Material Spec. <u>AWS D1.1 Table 3.1 Group 1, 2, 3</u> Type or Grade <u>(Except for Group 3 to Group 3)</u> Thickness Groove <u>Unlimited</u> Fillet <u>N/A</u> Diameter (Rebar) <u>N/A</u>		ELECTRICAL CHARACTERISTICS DC Transfer Mode (GMAW) Short - Circuiting () Globular () Spray () Current: AC () DCEP (X) DCEN () Pulsed () Power Source: CC () CV (X)	
FILLER METALS AWS Specification <u>A5.20</u> AWS Classification <u>E70T-9 (Lincoln's OSXLH-70)</u>		TECHNIQUE Stringer or Weave Bead <u>Stringer Bead</u> Multi - pass or Single Pass (per side) <u>Multi/Single</u> Number of electrodes <u>One</u> Longitudinal <u>N/A</u> Lateral <u>N/A</u> Angle <u>N/A</u>	
SHIELDING Flux <u>N/A</u> Gas <u>CO2</u> Composition <u>100%</u> Electrode - Flux (Class) <u>N/A</u> Flow Rate <u>50 CFH</u> Gas Cup Size <u>5/8"</u>		Contact Tube to Work Distance <u>1-1/8"</u> Peening: None Interpass Cleaning <u>Pneumatic Chipping Hammer or Brush</u>	
PREHEAT Preheat Temp., Min. See below * Interpass Temp., Min See below Max <u>550° F</u>		POSTWELD HEAT TREATMENT Temp. <u>None**</u> Time <u>N/A</u>	

AWES Jose W Garcia
 CWI 98010941
 QC1-EXP-12/1/2015

WELDING PROCEDURE

Pass or Weld Layer (s)	Process	Filler Metals		Current		In/Min Wire Feed Speed	Volts	In/Min Travel Speed	Joint Details								
		Class	Diam.	Type & Polarity	Amps												
ALL	FCAW-G	E70T-9	3/32"	DCEP	414-500	180-220	28-32	12"-20"									
Heat Input Range: 30 - 80 KJ/in																	
								TOLERANCES <table border="1"> <tr> <th>AS DETAILED</th> <th>AS FIT UP</th> </tr> <tr> <td>R = + 1/16, - 0</td> <td>+ 1/16, - 1/8</td> </tr> <tr> <td>F = + 1/16, - 0</td> <td>NOT LIMITED</td> </tr> <tr> <td>a = 10, - 0</td> <td>10, - 5</td> </tr> </table>		AS DETAILED	AS FIT UP	R = + 1/16, - 0	+ 1/16, - 1/8	F = + 1/16, - 0	NOT LIMITED	a = 10, - 0	10, - 5
AS DETAILED	AS FIT UP																
R = + 1/16, - 0	+ 1/16, - 1/8																
F = + 1/16, - 0	NOT LIMITED																
a = 10, - 0	10, - 5																

MINIMUM PREHEAT AND INTERPASS TEMPERATURE

UP TO 3/4"	OVER 3/4" - 1 1/2"	OVER 1 1/2" - 2 1/2"	OVER 2 1/2"
NONE *	50 °F	150 °F	225 °F

* When Base Metal is Below 32° F, preheat to at least 70° and maintain during welding.

**This procedure may vary due to fabrication sequence, fit-up, pass size, etc. within the limitation of variables given in the ANSI/AWS D1.1 (2010). See project welding specifications for additional notes.

Herrick

PROCEDURE QUALIFICATION RECORD (PQR)

THC-CP12

Company Name The Herrick Corporation
 Welding Process (es) FCAW-G

Identification # FCAW-CP-4b
 Revision _____ Date _____ By _____
 Authorized by [Signature] Date 04/10/02
 Type - Manual () Semi - Automatic (X)
 Machine () Automatic ()

JOINT DESIGN USED
 Type B-U4b-F
 Single (X) Double Weld ()
 Backing Yes () No (X)
 Backing Material N/A
 Root Opening 0 Root Face Dimension 0
 Groove Angle 30° Radius (J - U) N/A
 Back Gouging Yes (X) No () Method AIRARC

BASE METALS
 Material Spec. A572
 Type or Grade 50
 Thickness Groove 1" Fillet N/A
 Diameter (Pipe) N/A

FILLER METALS
 AWS Specification A5.20
 AWS Classification E70T-9 (Lincoln's OSXLH-70)

SHIELDING
 Flux N/A Gas CO2
 Composition 100%
 Electrode - Flux (Class) N/A Flow Rate 50 CFH
 Gas Cup Size 5/8

PREHEAT
 Preheat Temp., Min 70°F Max _____
 Interpass Temp., Min 70° F Max 550° F

POSITION
 Position of: Groove Horz (2G) Fillet N/A
 Vertical Progression: Up () Down ()

ELECTRICAL CHARACTERISTICS
 DC
 Transfer Mode (GMAW)
 Short - Circuiting () Globular () Spray ()
 Current: AC () DCEP (X) DCEN () Pulsed ()
 Power Source: CC (X) CV (X)
 Other _____

TECHNIQUE
 Stringer or Weave Bead Stringer Bead
 Multi - pass or Single Pass (per side) Multiple
 Number of electrodes One
 Electrode Spacing Longitudinal N/A
 Lateral N/A
 Angle N/A

Contact Tube to Work Distance 1-1/8"
 Peening NONE
 Interpass Cleaning Pneumatic Chipping Hammer or Brush

POSTWELD HEAT TREATMENT
 Temp. None
 Time. N/A

DETAIL



Pass or Weld Layer (s)	Process	Filler Metals		Current		Volts	In/Min Travel Speed
		Class	Diam.	Type & Polarity	Amps		
1-9 *10	FCAW-G	E70T-9	3/32	DCEP	460	30	16"
	FCAW-G	E70T-9	3/32	DCEP	460	30	16"

* Backgouge to sound metal prior to weld pass # 10

ACCURATE WELD TESTING LAB

5223 TWEEDY BLVD., SOUTH GATE, CA 90280 PH(323)564-5879 FX(323)564-3843

Date: April 18, 2002

SAN BERNARDINO STEEL/HERRICK CORP.
5454 N. INDUSTRIAL PARKWAY
SAN BERNARDINO, CA 92427

Test Date: 04/18/02

WPS#: FCAW CP-4b

Lab#: 759

PLATE SIZE: 1" A-572, GR. 50

RADIOGRAPHIC TEST RESULTS: SATISFACTORY**SIDE BENDS**

1	SIDE BEND	SATISFACTORY	2.	SIDE BEND	SATISFACTORY
3.	SIDE BEND	SATISFACTORY	4.	SIDE BEND	SATISFACTORY

TENSION TEST RESULTS

No.	W	T	Area	Load	P.S.I.	Location
1	.755"	1.000"	.7550"	65,800	87,152	P.M-DUCTILE
2	.765"	.996"	.7619"	65,700	86,231	P.M-DUCTILE

CHARPY "V" NOTCH

@THE WELD@ +70°F.

NOTCH LOCATION	IMPACT VALUE	% SHEAR	MILL. LAT. EXP
1. WELD METAL	91	90	.073"
2. WELD METAL	89	90	.065"
3. WELD METAL	90	90	.076"
4. WELD METAL	*87	90	.071"
5. WELD METAL	*99	90	.075"

AVG. FT. LBS.: 90.6

* LOW & HIGH READING, AVERAGE OF REMAINING THREE.

@THE WELD@ +70°F.

NOTCH LOCATION	IMPACT VALUE	% SHEAR	MILL. LAT. EXP
1. H.A.Z.	150	60	.082"
2. H.A.Z.	151	60	.093"
3. H.A.Z.	*176	100	.091"
4. H.A.Z.	166	90	.090"
5. H.A.Z.	*147	60	.085"

AVG. FT. LBS.: 155.6

* LOW & HIGH READING, AVERAGE OF REMAINING THREE.

@THE WELD@ -0°F.

NOTCH LOCATION	IMPACT VALUE	% SHEAR	MILL. LAT. EXP
1. WELD METAL	64	60	.052"
2. WELD METAL	*55	50	.041"
3. WELD METAL	61	60	.048"
4. WELD METAL	*66	60	.054"
5. WELD METAL	57	60	.045"

AVG. FT. LBS.: 60.6

* LOW & HIGH READING, AVERAGE OF REMAINING THREE.

ACCURATE WELD TESTING LAB

Ronald S. Mobley
04/18/02
RONALD S. MOBLEY, LAB MANAGER

WE CERTIFY THAT THE ABOVE INFORMATION IS TRUE AND CORRECT



Herrick

WELDING PROCEDURE SPECIFICATION (WPS) YES (X)
 PREQUALIFIED _____ QUALIFIED BY TESTING X _____

Company Name The Herrick Corporation
 Welding Process (es) FCAW-G
 Supporting PQR No. (s) FCAW-CP-4b

Identification # THC-CP13
 Revision # 2 Date 5/28/14 By Joe Kraft
 Authorized by _____ Date 10/11/12
 Type - Manual () Semi - Automatic (X)
 Machine () Automatic ()

JOINT DESIGN USED Type <u>TC-U4b-F</u> Single () Double Weld (X) Backing Yes () No (X) Backing Material <u>N/A</u> Root Opening <u>0-1/16"</u> Root Face Dimension <u>0-1/16"</u> Groove Angle <u>30°</u> Radius (J - U) <u>N/A</u> Back Gouging Yes (X) No () Method <u>AIRARC</u>		POSITION Position of Groove <u>(1G) & (2G)</u> Fillet <u>N/A</u> Vertical Progression Up () Down ()	
BASE METALS Material Spec. <u>AWS D1.1 Table 3.1 Group 1, 2, 3</u> Type or Grade <u>(Except for Group 3 to Group 3)</u> Thickness Groove <u>Unlimited</u> Fillet <u>N/A</u> Diameter (Rebar) <u>N/A</u>		ELECTRICAL CHARACTERISTICS DC Transfer Mode (GMAW) Short - Circuiting () Globular () Spray () Current: AC () DCEP (X) DCEN () Pulsed () Power Source: CC () CV (X)	
FILLER METALS AWS Specification <u>A5.20</u> AWS Classification <u>E70T-9</u> (Lincoln's OSXLH-70)		TECHNIQUE Stringer or Weave Bead <u>Stringer Bead</u> Multi - pass or Single Pass (per side) <u>Multi/Single</u> Number of electrodes <u>One</u> Longitudinal <u>N/A</u> Lateral <u>N/A</u> Angle <u>N/A</u>	
SHIELDING Flux <u>N/A</u> Gas <u>CO2</u> Composition <u>100%</u> Electrode - Flux (Class) <u>N/A</u> Flow Rate <u>50 CFH</u> Gas Cup Size <u>3/4"</u>		Contact Tube to Work Distance <u>1-1/8"</u> Peening: <u>None</u> Interpass Cleaning <u>Pneumatic Chipping Hammer or Brush</u>	
PREHEAT Preheat Temp., Min. <u>See below *</u> Interpass Temp., Min <u>See below</u> Max <u>550° F</u>		POSTWELD HEAT TREATMENT Temp. <u>None**</u> Time <u>N/A</u>	

Jose W Garcia
 CWI 98010941
 QC1 EXP. 12/1/2015

WELDING PROCEDURE

Pass or Weld Layer (s)	Process	Filler Metals		Current		In/Min Wire Feed Speed	Volts	In/Min Travel Speed	Joint Details										
		Class	Diam.	Type & Polarity	Amps														
ALL	FCAW-G	E70T-9	3/32"	DCEP	414-500	180-220	28-32	12"-20"											
Heat Input Range: 30 - 80 KJ/in																			
<table border="1"> <thead> <tr> <th colspan="2">TOLERANCES</th> </tr> <tr> <th>AS DETAILED</th> <th>AS FIT UP</th> </tr> </thead> <tbody> <tr> <td>R = + 1/16, - 0</td> <td>+ 1/16, - 1/8</td> </tr> <tr> <td>f = + 1/16, - 0</td> <td>NOT LIMITED</td> </tr> <tr> <td>a = + 10, - 0</td> <td>+ 10, - 5</td> </tr> </tbody> </table>										TOLERANCES		AS DETAILED	AS FIT UP	R = + 1/16, - 0	+ 1/16, - 1/8	f = + 1/16, - 0	NOT LIMITED	a = + 10, - 0	+ 10, - 5
TOLERANCES																			
AS DETAILED	AS FIT UP																		
R = + 1/16, - 0	+ 1/16, - 1/8																		
f = + 1/16, - 0	NOT LIMITED																		
a = + 10, - 0	+ 10, - 5																		

MINIMUM PREHEAT AND INTERPASS TEMPERATURE

UP TO 3/4"	OVER 3/4" - 1 1/2"	OVER 1 1/2" - 2 1/2"	OVER 2 1/2"
NONE *	50 °F	150 °F	225 °F

* When Base Metal is Below 32° F, preheat to at least 70° and maintain during welding.

**This procedure may vary due to fabrication sequence, fit-up, pass size, etc. within the limitation of variables given in the ANSI/AWS D1.1 (2010). See project welding specifications for additional notes.

Herrick

PROCEDURE QUALIFICATION RECORD (PQR)

THC-CP13

Company Name The Herrick Corporation
 Welding Process (es) FCAW-G

Identification # FCAW-CP-4b
 Revision _____ Date _____ By _____
 Authorized by [Signature] Date 04/10/02
 Type - Manual () Semi - Automatic (X)
 Machine () Automatic ()

JOINT DESIGN USED Type <u>B-U4b-F</u> Single (X) Double Weld () Backing Yes () No (X) Backing Material <u>N/A</u> Root Opening <u>0</u> Root Face Dimension <u>0</u> Groove Angle <u>30°</u> Radius (J - U) <u>N/A</u> Back Gouging Yes (X) No () Method <u>AIRARC</u>		POSITION Position of: Groove <u>Horz (2G)</u> Fillet <u>N/A</u> Vertical Progression: Up () Down ()	
BASE METALS Material Spec. <u>A572</u> Type or Grade <u>50</u> Thickness Groove <u>1"</u> Fillet <u>N/A</u> Diameter (Pipe) <u>N/A</u>		ELECTRICAL CHARACTERISTICS DC Transfer Mode (GMAW) Short - Circuiting () Globular () Spray () Current: AC () DCEP (X) DCEN () Pulsed () Other _____	
FILLER METALS AWS Specification <u>A5.20</u> AWS Classification <u>E70T-9 (Lincoln's OSXLH-70)</u>		TECHNIQUE Stringer or Weave Bead <u>Stringer Bead</u> Multi - pass or Single Pass (per side) <u>Multiple</u> Number of electrodes <u>One</u> Electrode Spacing Longitudinal <u>N/A</u> Lateral <u>N/A</u> Angle <u>N/A</u>	
SHIELDING Flux <u>N/A</u> Gas <u>CO2</u> Electrode - Flux (Class) <u>N/A</u> Composition <u>100%</u> Flow Rate <u>50 CFH</u> Gas Cup Size <u>3/4</u>		Contact Tube to Work Distance <u>1-1/8"</u> Peening: <u>NONE</u> Interpass Cleaning <u>Pneumatic Chipping Hammer or Brush</u>	
PREHEAT Preheat Temp., Min <u>70°F</u> Interpass Temp., Min <u>70° F</u> Max <u>550° F</u>		POSTWELD HEAT TREATMENT Temp. <u>None</u> Time. <u>N/A</u>	

DETAIL



Pass or Weld Layer (s)	Process	Filler Metals		Current		Volts	In/Min Travel Speed
		Class	Diam.	Type & Polarity	Amps		
1-9	FCAW-G	E70T-9	3/32	DCEP	460	30	16"
*10	FCAW-G	E70T-9	3/32	DCEP	460	30	16"

* Backgouged to sound metal prior to weld pass # 10

ACCURATE WELD TESTING LAB

5223 TWEEDY BLVD., SOUTH GATE, CA 90280 PH(323)564-5879 FX(323)564-3843

Date: April 18, 2002

SAN BERNARDINO STEEL/HERRICK CORP.
5454 N. INDUSTRIAL PARKWAY
SAN BERNARDINO, CA 92427

Test Date: 04/18/02

WPS#: FCAW CP-4b

Lab#: 759

PLATE SIZE : 1" A-572, GR. 50

RADIOGRAPHIC TEST RESULTS: SATISFACTORY

SIDE BENDS

1	SIDE BEND	SATISFACTORY	2.	SIDE BEND	SATISFACTORY
3.	SIDE BEND	SATISFACTORY	4.	SIDE BEND	SATISFACTORY

TENSION TEST RESULTS

No.	W	T	Area	Load	P.S.I.	Location
1	.755"	1.000"	.7550"	65,800	87,152	P.M -DUCTILE
2	.765"	.996"	.7619"	65,700	86,231	P.M- DUCTILE

CHARPY "V" NOTCH

@THE WELD@ +70°F.

	NOTCH LOCATION	IMPACT VALUE	% SHEAR	MILL. LAT. EXP
1.	WELD METAL	91	90	.073"
2.	WELD METAL	89	90	.065"
3.	WELD METAL	90	90	.076"
4.	WELD METAL	*87	90	.071"
5.	WELD METAL	*99	90	.075"

AVG. FT. LBS.: 90.6

* LOW & HIGH READING, AVERAGE OF REMAINING THREE.

@THE WELD@ +70°F.

	NOTCH LOCATION	IMPACT VALUE	% SHEAR	MILL. LAT. EXP
1.	H.A.Z.	150	60	.082"
2.	H.A.Z.	151	60	.093"
3.	H.A.Z.	*176	100	.091"
4.	H.A.Z.	166	90	.090"
5.	H.A.Z.	*147	60	.085"

AVG. FT. LBS.: 155.6

* LOW & HIGH READING, AVERAGE OF REMAINING THREE.

@THE WELD@ -0°F.

	NOTCH LOCATION	IMPACT VALUE	% SHEAR	MILL. LAT. EXP
1.	WELD METAL	64	60	.052"
2.	WELD METAL	*55	50	.041"
3.	WELD METAL	61	60	.048"
4.	WELD METAL	*66	60	.054"
5.	WELD METAL	57	60	.045"

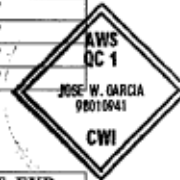
AVG. FT. LBS.: 60.6

* LOW & HIGH READING, AVERAGE OF REMAINING THREE.

ACCURATE WELD TESTING LAB

Ronald S. Mobley 04/18/02
RONALD S. MOBLEY, LAB MANAGER

WE CERTIFY THAT THE ABOVE INFORMATION IS TRUE AND CORRECT



Herrick

WELDING PROCEDURE SPECIFICATION (WPS) YES (X)
 PREQUALIFIED X QUALIFIED BY TESTING _____

Company Name The Herrick Corporation
 Welding Process (es) FCAW-G
 Supporting PQR No. (s) _____

Identification # THC - CP43
 Revision _____ Date _____ By _____
 Authorized by Joe Kraft Date 5/31/19
 Type - Manual () Semi - Automatic (X)
 Machine () Automatic ()

JOINT DESIGN USED Type <u>Dblr - F</u> Single (X) Double Weld () Backing Yes (X) No () Backing Material _____ Base Metal _____ Root Opening <u>As Rolled</u> Root Face Dimension <u>0</u> Groove Angle <u>30°</u> Radius (J - U) <u>J</u> Back Gouging Yes () No (X) Method <u>N/A</u>		POSITION Position of Groove <u>FLAT (1G)</u> Fillet <u>N/A</u> Vertical Progression Up () Down ()	
BASE METALS Material Spec. <u>AWS D1.1 Table 3.1 Group 1, 2, 3</u> Type or Grade <u>(Except for Group 3 to Group 3)</u> Thickness Groove <u>Unlimited</u> Fillet <u>N/A</u> Diameter (Rebar) _____ N/A		ELECTRICAL CHARACTERISTICS DC Transfer Mode (GMAW) Short - Circuiting () Globular () Spray () Current: AC () DCEP (X) DCEN () Pulsed () Power Source: CC () CV (X) Other: N/A	
FILLER METALS AWS Specification <u>A5.20</u> AWS Classification <u>E70T-9</u> (<u>Lincoln's OSXLH-70</u>)		TECHNIQUE Stringer or Weave Bead <u>Stringer Bead</u> Multi - pass or Single Pass (per side) <u>Multi-pass</u> Number of electrodes <u>One</u> Longitudinal <u>N/A</u> Lateral <u>N/A</u> Angle <u>N/A</u>	
SHIELDING Flux <u>N/A</u> Gas <u>CO2</u> Composition <u>100%</u> Electrode - Flux (Class) <u>N/A</u> Flow Rate <u>50 CFH</u> Gas Cup Size <u>5/8"</u>		Contact Tube to Work Distance <u>1-1/4"</u> Peening _____ Interpass Cleaning <u>Pneumatic Chipping Hammer or Brush</u>	
PREHEAT Preheat Temp., Min. <u>See below *</u> Interpass Temp., Min <u>See below</u> Max <u>550° F</u>		POSTWELD HEAT TREATMENT Temp. <u>None**</u> Time <u>N/A</u>	



WELDING PROCEDURE

Pass or Weld Layer (s)	Process	Filler Metals		Current		In/Min Wire Feed Speed	Volts	In/Min Travel Speed	Joint Details						
		Class	Diam.	Type & Polarity	Amps										
ALL	FCAW-G	E70T-9	3/32"	DCEP	414-500	180-220	28-32	12"-20"							
Heat Input Range: 35 - 80 KJ/in															
TOLERANCES <table border="1"> <tr> <th>AS DETAILED</th> <th>AS FIT UP</th> </tr> <tr> <td>R = +1/16", -0"</td> <td>+ 1/4", - 1/16"</td> </tr> <tr> <td>a = +10", -0"</td> <td>+ 10", -5"</td> </tr> </table>										AS DETAILED	AS FIT UP	R = +1/16", -0"	+ 1/4", - 1/16"	a = +10", -0"	+ 10", -5"
AS DETAILED	AS FIT UP														
R = +1/16", -0"	+ 1/4", - 1/16"														
a = +10", -0"	+ 10", -5"														

MINIMUM PREHEAT AND INTERPASS TEMPERATURE

UP TO 3/4"	OVER 3/4" - 1 1/2"	OVER 1 1/2" - 2 1/2"	OVER 2 1/2"
NONE *	50 °F	150 °F	225 °F

* When Base Metal is Below 32° F, preheat to at least 70° and maintain during welding.

**This procedure may vary due to fabrication sequence, fit-up, pass size, etc. within the limitation of variables given in the ANSI/AWS D1.1 (2015). See project welding specifications for additional notes.

Herrick

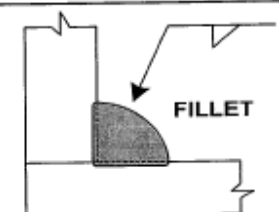
WELDING PROCEDURE SPECIFICATION (WPS) YES (X) PREQUALIFIED X QUALIFIED BY TESTING _____

Company Name The Herrick Corporation
 Welding Process (es) FCAW-G
 Supporting PQR No. (s) N/A

Identification # THC-F1
 Revision # 2 Date 5/28/14 By Joe Kraft
 Authorized by _____ Date 10/11/12
 Type - Manual () Semi - Automatic (X)
 Machine () Automatic ()

JOINT DESIGN USED Type <u>Fillet</u> Single (X) Double Weld () Backing Yes () No (X) Backing Material <u>N/A</u> Root Opening <u>N/A</u> Root Face Dimension <u>N/A</u> Groove Angle <u>N/A</u> Radius (J - U) <u>N/A</u> Back Gouging Yes () No (X) Method <u>N/A</u>		POSITION Position of Groove <u>N/A</u> Fillet <u>(1F) & (2F)</u> Vertical Progression Up () Down ()	
BASE METALS Material Spec. <u>AWS D1.1 Table 3.1 Group 1, 2, 3</u> Type or Grade <u>(Except for Group 3 to Group 3)</u> Thickness Groove <u>N/A</u> Fillet <u>Unlimited</u> Diameter (Rebar) <u>N/A</u>		ELECTRICAL CHARACTERISTICS DC Transfer Mode (GMAW) Short - Circuiting () Globular () Spray () Current: AC () DCEP (X) DCEN () Pulsed () Power Source: CC () CV (X)	
FILLER METALS AWS Specification <u>A5.20</u> AWS Classification <u>E70T-9 (Lincoln's OSXLH-70)</u>		TECHNIQUE Stringer or Weave Bead <u>Stringer Bead</u> Multi - pass or Single Pass (per side) <u>Multi/Single</u> Number of electrodes <u>One</u> Longitudinal <u>N/A</u> Lateral <u>N/A</u> Angle <u>N/A</u>	
SHIELDING Flux <u>N/A</u> Gas <u>CO2</u> Composition <u>100%</u> Electrode - Flux (Class) <u>N/A</u> Flow Rate <u>50 CFH</u> Gas Cup Size <u>5/8"</u>		Contact Tube to Work Distance <u>1-1/8"</u> Peening, None Interpass Cleaning <u>Pneumatic Chipping Hammer or Brush</u>	
PREHEAT Preheat Temp., Min. <u>See below *</u> Interpass Temp., Min <u>See below</u> Max <u>550° F</u>		POSTWELD HEAT TREATMENT Temp. <u>None**</u> Time <u>N/A</u> In Charge: <u>Jose W Garcia</u> CWI: <u>98010941</u> QC1 EXP: <u>12/1/2015</u>	

WELDING PROCEDURE

Pass or Weld Layer (s)	Process	Filler Metals		Current		In/Min Wire Feed Speed	Volts	In/Min Travel Speed	Joint Details
		Class	Diam.	Type & Polarity	Amps				
All	FCAW-G	E70T-9	3/32"	DCEP	311-379	135-165	23-27	8"-14"	 <p>FILLET</p> <p>Min. Weld Size See Table 5.8</p> <p>Base Metal Thickness of Thicker Part Joined (T) Minimum Size of Fillet Weld</p> <p>T<3/4 1/4 Single-Pass Weld Must be Used T>3/4 5/16</p>
Heat Input Range: 30 - 80 KJ/in									
All	FCAW-G	E70T-9	3/32"	DCEP	400-490	180-220	27-31	12"-20"	
Heat Input Range: 30 - 80 KJ/in									

MINIMUM PREHEAT AND INTERPASS TEMPERATURE

UP TO 3/4"	OVER 3/4" - 1 1/2"	OVER 1 1/2" - 2 1/2"	OVER 2 1/2"
NONE *	50 °F	150 °F	225 °F

* When Base Metal is Below 32° F, preheat to at least 70° and maintain during welding.

**This procedure may vary due to fabrication sequence, fit-up, pass size, etc. within the limitation of variables given in the ANSI/AWS D1.1 (2010). See project welding specifications for additional notes.

WELDING PROCEDURE SPECIFICATION (WPS) YES (X)
PREQUALIFIED X QUALIFIED BY TESTING _____

Company Name The Herrick Corporation
 Welding Process (es) FCAW-G
 Supporting PQR No. (s) N/A

Identification # THC-PP1
 Revision # 1 Date 5/28/14 By Joe Kraft
 Authorized by [Signature] Date 10/11/12
 Type - Manual () Semi - Automatic (X)
 Machine () Automatic ()

JOINT DESIGN USED Type <u>BTC-P4-F</u> Single (X) Double Weld () Backing Yes () No (X) Backing Material <u>N/A</u> Root Opening <u>0</u> Root Face Dimension <u>1/8" (Min)</u> Groove Angle <u>45°</u> Radius (J - U) <u>N/A</u> Back Gouging Yes () No (X) Method <u>N/A</u>		POSITION Position of Groove <u>(1G) & (2G)</u> Fillet <u>N/A</u> Vertical Progression Up () Down ()	
BASE METALS Material Spec. <u>AWS D1.1 Table 3.1 Group 1, 2, 3</u> Type or Grade <u>(Except for Group 3 to Group 3)</u> Thickness Groove <u>1/4" Min</u> Fillet <u>N/A</u> Diameter (Rebar) <u>N/A</u>		ELECTRICAL CHARACTERISTICS <u>DC</u> Transfer Mode (GMAW) Short - Circuling () Globular () Spray () Current: AC () DCEP (X) DCEN () Pulsed () Power Source: CC () CV (X)	
FILLER METALS AWS Specification <u>A5.20</u> AWS Classification <u>E70T-9 (Lincoln's OSXLH-70)</u>		TECHNIQUE Stringer or Weave Bead <u>Stringer Bead</u> Multi - pass or Single Pass (per side) <u>Multi/Single</u> Number of electrodes <u>One</u> Longitudinal <u>N/A</u> Lateral <u>N/A</u> Angle <u>N/A</u>	
SHIELDING Flux <u>N/A</u> Gas <u>CO2</u> Composition <u>100%</u> Electrode - Flux (Class) <u>50 CFH</u> Gas Cup Size <u>5/8"</u>		Contact Tube to Work Distance <u>1-1/8"</u> Peening: None Interpass Cleaning <u>Pneumatic Chipping Hammer or Brush</u>	
PREHEAT Preheat Temp., Min. <u>See below *</u> Interpass Temp., Min <u>See below</u> Max <u>550° F</u>		POSTWELD HEAT TREATMENT Temp. <u>None**</u> Time <u>N/A</u>	

Jose W Garcia
 CWI 98010941
 QCT EXP: 12/1/2015

WELDING PROCEDURE

Pass or Weld Layer (s)	Process	Filler Metals		Current			In/Min Wire Feed Speed	Volts	In/Min Travel Speed	Joint Details							
		Class	Diam.	Type & Polarity	Amps												
All	FCAW-G	E70T-9	3/32"	DCEP	311-379	135-165	23-27	8"-14"	<table border="1"> <caption>TOLERANCES</caption> <thead> <tr> <th>AS DETAILED</th> <th>AS FIT UP</th> </tr> </thead> <tbody> <tr> <td>R= +1/16", -0</td> <td>+1/16", -1/16"</td> </tr> <tr> <td>f= +U, -0</td> <td>± 1/16"</td> </tr> <tr> <td>a= +10", -0"</td> <td>+10", -6"</td> </tr> </tbody> </table> <p>*S" Minimum as per AWS D1.1</p>	AS DETAILED	AS FIT UP	R= +1/16", -0	+1/16", -1/16"	f= +U, -0	± 1/16"	a= +10", -0"	+10", -6"
AS DETAILED	AS FIT UP																
R= +1/16", -0	+1/16", -1/16"																
f= +U, -0	± 1/16"																
a= +10", -0"	+10", -6"																
Heat Input Range: 30 - 80 KJ/in																	
All	FCAW-G	E70T-9	3/32"	DCEP	400-490	180-220	27-31	12"-20"									
Heat Input Range: 30 - 80 KJ/in																	

MINIMUM PREHEAT AND INTERPASS TEMPERATURE

UP TO 3/4"	OVER 3/4" - 1 1/2"	OVER 1 1/2" - 2 1/2"	OVER 2 1/2"
NONE *	50 °F	150 °F	225 °F

* When Base Metal is Below 32° F, preheat to at least 70° and maintain during welding.

**This procedure may vary due to fabrication sequence, fit-up, pass size, etc. within the limitation of variables given in the ANSI/AWS D1.1 (2010). See project welding specifications for additional notes.

The Herrick Corporation SHOP Welding Procedure Specifications Index
Herrick Job #9870


WPS ID#	PROCESS	JOINT	TYPE WELD	POSITION	ELECT. DIA	ELECTRODE TYPE	CVN	PREQ	QUAL	D.I.S	REV.	DATE
PARTIAL PENETRATION WELDS												
THC-PP1	FCAW-G	BTC-P4	0-45 Deg PP	1G-2G	3/32"	OSXLH-70	YES	YES		YES	1	5/28/14
FILLET WELDS												
THC-F1	FCAW-G	FILLET	FILLET	1F-2F	3/32"	OSXLH-70	YES	YES		YES	2	5/28/14

Herrick

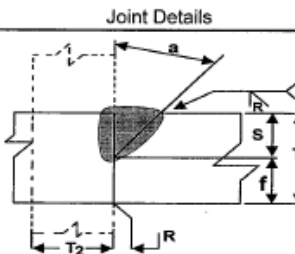
WELDING PROCEDURE SPECIFICATION (WPS) YES (X) PREQUALIFIED X QUALIFIED BY TESTING _____

Identification # THC-PP1
 Revision # 1 Date 5/28/14 By Joe Kraft
 Authorized by [Signature] Date 10/11/12
 Type - Manual () Semi - Automatic (X)
 Machine () Automatic ()

Company Name The Herrick Corporation
 Welding Process (es) FCAW-G
 Supporting PQR No. (s) N/A

JOINT DESIGN USED Type <u>BTC-P4-F</u> Single (X) Double Weld () Backing Yes () No (X) Backing Material <u>N/A</u> Root Opening <u>0</u> Root Face Dimension <u>1/8"</u> (Min) Groove Angle <u>45°</u> Radius (J - U) <u>N/A</u> Back Gouging Yes () No (X) Method <u>N/A</u>	POSITION Position of Groove <u>(1G) & (2G)</u> Fillet <u>N/A</u> Vertical Progression Up () Down ()
BASE METALS Material Spec. <u>AWS D1.1 Table 3.1 Group 1, 2, 3</u> Type or Grade <u>(Except for Group 3 to Group 3)</u> Thickness Groove <u>1/4" Min</u> Fillet <u>N/A</u> Diameter (Rebar) <u>N/A</u>	ELECTRICAL CHARACTERISTICS <u>DC</u> Transfer Mode (GMAW) Short - Circuiting () Globular () Spray () Current: AC () DCEP (X) DCEN () Pulsed () Power Source: CC () CV (X)
FILLER METALS AWS Specification <u>A5.20</u> AWS Classification <u>E70T-9 (Lincoln's OSXLH-70)</u>	TECHNIQUE Stringer or Weave Bead <u>Stringer Bead</u> Multi - pass or Single Pass (per side) <u>Multi/Single</u> Number of electrodes <u>One</u> Longitudinal <u>N/A</u> Lateral <u>N/A</u> Angle <u>N/A</u>
SHIELDING Flux <u>N/A</u> Gas <u>CO2</u> Composition <u>100%</u> Electrode - Flux (Class) <u>50 CFH</u> Gas Cup Size <u>5/8"</u>	Contact Tube to Work Distance <u>1-1/8"</u> Peening: None Interpass Cleaning <u>Pneumatic Chipping Hammer or Brush</u>
PREHEAT Preheat Temp., Min. See below * Interpass Temp., Min See below Max 550° F	POSTWELD HEAT TREATMENT Temp. None** Time <u>N/A</u>  Jose W Garcia CWI 98010941 QCI EXP. 12/1/2015

WELDING PROCEDURE

Pass or Weld Layer (s)	Process	Filler Metals		Current		In/Min Wire Feed Speed	Volts	In/Min Travel Speed	Joint Details										
		Class	Diam.	Type & Polarity	Amps														
All	FCAW-G	E70T-9	3/32"	DCEP	311-379	135-165	23-27	8"-14"	 <table border="1"> <thead> <tr> <th colspan="2">TOLERANCES</th> </tr> <tr> <th>AS DETAILED</th> <th>AS FIT UP</th> </tr> </thead> <tbody> <tr> <td>R= +1/16", -0</td> <td>+1/8", -1/16"</td> </tr> <tr> <td>f= +U, -0</td> <td>± 1/16"</td> </tr> <tr> <td>a= +10", -5"</td> <td>+10", -5"</td> </tr> </tbody> </table> <p>*S" Minimum as per AWS D1.1</p>	TOLERANCES		AS DETAILED	AS FIT UP	R= +1/16", -0	+1/8", -1/16"	f= +U, -0	± 1/16"	a= +10", -5"	+10", -5"
TOLERANCES																			
AS DETAILED	AS FIT UP																		
R= +1/16", -0	+1/8", -1/16"																		
f= +U, -0	± 1/16"																		
a= +10", -5"	+10", -5"																		
Heat Input Range: 30 - 80 KJ/in																			
All	FCAW-G	E70T-9	3/32"	DCEP	400-490	180-220	27-31	12"-20"											
Heat Input Range: 30 - 80 KJ/in																			

MINIMUM PREHEAT AND INTERPASS TEMPERATURE

UP TO 3/4"	OVER 3/4" - 1 1/2"	OVER 1 1/2" - 2 1/2"	OVER 2 1/2"
NONE *	50 °F	150 °F	225 °F

* When Base Metal is Below 32° F, preheat to at least 70° and maintain during welding.

**This procedure may vary due to fabrication sequence, fit-up, pass size, etc. within the limitation of variables given in the ANSI/AWS D1.1 (2010). See project welding specifications for additional notes.

Herrick

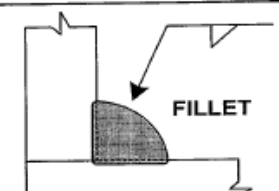
WELDING PROCEDURE SPECIFICATION (WPS) YES (X)
 PREQUALIFIED X QUALIFIED BY TESTING _____

Company Name The Herrick Corporation
 Welding Process (es) FCAW-G
 Supporting PQR No. (s) N/A

Identification # THC-F1
 Revision # 2 Date 5/28/14 By Joe Kraft
 Authorized by [Signature] Date 10/11/12
 Type - Manual () Semi - Automatic (X)
 Machine () Automatic ()

JOINT DESIGN USED Type <u>Fillet</u> Single (X) Double Weld () Backing Yes () No (X) Backing Material <u>N/A</u> Root Opening <u>N/A</u> Root Face Dimension <u>N/A</u> Groove Angle <u>N/A</u> Radius (J - U) <u>N/A</u> Back Gouging Yes () No (X) Method <u>N/A</u>		POSITION Position of Groove <u>N/A</u> Fillet <u>(1F) & (2F)</u> Vertical Progression Up () Down ()	
BASE METALS Material Spec. <u>AWS D1.1 Table 3.1 Group 1, 2, 3</u> Type or Grade <u>(Except for Group 3 to Group 3)</u> Thickness Groove <u>N/A</u> Fillet <u>Unlimited</u> Diameter (Rebar) <u>N/A</u>		ELECTRICAL CHARACTERISTICS DC Transfer Mode (GMAW) Short - Circuiting () Globular () Spray () Current: AC () DCEP (X) DCEN () Pulsed () Power Source: CC () CV (X)	
FILLER METALS AWS Specification <u>A5.20</u> AWS Classification <u>E70T-9 (Lincoln's OSXLH-70)</u>		TECHNIQUE Stringer or Weave Bead <u>Stringer Bead</u> Multi - pass or Single Pass (per side) <u>Multi/Single</u> Number of electrodes <u>One</u> Longitudinal <u>N/A</u> Lateral <u>N/A</u> Angle <u>N/A</u>	
SHIELDING Flux <u>N/A</u> Gas <u>CO2</u> Composition <u>100%</u> Electrode - Flux (Class) <u>N/A</u> Flow Rate <u>50 CFH</u> Gas Cup Size <u>5/8"</u>		Contact Tube to Work Distance <u>1-1/8"</u> Peening: None Interpass Cleaning <u>Pneumatic Chipping Hammer or Brush</u>	
PREHEAT Preheat Temp., Min. <u>See below *</u> Interpass Temp., Min <u>See below</u> Max <u>550° F</u>		POSTWELD HEAT TREATMENT Temp. <u>None**</u> Time <u>N/A</u>	

WELDING PROCEDURE

Pass or Weld Layer (s)	Process	Filler Metals		Current		In/Min Wire Feed Speed	Volts	In/Min Travel Speed	Joint Details	
		Class	Diam.	Type & Polarity	Amps					
All	FCAW-G	E70T-9	3/32"	DCEP	311-379	135-165	23-27	8"-14"	 <p>Min. Weld Size See Table 5.8 Base Metal Thickness of Thicker Part Joined (T) Minimum Size of Fillet Weld</p> <p>T < 3/4 1/4 Single-Pass T > 3/4 5/16 Weld Must be Used</p>	
Heat Input Range: 30 - 80 KJ/in										
All	FCAW-G	E70T-9	3/32"	DCEP	400-490	180-220	27-31	12"-20"		
Heat Input Range: 30 - 80 KJ/in										

MINIMUM PREHEAT AND INTERPASS TEMPERATURE

UP TO 3/4"	OVER 3/4" - 1 1/2"	OVER 1 1/2" - 2 1/2"	OVER 2 1/2"
NONE *	50 °F	150 °F	225 °F

* When Base Metal is Below 32° F, preheat to at least 70° and maintain during welding.
 **This procedure may vary due to fabrication sequence, fit-up, pass size, etc. within the limitation of variables given in the ANSI/AWS D1.1 (2010). See project welding specifications for additional notes.



FLUX-CORED GAS-SHIELDED (FCAW-G) WIRE

Outershield® XLH-70

Mild Steel, Flat & Horizontal • AWS E70T-1C-H8, E70T-9C-H8

Key Features

- ▶ Meets AWS D1.8 seismic lot waiver requirements for demand critical welds.
- ▶ H8 diffusible hydrogen levels - controlled for high resistance to hydrogen induced cracking.
- ▶ High deposition rates and excellent fast follow characteristics.
- ▶ Stiff wire enables feeding over long distances.
- ▶ Tolerates mild levels of surface contaminants.
- ▶ Designed for welding with CO₂ shielding gas.

Conformances

AWS A5.20/A5.20M: 2005 E70T-1C-H8, E70T-9C-H8
 ASME SFA-5.20: E70T-1C-H8, E70T-9C-H8
 ABS: 3YSA-H5
 FEMA 353
 AWS D1.8

Welding Positions

Flat & Horizontal

Typical Applications

- ▶ Structural fabrication
- ▶ Heavy equipment
- ▶ General fabrication
- ▶ Seismic applications
- ▶ Machinery fabrication

Shielding Gas

100% CO₂
 Flow Rate: 40-50 CFH

Outershield® XLH-70
(AWS E70T-1C, E70T-9C)

DIAMETERS / PACKAGING

Diameter in (mm)	50 lb (22.7 kg) Coil	500 lb (227 kg) Speed-Feed® Drum
3/32 (2.4)	ED030236	ED030360

NOTE: Speed-Feed® drums require rotation for proper payout.

MECHANICAL PROPERTIES⁽¹⁾ – As Required per AWS A5.20/A5.20M: 2005

	Yield Strength ⁽²⁾ MPa (ksi)	Tensile Strength MPa (ksi)	Elongation %	Charpy V-Notch J (ft•lbf)	
				① -18°C (0°F)	② -29°C (-20°F)
Requirements AWS E70T-1C-H8 AWS E70T-9C-H8	400 (58) min.	480-660 (70-95)	22 min.	27 (20) min. –	– 27 (20) min.
Typical Results⁽³⁾ As-Welded with 100% CO ₂	480-530 (70-77)	570-620 (82-89)	27-30	61-134 (45-99)	42-107 (31-79)

DEPOSIT COMPOSITION⁽¹⁾ – As Required per AWS A5.20/A5.20M: 2005

	%C	%Mn	%Si
Requirements - AWS E70T-1C-H8, E70T-9C-H8	0.12 max.	1.75 max.	0.90 max.
Test Results⁽²⁾ As-Welded with 100% CO ₂	0.06-0.07	1.40-1.60	0.48-0.58
	%S	%P	Diffusible Hydrogen (mL/100g weld deposit)
Requirements - AWS E70T-1C-H8, E70T-9C-H8	0.03 max.	0.03 max.	8.0 max.
Test Results⁽²⁾ As-Welded with 100% CO ₂	≤0.01	≤0.01	3-6

TYPICAL OPERATING PROCEDURES

Diameter, Polarity Shielding Gas	CTWD ⁽⁴⁾ mm (in)	Wire Feed Speed m/min (in/min)	Voltage (volts)	Approx. Current (amps)	Melt-Off Rate kg/hr (lb/hr)	Deposition Rate kg/hr (lb/hr)	Efficiency (%)
3/32 in. (2.4 mm), DC+ 100% CO ₂	32 (1-1/4)	3.8 (150)	23-26	345	6.5 (14.4)	5.6 (12.4)	86
		5.1 (200)	27-30	445	8.7 (19.2)	7.6 (16.8)	87
		6.4 (250)	28-31	510	10.9 (24.0)	9.5 (21.0)	87
		7.6 (300)	30-32	570	13.1 (28.8)	11.4 (25.2)	87
		8.3 (325)	31-33	600	14.2 (31.2)	12.4 (27.3)	87

⁽¹⁾Typical all weld metal. ⁽²⁾Measured with 0.2% offset. ⁽³⁾See test results disclaimer below. ⁽⁴⁾To estimate CTWD, subtract 1/4 in. (6.0 mm) from CTWD.

The Lincoln Electric Company
 22801 St. Clair Avenue
 Cleveland, Ohio 44117-1199

CERTIFICATE OF CONFORMANCE
 (APPLIES ONLY TO U.S. PRODUCTS)



Product: **Outershield® XLH70**
 Classification: **E70T-1C-H8, E70T-9C-H8**
E70T1-C1A2-CS1-H8
 Specification: **AWS A5.20:2005, ASME SFA-5.20**
AWS A5.36:2012, ASME SFA-5.36
 Date: **October 22, 2015**

This is to certify that the product named above and supplied on the referenced order number is of the same classification, manufacturing process, and material requirements as the material which was used for the test that was concluded on the date shown, the results of which are shown below. All tests required by the specifications shown for classification were performed at that time and the material tested met all requirements. It was manufactured and supplied according to the Quality System Program of the Lincoln Electric Company, Cleveland, Ohio, U.S.A., which meets the requirements of ISO9001, NCA3800, AWS A5.01, and other specification and Military requirements, as applicable. The Quality System Program has been approved by ASME, ABS, and VdTUV.

Operating Settings	E70T-9C-H8 Requirements	RESULTS
Electrode Size		3/32 inch
Polarity		DC+
Shielding Gas (per AWS A5.32)	100% CO ₂ (C1-C-100)	100% CO ₂ (C1-C-100)
Voltage, V		29
Wire Feed Speed, cm/min (in/min)		508 (200)
Current, A		435
Average Heat Input, kJ/mm (kJ/in)		1.9 (48)
Contact Tip to Work Distance, mm (in)		32 (1.25)
Postweld Heat Treatment	As-welded	As-welded
Pass/Layers		11/5
Preheat Temperature, °C (°F)	(60 min.)	20 (70)
Interpass Temperature, °C (°F)	(275 - 325)	165 (325)

Mechanical properties of weld deposits

Tensile Strength, MPa (ksi)	(70 - 95)	630 (91)
Yield Strength, 0.2% Offset, MPa (ksi)	(58 min.)	540 (78)
Elongation %	22 min.	27
Average Impact Energy Joules @ -29 °C (ft-lbs @ -20 °F)	(20 min.)	67 (50) 59,63,79 (44,46,58)
Average Hardness, HRB	Not Required	93

Chemical composition of weld deposits (weight %)

C	0.12 max.	0.07
Mn	1.75 max.	1.88
Si	0.90 max.	0.63
S	0.03 max.	0.01
P	0.03 max.	0.01

Diffusible Hydrogen (per AWS A4.3)	E70T-9C-H8 Requirements	RESULTS
Electrode Size		3/32 inch
Polarity		DC+
Shielding Gas (per AWS A5.32)		100% CO ₂ (C1-C-100)
Diffusible Hydrogen, mL/100g	8.0 max.	4.7
Absolute Humidity (grains moisture/lb dry air)		59

The Lincoln Electric Company
 22801 St. Clair Avenue
 Cleveland, Ohio 44117-1199

CERTIFICATE OF CONFORMANCE
 (APPLIES ONLY TO U.S. PRODUCTS)



Product: Outershield® XLH70
 Classification: E70T-1C-H8, E70T-9C-H8
 E70T1-C1A2-CS1-H8
 Specification: AWS A5.20:2005, ASME SFA-5.20
 AWS A5.36:2012, ASME SFA-5.36
 Date: October 22, 2015

Operating Settings	E70T1-C1A2-CS1-H8 Requirements	RESULTS
Electrode Size		3/32 inch
Polarity		DC+
Shielding Gas (per AWS A5.32)	100% CO2 (C1-C-100)	100% CO2 (C1-C-100)
Voltage, V		29
Wire Feed Speed, cm/min (in/min)		508 (200)
Current, A		435
Average Heat Input, kJ/mm (kJ/in)		1.9 (48)
Contact Tip to Work Distance, mm (in)		32 (1.25)
Postweld Heat Treatment	As-welded	As-welded
Pass/Layers		11/5
Preheat Temperature, °C (°F)	(60 min.)	20 (70)
Interpass Temperature, °C (°F)	(275 - 325)	165 (325)

Mechanical properties of weld deposits		
Tensile Strength, MPa (ksi)	(70 - 95)	630 (91)
Yield Strength, 0.2% Offset, MPa (ksi)	(58 min.)	540 (78)
Elongation %	22 min.	27
Average Impact Energy Joules @ -29 °C (ft-lbs @ -20 °F)	(20 min.)	67 (50) 59,63,79 (44,46,58)
Average Hardness, HRB	Not Required	93

Chemical composition of weld deposits (weight %)		
C	0.12 max.	0.07
Mn	1.75 max.	1.68
Si	0.90 max.	0.63
S	0.030 max.	0.006
P	0.030 max.	0.006

Diffusible Hydrogen (per AWS A4.3)	E70T1-C1A2-CS1-H8 Requirements	RESULTS
Electrode Size		3/32 inch
Polarity		DC+
Shielding Gas (per AWS A5.32)		100% CO2 (C1-C-100)
Diffusible Hydrogen, mL/100g	8 max.	5
Absolute Humidity (grains moisture/lb dry air)		59

- This certificate complies with the requirements of EN 10204, Type 2.2.
- Test assembly constructed of ASTM A36 steel.
- Filler Weld Test (positions as required): Met requirements.
- Radiographic inspection: Met requirements.
- The strength and elongation properties reported here were obtained from tensile specimens artificially aged at 105°C (220°F) for 48 hours.
- Results below the detection limits of the instrument or lower than the precision required by the specification are reported as zero. Strength values in SI units are reported to the nearest 10 MPa converted from actual data. Preheat and interpass temperature values in SI units are reported to the nearest 5 degrees.

Toronto Cunningham October 22, 2015
 Toronto Cunningham, Certification Supervisor Date

Marie Quintana October 22, 2015
 Marie Quintana, Director, Consumable Compliance Date



CERTIFICATE OF CONFORMANCE
(APPLIES ONLY TO U.S. PRODUCTS)

The Lincoln Electric Company
22801 St. Clair Avenue
Cleveland, Ohio 44117-1199

Product: **Outershield[®] XLH70**
Electrode Lot Number: **14017194**
Classification: **E70T-1C-H8, E70T-9C-H8**
Specification: **AWS D1.8:2009**
Date: **January 16, 2015**

This is to certify that the above listed product was manufactured to meet the Class 1H requirement of AWS A5.01 as required by clause 6.3.8.1 of AWS D1.8:2009.

The product stated herein was manufactured and supplied in accordance with the Quality System Program of The Lincoln Electric Co., Cleveland, Ohio, U.S.A. as outlined in our Quality Assurance Manual. The Quality System Program of The Lincoln Electric Co. has been accepted by ASME, ABS and approved by V>UV, and is certified to ISO 9001:2013

Operating Settings	AWS D1.8 Requirements	High Heat Input Results	Low Heat Input Results
Electrode Size Polarity Shielding Gas (per AWS A5.32) Wire Feed Speed, cm/min (in/min) Current, A Voltage, V Average Heat Input, kJ/mm (kJ/in) Contact Tip to Work Distance, mm (in) Travel Speed, cm/min (in/min) Pass/Layers Interpass Temperature, °C (°F) Preheat Temperature, °C (°F) Weld Position		3/32 inch DC+ 100% CO ₂ (C1-C-100) 762 (3000) 580 32 3.1 (79) 32 (1.25) 36 (1.4) 8/5 230 (450) 120 (250) 1G	3/32 inch DC+ 100% CO ₂ (C1-C-100) 381 (1500) 345 23 1.2 (30) 32 (1.25) 41 (1.6) 17/6 120 (250) 20 (70) 1G
Mechanical properties of weld deposits			
Tensile Strength, MPa (ksi) Yield Strength, 0.2% Offset, MPa (ksi) Elongation %	(70 min.) (58 min.) 22 min.	610 (88) 510 (74) 27	650 (94) 580 (85) 24
Average Impact Energy Joules @ 21 °C (ft-lbs @ 70 °F)	(40 min.)	119 (88) 117,120,120 (96,89,89)	160 (118) 155,159,167 (114,117,123)
Average Impact Energy Joules @ -18 °C (ft-lbs @ 0 °F)	(40 min.)	75 (55) 67,78,79 (49,58,58)	86 (65) 84,85,96 (62,63,71)

- This product satisfies the requirements of AWS D1.8:2009, Annex E, after exposure for 8 weeks at 60°F / 80% relative humidity.
- The Charpy V-notch impact values reported at -18 °C (0 °F) are required when the Lowest Anticipated Service Temperature (LAST) is -28 °C (-20 °F).
- The Charpy V-notch impact values reported at 21 °C (70 °F) are required when the Lowest Anticipated Service Temperature (LAST) is 10 °C (50 °F).
- Test assembly constructed of ASTM A36 steel.
- The strength and elongation properties reported here were obtained from tensile specimens artificially aged at 105°C (220°F) for 48 hours.
- Strength values in SI units are reported to the nearest 10 MPa converted from actual data. Preheat and interpass temperature values in SI units are reported to the nearest 5 degrees.

Toronto Cunningham, Certification Supervisor
January 16, 2015
Date

Dave Fink, Manager, Compliance Engineering, Consumable R&D
January 18, 2015
Date

The Lincoln Electric Company
22801 St. Clair Avenue
Cleveland, Ohio 44117-4199

CERTIFICATE OF CONFORMANCE
(APPLIES ONLY TO U.S. PRODUCTS)



Product: **Outershield® XLH70**
Electrode Lot Number: **14146087**
Classification: **E70T-1C-H8, E70T-9C-H8**
Specification: **AWS D1.8:2009**
Date: **January 30, 2015**

This is to certify that the above listed product was manufactured to meet the Class T4 requirement of AWS A5.01 as required by clause 6.3.8.1 of AWS D1.8:2009.

The product stated herein was manufactured and supplied in accordance with the Quality System Program of The Lincoln Electric Co., Cleveland, Ohio, U.S.A., as outlined in our Quality Assurance Manual. The Quality System Program of The Lincoln Electric Co. has been accepted by ASME, ABS and approved by VGTUV, and is certified to ISO 9001:2013

Operating Settings	AWS D1.8 Requirements	High Heat Input Results	Low Heat Input Results
Electrode Size Polarity Shielding Gas (per AWS A5.32) Wire Feed Speed, cm/min (in/min) Current, A Voltage, V Average Heat Input, kJ/mm (kJ/in) Contacted Tip to Work Distance, mm (in) Travel Speed, cm/min (in/min) Pass/Layers Preheat Temperature, °C (°F) Interpass Temperature, °C (°F) Weld Position	3/32 inch DC+ 100% CO ₂ (C1-C-100) 762 (3000) 555 32 3.0 (76) 32 (1.25) 36 (1.4) 7/4 120 (250) 230 (450) 1G	3/32 inch DC+ 100% CO ₂ (C1-C-100) 381 (150) 340 23 1.2 (31) 32 (1.25) 39 (1.5) 14/5 20 (70) 120 (250) 1G	3/32 inch DC+ 100% CO ₂ (C1-C-100) 381 (150) 340 23 1.2 (31) 32 (1.25) 39 (1.5) 14/5 20 (70) 120 (250) 1G
Mechanical properties of weld deposits			
Tensile Strength, MPa (ksi) Yield Strength, 0.2% Offset, MPa (ksi) Elongation %	(70 min.) (58 min.) 22 min.	580 (83) 470 (68) 30	630 (92) 560 (81) 28
Average Impact Energy Joules @ 21 °C (ft-lbs @ 70 °F)	(40 min.)	177 (130) 172,179,180 (127,132,132)	153 (113) 146,163,159 (106,113,117)
Average Impact Energy Joules @ -18 °C (ft-lbs @ 0 °F)	(40 min.)	112 (83) 111,112,113 (82,82,84)	95 (70) 89,93,103 (65,69,76)

- This product satisfies the requirements of AWS D1.8:2009, Annex E, after exposure for 8 weeks at 80°F / 80% relative humidity.
- The Charpy V-notch impact values reported at -18 °C (0 °F) are required when the Lowest Anticipated Service Temperature (LAST) is -29 °C (-20 °F).
- The Charpy V-notch impact values reported at 21 °C (70 °F) are required when the Lowest Anticipated Service Temperature (LAST) is 10 °C (50 °F).
- Test assembly constructed of ASTM A36 steel.
- The strength and elongation properties reported here were obtained from tensile specimens artificially aged at 105 °C (220 °F) for 48 hours.
- Strength values in SI units are reported to the nearest 10 MPa converted from actual data. Preheat and interpass temperature values in SI units are reported to the nearest 5 degrees.

Toronto Cunningham
Toronto Cunningham, Certification Supervisor
January 30, 2015
Date

David R. ...
Deve Fink, Manager, Compliance
Engineering, Consumable R&D
January 30, 2015
Date